Pacific Northwest
NATIONAL LABORATORY

PNNL-36617, Rev 1
EWG-RPT-049, Rev 1

Testing of High S Matrix Glasses to Expand DFHLW Glass Compositional Ranges

April 2026

JT Reiser
X Lu
S Chong
LM Seymour
NA Lumetta
JD Vienna
RL Russell
V Gervasio
J Bai
JJ Neeway
JL George

U.S. DEPARTMENT OF ENERGY

Prepared for the U.S. Department of Energy
under Contract DE-AC05-76RL01830

DISCLAIMER

PACIFIC NORTHWEST NATIONAL LABORATORY
operated by
BATTELLE
for the
UNITED STATES DEPARTMENT OF ENERGY
under Contract DE-AC05-76RL01830

Printed in the United States of America

Available to DOE and DOE contractors from
the Office of Scientific and Technical
Information,
P.O. Box 62, Oak Ridge, TN 37831-0062
www.osti.gov
ph: (865) 576-8401
fax: (865) 576-5728
email: reports@osti.gov

Available to the public from the National Technical Information Service
5301 Shawnee Rd., Alexandria, VA 22312
ph: (800) 553-NTIS (6847)
or (703) 605-6000
email: info@ntis.gov
Online ordering: http://www.ntis.gov

PNNL-36617, Rev 1
EWG-RPT-049, Rev 1

Testing of High S Matrix Glasses to Expand DFHLW Glass Compositional Ranges

April 2026

JT Reiser, RL Russell, X Lu, V Gervasio, S Chong,
J Bai, LM Seymour, JJ Neeway, NA Lumetta,
JL George, JD Vienna

Prepared for
the U.S. Department of Energy
under Contract DE-AC05-76RL01830

Pacific Northwest National Laboratory
Richland, Washington 99354

Abstract

Gaps in glass composition-property data for direct-feed high-level waste (DFHLW) have recently been identified. One such gap is the region of high sulfur solubility since previous, pretreated, high-level wastes contained very little sulfur. Filling this data gap will significantly broaden the range of process flowsheet options including minimal or no washing and will allow for optimized waste loading in DFHLW glasses for high S-containing wastes. This report summarizes the data collected during the characterization of the DFHLW High S Glass Matrix (HS24).

A glass matrix of 50 glass compositions was developed with a space filling design method to uniformly cover the DFHLW composition region for high sulfur glass. Matrix glasses were designed to expand the composition region outside the current component concentration and property limits to reduce uncertainties at the limits. The 50 matrix glasses were fabricated and tested for properties important to the success of DFHLW vitrification including: composition, canister centerline cooling (CCC) crystallinity and isothermal crystallinity, density, viscosity, electrical conductivity (EC), product consistency test (PCT) response, toxicity, and sulfate solubility. Melter materials corrosion testing is reported elsewhere.

These glasses were intentionally designed to have high SO_3 solubilities (0.7 to 2.2 SO_3 wt%) in compositional regions that had not been previously explored such as high Al_2O_3, Cr_2O_3, F and/or Li_2O regions. Twenty-five glasses showed the measured SO_3 content retained >90% of the target SO_3, and seventeen glasses had SO_3 retention between 80% and 90%. The densities of all the glasses ranged from 2.49 $g \cdot cm^{-3}$ to 2.74 $g \cdot cm^{-3}$. While the model predicted nepheline formation in 5 glasses, only one of the tested 50 CCC glasses formed nepheline, and 35 glasses formed Cr-containing phases such as spinels and eskolaite. Only five glasses were amorphous after CCC treatment where 44 glasses with detectable crystals contained ≤10 wt% crystals and only one glass had > 10 wt% crystals. None of the glasses exceeded the allowable $T_{2\%}$ for spinel crystal formation at 950 ºC (i.e., no glasses had >2 wt% spinel at 950 ºC) during isothermal crystal fraction tests where 10 glasses showed no crystalline phases at or below 950 ºC. All the glasses (except one which failed being slightly lower than the target) satisfied the SO_3 constraint (e.g., target SO_3 concentration in the final glass ≥ measured SO_3 solubility) while 98 glasses did not meet the viscosity constraints and 4 failed the EC constraints. Six quenched (Q) and six CCC glasses failed the Defense Waste Processing Facility (DWPF) Environmental Assessment (EA) glass PCT threshold (PCT $NC_B \leq 16.70$ $g \cdot L^{-1}$, PCT $NC_{Na} \leq 13.35$ $g \cdot L^{-1}$, and PCT $NC_{Li} \leq 9.57$ $g \cdot L^{-1}$,) and 3 Q and 4 CCC failed the PCT design constraint (PCT $NL_{ave} \leq 6.44$ $g \cdot m^{-2}$). One glass exceeded the WTP delisting limits for Cr via EPA Method 1311 (i.e., Toxicity Characteristic Leaching Procedure, TCLP). It should be emphasized that some of these glasses were specifically designed to approach or even exceed certain property constraints, as filling data gaps in these regions will provide the greatest benefit for future model development efforts by improving accuracy and reducing uncertainties. These insights will ultimately support the development of more robust glass formulation strategies, enabling higher waste loading, reducing operational risks, and expanding the processing envelope.

Acknowledgments

The authors gratefully acknowledge the financial support provided by the U.S. Department of Energy Office (DOE) of Environmental Management. We are thankful to Ming Zhu, John Kelley, and Albert Kruger (DOE) for their oversight and collaboration.

The following Pacific Northwest National Laboratory staff members are acknowledged for their contributions: Pavel Ferkl for technical review of the report, David MacPherson for quality assurance, Chrissy Charron, and Cassie Martin for programmatic support during the conduct of this work.

All of the other PNNL staff helping in the laboratory to complete this work are greatly appreciated and acknowledged: P Metheny, M Torres, JM Westman, JM Oshiro, JV Crum, J Kroll, S Choi, J Marcial, A Zwoster, ML Blazon, and D Wang.

Acronyms and Abbreviations

3TS	three times saturation (method)
ARM	Approved Reference Material
ASTM	ASTM International, formerly American Society for Testing and Materials
CCC	canister centerline cooling
CF	crystal fraction
DFHLW	direct-feed high-level waste
DOE	U.S. Department of Energy
DIW	de-ionized water
DWPF	Defense Waste Processing Facility
EA	Environmental Assessment
EC	electrical conductivity
EPMA	electron probe micro-analyzer(sis)
EWG	enhanced waste glass
EWG2	second iteration of enhanced waste glass
HLW	high-level waste
HS	high sulfur
IC	Ion Chromatography
ICP-OES	Inductively Coupled Plasma Optical Emission Spectroscopy
LAB	WTP Laboratory
LAW	low-activity waste
LIBS	Laser-Induced Breakdown Spectroscopy
MV	model validity
NC	normalized concentration by 7-day PCT in $g \cdot L^{-1}$
NL	normalized elemental mass loss by 7-day PCT in $g \cdot m^{-2}$
NP	nepheline
NQAP	Nuclear Quality Assurance Program
PCT	Product Consistency Test
PI	prediction interval
PNNL	Pacific Northwest National Laboratory
Q	quenched glasses
QA	quality assurance
RPD	relative percent difference
SCC	single-component constraint
SD_{pooled}	pooled standard deviation
SSM	sulfur-saturated melt
SwRI	Southwest Research Institute

$T_{1\%}$	temperature at 1 vol% spinel
$T_{2\%}$	temperature at 2 vol% spinel
T_L	liquidus temperature
T_M	melting temperature
TCLP	Toxic Leaching Characteristic Procedure
TPMF	tilt-pour melting furnace
vol%	volume percent
WC	tungsten carbide
w_{SO3}	SO_3 solubility
wt%	weight percent
WDS	Wavelength Dispersive Spectroscopy
WTP	Waste Treatment and Immobilization Plant
XRD	X-ray diffraction

Contents

Figures

Tables

1.0 Introduction

Baseline glass compositions have been developed and demonstrated for successful immobilization of Hanford high-level waste (HLW) (Vienna and Kim 2014). These formulations were developed to start up the Waste Treatment and Immobilization Plant (WTP) located at Hanford and therefore were developed over a narrow range of waste compositions based on fully leached and washed tank sludges with modest waste loading (Peeler et al. 2015). Recent enhanced waste glass (EWG) formulations have shown promise in increasing the waste loading of pretreated sludge compositions from a broader range of HLW feeds (Vienna et al. 2016). Advancements in formulations through the EWG program have recently led to the possibility that the WTP HLW Facility can be efficiently started under a direct feed high-level waste (DFHLW) mode (Vienna et al. 2023) using DFHLW feed vectors with various assumptions. Increasing the loading of minimally pretreated wastes in glass can decrease mission life by 5-10 years and reduce the cost of cleanup by $12.5B-$25.0B (Herman et al. 2022).

DFHLW feeds have several key compositional differences from those of leached and washed (e.g., pretreated) sludges that ultimately could limit waste loading:

1. DFHLW feeds may be retrieved with tank supernate to improve the ability to mobilize solids, reliably sample, and deliver them from tank farms to the HLW Facility. The supernate is rich in sodium (typically up to 4 mol·L^{-1} [Na]), sulfate, and other components (e.g., Cr_2O_3, F, P_2O_5, Cl, K_2O) that are generally washed out of pretreated sludge and managed in the low-activity waste (LAW) treatment flowsheet (Britton 2023). This results in higher ranges of Na_2O and SO_3 in DFHLW feed, requiring expanded composition bounds to allow for increased waste loading in glass. Expanding composition space allows for the compositional flexibility to efficiently treat the current DFHLW flowsheet wastes as well as accommodate wastes delivered through other possible strategies.

2. Aluminum leaching was a primary function of the pretreatment process. Caustic leaching removed a weighted average of 77% of the Al in tank waste sludge (Certa et al. 2005). Earlier baseline work did not include higher Al_2O_3 loadings due to challenges such as meeting the minimum glass production rate for the HLW Facility, and caustic leaching was therefore considered. The lack of leaching in the current scheme, suggests a need to consider broader Al_2O_3 compositional ranges in DFHLW glasses than those previously demonstrated.

3. The concentrations of other components (e.g., SO_3, Cr_2O_3, F, P_2O_5, Cl, K_2O) are increased by the reintroduction of DST supernates and lack of leaching anticipated in the DFHLW flowsheet. Efforts to increase Cr tolerance have been conducted (Gervasio et al. 2025) and are ongoing (Gervasio et al. 2026), resulting in mitigation of the previously reported unacceptable fissile load in the LAW pretreated feed baseline.

This project is aimed at increasing the loading of potential DFHLW feeds in glass by expanding the existing database (Lu et al. 2023) and improving the prediction accuracy of glass property-composition models (Vienna et al. 2016) in the high Al, high S, and high Na compositional region.

- Al_2O_3: As concentrations of Al_2O_3 and Na_2O increase in glass, so does the probability of nepheline [$NaAlSiO_4$] formation (Lu et al. 2021). Nepheline formation during slow cooling in the HLW glass canister is likely to cause the glass to fail to meet chemical durability requirements (Vienna et al. 2017). Although some data in the higher Al_2O_3 and Na_2O composition region has been developed, much more is required to expand the composition region and reduce the prediction uncertainty for nepheline models (Lu et al. 2021). Early estimates suggest that Al_2O_3 concentrations in HLW glass limited by nepheline can be increased from the Vienna et al. (2013)

limit of 23 wt% or the WTP baseline (Vienna and Kim 2014) of 13 wt% to over 24 wt% (Matlack et al. 2008, Matlack et al. 2010) or 30 wt% (Kroll et al. 2019).

- Na_2O: Increasing data and model validity for glasses with increased Na_2O content is paramount for minimizing impacts to the HLW flowsheet. At some point, increasing the concentration of Na_2O will decrease the chemical durability of glass, increase the corrosion rate of melter components, and increase the electrical conductivity of the melt, and decrease the melt viscosity. Several data sets exist for LAW formulations that can augment the current HLW models (Vienna et al. 2022). However, the composition regions are not the same, so data on additional glasses is required to bridge the gap. Early estimates suggest that Na_2O concentration in HLW glass can be increased from the Vienna et al. (2013) limit of 23 wt% or the WTP baseline (Vienna and Kim 2014) of 20 wt% to near 30 wt%.

- SO_3: As concentrations of SO_3, Cl, Cr_2O_3, F, and P_2O_5 increase, so does the propensity for molten salt accumulation in the melter (Vienna et al. 2014; Skidmore et al. 2019). As the concentrations of these components are higher in DFHLW feeds compared to pretreated feeds, the concentration ranges of these components need to be expanded and the solubility measured to improve loading of DFHLW in glass. Early estimates suggest that SO_3 concentration in HLW melter feed can be increased from the WTP baseline (Vienna and Kim 2014) of 0.44 wt% to 2 wt%.

This report documents the design and testing of a high sulfur matrix (HS24) to extend DFHLW glass compositional ranges, glass preparation, characterization and measured vs predicted values comparison using the EWG2.6 models (Vienna et al. 2025).

The designed HS24 glass compositions were batched using the appropriate chemicals and melted a minimum of 2 times to produce a glass of the designed composition. The glass compositions were measured to confirm target compositions.

In this report, the glasses were characterized for the following properties:

- Glass forming ability and melting temperature for each glass by visual observations.
- Elemental and oxide composition of quenched (Q) glasses will be analyzed by electron probe micro-analyzer (EPMA) and Inductively Coupled Plasma Optical Emission Spectroscopy (ICP-OES) to verify accurate batching for glasses selected.
- Secondary crystalline phase formation after slow cooling using the canister centerline cooling (CCC) profile.
- Isothermal crystal fraction formation as a function of temperature.
- Density of Q glasses.
- Viscosity and EC of melt as a function of temperature.
- Q and CCC glass PCT normalized boron, sodium, lithium, and silicon releases.
- Q and CCC glass TCLP responses.
- Sulfate solubility by the three times saturation (3TS) method.

1.1 Quality Assurance

This work was performed in accordance with the Pacific Northwest National Laboratory (PNNL) Nuclear Quality Assurance Program (NQAP). The NQAP complies with the United States Department of Energy Order 414.1D, *Quality Assurance*, and 10 CFR 830, Subpart A, *Quality Assurance Requirements*. The NQAP uses NQA-1-2012*, Quality Assurance Requirements for Nuclear Facility Applications*, as its consensus standard and NQA-1-2012, Subpart 4.2.1, as the basis for its graded approach to quality.

The NQAP works in conjunction with PNNL's laboratory-level Quality Management Program, which is based on the requirements as defined in DOE Order 414.1D and 10 CFR 830 Subpart A.

The work in this report was performed to a technology readiness level of 5.

2.0 Matrix Development

This section describes how the glasses were formulated for representative DFHLW feed composition estimates using the current state-of-the-art glass property-composition models and constraint sets applicable to DFHLW.

2.1 Design Method

The space-filling experimental design capabilities of JMP® were used to develop a glass composition matrix for HLW glass composition region. JMP® has a unique proprietary approach to space-filling designs that are not available in other software packages and are widely considered the most appropriate method for developing such a matrix (Joseph et al. 2015). Standard software default assumptions were used to design the matrix of glasses with a fixed set of single-component constraints (SCC's) for individual oxide concentration ranges. HLW glasses from an existing database of glasses in the same composition region were augmented by this design. The matrix design was required to meet pre-defined acceptance ranges defined by the SCC's and also a broad dispersion of points across the range compared to those of external vertices.

A successful matrix must meet two success criteria: 1) the dispersion value of each component must be below 0.90 and 2) relative range of individual components across the glasses in the matrix should be greater than or equal to 0.80 for components that can achieve their full design range. The methods for calculating these two values are given below.

1) The dispersion ratio of a matrix is defined by the following:
Given a vector x of n values for a particular component (so x is a vector of length n) that are sorted in increasing order, define the d to be the differences of the entries in x. So, d is a vector of length $n - 1$, such that Equation 2.1 applies:

$$d_i = x_{i+1} - x_i \text{ for } i = 1, 2, 3, \ldots, n - 1 \tag{2.1}$$

These d_i values are the lengths of the segments of the partition formed by the component values contained in vector x.

The formula for the dispersion metric is described in Equation 2.2:

$$D = \frac{\sum_{i=1}^{n-1} \left| d_i - \frac{R}{n-1} \right|}{R} \quad (2.2)$$

where D = the dispersion metric
R = the intended range of the particular component or predicted property
n = number of glasses in the matrix

Note that if the points formed an "ideal" uniform or regular partition of the range of the particular component, each d_i would have a length of $\frac{R}{n-1}$, and D would be 0. So, the dispersion metric describes the sum of absolute differences from a uniform or regular partition of the range of the particular component, relative to the range of the component. Thus, a value of D = 1.45 would mean that the absolute differences in the actual segment lengths of the partition formed by the vector x and the length of an "ideal" segment would sum to 1.45 times the intended range of the component.

Additionally, the dispersion metric, D, rewards sets of component values that are close to a uniform or regular partition. Smaller values of D are better in the sense that the corresponding x vector would be closer to a regular partition.

2) The relative range of each individual component across the glasses in the matrix is calculated according to $[\min(g_{matrix})\text{-}\max(g_{matrix})]/[\min(g_{target})\text{-}\max(g_{target})]$.

The matrix was designed following these general steps:

1. Identify compositional gaps;
2. Set component concentration boundaries and property boundaries (both within and outside the typical processing and product quality constraints so that constraints can be successfully predicted);
3. Generate a significant amount (e.g., 40,000) of simulated glasses by JMP® to fill in the space within boundaries;
4. Calculate the predicted properties using various models;
5. Select the glasses within the target property ranges among the 40,000 simulated glasses;
6. Combine the selected glasses with existing data that are within the component concentration boundaries, as well as adding duplicates from previously tested glass matrices;
7. Design candidate glass matrices using JMP® to back fill existing available data with a few different random seeds (e.g., 5);
8. Calculate matrix dispersion and range coverage to select one matrix for testing; and
9. Plot figures to check compositional coverage and property distribution.

2.2 Compositional Boundaries

Component concentration boundaries were obtained using the glasses reported by Lu et al. (2024). The boundaries were based on glasses formulated using the EWG2.5 modeling method from estimated DFHLW feeds (Vienna et al. 2024). Compositional ranges of the glasses that reach the SO_3 solubility limit were used in the high sulfur matrix design. A few exceptions were made to increase the maximum concentration in the high sulfur matrix, such as Cr_2O_3, Li_2O and Fe_2O_3.

Table 2.1 shows these boundaries and rationales of the matrix design ranges.

Table 2.2 shows the components contained in the "Others" component listed in Table 2.1. These minor components are based on average values in the glasses in Lu et al. (2024) and were grouped together with fixed concentrations in the "Others" component.

Table 2.1. Minimum and maximum values (wt%) of the matrix design ranges and rationales.

Component	Min	Max	Rationale
Al_2O_3	4.08	23.13	Range of S-limited glasses in Lu et al. (2024)
B_2O_3	4.71	22.00	Range of S-limited glasses in Lu et al. (2024)
CaO	0.00	8.34	Range of S-limited glasses in Lu et al. (2024)
Cr_2O_3	0.00	2.50	Max from Gervasio et al. (2025)
F	0.00	4.04	Range of S-limited glasses in Lu et al. (2024)
Fe_2O_3	0.00	12.50	TS-1.1 from Vienna and Kim (2014)
Li_2O	0.00	4.30	LAW algorithm from Lumetta et al. (2023)
Na_2O	13.10	25.06	Range of S-limited glasses in Lu et al. (2024)
P_2O_5	0.00	3.90	Range of S-limited glasses in Lu et al. (2024)
SiO_2	28.24	49.46	Range of S-limited glasses in Lu et al. (2024)
SO_3	0.00	1.58	Range of S-limited glasses in Lu et al. (2024)
V_2O_5	0.00	5.08	Range of S-limited glasses in Lu et al. (2024)
ZnO	0.00	4.00	Range of S-limited glasses in Lu et al. (2024)
ZrO_2	0.00	7.57	Range of S-limited glasses in Lu et al. (2024)
Others	0.00	0.15	Range of S-limited glasses in Lu et al. (2024)

Table 2.2. Minor components in "Others". These minor components were grouped together with fixed concentrations in the "Others" component.

Others	Median wt%	wt% in "Others"
Bi_2O_3	0.0096	1.11
Cl	0.1983	23.08
K_2O	0.1250	14.55

Others	Median wt%	wt% in "Others"
MgO	0.0070	0.81
MnO	0.2000	23.28
NiO	0.2125	24.74
PbO	0.0874	10.18
SrO	0.0100	1.16
TiO_2	0.0092	1.07
Total	0.08591	100

2.3 Property Constraints

Table 2.3 shows the property targets used to select glasses generated from the space filling step that bound the properties. These targets are 20% above and below the EWG2.5 model property limits (Vienna et al. 2024), so that the glasses that have predicted values on/near the limits can be included in the testing. The PCT is predicted as normalized elemental mass loss (NL in $g \cdot m^{-2}$) though experimental results are reported as normalized concentration (NC in $g \cdot L^{-1}$) for consistency with past reporting on HLW glasses.

Table 2.3. Property constraints used in the matrix design.

Property	Original EWG2.5 model constraints	Design targets
PCT (Vienna et al. 2024)	$NL_B \leq 4$ g/m^2	$NL_B \leq 4.8$ g/m^2
PCT (Crum and Vienna 2018)	$NL_{Ave} \leq 6.44$ g/m^2	$NL_{Ave} \leq 7.72$ g/m^2
TCLP	$C_{Cd} \leq 0.48$ mg/L	$C_{Cd} \leq 0.58$ mg/L
Nepheline formation (distance to the line)	$p \geq 0.028$	$p \geq 0.0224$
Temperature at 2 vol% spinel	$T_{2\%} \leq 950$ °C	$T_{2\%} \leq 1140$ °C
Zirconia liquidus temperature	T_L-Zr ≤ 1050 °C (for $g_{ZrO2} \geq 0.04$)	T_L-Zr ≤ 1260 °C (for $g_{ZrO2} \geq 0.04$)
Viscosity	$4 \leq \eta_{1150} \leq 6$ Pa·s, $\eta_{1100} < 15$ Pa·s	$3.2 \leq \eta_{1150} \leq 7.2$ Pa·s, $\eta_{1100} < 18$ Pa·s
EC	$\varepsilon_{1100} \geq 0.1$ S/cm, $\varepsilon_{1200} \leq 0.7$ S/cm	$\varepsilon_{1100} \geq 0.08$ S/cm, $\varepsilon_{1200} \leq 0.84$ S/cm
Sulfate solubility	$g_{SO3} \leq$ 3TS w_{SO3} - offset, wt%	$g_{SO3} \times 0.8 \leq$ 3TS w_{SO3} - offset, wt%
Immiscibility	$N_{NaLi} \geq 20$ wt%	$N_{NaLi} \geq 16$ wt%
K-3 refractory corrosion	$k_{1208} \leq 0.04$ in.	$k_{1208} \leq 0.048$ in.
Phosphate formation probability	$p \leq 0.24$	$p \leq 0.29$

PCT is Product Consistency Test; TCLP is Toxicity Characteristic Leaching Procedure; EC is electrical conductivity.

2.4 Compositions

Figure 2.1 shows the scatterplot matrix for the designed 50 high sulfur glasses. Table 2.4 to Table 2.8 list the compositions of the HS24 glasses. HS24-49 and HS24-50 are ORPLG27 (Muller et al. 2010) and HLW-APPS-05 (Gervasio et al. 2023), respectively used as replicates. Heatmaps showing the pair correlations of a few major glass components can be found in Appendix A. Those figures show the comparison between the design space, existing glasses, and the designed 50 high sulfur glasses.

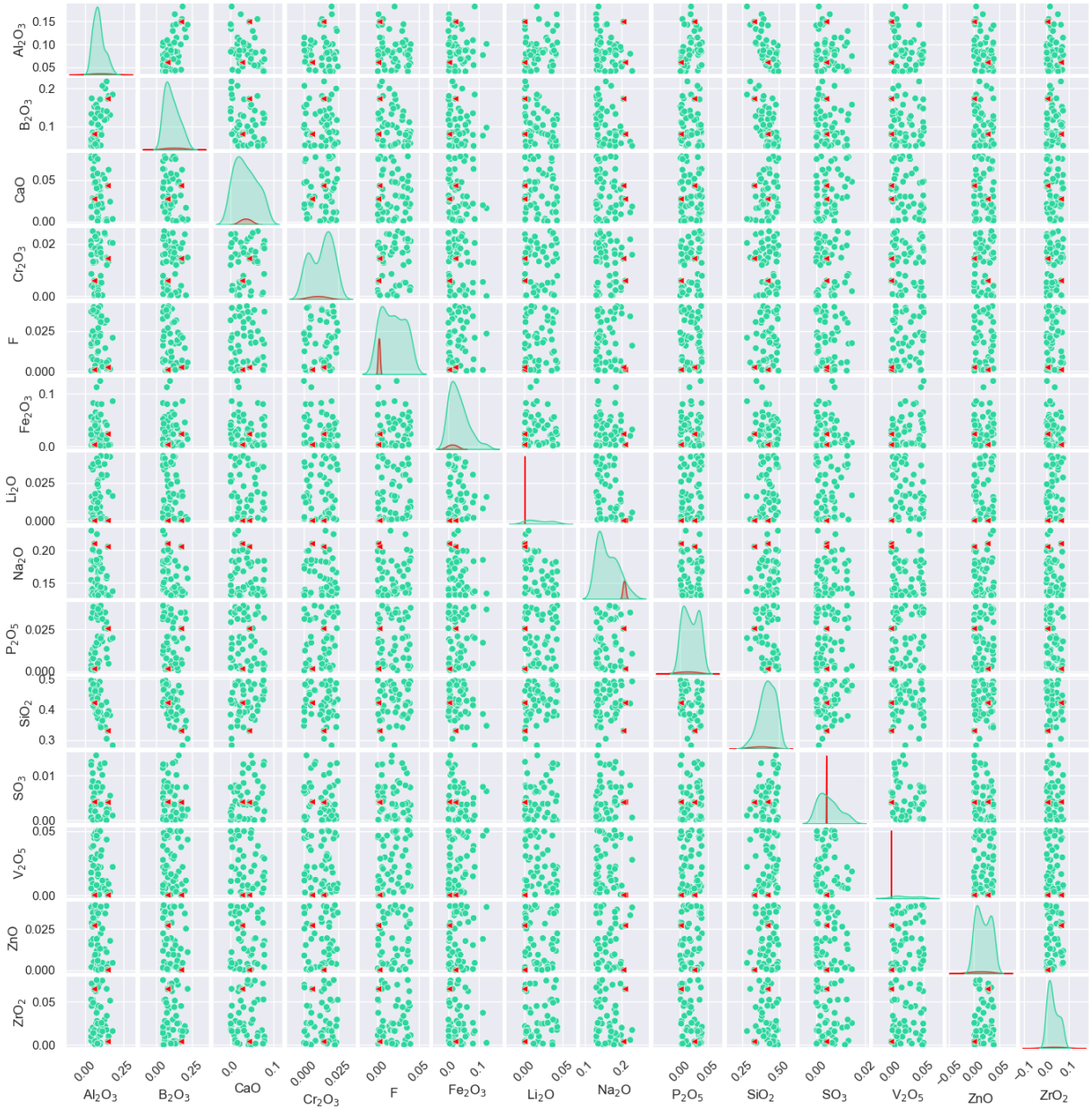

Figure 2.1. Scatterplot matrix for the designed 50 high sulfur glasses. Two red triangles represent the replicate glasses taken from previous studies.

Table 2.4. Glass compositions (mass fraction) for HS24-01 to HS24-10.

Glass ID	HS24-01	HS24-02	HS24-03	HS24-04	HS24-05	HS24-06	HS24-07	HS24-08	HS24-09	HS24-10
Al_2O_3	0.04421	0.06104	0.07015	0.08768	0.05837	0.08296	0.10006	0.16543	0.09412	0.11428
B_2O_3	0.17357	0.15154	0.11092	0.08731	0.05517	0.08325	0.0863	0.12975	0.09966	0.14125
CaO	0.00457	0.04622	0.0182	0.00859	0.02092	0.01109	0.03779	0.02374	0.03892	0.05601
Cr_2O_3	0.00399	0.00029	0.01313	0.00237	0.00339	0.02373	0.02105	0.02044	0.01581	0.01471
F	0.02229	0.02397	0.03858	0.0002	0.03972	0.01144	0.04027	0.00134	0.00624	0.00512
Fe_2O_3	0.00548	0.00552	0.06485	0.05974	0.04782	0.00295	0.0232	0.0027	0.02978	0.0074
Li_2O	0.01583	0.0013	0.00264	0.01803	0.01263	0.03627	0.00914	0.04198	0.01378	0.02839
Na_2O	0.13266	0.176	0.14139	0.19886	0.19924	0.16629	0.18794	0.13122	0.19776	0.14194
P_2O_5	0.00662	0.00045	0.00177	0.0337	0.00304	0.03815	0.03768	0.01891	0.00601	0.01773
SiO_2	0.45436	0.40629	0.38584	0.4272	0.49133	0.48467	0.39331	0.38044	0.41151	0.36524
SO_3	0.00311	0.00035	0.00016	0.00637	0.00736	0.00036	0.00343	0.00551	0.00627	0.01013
V_2O_5	0.03741	0.04447	0.04964	0.04529	0.04706	0.04648	0.00693	0.0024	0.0004	0.00664
ZnO	0.03868	0.00878	0.02904	0.00098	0.00499	0.00367	0.03656	0.01765	0.00378	0.00448
ZrO_2	0.04481	0.06939	0.06192	0.01124	0.00115	0.00286	0.01115	0.05103	0.07064	0.07415
Bi_2O_3	0.00014	0.00005	0.00013	0.00014	0.00009	0.00006	0.00006	0.00008	0.00006	0.00014
Cl	0.00287	0.00101	0.00271	0.00287	0.0018	0.00135	0.0012	0.00172	0.00123	0.00289
K_2O	0.00181	0.00064	0.00171	0.00181	0.00114	0.00085	0.00075	0.00109	0.00077	0.00182
MgO	0.0001	0.00004	0.0001	0.0001	0.00006	0.00005	0.00004	0.00006	0.00004	0.0001
MnO	0.00289	0.00102	0.00274	0.0029	0.00182	0.00136	0.00121	0.00174	0.00124	0.00292
NiO	0.00307	0.00108	0.00291	0.00308	0.00193	0.00144	0.00128	0.00184	0.00132	0.0031
PbO	0.00126	0.00045	0.0012	0.00127	0.0008	0.00059	0.00053	0.00076	0.00054	0.00128
SrO	0.00014	0.00005	0.00014	0.00014	0.00009	0.00007	0.00006	0.00009	0.00006	0.00015
TiO_2	0.00013	0.00005	0.00013	0.00013	0.00008	0.00006	0.00006	0.00008	0.00006	0.00013

Table 2.5. Glass compositions (mass fraction) for HS24-11 to HS24-20.

Glass ID	HS24-11	HS24-12	HS24-13	HS24-14	HS24-15	HS24-16	HS24-17	HS24-18	HS24-19	HS24-20
Al_2O_3	0.13309	0.07915	0.0416	0.04417	0.04251	0.08411	0.05132	0.07402	0.04081	0.06199
B_2O_3	0.1994	0.05945	0.04837	0.10846	0.1325	0.08684	0.0837	0.15704	0.05999	0.04987
CaO	0.00145	0.01089	0.01793	0.0751	0.07739	0.04817	0.02795	0.04772	0.07829	0.07263
Cr_2O_3	0.0236	0.02169	0.01582	0.01857	0.0085	0.01748	0.01856	0.00193	0.02106	0.00082
F	0.01429	0.03393	0.01583	0.00882	0.017	0.03646	0.03567	0.01736	0.03681	0.01956
Fe_2O_3	0.04538	0.01962	0.03183	0.00631	0.00194	0.03001	0.0113	0.00677	0.05597	0.05201
Li_2O	0.00073	0.00155	0.00538	0.00718	0.00076	0.0063	0.00366	0.01665	0.0084	0.03557
Na_2O	0.13479	0.22443	0.22965	0.14042	0.18416	0.18141	0.20102	0.13427	0.17078	0.14026
P_2O_5	0.03493	0.03488	0.01036	0.00338	0.03162	0.02067	0.01291	0.00306	0.00329	0.01223
SiO_2	0.34171	0.41893	0.49081	0.44507	0.4603	0.37096	0.47801	0.47694	0.4649	0.48096
SO_3	0.00098	0.0078	0.00062	0.00749	0.01307	0.00394	0.01055	0.01451	0.00217	0.00608
V_2O_5	0.00324	0.04415	0.0275	0.02946	0.01192	0.05058	0.00739	0.01845	0.01755	0.00204
ZnO	0.03414	0.03311	0.03789	0.0285	0.0018	0.00946	0.02623	0.00051	0.01756	0.03659
ZrO_2	0.02161	0.00568	0.0171	0.07077	0.00479	0.04091	0.01988	0.02516	0.00955	0.01693
Bi_2O_3	0.00012	0.00005	0.0001	0.00007	0.00013	0.00014	0.00013	0.00006	0.00014	0.00014
Cl	0.00246	0.0011	0.00215	0.00145	0.00271	0.00293	0.00273	0.00129	0.00297	0.00288
K_2O	0.00155	0.00069	0.00135	0.00092	0.00171	0.00185	0.00172	0.00082	0.00187	0.00181
MgO	0.00009	0.00004	0.00008	0.00005	0.0001	0.0001	0.0001	0.00005	0.0001	0.0001
MnO	0.00248	0.0011	0.00217	0.00147	0.00273	0.00296	0.00276	0.0013	0.003	0.0029
NiO	0.00264	0.00117	0.0023	0.00156	0.0029	0.00314	0.00293	0.00139	0.00319	0.00308
PbO	0.00109	0.00048	0.00095	0.00064	0.00119	0.00129	0.00121	0.00057	0.00131	0.00127
SrO	0.00012	0.00006	0.00011	0.00007	0.00014	0.00015	0.00014	0.00007	0.00015	0.00015
TiO_2	0.00011	0.00005	0.0001	0.00007	0.00013	0.00014	0.00013	0.00006	0.00014	0.00013

Table 2.6. Glass compositions (mass fraction) for HS24-21 to HS24-30.

Glass ID	HS24-21	HS24-22	HS24-23	HS24-24	HS24-25	HS24-26	HS24-27	HS24-28	HS24-29	HS24-30
Al_2O_3	0.10073	0.14111	0.05165	0.04104	0.09679	0.05462	0.08711	0.10372	0.08735	0.07677
B_2O_3	0.09662	0.11883	0.0571	0.06584	0.04722	0.04818	0.08188	0.04956	0.07935	0.04868
CaO	0.01591	0.00107	0.06287	0.07603	0.04175	0.06311	0.03028	0.02969	0.0033	0.03987
Cr_2O_3	0.00009	0.01464	0.02477	0.01931	0.00526	0.01271	0.00412	0.00778	0.00229	0.02179
F	0.02325	0.00165	0.02479	0.00035	0.03232	0.0074	0.02675	0.00568	0.03916	0.03671
Fe_2O_3	0.12456	0.02284	0.02081	0.02198	0.01308	0.08243	0.04854	0.00335	0.0367	0.03312
Li_2O	0.0156	0.04227	0.03351	0.03527	0.03636	0.0019	0.02261	0.04257	0.02666	0.04092
Na_2O	0.13447	0.1325	0.14169	0.15504	0.17959	0.18336	0.16829	0.16791	0.18401	0.14774
P_2O_5	0.03674	0.02918	0.03483	0.00113	0.03087	0.03829	0.03048	0.03897	0.01594	0.0323
SiO_2	0.34618	0.42364	0.43198	0.49376	0.48965	0.41158	0.44842	0.46238	0.42002	0.4233
SO_3	0.00648	0.00001	0.00877	0.01238	0.01168	0.00501	0.00833	0.01252	0.00068	0.00022
V_2O_5	0.05037	0.01094	0.00882	0.00523	0.00563	0.03839	0.01387	0.0218	0.02229	0.00777
ZnO	0.03807	0.03873	0.03466	0.01539	0.00141	0.03143	0.00005	0.02212	0.02805	0.0116
ZrO_2	0.00239	0.01724	0.05205	0.05241	0.00021	0.01373	0.02441	0.02084	0.04523	0.07478
Bi_2O_3	0.0001	0.00006	0.00013	0.00005	0.00009	0.00009	0.00005	0.00012	0.0001	0.00005
Cl	0.00197	0.00124	0.0027	0.00112	0.00189	0.00182	0.00112	0.00256	0.00207	0.00102
K_2O	0.00124	0.00078	0.0017	0.0007	0.00119	0.00114	0.00071	0.00162	0.00131	0.00064
MgO	0.00007	0.00004	0.0001	0.00004	0.00007	0.00006	0.00004	0.00009	0.00007	0.00004
MnO	0.00199	0.00125	0.00272	0.00113	0.0019	0.00183	0.00113	0.00259	0.00209	0.00103
NiO	0.00211	0.00132	0.00289	0.0012	0.00202	0.00195	0.0012	0.00275	0.00222	0.0011
PbO	0.00087	0.00054	0.00119	0.00049	0.00083	0.0008	0.0005	0.00113	0.00091	0.00045
SrO	0.0001	0.00006	0.00014	0.00006	0.0001	0.00009	0.00006	0.00013	0.0001	0.00005
TiO_2	0.00009	0.00006	0.00013	0.00005	0.00009	0.00008	0.00005	0.00012	0.0001	0.00005

Table 2.7. Glass compositions (mass fraction) for HS24-31 to HS24-40.

Glass ID	HS24-31	HS24-32	HS24-33	HS24-34	HS24-35	HS24-36	HS24-37	HS24-38	HS24-39	HS24-40
Al_2O_3	0.07942	0.05404	0.06833	0.12895	0.08378	0.0673	0.08404	0.08183	0.09968	0.155
B_2O_3	0.06189	0.07162	0.05317	0.11631	0.14697	0.12093	0.13432	0.1033	0.17102	0.17985
CaO	0.01131	0.05491	0.04721	0.05132	0.00064	0.07811	0.07494	0.05766	0.03125	0.06214
Cr_2O_3	0.01612	0.01321	0.02272	0.02411	0.0188	0.01824	0.0014	0.01693	0.01825	0.01326
F	0.00667	0.03782	0.02144	0.02995	0.01919	0.00343	0.00088	0.0178	0.02186	0.00667
Fe_2O_3	0.02729	0.00328	0.04298	0.00062	0.034	0.03952	0.08035	0.00538	0.00094	0.00202
Li_2O	0.04084	0.03721	0.01353	0.03716	0.02565	0.0176	0.01192	0.02393	0.00476	0.01888
Na_2O	0.18219	0.13526	0.15104	0.14217	0.14679	0.13236	0.13695	0.15605	0.14072	0.13158
P_2O_5	0.00284	0.00766	0.01505	0.02556	0.00211	0.01098	0.00457	0.03371	0.03479	0.00447
SiO_2	0.4787	0.48161	0.46439	0.37814	0.42992	0.45892	0.43168	0.43554	0.39019	0.3947
SO_3	0.00426	0.00003	0.00354	0.01277	0.00738	0.00199	0.00014	0.00368	0.00029	0.00251
V_2O_5	0.02049	0.02305	0.0485	0.00512	0.04975	0.02848	0.01467	0.03202	0.04984	0.00868
ZnO	0.03518	0.01881	0.0392	0.01264	0.00567	0.00928	0.01509	0.01928	0.01292	0.00369
ZrO_2	0.0277	0.04871	0.00001	0.02916	0.02459	0.00442	0.00146	0.0015	0.01649	0.00989
Bi_2O_3	0.00006	0.00014	0.0001	0.00007	0.00005	0.00009	0.00008	0.00013	0.00008	0.00007
Cl	0.00118	0.00295	0.00205	0.00139	0.0011	0.00195	0.00175	0.00263	0.00161	0.00154
K_2O	0.00074	0.00186	0.00129	0.00088	0.00069	0.00123	0.00111	0.00166	0.00102	0.00097
MgO	0.00004	0.0001	0.00007	0.00005	0.00004	0.00007	0.00006	0.00009	0.00006	0.00005
MnO	0.00119	0.00298	0.00207	0.0014	0.00111	0.00196	0.00177	0.00265	0.00163	0.00155
NiO	0.00126	0.00316	0.0022	0.00149	0.00118	0.00209	0.00188	0.00282	0.00173	0.00165
PbO	0.00052	0.0013	0.00091	0.00061	0.00048	0.00086	0.00077	0.00116	0.00071	0.00068
SrO	0.00006	0.00015	0.0001	0.00007	0.00006	0.0001	0.00009	0.00013	0.00008	0.00008
TiO_2	0.00005	0.00014	0.0001	0.00006	0.00005	0.00009	0.00008	0.00012	0.00008	0.00007

Table 2.8. Glass compositions (mass fraction) for HS24-41 to HS24-50.

Glass ID	HS24-41	HS24-42	HS24-43	HS24-44	HS24-45	HS24-46	HS24-47	HS24-48	HS24-49	HS24-50
Al_2O_3	0.11466	0.14243	0.14349	0.0763	0.10875	0.18212	0.08624	0.10366	0.0603	0.14895
B_2O_3	0.20683	0.21833	0.13933	0.07522	0.07745	0.18373	0.10381	0.12671	0.0792	0.17253
CaO	0.01636	0.00243	0.00031	0.01945	0.02138	0.0029	0.02056	0.03003	0.0269	0.04295
Cr_2O_3	0.00039	0.01477	0.01189	0.00543	0.00517	0.02028	0.00042	0.01658	0.0059	0.01436
F	0.00287	0.00546	0.03152	0.00082	0.03405	0.02072	0.01231	0.03044	0.0009	0.00238
Fe_2O_3	0.02106	0.0136	0.04015	0.11265	0.08036	0.08594	0.05573	0.06047	0.0028	0.0231
Li_2O	0.00237	0.00098	0.02993	0.00799	0.0302	0.01621	0.0384	0.00147	0	0.00005
Na_2O	0.17228	0.15751	0.16086	0.18542	0.13569	0.13773	0.1315	0.14411	0.21	0.20533
P_2O_5	0.03107	0.01325	0.00793	0.01692	0.0205	0.01974	0.03698	0.01952	0.0014	0.02533
SiO_2	0.36293	0.30414	0.38278	0.38472	0.41299	0.28252	0.39191	0.34102	0.4209	0.32994
SO_3	0.00742	0.00246	0.00168	0.00748	0.00366	0.00106	0.00082	0.00353	0.0041	0.00401
V_2O_5	0.01133	0.04333	0.00267	0.04631	0.03505	0.02199	0.01639	0.03047	0	0.00003
ZnO	0.02501	0.01084	0.0019	0.01878	0.00066	0.00434	0.03426	0.03827	0.0269	0.00007
ZrO_2	0.01568	0.06461	0.0335	0.03702	0.02544	0.01593	0.06628	0.04358	0.0644	0.0038
Bi_2O_3	0.00011	0.00007	0.00013	0.00006	0.0001	0.00005	0.00005	0.00011	0	0.0002
Cl	0.00225	0.00135	0.00278	0.00127	0.002	0.00111	0.00101	0.00234	0.0023	0.00256
K_2O	0.00142	0.00085	0.00176	0.0008	0.00126	0.0007	0.00064	0.00148	0.0575	0.01333
MgO	0.00008	0.00005	0.0001	0.00004	0.00007	0.00004	0.00004	0.00008	0.0044	0.0007
MnO	0.00227	0.00136	0.00281	0.00128	0.00201	0.00111	0.00102	0.00236	0	0.00122
NiO	0.00241	0.00145	0.00298	0.00136	0.00214	0.00118	0.00108	0.00251	0.0001	0.00142
PbO	0.00099	0.0006	0.00123	0.00056	0.00088	0.00049	0.00045	0.00103	0.0001	0.0008
SrO	0.00011	0.00007	0.00014	0.00006	0.0001	0.00006	0.00005	0.00012	0	0
TiO_2	0.0001	0.00006	0.00013	0.00006	0.00009	0.00005	0.00005	0.00011	0	0
Ag_2O	0	0	0	0	0	0	0	0	0	0.00013
Nd_2O_3	0	0	0	0	0	0	0	0	0	0.00681
SnO_2	0	0	0	0	0	0	0	0	0.0319	0

2.5 Predicted Properties

Figure 2.2 shows the predicted properties including η_{1150} (viscosity value at 1150 °C), ε_{1150} (electrical conductivity value at 1150 °C), PCT response, temperature at 2 vol% spinel ($T_{2\%}$), K-3 refractory corrosion, nepheline formation, three times saturation (3TS) sulfur solubility (w_{SO3} in SO_3 wt%), liquidus temperature of Zr-containing phases, and phosphate formation probability for the 50 HS24 designed glasses.

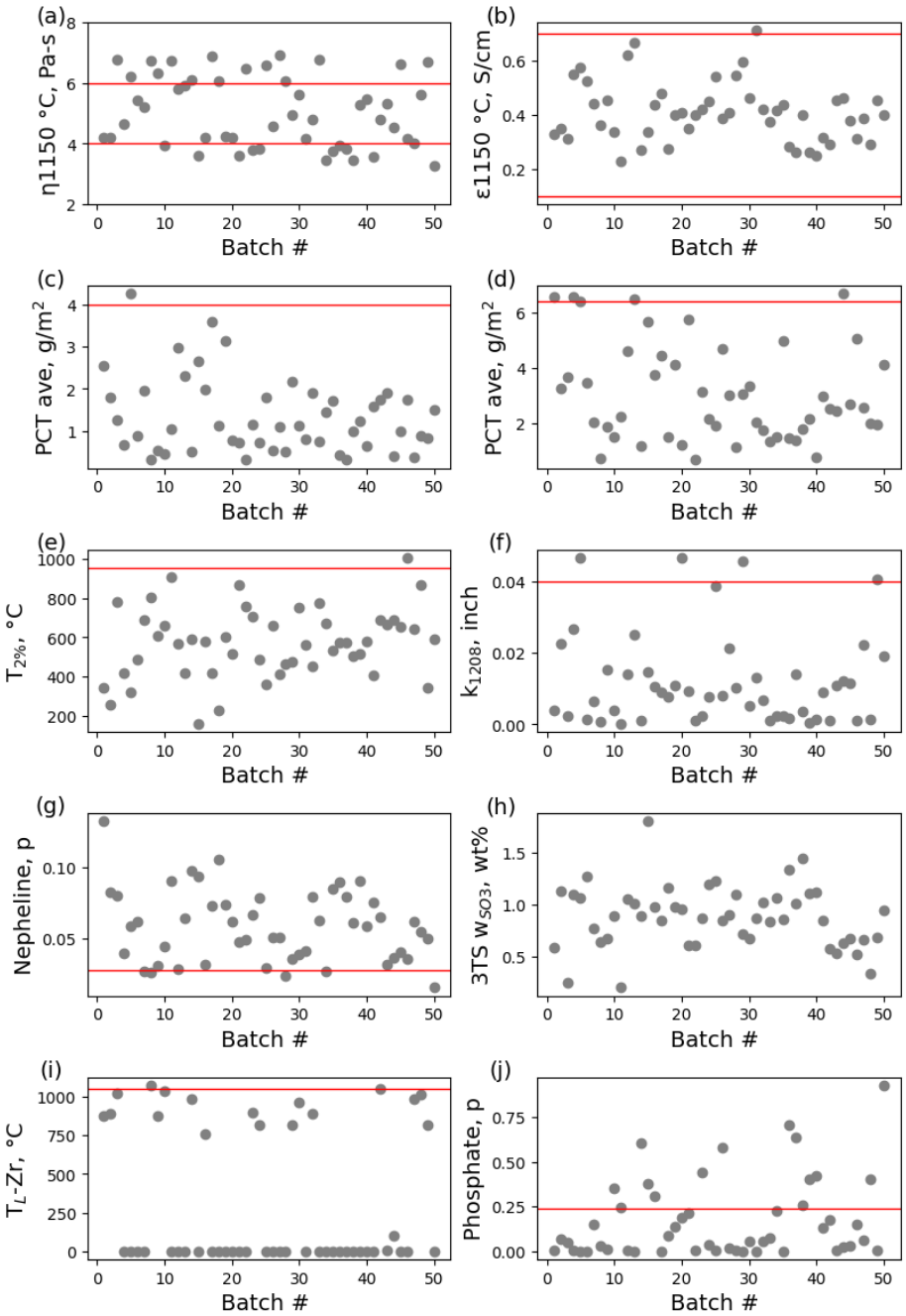

Figure 2.2. Predicted properties including η_{1150} (a), ε_{1150} (b), PCT response from model by Vienna and Crum (2018) (c), PCT response from model by Vienna et al. (2024) (d), spinel $T_{2\%}$ temperature (e), K-3

refractory corrosion (f), nepheline formation (g), 3TS w_{SO3} (h), liquidus temperature of Zr-containing phases, and (i) phosphate formation probability for the 50 designed glasses. Red lines represent the original EWG2.5 model constraints.

3.0 Experimental Methods

This section describes how the test matrix of 50 HS24 glasses was characterized. The descriptions include the methods for (1) glass fabrication and chemical composition analysis, (2) density (ρ) determination, (3) secondary phase identification from CCC treatment, (4) isothermal crystal fraction (CF) and liquidus temperature (T_L) measurement, (5) sulfur solubility measurement, (6) viscosity (η) measurement, (7) EC measurement, (8) PCT measurement, and (9) TCLP measurement. Refractory corrosion testing will be reported separately.

3.1 Glass Fabrication and Characterization

This section describes the fabrication method of the high sulfur glasses (HS24) and their characterization. Laboratory crucible-scale fabrication of glasses was intended to fabricate a glass sample with a controlled composition for property testing, and it was not intended to mimic the actual melter process or feed processability.

3.1.1 Glass Fabrication

These HS24 glasses were batched using appropriate masses of single-metal oxides, single-metal carbonates, sodium salts, and boric acid to form the target compositions. The batched powders were thoroughly mixed in a plastic bag for at least 30 s until the mixture obtained a uniform color. The powders were then transferred to an agate milling chamber and milled for 4 min in a vibratory mill (Angstrom TE110) and placed into a clean Pt-10%Rh crucible for melting. Two types of furnaces were used to increase production rates. The compositions of the resulting glasses were compared to the target compositions, and no difference in glass compositions was observed for using either furnace type.

Some glasses were melted in the Deltech furnace (Deltech Model DT-31-RS, Denver, Colorado) at least two times. First and second melts were performed at 1150 ± 10 °C for 1 h ± 10 min. After the first melt, the glass was air quenched on a stainless-steel pouring plate, ground to a fine powder for 5 min (+ 1 min if glass chunks were still present) in a tungsten carbide (WC) vibratory mill (AngstromTE110) and melted a second time. After each melt, the glass was observed under an optical microscope, and the presence of undissolved particles and/or salts was reported. When the glass presented large amounts of undissolved particles, a third melt was performed at 1200 °C for 1 h ± 10 min after the glass was reduced to powder as described above.

Some glasses were melted in the tilt-pour melting furnace (TPMF, UltraMELT, TLT-2P, Ronkonkoma, NY) where melting was performed by the *Operating Procedure for the Tilt-Pour Furnace*, EWG-OP-086, Rev. 1.0.[1] Melting with a tilt-pour furnace took about 1 h at 1150 ± 50 °C after charging the crucible with the chemical powder was complete. The melt was stirred every 10 to 15 min for < 1 min to obtain a homogeneous distribution of precursors. After the first melt was air quenched on a pouring plate, the glass was observed under an optical microscope and the presence of undissolved particles and/or salts was reported. A second melt was performed on the glasses with large amounts of undissolved particles and/or salts present.

[1] Neeway, JJ. 2024. *Operating Procedure for Tilt-Pour Furnace*. EWG-OP-086, Rev. 1.0.

Details on the furnace type used and number of melts are reported in Table 3.1. The glass compositions were checked using EPMA and ICP-OES, and the crystalline phases in the glass were identified and quantified using X-ray diffraction (XRD).

Table 3.1. Number of melts and type of furnace used. The first melts were all performed at 1150 °C. The second and third melts were done at 1150 °C or 1200 °C depending on glass quality. Glasses were melted at 1200 °C if they had undissolved particles after being melted at 1150 °C.

Glass ID	1st melt	2nd melt	3rd melt	Glass ID	1st melt	2nd melt	3rd melt
HS24-01	Tilt-pour			HS24-26	Deltech	Deltech	
HS24-02	Tilt-pour			HS24-27	Tilt-pour		
HS24-03	Tilt-pour			HS24-28	Deltech	Deltech	Deltech
HS24-04	Tilt-pour			HS24-29	Tilt-pour	Tilt-pour	
HS24-05	Tilt-pour	Tilt-pour		HS24-30	Tilt-pour		
HS24-06	Tilt-pour			HS24-31	Tilt-pour		
HS24-07	Tilt-pour			HS24-32	Deltech	Tilt-pour	
HS24-08	Tilt-pour	Tilt-pour		HS24-33	Tilt-pour		
HS24-09	Tilt-pour			HS24-34	Deltech	Tilt-pour	
HS24-10	Tilt-pour			HS24-35	Deltech	Deltech	
HS24-11	Tilt-pour			HS24-36	Tilt-pour		
HS24-12	Deltech	Deltech		HS24-37	Tilt-pour		
HS24-13	Deltech	Tilt-pour		HS24-38	Deltech	Tilt-pour	
HS24-14	Tilt-pour			HS24-39	Tilt-pour	Tilt-pour	
HS24-15	Deltech	Deltech		HS24-40	Deltech	Tilt-pour	
HS24-16	Tilt-pour	Tilt-pour		HS24-41	Deltech	Tilt-pour	
HS24-17	Tilt-pour			HS24-42	Deltech	Deltech	Deltech
HS24-18	Deltech	Deltech	Tilt-pour	HS24-43	Deltech	Deltech	
HS24-19	Deltech	Deltech		HS24-44	Deltech	Deltech	
HS24-20	Deltech	Deltech		HS24-45	Deltech	Deltech	
HS24-21	Tilt-pour	Tilt-pour		HS24-46	Deltech	Deltech	Deltech
HS24-22	Tilt-pour	Tilt-pour		HS24-47	Deltech	Deltech	
HS24-23	Deltech	Deltech	Tilt-pour	HS24-48	Deltech	Deltech	
HS24-24	Deltech	Deltech	Tilt-pour	HS24-49	Deltech	Deltech	
HS24-25	Tilt-pour	Tilt-pour		HS24-50	Deltech	Deltech	

3.1.2 Chemical Composition Analysis

The JEOL JXA-8530F Hyperprobe EPMA (JEOL USA Inc., Peadbody, MA) was used for chemical composition measurements performed on polished cross sections of the quenched HS24 glasses to confirm that the “as-fabricated” glasses corresponded to the specified target compositions. The glass pieces were mounted in 1” epoxy pucks and polished. The EPMA instrument uses a field-emission gun (FEG) equipped with five wavelength dispersive spectrometers (WDS), each with a take-off angle of 40°. The microprobe data was collected at an accelerating voltage of 15 kV, beam current of 5 nA, and beam size of 50 µm.

Appropriate standards were used for each of the elements analyzed. Interferences were identified and corrected by applying interference standards for each element. Oxygen and lithium were not directly

analyzed. Instead, oxygen was calculated based on stoichiometry of the oxides analyzed. Lithium cannot be detected by WDS, so the target value for each composition was assumed to be present when adjusting the wt% total for the measured glass.

Each sample was measured in ten different locations in a linear traverse with the intention of maximizing representation of the sample. The average of the 10 duplicate measured concentrations of components in weight percent in the quenched glasses were used for the remainder of the study, and they are compared to the target concentrations in Appendix C along with the relative percent difference. Due to the EPMA instrument failure, 6 samples were analyzed by ICP-OES at Southwest Research Institute (SwRI).

These results are discussed in Section 4.1.

3.1.3 Secondary Phase Investigation

XRD analysis was performed on all the quenched HS24 glasses to identify and quantify the crystalline phases within the glasses. The glass powders were mixed with ~5 mass% of an internal standard (e.g., CeO_2 or TiO_2-anatase) using a vibratory mill (Angstrom TE110) and loaded in the Bruker D8 Advance XRD (Bruker AXS Inc., Madison, Wisconsin) with Cu Kα emission. Samples were scanned at a 0.015 or 0.03° 2θ step size with 1.5-s dwell time from 5° to 75° 2θ scan range. The crystalline phases were identified using DIFFRAC.EVA (Bruker Corporation, Billerica, Massachusetts). The crystalline and amorphous fractions were refined and quantified using TOPAS (Bruker Corporation, Billerica, Massachusetts).

These results are discussed in Section 4.1.1.

3.2 Density

The densities of the quenched HS24 glasses were calculated using a helium pycnometer (MicroMetrics AccuPyc II 1340). Each glass was broken into small pieces (~2-8 mm), the mass of glass sample was measured and then placed in a tared 1-cm^3 sample cup. The pycnometer was purged 10 times with He gas prior to volume measurement, and the volume of each glass was measured 10 times at room temperature. An average of 10 volume measurements and the measured mass was used to calculate the glass density. The pycnometer calibration was verified before and after measurements for that day using a National Institute of Standards and Technology traceable standard tungsten carbide ball.

These results are discussed in Section 4.2.

3.3 Canister Centerline Cooling

A portion (~150 g) of each HS24 glass was heat-treated to the simulated CCC temperature profile shown in Table 3.2 and Figure 3.1.

Table 3.2. CCC profile for the DFHLW samples.

Segment	Start Temp (°C)	Stop Temp (°C)	Rate (°C/min)
1[(a)]	1150	1150	0.000
2[(b)]	1150	1050	free fall
3	1050	980	-1.556
4	980	930	-0.806
5	930	875	-0.591
6	875	825	-0.388
7	825	775	-0.253
8	775	725	-0.278
9	725	400	-0.304

(a) Segment 1 is a 30-min dwell at 1150 °C.
(b) Segment 2 free fall is at an estimated rate of -12.5 °C/min.

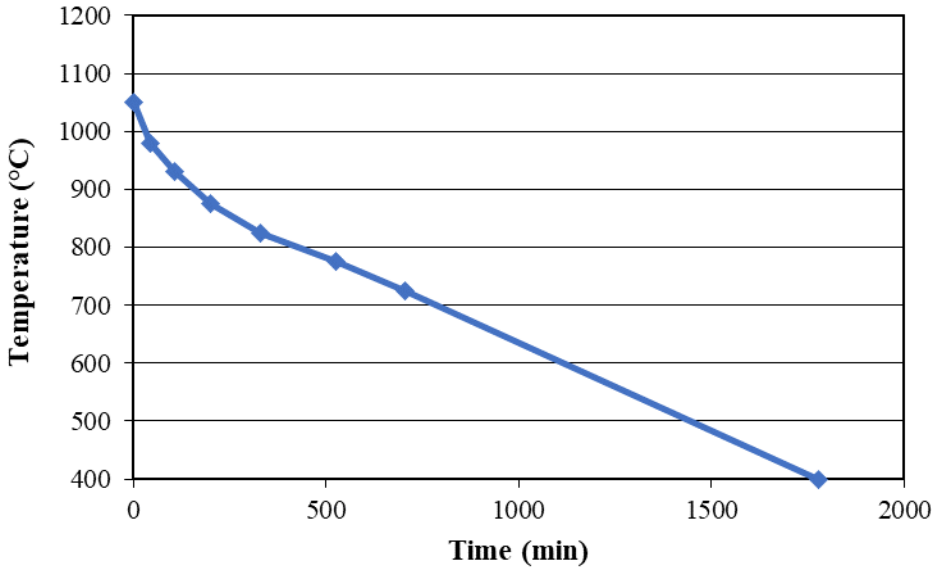

Figure 3.1. Plot of target temperature schedule during CCC treatment.

This profile is the temperature schedule of CCC treatment for Hanford HLW glasses planned for use at the WTP (Petkus 2003) and modified by PNNL to include a 30-min soak at 1150 °C before the cooling begins. Pieces of quenched glass, <3 cm in diameter, were placed in a Pt-alloy crucible and covered with a Pt-alloy lid. The glass samples were placed in a furnace preheated to 1150 °C. After 30 min at 1150 °C, the furnace temperature was quickly dropped to 1050 °C and the cooling profile started. It progressed down to at least 400 °C based on the seven cooling segments shown in Table 3.2 and Figure 3.1.

The amounts and types of crystalline phases that formed during CCC treatment were analyzed by XRD according to the ASTM C1720 procedure. XRD was performed as described in Section 3.1.3. These results are discussed in Section 4.3.

3.4 Isothermal Crystal Fraction and Liquidus Temperature (T_L)

Isothermal crystal fraction (CF) as a function of temperature was measured in Pt-alloy crucibles with tight-fitting lids to minimize volatility according to the ASTM C1720 procedure. Prior to measuring the CF, the furnace temperature accuracy was verified using ARG-1 glass (Smith 1993).

Isothermal CF heat treatments were completed on each HS24 glass by selecting pieces of glass between 4 mm and 425 µm, washing with deionized water (DIW) (three times) in a sonic bath, then performing a final wash with clean ethanol and drying in an appropriate flammable solvent drying oven at 90 °C for at least 2 h. These glass pieces were loaded into a Pt-alloy crucible of roughly 1 cm^3 prepared following the ASTM C1720 procedure. The crucible was first held for 30 min at 1150 °C prior to moving into a second furnace pre-heated to the desired temperature for the isothermal CF heat treatment. The heat treatment temperatures and duration are reported in Table 3.3. Upon the completion of the heat-treatment test, the Pt-alloy crucibles were removed from the furnace and placed on a ceramic brick to quickly cool in air. Due to the small sample size, water quenching was unnecessary to prevent crystal formation from cooling. The crystals that formed during heat treatment and the corresponding fraction (wt%) of each crystal were analyzed using XRD according to Section 3.1.3.

Table 3.3. Heat treatment temperatures and duration used for CF measurements HS24 samples.

Heat Treatment Temperatures and Duration	Glasses Tested
750 °C–72 h	-06, -09, -30, -32, -39
850 °C–48 h	All glasses
900 °C–24 h	-02, -04, -05, -06, -09, -16, -17, -20, -24, -25, -26, -27, -30, -32, -41, -43, -44, -47
950 °C–24 h	All glasses
1000 °C–24 h	-27
1050 °C–24 h	All glasses except for -04, -05, -20, -25, -27, -32, -44, -47

The liquidus temperature (T_L) of each crystal formed in the HS24 glasses was determined using the CF extrapolation method outlined in the ASTM C1720 procedure. This involved linear extrapolation of the measured CF data as a function of temperature, and the temperature projected at zero percent crystals is the T_L. The coefficient of determination (R-squared) was used to indicate how well temperature variations could predict crystallinity formation. Generally, an R-squared value near 1 suggests a strong predictive relationship. If the value significantly deviated from 1, a non-linear fit was also evaluated. The non-linear fit of the CF was calculated using a modified ideal-solution equation (Alton 2002) found in Equation 3.1:

$$C_0 = C_{\max}\left\{1 - \exp\left[-B_L\left(\frac{1}{T} - \frac{1}{T_L}\right)\right]\right\} \quad (3.1)$$

where C_0 is the crystalline mass fraction at equilibrium, C_{max} is the total solute mass fraction in glass, B_L is crystal phase solubility temperature coefficient in K, T is temperature in K from isothermal heat treatment, and T_L is glass liquidus temperature in K. The GRG Nonlinear Solver method in Excel was selected to adjust C_{max}, B_L, and T_L to minimize the sum of squares difference between the measured and calculated CFs as a function of temperature. T_L is listed as > 1300 °C if the fit resulted in values higher than 1300 °C.

The CF and T_L results are discussed in Section 4.4.

3.5 SO_3 Solubility

For all HS24 glasses, SO_3 solubility (w_{SO3}) was determined using the three times saturation (3TS) method (Jin et al. 2019) which was found to have an off-set of 0.33 wt% SO_3 higher than SO_3 expected from

melter operations for melter SO_3 tolerance. This off-set was applied during the design of these glasses (shown in Table 2.3). For each glass, ~52 g of the quenched HS24 glass was milled in a WC chamber for 3 min in the Angstrom mill to generate fines. Then 3.82 g of Na_2SO_4 (Fisher Chemical) was added to 50.00 g of the crushed quenched glass fraction and homogenized with the WC mill for 30 s. The Na_2SO_4 + glass mixtures were melted in Pt/Rh crucibles at 1150 °C for 1 h. After 1 h, each melt was quenched on a stainless-steel pouring plate resulting in a glass and a sulfate salt separated phase. Once cooled, each glass was crushed to fines in the WC mill for 2 min and remelted for 1 h at 1150 °C. This process continued until all three melts were completed to generate the sulfur-saturated melt (SSM) glasses.

The SSM glasses were prepared using the washed particle method where the glasses were crushed incrementally in the WC mill for 4 min and passed through a #120 sieve to obtain <125-µm fraction using a Ro-Tap shaker (RX-29 model, W.C. Tyler) for 6 min for each session. Any glass that did not pass through the sieve was reground in a small grinding chamber for 1.5 min. Grinding and sieving continued until less than 0.5 g remained. From the ~ 50 g of the <125-µm glass fraction, 2.0 g of SSM glass and 20 g of DIW were transferred into a centrifuge tube equipped with a 0.45-µm nylon filter. The centrifuge tube was closed and shaken by hand for ~2 min to ensure that the glass was completely exposed to the solution. After shaking, the centrifuge tubes were centrifuged at 3000 rpm for 5 min in a centrifuge (Sorvall Legend Mach 1.6 model, Thermo Electron Corporation). The centrifuge filter with the washed glass powder was removed, and the rinse solution was decanted and stored for potential future use. The filter with glass powder was returned to the centrifuge tube and the washing procedure was repeated. After the second washing, the filter with glass powder was dried overnight in an 80 °C oven. This procedure was duplicated for each glass to obtain a sufficient amount of final product for analysis. The dried powder was separated from the centrifuge filter and prepared for analysis. The samples were then analyzed by both ICP-OES and Ion Chromatography (IC).

These results are discussed in Section 4.5.

3.6 Viscosity

The viscosity of each glass was measured as a function of temperature using the viscosity dependance to the shear stress and shear rate according to Equation 3.2:

$$\eta = \frac{\tau}{\gamma} \tag{3.2}$$

where η is the viscosity, γ is the shear rate, and τ is the shear stress.

A rotating spindle digital viscometer capable of measuring viscosities from 1 to 100 Pa·s (Brookfield Digital Model LVTD) was staged above a high-temperature Deltech furnace (Deltech Model DT-31-RS, Denver, Colorado) equipped with a Pt/Rh spindle to fit through a hole in the top of the furnace. A 50 mL HS24 glass sample was added to a 100-mL Pt/Rh alloy crucible with approximate dimensions of 5 cm diameter × 6 cm height. The crucible was placed into the furnace, which was set at 1150 °C, and the glass was left to melt for about 20 min. The spindle was lowered into the molten glass in the center of the crucible with the lower end of the rod suspended 0.5 cm above the bottom of the crucible. The furnace was programmed to follow a set ramp schedule at the following temperatures: 1150, 1050, 950, 1150, 1200 °C, and back to 1150 °C. The soak time was 45 min at each temperature. This temperature profile allowed for the potential impacts of crystallization (at lower temperatures) and volatility (at higher temperatures) to be assessed (via reproducibility) at the repeated 1150 °C temperature. The viscometer was calibrated using the Defense Waste Processing Facility (DWPF) startup frit (Crum et al. 2012). At each target temperature, the maximum and minimum spindle torque values were recorded three times each at 3-min intervals. The average of the three measurements was used for data analysis. A secondary

thermocouple was placed below the crucible and temperature was recorded continuously during measurement to ensure thermal equilibrium was reached before measurement.

Results are discussed in Section 4.6.

3.7 Electrical Conductivity

Before conducting EC experiments on the glasses, the EC cell constant, a geometric factor, (K in m^{-1}) was established for the experimental system. The K of the system was calculated using Equation 3.3:

$$K = \varepsilon_s R_s \tag{3.3}$$

where R_s is the solution resistance obtained from the KCl calibration solutions in Ω and ε_s is the known conductivity of the KCl solution in $S \cdot m^{-1}$. R_s was determined by fitting impedance spectra (i.e., Nyquist plots) using 0.1 M and 1.0 M KCl solutions measured at the same volume in the same alumina crucible and Pt/Rh probe apparatus as used for measuring glasses. K was established over a small range of volumes (6.75-7.25 mL) to match the volume of glass used during measurements.

Glass EC measurements were conducted by adding approximately 18 g of quenched HS24 glass to an alumina crucible with the two-blade Pt/Rh probes attached perpendicular to one another 20 mm apart. The assembly was loaded into the furnace at room temperature. The furnace was then slowly (~10 °C/min) ramped to 900 °C to prevent thermal shock to the crucibles and was successively fast ramped to 1200 °C to complete glass melting. The furnace was then held (~30 min) at 1200 °C to homogenize the glass before taking the first measurement. A Biologic VSP-3E potentiostat connected to a two-blade Pt/Rh probe staged above a high-temperature Sentrotech furnace (Sentrotech Model ST-1200-7812, Strongsville, Ohio) was used to measure the molten glass impedance. The furnace was then set to 1150, 1050, and 950 °C using a slow rate (~10 °C/min). After roughly 30-min soaks at each temperature, allowing the program to collect impedance data at an applied voltage of 100 mV and frequencies of 0.5 Hz – $5x10^5$ Hz, measuring 25 data points per decade, and repeating the scan three times for a total of four measurements per glass per temperature. The impedance data was used to determine resistance of the glass (R' in Ω) which was used with the K calculated for the system with the KCl solutions to calculate the experimental conductivity of each glass (ε in $S \cdot m^{-1}$) using Equation 3.4

$$\varepsilon = K/R' \tag{3.4}.$$

These results are discussed in Section 4.7.

3.8 Product Consistency Test

The PCT responses were measured for both Q and CCC samples of each HS24 glass using Method A of ASTM C1285, *Standard Test Methods for Determining Chemical Durability of Nuclear, Hazardous, and Mixed Waste Glasses and Multiphase Glass Ceramics: The Product Consistency Test (PCT)*. Tests were performed in triplicate for each Q and CCC glass. Alongside each campaign of tests, the Approved Reference Material-1 (ARM-1, Mellinger and Daniel 1984) glass was also tested in triplicate. In addition, two blanks, which consisted of DIW in a clean vessel without glass, were added to each campaign. Glasses were ground, sieved to -100 +200 mesh, washed, and prepared according to Section 19.6 of ASTM C1285, and 1.5 g of the prepared glass was added to 15 mL of DIW. The Type 304L Parr stainless steel vessels with polytetrafluoroethylene (PTFE) gaskets were closed, sealed, and placed into an oven at 90 ± 2 °C for 7 days ± 3 h.

After 7 days, the vessels were removed from the oven and allowed to sit until they were cool to the touch. The final mass of the vessel and the solution pH were recorded. The maximum evaporation mass loss due

to evaporation to consider the results from a test vessel was 5% of the original leachant mass. The leachate from each test vessel was filtered through a 0.45-µm-size filter and acidified with concentrated, high-purity HNO_3 to 1 vol% acid before analysis. The leachates were analyzed using ICP-OES for Si, Na, Li and B at SwRI.

Normalized concentrations (NC_i, g L^{-1}) were calculated with the formula in Equation 3.5:

$$\mathrm{NC}_i = \frac{C_i}{f_i} \tag{3.5}$$

where: C_i = the concentration of element i in solution ($g_i \cdot L^{-1}$)
f_i = target mass fraction of element i in the glass ($g_i \cdot glass^{-1}$).

Per the WTP contract (DOE 2000) and the Waste Acceptance Product Specification (DOE 1996), the NC_B, NC_{Na}, and NC_{Li} values must be below the associated values of the DWPF Environmental Assessment (EA) glass (Jantzen et al 1993), which is presented in
Table 3.4. As per ASTM C1285, the $NC_{i,ave}$ values were determined from triplicate tests with the following expression defined in Equation 3.6:

$$\mathrm{NC}_{i,ave} = exp\,[avg\,\ln(\mathrm{NC}_i)] \tag{3.6}$$

Table 3.4. WTP PCT Normalized Release Limits to HLW Glass expressed as NC_i (g/L). The limits are based on the DWPF Environmental Assessment (EA) glass (Jantzen et al 1993).

Constraint Description	Value
PCT normalized B	NC_B <16.70 $g \cdot L^{-1}$ $\ln(NC_B)$ <2.82
PCT normalized Li	NC_{Li} <9.57 $g \cdot L^{-1}$ $\ln(NC_{Li,})$ <2.26
PCT normalized Na	NC_{Na} <13.35 $g \cdot L^{-1}$ $\ln(NC_{Na})$ <2.59
Average PCT normalized B, Li, Na	NC <12.87 $g \cdot L^{-1}$ ln(NC) <2.56

These results are discussed in Section 4.8.

3.9 Toxicity Characteristic Leaching Procedure

The TCLP based on EPA Method 1311 was performed on the Q and CCC glasses to measure the release of toxic elements present in the HS24 glasses (Cr, Ni, Pb, V, Zn) and the boron tracer. The measured TCLP concentrations of regulated elements were compared to their delisting limit concentrations provided in Table 3.5 and to predicted TCLP releases from various models discussed Section 4.9.

Table 3.5. WTP Delisting Limits (Blumenkranz 2006), Resource Conservation and Recovery Act (RCRA) Toxicity, and Universal Treatment Standards (UTS) Limits for TCLP (40 CFR 268. 2015)

Element	Ag	As	Ba	Cd	Cr	Hg	Ni	Pb	Se	V	Zn
WTP Delisting Limit (mg/L)	3.07	0.616	100	0.48	4.95	0.2	22.6	5	1	16.9	225
RCRA Toxicity Limit (mg/L)	5	5	100	1	5	0.2	--	5	1	--	--
RCRA UTS Limit (mg/L)	0.14	5	21	0.11	0.6	0.025	--	0.75	5.7	--	--

The TCLP tests performed on the HS24 glasses included modifications from the original EPA Method 1311 which are as follows:

1) the amount of glass tested was reduced from 100 g to 15 g and the corresponding extraction fluid volume was reduced from 2000 mL to 300 mL,

2) glasses were size-reduced to pass through a sieve < 5.0 mm according to ASTM D6323 rather than < 9.5 mm as described in EPA Method 1311.

3) 0.45-µm PTFE filters housed in polypropylene (PP) casing were used instead of 0.7-µm borosilicate glass fiber filters specified in EPA Method 1311.

These modifications to the EPA Method 1311 test method were agreed upon for application to Hanford HLW glasses between the Washington State Department of Ecology, the U.S. Department of Energy, Vanderbilt University, and PNNL (Kruger 2023).

A pretest was performed on each Q and CCC HS24 glass to identify the extraction fluid to be used for testing according to EPA Method 1311. The extraction fluid used for each glass is provided in Appendix L. Glasses were tested in duplicate. Each campaign of tests was conducted for 18 ± 2 h in ambient temperatures of 23 ± 2 °C. One blank vessel for each extraction fluid used in a campaign was tested in parallel with tests in the campaign. After 18 ± 2 h, the TCLP leachate was filtered with 0.45 µm PTFE filters, preserved with 100 µL Optima concentrated HNO_3, and refrigerated until the samples were ready for solution analysis. The solutions were analyzed by SwRI using ICP-OES.

The normalized concentrations of B (*NC(B)*) and the hazardous metals were calculated using Equation 3.5 from Section 3.8.

The TCLP results are discussed in Section 4.9.

4.0 Results and Discussion

This section describes the results for the chemical composition, CCC, CF and T_L, sulfur solubility, density, viscosity, EC, PCT, and TCLP results.

4.1 Glass Composition

Optical images of the quenched HS24 glasses are provided in Appendix B.

The comparison of the target and measured compositions of HS24 glasses in wt% are provided in Appendix C. The EPMA analysis was done on 44 out of 50 HS24 glasses, and ICP-OES was performed on the remaining 6 glasses. The EPMA results showed that the sums of the measured oxides for all glasses were between 93.8 wt% and 101.6 wt% with added Li_2O target wt%. For the 6 glasses with the ICP-OES results, the sums of the measured oxides were between 96.3 wt% and 100.6 wt% excluding F and Cl.

The summary of measured composition results include the following:

- The relative precent difference (RPD) of the main components including Al_2O_3, Na_2O, and SiO_2 were ≤ 4.8%, ≤ 5.0%, and ≤ 5.4%, respectively.
- RPD values of Cl were in the range of -8.1% to -34.4% where negative RPDs imply that the measured concentrations were lower than the target concentrations.
- RPD values of F were in the range of -100% to 9.7%. Three glasses including HS24-04, HS24-37, and HS24-44 showed the highest RPD (-100%), and their target F masses were relatively low ranging from 0.02 to 0.09 wt%. The median RPD was -8.6%.
- Twenty-five glasses showed the SO_3 retention of > 90%, and 17 glasses showed SO_3 retention between 80 and 90%.

The Cr_2O_3 or Cr-containing spinels were observed in most HS24 glasses, indicating that the solubility limit was surpassed or Cr_2O_3 was not fully dissolved. Relatively high fluctuation of RPD values for Cl and F were due to their volatilities during the melting process. The RPD values were inconsistent or high for the components with low target wt% (<0.2 wt%). These inconsistencies in RPD are likely due to instrumental uncertainties near the detection limits. Overall, the measured compositions of HS24 glasses were close to the target compositions with reasonable expectation.

4.1.1 Secondary Phase Investigation in Quenched Glasses

The refined XRD patterns with crystalline phase wt% are provided in Appendix D. The normalized wt% was calculated using Equation 4.1, where *P* is the phase wt%, *C* is the crystallinity of 51.28% in the CeO_2 standard, and *S* is the added standard wt%.

$$\text{Normalized wt\% of a Phase} = \frac{P \times C}{100 - S} \tag{4.1}$$

Table 4.1 provides a summary of crystalline phases found in the HS24 glasses. Eleven glasses were fully amorphous. The XRD results showed the presence of CaF_2, Cr_2O_3, $Na_2Ca(PO_4)F$, $ZnSiO_4$, $CaAl_4O_7$, Li_3PO_4, $Ca_{10}(PO_4)_6F_2$, $Ca_2Fe_2O_5$, ZrO_2, $Cr_{0.75}Fe_{1.25}O_3$, Fe_3O_4 (spinel), and Cr-containing spinel phases as expected. Lower RPD values of Cr in the glass matrix were due to the removal of Cr from the glass matrix because

of crystallization of Cr_2O_3, $Cr_{0.75}$ $Fe_{1.25}O_3$, or spinel phases. The $Cr_{0.75}$ $Fe_{1.25}O_3$ phase has the same structure as Cr_2O_3, and the Cr site is partially occupied by the Fe cation. The Cr-spinel phases, $Zn(Fe_{1.9}Cr_{0.1})O_4$ and $ZnCr_2O_4$ were observed and their structures are shown in Figure 4.1. These two phases are isostructural, but the 3+ site is occupied by either the Cr cation or partially occupied by both Fe and Cr cations, and the unit cell parameters are slightly different, resulting in a small difference in diffraction peak positions. With small amounts of spinel phases in the glasses, only two small peaks from diffraction from (h k l) planes of (2 2 0) and (3 1 1) were generally observed in the XRD patterns. Different elements in the spinel phases affect the unit cell parameters and shifts in peak positions, but it is difficult to identify the exact chemistries of the spinel phases solely based on XRD analysis. The +2 sites of spinel crystals can be occupied by either +2 or +3 cations including Al, Cr, Ni, Fe, Mg, Mn, Zn, etc. whereas +3 sites are only occupied by +3 cations.

Table 4.1. Crystalline phases and wt% in Q HS24 glasses.

Glass ID	Crystalline Phase	wt%	Glass ID	Crystalline Phase	wt%
HS24-01	None	-	HS24-26	$CaAl_4O_7$	2.0
HS24-02	None	-	HS24-27	$CaAl_4O_7$	2.1
HS24-03	$Zn(Fe_{1.9}Cr_{0.1})O_4$, CaF_2	1.0, 2.1	HS24-28	$Zn(Fe_{1.9}Cr_{0.1})O_4$, Li_3PO_4	0.3, 3.4
HS24-04	None	-	HS24-29	None	-
HS24-05	None	-	HS24-30	Cr_2O_3	0.9
HS24-06	Cr_2O_3, Li_3PO_4	1.1, 3.3	HS24-31	$Zn(Fe_{1.9}Cr_{0.1})O_4$	0.8
HS24-07	$Zn(Fe_{1.9}Cr_{0.1})O_4$, $Na_2Ca(PO_4)F$	1.3, 4.5	HS24-32	Cr_2O_3	0.4
HS24-08	$ZnCr_2O_4$	1.3	HS24-33	$Zn(Fe_{1.9}Cr_{0.1})O_4$	1.5
HS24-09	Cr_2O_3	0.6	HS24-34	Cr_2O_3, $Ca_{10}(PO_4)_6F_2$	0.9, 1.6
HS24-10	Cr_2O_3	0.7	HS24-35	Cr_2O_3	0.8
HS24-11	$Zn(Fe_{1.9}Cr_{0.1})O_4$	2.1	HS24-36	Cr_2O_3	0.6
HS24-12	$Zn(Fe_{1.9}Cr_{0.1})O_4$, $ZnSiO_4$	1.1, 1.7	HS24-37	None	-
HS24-13	$Zn(Fe_{1.9}Cr_{0.1})O_4$	0.5	HS24-38	Cr_2O_3, $Ca_{10}(PO_4)_6F_2$	0.6, 3.8
HS24-14	Cr_2O_3	0.7	HS24-39	Cr_2O_3, $Ca_{10}(PO_4)_6F_2$	0.8, 3.5
HS24-15	$Ca_{10}(PO_4)_6F_2$, $Na_2Ca(PO_4)F$	2.3, 0.8	HS24-40	Cr_2O_3	0.6
HS24-16	Cr_2O_3, CaF_2, $Na_2Ca(PO_4)F$	0.7, 3.0, 5.1	HS24-41	$Ca_{10}(PO_4)_6F_2$, $Ca_2Fe_2O_5$	0.9, 1.1
HS24-17	Cr_2O_3	0.5	HS24-42	$Zn(Fe_{1.9}Cr_{0.1})O_4$, ZrO_2	1.1, 0.6
HS24-18	None	-	HS24-43	Cr_2O_3	0.6
HS24-19	$Zn(Fe_{1.9}Cr_{0.1})O_4$	0.9	HS24-44	$Zn(Fe_{1.9}Cr_{0.1})O_4$	0.2
HS24-20	None	-	HS24-45	None	-
HS24-21	Fe_3O_4	2.4	HS24-46	$Zn(Fe_{1.9}Cr_{0.1})O_4$, $Cr_{0.75}Fe_{1.25}O_3$	0.5, 2.6
HS24-22	$Zn(Fe_{1.9}Cr_{0.1})O_4$	1.2	HS24-47	None	-
HS24-23	$Zn(Fe_{1.9}Cr_{0.1})O_4$, $Ca_{10}(PO_4)_6F_2$	1.5, 2.4	HS24-48	$Zn(Fe_{1.9}Cr_{0.1})O_4$, CaF_2	1.4, 2.2
HS24-24	Cr_2O_3	0.5	HS24-49	None	-
HS24-25	$Zn(Fe_{1.9}Cr_{0.1})O_4$, $Ca_2Fe_2O_5$	0.8, 2.7	HS24-50	Cr_2O_3	0.5

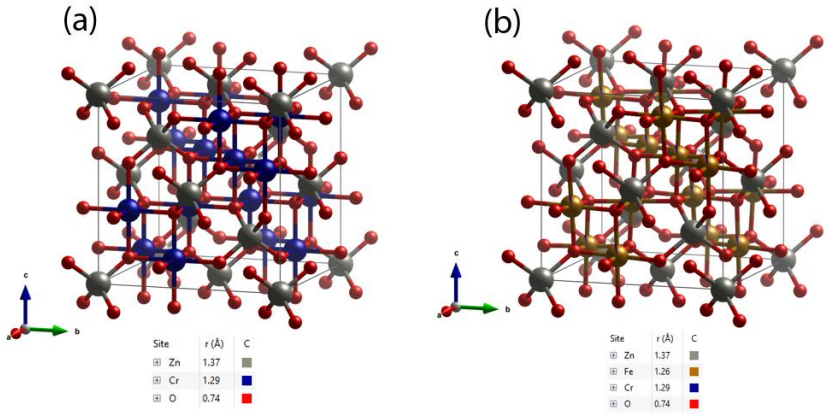

Figure 4.1. Structures of (a) $ZnCr_2O_4$ and (b) $Zn(Fe_{1.9}Cr_{0.1})O_4$ in HS24 glasses.

4.2 Density

Room temperature densities of the HS24 glasses were obtained using the method discussed in Section 3.2 and are provided in Table 4.2. The densities of these glasses ranged from 2.49 g·cm^{-3} to 2.74 g·cm^{-3}. The average density of the 50 HS24 glasses was 2.61 g·cm^{-3}. Comparison of measured and predicted densities is provided in Figure 4.2, and the predicted values from a model by Vienna et al. (2002) were closer to measured density values compared to the Hanford Tank Waste Optimization Simulator (HTWOS)(Vienna et al. 2009) model, indicating a better fit.

Table 4.2. Measured densities of HS24 glasses in g·cm^{-3}.

Glass ID	Density (g·cm^{-3})	Standard Deviation (g·cm^{-3})
HS24-01	2.58	0.01
HS24-02	2.63	0.00
HS24-03	2.67	0.00
HS24-04	2.59	0.00
HS24-05	2.59	0.00
HS24-06	2.52	0.00
HS24-07	2.63	0.00
HS24-08	2.51	0.00
HS24-09	2.67	0.00
HS24-10	2.65	0.00
HS24-11	2.52	0.00
HS24-12	2.64	0.00
HS24-13	2.67	0.00
HS24-14	2.71	0.00
HS24-15	2.61	0.00
HS24-16	2.69	0.01
HS24-17	2.64	0.00
HS24-18	2.55	0.00
HS24-19	2.71	0.00
HS24-20	2.69	0.00
HS24-21	2.69	0.00
HS24-22	2.56	0.00
HS24-23	2.64	0.00
HS24-24	2.67	0.00
HS24-25	2.54	0.00
HS24-26	2.74	0.01
HS24-27	2.58	0.00

Glass ID	Density ($g \cdot cm^{-3}$)	Standard Deviation ($g \cdot cm^{-3}$)
HS24-28	2.57	0.00
HS24-29	2.63	0.00
HS24-30	2.69	0.00
HS24-31	2.64	0.00
HS24-32	2.66	0.00
HS24-33	2.67	0.00
HS24-34	2.59	0.00
HS24-35	2.56	0.00
HS24-36	2.63	0.00
HS24-37	2.64	0.00
HS24-38	2.60	0.00
HS24-39	2.53	0.00
HS24-40	2.54	0.00
HS24-41	2.52	0.00
HS24-42	2.49	0.00
HS24-43	2.57	0.00
HS24-44	2.71	0.00
HS24-45	2.59	0.00
HS24-46	2.56	0.00
HS24-47	2.68	0.00
HS24-48	2.65	0.00
HS24-49	2.55	0.00
HS24-50	2.57	0.00

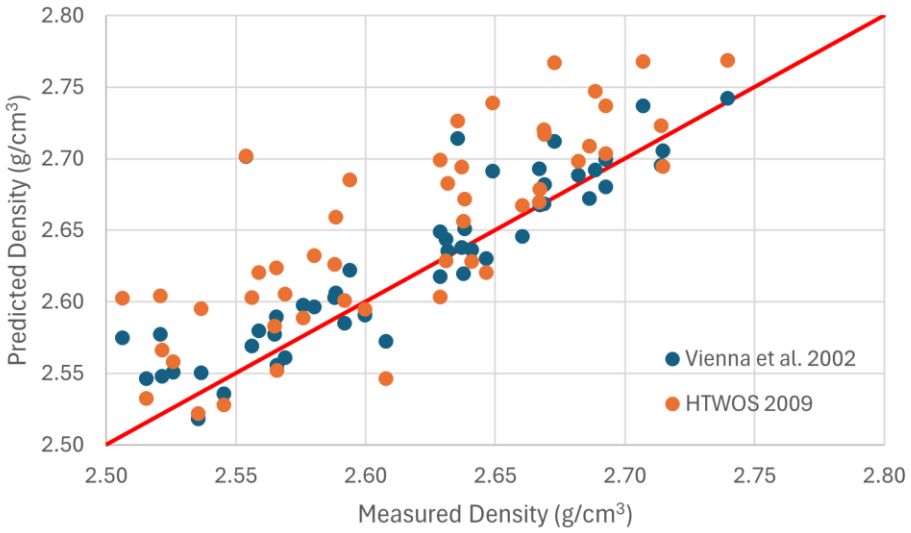

Figure 4.2. Comparison of predicted and measured densities of HS24 glasses.

4.3 Crystal Identification in Canister Centerline Cooling Glasses

The CCC treatment simulates the slow cooling profile of the molten glass inside the canister core. Crystal formation during the slow cooling might impact glass durability by altering the residual glass composition depending on the type of crystals formed (Kim et al. 1995; Kroll et al. 2019). Not all crystals affect glass durability in the same way, so identifying the crystal type and content after CCC is an important step toward understanding crystallization impacts on glass durability. Moreover, property-prediction models were formulated using quenched data; therefore, differences in PCT and TCLP responses after CCC were evaluated.

This section presents and discusses crystallinity in the CCC-treated HS24 glasses obtained using the methods discussed in Section 3.3. The effects of CCC on PCT and TCLP are reported in Sections 4.8 and 4.9, respectively.

Among the 50 glasses, there were five glasses observed without any crystal formation from CCC heat-treatment including HS24-01, HS24-02, HS24-20, HS24-37, and HS24-49. Of the remaining glasses, twenty-one had CF ≤ 4 wt%, twenty-three had 4 wt% ≤ CF ≤ 10 wt%, and one had CF > 10 wt%. XRD analysis revealed a range of different crystal phases with moderate variance in the CF values (wt%). In all the crystalized glasses, common crystalline phases were Franklinite ($ZnFe_{1.9}Cr_{0.1}O_4$) appearing in 19 glasses, Fluorapatite ($Ca_{10}(PO_4)_6F_2$) appearing in 20 glasses, and Eskolaite (Cr_2O_3) appearing in 14 glasses. Less common phases observed were calcium fluoride (CaF_2) found in 6 glasses, Hematite (Fe_2O_3) found in 4 glasses, and lithium phosphate (Li_3PO_4) found in 3 glasses. Additional crystalline phases such as Magnetite (Fe_3O_4), Nacaphite ($Na_2Ca(PO_4)F$), chromium iron oxide ($Cr_{0.75}Fe_{1.25}O_3$), and Zincochromite ($ZnCr_2O_4$) were each found in 2 glasses. Other phases included Baddeleyite (ZrO_2), lithium iron silicate (Li_2FeSiO_4), iron aluminum oxide ($FeAlO_3$), Nosean ($Na_8(Al_6Si_6O_{24})(SO_4)$), sodium silicate ($Na_2Si_3O_7$), zinc ferrite ($ZnFe_2O_4$), and nepheline ($NaAlSiO_4$) with each phase only appearing in 1 glass. The highest CF of a single phase was observed in glass HS24-50, which contained 19.1 wt% of nepheline. The other common phases, $ZnFe_{1.9}Cr_{0.1}O_4$ and $Ca_{10}(PO_4)_6F_2$, had the highest CF of 3.3 wt% in HS24-03 and 6.1 wt% in HS24-26, respectively. The highest CF for Cr_2O_3 was 1.6 wt% in HS24-06. Notable formation of phosphate crystalline phases ($Ca_{10}(PO_4)_6F_2$, Li_3PO_4 and $Na_2Ca(PO_4)F$) were observed in 23 out of the total 45 crystallized glasses. Overall, the diverse distribution of crystalline phases underscores the distinct

crystallization behavior across the compositional range of the glass matrix with certain dominating phases like Franklinite ($ZnFe_{1.9}Cr_{0.1}O_4$) and Fluorapatite ($Ca_{10}(PO_4)_6F_2$) formed during the CCC treatment. For 49 HS24 CCC glasses, no nepheline phase was observed, and 4 of these 49 glasses were predicted to have nepheline formation. Prediction of nepheline formation is based on the P values of pseudo-ternary phase gram from Lu et al. (2021) where glasses with P>0.028 are predicted not to from nepheline. Four glasses had P values ranging from 0.024 to 0.027. HS24-50 had a P value of 0.016 and showed nepheline phase in the CCC glass as predicted.

The XRD phases and wt% crystallinity results are summarized in Table 4.3. Appendix E and Appendix F present images of the glasses after CCC and XRD scans when applicable, respectively.

Table 4.3. Crystalline phases and wt% in CCC glasses.

Glass ID	Crystalline Phase	wt%
HS24-01	None	-
HS24-02	None	-
HS24-03	$ZnFe_{1.9}Cr_{0.1}O_4$, CaF_2	3.3, 1.7
HS24-04	$Na_2Ca(PO_4)F$	0.7
HS24-05	CaF_2	0.4
HS24-06	Cr_2O_3, Li_3PO_4	1.6, 4.3
HS24-07	$ZnFe_{1.9}Cr_{0.1}O_4$, $Ca_{10}(PO_4)_6F_2$	2.1, 4.2
HS24-08	$ZnCr_2O_4$	1.9
HS24-09	Cr_2O_3	1.2
HS24-10	Cr_2O_3, $Ca_{10}(PO_4)_6F_2$	1.1, 3.1
HS24-11	$ZnFe_{1.9}Cr_{0.1}O_4$, Fe_3O_4	2.5, 2.4
HS24-12	$ZnFe_{1.9}Cr_{0.1}O_4$, $Na_2Ca(PO_4)F$	1.9, 3.9
HS24-13	$ZnFe_{1.9}Cr_{0.1}O_4$	1.2
HS24-14	Cr_2O_3	1.0
HS24-15	$Ca_{10}(PO_4)_6F_2$	4.9
HS24-16	Cr_2O_3, CaF_2, $Ca_{10}(PO_4)_6F_2$	1.0, 1.7, 3.9
HS24-17	Cr_2O_3, CaF_2	0.9, 0.9
HS24-18	$Ca_{10}(PO_4)_6F_2$, CaF_2	0.7, 0.3
HS24-19	$ZnFe_{1.9}Cr_{0.1}O_4$	2.1
HS24-20	None	-
HS24-21	Fe_3O_4, $Ca_{10}(PO_4)_6F_2$, Fe_2O_3	2.4, 2.4, 4.1
HS24-22	$ZnFe_{1.9}Cr_{0.1}O_4$, Li_2FeSiO_4	1.7, 7.9
HS24-23	$ZnFe_{1.9}Cr_{0.1}O_4$, $Ca_{10}(PO_4)_6F_2$	2.4, 5.7
HS24-24	Cr_2O_3	0.9
HS24-25	$Ca_{10}(PO_4)_6F_2$	2.1
HS24-26	$ZnFe_{1.9}Cr_{0.1}O_4$, $Ca_{10}(PO_4)_6F_2$	1.5, 6.1

Glass ID	Crystalline Phase	wt%
HS24-27	$Ca_{10}(PO_4)_6F_2$	3.4
HS24-28	$ZnFe_{1.9}Cr_{0.1}O_4$, Li_3PO_4, $Ca_{10}(PO_4)_6F_2$	0.7, 4.2, 2.5
HS24-29	$FeAlO_3$	0.7
HS24-30	Cr_2O_3, $Ca_{10}(PO_4)_6F_2$	1.4, 4.4
HS24-31	Cr_2O_3, CaF_2	0.6, 1.2
HS24-32	$ZnFe_{1.9}Cr_{0.1}O_4$	1.3
HS24-33	$ZnFe_{1.9}Cr_{0.1}O_4$, $Ca_{10}(PO_4)_6F_2$	2.3, 2.7
HS24-34	Cr_2O_3, $Ca_{10}(PO_4)_6F_2$, $ZnCr_2O_4$, $Na_8(Al_6Si_6O_{24})(SO_4)$	0.9, 4.3, 0.7, 2.9
HS24-35	Cr_2O_3	1.3
HS24-36	Cr_2O_3	1.1
HS24-37	None	-
HS24-38	$ZnFe_{1.9}Cr_{0.1}O_4$, $Ca_{10}(PO_4)_6F_2$	1.2, 5.1
HS24-39	Cr_2O_3, $ZnFe_{1.9}Cr_{0.1}O_4$, $Ca_{10}(PO_4)_6F_2$	1.1, 0.3, 4.3
HS24-40	Cr_2O_3	0.8
HS24-41	$Ca_{10}(PO_4)_6F_2$, $Na_2Si_3O_7$	2.4, 2.7
HS24-42	$ZnFe_{1.9}Cr_{0.1}O_4$, ZrO_2	1.6, 2.2
HS24-43	$Cr_{0.75}Fe_{1.25}O_3$	1.2
HS24-44	$ZnFe_{1.9}Cr_{0.1}O_4$	0.7
HS24-45	$ZnFe_{1.9}Cr_{0.1}O_4$, $Ca_{10}(PO_4)_6F_2$, Fe_2O_3	0.3, 2.7, 1.6
HS24-46	$ZnFe_{1.9}Cr_{0.1}O_4$, Fe_2O_3	0.7, 7.0
HS24-47	$Ca_{10}(PO_4)_6F_2$, Li_3PO_4	2.0, 3.4
HS24-48	$ZnFe_{1.9}Cr_{0.1}O_4$, $Ca_{10}(PO_4)_6F_2$, $ZnFe_2O_4$	2.2, 3.4, 3.0
HS24-49	None	-
HS24-50	$Cr_{0.75}Fe_{1.25}O_3$, Fe_2O_3, $NaAlSiO_4$	1.8, 0.7, 19.1

4.4 Isothermal Crystal Fraction (CF) and Liquidus Temperature (T_L)

The long idling of the melter at low temperatures may promote crystal formation, impacting glass processability by settling in the melter and clogging the pour spout (Vienna et al. 2001). Therefore, the study of crystalline phases, quantities, and T_L in isothermal heat-treatments is part of the regular investigation of HLW glasses.

This section presents and discusses the isothermal CF and T_L results obtained using the methodologies detailed in Section 3.4. When the T_L was predicted to be greater than 850 °C, the analysis results included the measured temperatures (°C), crystalline phases, and CF (wt%) of each phase. T_L plots of the primary crystalline phase and XRD scans are shown in Appendix G.

Table 4.4 summarizes the isothermal temperature runs, identified phases, CF (wt%), converted CF to vol% at 950 °C, and T_L values of each HS24 glass. It is important to note that the T_L of glass is determined based on the primary crystal phase when multiple crystal phases are present. Generally, crystal formation is favored at lower heat-treatment temperatures with longer testing periods. The crucial criteria are to avoid the formation of undesirable crystalline phases at or near 950 °C without compromising other glass properties such chemical durability and electrical conductivity. For samples heat-treated at 950 °C, zero or minimal CF suggest the sample is in a vitreous state and no crystal formation is expected at higher temperatures for the same glass composition.

Among all 50 glass compositions tested by isothermal heat-treatment, 10 compositions showed no crystal phases at or below 950 °C including HS24-02, -04, -05, -18, -20, -29, -37, -41, -47, and -49. A diverse group of crystalline phases was identified across the other glass compositions in the matrix. The commonly observed phases were Eskolaite (Cr_2O_3) found in 16 compositions, Franklinite ($ZnFe_{1.9}Cr_{0.1}O_4$) found in 28 compositions, and Fluorapatite ($Ca_{10}(PO_4)_6F_2$) found in 20 compositions. Less common phases were lithium phosphate (Li_3PO_4) found in 2 compositions, Nosean ($Na_8(Al_6Si_6O_{24})(SO_4)$), Hematite ($Fe_2O_3$), Buchwaldite ($NaCaPO_4$), and Baddeleyite ($ZrO_2$) each found in one composition. Franklinite ($ZnFe_{1.9}Cr_{0.1}O_4$) was observed as the primary phase in 21 glasses to determine the T_L of glass, and the highest CF value of $ZnFe_{1.9}Cr_{0.1}O_4$ was 4.7 wt% in HS24-48 at 850 °C. Fluorapatite ($Ca_{10}(PO_4)_6F_2$) was observed as the primary phase in 10 glasses to determine the T_L of glass, and the highest CF value of $Ca_{10}(PO_4)_6F_2$ was 5.7 wt% in HS24-15 at 850 °C. Eskolaite (Cr_2O_3) was observed as the primary phase in 8 glasses to determine the T_L of glass, and the highest CF value of Cr_2O_3 was 1.8 wt% in HS24-50 at 850 °C. It was noted that in HS24-17 and HS24-24, Eskolaite is the primary phase ≤ 950 °C, while Franklinite is the only phase observed at 1050 °C. Lithium phosphate (Li_3PO_4) was observed as the primary phase in 2 glasses to determine the T_L of glass, and the highest CF value of Li_3PO_4 was 4.7 wt% in HS24-06 at 850 °C. Hematite (Fe_2O_3) and Buchwaldite ($NaCaPO_4$) were each observed as the primary phase in one glass to determine the T_L of glass. The highest CF value of Fe_2O_3 and $NaCaPO_4$ was 6.7 wt% in HS24-46 at 850 °C and 2.6 wt% in HS24-50 at 850 °C, respectively. These results highlight the disparity in crystal formation within compositional variation of the HS24 glass matrix.

Table 4.4. Crystalline phases, wt%, vol% at 950 °C, and T_L for isothermally heat-treated glasses.

Glass ID	T (°C)	Phases	wt%	$C_{950,}$ vol%	T_L (°C)
HS24-01	850	$ZnFe_{1.9}Cr_{0.1}O_4$	0.65	0.16	1154 or 1152 (non-linear)
	950	$ZnFe_{1.9}Cr_{0.1}O_4$	0.34		
	1050	$ZnFe_{1.9}Cr_{0.1}O_4$	0.25		
HS24-02	850	None	NA	NA	T_L <850
	900	None	NA		
	950	None	NA		
	1050	None	NA		
HS24-03	850	$ZnFe_{1.9}Cr_{0.1}O_4$	3.02	1.11	1318 or 1321 (non-linear)
	950	$ZnFe_{1.9}Cr_{0.1}O_4$	2.30		
	1050	$ZnFe_{1.9}Cr_{0.1}O_4$	1.71		
HS24-04	850	None	NA	NA	T_L <850
	900	None	NA		
	950	None	NA		
HS24-05	850	None	NA	NA	T_L <850
	900	None	NA		
	950	None	NA		

Glass ID	T (°C)	Phases	wt%	$C_{950,}$ vol%	T_L (°C)
HS24-06	750	Li_3PO_4, Cr_2O_3	4.64, 1.76	4.92, 0.72	1334 (non-linear)
	850	Li_3PO_4, Cr_2O_3	4.67, 1.76		
	900	Li_3PO_4, Cr_2O_3	4.48, 1.64		
	950	Li_3PO_4, Cr_2O_3	4.50, 1.42		
	1050	Li_3PO_4, Cr_2O_3	4.06, 1.59		
HS24-07	850	$Ca_{10}(PO_4)_6F_2$, $ZnFe_{1.9}Cr_{0.1}O_4$	3.43, 2.53	1.18, 1.16	1558 (non-linear)
	950	$Ca_{10}(PO_4)_6F_2$, $ZnFe_{1.9}Cr_{0.1}O_4$	1.40, 2.38		
	1050	$Ca_{10}(PO_4)_6F_2$, $ZnFe_{1.9}Cr_{0.1}O_4$	1.47, 2.18		
HS24-08	850	$ZnFe_{1.9}Cr_{0.1}O_4$	2.72	1.24	1388 (non-linear)
	950	$ZnFe_{1.9}Cr_{0.1}O_4$	2.56		
	1050	$ZnFe_{1.9}Cr_{0.1}O_4$	2.29		
HS24-09	750	$Na_8(Al_6Si_6O_{24})(SO_4)$, Cr_2O_3	5.69, 0.98	0.43	1098 (non-linear)
	850	Cr_2O_3	1.07		
	900	Cr_2O_3	1.15		
	950	Cr_2O_3	0.84		
	1050	Cr_2O_3	0.42		
HS24-10	850	$Ca_{10}(PO_4)_6F_2$, Cr_2O_3	2.62, 1.24	0.45	1318 or 1319 (non-linear)
	950	Cr_2O_3	0.89		
	1050	Cr_2O_3	0.73		
HS24-11	850	$ZnFe_{1.9}Cr_{0.1}O_4$	4.31	1.70	1566 or 1579 (non-linear)
	950	$ZnFe_{1.9}Cr_{0.1}O_4$	3.49		
	1050	$ZnFe_{1.9}Cr_{0.1}O_4$	3.13		
HS24-12	850	$ZnFe_{1.9}Cr_{0.1}O_4$	2.17	0.89	1589 or 1604 (non-linear)
	950	$ZnFe_{1.9}Cr_{0.1}O_4$	1.84		
	1050	$ZnFe_{1.9}Cr_{0.1}O_4$	1.59		
HS24-13	850	$ZnFe_{1.9}Cr_{0.1}O_4$	1.48	0.61	1175 or 1086 (non-linear)
	950	$ZnFe_{1.9}Cr_{0.1}O_4$	1.26		
	1050	$ZnFe_{1.9}Cr_{0.1}O_4$	0.52		
HS24-14	850	Cr_2O_3	1.39	0.60	1352 or 1205 (non-linear)
	950	Cr_2O_3	1.18		
	1050	Cr_2O_3	0.83		
HS24-15	850	$Ca_{10}(PO_4)_6F_2$	5.66	3.71	1146 or 1087 (non-linear)
	950	$Ca_{10}(PO_4)_6F_2$	4.44		
	1050	$Ca_{10}(PO_4)_6F_2$	1.67		
HS24-16	850	$Ca_{10}(PO_4)_6F_2$, Cr_2O_3	3.32, 1.34	1.34, 0.58	1134
	900	$Ca_{10}(PO_4)_6F_2$, Cr_2O_3	2.51, 1.28		
	950	$Ca_{10}(PO_4)_6F_2$, Cr_2O_3	1.61, 1.13		
	1050	$Ca_{10}(PO_4)_6F_2$	1.12		
HS24-17	850	Cr_2O_3	0.78	0.35	$1050 < T_L$
	900	Cr_2O_3	0.73		
	950	Cr_2O_3	0.70		
	1050	$ZnFe_{1.9}Cr_{0.1}O_4$	0.27		
HS24-18	850	None	NA	NA	T_L <850

Glass ID	T (°C)	Phases	wt%	$C_{950,}$ vol%	T_L (°C)
	950	None	NA		
	1050	None	NA		
HS24-19	850	$ZnFe_{1.9}Cr_{0.1}O_4$	2.43	0.92	1304 or 1281 (non-linear)
	950	$ZnFe_{1.9}Cr_{0.1}O_4$	1.91		
	1050	$ZnFe_{1.9}Cr_{0.1}O_4$	1.36		
HS24-20	850	$Ca_{10}(PO_4)_6F_2$	1.13	NA	850 < T_L <900
	900	None	NA		
	950	None	NA		
HS24-21	850	$Ca_{10}(PO_4)_6F_2$, $ZnFe_{1.9}Cr_{0.1}O_4$	2.30, 3.23	0.21, 0.70	1064
	950	$Ca_{10}(PO_4)_6F_2$, $ZnFe_{1.9}Cr_{0.1}O_4$	0.25, 1.46		
	1050	$ZnFe_{1.9}Cr_{0.1}O_4$	0.32		
HS24-22	850	$ZnFe_{1.9}Cr_{0.1}O_4$	1.95	0.85	1727 (non-linear)
	950	$ZnFe_{1.9}Cr_{0.1}O_4$	1.77		
	1050	$ZnFe_{1.9}Cr_{0.1}O_4$	1.74		
HS24-23	850	$Ca_{10}(PO_4)_6F_2$, $ZnFe_{1.9}Cr_{0.1}O_4$	4.90, 2.65	2.03, 1.23	1727 (non-linear)
	950	$Ca_{10}(PO_4)_6F_2$, $ZnFe_{1.9}Cr_{0.1}O_4$	2.41, 2.52		
	1050	$ZnFe_{1.9}Cr_{0.1}O_4$	2.48		
HS24-24	850	Cr_2O_3, $ZnFe_{1.9}Cr_{0.1}O_4$	0.88, 0.24	0.27, 0.24	1050 < T_L
	900	Cr_2O_3, $ZnFe_{1.9}Cr_{0.1}O_4$	0.91, 0.25		
	950	Cr_2O_3, $ZnFe_{1.9}Cr_{0.1}O_4$	0.54, 0.50		
	1050	$ZnFe_{1.9}Cr_{0.1}O_4$	0.46		
HS24-25	850	$Ca_{10}(PO_4)_6F_2$	1.96	0.90	990 (non-linear)
	900	$Ca_{10}(PO_4)_6F_2$	1.72		
	950	$Ca_{10}(PO_4)_6F_2$	1.09		
HS24-26	850	$Ca_{10}(PO_4)_6F_2$, $ZnFe_{1.9}Cr_{0.1}O_4$	5.57, 1.73	3.01, 0.76	1191
	900	$Ca_{10}(PO_4)_6F_2$, $ZnFe_{1.9}Cr_{0.1}O_4$	4.15, 1.53		
	950	$Ca_{10}(PO_4)_6F_2$, $ZnFe_{1.9}Cr_{0.1}O_4$	3.58, 1.57		
	1050	$Ca_{10}(PO_4)_6F_2$, $ZnFe_{1.9}Cr_{0.1}O_4$	2.32, 0.93		
HS24-27	850	$Ca_{10}(PO_4)_6F_2$	2.48	1.24	1116
	900	$Ca_{10}(PO_4)_6F_2$	1.86		
	950	$Ca_{10}(PO_4)_6F_2$	1.49		
	1000	$Ca_{10}(PO_4)_6F_2$	1.09		
HS24-28	850	Li_3PO_4, $ZnFe_{1.9}Cr_{0.1}O_4$	2.85, 0.70	2.89, 0.30	1967 or 1401 (non-linear)
	950	Li_3PO_4, $ZnFe_{1.9}Cr_{0.1}O_4$	2.65, 0.62		
	1050	Li_3PO_4	2.33		
HS24-29	850	None	NA	NA	T_L <850
	950	None	NA		
	1050	None	NA		
HS24-30	750	$Ca_{10}(PO_4)_6F_2$, Cr_2O_3, $ZnFe_{1.9}Cr_{0.1}O_4$	3.72, 1.56, 0.41	0.32, 0.35	1050 < T_L
	850	$Ca_{10}(PO_4)_6F_2$, Cr_2O_3, $ZnFe_{1.9}Cr_{0.1}O_4$	2.49, 1.32, 0.60		
	900	$Ca_{10}(PO_4)_6F_2$, Cr_2O_3, $ZnFe_{1.9}Cr_{0.1}O_4$	1.09, 1.22, 0.48		

Glass ID	T (°C)	Phases	wt%	$C_{950,}$ vol%	T_L (°C)
	950	Cr_2O_3, $ZnFe_{1.9}Cr_{0.1}O_4$	0.63, 0.74		
	1050	$ZnFe_{1.9}Cr_{0.1}O_4$	1.14		
HS24-31	850	$ZnFe_{1.9}Cr_{0.1}O_4$	1.79	0.85	1081 (non-linear)
	950	$ZnFe_{1.9}Cr_{0.1}O_4$	1.75		
	1050	$ZnFe_{1.9}Cr_{0.1}O_4$	1.03		
HS24-32	750	Cr_2O_3	0.66	0.23, 0.15	1387 or 1117 (non-linear)
	850	Cr_2O_3	0.58		
	900	Cr_2O_3, $ZnFe_{1.9}Cr_{0.1}O_4$	0.68, 0.26		
	950	Cr_2O_3, $ZnFe_{1.9}Cr_{0.1}O_4$	0.45, 0.31		
HS24-33	850	$Ca_{10}(PO_4)_6F_2$, $ZnFe_{1.9}Cr_{0.1}O_4$	2.26, 2.85	0.90, 1.33	1166 (non-linear)
	950	$Ca_{10}(PO_4)_6F_2$, $ZnFe_{1.9}Cr_{0.1}O_4$	1.07, 2.73		
	1050	$ZnFe_{1.9}Cr_{0.1}O_4$	2.22		
HS24-34	850	$Ca_{10}(PO_4)_6F_2$, Cr_2O_3, $ZnFe_{1.9}Cr_{0.1}O_4$	3.81, 0.88, 1.10	1.82, 0.36, 0.52	1309 (non-linear)
	950	$Ca_{10}(PO_4)_6F_2$, Cr_2O_3, $ZnFe_{1.9}Cr_{0.1}O_4$	2.17, 0.70, 1.07		
	1050	Cr_2O_3, $ZnFe_{1.9}Cr_{0.1}O_4$	0.46, 0.99		
HS24-35	850	Cr_2O_3	1.38	0.67	1125 (non-linear)
	950	Cr_2O_3	1.32		
	1050	Cr_2O_3	0.97		
HS24-36	850	$Ca_{10}(PO_4)_6F_2$, Cr_2O_3	1.86, 1.35	0.49, 0.60	1450 or 1222 (non-linear)
	950	$Ca_{10}(PO_4)_6F_2$, Cr_2O_3	0.59, 1.18		
	1050	Cr_2O_3	0.89		
HS24-37	850	None	NA	NA	T_L <850
	950	None	NA		
	1050	None	NA		
HS24-38	850	$Ca_{10}(PO_4)_6F_2$, $ZnFe_{1.9}Cr_{0.1}O_4$	4.99, 1.64	2.48, 0.71	1415 or 1169 (non-linear)
	950	$Ca_{10}(PO_4)_6F_2$, $ZnFe_{1.9}Cr_{0.1}O_4$	2.96, 1.46		
	1050	$Ca_{10}(PO_4)_6F_2$, $ZnFe_{1.9}Cr_{0.1}O_4$	3.61, 1.05		
HS24-39	750	$Ca_{10}(PO_4)_6F_2$, Cr_2O_3, $ZnFe_{1.9}Cr_{0.1}O_4$	4.80, 1.24, 0.52	3.24, 0.40, 0.45	1778 or 1209 (non-linear)
	850	$Ca_{10}(PO_4)_6F_2$, Cr_2O_3, $ZnFe_{1.9}Cr_{0.1}O_4$	4.46, 1.01, 0.68		
	950	$Ca_{10}(PO_4)_6F_2$, Cr_2O_3, $ZnFe_{1.9}Cr_{0.1}O_4$	3.85, 0.77, 0.93		
	1050	$Ca_{10}(PO_4)_6F_2$, Cr_2O_3, $ZnFe_{1.9}Cr_{0.1}O_4$	4.43, 0.49, 1.13		
HS24-40	850	Cr_2O_3	0.93	0.44	1844 or 1242 (non-linear)
	950	Cr_2O_3	0.87		
	1050	Cr_2O_3	0.74		
HS24-41	850	$Ca_{10}(PO_4)_6F_2$	0.89	NA	900 < T_L <950
	900	$Ca_{10}(PO_4)_6F_2$	0.58		
	950	None	NA		
	1050	None	NA		
HS24-42	850	ZrO_2, $ZnFe_{1.9}Cr_{0.1}O_4$	2.81, 1.86	0.96, 0.87	

Glass ID	T (°C)	Phases	wt%	$C_{950,}$ vol%	T_L (°C)
	950	ZrO_2, $ZnFe_{1.9}Cr_{0.1}O_4$	2.07, 1.78		1235 (non-linear)
	1050	ZrO_2, $ZnFe_{1.9}Cr_{0.1}O_4$	1.21, 1.57		
HS24-43	850	Cr_2O_3, $ZnFe_{1.9}Cr_{0.1}O_4$	0.54, 0.71	0.44	1166 or 1092 (non-linear)
	900	Cr_2O_3, $ZnFe_{1.9}Cr_{0.1}O_4$	0.94, 0.15		
	950	Cr_2O_3	0.86		
	1050	Cr_2O_3	0.41		
HS24-44	850	$ZnFe_{1.9}Cr_{0.1}O_4$	0.65	0.08	993 or 965 (non-linear)
	900	$ZnFe_{1.9}Cr_{0.1}O_4$	0.51		
	950	$ZnFe_{1.9}Cr_{0.1}O_4$	0.18		
HS24-45	850	$Ca_{10}(PO_4)_6F_2$, $ZnFe_{1.9}Cr_{0.1}O_4$	1.36, 0.99	0.15	995 or 992 (non-linear)
	900	$Ca_{10}(PO_4)_6F_2$, $ZnFe_{1.9}Cr_{0.1}O_4$	0.64, 0.65		
	950	$ZnFe_{1.9}Cr_{0.1}O_4$	0.31		
HS24-46	850	Fe_2O_3, $ZnFe_{1.9}Cr_{0.1}O_4$	6.70, 0.74	2.17, 0.34	1567 (non-linear)
	950	Fe_2O_3, $ZnFe_{1.9}Cr_{0.1}O_4$	4.26, 0.69		
	1050	Fe_2O_3, $ZnFe_{1.9}Cr_{0.1}O_4$	3.00, 0.64		
HS24-47	850	$Ca_{10}(PO_4)_6F_2$	0.87	NA	$850 < T_L < 900$
	900	None	NA		
	950	None	NA		
HS24-48	850	$Ca_{10}(PO_4)_6F_2$, $ZnFe_{1.9}Cr_{0.1}O_4$	3.50, 4.71	1.93, 1.59	1335
	950	$Ca_{10}(PO_4)_6F_2$, $ZnFe_{1.9}Cr_{0.1}O_4$	2.28, 3.26		
	1050	$Ca_{10}(PO_4)_6F_2$, $ZnFe_{1.9}Cr_{0.1}O_4$	2.04, 2.84		
HS24-49	850	None	NA	NA	$850 < T_L$
	950	None	NA		
	1050	None	NA		
	850	$NaCaPO_4$, Cr_2O_3	2.62, 1.77		
HS24-50	950	$NaCaPO_4$, Cr_2O_3	2.13, 0.85	1.83, 0.43	1326 or 1239 (non-linear)
	1050	$NaCaPO_4$	1.51		

Predicted properties of phosphate liquidus temperature (T_L-P), temperature of 1 vol% ($T_{1\%}$) of spinel, and liquidus temperature of Zr-bearing phases (T_L-Zr) of HS24 glasses were compared to the determined values by the isothermal heat-treatment test as shown in Figure 4.3, Figure 4.4, and Figure 4.5, respectively. The predicted properties were calculated using the EWG2.6 models (Vienna et al. 2025) and the 95% prediction interval (PI) was included in each plot. Measured values were determined using the linear-fit extrapolation method. For some glasses, the properties could not be determined by extrapolation and were instead bracketed within a certain temperature range (e.g., 850 ºC<T_L-P<950 ºC). These property data were referred to as "censored" values, and the corresponding temperature range was indicated by an extended bar in the plot. For T_L-P (Figure 4.3), five out of the eleven HS24 glasses with measured values show good agreement with model prediction, while the remaining six glasses have higher measured T_L-P than model prediction. This could be related to the liquid-liquid phase separation of phosphorus in borosilicate glass melt due to immiscibility. For the censored data, eighteen out of thirty-nine show partial overlapping with the model PI range. For $T_{1\%}$ spinel (Figure 4.4), eight out of sixteen HS24 glasses with measured values show good agreement with model prediction. For the censored data, thirty-one out of thirty-four HS24 glasses show partial overlapping with the model PI range. Only one HS24 glass (HS24-42) showed Zr-bearing phase during the isothermal heat-treatment test, and the

measured T_L-Zr is in good agreement with model prediction (Figure 4.5). All remaining glasses have censored data on T_L-Zr (i.e., <750 ºC or <850 ºC).

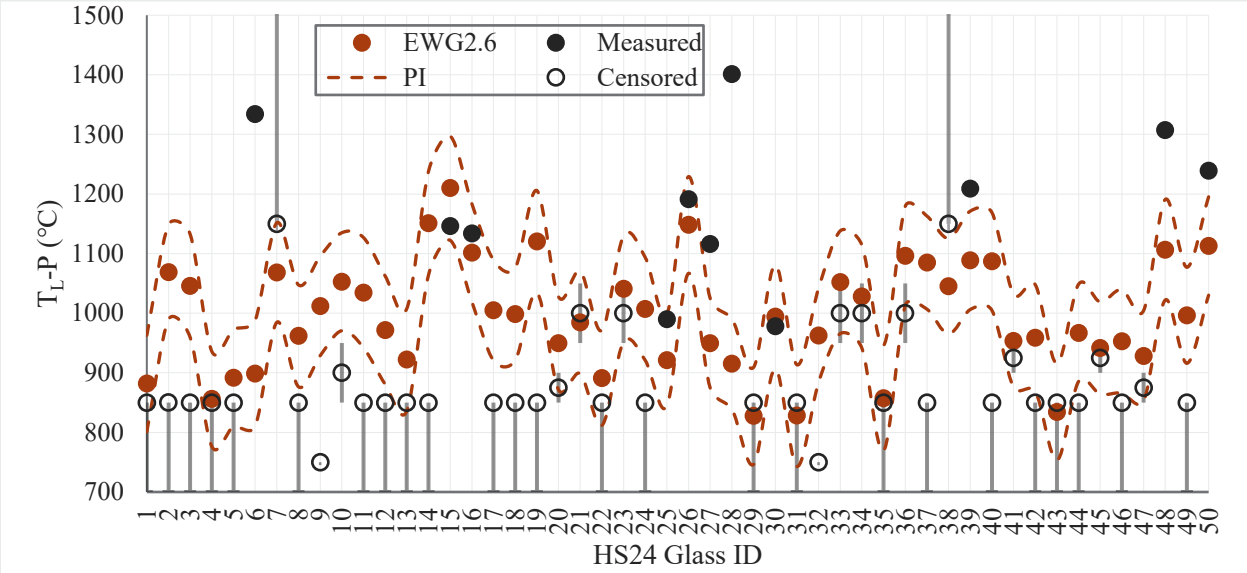

Figure 4.3. Comparison of predicted T_L-P by EWG2.6 model (Vienna et al. 2025) and the measured T_L-P of HS24 glass.

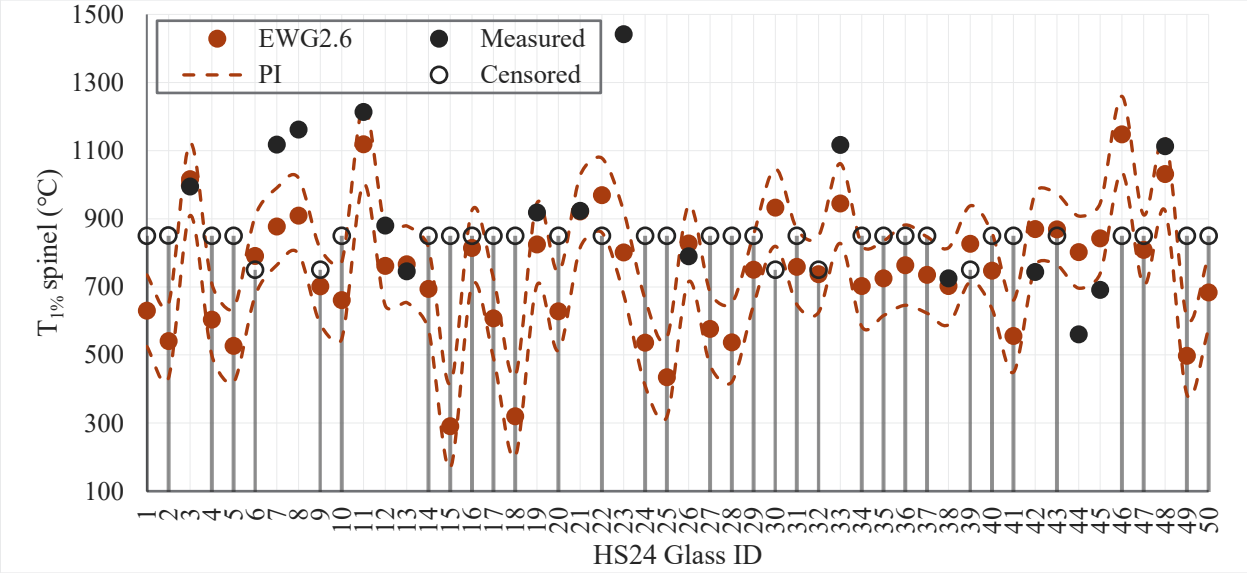

Figure 4.4. Comparison of predicted $T_{1\%}$ spinel by EWG2.6 model (Vienna et al. 2025) and the measured $T_{1\%}$ spinel of HS24 glass.

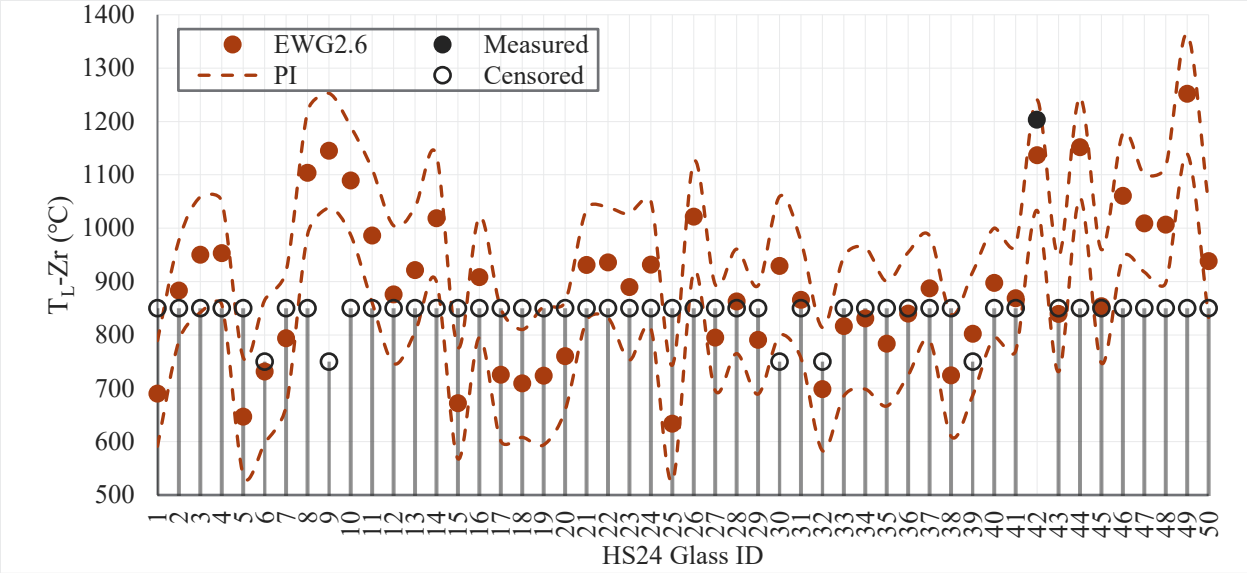

Figure 4.5. Comparison of predicted T_L-Zr by EWG2.6 model (Vienna et al. 2025) and the measured T_L-Zr of HS24 glass.

4.5 SO_3 Solubility

The SO_3 saturation concentration is controlled to avoid excessive corrosion of melter materials at the melt-line. This section summarizes the SSM study on the HS24 glasses. The SO_3 concentrations of SSM and Q glasses were compared. In addition, the predicted SO_3 solubilities from different models were compared.

4.5.1 SSM SO_3 Concentrations

For each HS24 glass, the excess salt phase was easily observed in the final melts for 44 of the 50 glasses (exceptions include HS24-03, HS24-11, HS24-40, HS24-42, HS24-45, HS24-48) as seen in sample HS24-43 in Figure 4.6 as the bright yellow and orange deposits on the black glass and inner crucible walls. An excess phase was expected for all three melts in all glasses as the amount of Na_2SO_4 added exceeds the conservative sulfur solubility limit for the WTP used in the 2014 algorithm by nine times (4 wt% vs. 0.44 wt% SO_4) (Kim et al. 2014). However, while the excess phase may form for the first two melts, Jin et al. (2019) provided evidence that the glass is not completely saturated with SO_3 until the third melt.

As seen in Figure 4.6, most glasses in this study exhibited an undissolved portion usually in a white, yellow, orange, tan or pink color and in a quantity that visibly decreased with each successive melt. Sulfur solubility was experimentally determined for each glass sample by measuring SO_3 retention after three saturation cycles as demonstrated in Jin et al. (2019) with the specifics outlined in Section 3.5. The saturation results, expressed as SO_3 content in wt%, are summarized in Table 4.5, ranging from 0.81 to 1.99 wt% across all saturated glasses.

Figure 4.6. Photos of the three melts (left to right: melts 1, 2, and 3, i.e., the SSM) for HS24-43.

Table 4.5. Measured SO_3 content in the SSM glasses are an average of both ICP-OES and IC which were both analyzed from a portion of the same sample supplied to SwRI. The individual ICP-OES and IC results are provided in Appendix H.

Glass ID	Average SO_3 Content (wt%)	SD_{ICP+IC} (wt%)	Glass ID	SO_3 Content (wt%)	SD_{ICP+IC} (wt%)
HS24-01-SSM	0.97	0.198	HS24-26-SSM	1.36	0.019
HS24-02-SSM	1.56	0.039	HS24-27-SSM	1.00	0.021
HS24-03-SSM	1.08	0.006	HS24-28-SSM	1.48	0.005
HS24-04-SSM	1.39	0.025	HS24-29-SSM	1.05	0.040
HS24-05-SSM	1.42	0.028	HS24-30-SSM	0.96	0.017
HS24-06-SSM	1.62	0.034	HS24-31-SSM	1.43	0.044
HS24-07-SSM	1.14	0.004	HS24-32-SSM	1.48	0.009
HS24-08-SSM	1.15	0.099	HS24-33-SSM	1.37	0.028
HS24-09-SSM	1.04	0.043	HS24-34-SSM	1.36	0.021
HS24-10-SSM	1.44	0.053	HS24-35-SSM	1.11	0.043
HS24-11-SSM	0.88	0.020	HS24-36-SSM	1.81	0.059
HS24-12-SSM	1.12	0.035	HS24-37-SSM	1.44	0.025
HS24-13-SSM	1.37	0.101	HS24-38-SSM	1.75	0.018
HS24-14-SSM	1.44	0.030	HS24-39-SSM	1.47	0.030
HS24-15-SSM	1.99	0.188	HS24-40-SSM	1.19	0.076
HS24-16-SSM	1.29	0.140	HS24-41-SSM	1.00	0.072
HS24-17-SSM	1.04	0.026	HS24-42-SSM	0.91	0.074
HS24-18-SSM	1.47	0.032	HS24-43-SSM	0.81	0.022
HS24-19-SSM	1.28	0.013	HS24-44-SSM	1.14	0.035
HS24-20-SSM	1.56	0.029	HS24-45-SSM	1.01	0.033
HS24-21-SSM	1.26	0.003	HS24-46-SSM	0.89	0.003
HS24-22-SSM	1.19	0.352	HS24-47-SSM	1.11	0.247
HS24-23-SSM	1.19	0.058	HS24-48-SSM	1.14	0.095
HS24-24-SSM	1.60	0.041	HS24-49-SSM	1.21	0.017
HS24-25-SSM	1.33	0.035	HS24-50-SSM	1.24	0.011

The standard deviation (SD_{ICP+IC}) in Table 4.5 is determined from the average of the two analysis methods, ICP-OES and IC, taken from the same sample. The individual differences are small between the two methods (typically within ± 0.1 - 0.15 wt%), indicating good agreement and suitable precision for routine SO_3 determination.

In most glasses examined, the SSM melts increased SO_3 (wt%) above the original target values (Figure 4.7), indicating that these compositions can dissolve additional SO_3 under the experimental conditions.

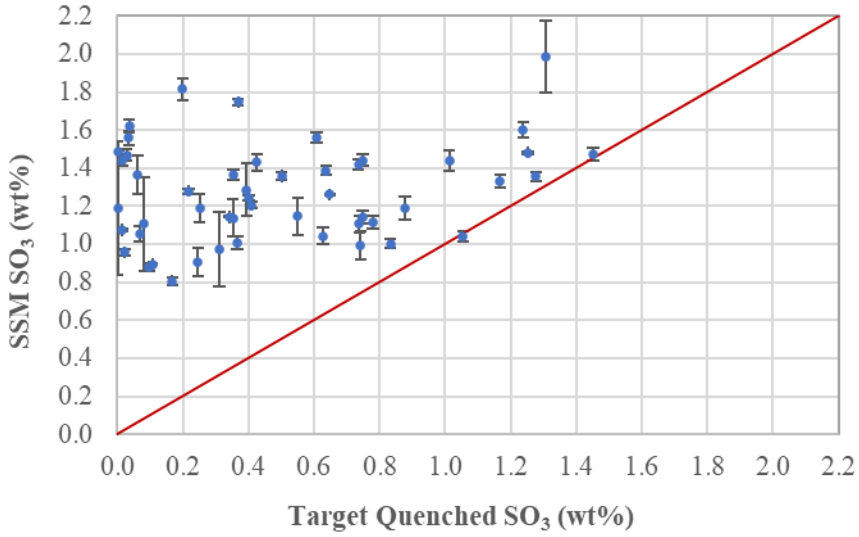

Figure 4.7. Measured SO_3 content in SSM and target quenched glasses for the HS24 matrix. Uncertainties are represented by SD_{ICP+IC}. The red line represents the 1-1 correlation between the measured and original target values.

The glasses with the lowest initial SO_3 contents exhibited the largest increases and thus the greatest capacity for further sulfate uptake. In contrast, two glasses (HS24-17-SSM and HS24-18-SSM) plot on the 1:1 line, suggesting that their starting "as-quenched" compositions were already at sulfate saturation. In these cases, the measured SO_3 contents can be considered effectively unchanged, with the small differences between the quenched and SSM values falling within experimental error. Of the three glasses with the greatest sulfate uptake after SSM compared to their initial "as-quenched" sulfate values were HS24-36-SSM (from 0.20 to 1.82 wt% SO_3), HS24-38-SSM (from 0.37 to 1.75 wt% SO_3), and HS24-15-SSM (from 1.31 to 1.99 wt% SO_3).

4.5.2 Comparisons to Predicted SO_3 Saturation Concentrations

The EWG 2.6 Sulfur Tolerance Model, (wt% with 0.33 Offset), was used for the predicted SO_3 solubility values and associated PI was utilized to quantify the uncertainty of the predicted values (Vienna et al. 2025). The uncertainties in the measured values were calculated using the 90% confidence interval, assuming a Gaussian distribution (1.645), and the pooled standard deviation (SD_{pooled} = 0.1067) based on 22 replicate data sets from Table 7.2 of Vienna et al. (2022). The calculation, 1.645 x $SD_{pooled,SSM}$, resulted in 0.1755 wt%. This approach provides a more comprehensive representation of uncertainty for measured SO_3 solubilities as it accounts for variations in glass batching, melting, melt saturation, glass washing, and chemical analyses conducted by multiple laboratories over approximately five years. In comparison, the

uncertainties for ICP-OES and IC measurements (SD_{ICP+IC}) only reflects the standard deviation of the average from the two methods for each individual glass.

As shown in Figure 4.8, the relationship between predicted and measured SO_3 wt% values from the SSM lies generally close to the 1:1 line when considering the standard deviations.

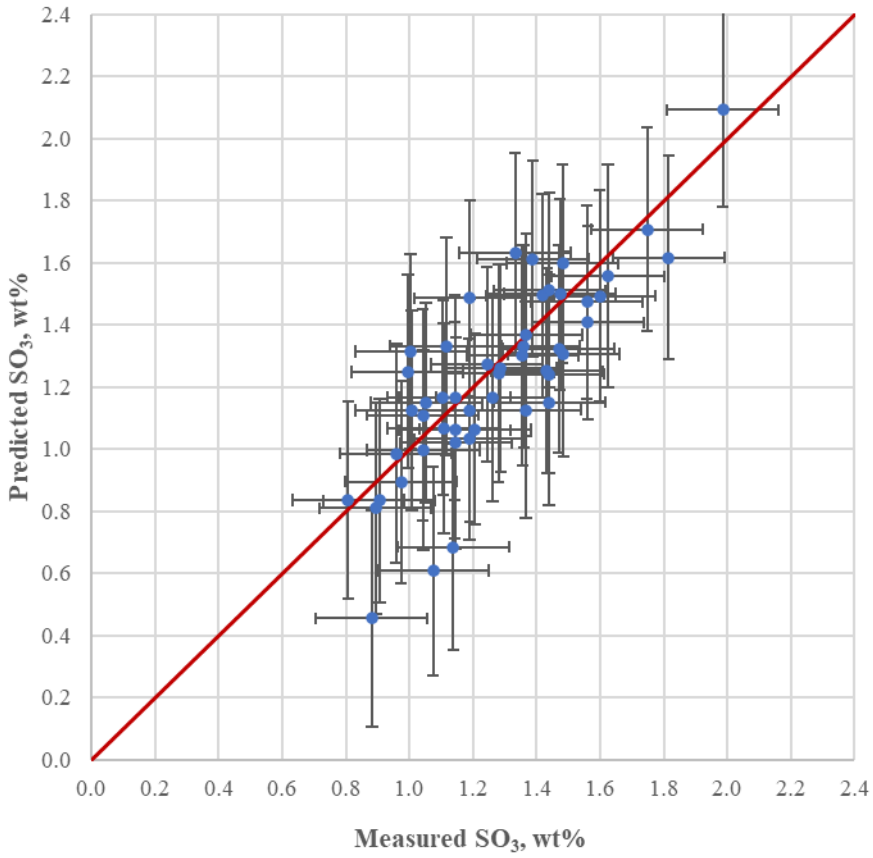

Figure 4.8. Correlation between Predicted and Measured SO_3 wt% of the SSM glasses. The red line represents the 1-1 correlation between the measured and predicted SO_3 values.

Overall, these results indicate that the model predicts SO_3 reasonably well and that the upper limit of sulfur saturation for the model's sulfate compositional region can likely be increased. They enable us to investigate even higher sulfur solubility regions by extrapolating with the existing model to this new composition domain.

4.6 Viscosity

This section presents the viscosity results obtained using the methods discussed in Section 3.6. The results are summarized in Table 4.6 and individually reported in Appendix I. Note the reported temperatures may be different than target temperatures listed in Section 3.6 because of a difference between the furnace control thermocouple and the viscosity measurement thermocouple. For some glasses, readings at 950 and 1050 °C were outside of the limitations of the viscometer because the viscosity of the glass was too high, likely due to these glasses crystallizing at lower temperatures. For all such glasses, raising the temperature

back to 1150 °C allowed for a measurement again. HS24-11 showed a relatively higher viscosity value at the last 1150 °C reading, indicating that alkali may have volatilized from the glass at the previous 1250 °C reading. Most glasses showed good agreement between the three 1150 °C readings and good Arrhenius fits, which are reported in Appendix I.

Table 4.6. Measured ln η (Pa-s) values versus target temperature (in the sequence of measurement). The temperature profile was set to investigate the impact of crystallization and volatility on the viscosity.

Target *T*, °C	1150	1050	950	1150	1250	1150
Glass ID	ln η (Pa-s)[a]	ln η (Pa-s)[a]	ln η (Pa-s)[a]	ln η (Pa-s)[a]	ln η (Pa-s)[a]	ln η (Pa-s)[a]
HS24-01	1.508	2.341	3.391	1.534	0.877	1.563
HS24-02	1.141	1.953	3.007	1.107	0.437	1.153
HS24-03	1.953	2.868	3.884	2.000	1.225	1.967
HS24-04	1.729	2.453	3.393	1.703	1.126	1.710
HS24-05	0.583	1.256	2.124	0.632	0.080	0.669
HS24-06	1.530	2.279	3.150	1.574	0.924	1.578
HS24-07	1.491	2.324	3.315	1.510	0.795	1.399
HS24-08	2.285	3.111	4.210	2.321	1.665	2.304
HS24-09	1.900	2.812	3.976	1.884	1.025	1.796
HS24-10	1.582	2.428	3.531	1.527	0.728	1.433
HS24-11	2.908	3.821	5.200	2.982	2.361	3.110
HS24-12	1.219	1.889	2.791	1.171	0.579	1.251
HS24-13	1.702	2.515	3.488	1.717	1.025	1.704
HS24-14	2.014	2.997	4.252	2.026	1.218	2.003
HS24-15	1.239	2.022	--[b]	1.191	0.541	1.199
HS24-16	1.014	1.780	4.686	0.980	0.353	1.037
HS24-17	1.531	2.361	3.435	1.573	0.943	1.626
HS24-18	2.219	3.048	4.994	2.233	1.601	2.286
HS24-19	1.362	2.125	3.119	1.324	0.658	1.370
HS24-20	1.464	2.246	3.201	1.479	0.840	1.517
HS24-21	1.392	2.112	3.020	1.416	0.764	1.416
HS24-22	2.361	3.156	4.133	2.347	1.689	2.351
HS24-23	1.915	2.694	3.034	1.722	0.972	1.721
HS24-24	1.956	2.828	3.883	1.877	1.138	1.860
HS24-25	1.751	2.519	3.434	1.777	1.189	1.850
HS24-26	1.758	2.709	--[b]	1.762	0.990	1.742
HS24-27	1.792	2.591	--[b]	1.808	1.187	1.854
HS24-28	1.923	2.748	3.724	1.923	1.235	1.935
HS24-29	1.084	1.779	2.713	1.053	0.460	1.157
HS24-30	1.519	2.377	3.442	1.452	0.802	1.545
HS24-31	1.608	2.365	3.312	1.567	0.905	1.587
HS24-32	1.228	2.076	3.049	1.236	0.566	1.263
HS24-33	2.119	2.777	3.800	2.095	1.449	2.119
HS24-34	1.235	1.961	--[b]	1.166	0.579	1.268
HS24-35	1.377	2.214	3.155	1.448	0.756	1.384
HS24-36	1.583	2.436	3.534	1.582	0.845	1.552

Target T, °C	1150	1050	950	1150	1250	1150
Glass ID	ln η (Pa-s)[a]	ln η (Pa-s)[a]	ln η (Pa-s)[a]	ln η (Pa-s)[a]	ln η (Pa-s)[a]	ln η (Pa-s)[a]
HS24-37	1.442	2.246	3.316	1.442	0.768	1.431
HS24-38	1.142	1.897	--[b]	1.177	0.556	1.233
HS24-39	1.743	--[b]	--[b]	1.752	1.145	1.778
HS24-40	1.745	2.704	3.929	1.737	1.089	1.697
HS24-41	1.477	2.311	3.388	1.481	0.820	1.474
HS24-42	2.186	3.082	4.319	2.157	1.373	2.095
HS24-43	1.190	1.920	2.830	1.203	0.646	1.262
HS24-44	1.670	2.606	3.723	1.683	0.921	1.640
HS24-45	1.603	2.410	3.401	--[c]	0.952	1.659
HS24-46	2.482	3.397	4.614	2.569	1.764	2.235
HS24-47	1.312	2.026	3.035	1.211	0.546	1.251
HS24-48	1.961	2.838	--[b]	1.800	1.179	1.879
HS24-49	1.844	2.795	4.042	1.754	0.954	1.807
HS24-50	1.048	1.885	3.010	1.102	0.445	1.050

(a) Average of three measurements.
(b) Too thick to get a reading.
(c) Not Measured

The Arrhenius model was used to fit the viscosity-temperature data for each waste glass. The model form is the Arrhenius equation shown in Equation 4.2:

$$\ln(\eta) = A + \frac{B}{T_K} \tag{4.2}$$

where A and B are independent of temperature (T_K), which is in Kelvin (T(°C) + 273.15). For each glass, Table 4.7 provides the values for the A and B coefficients and summarizes the viscosity results at six target temperatures calculated using Equation 4.2.

Table 4.7. Fit of Arrhenius coefficients and calculated η for various temperatures.

	Arrhenius Coefficients			Temperature (°C)					
Glass ID	A (ln Pa-s)	B (ln Pa-s*K)	η_{1150} (Pa-s)	950	1050	1100	1150	1200	1250
				ln η [Pa-s]					
HS24-01	-10.9846	17709.3	4.31	3.496	2.401	1.914	1.460	1.038	0.643
HS24-02	-11.5573	17933.4	2.84	3.106	1.998	1.504	1.045	0.617	0.218
HS24-03	-10.9355	18237.7	6.56	3.977	2.850	2.348	1.881	1.446	1.039
HS24-04	-9.7004	16165.4	5.26	3.517	2.518	2.073	1.660	1.274	0.914
HS24-05	-9.3493	14129.3	1.79	2.204	1.330	0.942	0.580	0.243	-0.072
HS24-06	-9.2857	15352.8	4.50	3.268	2.319	1.896	1.503	1.137	0.795
HS24-07	-10.9761	17688.7	4.28	3.487	2.394	1.907	1.454	1.032	0.638
HS24-08	-10.2651	17860.1	9.84	4.338	3.235	2.743	2.286	1.860	1.462
HS24-09	-12.7146	20667.9	6.11	4.185	2.907	2.338	1.810	1.317	0.856
HS24-10	-12.2386	19513.6	4.37	3.717	2.511	1.974	1.474	1.009	0.574
HS24-11	-11.0267	19938.9	19.79	5.277	4.044	3.495	2.985	2.510	2.065
HS24-12	-9.4744	15197.0	3.34	2.952	2.012	1.594	1.205	0.843	0.504
HS24-13	-10.3581	17143.8	5.42	3.660	2.600	2.128	1.690	1.281	0.898
HS24-14	-12.9640	21346.1	7.67	4.490	3.171	2.583	2.037	1.528	1.052
HS24-15	-10.6425	16890.3	3.41	3.168	2.124	1.659	1.227	0.824	0.448
HS24-16	-10.4764	16347.5	2.75	2.890	1.880	1.430	1.012	0.622	0.257
HS24-17	-10.6068	17374.2	4.97	3.599	2.526	2.047	1.603	1.188	0.801
HS24-18	-9.3716	16436.4	8.84	4.068	3.052	2.600	2.179	1.787	1.421
HS24-19	-10.8565	17265.7	3.59	3.261	2.194	1.719	1.277	0.865	0.480
HS24-20	-10.2052	16547.0	4.15	3.325	2.302	1.847	1.423	1.028	0.660
HS24-21	-9.8057	15872.3	3.85	3.173	2.192	1.755	1.348	0.970	0.616
HS24-22	-9.7053	17091.6	10.03	4.270	3.214	2.743	2.306	1.898	1.517
HS24-23	-10.7651	17736.7	5.47	3.737	2.641	2.153	1.699	1.276	0.881
HS24-24	-11.8975	19532.6	6.23	4.074	2.866	2.329	1.829	1.363	0.928
HS24-25	-9.3811	15845.6	5.78	3.575	2.596	2.160	1.754	1.376	1.023
HS24-26	-11.8953	19378.7	5.60	3.950	2.752	2.219	1.723	1.261	0.829
HS24-27	-9.4491	15981.2	5.94	3.618	2.630	2.190	1.782	1.400	1.044
HS24-28	-10.2861	17435.7	7.15	3.970	2.893	2.413	1.967	1.551	1.162
HS24-29	-9.7410	15427.2	3.00	2.873	1.920	1.495	1.100	0.732	0.389
HS24-30	-11.3307	18327.6	4.71	3.655	2.522	2.018	1.549	1.112	0.703
HS24-31	-9.8102	16231.6	4.93	3.462	2.459	2.012	1.596	1.209	0.847
HS24-32	-10.9900	17461.4	3.60	3.288	2.208	1.728	1.281	0.864	0.475
HS24-33	-9.2258	16151.6	8.37	3.981	2.982	2.538	2.125	1.739	1.379
HS24-34	-9.6823	15546.8	3.47	3.030	2.069	1.641	1.243	0.872	0.526
HS24-35	-10.2102	16579.1	4.22	3.346	2.321	1.865	1.441	1.045	0.676
HS24-36	-11.5345	18676.7	4.90	3.737	2.582	2.068	1.590	1.145	0.729
HS24-37	-10.9813	17707.1	4.31	3.497	2.403	1.915	1.462	1.040	0.645
HS24-38	-9.3618	15019.1	3.30	2.919	1.990	1.577	1.193	0.834	0.500
HS24-39	-8.2809	14328.8	5.98	3.435	2.550	2.155	1.789	1.447	1.127
HS24-40	-12.3304	20128.1	6.13	4.128	2.884	2.329	1.814	1.334	0.886
HS24-41	-11.0988	17944.7	4.54	3.574	2.465	1.971	1.512	1.084	0.684
HS24-42	-12.0422	20252.1	8.94	4.517	3.265	2.708	2.190	1.707	1.255
HS24-43	-9.4661	15238.2	3.46	2.994	2.052	1.632	1.242	0.879	0.539
HS24-44	-12.0236	19536.0	5.50	3.950	2.743	2.205	1.705	1.239	0.804
HS24-45	-10.1590	16805.7	5.21	3.582	2.544	2.081	1.651	1.250	0.876

	Arrhenius Coefficients			Temperature (°C)					
Glass ID	A (ln Pa-s)	B (ln Pa-s*K)	η_{1150} (Pa-s)	950	1050	1100	1150	1200	1250
				ln η [Pa-s]					
HS24-46	-11.6911	20186.6	12.12	4.815	3.567	3.012	2.495	2.013	1.563
HS24-47	-10.7569	17105.4	3.54	3.230	2.172	1.702	1.264	0.856	0.475
HS24-48	-11.1546	18620.6	6.90	4.071	2.920	2.407	1.931	1.487	1.072
HS24-49	-13.1896	21359.0	6.17	4.275	2.955	2.367	1.820	1.311	0.835
HS24-50	-11.4717	17909.9	3.05	3.173	2.066	1.573	1.114	0.687	0.288

The η_{1150} values interpolated from measured data were compared to predicted values calculated using the EWG 2.5 Viscosity VFT RLM Model (Vienna et al. 2024) shown in Figure 4.9. The pooled standard deviation for the measured viscosity values (0.1655 ln(Pa-s)) is from Vienna et al. (2022). Large differences between the predicted and measured viscosity values were observed in HS24-05, HS24-11, and HS24-46. The predicted viscosity value of HS24-05 was ~3 times higher than the measured value. HS24-05 was fully amorphous and contained relatively high F (~4 wt%) compared to the average F content (~1.8 wt%), resulting in fluoroapatite crystals which increased viscosity. Both HS24-11 and HS24-46 showed higher viscosity values compared to the predicted values, and these two glasses contained higher Cr and Fe contents compared to the average values, resulting in crystallization of spinel compounds at 1150°C. Overall, the glasses were designed to have a narrow range of predicted viscosities of 4-6 Pa-s, but due to expanding the compositional ranges of the prediction models, the range of measured values was larger than the predicted range.

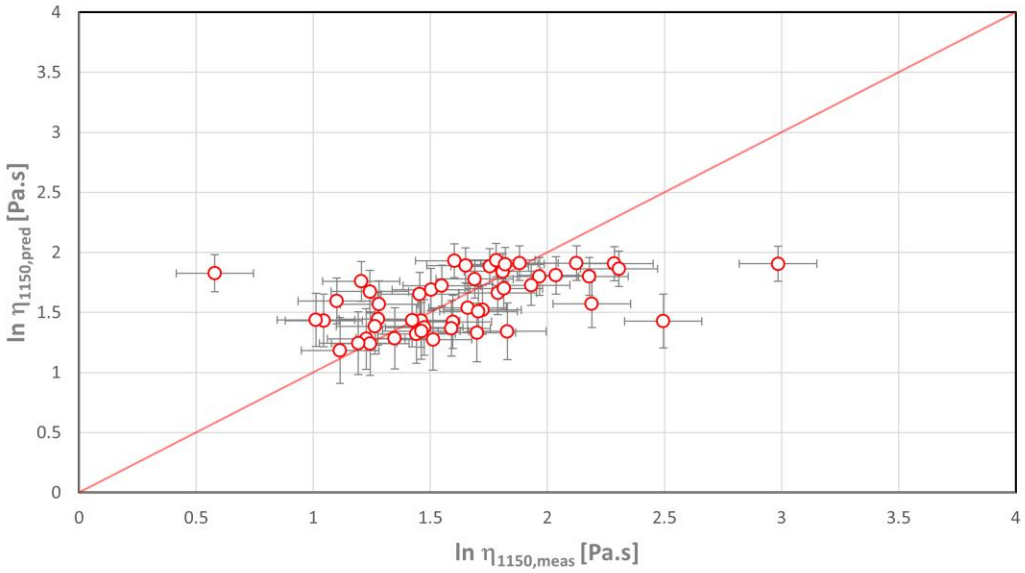

Figure 4.9. ln η values of predicted ln η vs. measured ln η at 1150 °C of HS24 glasses.

4.7 Electrical Conductivity

This section presents the EC results obtained using the methods discussed in Section 3.7. The results are summarized in Table 4.8. Measured EC (S/m) values versus temperatures are individually reported in Appendix J. The Arrhenius equation (Equation 4.2) was used to fit EC-temperature data for each waste glass. Arrhenius coefficients and calculated ε_{1150} are reported in Table 4.9. Most of HS24 glasses showed similar electrical conductivity values between measured and fitted values. However, HS24-41 and HS24-48 glasses showed a noticeable difference between the measured and fitted values, and these two glasses

had linear fitting with R^2 of < 0.81. Figure 4.10 shows a comparison between measured and predicted values using the EWG 2.5 Electrical Conductivity VFT RLM Model (Vienna et al. 2024). Overall, 37 glasses of HS24 glasses at 1150 °C were within the predicted interval ranges whereas the predicted values of remaining 13 samples were out of the predicted interval ranges by 1 to 74%.

Table 4.8. Measured electrical conductivity (S/m) values versus temperatures.

Target *T*, °C	950	1050	1100	1150	1200	1250
Glass ID			S/m			
HS24-01	13.566	21.414	26.242	31.702	37.810	44.576
HS24-02	9.534	11.652	12.741	13.845	14.959	16.081
HS24-03	15.819	19.792	21.868	23.994	26.162	28.363
HS24-04	19.637	21.974	23.102	24.203	25.277	26.323
HS24-05	29.436	41.728	48.744	56.322	64.443	73.085
HS24-06	23.941	31.851	36.170	40.709	45.452	50.381
HS24-07	29.212	40.322	46.546	53.191	60.237	67.661
HS24-08	17.351	26.329	31.703	37.679	44.259	51.441
HS24-09	27.937	40.249	47.357	55.088	63.425	72.352
HS24-10	16.840	26.089	31.705	38.006	45.002	52.698
HS24-11	9.633	14.115	16.733	19.601	22.716	26.071
HS24-12	45.134	59.334	67.021	75.059	83.417	92.065
HS24-13	53.079	71.471	81.597	92.294	103.525	115.249
HS24-14	9.444	16.283	20.754	26.006	32.092	39.059
HS24-15	12.399	16.468	18.687	21.017	23.450	25.977
HS24-16	19.124	23.175	25.245	27.335	29.439	31.551
HS24-17	23.957	34.293	40.233	46.675	53.605	61.007
HS24-18	12.848	20.762	25.709	31.361	37.742	44.874
HS24-19	21.177	32.448	39.239	46.823	55.206	64.391
HS24-20	26.706	40.861	49.383	58.892	69.399	80.902
HS24-21	15.343	22.542	26.754	31.375	36.397	41.813
HS24-22	18.379	27.776	33.385	39.610	46.455	53.915
HS24-23	17.838	27.034	32.533	38.644	45.370	52.709
HS24-24	17.869	28.322	34.771	42.078	50.265	59.348
HS24-25	39.729	54.424	62.613	71.328	80.541	90.221
HS24-26	18.474	27.056	32.068	37.556	43.515	49.934
HS24-27	30.005	42.208	49.137	56.594	64.562	73.016
HS24-28	31.670	45.410	53.316	61.897	71.134	81.006
HS24-29	27.799	39.114	45.539	52.456	59.846	67.690
HS24-30	22.876	32.694	38.331	44.440	51.007	58.018
HS24-31	26.072	35.286	40.378	45.768	51.439	57.371
HS24-32	11.181	12.765	13.541	14.305	15.055	15.792
HS24-33	15.501	23.380	28.075	33.283	39.004	45.234
HS24-34	23.130	34.130	40.586	47.680	55.404	63.748
HS24-35	20.547	29.598	34.823	40.505	46.633	53.193
HS24-36	14.623	25.290	32.279	40.499	50.035	60.964
HS24-37	11.105	18.653	23.499	29.128	35.584	42.902

Target *T*, °C	950	1050	1100	1150	1200	1250
Glass ID			S/m			
HS24-38	17.126	23.610	27.239	31.112	35.216	39.539
HS24-39	14.632	21.353	25.268	29.549	34.190	39.183
HS24-40	10.415	17.444	21.949	27.174	33.160	39.938
HS24-41	20.564	27.251	30.891	34.711	38.695	42.830
HS24-42	15.858	23.693	28.332	33.456	39.064	45.150
HS24-43	25.920	38.147	45.311	53.174	61.727	70.957
HS24-44	23.086	32.907	38.534	44.625	51.167	58.143
HS24-45	27.277	42.160	51.182	61.294	72.512	84.840
HS24-46	15.197	23.225	28.054	33.440	39.388	45.898
HS24-47	18.138	27.357	32.852	38.947	45.642	52.934
HS24-48	2.961	4.159	4.839	5.569	6.350	7.177
HS24-49	14.252	16.144	17.066	17.970	18.855	19.722
HS24-50	22.305	33.537	40.217	47.616	55.734	64.565

Table 4.9. Fitted coefficients of Arrhenius model for ε_{1150}.

	Arrhenius Coefficients		
Glass ID	A, ln[S/m]	B, ln[S/m]·K	ε_{1150} (S/m)
HS24-01	8.647	-7386.2	32.01
HS24-02	4.909	-3245.5	14.01
HS24-03	5.725	-3625.2	24.97
HS24-04	4.465	-1819.3	24.06
HS24-05	7.999	-5646.3	56.36
HS24-06	6.953	-4619.6	41.12
HS24-07	7.639	-5214.9	53.79
HS24-08	8.371	-6747.5	37.21
HS24-09	8.161	-5908.3	55.49
HS24-10	8.615	-7083.2	38.12
HS24-11	7.320	-6181.7	19.59
HS24-12	7.429	-4426.0	73.92
HS24-13	7.908	-4813.7	94.46
HS24-14	9.453	-8814.7	25.90
HS24-15	6.272	-4591.8	21.03
HS24-16	5.493	-3108.5	27.72
HS24-17	7.922	-5803.6	46.77
HS24-18	8.902	-7764.9	31.52
HS24-19	8.698	-6904.5	46.94
HS24-20	8.912	-6881.6	58.42
HS24-21	7.820	-6224.5	31.54
HS24-22	8.375	-6681.9	38.65
HS24-23	8.382	-6726.9	38.65
HS24-24	8.977	-7452.8	42.37
HS24-25	7.846	-5092.4	71.60

	Arrhenius Coefficients		
Glass ID	A, ln[S/m]	B, ln[S/m]·K	ε_{1150} (S/m)
HS24-26	7.964	-6173.5	37.49
HS24-27	7.916	-5521.5	57.13
HS24-28	8.223	-5831.0	62.60
HS24-29	7.843	-5525.5	52.25
HS24-30	7.855	-5778.3	44.45
HS24-31	7.265	-4896.6	44.63
HS24-32	4.167	-2143.7	14.65
HS24-33	8.178	-6649.1	33.09
HS24-34	8.288	-6294.4	47.50
HS24-35	7.852	-5906.0	40.63
HS24-36	9.931	-8864.3	40.17
HS24-37	9.269	-8391.4	28.76
HS24-38	7.088	-5194.9	27.60
HS24-39	7.684	-6115.9	29.46
HS24-40	9.167	-8345.1	27.36
HS24-41	6.748	-4555.5	40.39
HS24-42	8.076	-6496.4	33.61
HS24-43	8.368	-6252.6	52.44
HS24-44	7.828	-5734.9	44.90
HS24-45	9.067	-7045.1	62.14
HS24-46	8.333	-6862.9	32.92
HS24-47	8.335	-6649.9	38.79
HS24-48	5.580	-5496.2	8.12
HS24-49	4.306	-2017.1	18.69
HS24-50	8.501	-6599.1	48.39

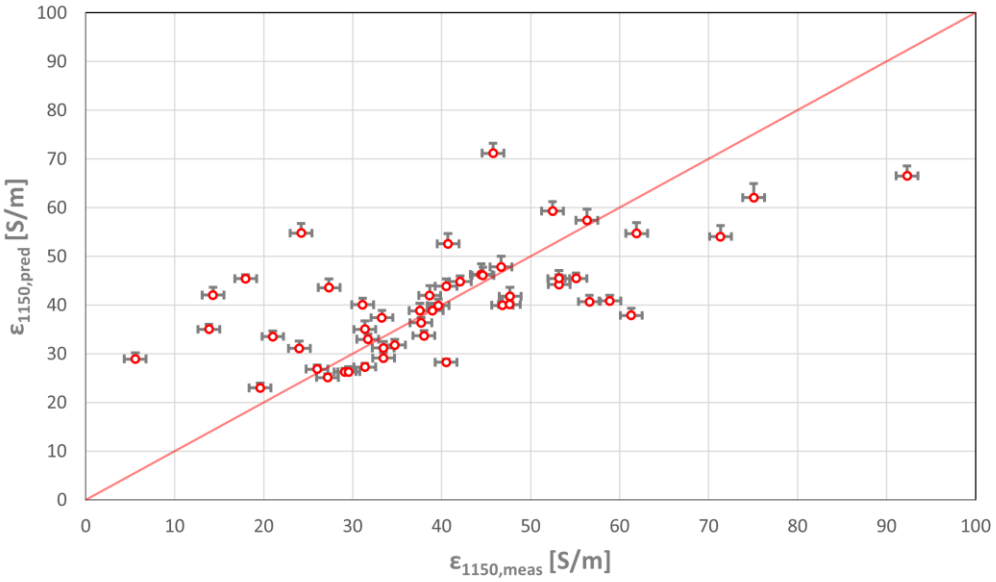

Figure 4.10. Predicted vs. measured EC values of HS24 glasses.

4.8 Product Consistency Test

This section presents the PCT results obtained using the methods discussed in Section 3.8. The average normalized concentrations ($NC_{i,ave}$) for B, Na, Si, and Li for Q and CCC glass are reported in Table 4.10 and Table 4.11, respectively. The NC_i for the individual tests are presented in Appendix K. The relative standard deviation between triplicate samples was less than 5%.

Table 4.10. Average normalized concentrations ($NC_{i,ave}$) in g/L for the HS24 Q glasses along with the average of $NC_{B, Na, Li,}$. Values exceeding the DWPF EA glass threshold listed in Table 3.4 are in bold red font. Silicon values are shown even though there are no WTP HLW PCT limits assigned for this element.

Glass ID	Boron	Silicon	Sodium	Lithium	Average (B, Na, Li)
HS24-01	14.47	0.44	9.00	**12.61**	11.80
HS24-02	5.91	0.28	4.93	6.00	5.59
HS24-03	0.59	0.18	0.62	0.67	0.63
HS24-04	1.39	0.43	1.43	0.64	1.08
HS24-05	2.10	0.53	2.07	1.51	1.87
HS24-06	2.34	0.50	2.08	1.26	1.83
HS24-07	0.65	0.27	0.87	0.45	0.63
HS24-08	0.38	0.24	0.45	0.60	0.47
HS24-09	0.53	0.24	0.85	0.30	0.52
HS24-10	0.61	0.18	0.71	0.68	0.66
HS24-11	14.45	0.17	6.53	**10.68**	10.03
HS24-12	1.37	0.42	1.27	1.06	1.23
HS24-13	3.32	1.27	3.40	1.66	2.66
HS24-14	1.01	0.30	1.24	1.11	1.11
HS24-15	6.69	1.23	6.58	5.46	6.21
HS24-16	0.59	0.24	0.76	0.49	0.60
HS24-17	2.26	0.53	2.20	1.43	1.92
HS24-18	2.99	0.37	2.71	3.30	2.99
HS24-19	1.10	0.46	1.61	1.19	1.28
HS24-20	0.41	0.28	0.81	0.69	0.61
HS24-21	0.57	0.31	0.64	0.71	0.64
HS24-22	0.60	0.35	0.57	0.15	0.37
HS24-23	0.62	0.32	0.91	0.64	0.71
HS24-24	1.35	0.62	1.81	1.52	1.55
HS24-25	0.44	0.35	0.91	0.43	0.55
HS24-26	0.73	0.39	1.15	0.87	0.90
HS24-27	0.42	0.26	0.61	0.37	0.46
HS24-28	0.46	0.34	0.96	0.46	0.59
HS24-29	0.75	0.26	0.88	0.41	0.65
HS24-30	0.38	0.23	0.76	0.36	0.47
HS24-31	0.95	0.48	1.45	0.77	1.02
HS24-32	1.67	0.50	1.70	1.68	1.69
HS24-33	0.40	0.28	0.70	0.52	0.53
HS24-34	0.68	0.22	0.70	0.59	0.66
HS24-35	9.41	0.27	4.81	7.71	7.04
HS24-36	0.43	0.20	0.58	0.54	0.51
HS24-37	0.32	0.17	0.52	0.48	0.43
HS24-38	1.57	0.40	1.49	1.36	1.47
HS24-39	**21.87**	0.19	10.30	**17.93**	**15.92**
HS24-40	1.09	0.18	1.07	1.25	1.13
HS24-41	**17.79**	0.17	9.23	**14.06**	**13.22**
HS24-42	**19.49**	0.15	8.43	**14.05**	**13.21**
HS24-43	2.98	0.20	1.90	2.74	2.50

Glass ID	Boron	Silicon	Sodium	Lithium	Average (B, Na, Li)
HS24-44	0.65	0.33	1.00	0.55	0.71
HS24-45	0.36	0.23	0.52	0.49	0.45
HS24-46	6.95	0.19	3.86	5.95	5.42
HS24-47	0.48	0.26	0.58	0.63	0.56
HS24-48	0.95	0.21	0.86	1.11	0.97
HS24-49	1.40	0.47	2.05	1.00	1.42
HS24-50	5.09	0.26	4.09	**32.53**	8.78

Table 4.11. Average normalized concentrations (NC_i) in g/L for the HS24 CCC glasses along with the average of $NC_{B, Na, Li,}$. Values exceed the DWPF EA glass threshold listed in Table 3.4 are in bold. Silicon values are shown even though there are no WTP HLW PCT limits assigned for this element.

Glass ID	Boron	Silicon	Sodium	Lithium	Average (B, Na, Li)
HS24-01	4.75	0.29	6.07	0.43	2.31
HS24-02	12.93	0.51	5.44	**119.11**	**20.31**
HS24-03	0.58	0.20	0.61	0.64	0.61
HS24-04	0.55	0.36	1.02	0.67	0.72
HS24-05	1.99	0.55	2.01	1.62	1.87
HS24-06	2.51	0.55	2.31	2.80	2.53
HS24-07	1.33	0.26	2.39	1.22	1.57
HS24-08	0.42	0.27	0.50	0.84	0.56
HS24-09	0.52	0.23	0.80	0.37	0.53
HS24-10	0.98	0.21	0.91	1.05	0.98
HS24-11	15.34	0.16	6.66	**10.87**	10.35
HS24-12	1.12	0.36	1.87	1.06	1.30
HS24-13	2.28	1.07	2.70	1.32	2.01
HS24-14	0.94	0.31	1.15	1.15	1.08
HS24-15	6.60	1.29	6.50	6.57	6.56
HS24-16	1.01	0.24	1.13	0.76	0.95
HS24-17	2.57	0.57	2.40	2.01	2.31
HS24-18	2.77	0.40	2.50	3.08	2.77
HS24-19	1.12	0.43	1.50	1.24	1.28
HS24-20	0.41	0.26	0.77	0.71	0.61
HS24-21	1.97	0.39	1.75	6.61	2.83
HS24-22	0.49	0.34	0.57	1.15	0.68
HS24-23	0.83	0.36	0.97	0.80	0.86
HS24-24	1.20	0.55	1.50	1.35	1.35
HS24-25	0.87	0.47	1.59	4.45	1.83
HS24-26	0.69	0.44	1.19	0.86	0.89
HS24-27	0.47	0.28	1.19	2.78	1.16
HS24-28	0.52	0.39	1.04	1.52	0.93
HS24-29	0.55	0.27	0.76	0.49	0.59
HS24-30	0.44	0.30	1.09	2.14	1.01
HS24-31	2.36	0.44	1.12	1.39	1.54
HS24-32	1.20	0.52	2.00	1.08	1.38
HS24-33	0.61	0.35	0.79	0.65	0.68
HS24-34	2.18	0.27	1.44	2.27	1.93
HS24-35	7.32	0.28	3.98	6.30	5.68
HS24-36	0.35	0.20	0.54	0.53	0.47
HS24-37	0.30	0.17	0.47	0.45	0.40
HS24-38	2.19	0.46	1.92	2.12	2.07
HS24-39	**20.68**	0.19	9.69	**17.39**	**15.16**
HS24-40	0.91	0.18	0.90	1.06	0.96

Glass ID	Boron	Silicon	Sodium	Lithium	Average (B, Na, Li)
HS24-41	15.87	0.17	8.61	**13.41**	12.24
HS24-42	**20.67**	0.16	8.68	**15.76**	**14.14**
HS24-43	1.95	0.22	1.29	1.78	1.65
HS24-44	0.59	0.31	0.88	0.69	0.71
HS24-45	0.34	0.24	0.90	8.48	1.37
HS24-46	9.11	0.19	4.37	7.12	6.57
HS24-47	0.47	0.27	0.58	1.38	0.72
HS24-48	2.54	0.17	1.76	2.56	2.25
HS24-49	1.00	0.40	1.57	1.00	1.16
HS24-50	**60.51**	0.44	**33.54**	**51.47**	**47.10**

Three of the 50 Q glasses exceeded the WTP HLW contract limit for B and five of the Q glasses exceeded the limit for Li. None of the Q glasses exceeded the limit for Na. Three of the 50 CCC glasses exceeded the contract requirement for B, one for Na, and six for Li. The glasses that exceed the PCT limit for at least one element for both the Q and CCC samples are HS24-11, HS24-39, HS24-41, HS24-42, and HS24-50.

A method that relies on a pooled standard deviation of PCT responses can be employed to determine if the difference between Q and CCC heat treated glasses are within experimental error (Russell et al. 2025). Briefly, the method creates a range for $\ln(NC_{Na})$ and $\ln(NC_{Li})$ where if the measured $\ln(NC_{Na})$ and $\ln(NC_{Li})$ for Q and CCC glasses fall within that range, then the Q and CCC responses can be considered to be within experimental uncertainty. Ten of the 50 HS24 glasses did not have Q PCT responses that were within experimental uncertainty for B, while eight of the 50 HS24 glasses did not have CCC PCT responses that were within experimental uncertainty for Na.

The differences between $\ln(NC_i)$ values for Q and CCC glasses are presented in Figure 4.11. The presence of crystals may cause disruption to the glass network connectivity and less durable glass. For this reason, the CCC responses are typically greater than or equivalent to the Q glass responses.

For the HS24 glasses, there seems to be little correlation between the crystalline phases that formed and the PCT response. In the Q glasses, the crystalline phases that formed were largely spinels, which have little impact on durability. None of the five Q glasses with the highest PCT response (HS24-01, HS24-11, HS24-39, HS24-41, and HS24-42) had Si- or Al-containing phases and one (HS-24-01) had no measurable crystalline phases. The only Si-containing phase for the Q glasses was in HS24-12, which contained a $ZnSiO_4$ phase at 1.7 wt%, but the glass did not have a relatively high PCT response. The CCC glasses resulted in Si- or Al-containing crystalline phases for HS24-22, HS24-37, HS24-41, and HS24-50. Though these CCC glasses had the same or higher PCT responses compared to their Q counterpart within uncertainty, the presence of the $NaAlSiO_4$ (presumably nepheline) phase in HS24-50 accounted for the largest relative difference between the Q and CCC glasses. HS24-02, which had the second highest PCT response for the CCC glass, did not contain measurable crystalline phases. There are a few cases where the Q glass had a response that was noticeably higher than the CCC glass. This includes HS24-01 for Li and B and HS24-04 for B. It is unclear why these two glasses are outliers.

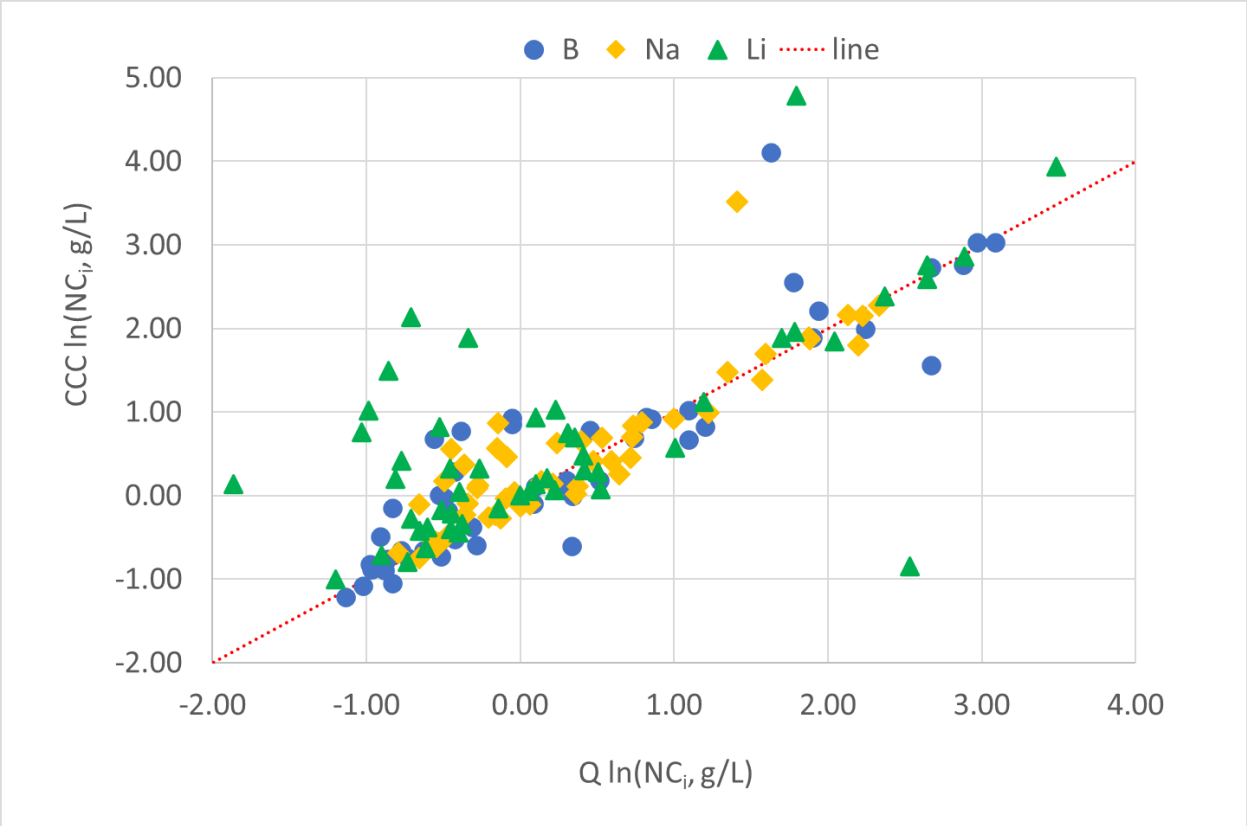

Figure 4.11. Average normalized NC_B, NC_{Li}, and NC_{Na} release in natural logarithm scale of Q vs. CCC for HS24 glasses. The red dotted line is the 1:1 line and is used to guide the eye.

Figure 4.12 shows the measured average $\ln(NC_B)$, $\ln(NC_{Na})$, and $\ln(NC_{Li})$ values plotted against model predictions from Vienna et al. (2024) and Vienna and Crum (2018). When $\ln(NC_B)$, $\ln(NC_{Na})$, and $\ln(NC_{Li})$ values are averaged, all glasses meet the PCT limit except for HS24-39 and HS24-42. Visually, the models adequately predict the average $\ln(NC_B)$, $\ln(NC_{Na})$, $\ln(NC_{Li})$ values with the Vienna and Crum (2018) values being slightly closer to the 1:1 line.

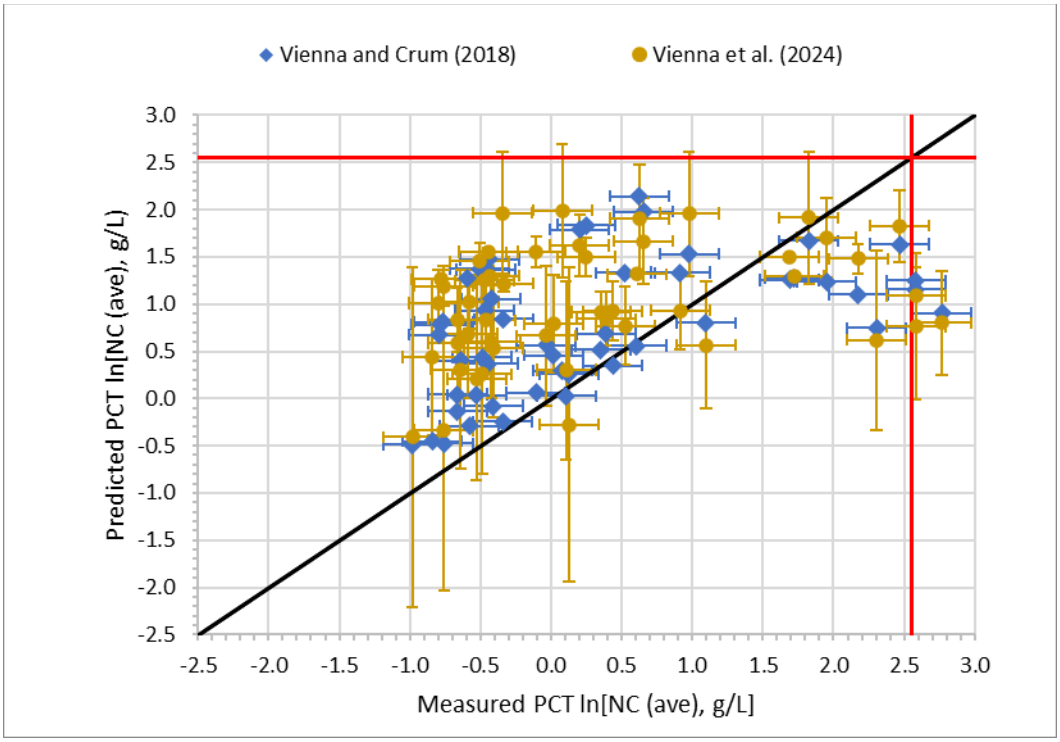

Figure 4.12. Average quenched glass $\ln(NC_B)$ and $\ln(NC_{Na})$ values plotted against model predictions from Vienna et al. (2024) and Crum and Vienna (2018).

4.9 Toxicity Characteristic Leaching Procedure

Figure 4.13 provides a summary of the measured TCLP leachate concentrations of B, Cr, Ni, Pb, V, and Zn for Q and CCC HS24 glasses compared to the analytical detection limits and the constituent of concerns' delisting limits (Blumenkranz 2006). The detection limit value is provided for tests that returned concentrations below detection limits. Full results are provided in Appendix L.

Many glasses had concentrations below detection limits for most regulated species, especially Ni and Pb. When TCLP leachate concentrations registered above detection limits, they primarily originated from the CCC glasses (see Cr as an example in Figure 4.13). All glasses, with the exception of HS24-15, remained below the delisting limits for the constituents of concern (Cr, Ni, Pb, V, Zn). The HS24-15 CCC glass was the only case that exceeded the Cr limit and, more broadly, exhibited elevated releases for most elements except Pb in both the Q and CCC samples. While the target Cr concentration was consistent with the matrix average, sulfur was present at the higher end of the range, suggesting the potential formation of S–Cr salts and associated Cr leaching. However, no salt layer was observed during optical inspection of the samples. XRD analysis of the CCC sample identified ~5 wt% of a Ca-P-F crystalline phase ($Ca_{10}(PO_4)_6F_2$), which is not known to compromise glass durability, and therefore does not explain the observed Cr release.

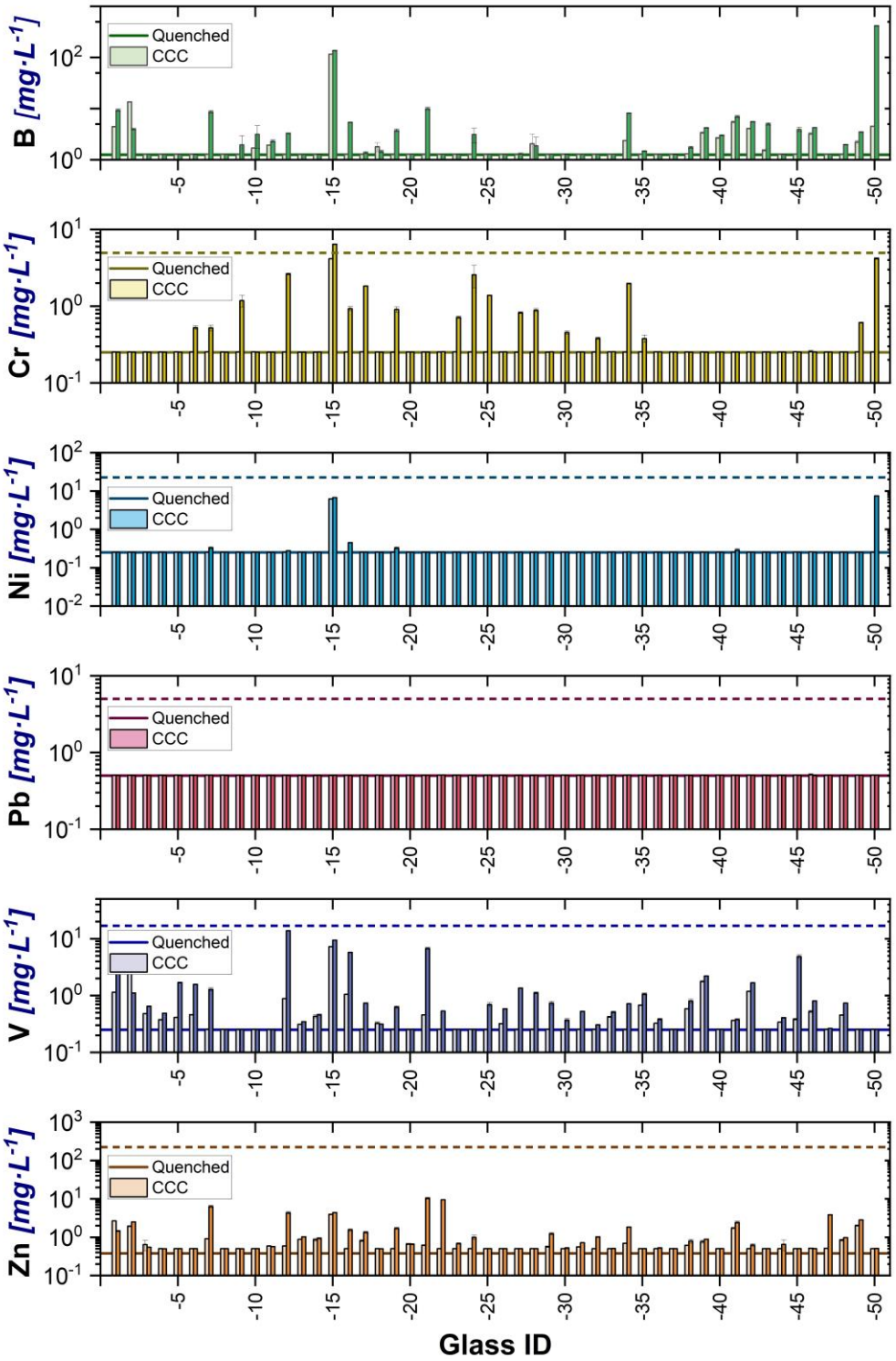

Figure 4.13. TCLP leachate concentrations for B, Cr, Ni, Pb, V, and Zn for Q and CCC HS24 glasses. The dashed lines represent the delisting limits while the solid lines specify the analytical detection limit.

Figure 4.14 compares the CCC and Q TCLP ln(NC_i) for element *i*. In general, the CCC glasses released higher concentrations of B, Cr, Ni, V, and Zn than the Q glasses. The TCLP responses do not appear to be

correlated to crystal presence (e.g., glasses HS24-01 and HS24-02 Q and CCC glasses did not have crystals; nevertheless, they had higher TCLP B, V, and Zn concentrations in CCC than Q). No other correlations were observed to explain the TCLP response.

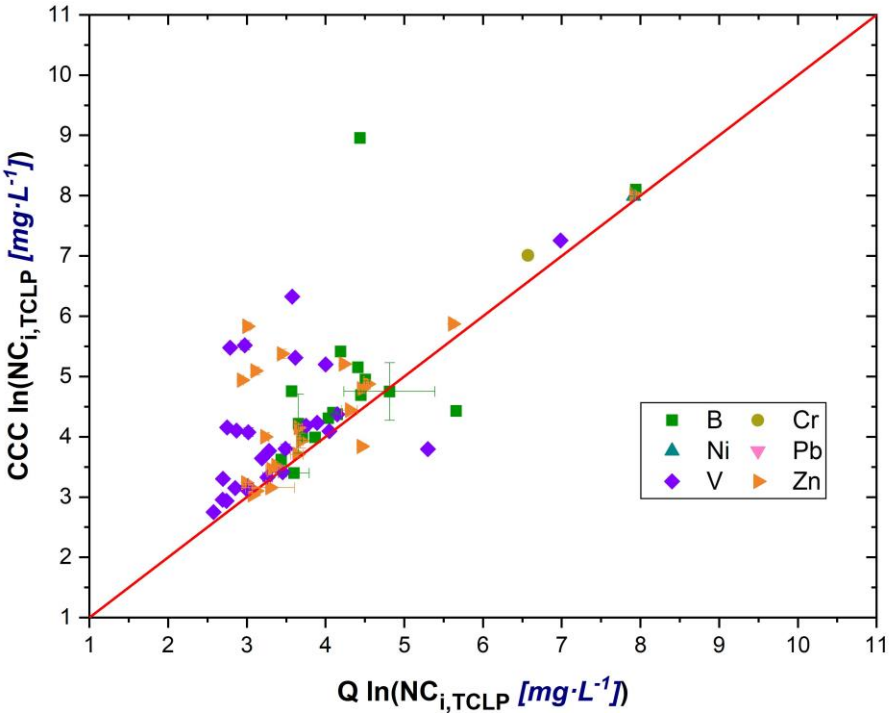

Figure 4.14. TCLP ln(NC_i) for B, Cr, Ni, Pb, V, and Zn for Q and CCC HS24 glasses. The uncertainties are represented by one standard deviation of the average of the replicate tests for the Q and CCC glasses, respectively. All results that were below detections were excluded. The red line represents the 1-1 correlation between the Q and CCC values.

Figure 4.15 shows ln(NC_i) for Cr, Ni, Pb, V, and Zn compared to ln(NC_B) for the Q glasses where concentrations were measured above detection limits for B and the selected element. In all instances, ln(NC_i) was within uncertainty or lower than ln(NC_B) which indicates that the B is reliable tracer of the toxic elements (which are congruent or mostly congruent with B) and thus a representative indicator of TCLP response in modeling.

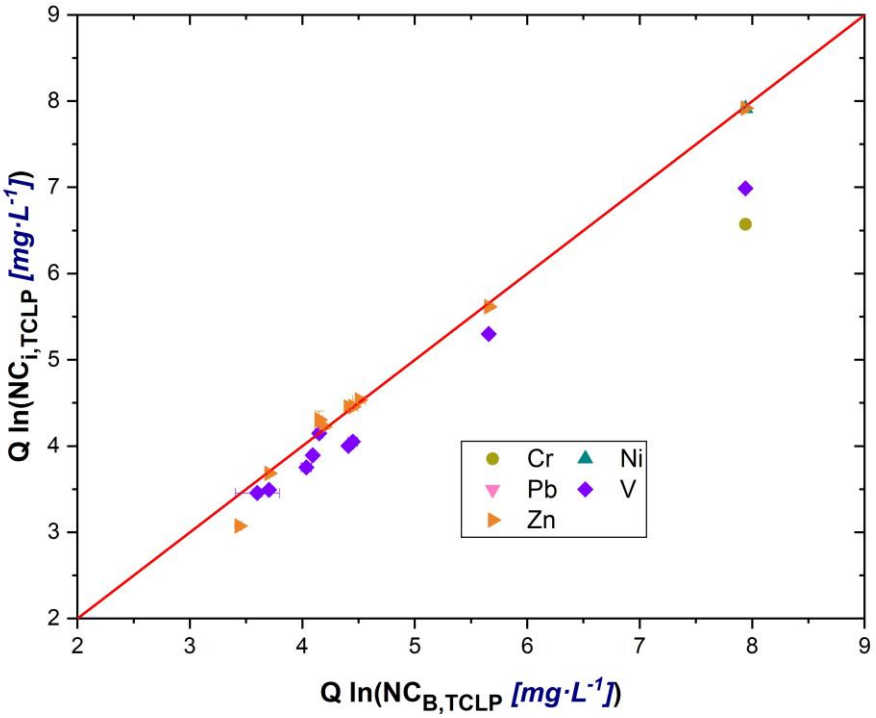

Figure 4.15. TCLP ln(NC_i) for Cr, Ni, Pb, V, and Zn compared to ln(NC_B). The uncertainties are represented by one standard deviation of the average of the replicate tests for each element. All results that were below detections were excluded. The red line represents the 1-1 correlation between the ln(NC_i) and ln(NC_B) values.

The NC_B from the Q glasses determined experimentally for the HS24 matrix were compared to predicted NC_B generated from the TCLP models in Vienna et al. (2009) and Kim and Vienna (2002) and are presented in Figure 4.16.

The predicted TCLP leachate concentration of element i ($c_{i,pred}$) was determined using Equation 4.3 originally from Kim and Vienna (2004):

$$c_{i,pred} = NC_{B,pred} \cdot f_i \tag{4.3}$$

where $NC_{B,pred}$ is the predicted NC_B using the Kim and Vienna (2002) and Vienna et al. (2009) models and f_i is the mass fraction of element i in the unaltered glass.

Both models overpredict NC_B providing conservative estimates. The Vienna et al. (2009) model generated predictions slightly closer to measured values. However, some HS24 glass compositions exceeded the model validation range. A new model accounting for a wider compositional range may improve agreement between model predictions and experimental measurements.

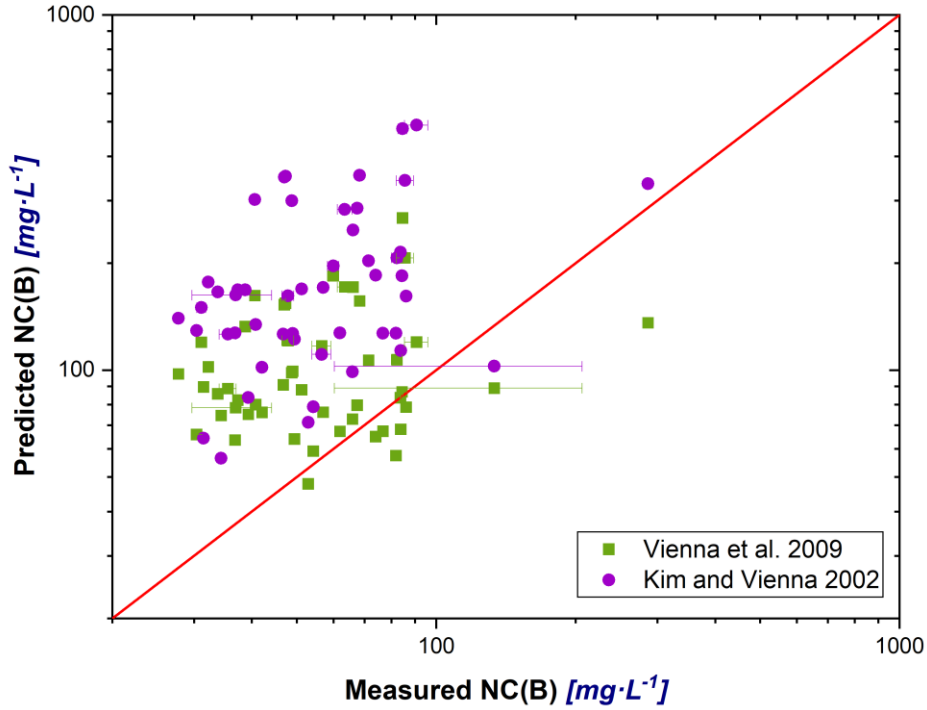

Figure 4.16. Measured NC_B results from HS24 Q glasses and their respective predicted NC_B values from the Vienna et al. (2009) and Kim and Vienna (2002) models. Results are only provided for measured NC(B) with results above the detection limits. The uncertainties are represented by one standard deviation of the average of the replicate tests for the measured Q glasses. The red line represents the 1-1 correlation between the measured and predicted values.

Figure 4.17 shows measured Q glasses and corresponding predicted TCLP releases from a) Kim and Vienna (2002) and b) Vienna et al. (2009) for Cr, Ni, Pb, V, and Zn. All measured values below the detection limit were excluded. As a result, fewer results are available for some species such as Cr and Pb compared to other species such as V and Zn. The predicted values are higher than the measured Q values in most instances. The exceptions are HS25-15 for the Kim and Vienna (2002) model and HS25-15 and HS25-02 for the Vienna et al. (2009) model. However, since both models have higher predicted values than measured values, the estimates are conservative.

In general, the Vienna et al. (2009) model provides predictions closer to experimental results, but a new TCLP model which includes the higher S compositional space would be ideal to further reduce excessive conservativity.

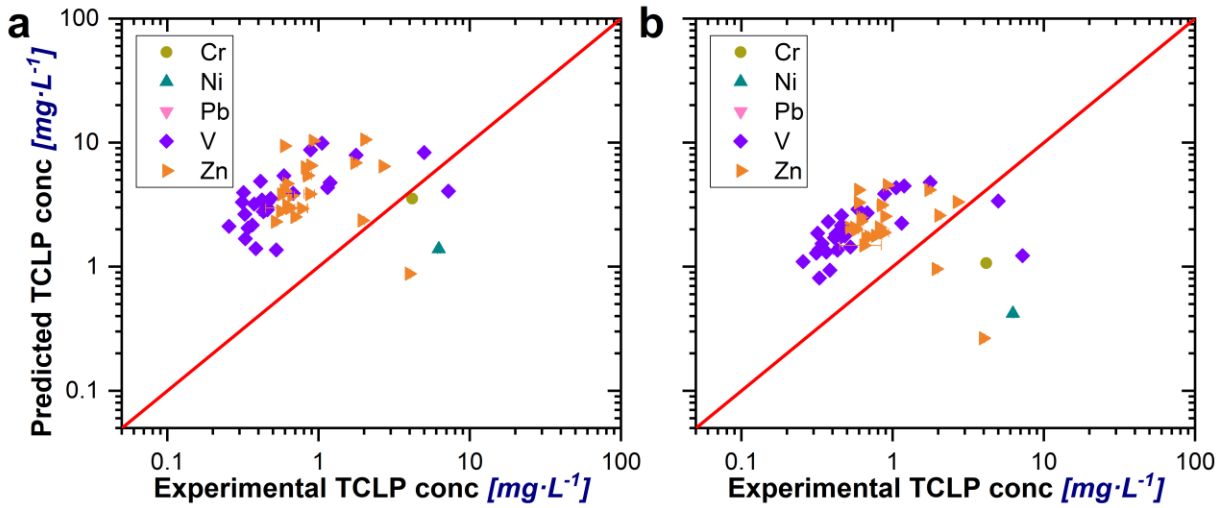

Figure 4.17. Measured Q and predicted TCLP releases from a) Kim and Vienna (2002) and b) Vienna et al. (2009) for Cr, Ni, Pb, V, and Zn. The uncertainties are represented by one standard deviation of the average of the replicate tests for the measured Q glasses. All measured values below detection limits were excluded. The red line represents the 1-1 correlation between the measured and predicted values.

5.0 Conclusions

A matrix of 50 glasses with a wide range of SO_3 content (0 – 1.58 SO_3 wt%) was designed to expand DFHLW glass compositional ranges. This matrix was designed using a space-filling method with component concentration boundaries obtained by expanding the existing database and results from EWG-based formulations. This 50-glass matrix satisfied the success criteria for the dispersion ratio and range of coverage. The designed glass compositions were fabricated and tested, including compositions, CCC and isothermal heat treatments, density, viscosity, EC, PCT, TCLP, and sulfate solubility.

Table 5.1 summarizes the HS24 glasses passing or failing the property constraints. Out of the 50 glasses tested, only one glass formed nepheline, while the model predicted nepheline formation in 5 glasses. Six glasses (both Q and CCC) failed the DWPF EA PCT threshold; while 3 Q and 4 CCC glasses failed the PCT design constraint. Additionally, 8 glasses did not satisfy the viscosity constraints, 4 failed the EC constraints, while none exceeded the allowable $T_{2\%}$ for spinel crystal formation. All the glasses (except one which failed being slightly lower than the target) satisfied the SO_3 constraint. No constraint is provided for TCLP as the typical constraint is based on Cd release (limit is Cd release < 0.48 mg·L^{-1}), and the glasses were fabricated without Cd. The failures in specific properties were intentionally incorporated during matrix design and are essential for defining acceptable processing envelopes for DFHLW operations. Data generated near property constraint boundaries are particularly critical, as they improve model accuracy and robustness, increase predictive accuracy in boundary regions, and reduce uncertainties in defining processing limits.

These glasses were intentionally designed with high sulfur solubilities (~1 to 2 wt%) to address glass compositional regions that previously lacked experimental data. Although some of these glasses exhibit relatively low SO_3 solubility compared with existing data, particularly when compared with certain LAW glasses, this is expected because the HS24 glasses were designed for DFHLW regions using DFHLW-specific property models and constraints. Some glasses were expected to either fail or approach property constraints to fill data gaps in poorly understood regions of the compositional space due to lack of data.

The resulting dataset provides valuable information to improve model accuracy and reduce prediction uncertainty. These insights will ultimately support the development of more robust glass formulation strategies, enabling higher waste loading, reducing operational risks, and expanding the processing envelope.

Table 5.1. Summary of the 50 HS24 glasses passing or failing property design constraints without considering uncertainties. Property constraints were taken from Vienna et al. (2025). This table is for information only.

Glass ID	w_{SO3}	η_{1150}	ε_{1150}	PCT Q	PCT CCC	Pred NP F/P	Meas NP F/P	Spinel $T_{2\%}$
Constraints	SO_3 in glass < w_{SO3}	2 to 8 Pa s	10 to 70 S/m	<6.44 $g/m^{2(a)}$	<6.44 $g/m^{2(a)}$	nepheline formation (>0.028)	Measured nepheline formation (>0 wt%)	F if spinel vol% >2% at 950 °C
HS24-01	P	P	P	P	P	P	P	P
HS24-02	P	P	P	P	F	P	P	P
HS24-03	P	P	P	P	P	P	P	P
HS24-04	P	P	P	P	P	P	P	P
HS24-05	P	F	P	P	P	P	P	P
HS24-06	P	P	P	P	P	P	P	P
HS24-07	P	P	P	P	P	F	P	P
HS24-08	P	F	P	P	P	F	P	P
HS24-09	P	P	P	P	P	P	P	P
HS24-10	P	P	P	P	P	P	P	P
HS24-11	P	F	P	P	P	P	P	P
HS24-12	P	P	F	P	P	P	P	P
HS24-13	P	P	F	P	P	P	P	P
HS24-14	P	P	P	P	P	P	P	P
HS24-15	P	P	P	P	P	P	P	P
HS24-16	P	P	P	P	P	P	P	P
HS24-17	F	P	P	P	P	P	P	P
HS24-18	P	F	P	P	P	P	P	P
HS24-19	P	P	P	P	P	P	P	P
HS24-20	P	P	P	P	P	P	P	P
HS24-21	P	P	P	P	P	P	P	P
HS24-22	P	F	P	P	P	P	P	P
HS24-23	P	P	P	P	P	P	P	P
HS24-24	P	P	P	P	P	P	P	P

Glass ID	w_{SO3}	η_{1150}	ε_{1150}	PCT Q	PCT CCC	Pred NP F/P	Meas NP F/P	Spinel $T_{2\%}$
HS24-25	P	P	F	P	P	P	P	P
HS24-26	P	P	P	P	P	P	P	P
HS24-27	P	P	P	P	P	P	P	P
HS24-28	P	P	P	P	P	F	P	P
HS24-29	P	P	P	P	P	P	P	P
HS24-30	P	P	P	P	P	P	P	P
HS24-31	P	P	P	P	P	P	P	P
HS24-32	P	P	P	P	P	P	P	P
HS24-33	P	F	P	P	P	P	P	P
HS24-34	P	P	P	P	P	F	P	P
HS24-35	P	P	P	P	P	P	P	P
HS24-36	P	P	P	P	P	P	P	P
HS24-37	P	P	P	P	P	P	P	P
HS24-38	P	P	P	P	P	P	P	P
HS24-39	P	P	P	F	F	P	P	P
HS24-40	P	P	P	P	P	P	P	P
HS24-41	P	P	P	F	P	P	P	P
HS24-42	P	F	P	F	F	P	P	P
HS24-43	P	P	P	P	P	P	P	P
HS24-44	P	P	P	P	P	P	P	P
HS24-45	P	P	P	P	P	P	P	P
HS24-46	P	F	P	P	P	P	P	P
HS24-47	P	P	P	P	P	P	P	P
HS24-48	P	P	F	P	P	P	P	P
HS24-49	P	P	P	P	P	P	P	P
HS24-50	P	P	P	P	F	F	F	P
Total F	1	8	4	3	4	5	1	0

(a) The value of 6.44 is calculated from the average ln[NL] of the Defense Waste Processing Facility (DWPF) EA glass [= (ln[16.70/2] + ln[13.35/2] + ln[9.57/2])/3 = 1.86; for B, Na, and Li, respectively, see Table 3.4] and applying an exponential function to the average ln[NL], which yields an average of NL of 6.44 g/m^2, or average NC of 12.78 g/L, where NC is assumed to be equal to two times NL. The glass may pass the design constraint but the requirement states that the glass needs to meet the limit for B, Na, and Li. See Section 4.8 for a discussion on the glasses that did not meet the individual element requirements.

6.0 References

Alton J, J Plaisted, and P Hrma. 2002. “Kinetics of Growth of Spinel Crystals in a Borosilicate Glass.” *Chemical Engineering Science* 57:2503-2509.

ASTM C1285-21, *Standard Test Methods for Determining Chemical Durability of Nuclear, Hazardous, and Mixed Waste Glasses and Multiphase Glass Ceramics: The Product Consistency Test (PCT)*. ASTM International, West Conshohocken, PA.

ASTM C1720-21, *Standard Test Method for Determining Liquidus Temperature of Immobilized Waste Glasses and Simulated Waste Glasses.* ASTM International, West Conshohocken, PA.

ASTM D6323-19, *Standard Guide for Laboratory Subsampling of Media Related to Waste Management Activities.* ASTM International, West Conshohocken, PA.

Blumenkranz DB. 2006. *Petition to Delist Immobilized High-Level Waste Generated at the Hanford Tank Waste Treatment and Immobilization Plant.* 24590-WTP-RPT- DB ENV-06-001, Rev. 0, River Protection Project, Hanford Tank Waste Treatment and Immobilization Plant, Richland, WA.

Britton, MD. 2023. "Preliminary Direct-Feed High-Level Waste Washing and Blending Study Results." Memo to T Wagnon, dtd Jan 27, 2023, WRPS-2300408, Washington River Protection Solutions, Richland, WA.

Certa, PJ, TM Hohl, AM Johnson, SL Orcutt, RS Wittman, and DS Kim. 2005. Sensitivity of Hanford Immobilized High Level Waste Glass Mass to Chromium and Aluminum Partitioning Assumptions, RPP-20003, Rev. 1, CH2MHill Hanford Group, Richland, WA.

Crum, JV, TB Edwards, RL Russell, PJ Workman, MJ Schweiger, RF Schumacher, DE Smith, DK Peeler, JD Vienna. DWPF Startup Frit Viscosity Measurement Round Robin Results, *Journal of the American Ceramic Society*, 95 (2012) 2196–2205. https://doi.org/10.1111/j.1551-2916.2012.05220.x.

DOE. 1996. *Waste Acceptance Product Specifications for Vitrified High-Level Waste Forms (WAPS)*. DOE/EM-0093, U.S. Department of Energy, Office of Environmental Management, Washington, D.C.

DOE. 2000. *Design, Construction, and Commissioning of the Hanford Tank Waste Treatment and Immobilization Plant*. Contract DE-AC27-01RV14136, as amended, U.S. Department of Energy, Office of River Protection, Richland, WA.

EPA Method 1311, “Toxicity Characteristic Leaching Procedure (TCLP).” In *Test Methods for Evaluating Solid Waste, Physical/Chemical Methods*, EPA Publication SW–846.

Gervasio, V, X Lu, J Reiser, M Peterson, NL Canfield, JB Lang, and JC Rigby, et al. 2023. Direct Feed High-Level Waste APPS Model Glass Testing (DFHLW APPS) Matrix, PNNL-35503, Pacific Northwest National Laboratory, Richland, WA.

Gervasio, V, JD Vienna, S Saslow, J George, S Baird, J Bonnet, R Russel, DS Kim, J Lang, B Westmen, S Sannoh, and D. Cutforth. 2021. Chromium content and redox effects on high-level waste glass properties. PNNL-30852, Pacific Northwest National Laboratory, Richland, WA.

Gervasio, V., Saslow, S. A., Lang, J. B., Westman, B. E., Cutforth, D. A., Baird, S. M., ... & Vienna, J. D. (2025). Impacts of Cr (III) and Cr (VI) concentrations on key high-level waste glass properties. *International Journal of Applied Glass Science*, e16708.

Gervasio V., X. Lu, N.A. Bontha, T. Jin, J. Crum, B.J. Riley, & N.A. Lumetta, et al. (2026). Effects of B_2O_3, CaO, and Fe_2O_3 on the solubility of Cr_2O_3 in high-level waste glasses. *International Journal of Applied Glass Science*. Under review.

Herman, CC, PR Dixon, TM Brouns, ME Stone, RT Jubin, KG Picha, MS Vassiliou, RP Miklos, SM Robinson, MJ Rigali, J Manna, S Venkatesh, and DM Tate. 2022. R&D Roadmap for Hanford Tank Waste Mission Acceleration, NNLEMS-2022-00005, Rev. 0, Network of National Laboratories for Environmental Management and Stewardship, Washington, D.C.

Jantzen CM, NE Bibler, DC Beam, CL Crawford, and MA Pickett. 1993. *Characterization of the Defense Waste Processing Facility (DWPF) Environmental Assessment (EA) Glass Standard Reference Material (U)*. WSRC-TR-92-346, Rev. 1, Westinghouse Savannah River Company, Aiken, SC.Jin T, Kim D, Darnell LP, Weese BL, Canfield NL, Bliss M, Schweiger MJ, Vienna JD, Kruger AA. A crucible salt saturation method for determining sulfur solubility in glass melt. *Int J Appl Glass Sci*. 2018; 10: 92–102. **https://doi.org/10.1111/ijag.12366**

Joseph, R, E Gui, and S Ba. 2015. Maximum Projection Designs for Computer Experiments," Biometrika. 102:2. 37 1-380.

Kim D, Peeler D, Hrma P, editors. Effect of Crystallization on the Chemical Durability of Simulated Nuclear Waste Glasses1995; Westerville, OH: American Ceramic Society.

Kim DS and JD Vienna. 2002. *Model for TCLP Releases from Waste Glasses*. PNNL-14061, Pacific Northwest National Laboratory, Richland, WA.

Kim DS and JD Vienna 2004. Glass composition-TCLP response model for waste glasses. In *Environmental Issues and Waste Management Technologies in the Ceramic & Nuclear Industries IX*: 297-305, American Ceramic Society.

Kim D, JD Vienna, and AA Kruger. 2012. *Preliminary ILAW Formulation Algorithm Description*. 24590-LAW-RPT-RT-04-0003. Rev. 1, River Protection Project, Waste Treatment Plant, Richland, WA.

Kot WK, K Gilbo, H Gan, and IL Pegg. 2019. *Enhancement of HLW Glass Property-Composition Models*. VSL-19R4480-1, Vitreous State Laboratory, The Catholic University of America, Washington, D.C.

Kroll, JO, ZJ Nelson, CH Skidmore, DA Dixon and JD Vienna. "Formulation of High-Al_2O_3 Waste Glasses From Projected Hanford Waste Compositions and Assessment of Current Glass Property Models." Journal of Non-Crystalline Solids 517:17-25 (2019).

Kruger, A. *Toxicity Characteristic Leaching Procedure (TCLP) Testing of Selected High-Level Waste (HLW) Simulant Glasses*. QAPP ID# CRESP-VU-ORP-2023-0001.

Lu, X., I. Sargin, and J. D. Vienna. 2021. "Predicting nepheline precipitation in waste glasses using ternary submixture model and machine learning." Journal of American Ceramic Society 104: 5636-5647. https://doi.org/10.1111/jace.17983

Lu, X, T Jin, JD Vienna, and CL Trivelpiece. 2023. Waste Glass Property Database and Data Qualification Plan, PNNL-34447, Pacific Northwest National Laboratory, Richland, WA.

Lu, X., JD Vienna, and P Ferkl. 2024. Evaluation of DFHLW EWG Formulations and Processing Rates. PNNL-36196. Pacific Northwest National Laboratory, Richland, WA

Lumetta, NA, DS Kim, and JD Vienna. 2023. Preliminary enhanced LAW glass formulation algorithm. PNNL-29475 Rev 2. Pacific Northwest National Laboratory, Richland, WA.

Matlack, KS, H Gan, M Chaudhuri, W Kot, W Gong, T Bardakci, and IL Pegg. 2008. Melt Rate Enhancement for High Aluminum HLW Glass Formulations. VSL-08R1360-1. Vitreous State Laboratory, The Catholic University of America, Washington, DC.

Matlack, KS, H Gan, M Chaudhuri, W Kot, W Gong, T Bardakci, and IL Pegg. 2010. DM100 and DM1200 Melter Testing with High Waste Loading Glass Formulations for Hanford High-Aluminum HLW Streams. VSL-10R1690-1. Vitreous State Laboratory, The Catholic University of America, Washington, DC.

Mellinger GB and JL Daniel. 1984. Approved Reference and Testing Materials for Use in Nuclear Waste Management Research and Development Programs. PNL-4955-2, Pacific Northwest Laboratory, Richland, WA. https://doi.org/10.2172/6224421

Muller, IS, I Joseph, AA Kruger, KS Matlack, H Gan and IL Pegg. 2010. Waste Loading Enhancements for Hanford LAW Glasses, VLS-10R1790-1, Vitreous State Laboratory, The Catholic University of America, Washington, DC.

Peeler, DK, JD Vienna, MJ Schweiger, and KM Fox. 2015. Advanced High-Level Waste Glass Research and Development Plan, PNNL-24450, Pacific Northwest National Laboratory, Richland, WA.

Petkus LL. 2003. “Canister Centerline Cooling Data, Revision 1.” To CA Musick, Oct 29, 2003. CCN 074851, River Protection Project, Waste Treatment and Immobilization Plant, Richland, WA.

Russell RL, V Gervasio, X Lu, S Chong, JT Reiser, NL Canfield, JL George, NA Lumetta, J Neeway, LM Seymour. 2025. *Direct Feed High Level Waste APPS Model Glass Testing (DFHLW APPS) Matrix, Phase 2*. PNNL-37506, Pacific Northwest National Laboratory, Richland, WA.

Skidmore, CH, JD Vienna, T Jin, D Kim, BA Stanfill, KM Fox, and AA Kruger. “Sulfur solubility in low activity waste glass and its correlation to melter tolerance”. International Journal of Applied Glass Science, 10(4), pp.558-568 (2019).

Smith GL. 1993. *Characterization of Analytical Reference Glass-1 (ARG-1)*. PNL-8992, Pacific Northwest Laboratory, Richland, WA.

U.S. Environmental Protection Agency. Land Disposal Restrictions. *Code of Federal Regulations*, Title 40, Part 268; U.S. Government Publishing Office: Washington, DC, 2015. U.S. Environmental Protection Agency. Land Disposal Restrictions. Code of Federal Regulations, Title 40, Part 268; U.S. Government Publishing Office: Washington, DC, 2015.

Vienna, John D., Dong-Sang Kim, and Pavel R. Hrma. 2002. *Database and Interim Glass Property Models for Hanford HLW and LAW Glasses*. PNNL-14060. Pacific Northwest National Lab., Richland, WA.

Vienna JD, Hrma P, Crum JV, Mika M. Liquidus temperature-composition model for multi-component glasses in the Fe, Cr, Ni, and Mn spinel primary phase field. Journal of Non-Crystalline Solids. 2001;292:1-24.

Vienna JD, A Fluegel, DS Kim, and P Hrma. 2009. *Glass Property Data and Models for Estimating High-Level Waste Glass Volume*. PNNL-18501, Pacific Northwest National Laboratory, Richland, WA.

Vienna, JD, DC Skorski, DS Kim, and J Matyáš. 2013. Glass Property Models and Constraints for Estimating the Glass to be Produced at Hanford by Implementing Current Advanced Glass Formulation Efforts, PNNL-22631, Pacific Northwest National Laboratory, Richland, WA.

Vienna, JD and DS Kim. 2014. Preliminary IHLW Formulation Algorithm Description, 24590-HLW-RPT-RT-05-001, Rev. 1, River Protection Project, Hanford Tank Waste Treatment and Immobilization Plant, Richland, WA.

Vienna, J. D., Kim, D. S., Muller, I. S., Piepel, G. F., & Kruger, A. A. 2014. “Toward understanding the effect of low-activity waste glass composition on sulfur solubility.” Journal of the American Ceramic Society, 97(10), 3135-3142. https://doi.org/10.1111/jace.13125

Vienna, JD, GF Piepel, DS Kim, JV Crum, CE Lonergan, BA Stanfill, BJ Riley, SK Cooley, and T Jin. 2016. 2016 Update of Hanford Glass Property Models and Constraints for Use in Estimating the Glass Mass to be Produced at Hanford by Implementing Current Enhanced Glass Formulation Efforts, PNNL-25835, Pacific Northwest National Laboratory, Richland, WA.

Vienna, JD, JO Kroll, PR Hrma, JB Lang, and JV Crum. “Submixture model to predict nepheline precipitation in waste glasses”. International Journal of Applied Glass Science, 8(2), pp.143-157 (2017).

Vienna, JD and JV Crum "Non-linear effects of alumina concentration on Product Consistency Test response of waste glasses." Journal of Nuclear Materials 511: 396–405 (2018).

Vienna, JD, A Heredia-Langner, SK Cooley, AE Holmes, DS Kim, and NA Lumetta. 2022. Glass Property-Composition Models for Support of Hanford WTP LAW Facility Operation, PNNL-30932, Rev. 2, Pacific Northwest National Laboratory, Richland, WA.

Vienna, JD, X Lu, P Ferkl, J Marcial, MS Fountain, M Trenidad, R Hanson, MD Britton, L Cree, and W Abdul. 2023. "High-Level Waste Glass Processing over Broad Range of Alternative Feed Compositions," Waste Management 2023, WMSymp. Inc.

Vienna, JD, X Lu, P Ferkl, LL Gunnell, A Heredia-Langner, NA Lumetta, and T Jin, et al. 2024. Glass Property-Composition Models Update for use in Direct Feed High-Level Waste Flowsheet Development. PNNL-35884, Pacific Northwest National Laboratory, Richland, WA.

Vienna, J. D., X. Lu, P. Ferkl, D. Kim, J. Marcial, J. Bai, and J.V. Crum, et al. 2025. Glass Property-Composition Models Update for use in Direct Feed High-Level Waste Flowsheet Development: EWG2.6. Pacific Northwest National Laboratory, PNNL-37762. Richland, WA

Appendix A – Heatmap and scatter plots

The information in this appendix is to be used for information only. These figures show the pair correlations of a few major glass components (e.g., Al_2O_3, B_2O_3, SiO_2, Na_2O). Figures (a) on the left show the design space (whole ranges) as blue heatmaps. Orange triangles represent existing glasses that have both 3TS and K-3 data. Figures (b) on the right show the design space (where glasses pass the property constraints) as blue heatmaps, and 50 glasses for tests as black x's. Orange triangles in Figures (b) represent existing glasses that have both 3TS and K-3 data and fall within the matrix design ranges. Orange squares represent the two replicate glasses.

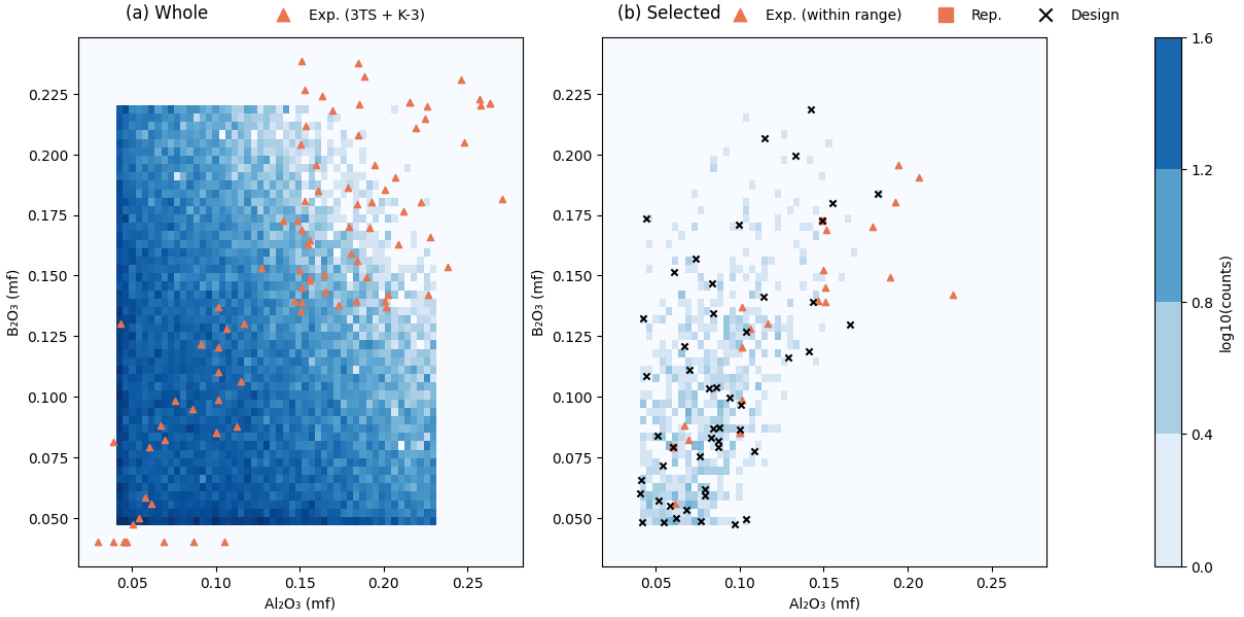

Figure A.1. Heatmaps for B_2O_3 compared to Al_2O_3

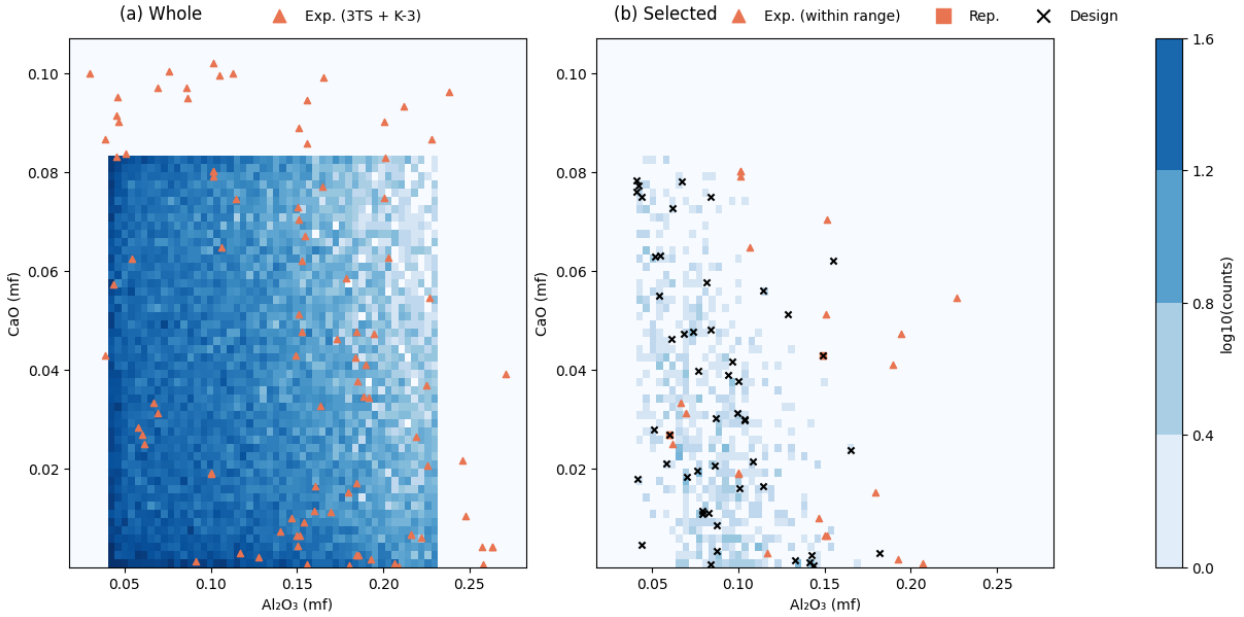

Figure A.2. Heatmaps for CaO compared to Al_2O_3

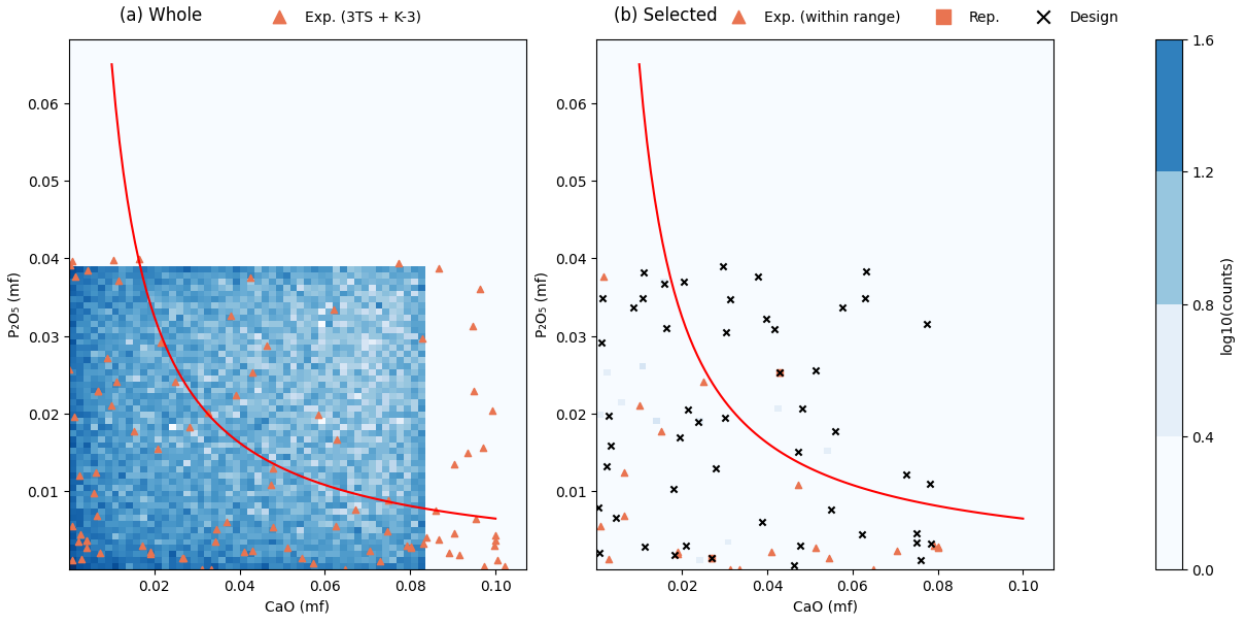

Figure A.3. Heatmaps for P_2O_5 compared to CaO

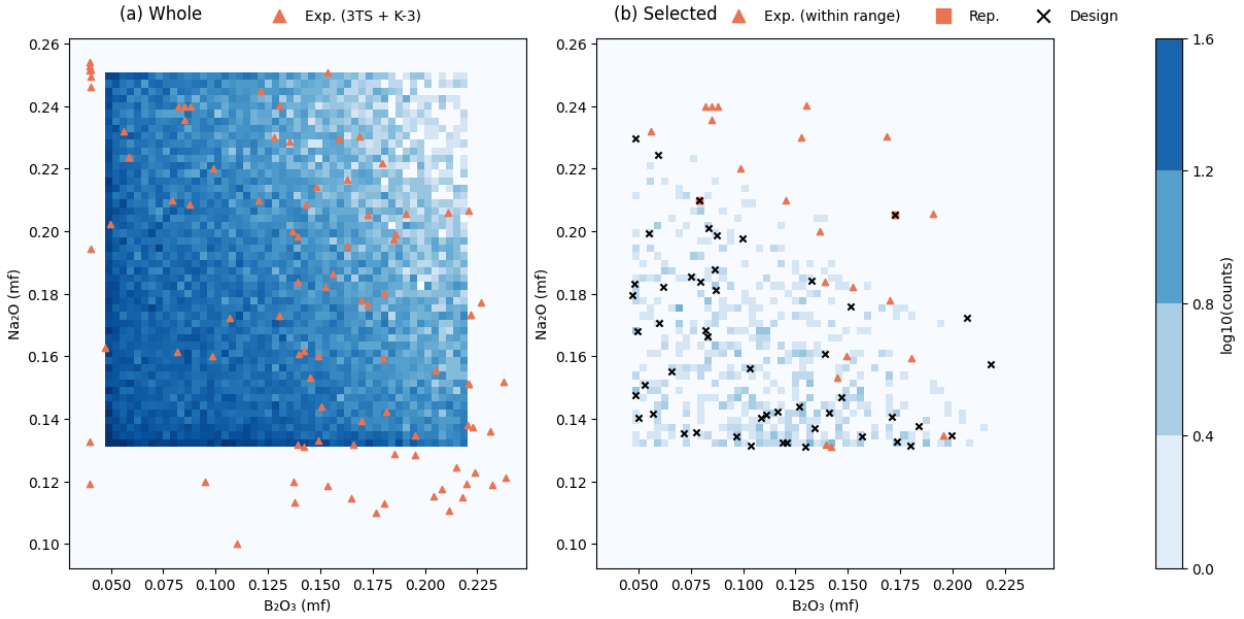

Figure A.4. Heatmaps for Na_2O compared to B_2O_3

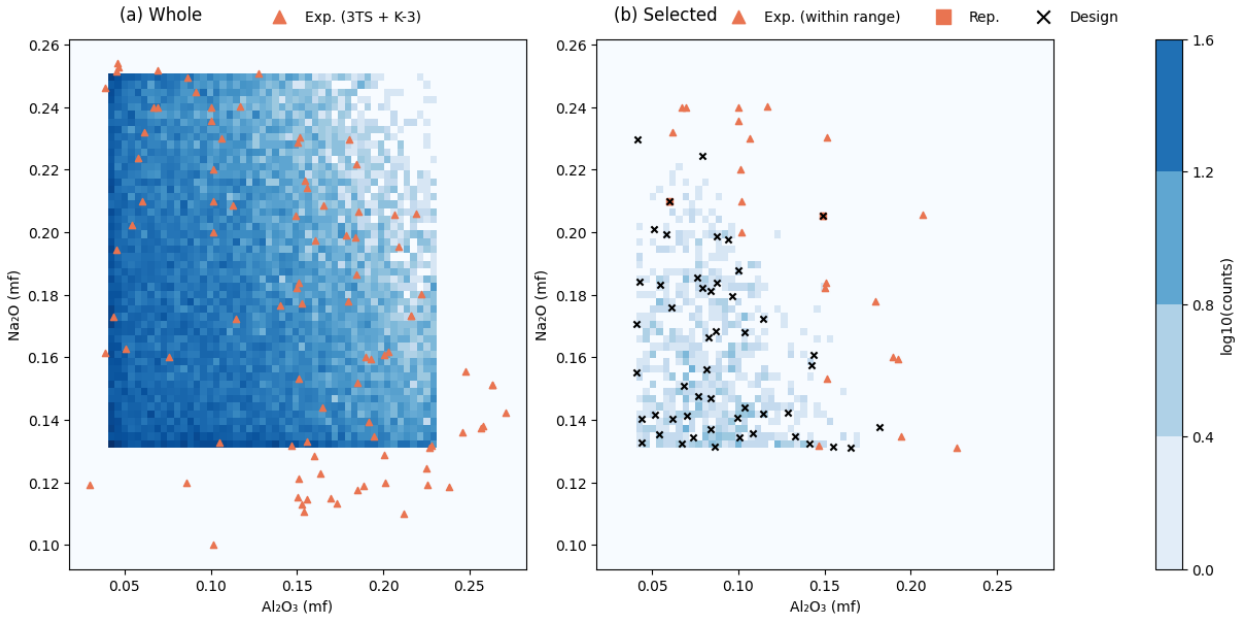

Figure A.5. Heatmaps for Na_2O compared to Al_2O_3

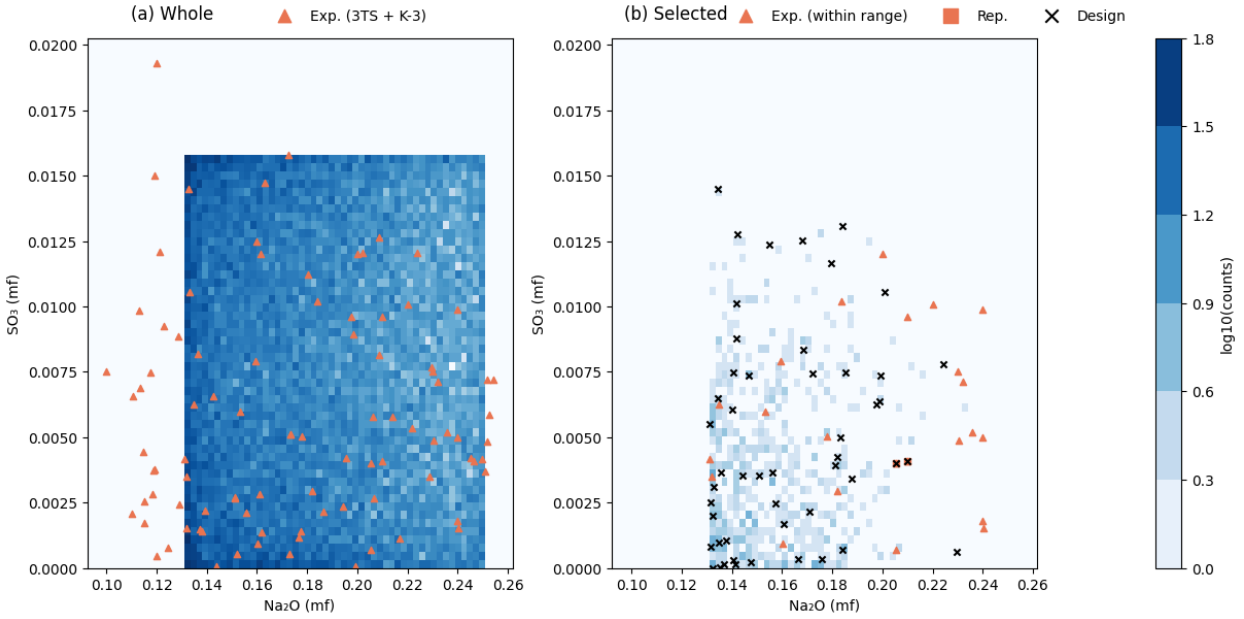

Figure A.6. Heatmaps for SO_3 compared to Na_2O

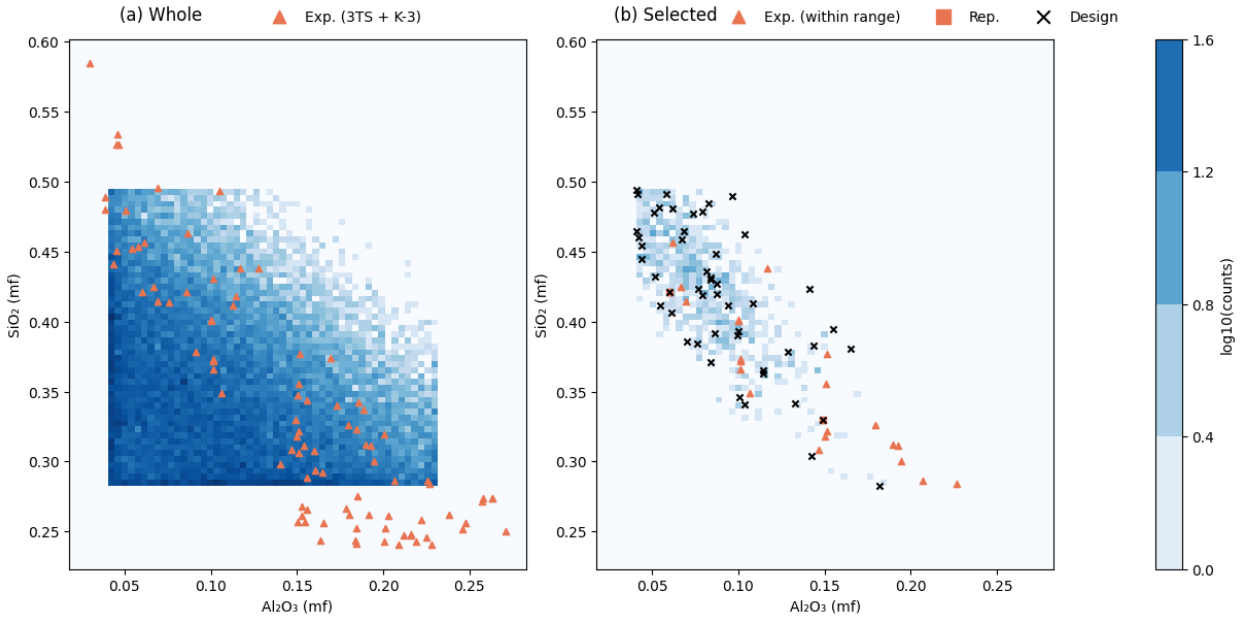

Figure A.7. Heatmaps for SiO_2 compared to Al_2O_3

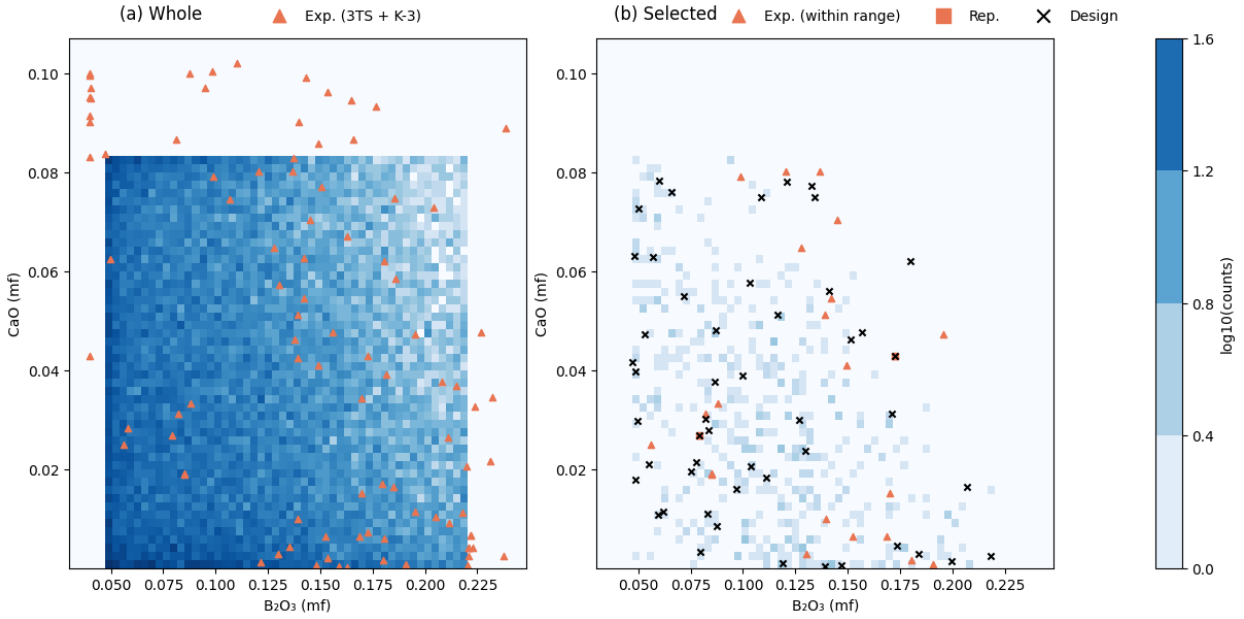

Figure A.8. Heatmaps for CaO compared to B_2O_3

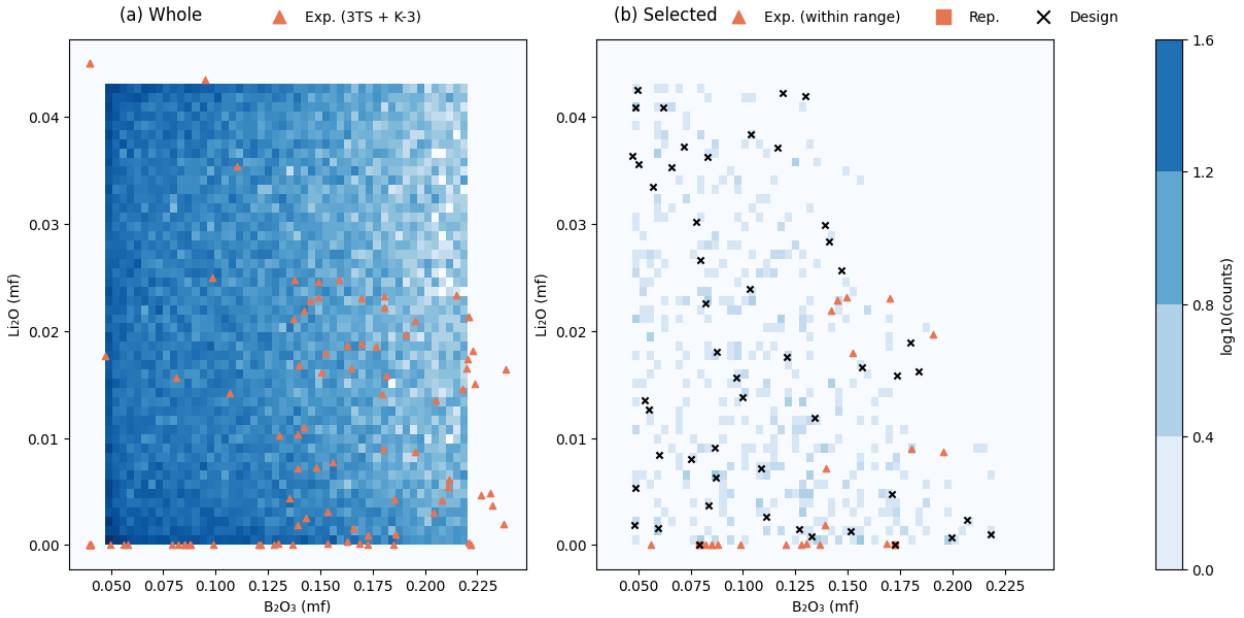

Figure A.9. Heatmaps for Li_2O compared to B_2O_3

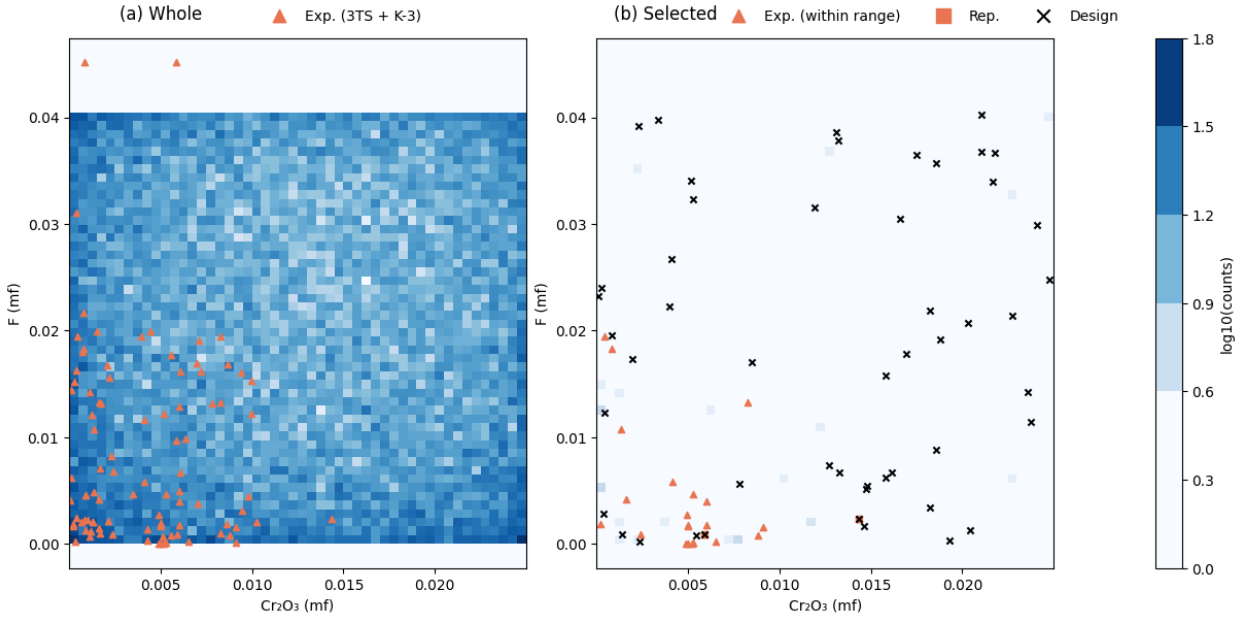

Figure A.10. Heatmaps for F compared to Cr_2O_3

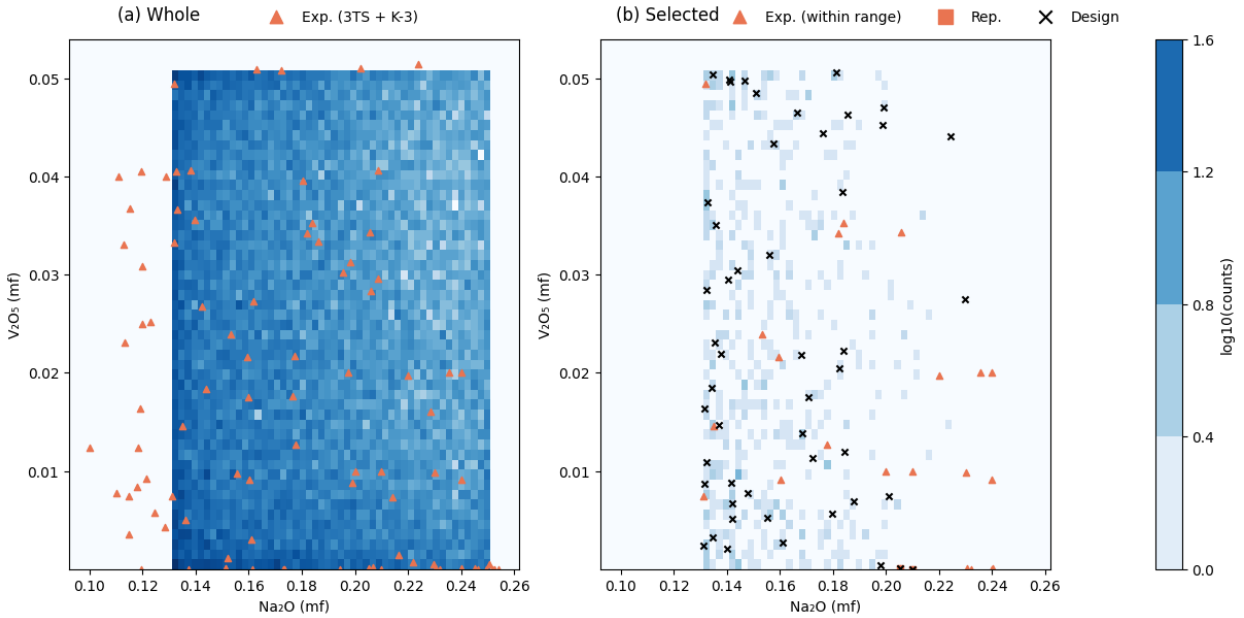

Figure A.11. Heatmaps for V_2O_5 compared to Na_2O

Appendix B – Optical Images of HS24 glasses

The optical images of the fabricated HS24 glasses are presented in this Appendix. Details of batching and melting are discussed in Section 3.1.1.

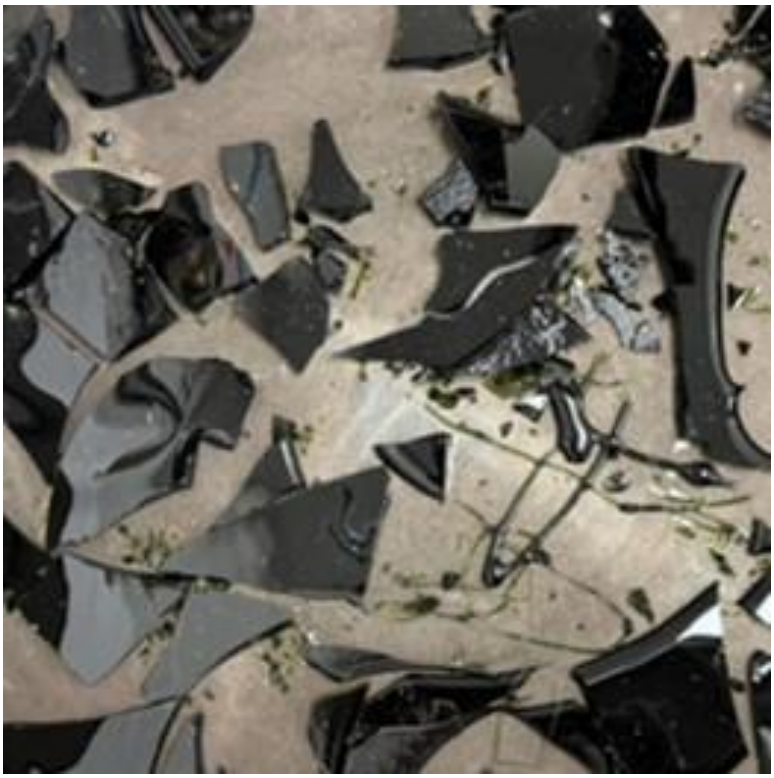

Figure B.1. Photographs of HS24-01 after the first melt using a tilt-pour furnace.

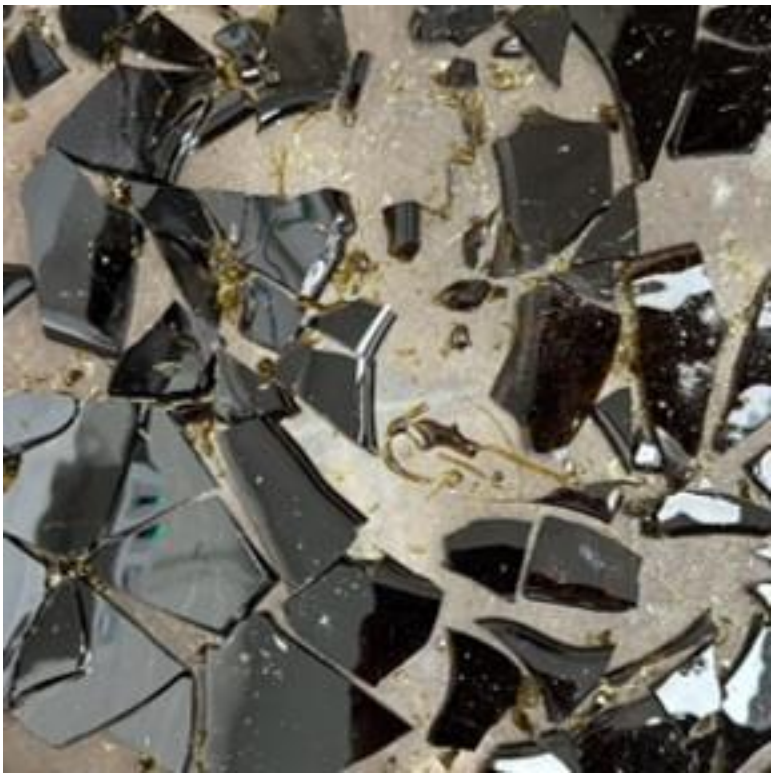

Figure B.2. Photographs of HS24-02 after the first melt using a tilt-pour furnace.

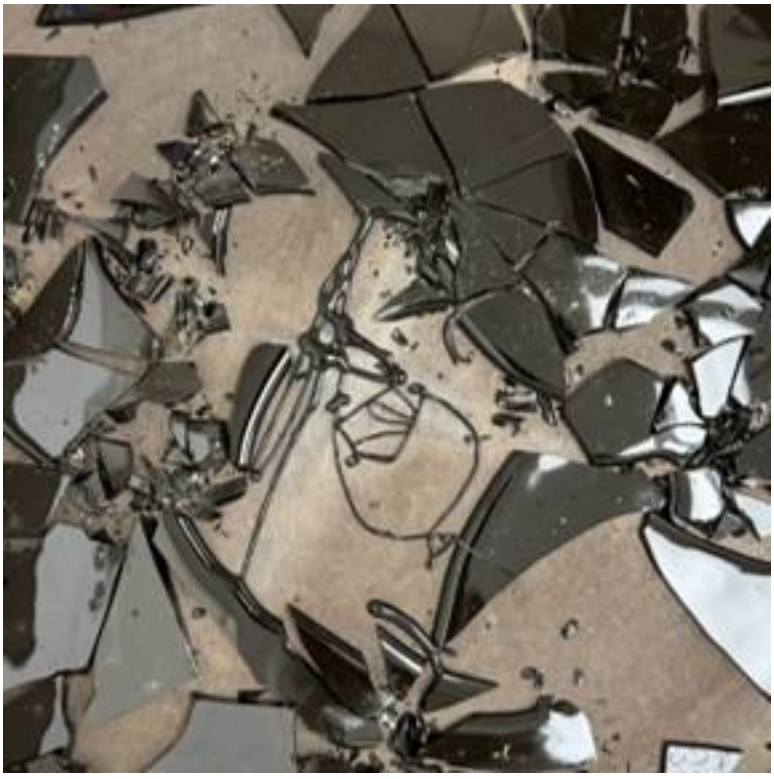

Figure B.3. Photographs of HS24-03 after the first melt using a tilt-pour furnace.

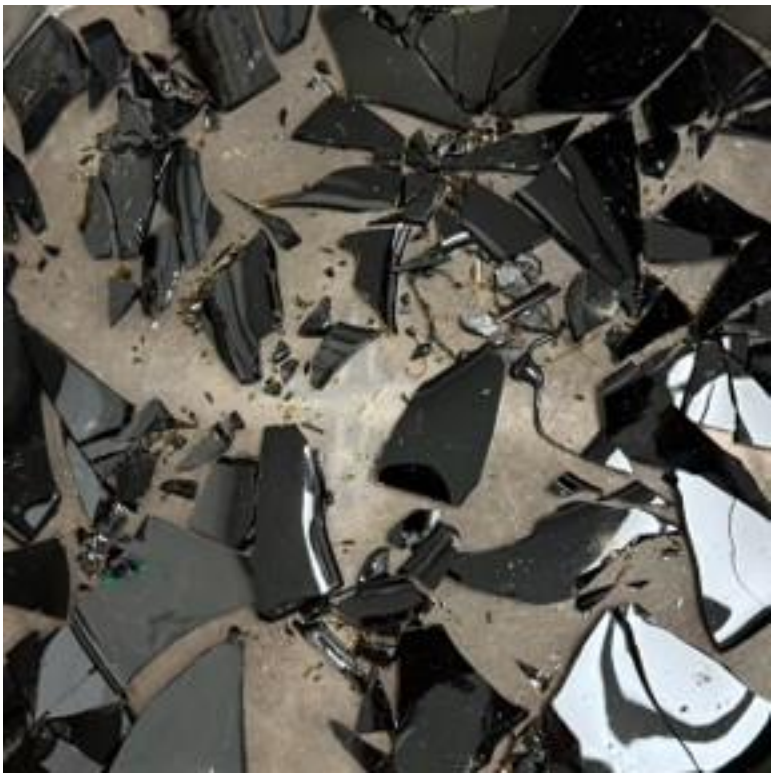

Figure B.4. Photographs of HS24-04 after the first melt using a tilt-pour furnace.

Figure B.5. Photographs of HS24-05 after the second melt using a tilt-pour furnace.

Figure B.6. Photographs of HS24-06 after the first melt using a tilt-pour furnace.

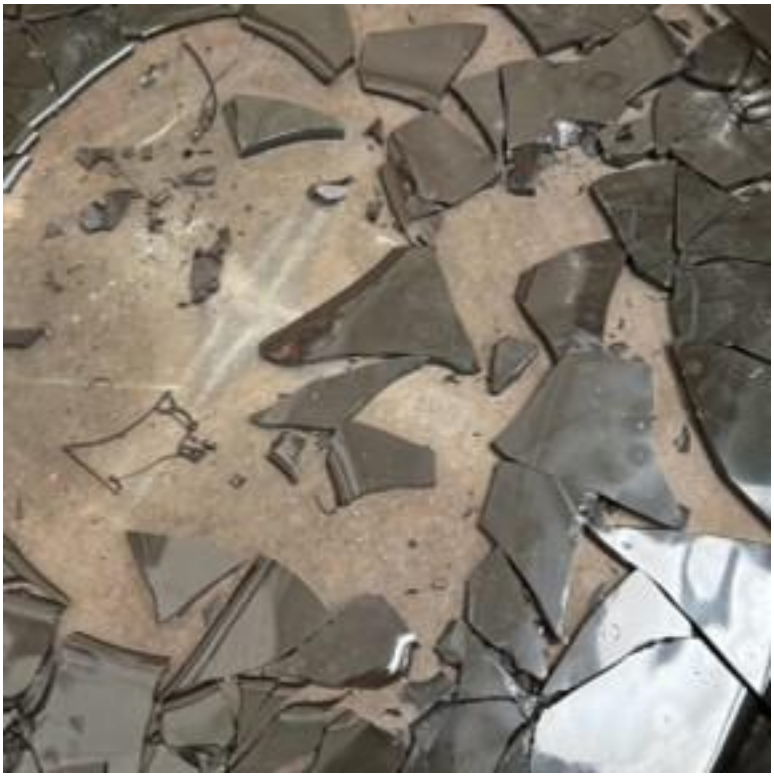

Figure B.7. Photographs of HS24-07 after the first melt using a tilt-pour furnace.

Figure B.8. Photographs of HS24-08 after the first melt using a tilt-pour furnace.

Figure B.9. Photographs of HS24-09 after the first melt using a tilt-pour furnace.

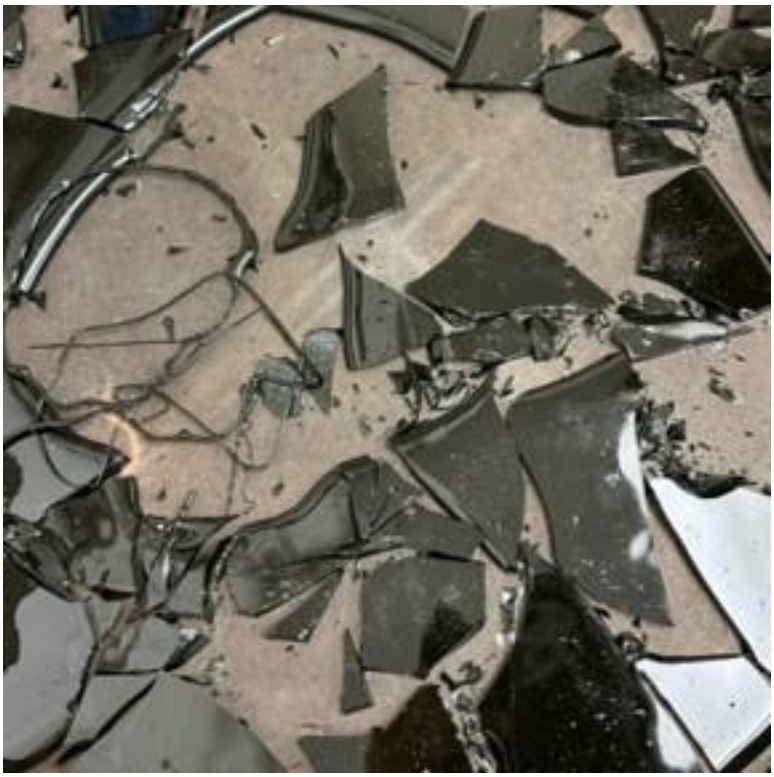

Figure B.10. Photographs of HS24-10 after the first melt using a tilt-pour furnace.

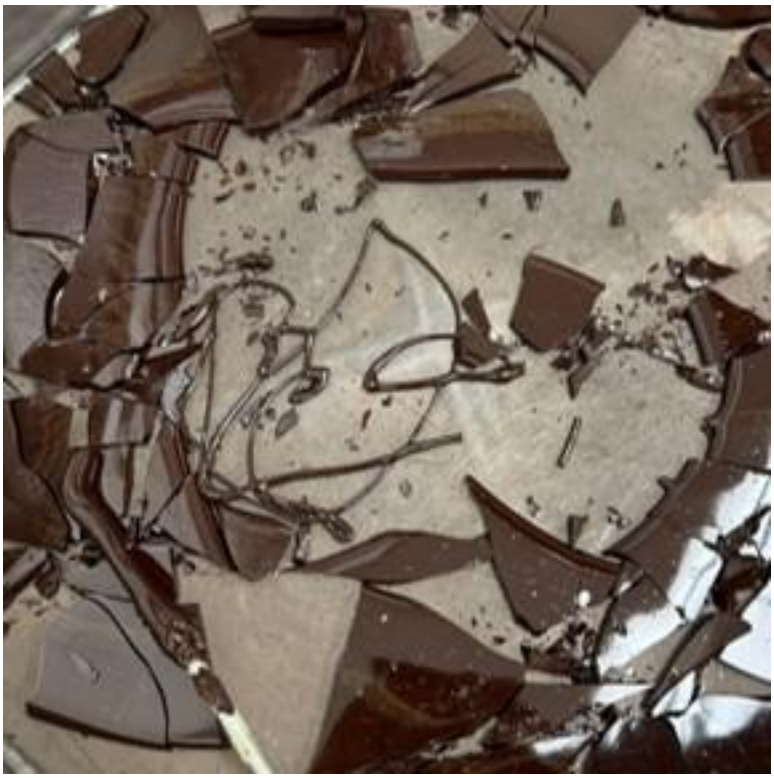

Figure B.11. Photographs of HS24-11 after the first melt using a tilt-pour furnace.

Figure B.12. Photographs of HS24-12 after the second melt using a Deltech furnace.

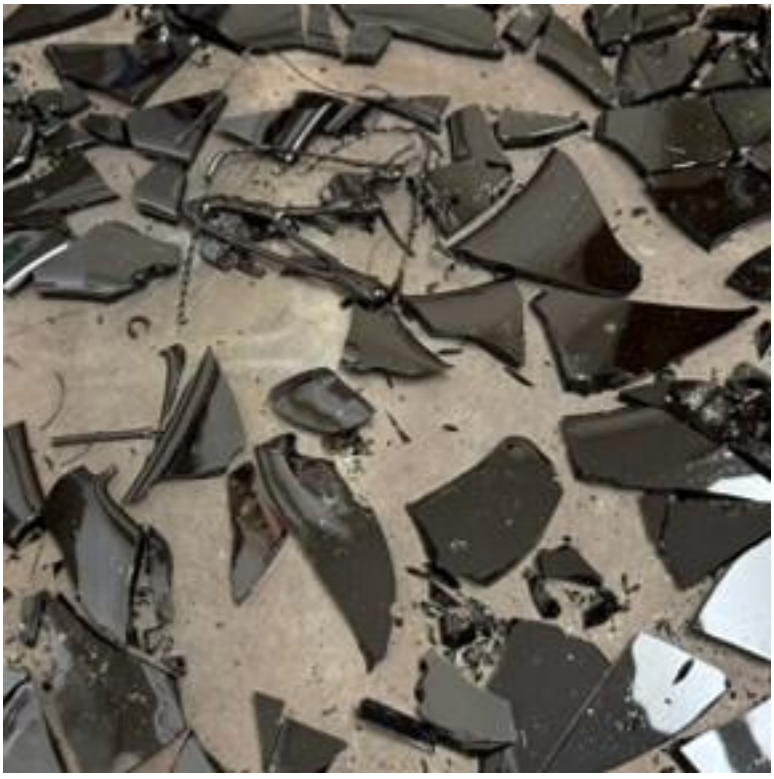

Figure B.13. Photographs of HS24-13 after the second melt using a tilt-pour furnace.

Figure B.14. Photographs of HS24-14 after the first melt using a tilt-pour furnace.

Figure B.15. Photographs of HS24-15 after the second melt using a Deltech furnace.

Figure B.16. Photographs of HS24-16 after the second melt using a tilt-pour furnace.

Figure B.17. Photographs of HS24-17 after the first melt using a tilt-pour furnace.

Figure B.18. Photographs of HS24-18 after the third melt using a tilt-pour furnace.

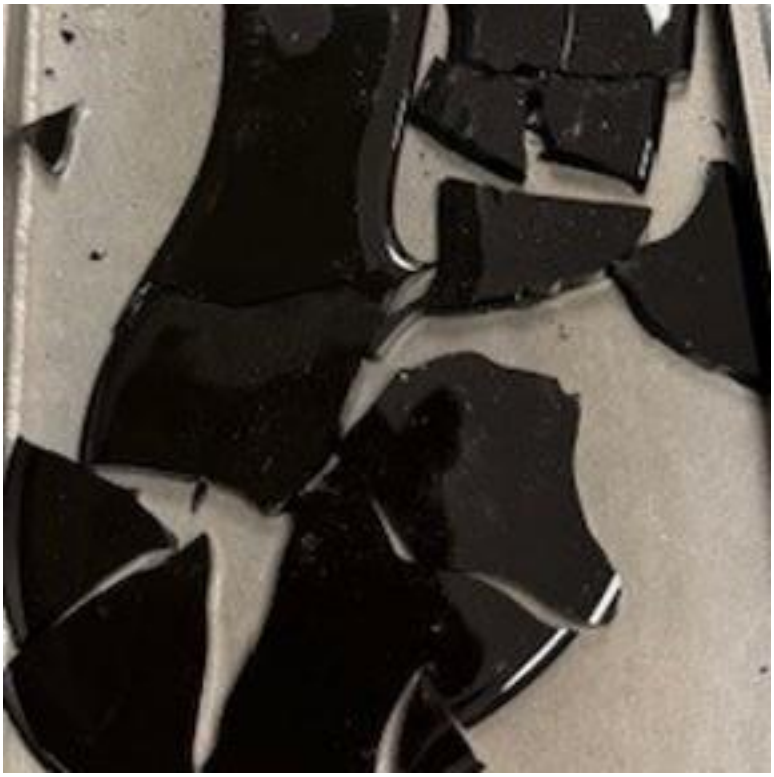

Figure B.19. Photographs of HS24-19 after the second melt using a Deltech furnace.

Figure B.20. Photographs of HS24-20 after the second melt using a Deltech furnace.

Figure B.21. Photographs of HS24-21 after the second melt using a tilt-pour furnace.

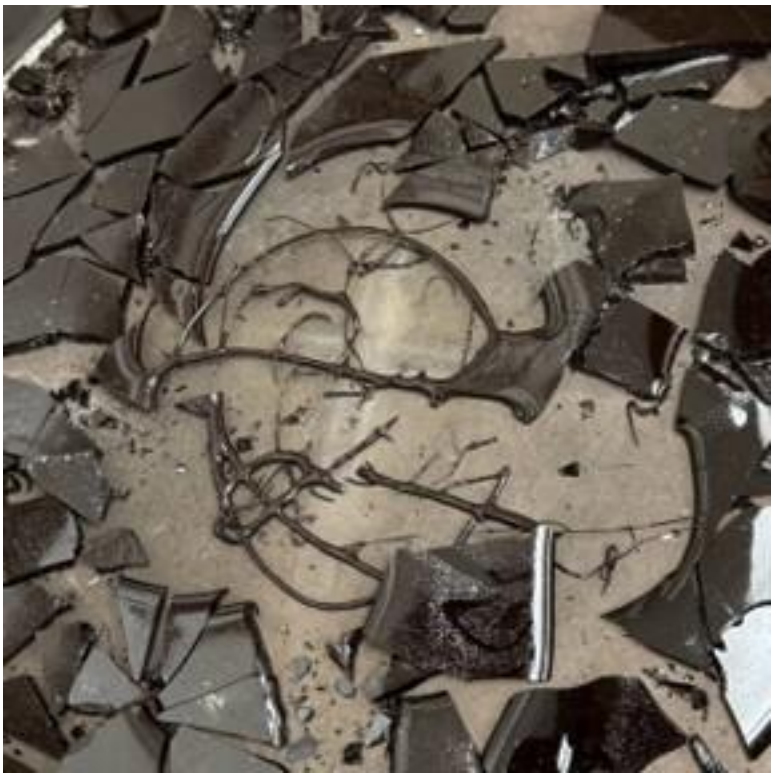

Figure B.22. Photographs of HS24-22 after the second melt using a tilt-pour furnace.

Figure B.23. Photographs of HS24-23 after the second melt using a Deltech furnace.

Figure B.24. Photographs of HS24-24 after the second melt using a Deltech furnace.

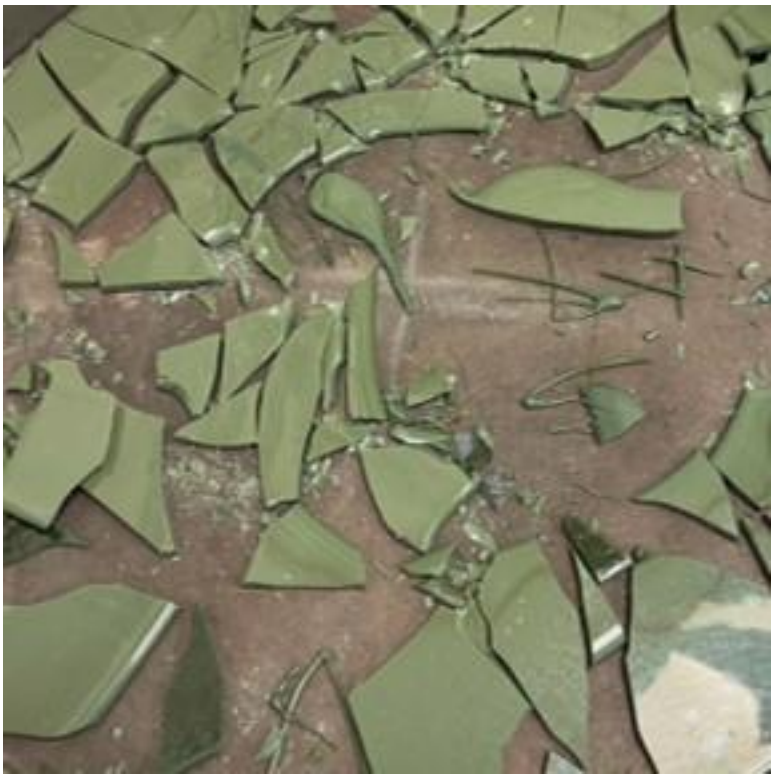

Figure B.25. Photographs of HS24-25 after the second melt using a tilt-pour furnace.

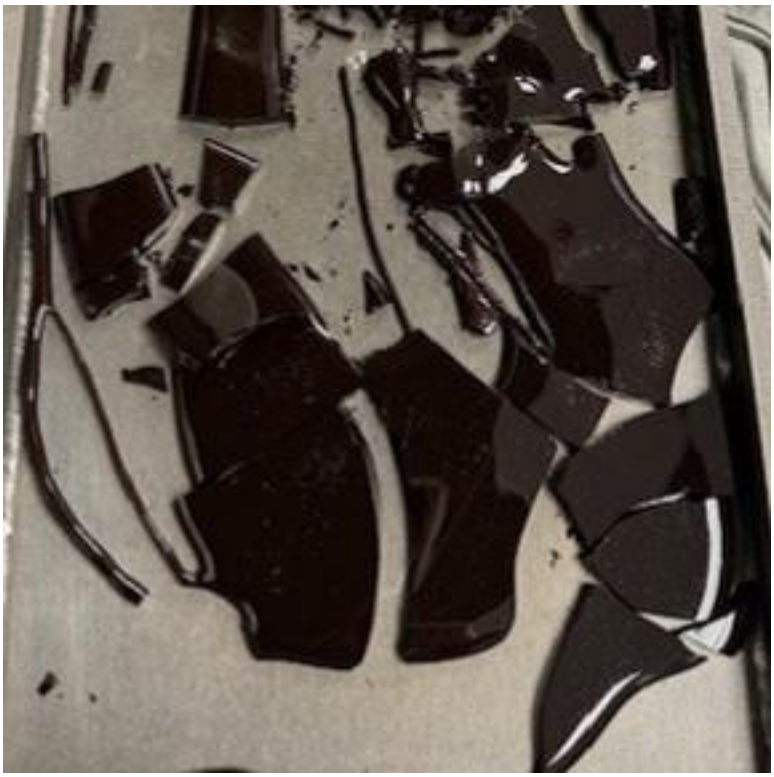

Figure B.26. Photographs of HS24-26 after the second melt using a Deltech furnace.

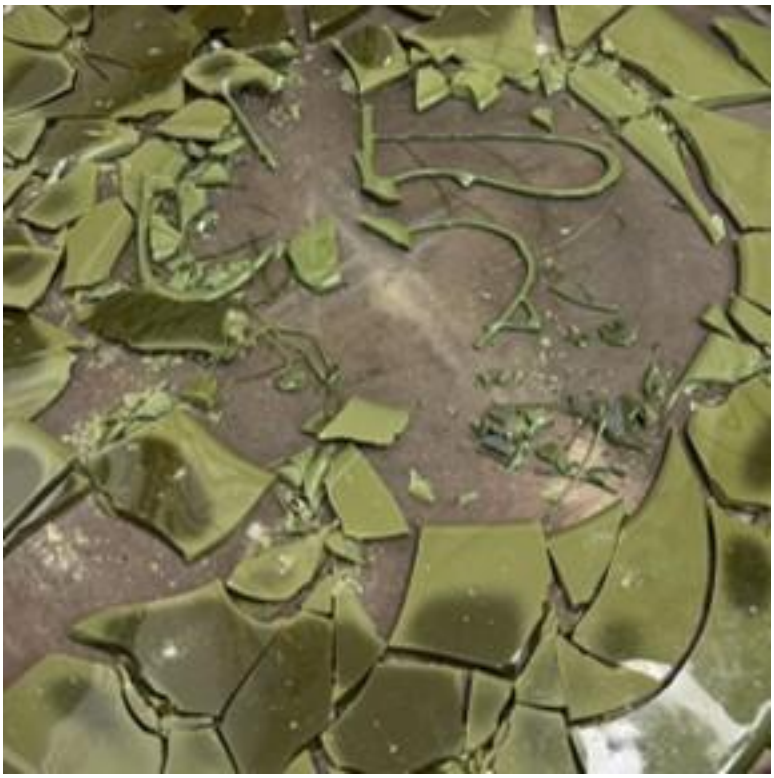

Figure B.27. Photographs of HS24-27 after the first melt using a tilt-pour furnace.

Figure B.28. Photographs of HS24-28 after the third melt using a Deltech furnace.

Figure B.29. Photographs of HS24-29 after the second melt using a tilt-pour furnace.

Figure B.30. Photographs of HS24-30 after the first melt using a tilt-pour furnace.

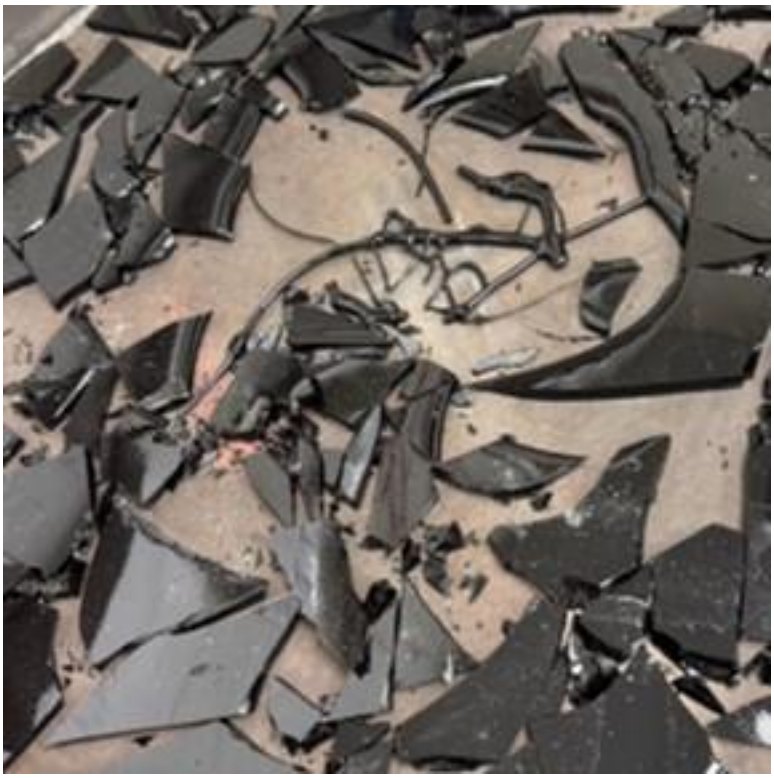

Figure B.31. Photographs of HS24-31 after the first melt using a tilt-pour furnace.

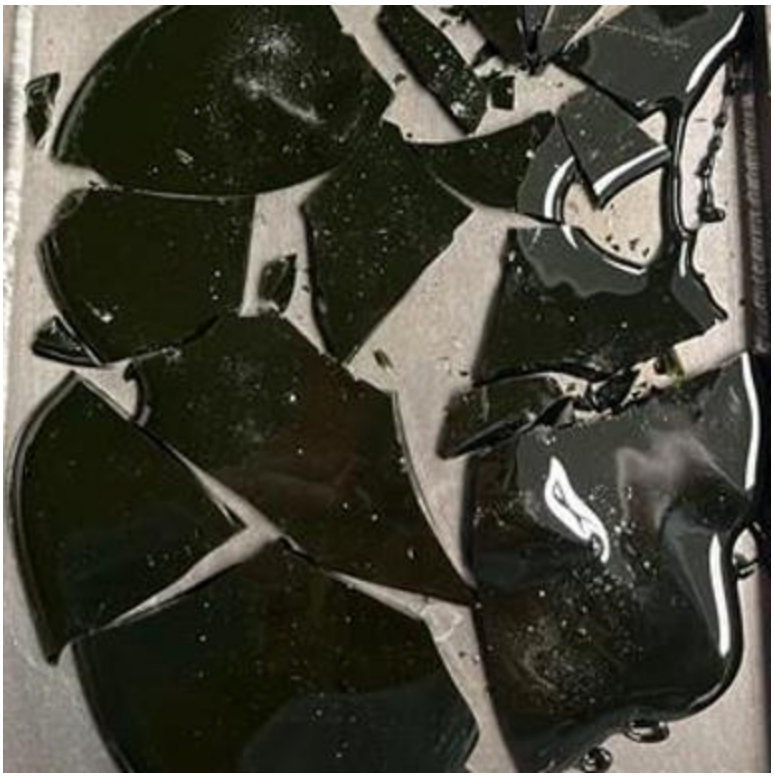

Figure B.32. Photographs of HS24-32 after the first melt using a Deltech furnace.

Figure B.33. Photographs of HS24-33 after the first melt using a tilt-pour furnace.

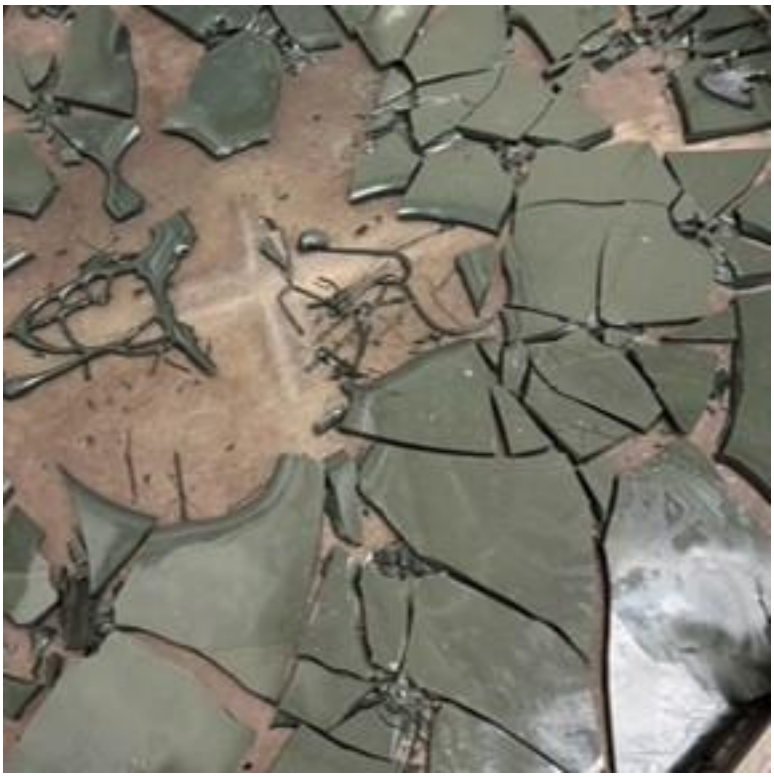

Figure B.34. Photographs of HS24-34 after the second melt using a tilt-pour furnace.

Figure B.35. Photographs of HS24-35 after the second melt using a Deltech furnace.

Figure B.36. Photographs of HS24-36 after the first melt using a tilt-pour furnace.

Figure B.37. Photographs of HS24-37 after the first melt using a tilt-pour furnace.

Figure B.38. Photographs of HS24-38 after the second melt using a tilt-pour furnace.

Figure B.39. Photographs of HS24-39 after the second melt using a tilt-pour furnace.

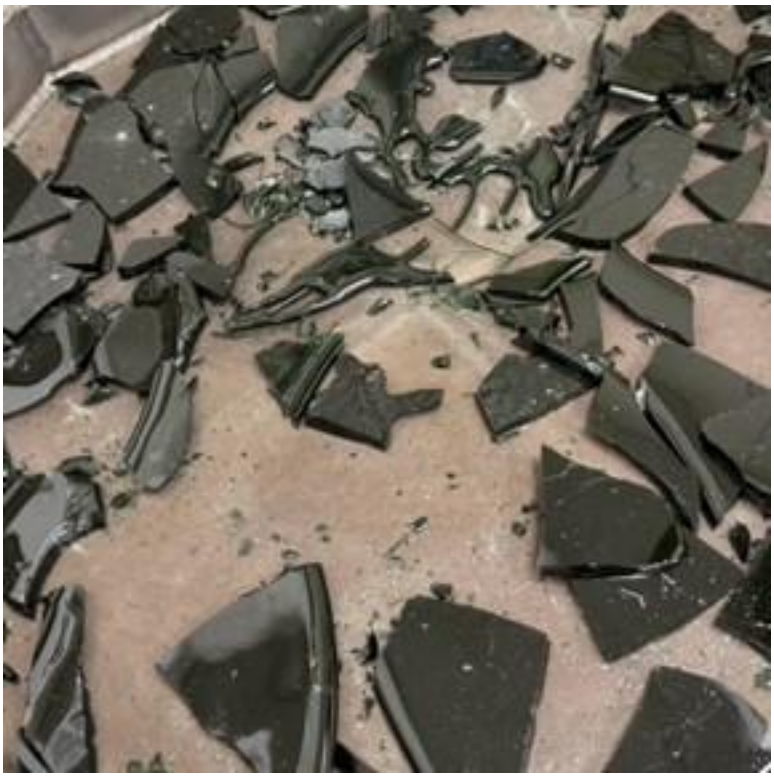

Figure B.40. Photographs of HS24-40 after the second melt using a tilt-pour furnace.

Figure B.41. Photographs of HS24-41 after the second melt using a tilt-pour furnace.

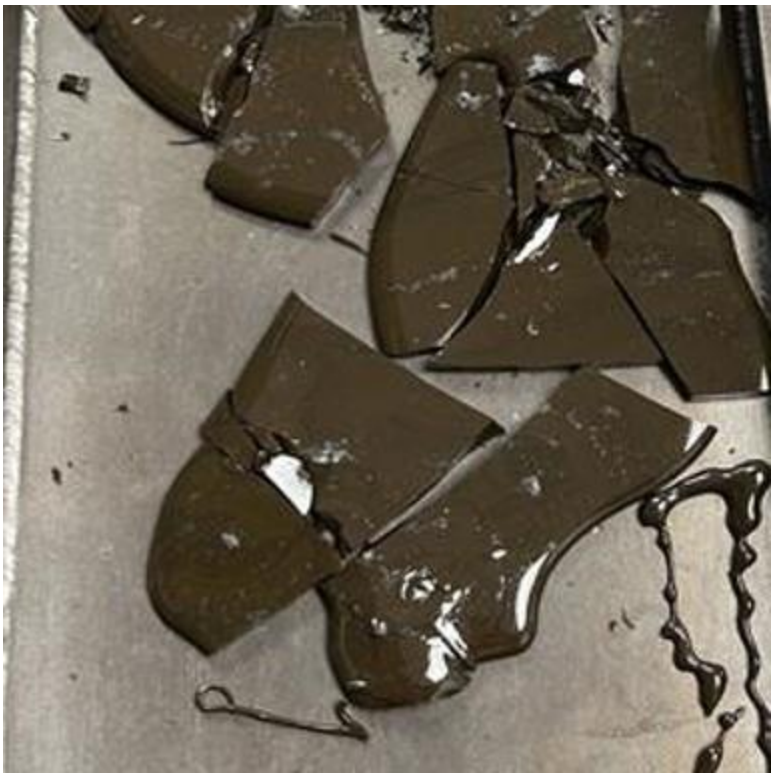

Figure B.42. Photographs of HS24-42 after the first melt using a Deltech furnace.

Figure B.43. Photographs of HS24-43 after the second melt using a Deltech furnace.

Figure B.44. Photographs of HS24-44 after the second melt using a Deltech furnace.

Figure B.45. Photographs of HS24-45 after the second melt using a Deltech furnace.

Figure B.46. Photographs of HS24-46 after the second melt using a Deltech furnace.

Figure B.47. Photographs of HS24-47 after the second melt using a Deltech furnace.

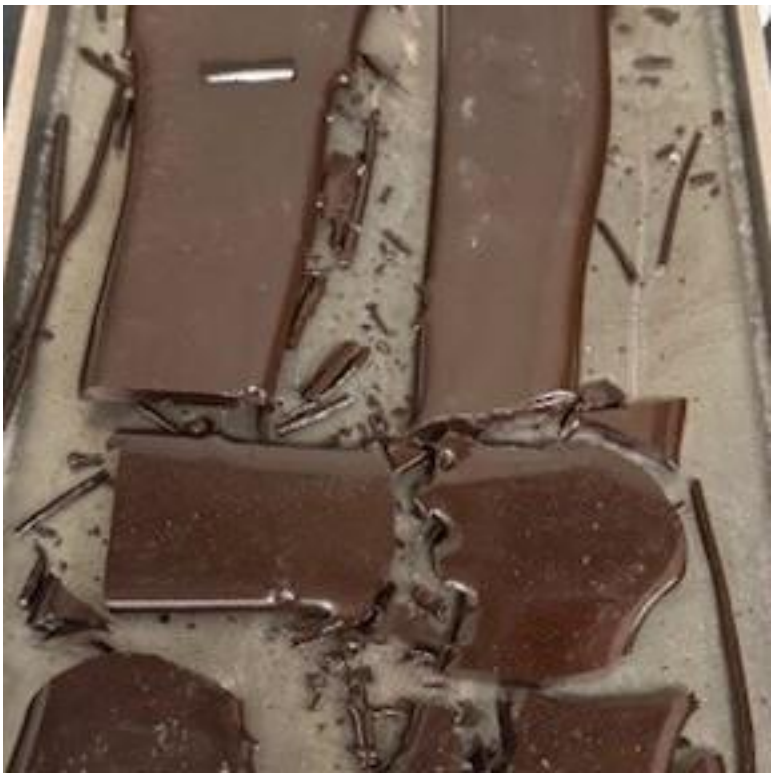

Figure B.48. Photographs of HS24-48 after the second melt using a Deltech furnace.

Figure B.49. Photographs of HS24-49 after the second melt using a Deltech furnace.

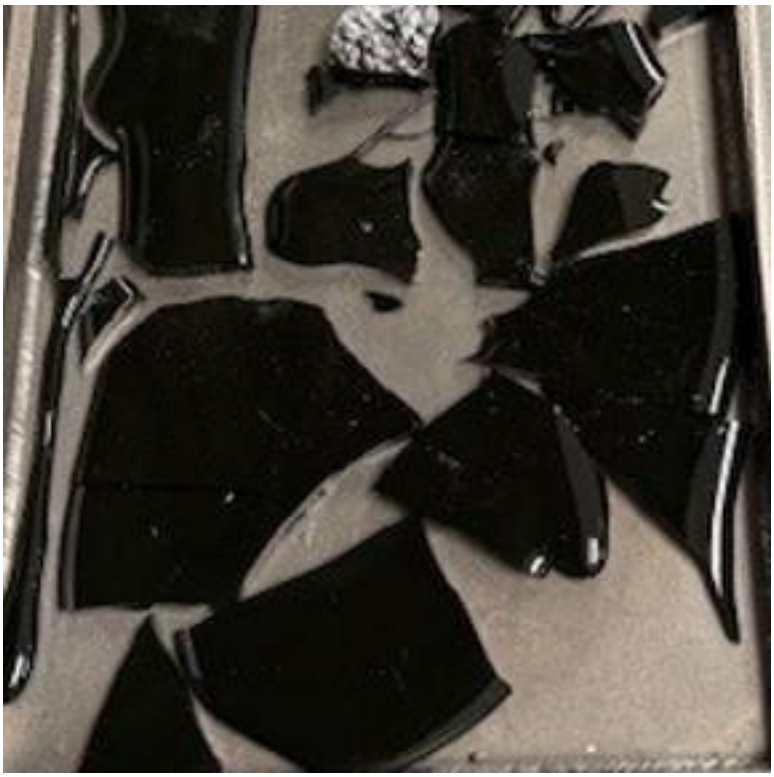

Figure B.50. Photographs of HS24-50 after the second melt using a Deltech furnace.

Appendix C – Glass Compositions

The tables in this appendix provide the target glass compositions and the analyzed glass compositions and the relative percent differences. EPMA analysis was performed for HS24-01 through HS24-44, and ICP-OES was performed for HS24-45 through HS24-50.

Table C.1. Target and analyzed compositions of HS24-01 and HS24-02 glasses.

	HS24-01			HS24-02		
Oxide	Target (wt%)	Measured (wt%)	RPD* (%)	Target (wt%)	Measured (wt%)	RPD* (%)
Al_2O_3	4.421	4.48	1.4	6.104	6.03	-1.2
B_2O_3	17.357	15.31	-11.8	15.154	14.88	-1.8
Bi_2O_3	0.014	0.01	-6.3	0.005	0.02	266.7
CaO	0.457	0.48	4.5	4.622	4.70	1.6
Cl	0.287	0.23	-19.0	0.101	0.08	-20.2
Cr_2O_3	0.399	0.39	-2.0	0.029	0.05	72.7
F	2.229	1.91	-14.3	2.397	2.13	-11.1
Fe_2O_3	0.548	0.57	3.1	0.552	0.57	2.6
K_2O	0.181	0.23	27.2	0.064	0.17	158.7
Li_2O	1.583	NM	NM	0.13	NM	NM
MgO	0.01	0.01	3.3	0.004	0.00	-100.0
MnO	0.289	0.33	13.5	0.102	0.11	7.4
Na_2O	13.266	13.33	0.5	17.6	17.64	0.2
NiO	0.307	0.32	4.6	0.108	0.11	2.8
P_2O_5	0.662	0.63	-4.7	0.045	0.06	42.5
PbO	0.126	0.10	-20.9	0.045	0.03	-37.7
SiO_2	45.436	46.93	3.3	40.629	41.20	1.4
SO_3	0.311	0.29	-6.4	0.035	0.04	10.4
SrO	0.014	0.05	224.4	0.005	0.02	385.2
TiO_2	0.013	0.05	316.7	0.005	0.04	641.5
V_2O_5	3.741	3.71	-0.9	4.447	4.38	-1.5
ZnO	3.868	4.01	3.5	0.878	0.91	4.2
ZrO_2	4.481	4.10	-8.4	6.939	6.41	-7.7
Total	100	97.47, 99.05**		100	99.58, 99.71**	

* RPD - Relative precent difference
**total with Li_2O target mass
NM- Not measured

Table C.2. Target and analyzed compositions of HS24-03 and HS24-04 glasses.

	HS24-03			HS24-04		
Oxide	Target (wt%)	Measured (wt%)	RPD* (%)	Target (wt%)	Measured (wt%)	RPD* (%)
Al_2O_3	7.015	7.08	0.9	8.768	8.52	-2.8
B_2O_3	11.092	9.97	-10.1	8.731	7.36	-15.7
Bi_2O_3	0.013	0.03	100.3	0.014	0.02	35.2
CaO	1.82	1.94	6.4	0.859	0.90	4.9
Cl	0.271	0.23	-16.8	0.287	0.24	-15.2
Cr_2O_3	1.313	1.07	-18.8	0.237	0.25	3.5
F	3.858	3.70	-4.2	0.02	0.00	-100.0
Fe_2O_3	6.485	6.45	-0.5	5.974	5.88	-1.6
K_2O	0.171	0.21	22.2	0.181	0.22	19.0
Li_2O	0.264	NM	NM	1.803	NM	NM
MgO	0.01	0.00	-89.0	0.01	0.01	-40.7
MnO	0.274	0.33	21.5	0.29	0.33	14.5
Na_2O	14.139	14.46	2.3	19.886	19.75	-0.7
NiO	0.291	0.29	1.0	0.308	0.32	4.3
P_2O_5	0.177	0.19	8.3	3.37	3.36	-0.4
PbO	0.12	0.12	4.1	0.127	0.09	-26.5
SiO_2	38.584	40.67	5.4	42.72	43.76	2.4
SO_3	0.016	0.02	14.0	0.637	0.61	-4.0
SrO	0.014	0.03	89.6	0.014	0.04	195.1
TiO_2	0.013	0.04	176.6	0.013	0.07	436.3
V_2O_5	4.964	4.97	0.1	4.529	4.46	-1.5
ZnO	2.904	2.95	1.7	0.098	0.12	24.0
ZrO_2	6.192	6.05	-2.3	1.124	1.07	-5.0
Total	100	100.79, 101.06**		100	97.38, 99.18**	

* RPD - Relative precent difference
**total with Li_2O target mass
NM- Not measured

Table C.3. Target and analyzed compositions of HS24-05 and HS24-06 glasses.

	HS24-05			HS24-06		
Oxide	Target (wt%)	Measured (wt%)	RPD* (%)	Target (wt%)	Measured (wt%)	RPD* (%)
Al_2O_3	5.837	5.84	0.0	8.296	8.11	-2.2
B_2O_3	5.517	4.93	-10.6	8.325	7.78	-6.5
Bi_2O_3	0.009	0.02	101.9	0.006	0.01	80.2
CaO	2.092	2.19	4.7	1.109	1.17	5.5
Cl	0.18	0.15	-18.0	0.135	0.12	-10.5
Cr_2O_3	0.339	0.36	7.1	2.373	1.47	-37.8
F	3.972	3.98	0.2	1.144	1.07	-6.2
Fe_2O_3	4.782	4.73	-1.0	0.295	0.29	-1.4
K_2O	0.114	0.17	53.5	0.085	0.13	48.8
Li_2O	1.263	NM	NM	3.627	NM	NM
MgO	0.006	0.00	-88.7	0.005	0.00	-51.4
MnO	0.182	0.22	20.3	0.136	0.14	-0.4
Na_2O	19.924	19.94	0.1	16.629	16.84	1.3
NiO	0.193	0.21	6.7	0.144	0.15	4.5
P_2O_5	0.304	0.32	4.1	3.815	3.73	-2.1
PbO	0.08	0.09	9.1	0.059	0.06	1.6
SiO_2	49.133	50.56	2.9	48.467	49.26	1.6
SO_3	0.736	0.70	-4.2	0.036	0.05	30.0
SrO	0.009	0.02	170.9	0.007	0.05	583.9
TiO_2	0.008	0.04	427.7	0.006	0.05	739.4
V_2O_5	4.706	4.66	-1.0	4.648	4.56	-1.8
ZnO	0.499	0.50	0.9	0.367	0.45	21.8
ZrO_2	0.115	0.13	13.8	0.286	0.27	-7.3
Total	100	99.78, 101.04**		100	95.77, 99.40**	

* RPD - Relative precent difference
**total with Li_2O target mass
NM- Not measured

Table C.4. Target and analyzed compositions of HS24-07 and HS24-08 glasses.

	HS24-07			HS24-08		
Oxide	Target (wt%)	Measured (wt%)	RPD* (%)	Target (wt%)	Measured (wt%)	RPD* (%)
Al_2O_3	10.006	10.02	0.2	16.543	16.14	-2.4
B_2O_3	8.63	7.85	-9.0	12.975	11.66	-10.1
Bi_2O_3	0.006	0.02	303.8	0.008	0.02	125.2
CaO	3.779	3.88	2.7	2.374	2.45	3.4
Cl	0.12	0.10	-15.3	0.172	0.16	-8.7
Cr_2O_3	2.105	1.43	-32.0	2.044	0.48	-76.5
F	4.027	4.20	4.3	0.134	0.00	-99.8
Fe_2O_3	2.32	2.31	-0.2	0.27	0.26	-5.0
K_2O	0.075	0.11	50.6	0.109	0.16	46.1
Li_2O	0.914	NM	NM	4.198	NM	NM
MgO	0.004	0.00	-100.0	0.006	0.00	-20.5
MnO	0.121	0.13	11.5	0.174	0.15	-13.0
Na_2O	18.794	19.69	4.8	13.122	12.95	-1.3
NiO	0.128	0.11	-12.8	0.184	0.17	-10.3
P_2O_5	3.768	3.69	-2.0	1.891	1.87	-1.2
PbO	0.053	0.05	-6.5	0.076	0.07	-14.2
SiO_2	39.331	41.33	5.1	38.044	38.57	1.4
SO_3	0.343	0.33	-4.0	0.551	0.49	-11.7
SrO	0.006	0.05	729.0	0.009	0.06	538.2
TiO_2	0.006	0.03	434.8	0.008	0.05	563.7
V_2O_5	0.693	0.70	1.3	0.24	0.23	-6.1
ZnO	3.656	3.59	-1.9	1.765	1.22	-30.8
ZrO_2	1.115	1.03	-7.3	5.103	4.66	-8.6
Total	100	100.69, 101.61**		100	91.80, 96.00**	

* RPD - Relative precent difference
**total with Li_2O target mass
NM- Not measured

Table C.5. Target and analyzed compositions of HS24-09 and HS24-10 glasses.

	HS24-09			HS24-10		
Oxide	Target (wt%)	Measured (wt%)	RPD* (%)	Target (wt%)	Measured (wt%)	RPD* (%)
Al_2O_3	9.412	9.34	-0.7	11.428	11.09	-2.9
B_2O_3	9.966	9.19	-7.8	14.125	13.06	-7.5
Bi_2O_3	0.006	0.02	207.6	0.014	0.01	-37.0
CaO	3.892	3.98	2.2	5.601	5.66	1.0
Cl	0.123	0.10	-14.7	0.289	0.24	-18.2
Cr_2O_3	1.581	0.50	-68.5	1.471	0.88	-40.4
F	0.624	0.32	-48.9	0.512	0.31	-39.1
Fe_2O_3	2.978	2.88	-3.4	0.74	0.72	-3.1
K_2O	0.077	0.10	31.4	0.182	0.21	17.7
Li_2O	1.378	NM	NM	2.839	NM	NM
MgO	0.004	0.00	-100.0	0.01	0.00	-100.0
MnO	0.124	0.12	0.3	0.292	0.29	-1.4
Na_2O	19.776	19.46	-1.6	14.194	13.84	-2.5
NiO	0.132	0.13	1.2	0.31	0.30	-3.8
P_2O_5	0.601	0.58	-2.8	1.773	1.73	-2.7
PbO	0.054	0.07	32.4	0.128	0.16	26.6
SiO_2	41.151	40.90	-0.6	36.524	36.41	-0.3
SO_3	0.627	0.52	-17.8	1.013	0.85	-16.3
SrO	0.006	0.03	449.3	0.015	0.05	206.5
TiO_2	0.006	0.06	977.7	0.013	0.07	474.0
V_2O_5	0.04	0.02	-55.2	0.664	0.66	-1.2
ZnO	0.378	0.39	3.9	0.448	0.50	11.7
ZrO_2	7.064	6.49	-8.2	7.415	6.71	-9.6
Total	100	95.21, 96.58**		100	93.73, 96.57**	

* RPD - Relative precent difference
**total with Li_2O target mass
NM- Not measured

Table C.6. Target and analyzed compositions of HS24-11 and HS24-12 glasses.

	HS24-11			HS24-12		
Oxide	Target (wt%)	Measured (wt%)	RPD* (%)	Target (wt%)	Measured (wt%)	RPD* (%)
Al_2O_3	13.309	13.47	1.2	7.915	8.24	4.2
B_2O_3	19.94	16.42	-17.7	5.945	5.80	-2.4
Bi_2O_3	0.012	0.02	63.4	0.005	0.03	485.0
CaO	0.145	0.19	27.9	1.089	1.15	5.7
Cl	0.246	0.22	-11.8	0.11	0.09	-14.7
Cr_2O_3	2.36	0.46	-80.4	2.169	0.85	-60.7
F	1.429	1.18	-17.4	3.393	3.72	9.7
Fe_2O_3	4.538	4.27	-5.8	1.962	1.98	0.7
K_2O	0.155	0.19	23.3	0.069	0.09	37.6
Li_2O	0.073	NM	NM	0.155	NM	NM
MgO	0.009	0.02	95.8	0.004	0.01	177.4
MnO	0.248	0.24	-3.2	0.11	0.11	1.4
Na_2O	13.479	13.78	2.2	22.443	23.09	2.9
NiO	0.264	0.20	-25.5	0.117	0.11	-5.4
P_2O_5	3.493	3.38	-3.1	3.488	3.35	-4.1
PbO	0.109	0.09	-17.5	0.048	0.09	83.5
SiO_2	34.171	34.41	0.7	41.893	42.08	0.4
SO_3	0.098	0.08	-14.4	0.78	0.73	-6.9
SrO	0.012	0.05	357.9	0.006	0.03	430.7
TiO_2	0.011	0.05	365.5	0.005	0.06	1197.1
V_2O_5	0.324	0.30	-8.9	4.415	4.47	1.3
ZnO	3.414	2.67	-21.9	3.311	2.78	-15.9
ZrO_2	2.161	2.08	-3.7	0.568	0.55	-3.7
Total	100	93.77, 93.84**		100	99.42, 99.58**	

* RPD - Relative precent difference
**total with Li_2O target mass
NM- Not measured

Table C.7. Target and analyzed compositions of HS24-13 and HS24-14 glasses.

	HS24-13			HS24-14		
Oxide	Target (wt%)	Measured (wt%)	RPD* (%)	Target (wt%)	Measured (wt%)	RPD* (%)
Al_2O_3	4.16	4.36	4.8	4.417	4.46	0.9
B_2O_3	4.837	4.40	-9.1	10.846	9.71	-10.5
Bi_2O_3	0.01	0.01	-12.9	0.007	0.03	307.1
CaO	1.793	1.85	3.4	7.51	7.53	0.3
Cl	0.215	0.17	-20.7	0.145	0.12	-16.4
Cr_2O_3	1.582	1.37	-13.1	1.857	0.59	-68.2
F	1.583	1.45	-8.5	0.882	0.63	-28.2
Fe_2O_3	3.183	3.14	-1.3	0.631	0.65	3.2
K_2O	0.135	0.18	31.8	0.092	0.11	23.9
Li_2O	0.538	NM	NM	0.718	NM	NM
MgO	0.008	0.00	-94.4	0.005	0.00	-100.0
MnO	0.217	0.22	0.9	0.147	0.13	-11.4
Na_2O	22.965	23.00	0.2	14.042	14.02	-0.2
NiO	0.23	0.23	-1.9	0.156	0.15	-3.1
P_2O_5	1.036	0.98	-5.5	0.338	0.31	-8.9
PbO	0.095	0.12	30.4	0.064	0.08	23.6
SiO_2	49.081	47.57	-3.1	44.507	44.61	0.2
SO_3	0.062	0.07	8.5	0.749	0.64	-14.6
SrO	0.011	0.05	349.0	0.007	0.04	490.7
TiO_2	0.01	0.03	152.7	0.007	0.08	1039.8
V_2O_5	2.75	2.73	-0.8	2.946	2.88	-2.2
ZnO	3.789	3.85	1.7	2.85	2.86	0.2
ZrO_2	1.71	1.59	-7.1	7.077	6.47	-8.6
Total	100	97.37, 97.91**		100	96.09, 96.81**	

* RPD - Relative precent difference
**total with Li_2O target mass
NM- Not measured

Table C.8. Target and analyzed compositions of HS24-15 and HS24-16 glasses.

	HS24-15			HS24-16		
Oxide	Target (wt%)	Measured (wt%)	RPD* (%)	Target (wt%)	Measured (wt%)	RPD* (%)
Al_2O_3	4.251	4.23	-0.4	8.411	8.40	-0.1
B_2O_3	13.25	11.02	-16.8	8.684	6.31	-27.3
Bi_2O_3	0.013	0.03	132.9	0.014	0.03	91.5
CaO	7.739	7.88	1.8	4.817	5.00	3.9
Cl	0.271	0.20	-25.2	0.293	0.24	-16.6
Cr_2O_3	0.85	0.83	-2.9	1.748	0.61	-65.1
F	1.7	1.56	-8.0	3.646	3.48	-4.7
Fe_2O_3	0.194	0.21	6.1	3.001	3.02	0.6
K_2O	0.171	0.19	10.1	0.185	0.22	17.3
Li_2O	0.076	NM	NM	0.63	NM	NM
MgO	0.01	0.00	-100.0	0.01	0.00	-96.4
MnO	0.273	0.27	-2.3	0.296	0.33	12.0
Na_2O	18.416	17.91	-2.7	18.141	18.64	2.7
NiO	0.29	0.30	3.0	0.314	0.33	6.6
P_2O_5	3.162	3.02	-4.4	2.067	2.11	2.0
PbO	0.119	0.10	-13.6	0.129	0.11	-12.2
SiO_2	46.03	46.80	1.7	37.096	38.67	4.2
SO_3	1.307	1.14	-12.5	0.394	0.36	-9.3
SrO	0.014	0.06	347.8	0.015	0.04	174.8
TiO_2	0.013	0.03	127.8	0.014	0.08	436.5
V_2O_5	1.192	1.13	-5.1	5.058	4.99	-1.4
ZnO	0.18	0.17	-6.7	0.946	1.00	6.1
ZrO_2	0.479	0.42	-11.4	4.091	3.94	-3.6
Total	100	97.51, 97.59**		100	97.92, 98.55**	

* RPD - Relative precent difference
**total with Li_2O target mass
NM- Not measured

Table C.9. Target and analyzed compositions of HS24-17 and HS24-18 glasses.

	HS24-17			HS24-18		
Oxide	Target (wt%)	Measured (wt%)	RPD* (%)	Target (wt%)	Measured (wt%)	RPD* (%)
Al_2O_3	5.132	5.19	1.1	7.402	7.18	-2.9
B_2O_3	8.37	5.68	-32.1	15.704	12.04	-23.4
Bi_2O_3	0.013	0.02	85.0	0.006	0.03	383.6
CaO	2.795	2.90	3.9	4.772	4.90	2.7
Cl	0.273	0.23	-14.2	0.129	0.08	-34.4
Cr_2O_3	1.856	0.95	-48.6	0.193	0.20	5.3
F	3.567	3.37	-5.5	1.736	1.44	-16.9
Fe_2O_3	1.13	1.19	5.4	0.677	0.66	-3.1
K_2O	0.172	0.21	23.2	0.082	0.11	34.3
Li_2O	0.366	NM	NM	1.665	NM	NM
MgO	0.01	0.00	-97.0	0.005	0.00	-73.8
MnO	0.276	0.32	16.8	0.13	0.13	0.9
Na_2O	20.102	20.72	3.1	13.427	13.40	-0.2
NiO	0.293	0.30	1.7	0.139	0.15	7.4
P_2O_5	1.291	1.30	0.6	0.306	0.29	-6.3
PbO	0.121	0.09	-25.0	0.057	0.06	3.8
SiO_2	47.801	49.46	3.5	47.694	48.65	2.0
SO_3	1.055	0.89	-15.2	1.451	1.08	-25.7
SrO	0.014	0.07	378.6	0.007	0.03	336.9
TiO_2	0.013	0.08	502.1	0.006	0.02	282.4
V_2O_5	0.739	0.67	-9.1	1.845	1.77	-3.9
ZnO	2.623	2.78	5.8	0.051	0.05	-10.1
ZrO_2	1.988	1.92	-3.5	2.516	2.32	-7.7
Total	100	98.36, 98.72**		100	94.61, 96.27**	

* RPD - Relative precent difference
**total with Li_2O target mass
NM- Not measured

Table C.10. Target and analyzed compositions of HS24-19 and HS24-20 glasses.

	HS24-19			HS24-20		
Oxide	Target (wt%)	Measured (wt%)	RPD* (%)	Target (wt%)	Measured (wt%)	RPD* (%)
Al_2O_3	4.081	4.20	2.9	6.199	6.12	-1.2
B_2O_3	5.999	5.26	-12.4	4.987	4.08	-18.2
Bi_2O_3	0.014	0.03	140.8	0.014	0.03	122.4
CaO	7.829	8.16	4.2	7.263	7.44	2.4
Cl	0.297	0.24	-17.7	0.288	0.22	-23.4
Cr_2O_3	2.106	1.38	-34.6	0.082	0.07	-18.7
F	3.681	3.49	-5.2	1.956	1.79	-8.6
Fe_2O_3	5.597	5.62	0.4	5.201	5.13	-1.4
K_2O	0.187	0.21	13.4	0.181	0.19	7.4
Li_2O	0.84	NM	NM	3.557	NM	NM
MgO	0.01	0.00	-100.0	0.01	0.00	-100.0
MnO	0.3	0.30	0.4	0.29	0.32	9.5
Na_2O	17.078	17.69	3.6	14.026	14.33	2.2
NiO	0.319	0.29	-10.2	0.308	0.31	0.2
P_2O_5	0.329	0.33	0.1	1.223	1.15	-6.3
PbO	0.131	0.11	-16.8	0.127	0.07	-41.2
SiO_2	46.49	48.61	4.6	48.096	49.66	3.2
SO_3	0.217	0.21	-1.3	0.608	0.62	1.5
SrO	0.015	0.03	112.3	0.015	0.08	440.5
TiO_2	0.014	0.06	330.9	0.013	0.06	397.5
V_2O_5	1.755	1.77	1.1	0.204	0.16	-20.0
ZnO	1.756	1.60	-9.0	3.659	3.72	1.7
ZrO_2	0.955	0.94	-2.0	1.693	1.55	-8.2
Total	100	100.53, 101.37**		100	97.11, 100.66**	

* RPD - Relative precent difference
**total with Li_2O target mass
NM- Not measured

Table C.11. Target and analyzed compositions of HS24-21 and HS24-22 glasses.

	HS24-21			HS24-22		
Oxide	Target (wt%)	Measured (wt%)	RPD* (%)	Target (wt%)	Measured (wt%)	RPD* (%)
Al_2O_3	10.073	9.90	-1.7	14.111	13.69	-3.0
B_2O_3	9.662	7.57	-21.7	11.883	9.19	-22.6
Bi_2O_3	0.01	0.03	181.6	0.006	0.01	8.7
CaO	1.591	1.63	2.6	0.107	0.13	16.9
Cl	0.197	0.16	-19.5	0.124	0.10	-19.0
Cr_2O_3	0.009	0.02	143.8	1.464	1.17	-19.9
F	2.325	1.90	-18.1	0.165	0.12	-30.0
Fe_2O_3	12.456	12.14	-2.5	2.284	2.20	-3.5
K_2O	0.124	0.16	27.4	0.078	0.10	34.5
Li_2O	1.56	NM	NM	4.227	NM	NM
MgO	0.007	0.01	-24.9	0.004	0.02	337.7
MnO	0.199	0.23	14.8	0.125	0.12	-3.1
Na_2O	13.447	13.78	2.5	13.25	13.65	3.1
NiO	0.211	0.21	-0.3	0.132	0.14	3.0
P_2O_5	3.674	3.64	-0.9	2.918	2.91	-0.3
PbO	0.087	0.08	-3.6	0.054	0.08	41.3
SiO_2	34.618	35.44	2.4	42.364	43.22	2.0
SO_3	0.648	0.57	-12.4	0.001	0.03	2766.4
SrO	0.01	0.06	474.6	0.006	0.04	619.8
TiO_2	0.009	0.11	1080.8	0.006	0.06	910.5
V_2O_5	5.037	4.91	-2.6	1.094	1.01	-8.1
ZnO	3.807	3.82	0.4	3.873	3.90	0.6
ZrO_2	0.239	0.22	-8.5	1.724	1.53	-11.2
Total	100	96.59, 98.15**		100	93.41, 97.64**	

* RPD - Relative precent difference
**total with Li_2O target mass
NM- Not measured

Table C.12. Target and analyzed compositions of HS24-23 and HS24-24 glasses.

	HS24-23			HS24-24		
Oxide	Target (wt%)	Measured (wt%)	RPD* (%)	Target (wt%)	Measured (wt%)	RPD* (%)
Al_2O_3	5.165	5.28	2.2	4.104	4.01	-2.3
B_2O_3	5.71	4.81	-15.7	6.584	5.70	-13.5
Bi_2O_3	0.013	0.02	70.5	0.005	0.02	205.3
CaO	6.287	6.53	3.9	7.603	7.49	-1.5
Cl	0.27	0.20	-26.7	0.112	0.08	-27.4
Cr_2O_3	2.477	1.73	-30.3	1.931	2.36	22.0
F	2.479	2.31	-6.7	0.035	0.01	-68.4
Fe_2O_3	2.081	2.04	-1.9	2.198	2.05	-6.7
K_2O	0.17	0.19	13.6	0.07	0.10	46.3
Li_2O	3.351	NM	NM	3.527	NM	NM
MgO	0.01	0.00	-100.0	0.004	0.00	-29.2
MnO	0.272	0.26	-3.5	0.113	0.11	-0.6
Na_2O	14.169	14.88	5.0	15.504	15.48	-0.2
NiO	0.289	0.28	-4.3	0.12	0.12	0.2
P_2O_5	3.483	3.47	-0.3	0.113	0.10	-11.5
PbO	0.119	0.08	-34.8	0.049	0.07	46.9
SiO_2	43.198	45.38	5.0	49.376	49.31	-0.1
SO_3	0.877	0.80	-8.6	1.238	1.07	-13.3
SrO	0.014	0.05	279.0	0.006	0.04	611.4
TiO_2	0.013	0.08	537.7	0.005	0.04	792.3
V_2O_5	0.882	0.85	-3.4	0.523	0.48	-7.4
ZnO	3.466	3.23	-6.7	1.539	1.49	-3.2
ZrO_2	5.205	4.87	-6.5	5.241	4.75	-9.4
Total	100	97.36, 100.71**		100	94.90, 98.42**	

* RPD - Relative precent difference
**total with Li_2O target mass
NM- Not measured

Table C.13. Target and analyzed compositions of HS24-25 and HS24-26 glasses.

	HS24-25			HS24-26		
Oxide	Target (wt%)	Measured (wt%)	RPD* (%)	Target (wt%)	Measured (wt%)	RPD* (%)
Al_2O_3	9.679	9.48	-2.0	5.462	5.56	1.7
B_2O_3	4.722	4.28	-9.3	4.818	3.98	-17.5
Bi_2O_3	0.009	0.01	41.2	0.009	0.01	1.4
CaO	4.175	4.28	2.4	6.311	6.53	3.4
Cl	0.189	0.16	-17.0	0.182	0.14	-20.4
Cr_2O_3	0.526	0.53	0.3	1.271	0.93	-26.9
F	3.232	3.09	-4.4	0.74	0.51	-31.5
Fe_2O_3	1.308	1.33	1.9	8.243	7.95	-3.6
K_2O	0.119	0.15	25.0	0.114	0.14	25.1
Li_2O	3.636	NM	NM	0.19	NM	NM
MgO	0.007	0.00	-96.6	0.006	0.00	-100.0
MnO	0.19	0.19	-1.3	0.183	0.18	-1.8
Na_2O	17.959	18.26	1.7	18.336	18.19	-0.8
NiO	0.202	0.23	13.2	0.195	0.18	-8.9
P_2O_5	3.087	2.92	-5.3	3.829	3.76	-1.7
PbO	0.083	0.12	39.2	0.08	0.13	68.6
SiO_2	48.965	50.88	3.9	41.158	41.12	-0.1
SO_3	1.168	1.08	-7.3	0.501	0.48	-4.1
SrO	0.01	0.05	355.5	0.009	0.05	407.3
TiO_2	0.009	0.06	544.3	0.008	0.05	570.2
V_2O_5	0.563	0.56	-0.3	3.839	3.85	0.2
ZnO	0.141	0.17	19.6	3.143	3.00	-4.5
ZrO_2	0.021	0.02	-9.5	1.373	1.26	-8.0
Total	100	97.84, 101.48**		100	98.00, 98.19**	

* RPD - Relative precent difference
**total with Li_2O target mass
NM- Not measured

Table C.14. Target and analyzed compositions of HS24-27 and HS24-28 glasses.

	HS24-27			HS24-28		
Oxide	Target (wt%)	Measured (wt%)	RPD* (%)	Target (wt%)	Measured (wt%)	RPD* (%)
Al_2O_3	8.711	8.78	0.8	10.372	10.49	1.2
B_2O_3	8.188	6.96	-15.0	4.956	4.05	-18.3
Bi_2O_3	0.005	0.02	316.7	0.012	0.02	34.4
CaO	3.028	3.10	2.4	2.969	3.07	3.4
Cl	0.112	0.10	-11.9	0.256	0.19	-25.5
Cr_2O_3	0.412	0.41	0.6	0.778	0.56	-27.7
F	2.675	2.45	-8.4	0.568	0.56	-1.4
Fe_2O_3	4.854	4.78	-1.5	0.335	0.35	4.9
K_2O	0.071	0.10	41.4	0.162	0.19	14.5
Li_2O	2.261	NM	NM	4.257	NM	NM
MgO	0.004	0.00	-78.4	0.009	0.00	-95.6
MnO	0.113	0.11	-6.2	0.259	0.26	2.3
Na_2O	16.829	16.71	-0.7	16.791	16.74	-0.3
NiO	0.12	0.12	2.1	0.275	0.26	-4.5
P_2O_5	3.048	2.84	-6.8	3.897	3.80	-2.5
PbO	0.05	0.07	49.9	0.113	0.14	19.9
SiO_2	44.842	44.97	0.3	46.238	45.45	-1.7
SO_3	0.833	0.81	-3.4	1.252	1.10	-12.4
SrO	0.006	0.04	565.7	0.013	0.03	142.6
TiO_2	0.005	0.04	664.9	0.012	0.05	298.4
V_2O_5	1.387	1.35	-2.8	2.18	2.14	-1.7
ZnO	0.005	0.01	194.2	2.212	2.16	-2.5
ZrO_2	2.441	2.30	-5.8	2.084	1.88	-9.7
Total	100	96.08, 98.34**		100	93.49, 97.75**	

* RPD - Relative precent difference
**total with Li_2O target mass
NM- Not measured

Table C.15. Target and analyzed compositions of HS24-29 and HS24-30 glasses.

	HS24-29			HS24-30		
Oxide	Target (wt%)	Measured (wt%)	RPD* (%)	Target (wt%)	Measured (wt%)	RPD* (%)
Al_2O_3	8.735	8.98	2.8	7.677	7.73	0.8
B_2O_3	7.935	6.47	-18.4	4.868	3.98	-18.3
Bi_2O_3	0.01	0.03	164.3	0.005	0.01	175.7
CaO	0.33	0.39	18.1	3.987	4.16	4.3
Cl	0.207	0.17	-16.2	0.102	0.09	-9.3
Cr_2O_3	0.229	0.22	-3.8	2.179	2.17	-0.3
F	3.916	3.78	-3.5	3.671	3.74	2.0
Fe_2O_3	3.67	3.60	-2.0	3.312	3.27	-1.1
K_2O	0.131	0.18	33.6	0.064	0.09	35.8
Li_2O	2.666	NM	NM	4.092	NM	NM
MgO	0.007	0.01	85.8	0.004	0.00	-93.9
MnO	0.209	0.21	-0.6	0.103	0.10	-7.4
Na_2O	18.401	18.56	0.9	14.774	14.97	1.3
NiO	0.222	0.23	5.6	0.11	0.10	-9.4
P_2O_5	1.594	1.55	-2.8	3.23	3.08	-4.7
PbO	0.091	0.11	20.1	0.045	0.11	150.0
SiO_2	42.002	42.26	0.6	42.33	43.70	3.2
SO_3	0.068	0.07	5.0	0.022	0.05	110.4
SrO	0.01	0.04	274.4	0.005	0.07	1213.3
TiO_2	0.01	0.07	605.7	0.005	0.07	1234.7
V_2O_5	2.229	2.21	-0.8	0.777	0.76	-2.4
ZnO	2.805	2.89	3.0	1.16	1.19	2.4
ZrO_2	4.523	4.29	-5.2	7.478	6.96	-6.9
Total	100	96.32, 98.98**		100	96.40, 100.49**	

* RPD - Relative precent difference
**total with Li_2O target mass
NM- Not measured

Table C.16. Target and analyzed compositions of HS24-31 and HS24-32 glasses.

	HS24-31			HS24-32		
Oxide	Target (wt%)	Measured (wt%)	RPD* (%)	Target (wt%)	Measured (wt%)	RPD* (%)
Al_2O_3	7.942	7.93	-0.1	5.404	5.65	4.5
B_2O_3	6.189	5.45	-12.0	7.162	5.62	-21.5
Bi_2O_3	0.006	0.01	115.5	0.014	0.02	36.4
CaO	1.131	1.19	5.3	5.491	5.71	4.0
Cl	0.118	0.11	-8.1	0.295	0.24	-20.3
Cr_2O_3	1.612	1.00	-38.2	1.321	0.59	-55.0
F	0.667	0.62	-6.9	3.782	3.74	-1.1
Fe_2O_3	2.729	2.68	-2.0	0.328	0.38	14.7
K_2O	0.074	0.13	71.6	0.186	0.21	15.2
Li_2O	4.084	NM	NM	3.721	NM	NM
MgO	0.004	0.01	135.3	0.01	0.00	-100.0
MnO	0.119	0.12	-0.8	0.298	0.30	-0.2
Na_2O	18.219	18.22	0.0	13.526	13.51	-0.1
NiO	0.126	0.12	-6.5	0.316	0.31	-0.6
P_2O_5	0.284	0.27	-3.7	0.766	0.75	-2.3
PbO	0.052	0.06	8.8	0.13	0.13	-2.7
SiO_2	47.87	49.93	4.3	48.161	48.14	0.0
SO_3	0.426	0.40	-6.1	0.003	0.04	1200.1
SrO	0.006	0.05	802.6	0.015	0.05	202.8
TiO_2	0.005	0.08	1437.2	0.014	0.05	276.5
V_2O_5	2.049	1.98	-3.5	2.305	2.30	0.0
ZnO	3.518	3.36	-4.6	1.881	1.91	1.3
ZrO_2	2.77	2.60	-6.0	4.871	4.55	-6.7
Total	100	96.31, 100.39**		100	94.19, 97.91**	

* RPD - Relative precent difference
**total with Li_2O target mass
NM- Not measured

Table C.17. Target and analyzed compositions of HS24-33 and HS24-34 glasses.

	HS24-33			HS24-34		
Oxide	Target (wt%)	Measured (wt%)	RPD* (%)	Target (wt%)	Measured (wt%)	RPD* (%)
Al_2O_3	6.833	6.97	2.0	12.895	12.84	-0.4
B_2O_3	5.317	4.69	-11.7	11.631	10.23	-12.0
Bi_2O_3	0.01	0.02	83.5	0.007	0.01	70.7
CaO	4.721	4.92	4.3	5.132	5.35	4.2
Cl	0.205	0.18	-13.0	0.139	0.11	-23.5
Cr_2O_3	2.272	1.45	-36.2	2.411	1.99	-17.5
F	2.144	2.10	-1.9	2.995	2.78	-7.3
Fe_2O_3	4.298	4.24	-1.3	0.062	0.06	4.6
K_2O	0.129	0.16	25.0	0.088	0.12	33.0
Li_2O	1.353	NM	NM	3.716	NM	NM
MgO	0.007	0.00	-100.0	0.005	0.01	86.9
MnO	0.207	0.21	1.3	0.14	0.16	14.8
Na_2O	15.104	15.31	1.4	14.217	14.22	0.0
NiO	0.22	0.19	-15.3	0.149	0.16	4.7
P_2O_5	1.505	1.53	1.5	2.556	2.50	-2.0
PbO	0.091	0.08	-9.2	0.061	0.08	26.6
SiO_2	46.439	47.71	2.7	37.814	39.51	4.5
SO_3	0.354	0.38	6.0	1.277	1.10	-13.6
SrO	0.01	0.04	302.7	0.007	0.04	443.8
TiO_2	0.01	0.05	434.2	0.006	0.03	473.3
V_2O_5	4.85	4.88	0.6	0.512	0.50	-2.8
ZnO	3.92	3.60	-8.1	1.264	1.31	3.8
ZrO_2	0.001	0.02	1650.1	2.916	2.71	-7.0
Total	100	98.74, 100.10**		100	95.81, 99.53**	

* RPD - Relative precent difference
**total with Li_2O target mass
NM- Not measured

Table C.18. Target and analyzed compositions of HS24-35 and HS24-36 glasses.

	HS24-35			HS24-36		
Oxide	Target (wt%)	Measured (wt%)	RPD* (%)	Target (wt%)	Measured (wt%)	RPD* (%)
Al_2O_3	8.378	8.31	-0.8	6.73	6.56	-2.6
B_2O_3	14.697	12.73	-13.4	12.093	9.27	-23.4
Bi_2O_3	0.005	0.01	173.7	0.009	0.02	134.4
CaO	0.064	0.08	20.4	7.811	8.05	3.1
Cl	0.11	0.09	-22.5	0.195	0.17	-13.8
Cr_2O_3	1.88	1.44	-23.5	1.824	1.51	-17.1
F	1.919	1.62	-15.3	0.343	0.25	-26.9
Fe_2O_3	3.4	3.39	-0.3	3.952	3.83	-3.0
K_2O	0.069	0.09	29.3	0.123	0.15	24.4
Li_2O	2.565	NM	NM	1.76	NM	NM
MgO	0.004	0.01	92.2	0.007	0.02	141.7
MnO	0.111	0.14	25.1	0.196	0.23	14.9
Na_2O	14.679	14.50	-1.2	13.236	13.05	-1.4
NiO	0.118	0.12	1.1	0.209	0.22	3.6
P_2O_5	0.211	0.21	-1.4	1.098	1.05	-4.4
PbO	0.048	0.09	80.5	0.086	0.10	17.4
SiO_2	42.992	43.97	2.3	45.892	46.46	1.2
SO_3	0.738	0.67	-9.0	0.199	0.21	7.4
SrO	0.006	0.04	554.6	0.01	0.02	139.6
TiO_2	0.005	0.02	236.3	0.009	0.02	167.5
V_2O_5	4.975	4.90	-1.5	2.848	2.75	-3.6
ZnO	0.567	0.58	2.1	0.928	0.95	2.1
ZrO_2	2.459	2.32	-5.6	0.442	0.42	-4.9
Total	100	95.31, 97.87**		100	95.30, 97.06**	

* RPD - Relative precent difference
**total with Li_2O target mass
NM- Not measured

Table C.19. Target and analyzed compositions of HS24-37 and HS24-38 glasses.

	HS24-37			HS24-38		
Oxide	Target (wt%)	Measured (wt%)	RPD* (%)	Target (wt%)	Measured (wt%)	RPD* (%)
Al_2O_3	8.404	8.04	-4.3	8.183	7.99	-2.3
B_2O_3	13.432	11.10	-17.3	10.33	9.38	-9.2
Bi_2O_3	0.008	0.03	250.7	0.013	0.03	95.2
CaO	7.494	7.76	3.6	5.766	5.95	3.2
Cl	0.175	0.15	-13.3	0.263	0.22	-17.8
Cr_2O_3	0.14	0.14	2.7	1.693	2.04	20.5
F	0.088	0.00	-100.0	1.78	1.68	-5.5
Fe_2O_3	8.035	7.74	-3.7	0.538	0.54	0.9
K_2O	0.111	0.14	24.9	0.166	0.20	18.0
Li_2O	1.192	NM	NM	2.393	NM	NM
MgO	0.006	0.02	221.1	0.009	0.01	37.4
MnO	0.177	0.18	3.6	0.265	0.31	17.6
Na_2O	13.695	13.42	-2.0	15.605	15.48	-0.8
NiO	0.188	0.18	-5.5	0.282	0.28	-1.4
P_2O_5	0.457	0.42	-8.6	3.371	3.26	-3.3
PbO	0.077	0.08	7.5	0.116	0.14	18.9
SiO_2	43.168	43.24	0.2	43.554	43.80	0.6
SO_3	0.014	0.04	161.8	0.368	0.32	-13.3
SrO	0.009	0.03	218.7	0.013	0.03	122.2
TiO_2	0.008	0.02	184.0	0.012	0.05	289.4
V_2O_5	1.467	1.37	-6.6	3.202	3.13	-2.3
ZnO	1.509	1.55	2.5	1.928	1.98	2.9
ZrO_2	0.146	0.09	-36.0	0.15	0.16	4.7
Total	100	95.75, 96.94**		100	96.97, 99.36**	

* RPD - Relative precent difference
**total with Li_2O target mass
NM- Not measured

Table C.20. Target and analyzed compositions of HS24-39 and HS24-40 glasses.

	HS24-39			HS24-40		
Oxide	Target (wt%)	Measured (wt%)	RPD* (%)	Target (wt%)	Measured (wt%)	RPD* (%)
Al_2O_3	9.968	9.86	-1.1	15.5	15.02	-3.1
B_2O_3	17.102	14.93	-12.7	17.985	15.35	-14.7
Bi_2O_3	0.008	0.01	60.0	0.007	0.01	97.3
CaO	3.125	3.18	1.7	6.214	6.44	3.7
Cl	0.161	0.14	-15.6	0.154	0.12	-20.4
Cr_2O_3	1.825	1.15	-37.0	1.326	0.90	-31.8
F	2.186	2.02	-7.8	0.667	0.61	-8.6
Fe_2O_3	0.094	0.09	-1.7	0.202	0.21	2.5
K_2O	0.102	0.13	26.1	0.097	0.13	35.2
Li_2O	0.476	NM	NM	1.888	NM	NM
MgO	0.006	0.02	213.6	0.005	0.02	234.0
MnO	0.163	0.19	18.9	0.155	0.18	14.0
Na_2O	14.072	14.17	0.7	13.158	12.97	-1.4
NiO	0.173	0.17	-3.4	0.165	0.18	6.5
P_2O_5	3.479	3.37	-3.3	0.447	0.41	-7.9
PbO	0.071	0.08	19.7	0.068	0.05	-28.3
SiO_2	39.019	39.08	0.1	39.47	39.73	0.7
SO_3	0.029	0.05	69.7	0.251	0.24	-4.5
SrO	0.008	0.03	240.3	0.008	0.02	137.4
TiO_2	0.008	0.05	486.3	0.007	0.04	541.3
V_2O_5	4.984	4.99	0.1	0.868	0.82	-5.2
ZnO	1.292	1.35	4.4	0.369	0.37	0.2
ZrO_2	1.649	1.47	-10.9	0.989	0.87	-11.6
Total	100	96.51, 96.98**		100	94.71, 196.59**	

* RPD - Relative precent difference
**total with Li_2O target mass
NM- Not measured

Table C.21. Target and analyzed compositions of HS24-41 and HS-42 glasses.

	HS24-41			HS24-42		
Oxide	Target (wt%)	Measured (wt%)	RPD* (%)	Target (wt%)	Measured (wt%)	RPD* (%)
Al_2O_3	11.466	11.04	-3.7	14.243	13.95	-2.0
B_2O_3	20.683	17.66	-14.6	21.833	19.04	-12.8
Bi_2O_3	0.011	0.01	7.7	0.007	0.01	15.9
CaO	1.636	1.70	4.0	0.243	0.26	6.2
Cl	0.225	0.17	-23.1	0.135	0.11	-21.9
Cr_2O_3	0.039	0.04	10.7	1.477	1.24	-15.7
F	0.287	0.18	-35.7	0.546	0.38	-30.3
Fe_2O_3	2.106	2.11	0.2	1.36	1.35	-1.0
K_2O	0.142	0.16	16.1	0.085	0.10	12.4
Li_2O	0.237	NM	NM	0.098	NM	NM
MgO	0.008	0.01	73.2	0.005	0.01	37.8
MnO	0.227	0.26	15.5	0.136	0.16	17.4
Na_2O	17.228	16.97	-1.5	15.751	15.57	-1.2
NiO	0.241	0.24	-1.4	0.145	0.13	-13.7
P_2O_5	3.107	3.01	-3.1	1.325	1.29	-3.0
PbO	0.099	0.08	-17.5	0.06	0.08	36.4
SiO_2	36.293	35.63	-1.8	30.414	30.22	-0.6
SO_3	0.742	0.55	-25.5	0.246	0.20	-18.6
SrO	0.011	0.02	93.6	0.007	0.02	140.2
TiO_2	0.01	0.05	448.3	0.006	0.05	727.4
V_2O_5	1.133	1.09	-3.9	4.333	4.25	-1.9
ZnO	2.501	2.63	5.0	1.084	1.08	-0.8
ZrO_2	1.568	1.46	-7.0	6.461	5.40	-16.3
Total	100	95.09, 95.33**		100	94.88, 94.88**	

* RPD - Relative precent difference
**total with Li_2O target mass
NM- Not measured

Table C.22. Target and analyzed compositions of HS24-43 and HS24-44 glasses.

	HS24-43			HS24-44		
Oxide	Target (wt%)	Measured (wt%)	RPD* (%)	Target (wt%)	Measured (wt%)	RPD* (%)
Al_2O_3	14.349	14.37	0.2	7.63	7.54	-1.2
B_2O_3	13.933	11.43	-18.0	7.522	7.67	1.9
Bi_2O_3	0.013	0.01	10.2	0.006	0.01	50.1
CaO	0.031	0.05	52.0	1.945	2.04	5.1
Cl	0.278	0.22	-20.2	0.127	0.10	-21.3
Cr_2O_3	1.189	0.50	-58.1	0.543	0.52	-5.1
F	3.152	2.84	-9.9	0.082	0.00	-100.0
Fe_2O_3	4.015	4.01	-0.1	11.265	11.12	-1.3
K_2O	0.176	0.20	11.1	0.08	0.09	18.2
Li_2O	2.993	NM	NM	0.799	NM	NM
MgO	0.01	0.00	-52.6	0.004	0.01	102.8
MnO	0.281	0.30	5.9	0.128	0.15	20.4
Na_2O	16.086	16.09	0.0	18.542	18.32	-1.2
NiO	0.298	0.31	3.3	0.136	0.13	-5.8
P_2O_5	0.793	0.77	-2.9	1.692	1.69	0.0
PbO	0.123	0.11	-14.1	0.056	0.08	49.4
SiO_2	38.278	38.83	1.5	38.472	38.09	-1.0
SO_3	0.168	0.14	-17.3	0.748	0.65	-13.5
SrO	0.014	0.07	384.7	0.006	0.03	434.2
TiO_2	0.013	0.06	381.3	0.006	0.06	930.0
V_2O_5	0.267	0.27	0.8	4.631	4.50	-2.7
ZnO	0.19	0.21	12.2	1.878	1.91	1.9
ZrO_2	3.35	3.26	-2.7	3.702	3.38	-8.8
Total	100	94.06, 97.05**		100	98.10, 98.90**	

* RPD - Relative precent difference
**total with Li_2O target mass
NM- Not measured

Table C.23. Target and analyzed compositions of HS24-45 and HS24-46 glasses.

	HS24-45			HS24-46		
Oxide	Target (wt%)	Measured (wt%)	RPD* (%)	Target (wt%)	Measured (wt%)	RPD* (%)
Al_2O_3	10.875	10.279	-5.5	18.212	17.327	-4.9
B_2O_3	7.745	8.179	5.6	18.373	19.901	8.3
Bi_2O_3	0.01	0.013	30.0	0.005	0.000	-100.0
CaO	2.138	2.113	-1.2	0.29	0.217	-25.2
Cl	0.2	NM	NM	0.111	NM	NM
Cr_2O_3	0.517	0.491	-5.0	2.028	1.900	-6.3
F	3.405	NM	NM	2.072	NM	NM
Fe_2O_3	8.036	7.477	-7.0	8.594	7.720	-10.2
K_2O	0.126	0.148	17.5	0.07	0.090	28.6
Li_2O	3.02	3.078	1.9	1.621	1.686	4.0
MgO	0.007	0.015	114.3	0.004	0.003	-25.0
MnO	0.201	0.212	5.5	0.111	0.118	6.3
Na_2O	13.569	14.019	3.3	13.773	14.558	5.7
NiO	0.214	0.207	-3.3	0.118	0.117	-0.8
P_2O_5	2.05	1.845	-10.0	1.974	1.881	-4.7
PbO	0.088	0.080	-9.1	0.049	0.044	-10.2
SiO_2	41.299	38.720	-6.2	28.252	25.670	-9.1
SO_3	0.366	0.367	0.3	0.106	0.121	14.2
SrO	0.01	0.010	0.0	0.006	0.004	-33.3
TiO_2	0.009	0.040	344.4	0.005	0.055	1000.0
V_2O_5	3.505	3.499	-0.2	2.199	2.249	2.3
ZnO	0.066	0.067	1.5	0.434	0.434	0.0
ZrO_2	2.544	2.350	-7.6	1.593	1.594	0.1
Total	100	93.21, 96.81**		100	95.69, 97.87**	

* RPD - Relative precent difference
**total with F and Cl target masses
NM- Not measured

Table C.24. Target and analyzed compositions of HS24-47 and HS24-48 glasses.

	HS24-47			HS24-48		
Oxide	Target (wt%)	Measured (wt%)	RPD* (%)	Target (wt%)	Measured (wt%)	RPD* (%)
Al_2O_3	8.624	8.276	-4.0	10.366	9.901	-4.5
B_2O_3	10.381	10.691	3.0	12.671	13.171	3.9
Bi_2O_3	0.005	0.000	-100.0	0.011	0.000	-100.0
CaO	2.056	2.085	1.4	3.003	3.106	3.4
Cl	0.101	NM	NM	0.234	NM	NM
Cr_2O_3	0.042	0.049	16.7	1.658	1.371	-17.3
F	1.231	NM	NM	3.044	NM	NM
Fe_2O_3	5.573	5.133	-7.9	6.047	5.847	-3.3
K_2O	0.064	0.082	28.1	0.148	0.173	16.9
Li_2O	3.84	3.875	0.9	0.147	0.157	6.8
MgO	0.004	0.013	225.0	0.008	0.021	162.5
MnO	0.102	0.108	5.9	0.236	0.248	5.1
Na_2O	13.15	13.615	3.5	14.411	15.232	5.7
NiO	0.108	0.105	-2.8	0.251	0.233	-7.2
P_2O_5	3.698	3.552	-3.9	1.952	1.762	-9.7
PbO	0.045	0.040	-11.1	0.103	0.096	-6.8
SiO_2	39.191	39.147	-0.1	34.102	29.521	-13.4
SO_3	0.082	0.076	-7.3	0.353	0.322	-8.8
SrO	0.005	0.005	0.0	0.012	0.013	8.3
TiO_2	0.005	0.025	400.0	0.011	0.044	300.0
V_2O_5	1.639	1.594	-2.7	3.047	3.071	0.8
ZnO	3.426	3.436	0.3	3.827	3.784	-1.1
ZrO_2	6.628	3.742	-43.5	4.358	3.904	-10.4
Total	100	95.65, 96.98**		100	91.98, 95.26**	

* RPD - Relative precent difference
**total with F and Cl target masses
NM- Not measured

Table C.25. Target and analyzed compositions of HS24-49 and HS24-50 glasses.

	HS24-49			HS24-50		
Oxide	Target (wt%)	Measured (wt%)	RPD* (%)	Target (wt%)	Measured (wt%)	RPD* (%)
Ag_2O	0	0.000	0.0	0.013	0.012	-7.7
Al_2O_3	6.03	5.839	-3.2	14.895	13.982	-6.1
B_2O_3	7.92	8.244	4.1	17.253	17.969	4.2
Bi_2O_3	0	0.000	0.0	0.02	0.020	0.0
CaO	2.69	2.728	1.4	4.295	4.324	0.7
Cl	0.23	NM	NM	0.256	NM	NM
Cr_2O_3	0.59	0.563	-4.6	1.436	1.352	-5.8
F	0.09	NM	NM	0.238	NM	NM
Fe_2O_3	0.28	0.266	-5.0	2.31	2.173	-5.9
K_2O	5.75	5.397	-6.1	1.333	1.337	0.3
Nd_2O_3	0	NM	NM	0.681	NM	NM
Li_2O	0	0.000	0.0	0.005	0.008	60.0
MgO	0.44	0.410	-6.8	0.07	0.080	14.3
MnO	0	0.001	0.0	0.122	0.126	3.3
Na_2O	21	21.029	0.1	20.533	20.759	1.1
NiO	0.01	0.010	0.0	0.142	0.134	-5.6
P_2O_5	0.14	0.136	-2.9	2.533	2.475	-2.3
PbO	0.01	0.009	-10.0	0.08	0.074	-7.5
SiO_2	42.09	39.789	-5.5	32.994	29.735	-9.9
SnO_2	3.19	2.247	-29.6	0	0.000	00.0
SO_3	0.41	0.405	-1.2	0.401	0.415	3.5
TiO_2	0	0.027	ND	0	0.038	ND
V_2O_5	0	0.001	ND	0.003	0.005	66.7
ZnO	2.69	2.676	-0.5	0.007	0.008	14.3
ZrO_2	6.44	5.944	-7.7	0.38	0.385	1.3
Total	100	95.72, 96.04**		100	95.41, 95.91**	

* RPD - Relative precent difference
**total with F and Cl target masses
NM- Not measured
ND-Not defined

Appendix D – XRD patterns of quenched glasses

The refined XRD patterns with wt% of crystalline phases are shown in this appendix for the quenched glasses. CeO_2 was added as a standard to quantify the crystalline phases. Red is calculated, and blue is experimental data. The gray line shows the difference between calculated and experimental data.

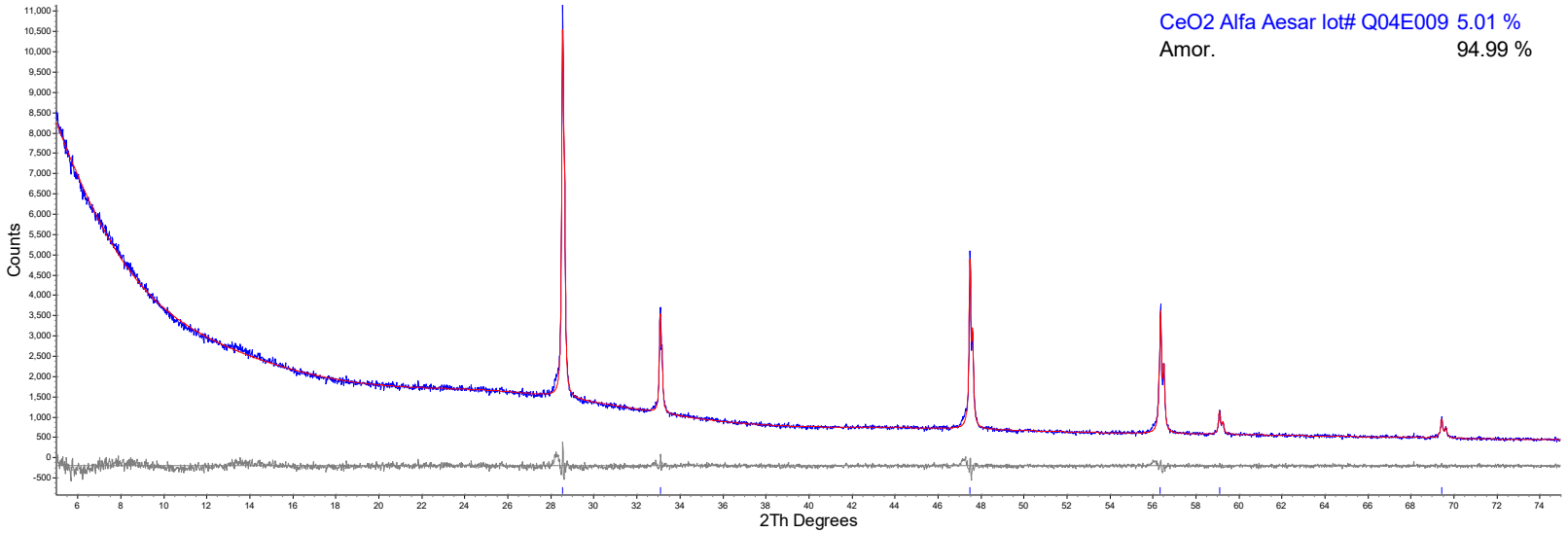

Figure D.1. Refined XRD data of HS24-01

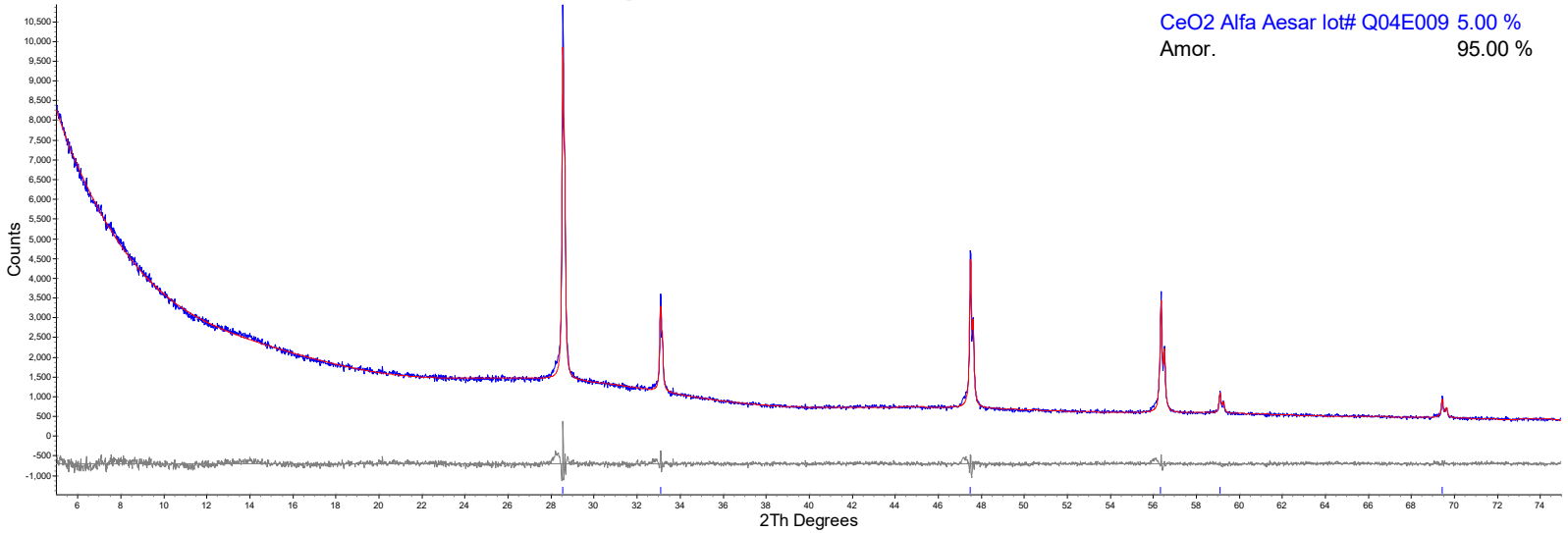

Figure D.2. Refined XRD data of HS24-02

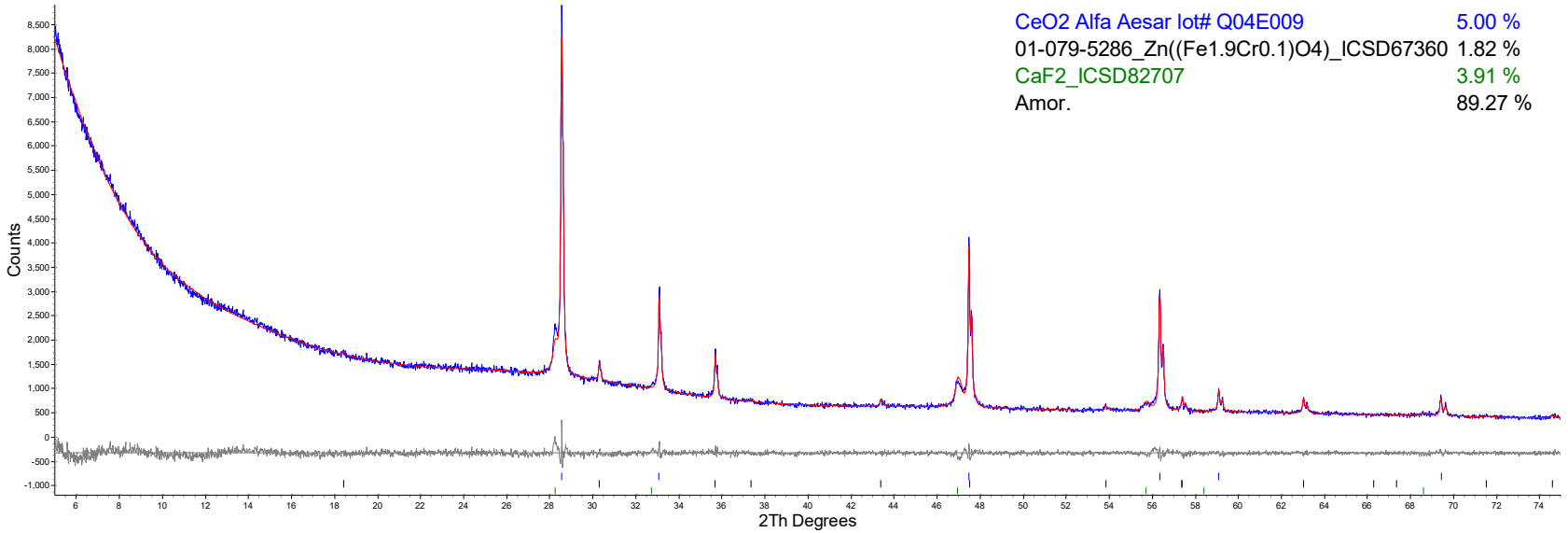

Figure D.3. Refined XRD data of HS24-03

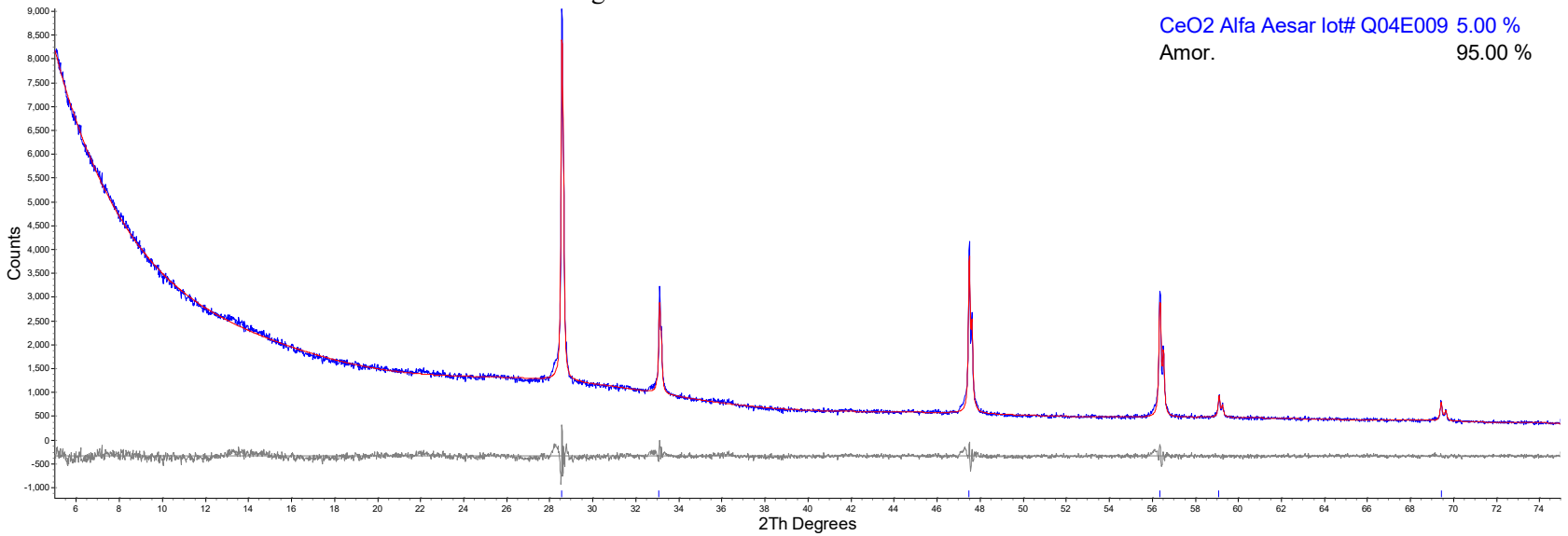

Figure D.4. Refined XRD data of HS24-04

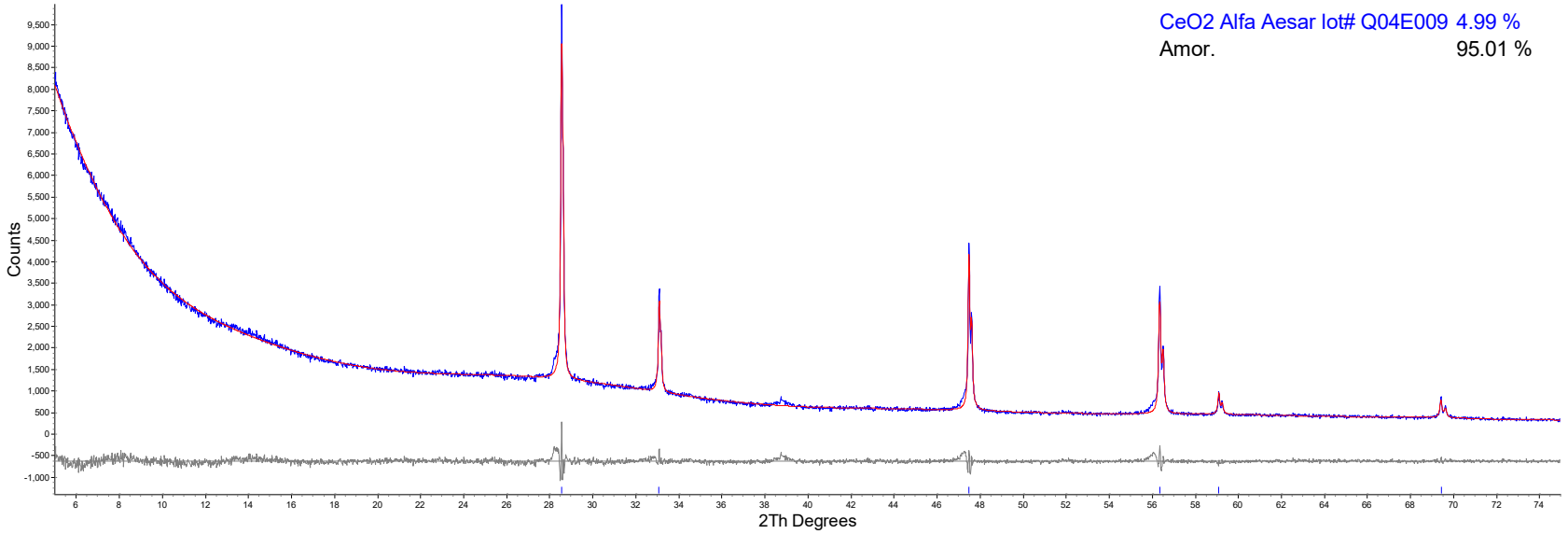

Figure D.5. Refined XRD data of HS24-05

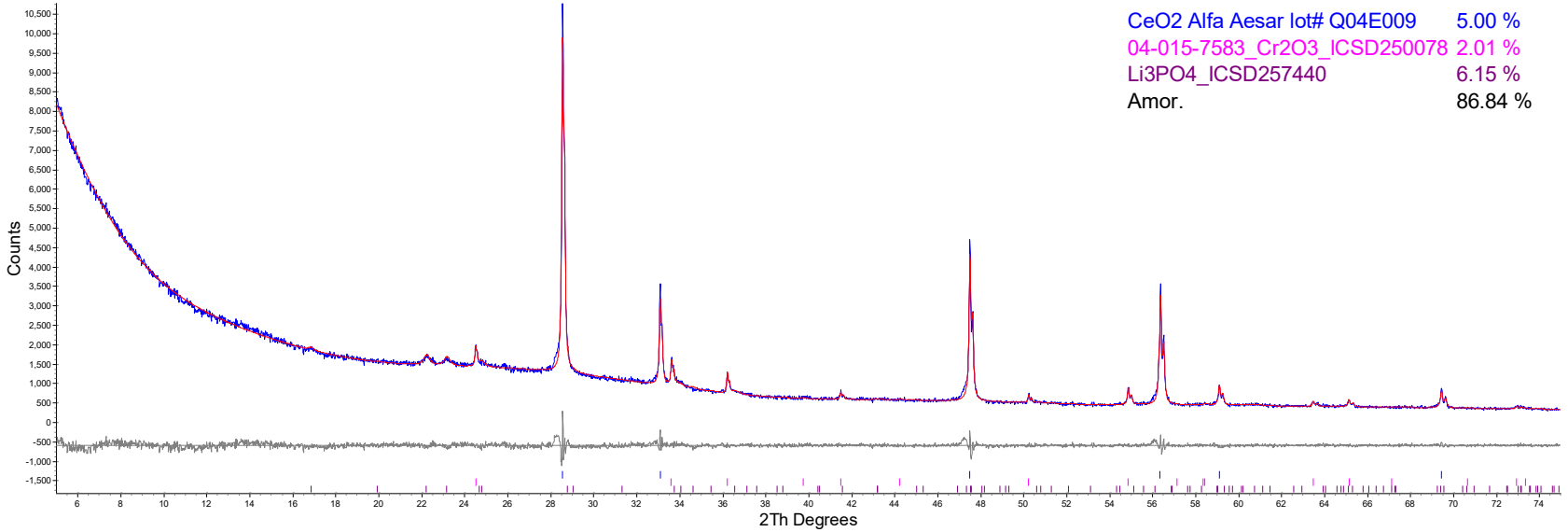

Figure D.6. Refined XRD data of HS24-06

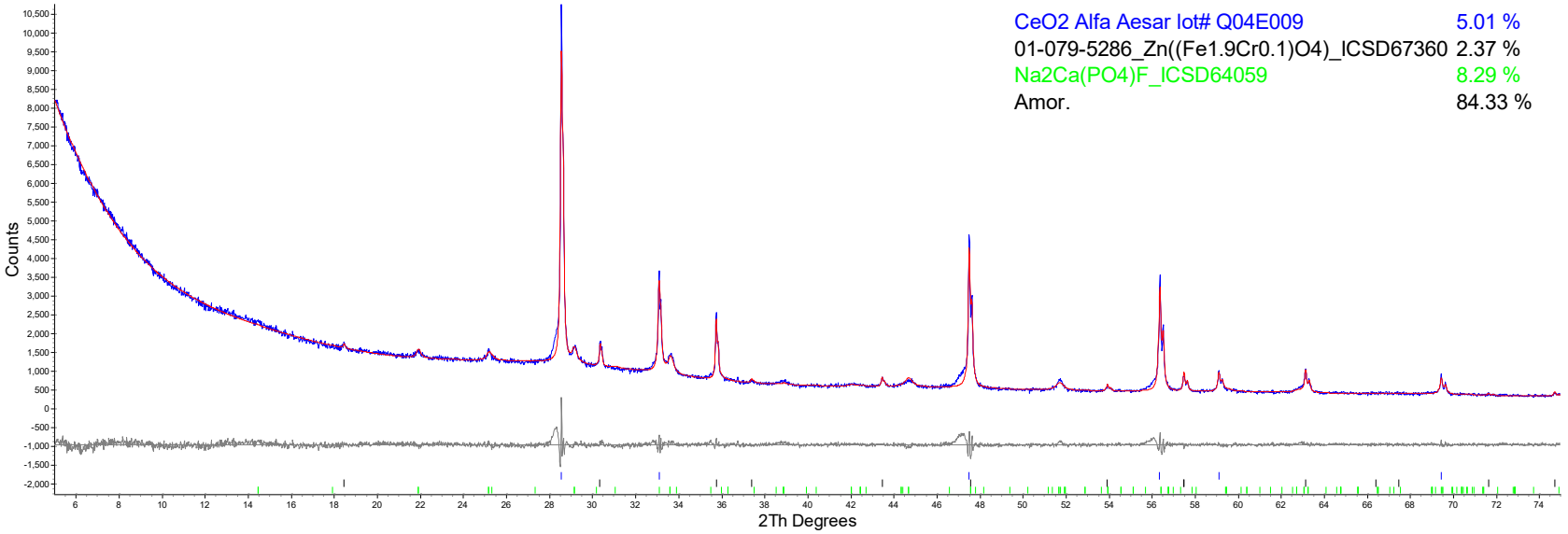

Figure D.7. Refined XRD data of HS24-07

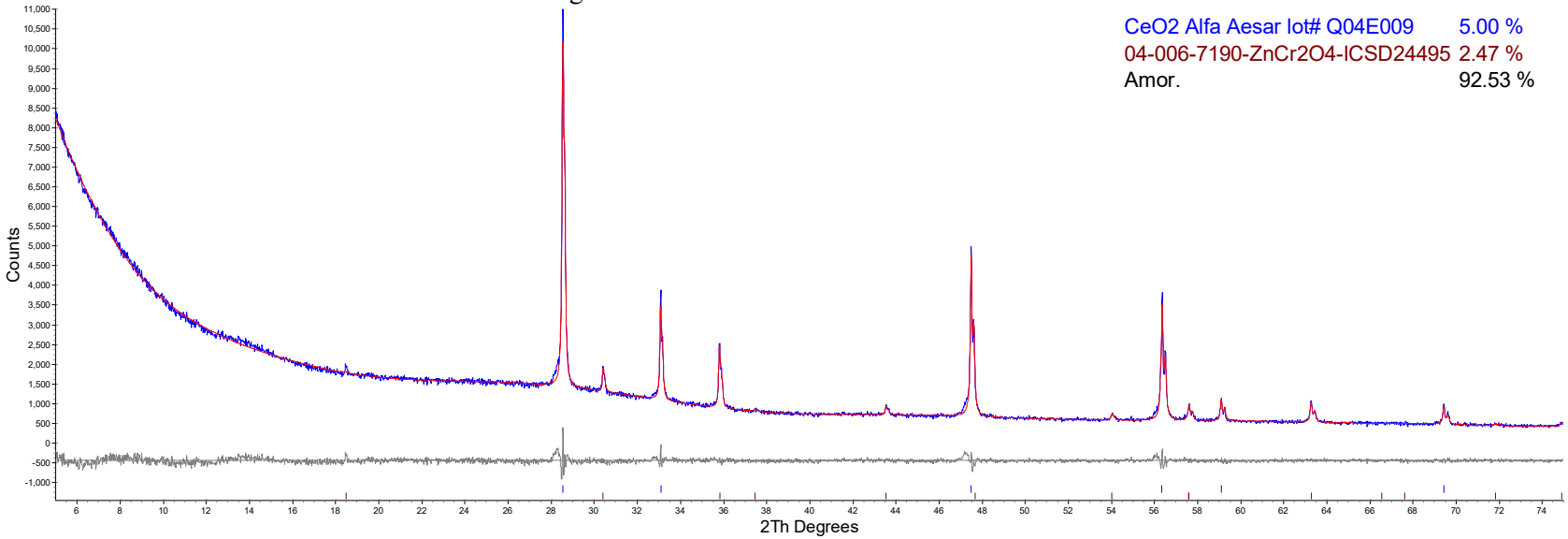

Figure D.8. Refined XRD data of HS24-08

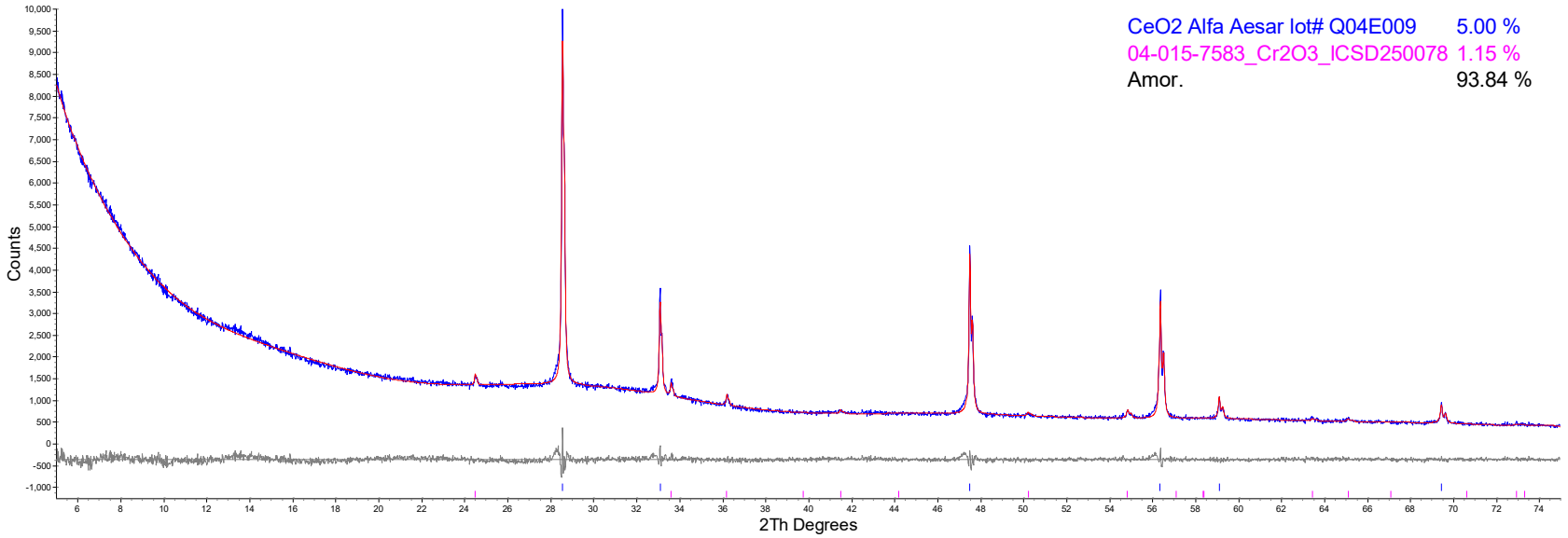

Figure D.9. Refined XRD data of HS24-09

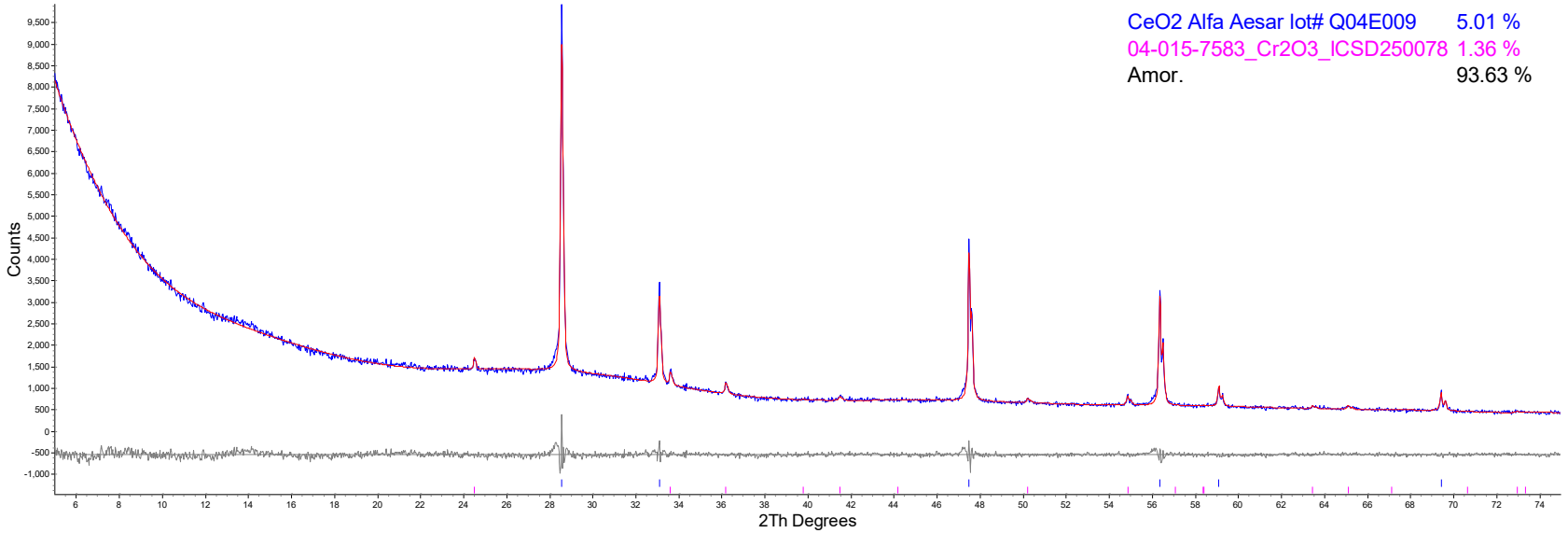

Figure D.10. Refined XRD data of HS24-10

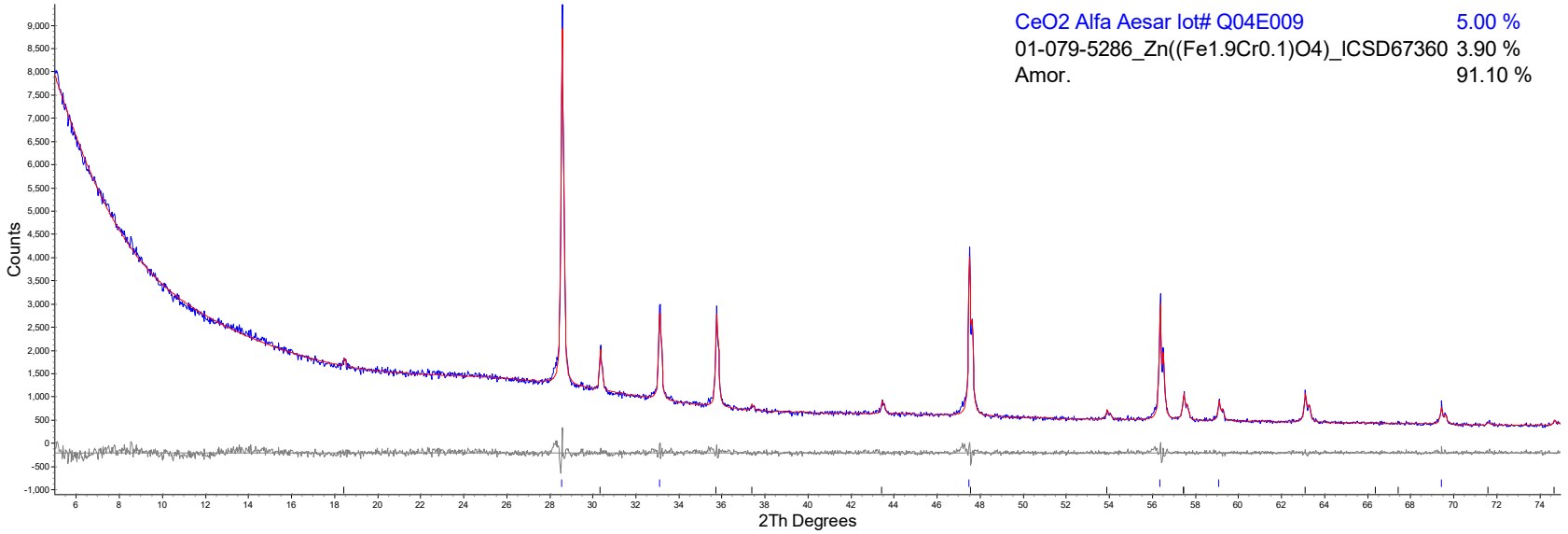

Figure D.11. Refined XRD data of HS24-11

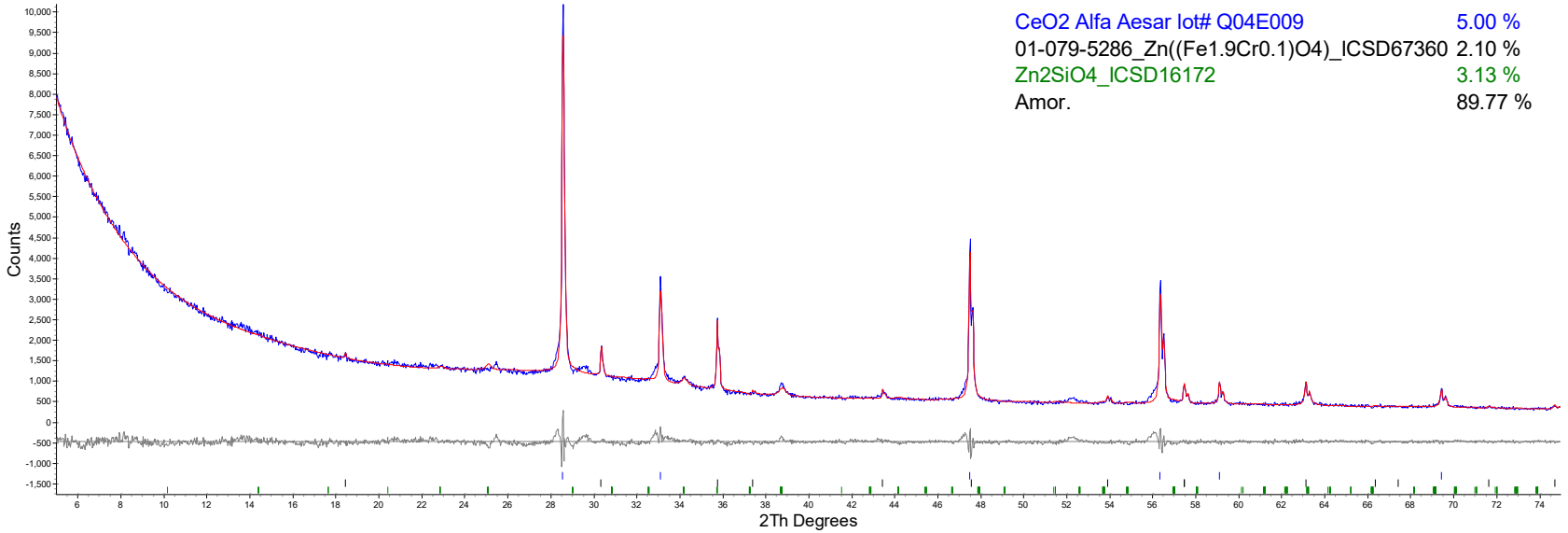

Figure D.12. Refined XRD data of HS24-12

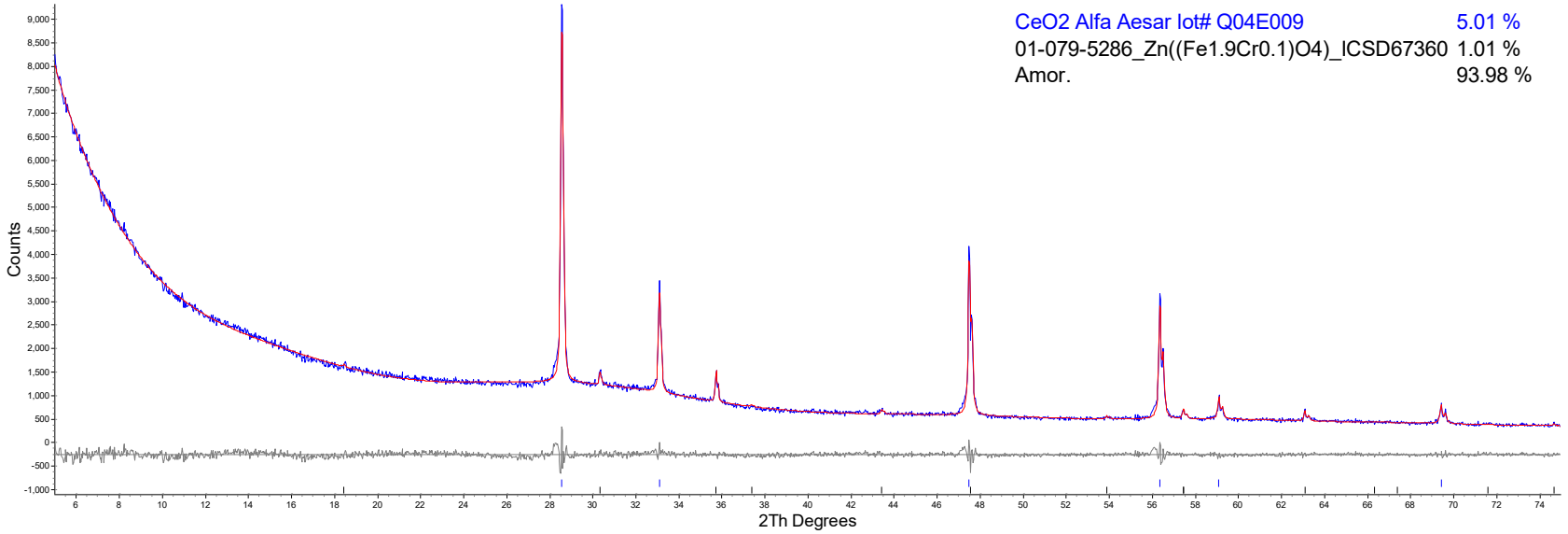

Figure D.13. Refined XRD data of HS24-13

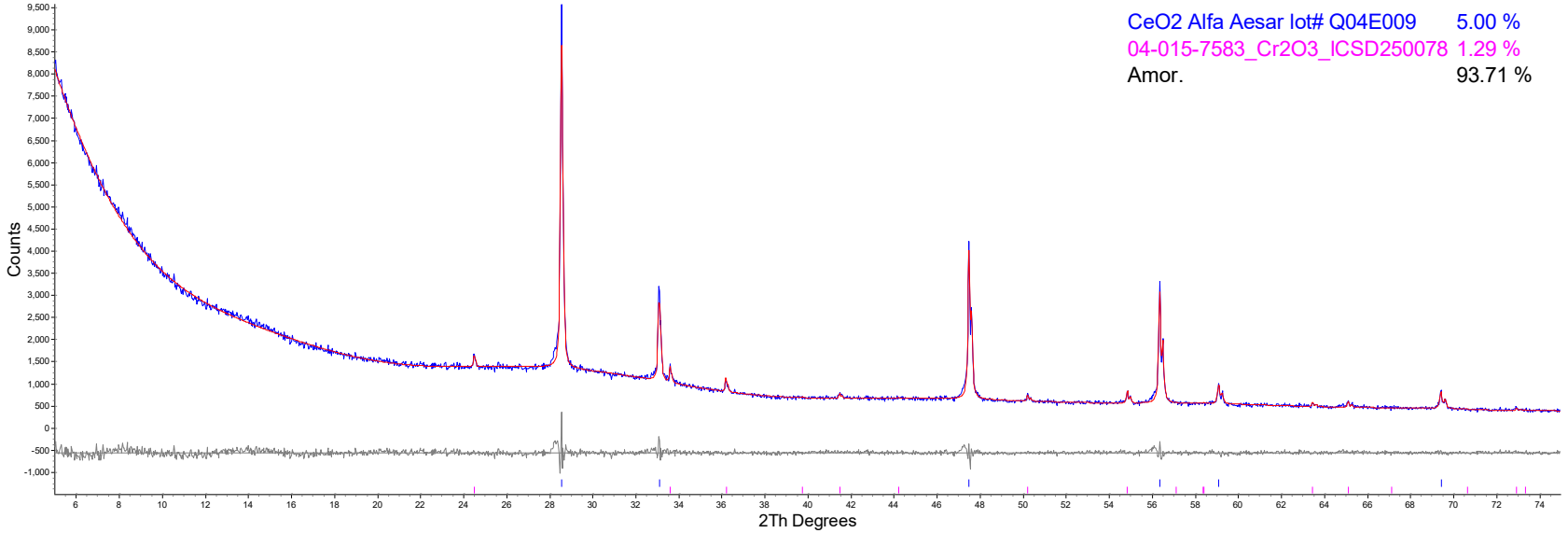

Figure D.14. Refined XRD data of HS24-14

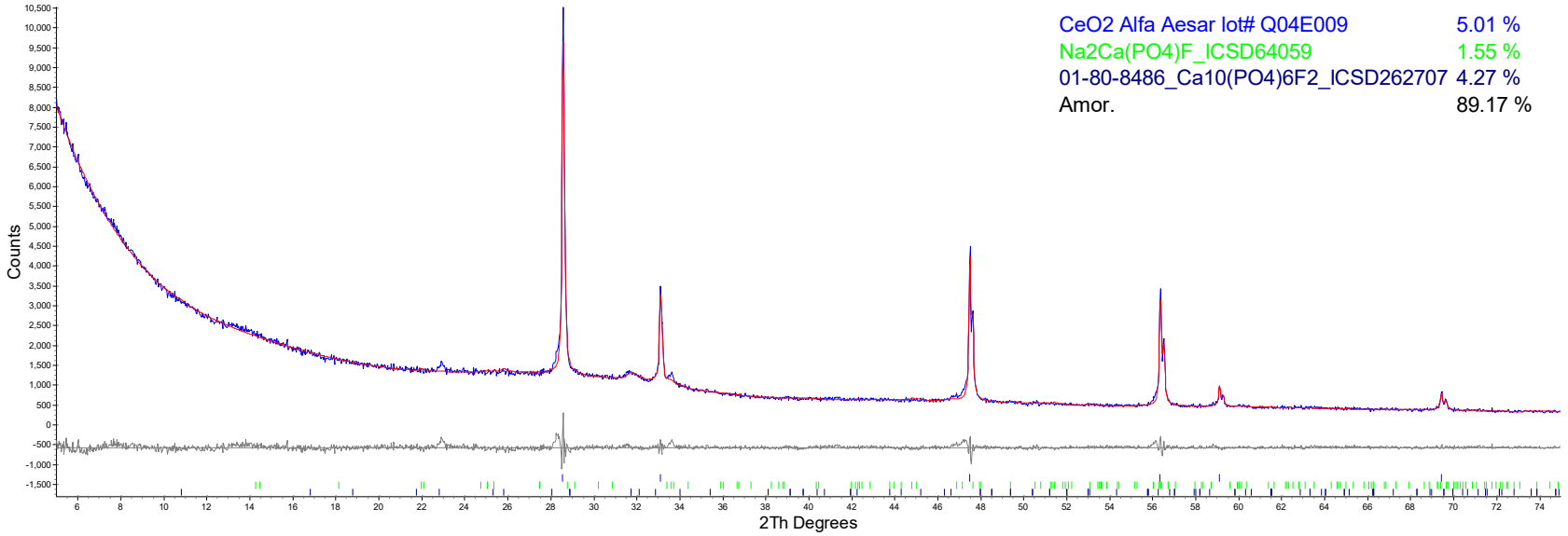

Figure D.15. Refined XRD data of HS24-15

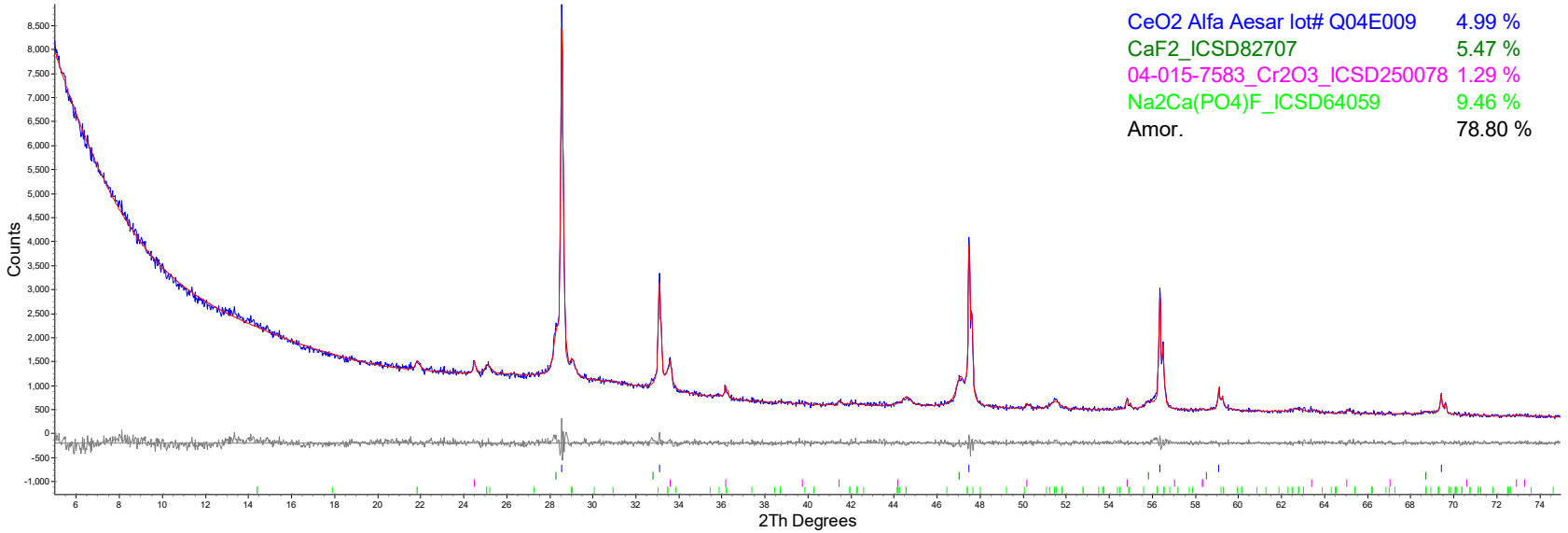

Figure D.16. Refined XRD data of HS24-16

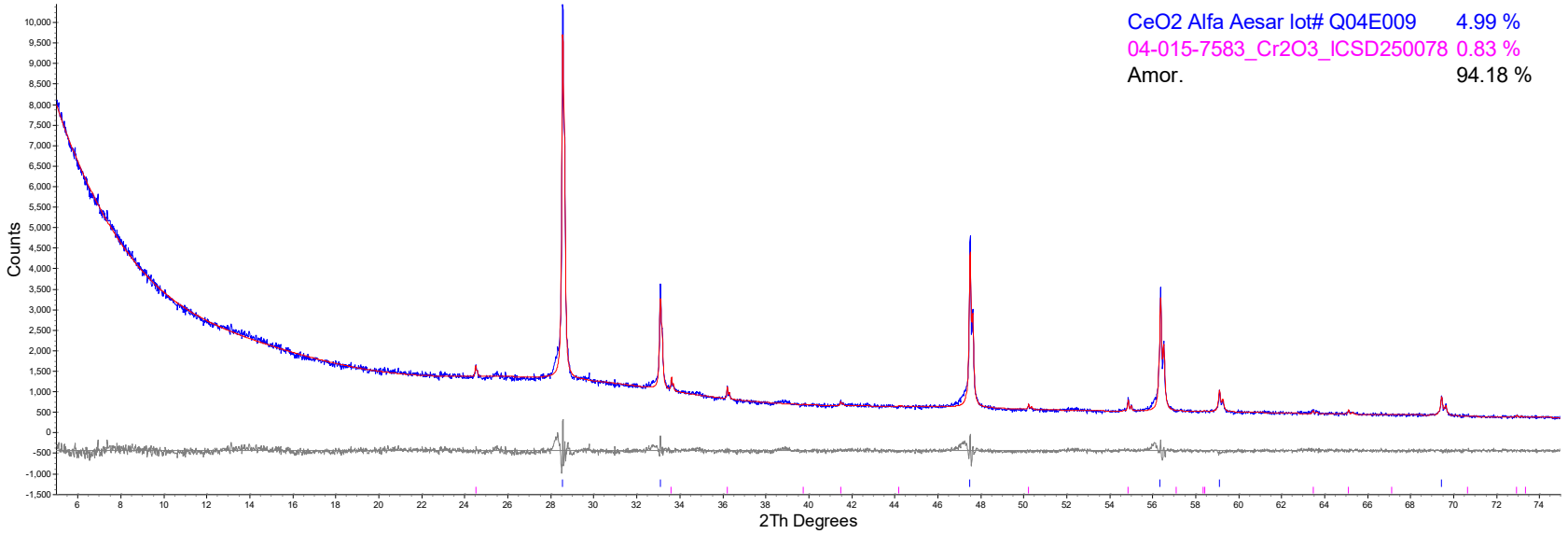

Figure D.17. Refined XRD data of HS24-17

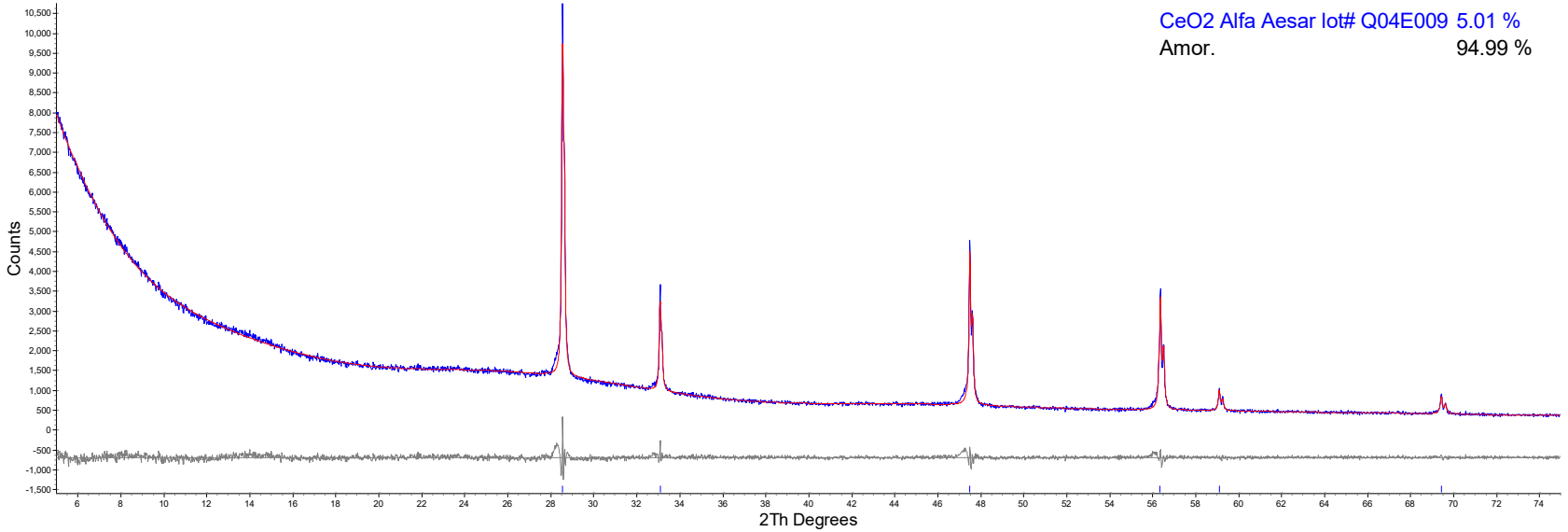

Figure D.18. Refined XRD data of HS24-18

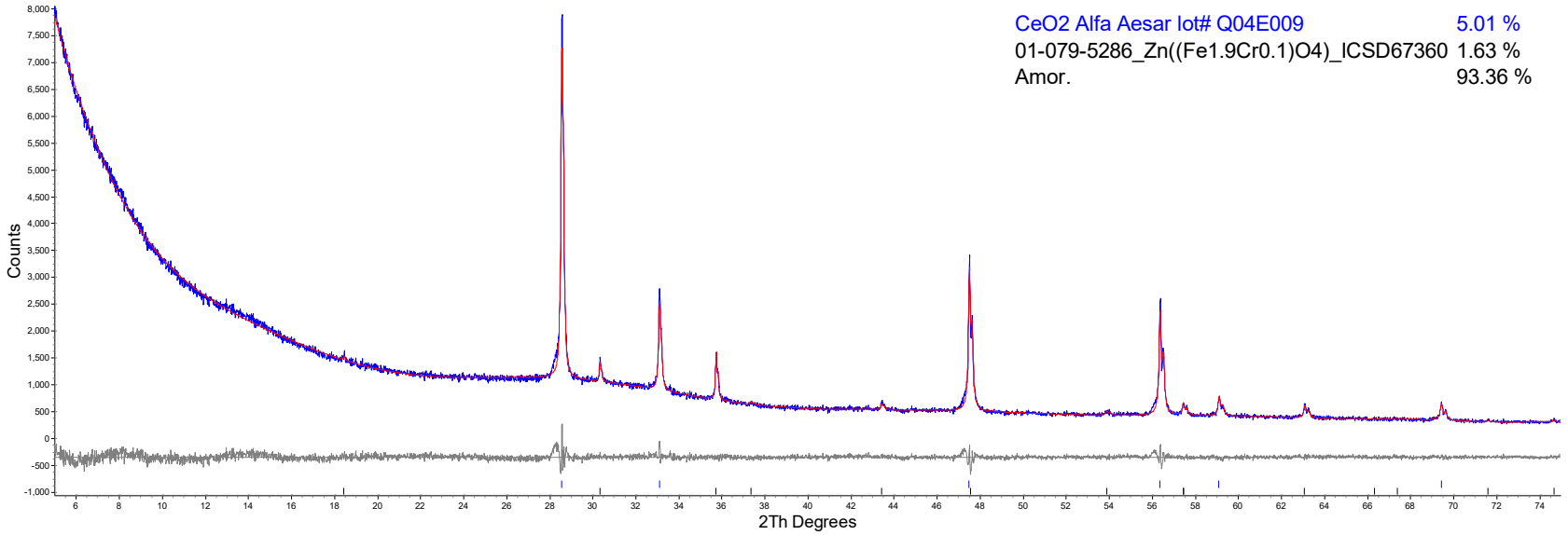

Figure D.19. Refined XRD data of HS24-19

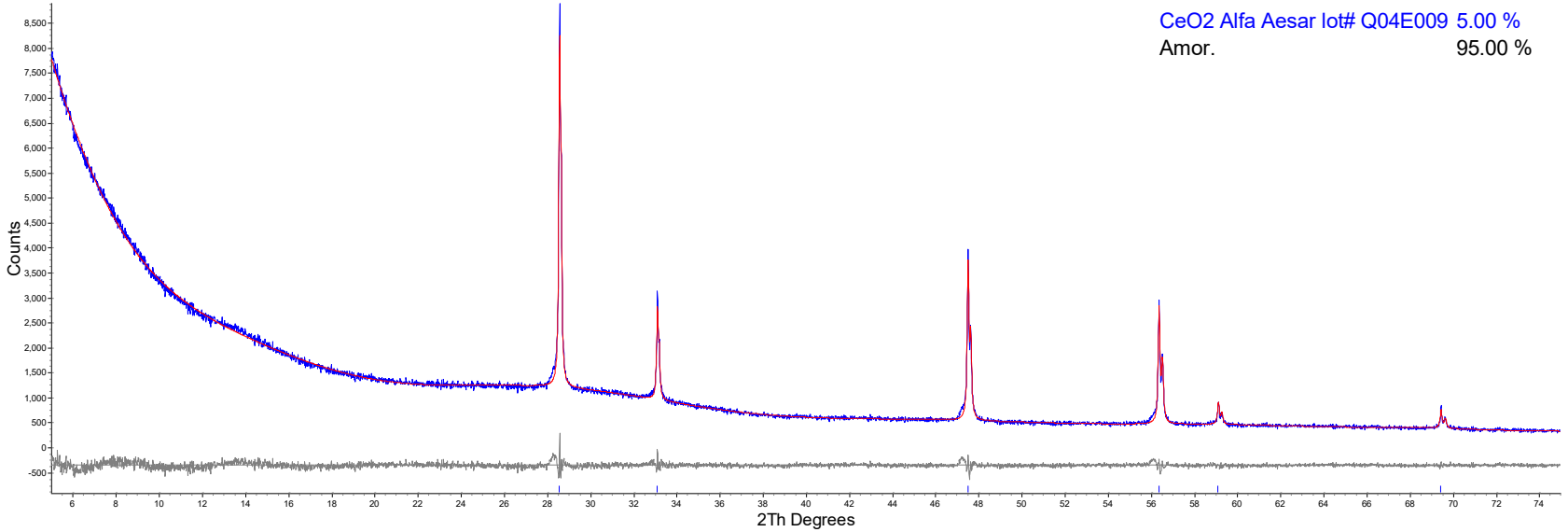

Figure D.20. Refined XRD data of HS24-20

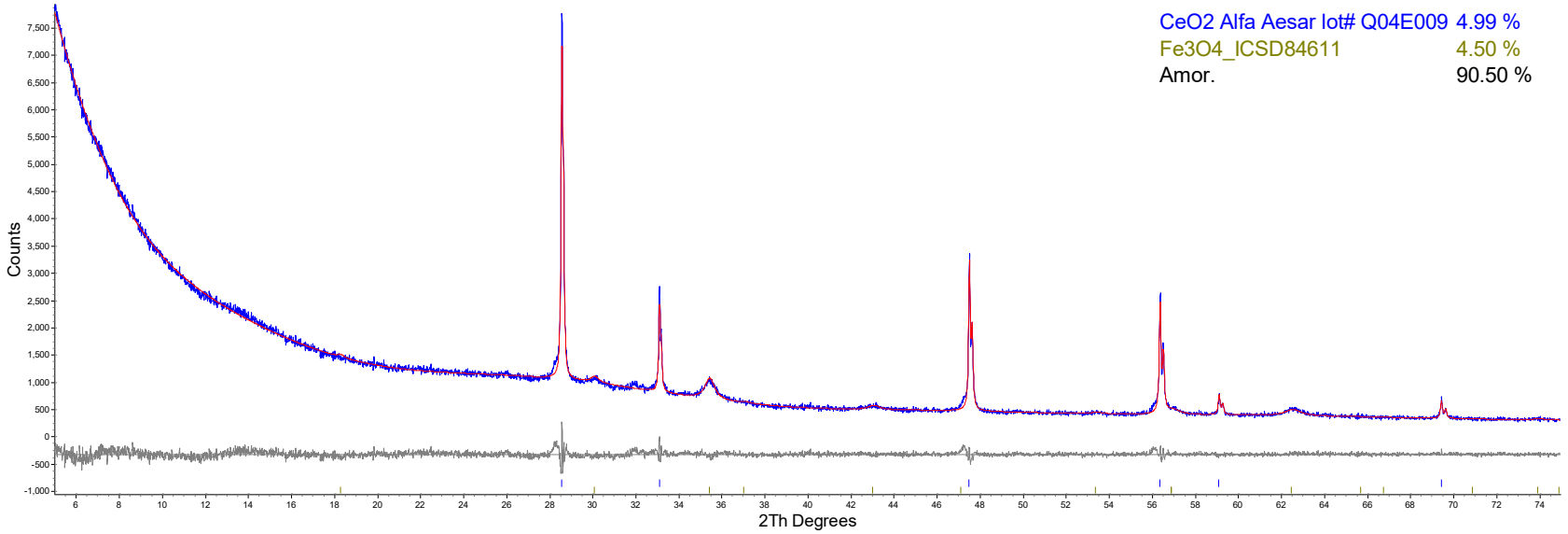

Figure D.21. Refined XRD data of HS24-21

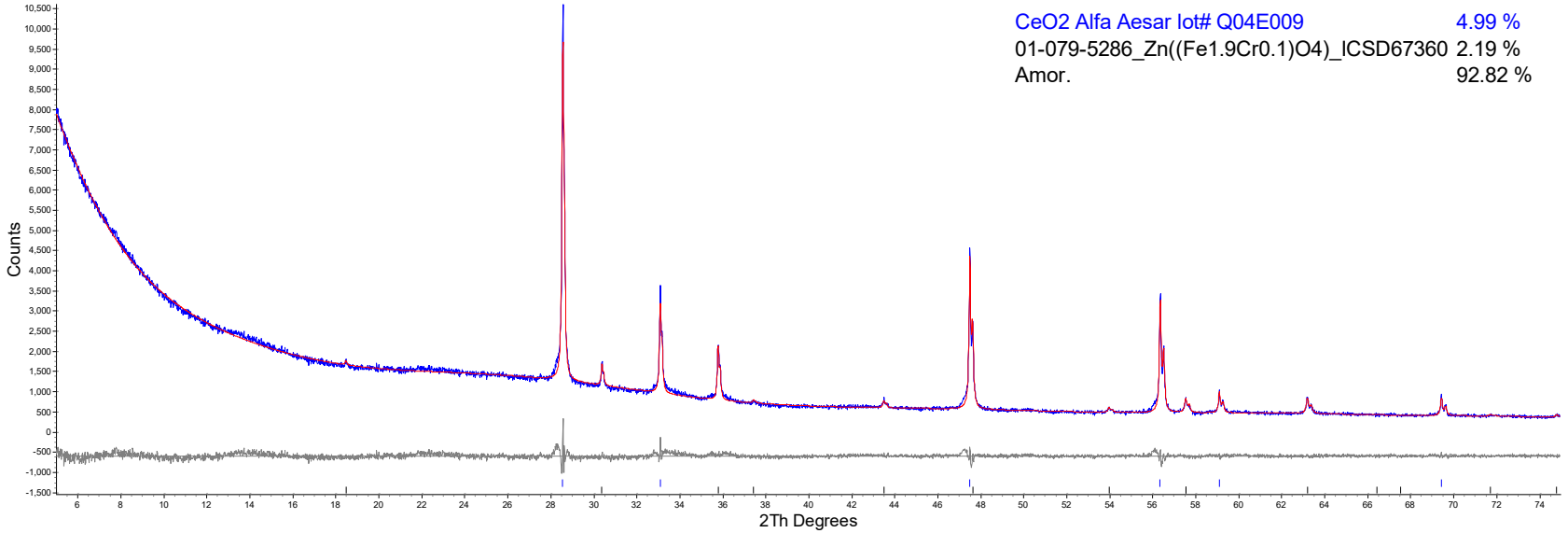

Figure D.22. Refined XRD data of HS24-22

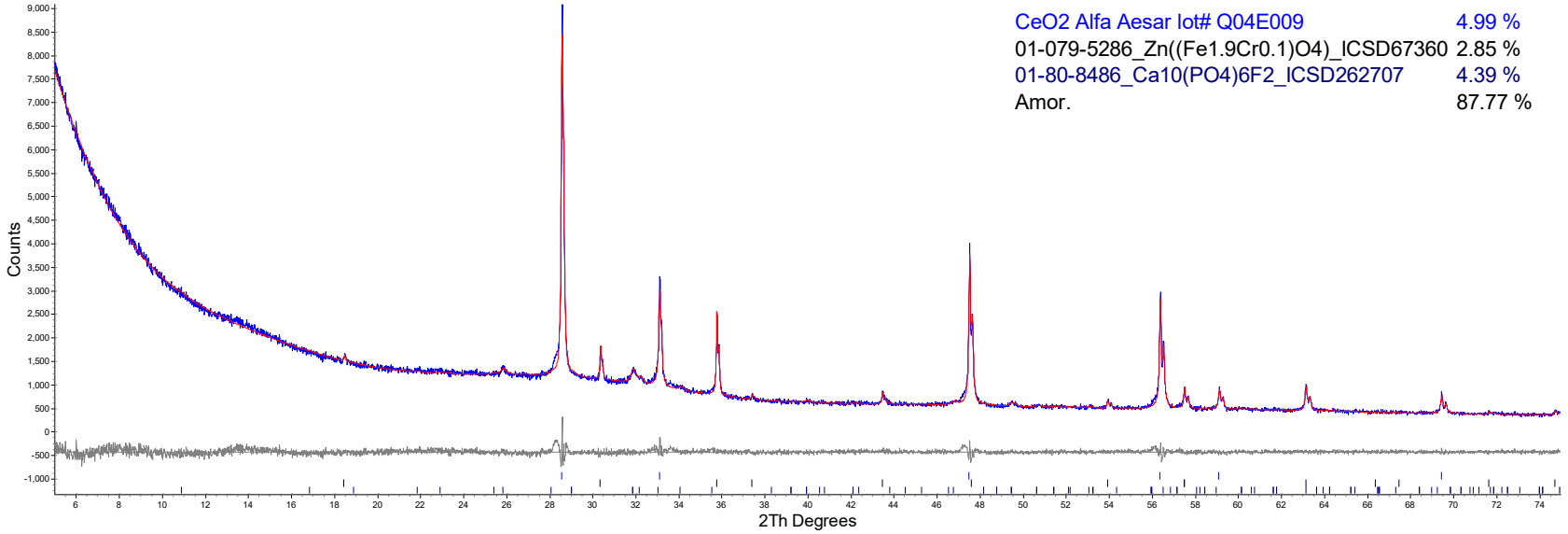

Figure D.23. Refined XRD data of HS24-23

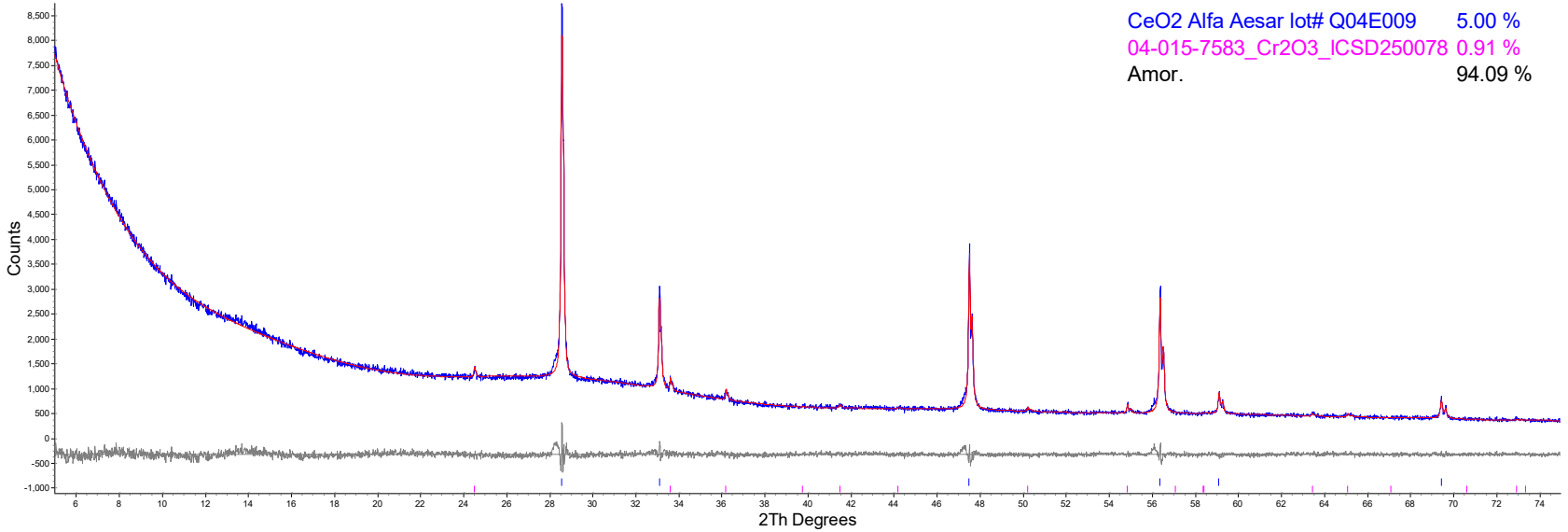

Figure D.24. Refined XRD data of HS24-24

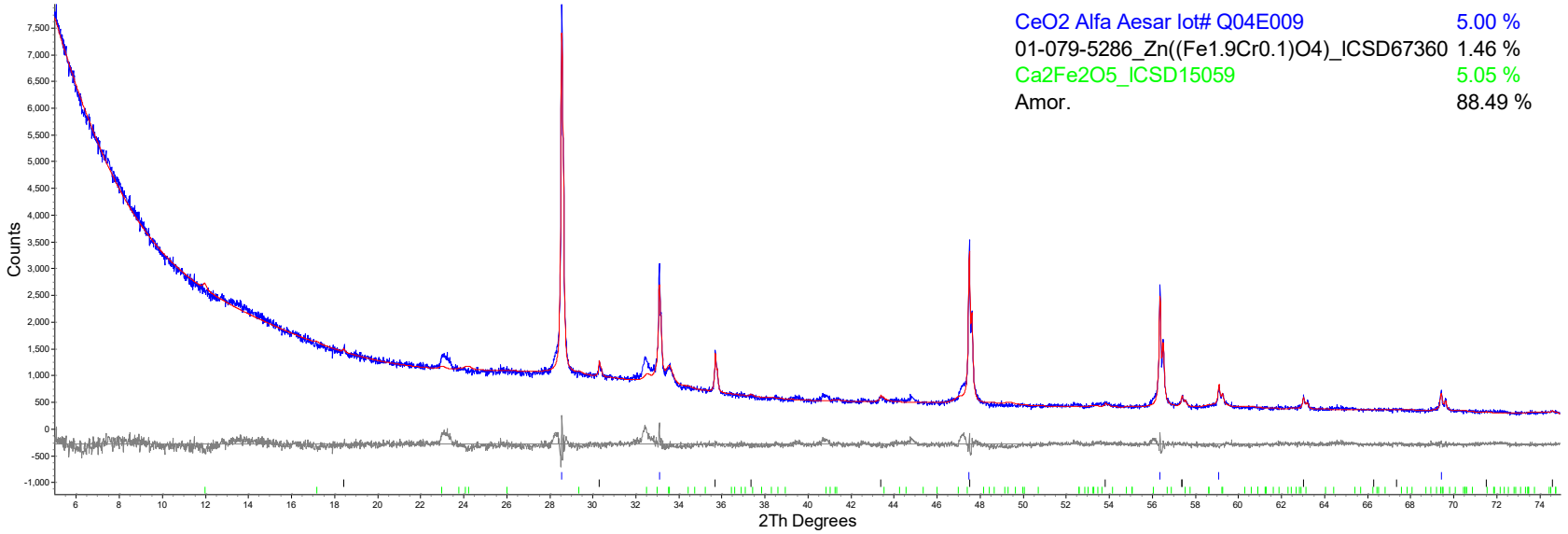

Figure D.25. Refined XRD data of HS24-25

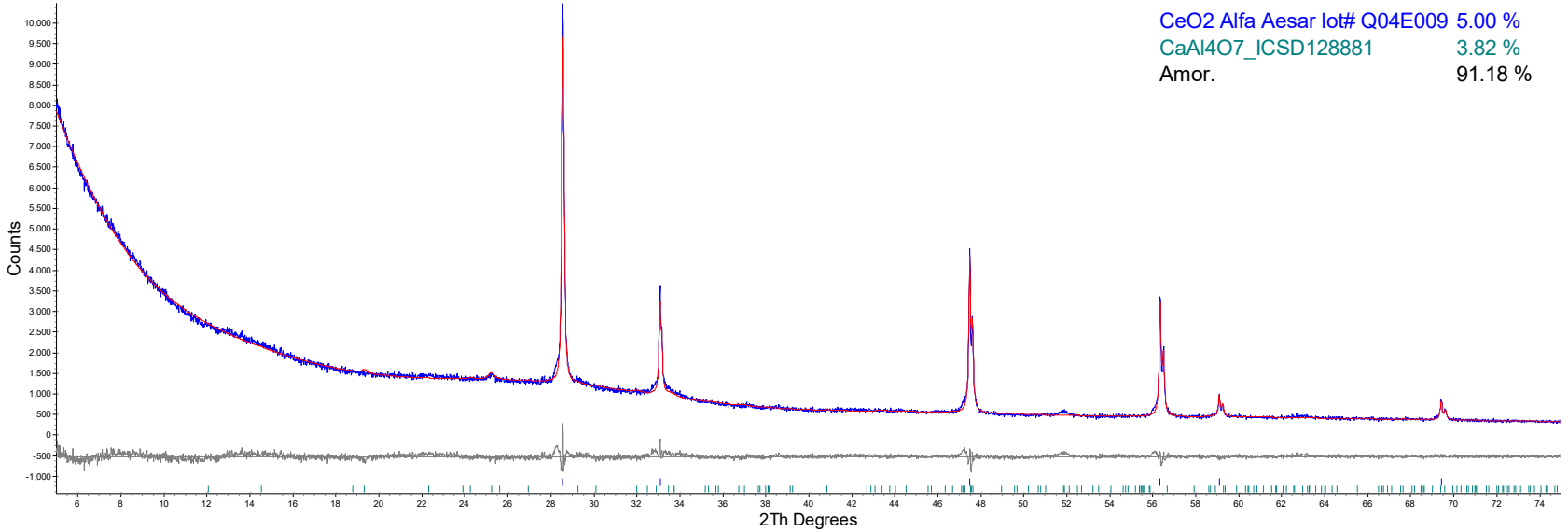

Figure D.26. Refined XRD data of HS24-26

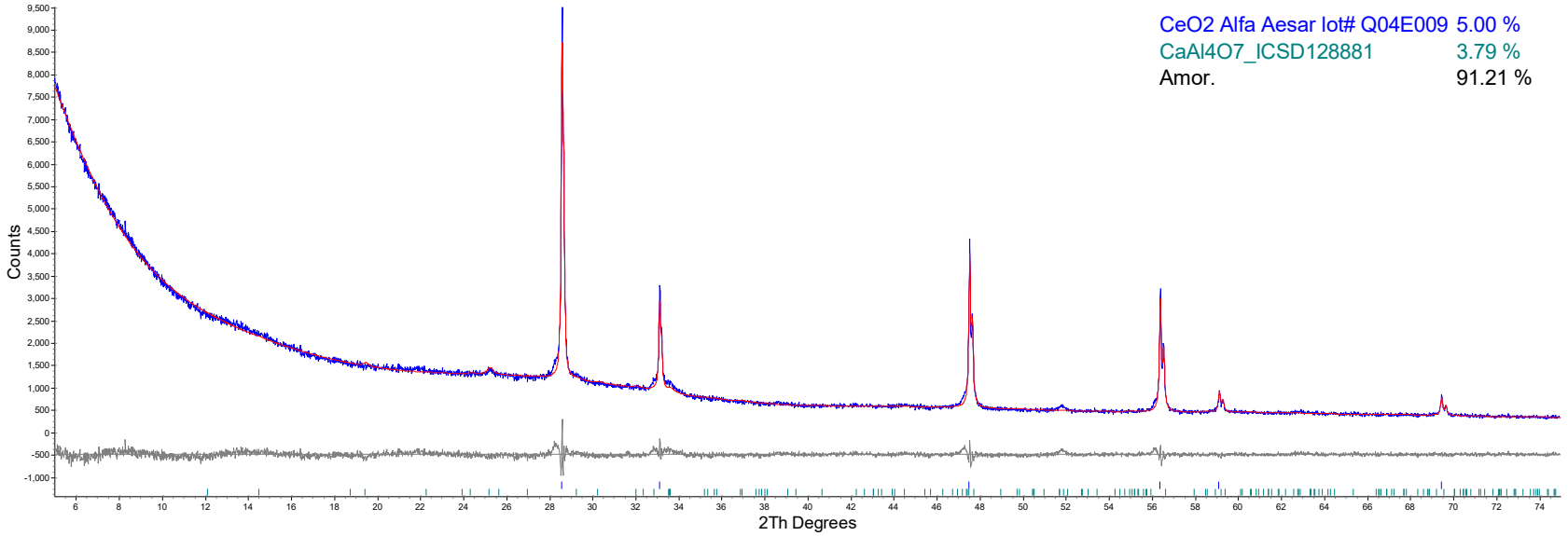

Figure D.27. Refined XRD data of HS24-27

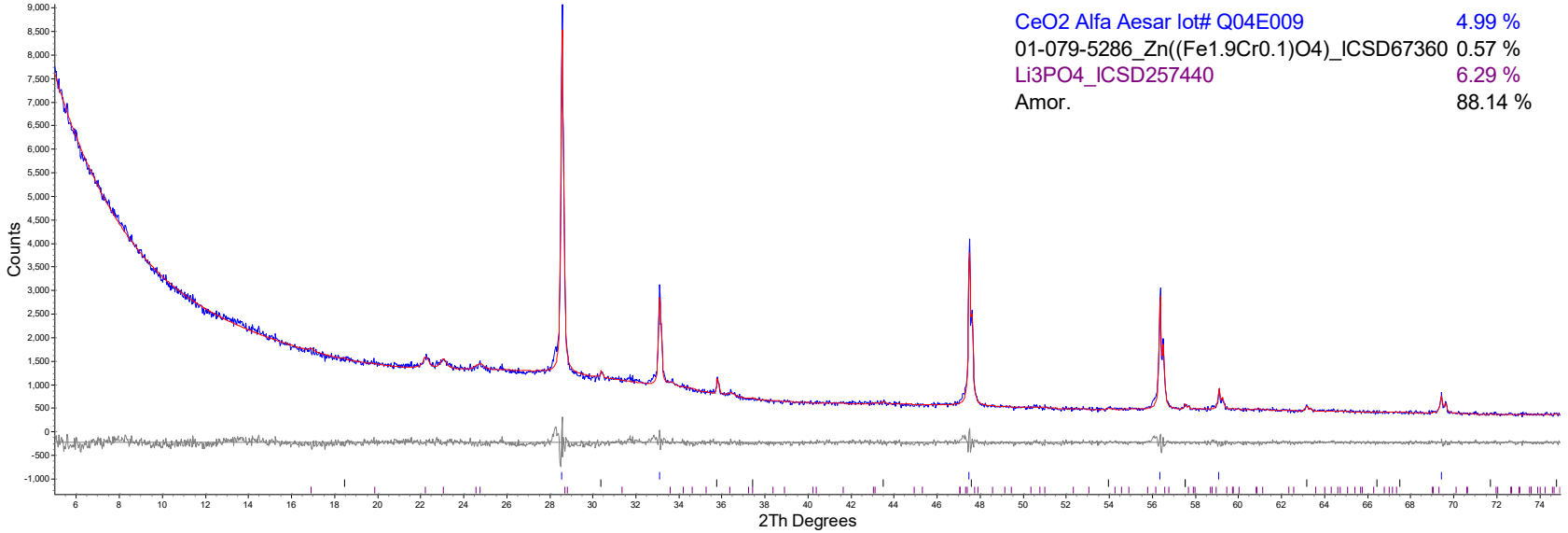

Figure D.28. Refined XRD data of HS24-28

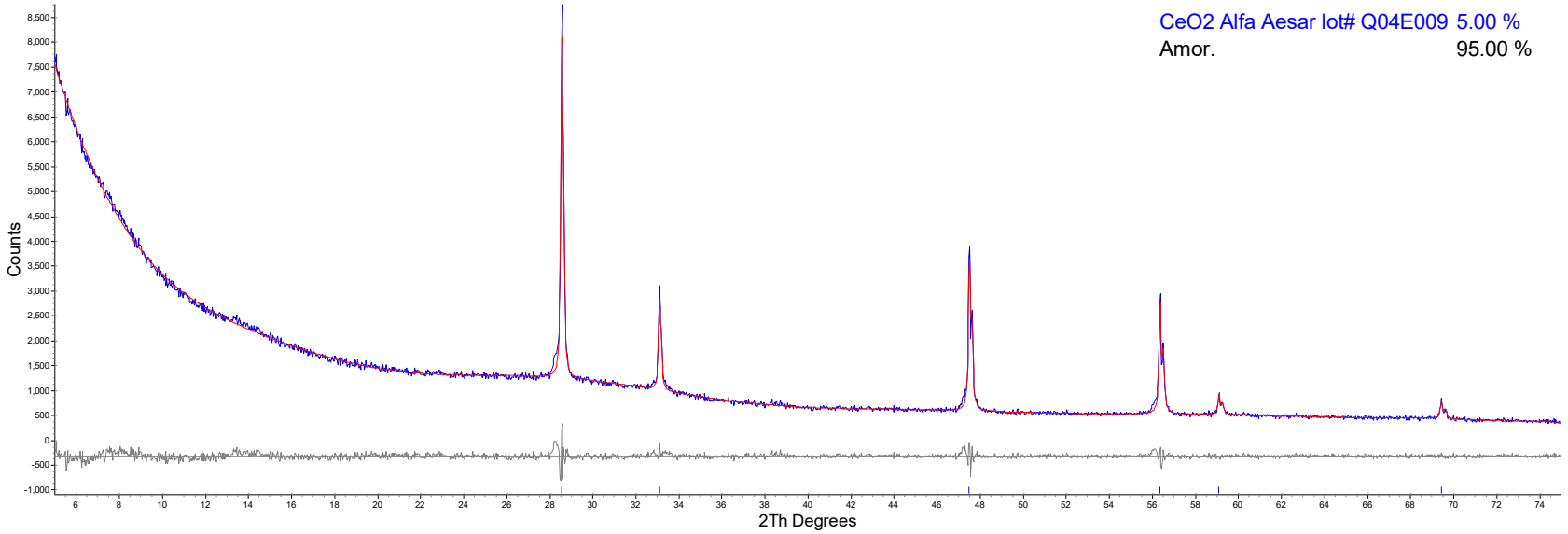

Figure D.29. Refined XRD data of HS24-29

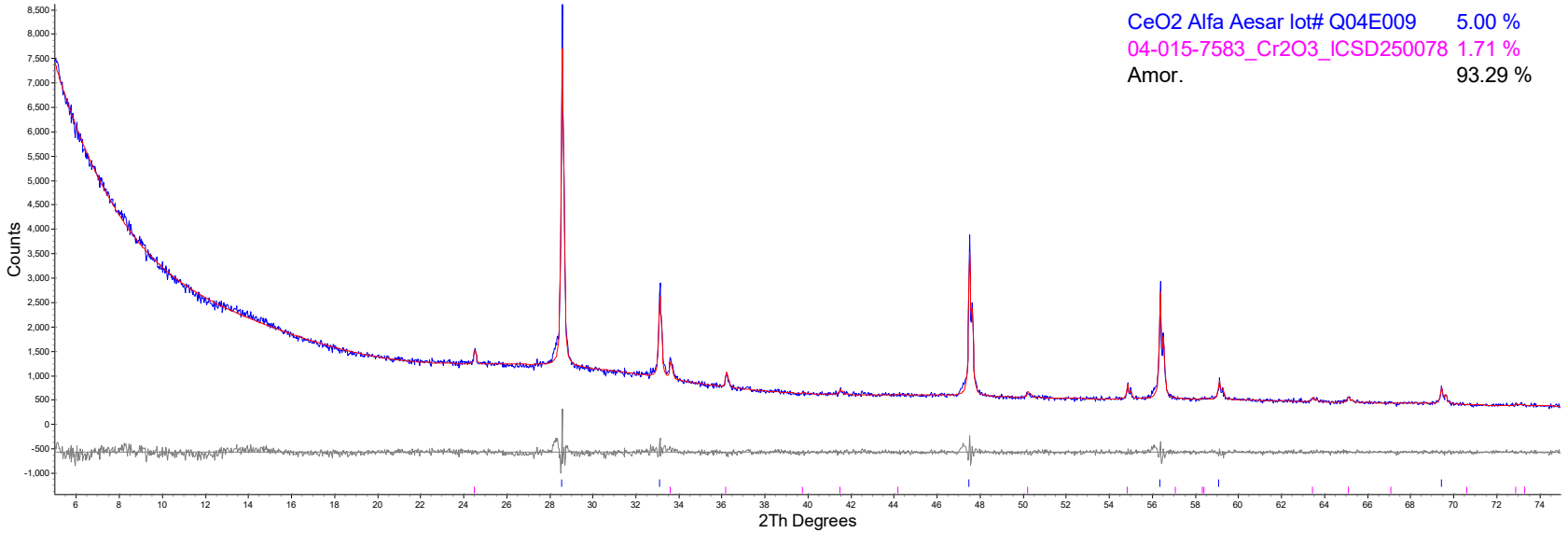

Figure D.30. Refined XRD data of HS24-30

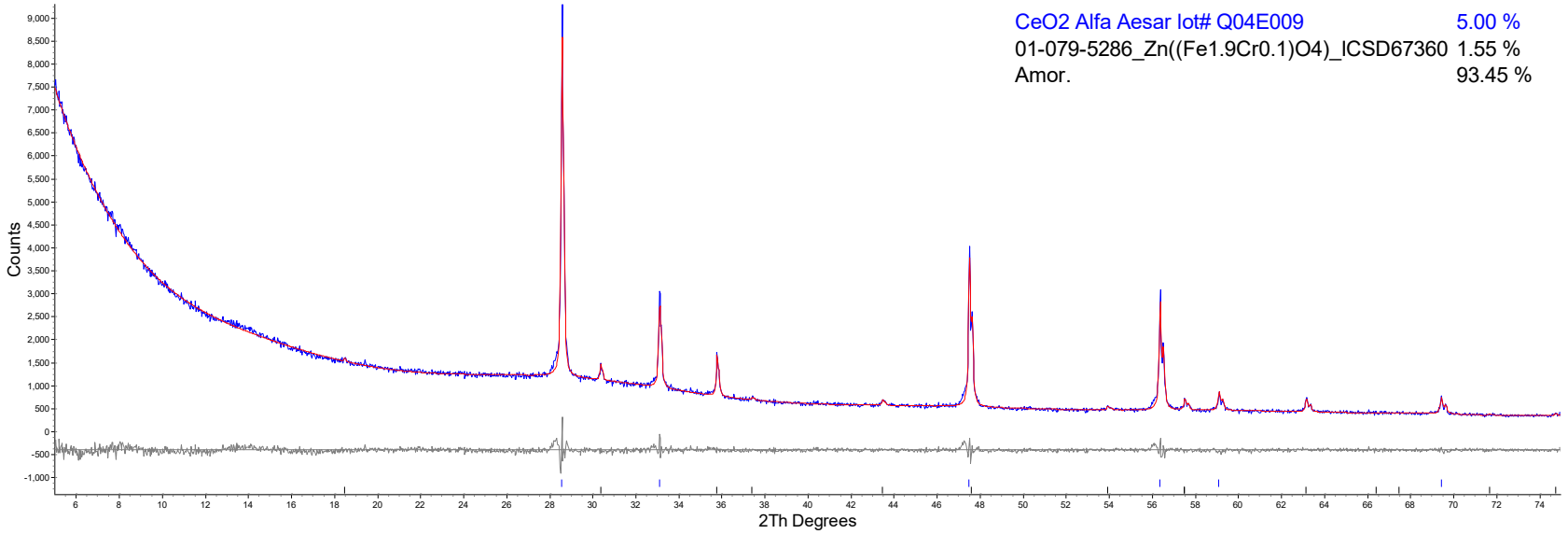

Figure D.31. Refined XRD data of HS24-31

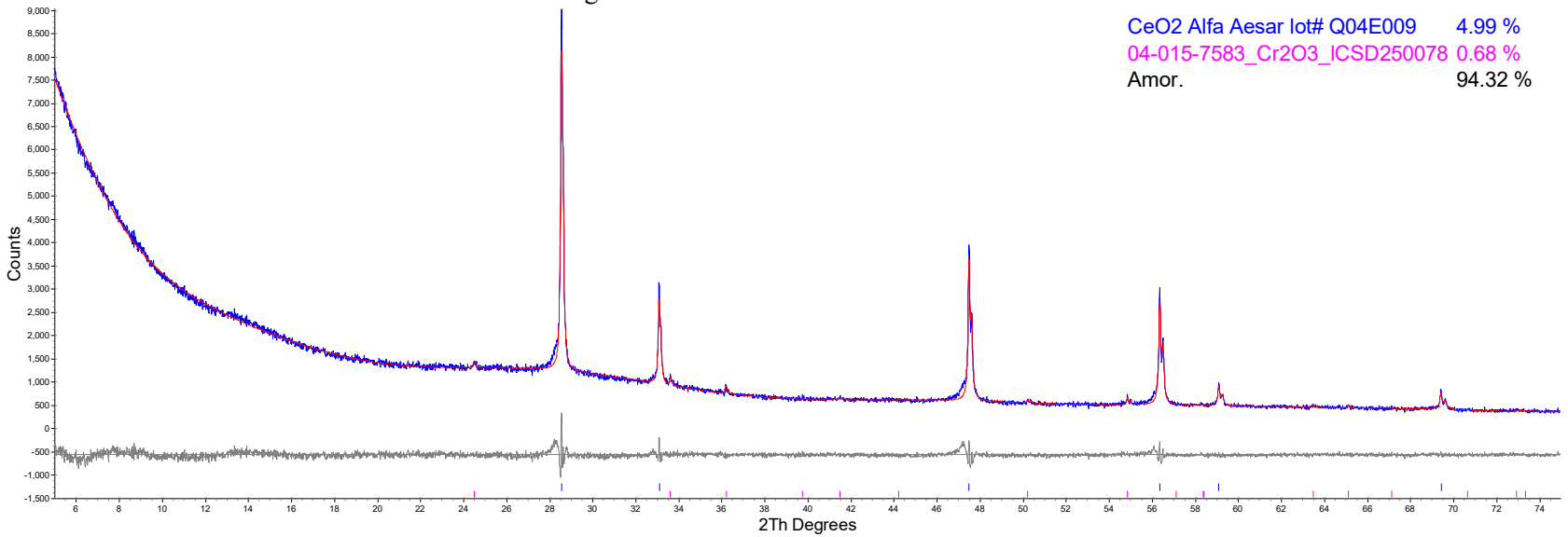

Figure D.32. Refined XRD data of HS24-32

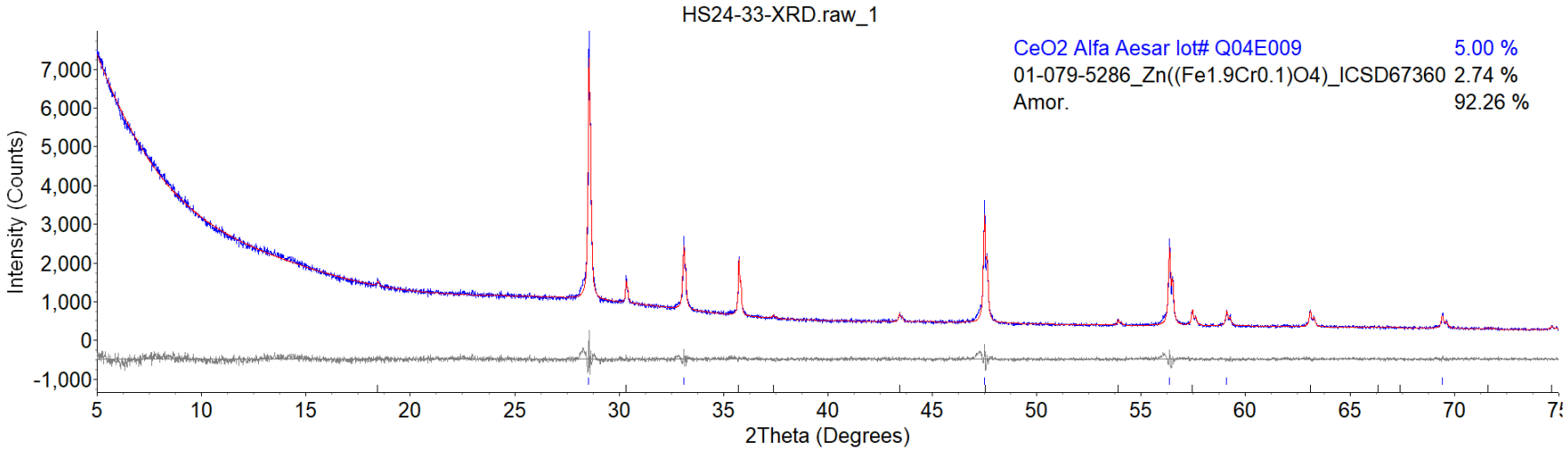

Figure D.33. Refined XRD data of HS24-33

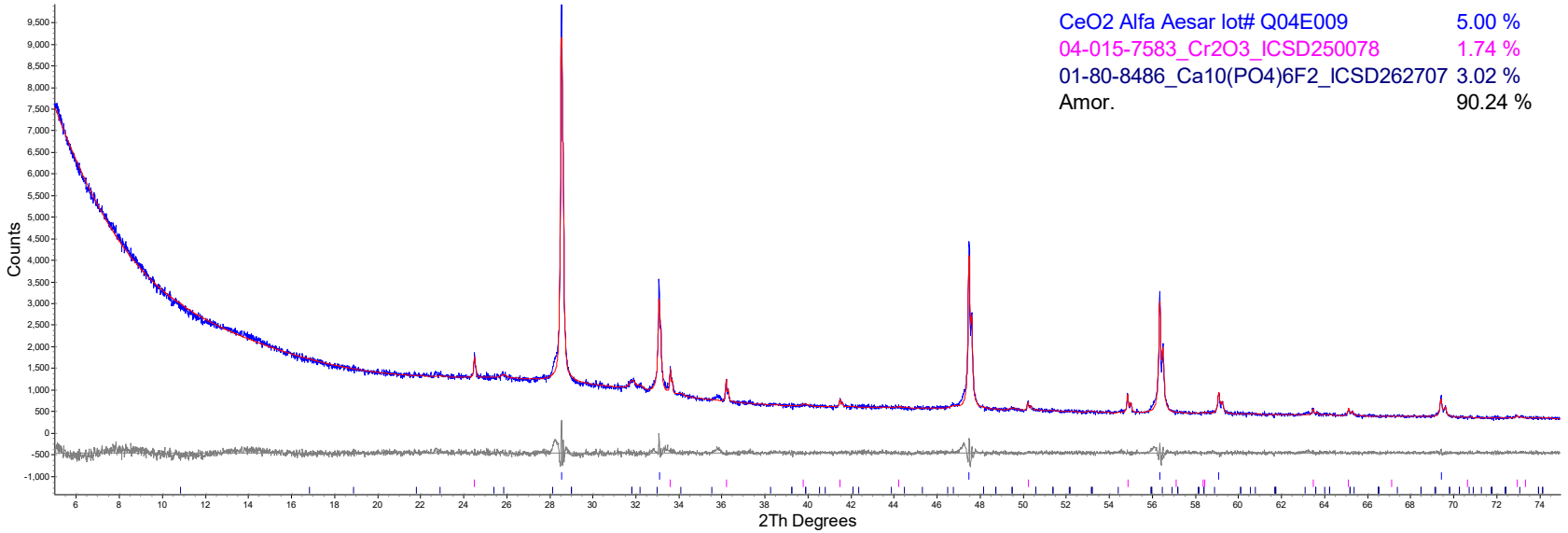

Figure D.34. Refined XRD data of HS24-34

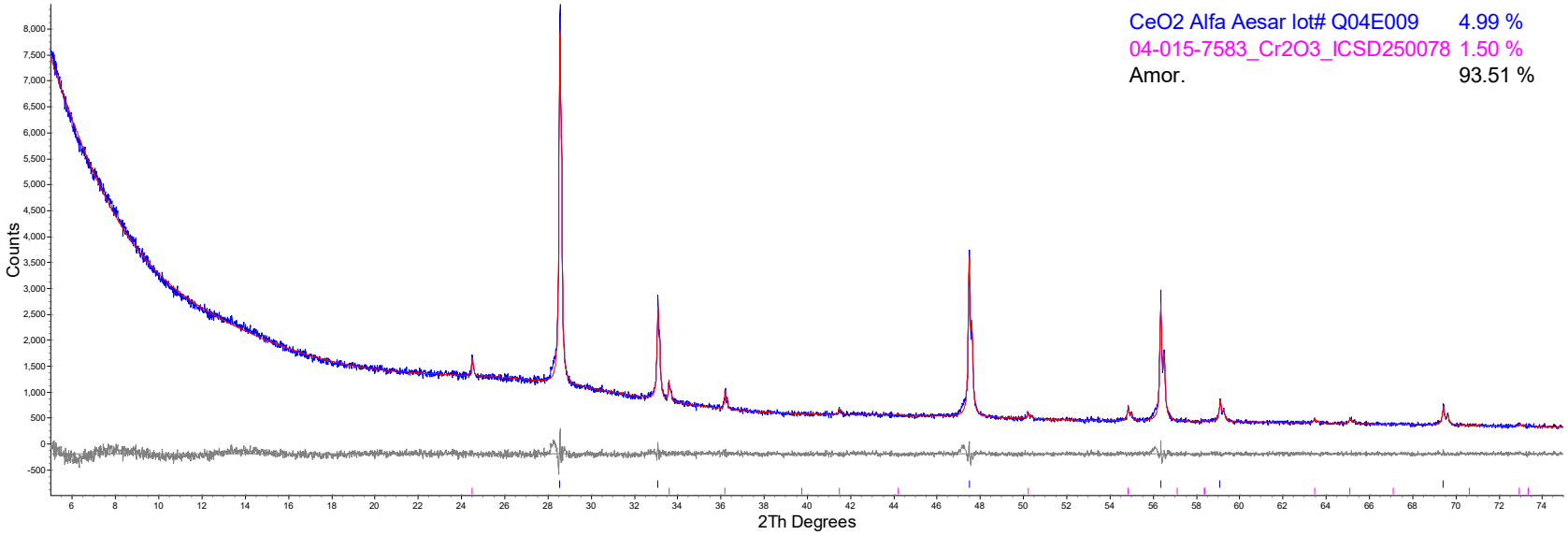

Figure D.35. Refined XRD data of HS24-35

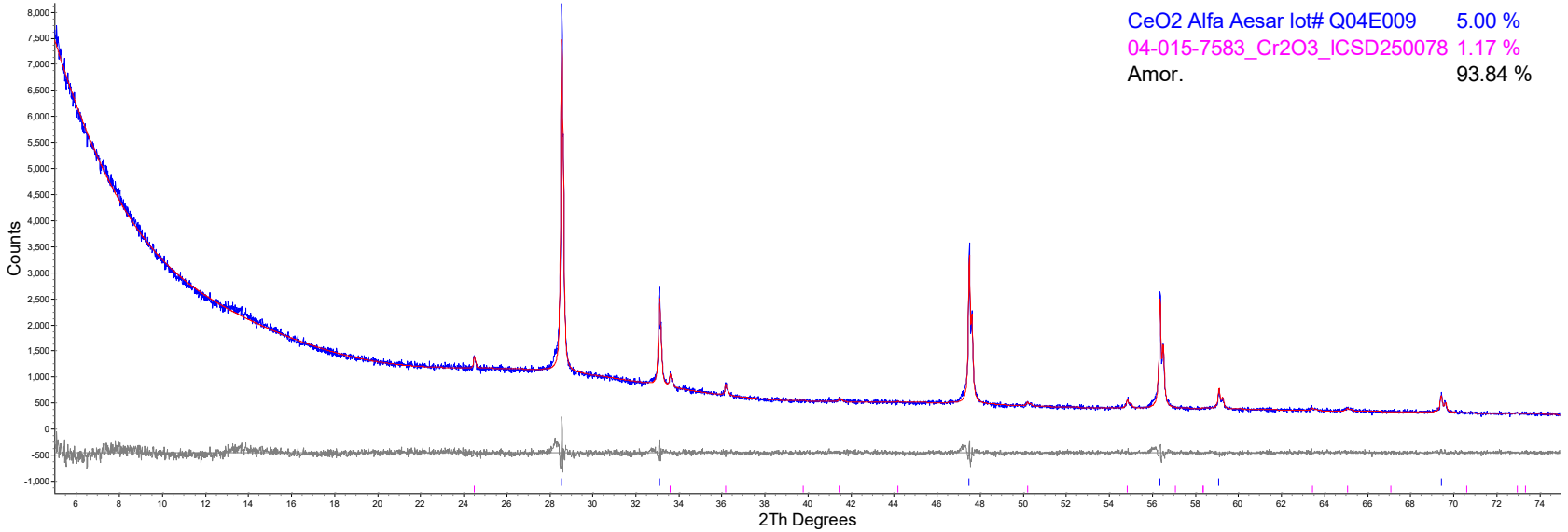

Figure D.36. Refined XRD data of HS24-36

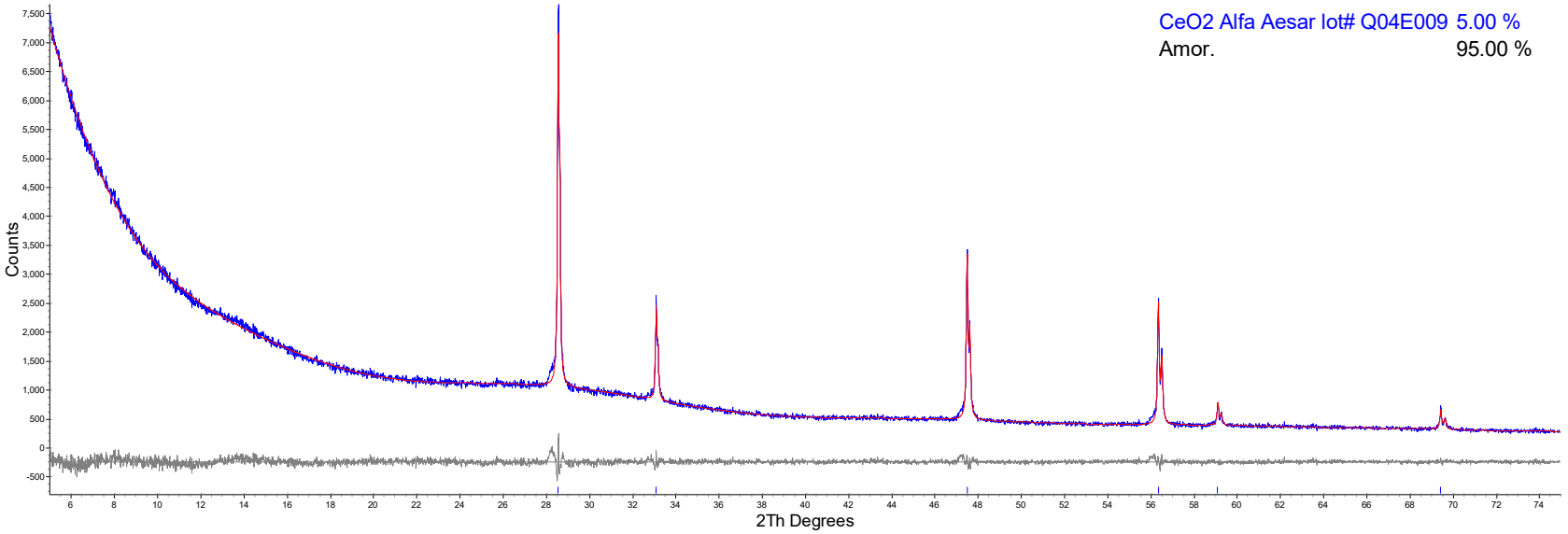

Figure D.37. Refined XRD data of HS24-37

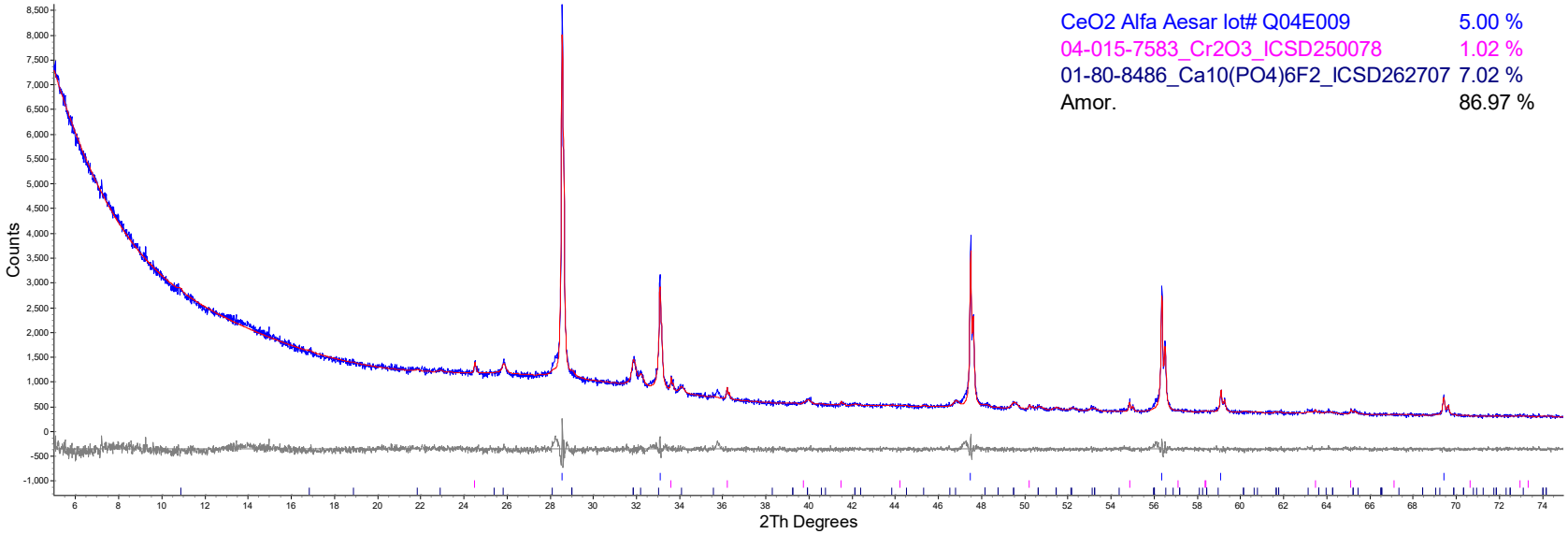

Figure D.38. Refined XRD data of HS24-38

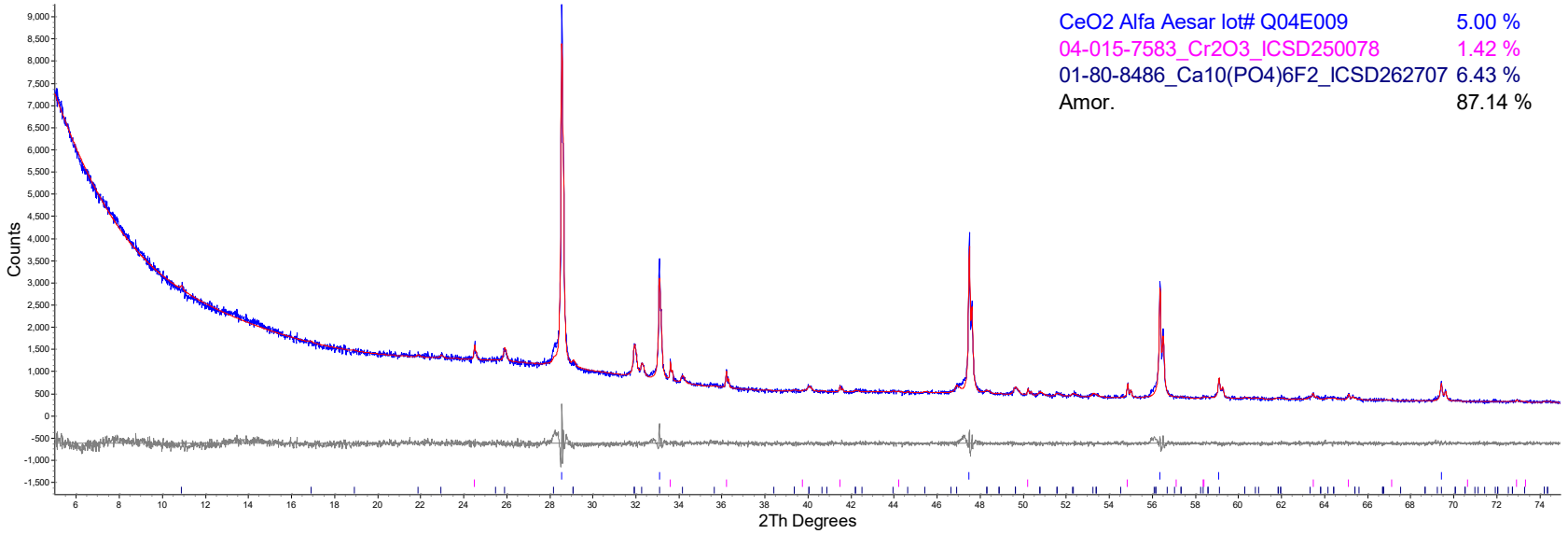

Figure D.39. Refined XRD data of HS24-39

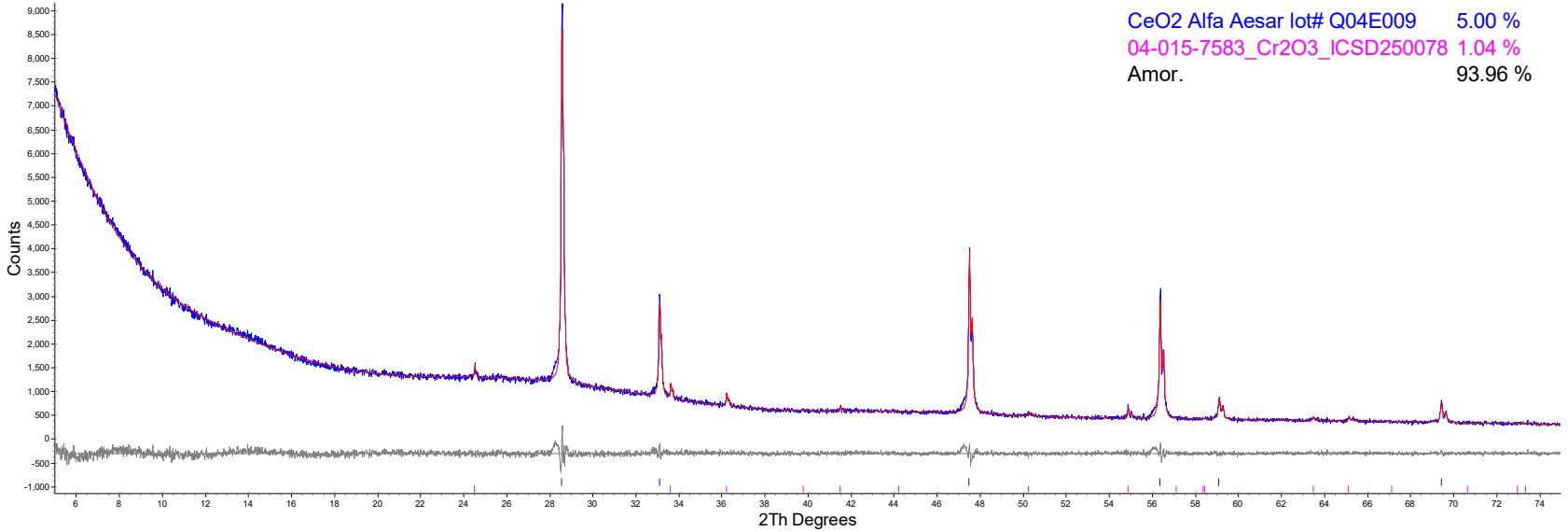

Figure D.40. Refined XRD data of HS24-40

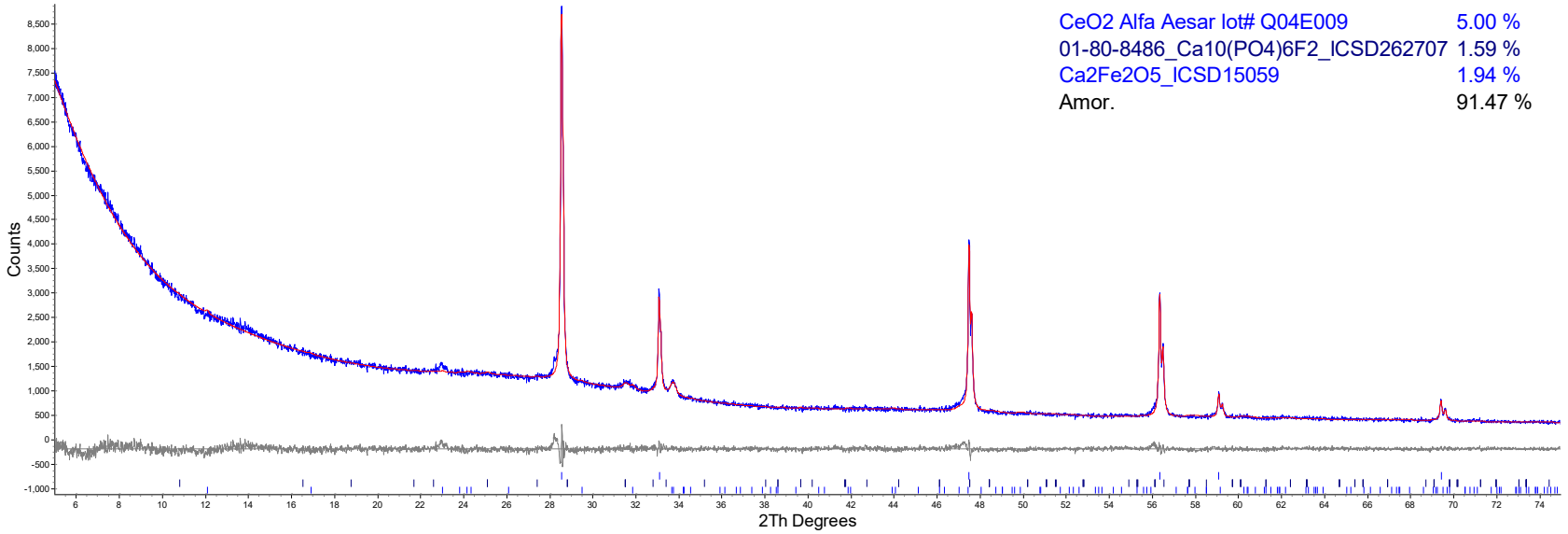

Figure D.41. Refined XRD data of HS24-41

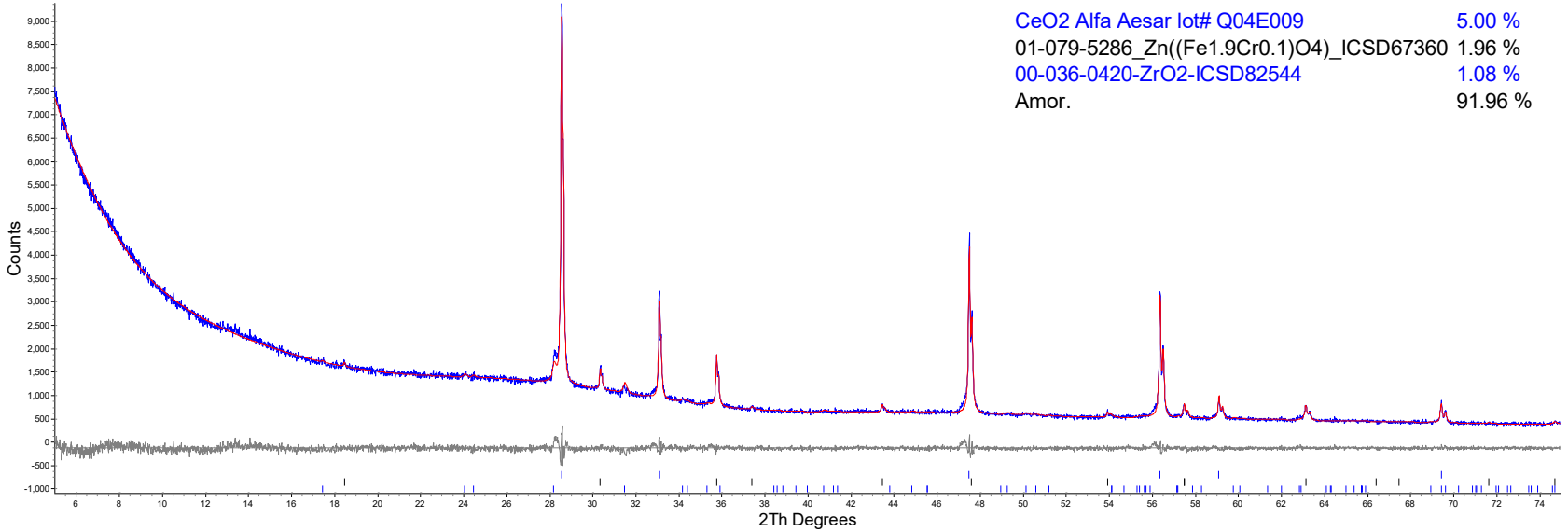

Figure D.42. Refined XRD data of HS24-42

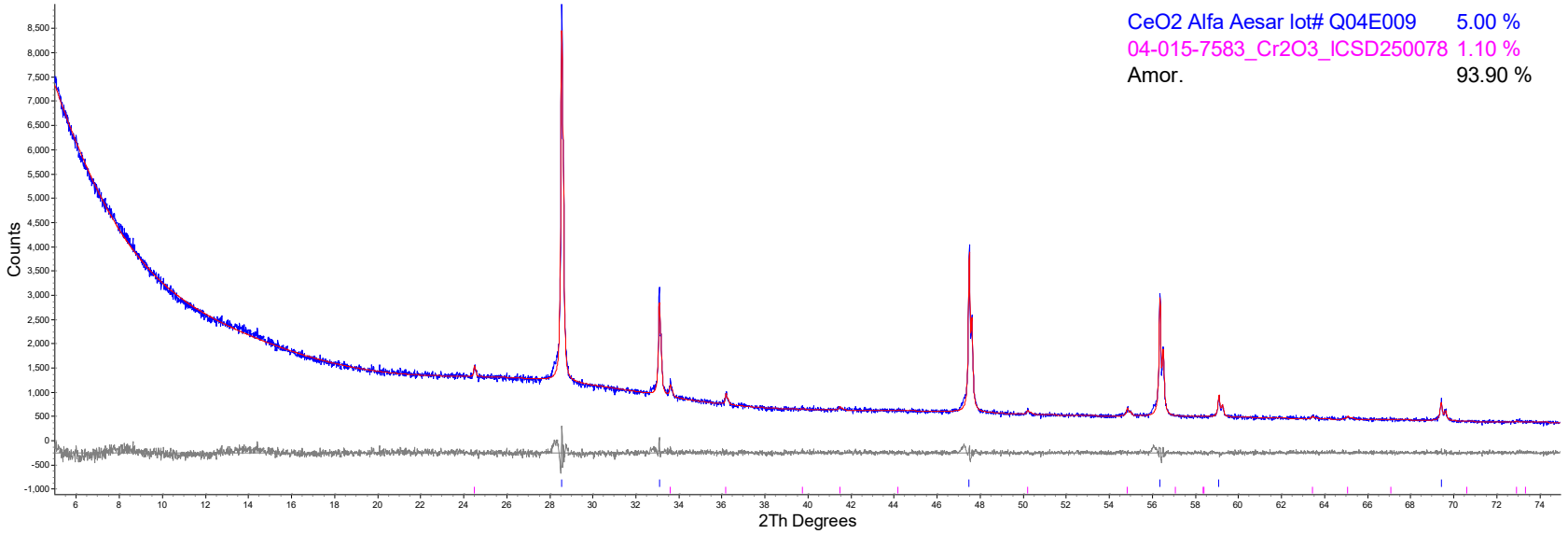

Figure D.43. Refined XRD data of HS24-43

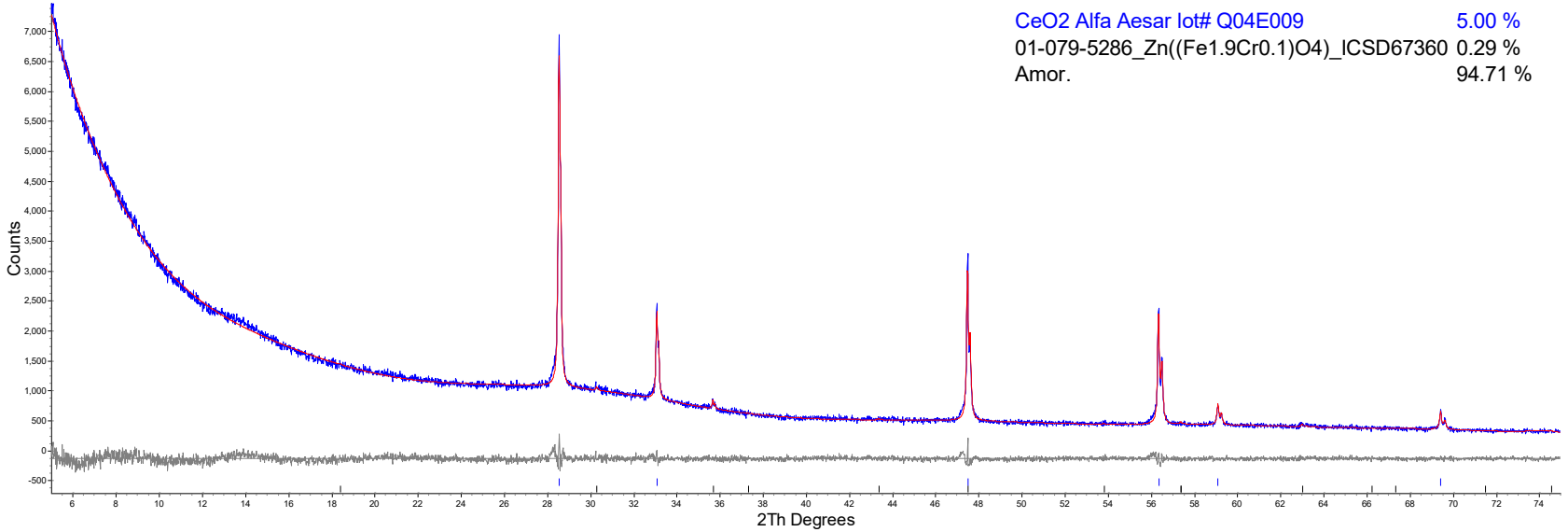

Figure D.44. Refined XRD data of HS24-44

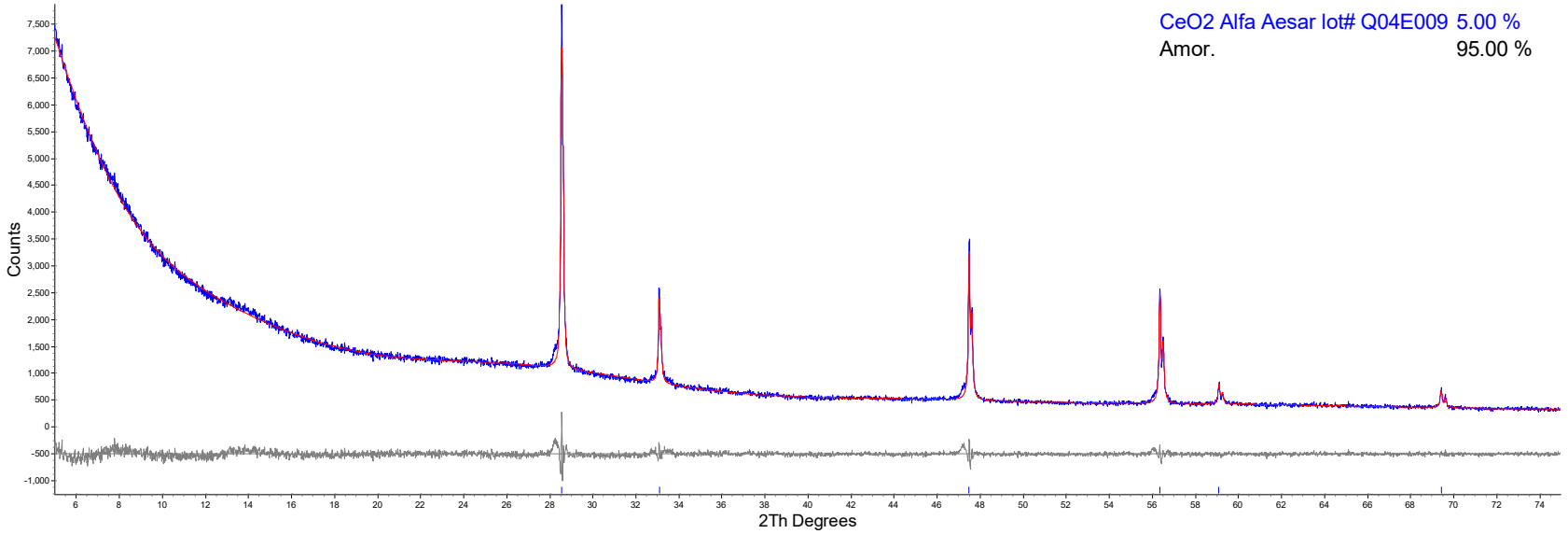

Figure D.45. Refined XRD data of HS24-45

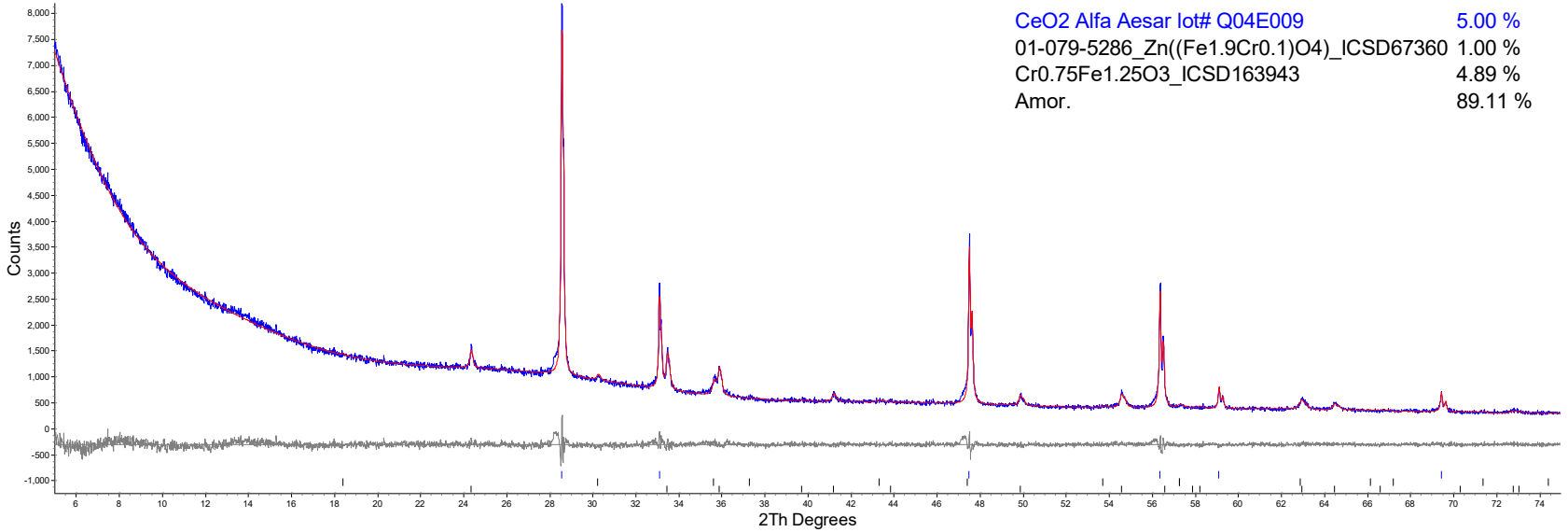

Figure D.46. Refined XRD data of HS24-46

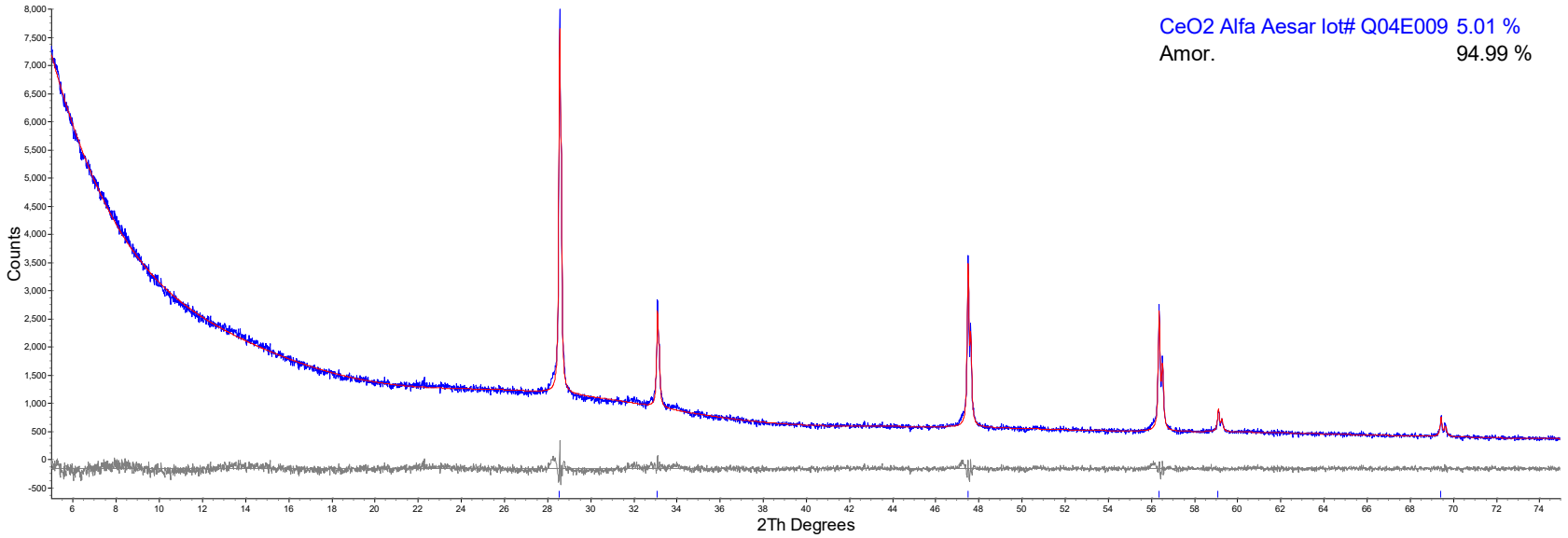

Figure D.47. Refined XRD data of HS24-47

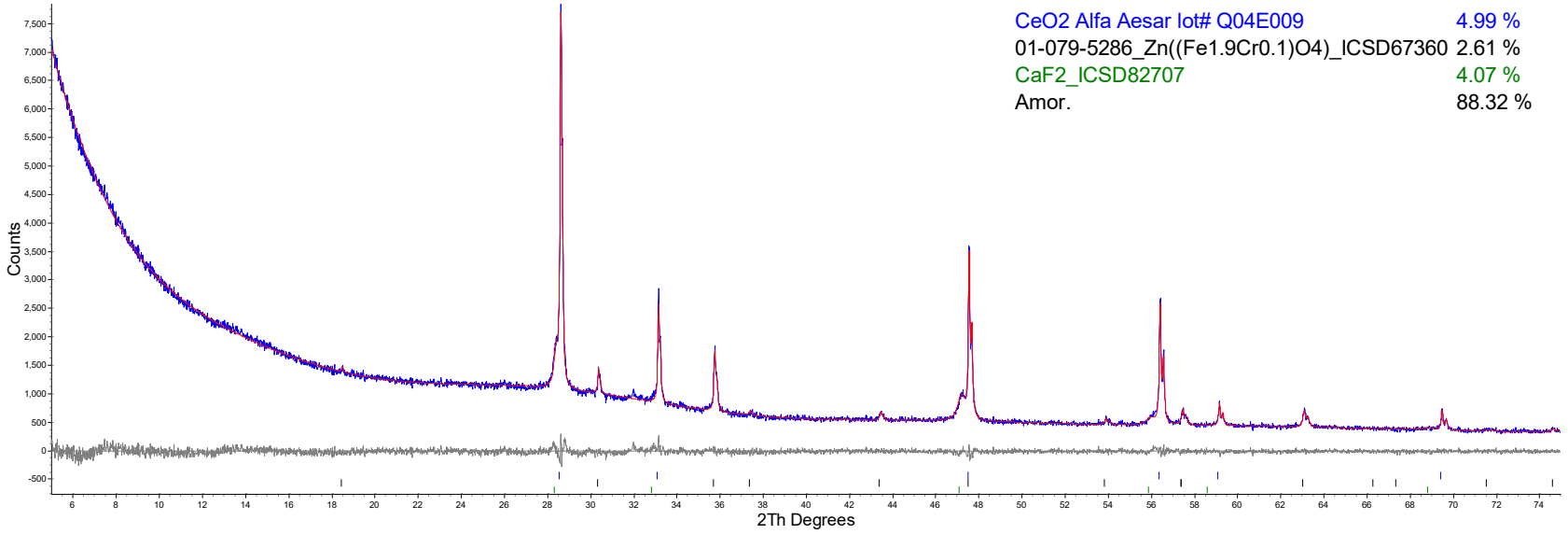

Figure D.48. Refined XRD data of HS24-48

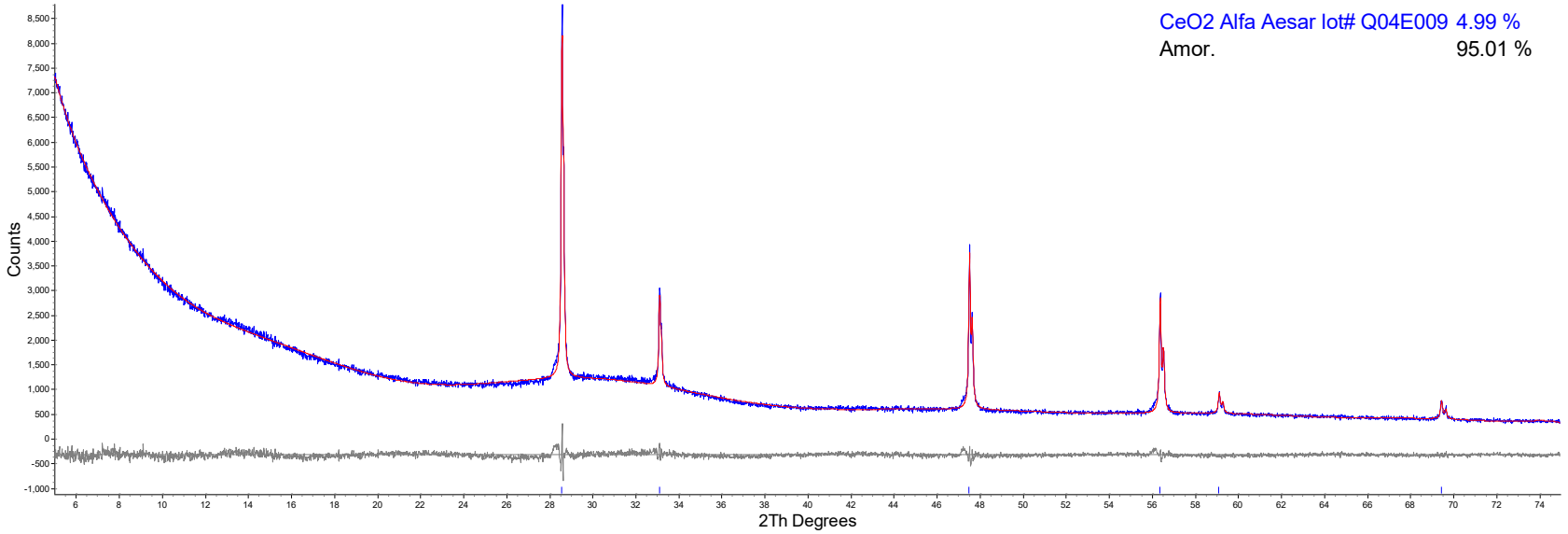

Figure D.49. Refined XRD data of HS24-49

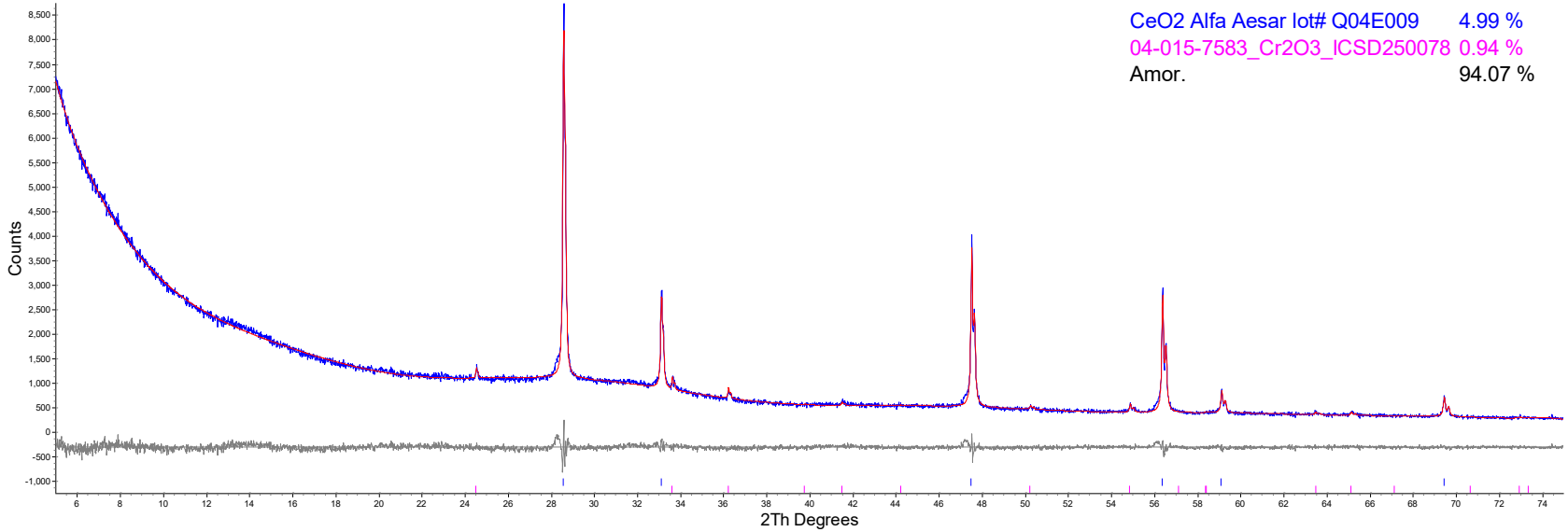

Figure D.50. Refined XRD data of HS24-50

Appendix E – Optical images of CCC glasses

The photographs in this appendix show each glass after canister centerline cooling (CCC) as described in Section 3.3. When applicable, X-ray diffraction (XRD) scans are reported in Appendix F.

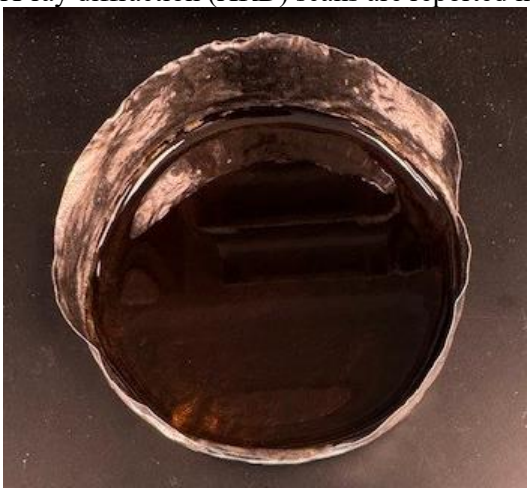

Figure E.1. Glass HS24-01 morphology after CCC.

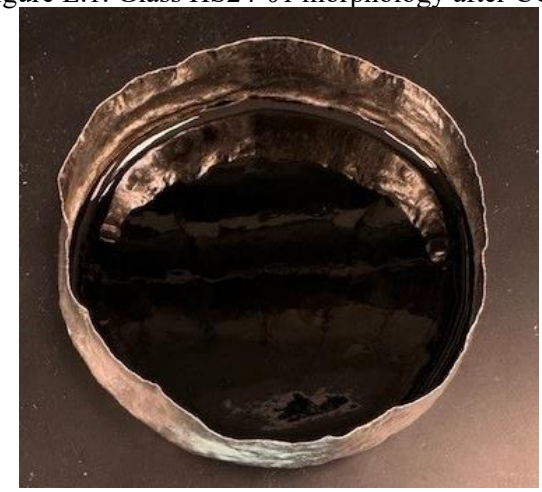

Figure E.2. Glass HS24-02 morphology after CCC.

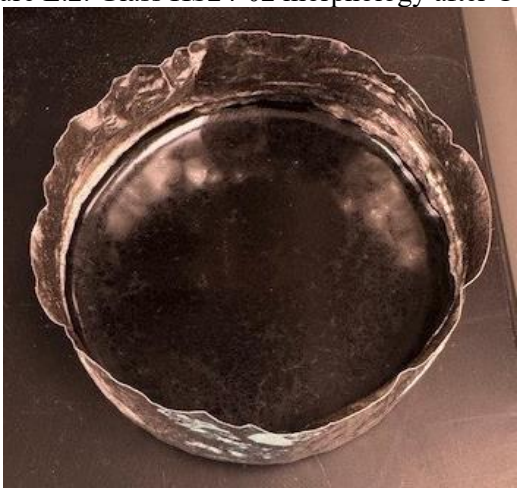

Figure E.3. Glass HS24-03 morphology after CCC.

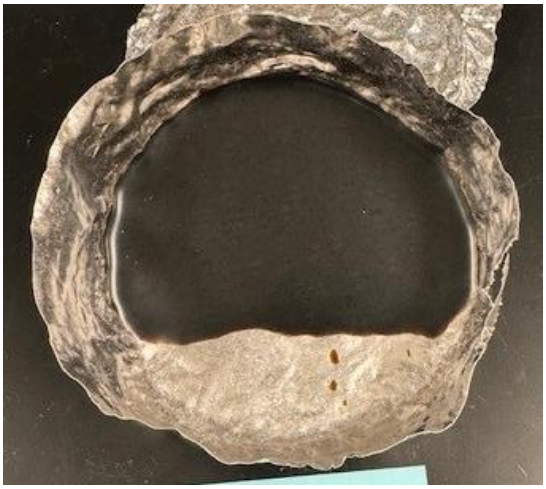

Figure E.4. Glass HS24-04 morphology after CCC.

Figure E.5. Glass HS24-05 morphology after CCC.

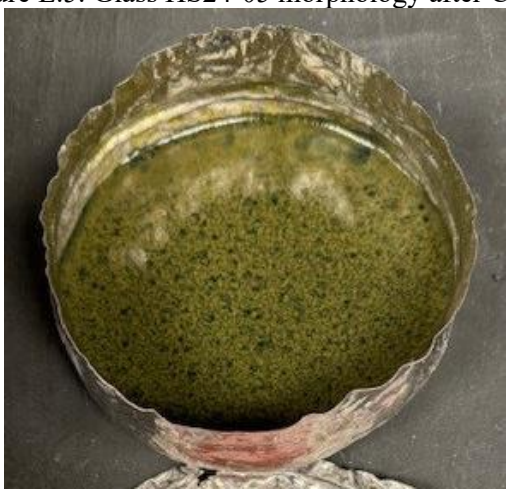

Figure E.6. Glass HS24-06 morphology after CCC.

Figure E.7. Glass HS24-07 morphology after CCC.

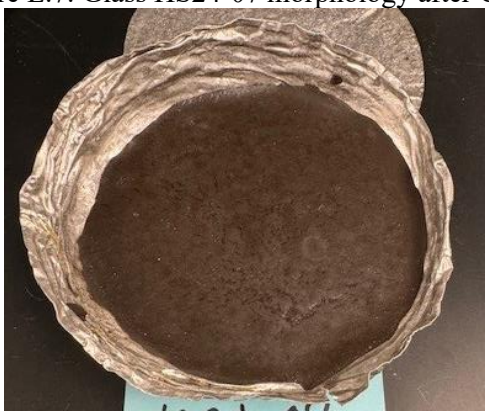

Figure E.8. Glass HS24-08 morphology after CCC.

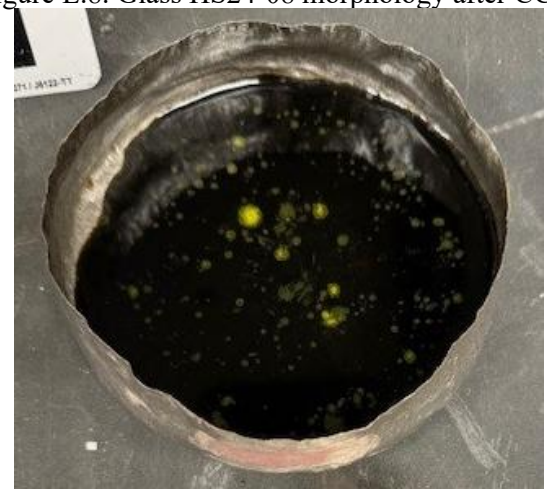

Figure E.9. Glass HS24-09 morphology after CCC.

Figure E.10. Glass HS24-10 morphology after CCC.

Figure E.11. Glass HS24-11 morphology after CCC.

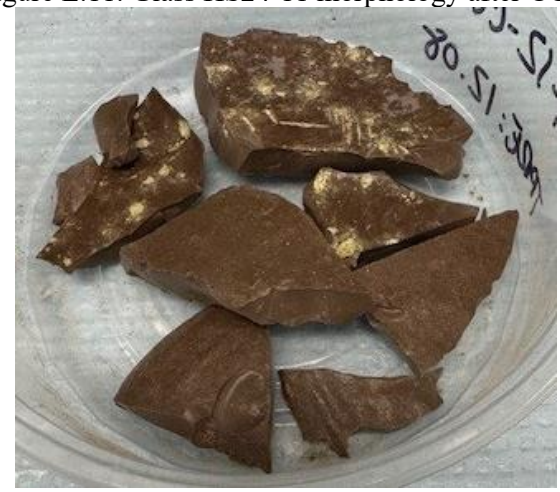

Figure E.12. Glass HS24-12 morphology after CCC.

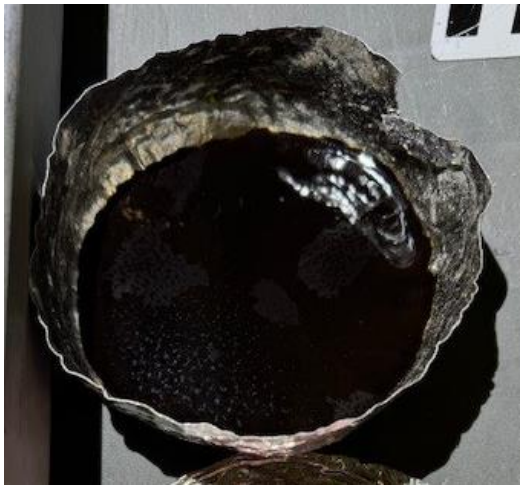

Figure E.13. Glass HS24-13 morphology after CCC.

Figure E.14. Glass HS24-14 morphology after CCC.

Figure E.15. Glass HS24-15 morphology after CCC.

Figure E.16. Glass HS24-16 morphology after CCC.

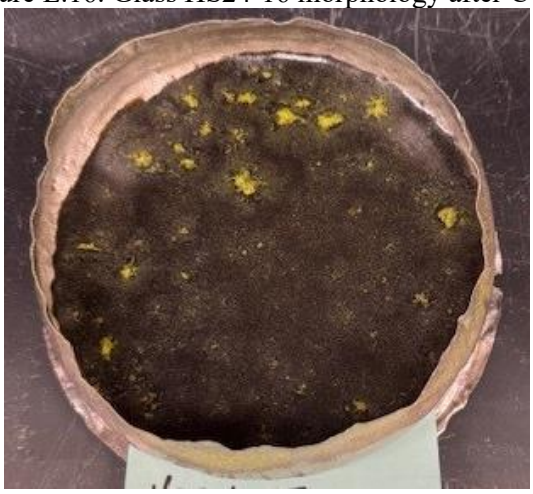

Figure E.17. Glass HS24-17 morphology after CCC.

Figure E.18. Glass HS24-18 morphology after CCC.

Figure E.19. Glass HS24-19 morphology after CCC.

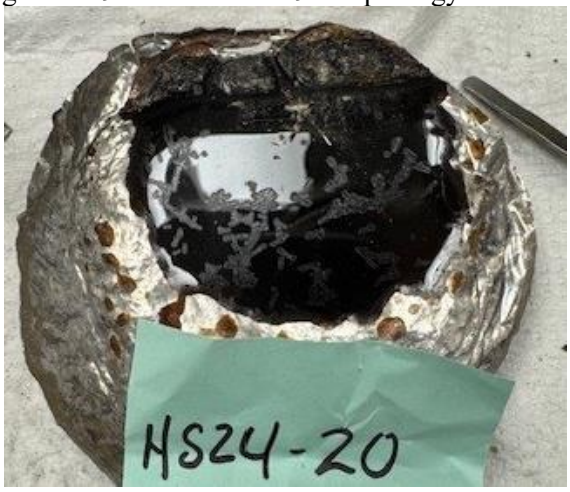

Figure E.20. Glass HS24-20 morphology after CCC.

Figure E.21. Glass HS24-21 morphology after CCC.

Figure E.22. Glass HS24-22 morphology after CCC.

Figure E.23. Glass HS24-23 morphology after CCC.

Figure E.24. Glass HS24-24 morphology after CCC.

Figure E.25. Glass HS24-25 morphology after CCC.

Figure E.26. Glass HS24-26 morphology after CCC.

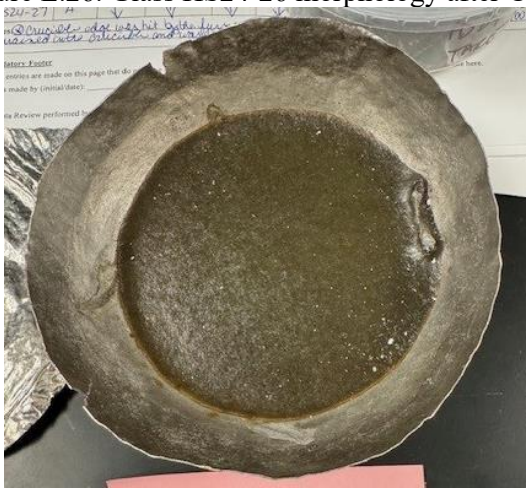

Figure E.27. Glass HS24-27 morphology after CCC.

Figure E.28. Glass HS24-28 morphology after CCC.

Figure E.29. Glass HS24-29 morphology after CCC.

Figure E.30. Glass HS24-30 morphology after CCC.

Figure E.31. Glass HS24-31 morphology after CCC.

Figure E.32. Glass HS24-32 morphology after CCC.

Figure E.33. Glass HS24-33 morphology after CCC.

Figure E.34. Glass HS24-34 morphology after CCC.

Figure E.35. Glass HS24-35 morphology after CCC.

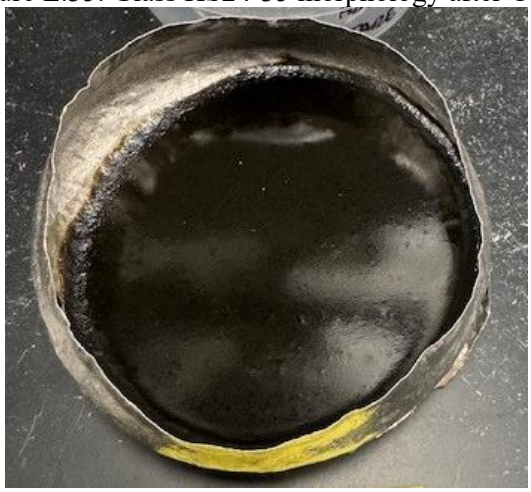

Figure E.36. Glass HS24-36 morphology after CCC.

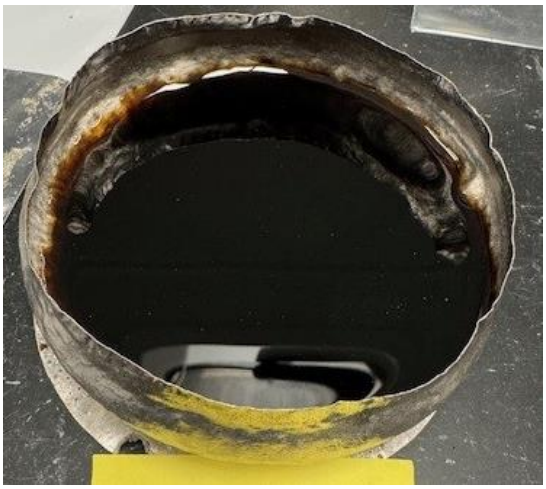

Figure E.37. Glass HS24-37 morphology after CCC.

Figure E.38. Glass HS24-38 morphology after CCC.

Figure E.39. Glass HS24-39 morphology after CCC.

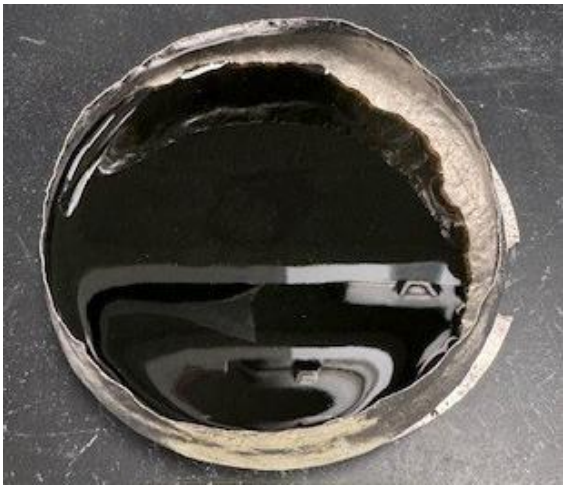

Figure E.40. Glass HS24-40 morphology after CCC.

Figure E.41. Glass HS24-41 morphology after CCC.

Figure E.42. Glass HS24-42 morphology after CCC.

Figure E.43. Glass HS24-43 morphology after CCC.

Figure E.44. Glass HS24-44 morphology after CCC.

Figure E.45. Glass HS24-45 morphology after CCC.

Figure E.46. Glass HS24-46 morphology after CCC.

Figure E.47. Glass HS24-47 morphology after CCC.

Figure E.48. Glass HS24-48 morphology after CCC.

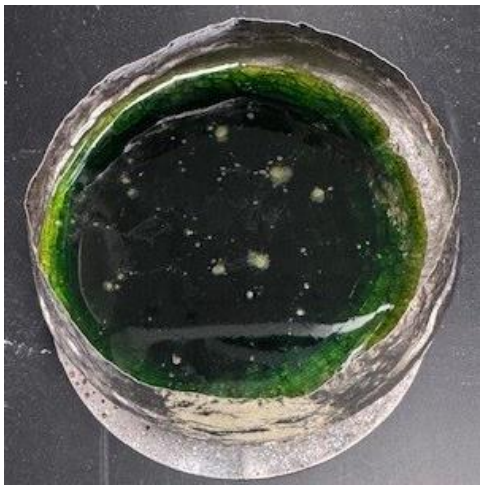

Figure E.49. Glass HS24-49 morphology after CCC.

Figure E.50. Glass HS24-50 morphology after CCC.

Appendix F – XRD results of CCC glasses

These are the X-ray diffraction (XRD) scans showing the main crystal phases present after canister centerline cooling (CCC) of the glasses photographed in Appendix E. The percentage of crystal content (wt%) reported in the XRD scans is presented before any adjustments were made from spiking with 5 wt% of high-purity TiO_2 anatase as an internal standard. XRD scans are not included when the glass maintains an amorphous structure.

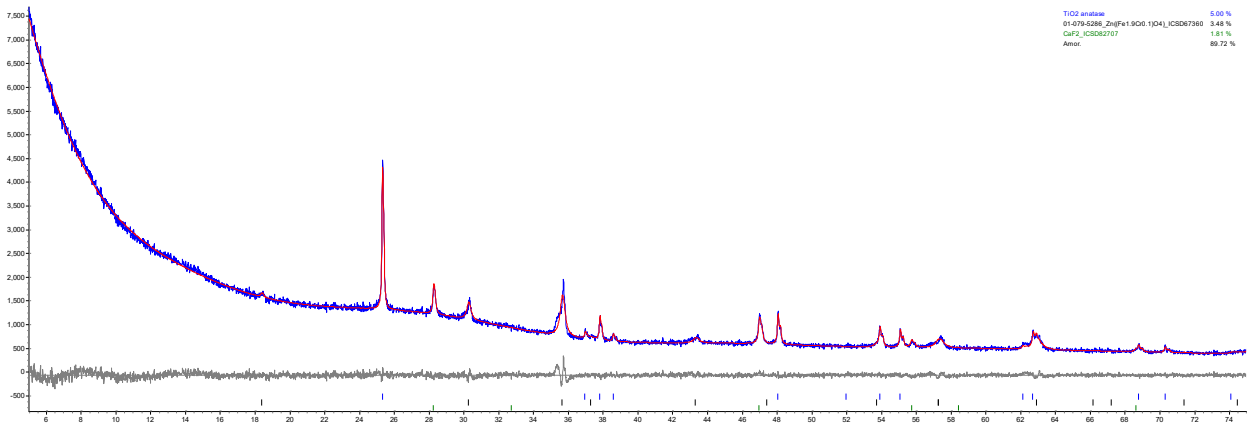

Phase Name	Wt% Measured	Wt% Corrected	Wt% Normalized
TiO_2 anatase	5.00	4.56	-
$ZnFe_{1.9}Cr_{0.1}O_4$	3.48	3.17	3.34
CaF_2	1.81	1.65	1.74

Figure F.1. XRD scan of glass HS24-03 after CCC.

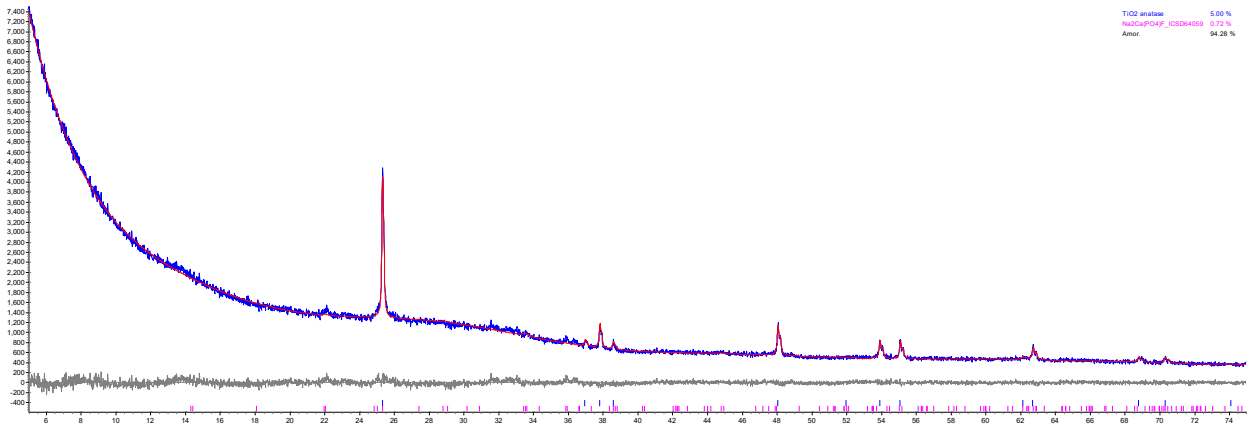

Phase Name	Wt% Measured	Wt% Corrected	Wt% Normalized
TiO_2 anatase	5.00	4.56	-
$Na_2Ca(PO_4)F$	0.72	0.66	0.69

Figure F.2. XRD scan of glass HS24-04 after CCC.

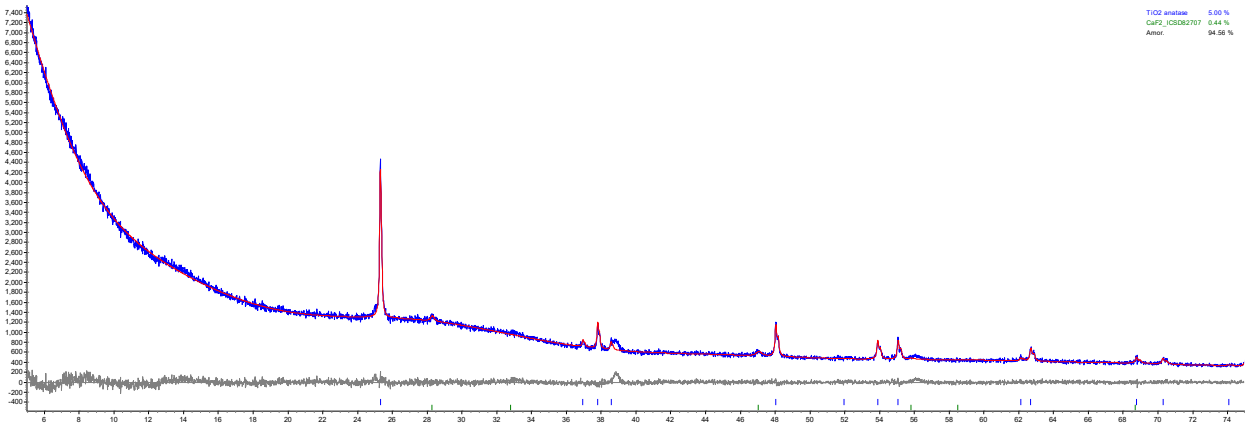

Phase Name	Wt% Measured	Wt% Corrected	Wt% Normalized
TiO_2 anatase	5.00	4.56	-
CaF_2	0.44	0.40	0.42

Figure F.3. XRD scan of glass HS24-05 after CCC.

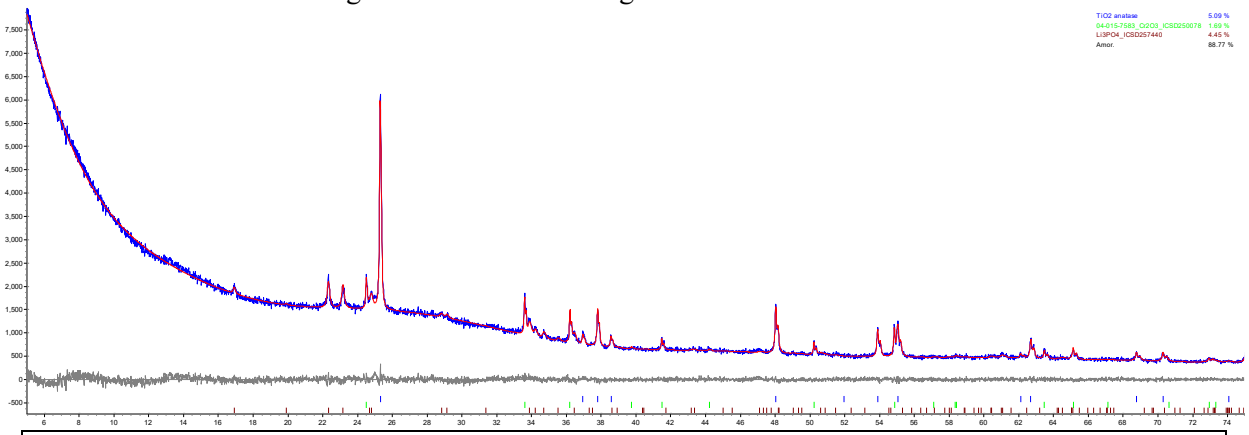

Phase Name	Wt% Measured	Wt% Corrected	Wt% Normalized
TiO_2 anatase	5.09	4.64	-
Cr_2O_3	1.69	1.55	1.63
Li_3PO_4	4.45	4.06	4.28

Figure F.4. XRD scan of glass HS24-06 after CCC.

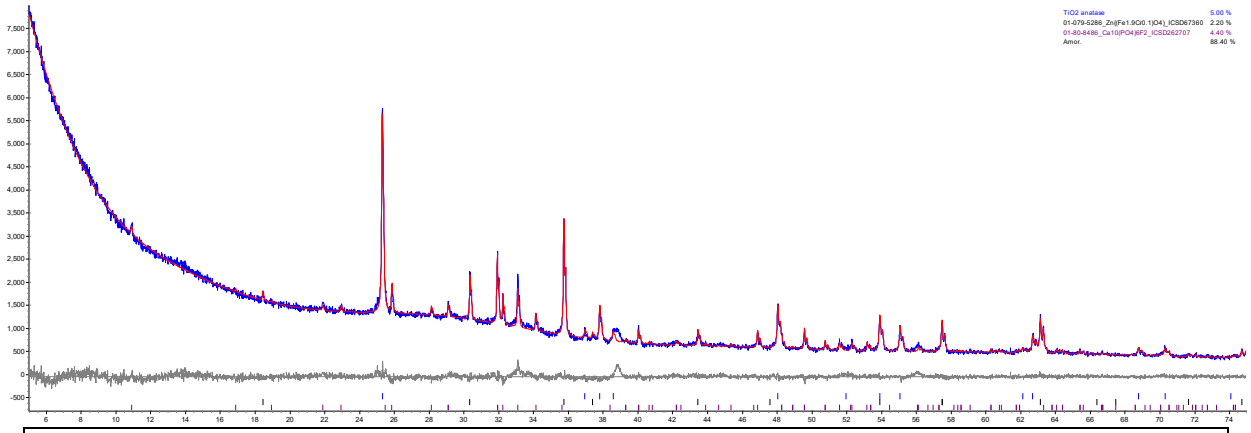

Phase Name	Wt% Measured	Wt% Corrected	Wt% Normalized
TiO_2 anatase	5.00	4.56	-
$ZnFe_{1.9}Cr_{0.1}O_4$	2.20	2.01	2.11
$Ca_{10}(PO_4)_6F_2$	4.40	4.01	4.23

Figure F.5. XRD scan of glass HS24-07 after CCC.

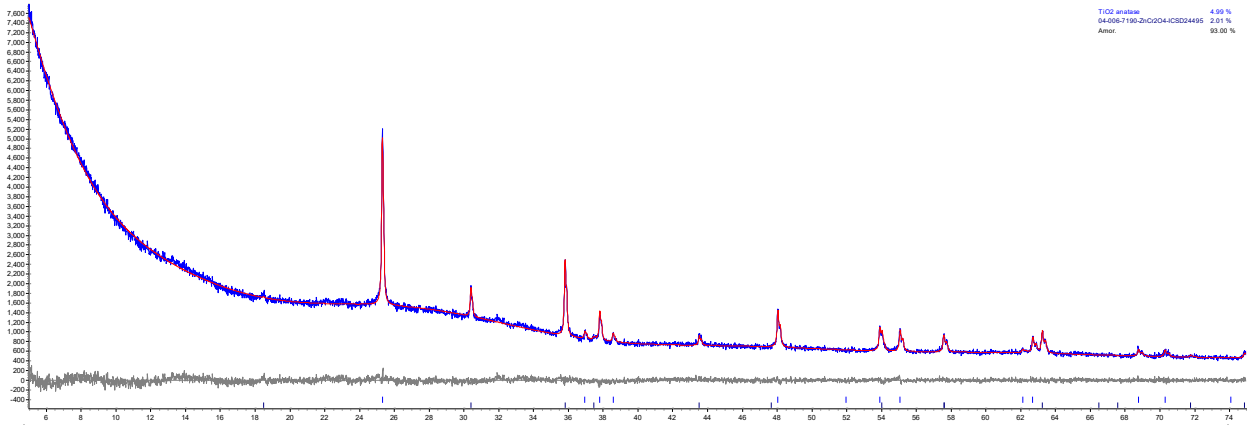

Phase Name	Wt% Measured	Wt% Corrected	Wt% Normalized
TiO_2 anatase	4.99	4.56	-
$ZnCr_2O_4$	2.01	1.84	1.93

Figure F.6. XRD scan of glass HS24-08 after CCC.

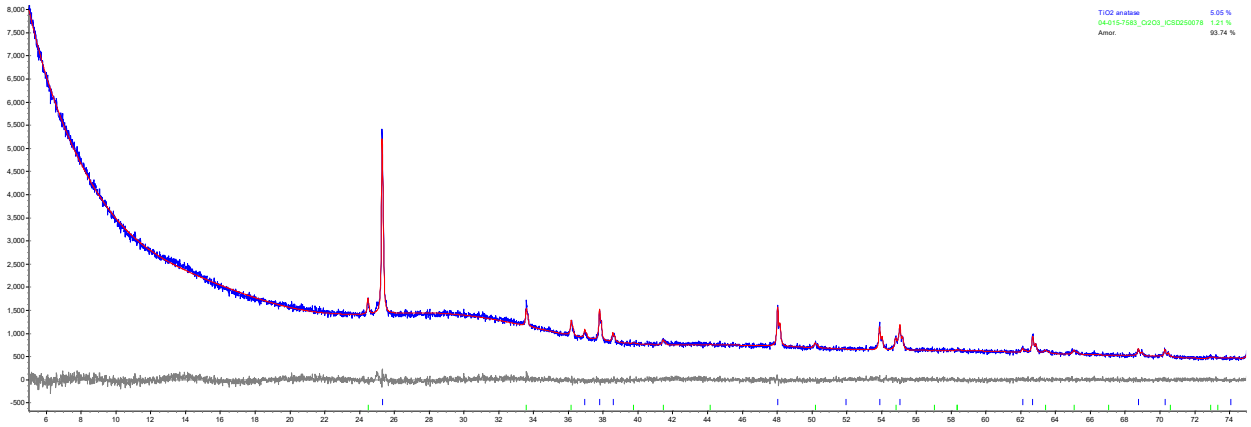

Phase Name	Wt% Measured	Wt% Corrected	Wt% Normalized
TiO_2 anatase	5.05	4.61	-
Cr_2O_3	1.21	1.10	1.16

Figure F.7. XRD scan of glass HS24-09 after CCC.

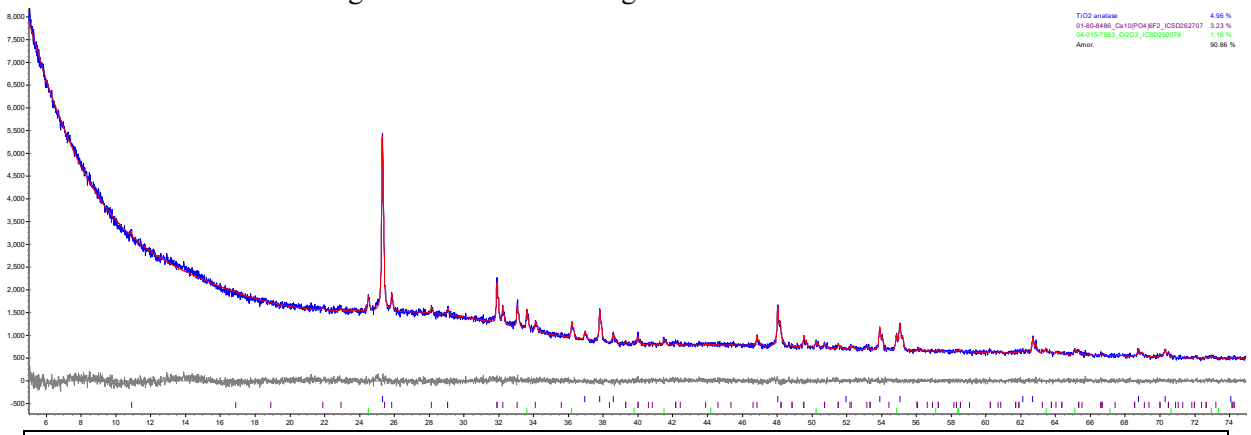

Phase Name	Wt% Measured	Wt% Corrected	Wt% Normalized
TiO_2 anatase	4.96	4.52	-
Cr_2O_3	1.16	1.06	1.11
$Ca_{10}(PO_4)_6F_2$	3.23	2.95	3.10

Figure F.8. XRD scan of glass HS24-10 after CCC.

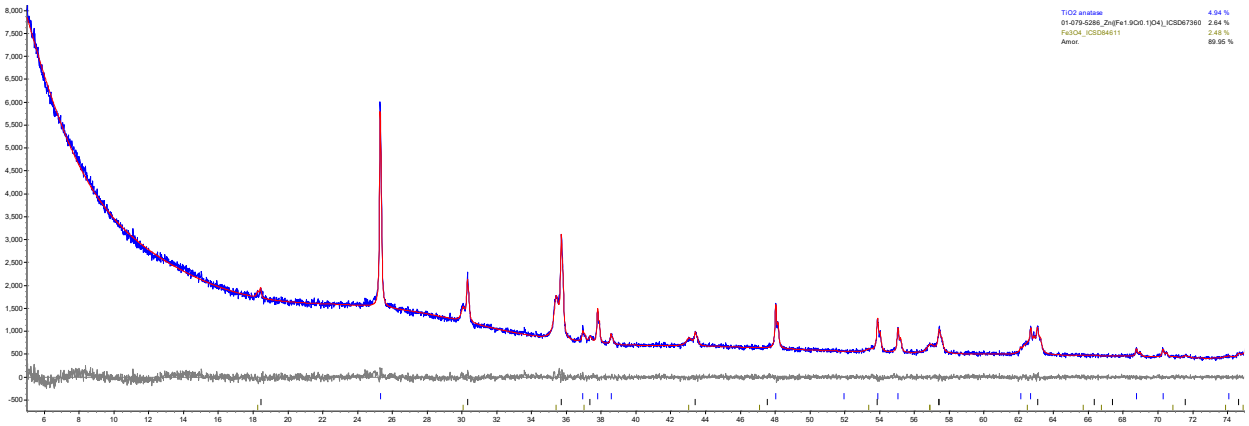

Phase Name	Wt% Measured	Wt% Corrected	Wt% Normalized
TiO_2 anatase	4.94	4.50	-
$ZnFe_{1.9}Cr_{0.1}O_4$	2.64	2.41	2.53
Fe_3O_4	2.48	2.26	2.38

Figure F.9. XRD scan of glass HS24-11 after CCC.

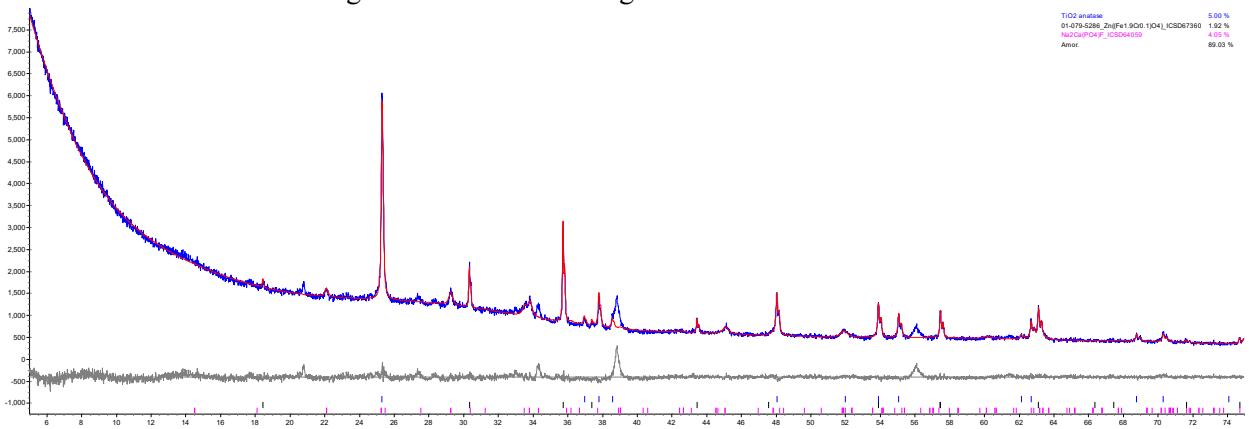

Phase Name	Wt% Measured	Wt% Corrected	Wt% Normalized
TiO_2 anatase	5.00	4.56	-
$ZnFe_{1.9}Cr_{0.1}O_4$	1.92	1.75	1.85
$Na_2Ca(PO_4)F$	4.05	3.70	3.89

Figure F.10. XRD scan of glass HS24-12 after CCC.

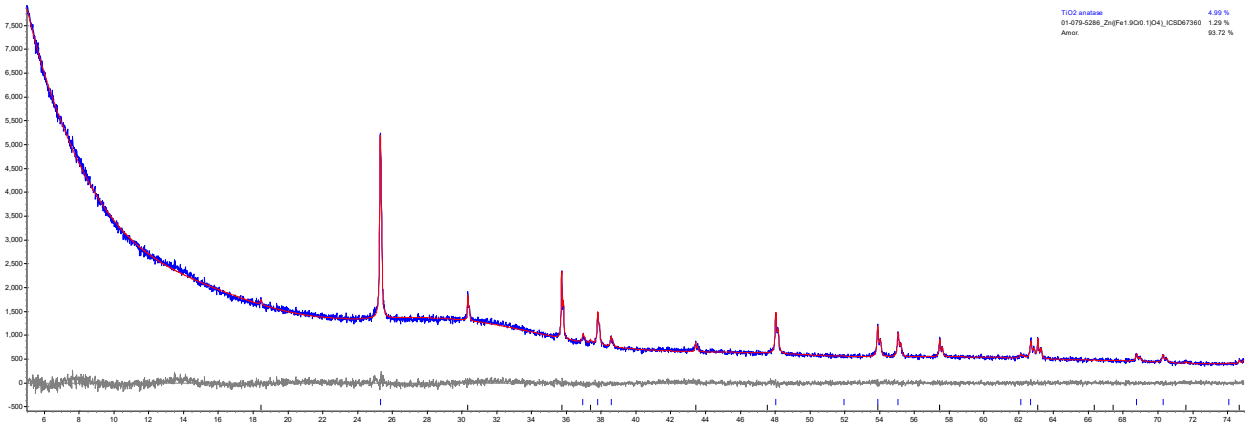

Phase Name	Wt% Measured	Wt% Corrected	Wt% Normalized
TiO_2 anatase	4.99	4.56	-
$ZnFe_{1.9}Cr_{0.1}O_4$	1.29	1.18	1.24

Figure F.11. XRD scan of glass HS24-13 after CCC.

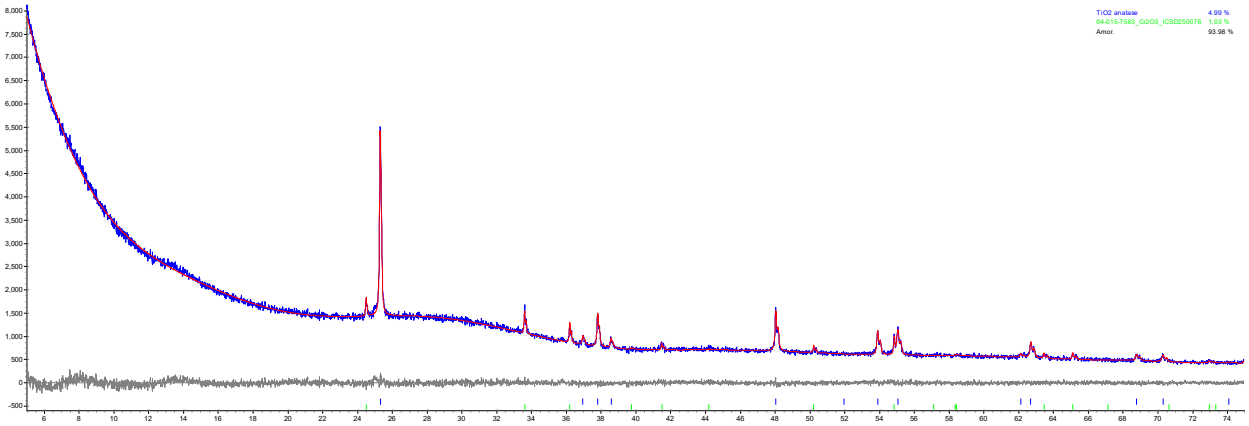

Phase Name	Wt% Measured	Wt% Corrected	Wt% Normalized
TiO_2 anatase	4.99	4.55	-
Cr_2O_3	1.03	0.94	0.99

Figure F.12. XRD scan of glass HS24-14 after CCC.

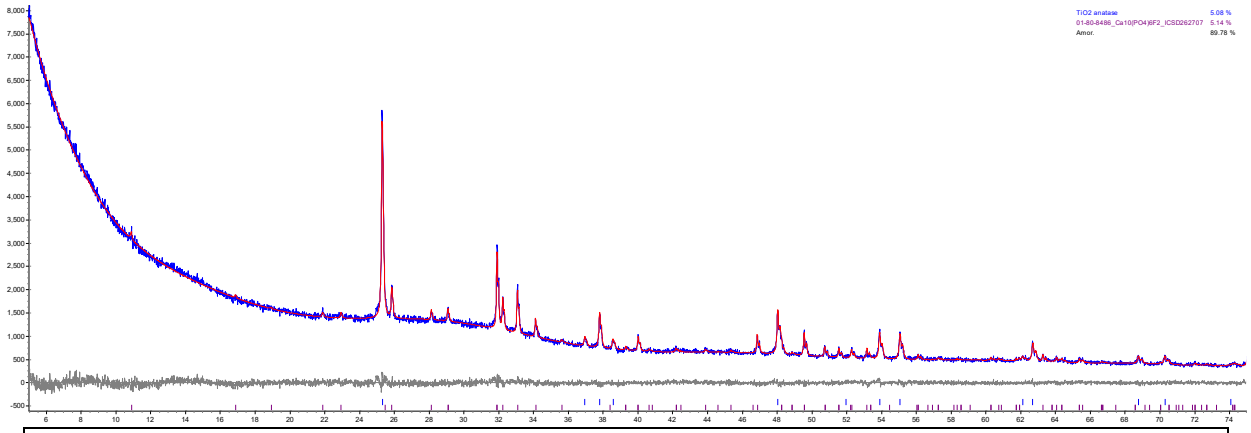

Phase Name	Wt% Measured	Wt% Corrected	Wt% Normalized
TiO_2 anatase	5.08	4.64	-
$Ca_{10}(PO_4)_6F_2$	5.14	4.69	4.94

Figure F.13. XRD scan of glass HS24-15 after CCC.

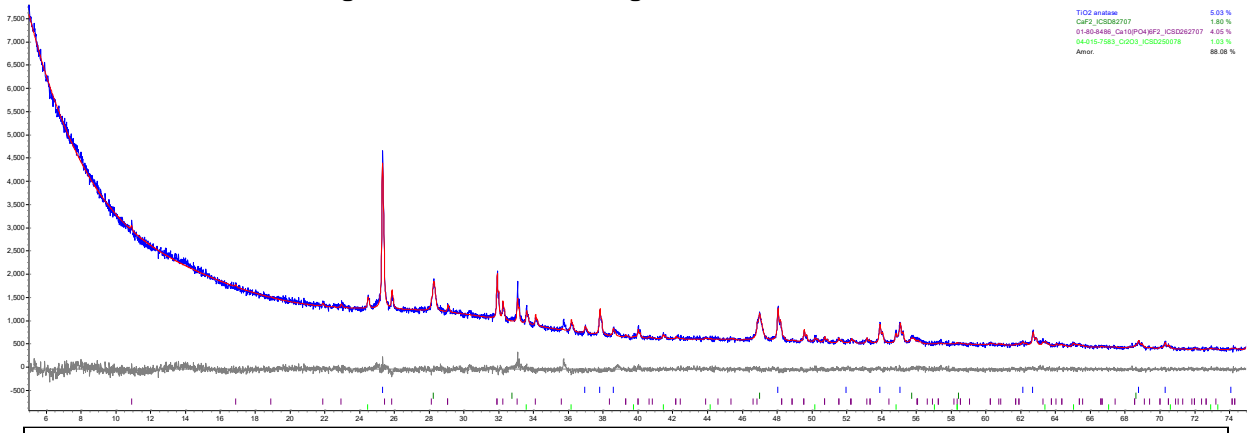

Phase Name	Wt% Measured	Wt% Corrected	Wt% Normalized
TiO_2 anatase	5.03	4.59	-
$Ca_{10}(PO_4)_6F_2$	4.05	3.70	3.90
CaF_2	1.80	1.65	1.73
Cr_2O_3	1.03	0.94	0.99

Figure F.14. XRD scan of glass HS24-16 after CCC.

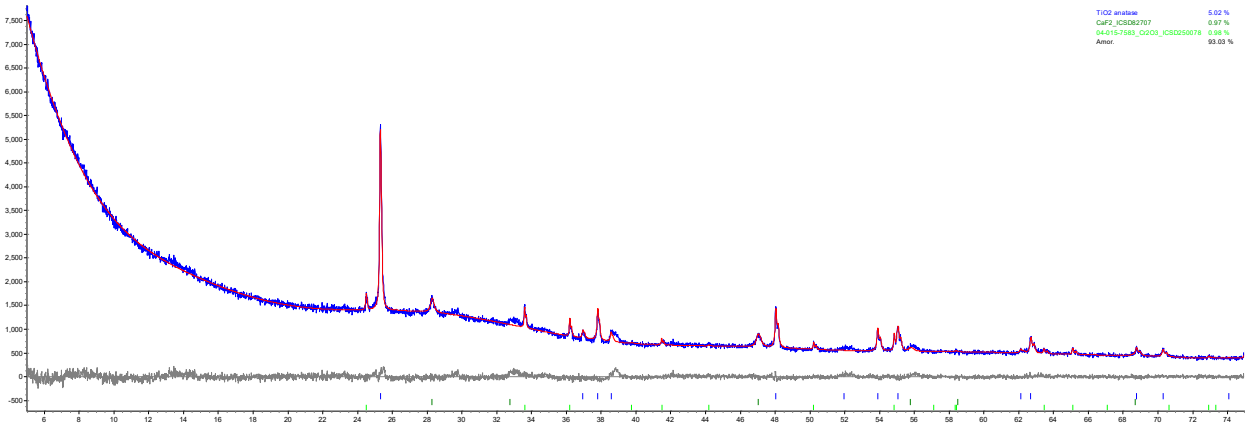

Phase Name	Wt% Measured	Wt% Corrected	Wt% Normalized
TiO_2 anatase	5.02	4.58	-
Cr_2O_3	0.98	0.89	0.94
CaF_2	0.97	0.88	0.93

Figure F.15. XRD scan of glass HS24-17 after CCC.

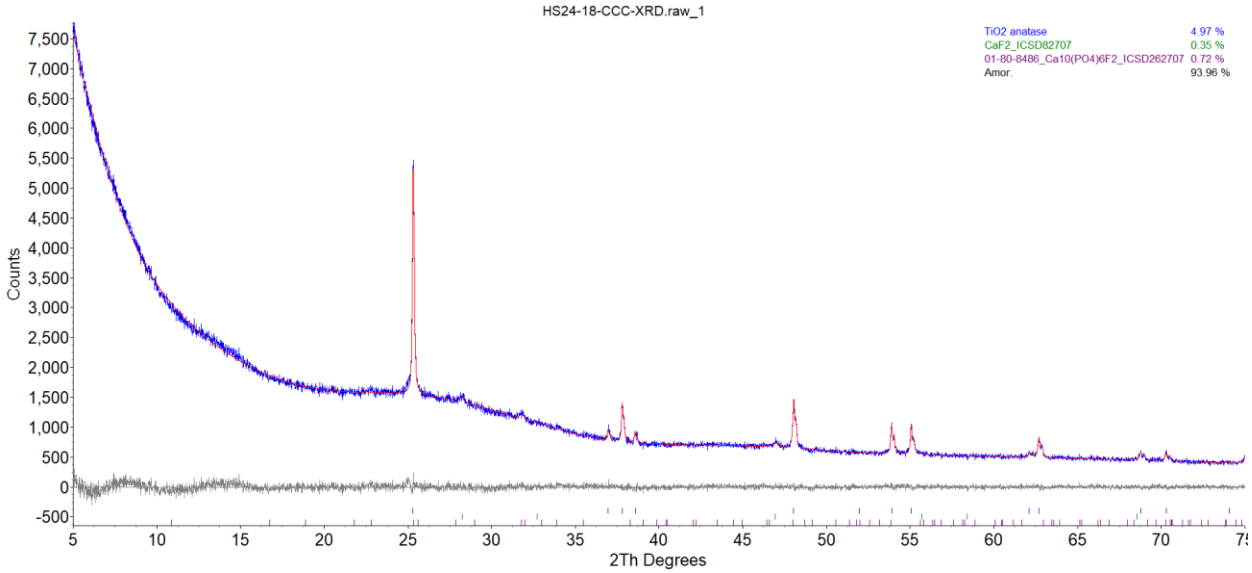

Phase Name	Wt% Measured	Wt% Corrected	Wt% Normalized
TiO_2 anatase	4.97	4.54	-
$Ca_{10}(PO_4)_6F_2$	0.72	0.66	0.69
CaF_2	0.35	0.32	0.34

Figure F.16. XRD scan of glass HS24-18 after CCC.

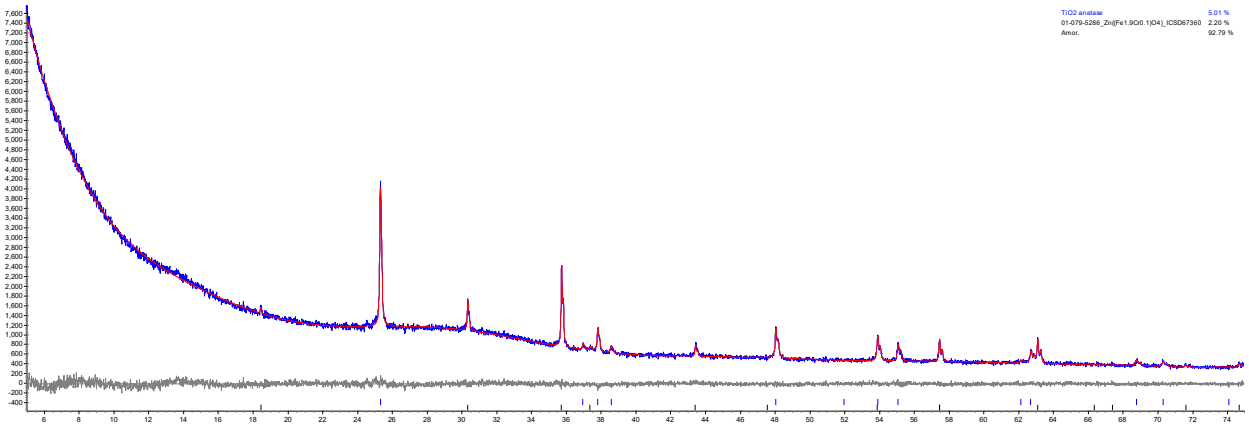

Phase Name	Wt% Measured	Wt% Corrected	Wt% Normalized
TiO_2 anatase	5.01	4.58	-
$ZnFe_{1.9}Cr_{0.1}O_4$	2.20	2.01	2.11

Figure F.17. XRD scan of glass HS24-19 after CCC.

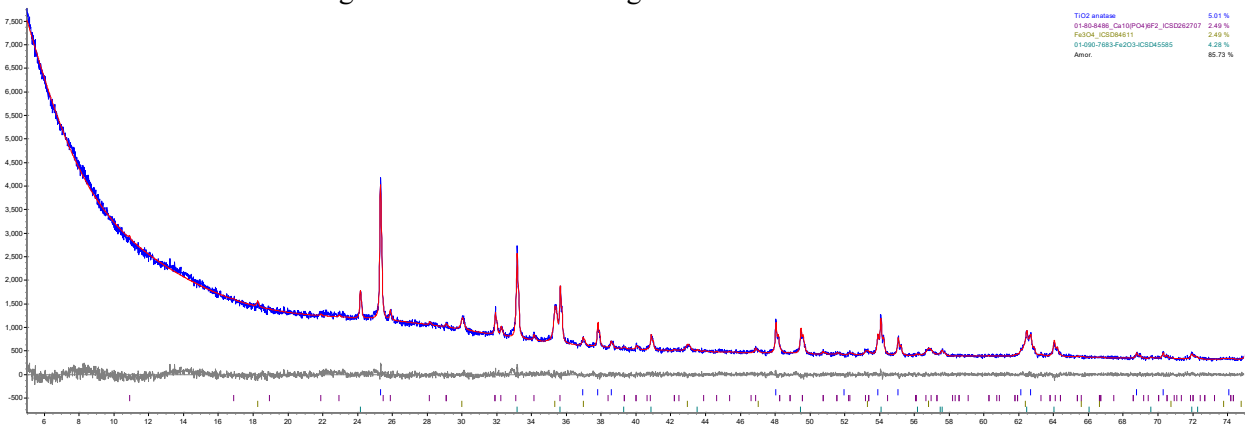

Phase Name	Wt% Measured	Wt% Corrected	Wt% Normalized
TiO_2 anatase	5.01	4.57	-
Fe_3O_4	2.49	2.27	2.39
$Ca_{10}(PO_4)_6F_2$	2.49	2.28	2.40
Fe_2O_3	4.28	3.91	4.11

Figure F.18. XRD scan of glass HS24-21 after CCC.

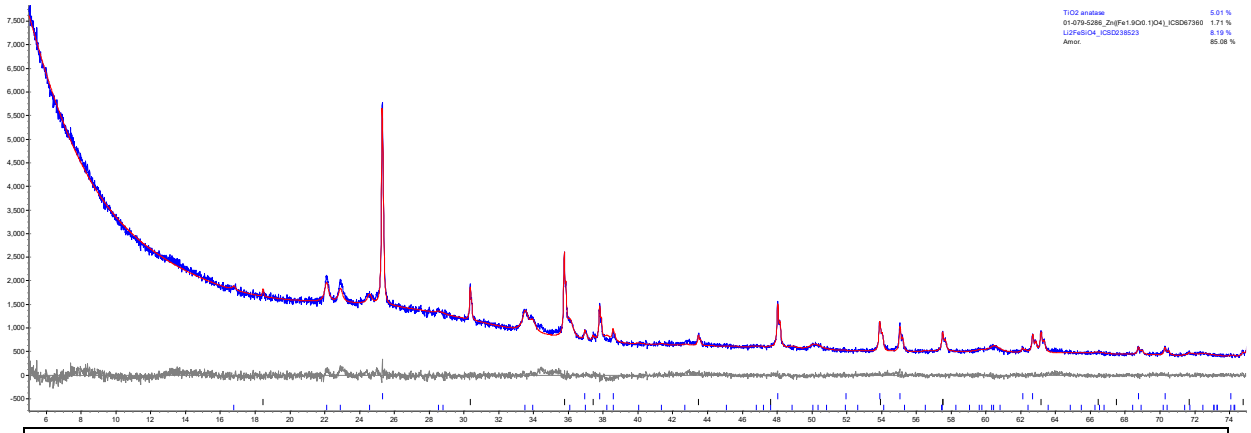

Phase Name	Wt% Measured	Wt% Corrected	Wt% Normalized
TiO_2 anatase	5.01	4.57	-
$ZnFe_{1.9}Cr_{0.1}O_4$	1.71	1.56	1.65
Li_2FeSiO_4	8.19	7.48	7.87

Figure F.19. XRD scan of glass HS24-22 after CCC.

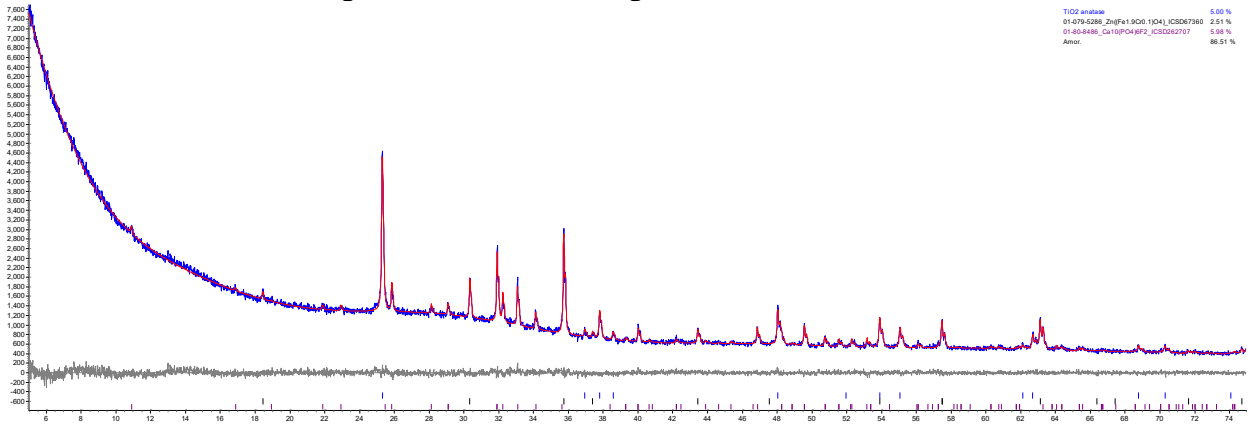

Phase Name	Wt% Measured	Wt% Corrected	Wt% Normalized
TiO_2 anatase	5.00	4.56	-
$ZnFe_{1.9}Cr_{0.1}O_4$	2.51	2.29	2.42
$Ca_{10}(PO_4)_6F_2$	5.98	5.46	5.74

Figure F.20. XRD scan of glass HS24-23 after CCC.

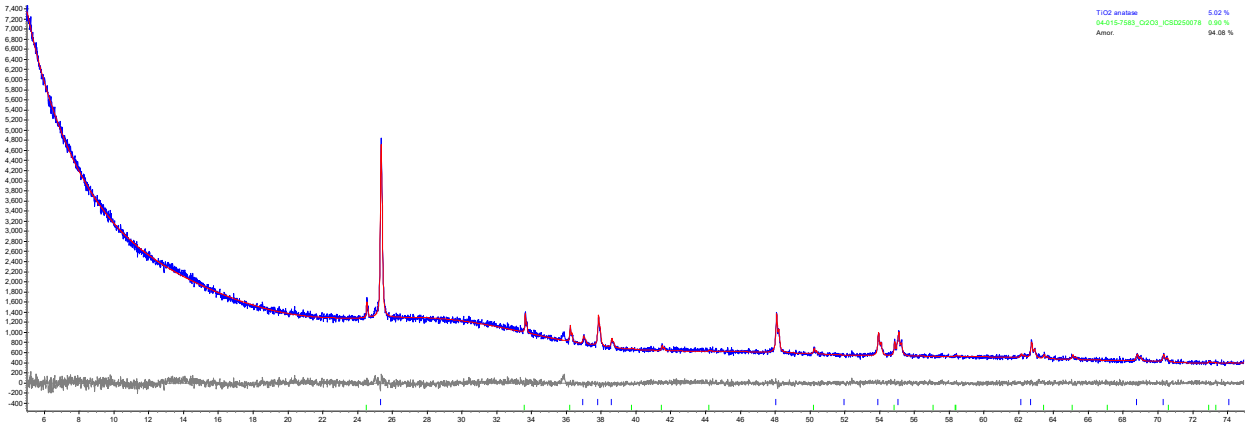

Phase Name	Wt% Measured	Wt% Corrected	Wt% Normalized
TiO_2 anatase	5.02	4.58	-
Cr_2O_3	0.90	0.82	0.86

Figure F.21. XRD scan of glass HS24-24 after CCC.

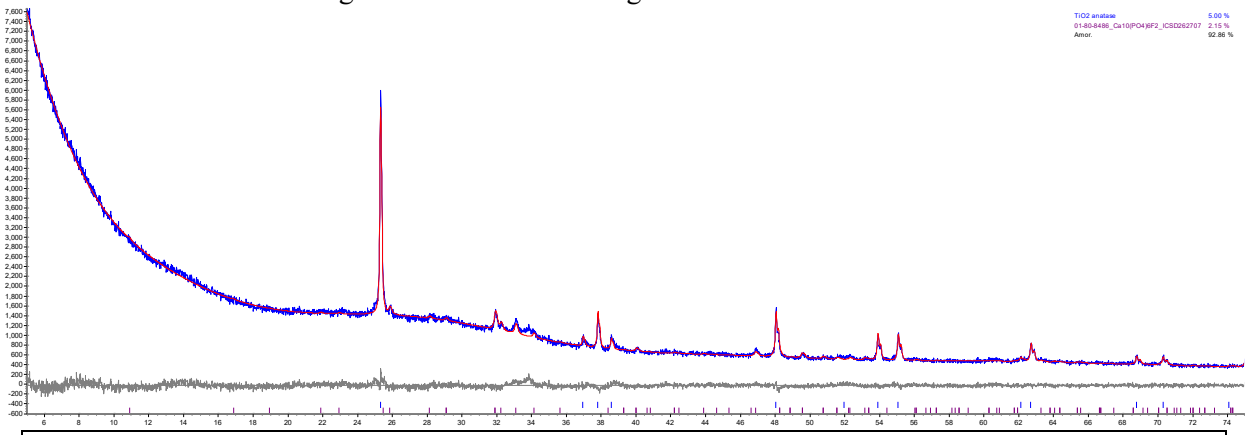

Phase Name	Wt% Measured	Wt% Corrected	Wt% Normalized
TiO_2 anatase	5.00	4.56	-
$Ca_{10}(PO_4)_6F_2$	2.15	1.96	2.06

Figure F.22. XRD scan of glass HS24-25 after CCC.

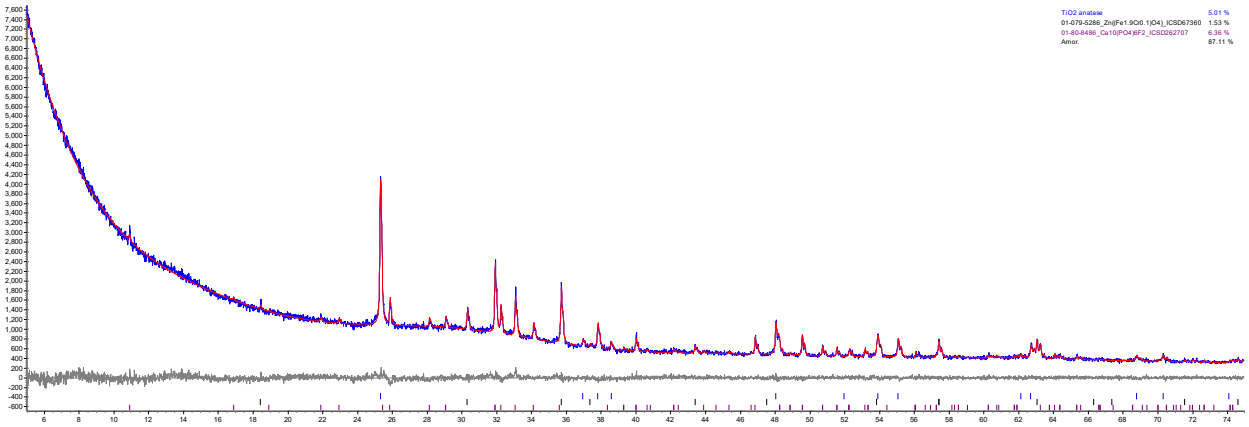

Phase Name	Wt% Measured	Wt% Corrected	Wt% Normalized
TiO_2 anatase	5.01	4.57	-
$ZnFe_{1.9}Cr_{0.1}O_4$	1.53	1.39	1.47
$Ca_{10}(PO_4)_6F_2$	6.36	5.80	6.11

Figure F.23. XRD scan of glass HS24-26 after CCC.

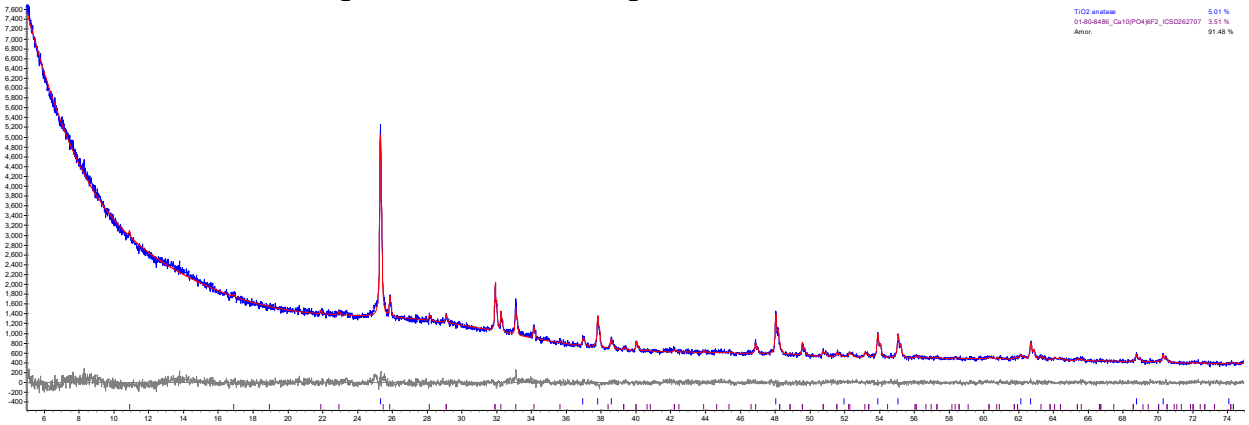

Phase Name	Wt% Measured	Wt% Corrected	Wt% Normalized
TiO_2 anatase	5.01	4.57	-
$Ca_{10}(PO_4)_6F_2$	3.51	3.20	3.37

Figure F.24. XRD scan of glass HS24-27 after CCC.

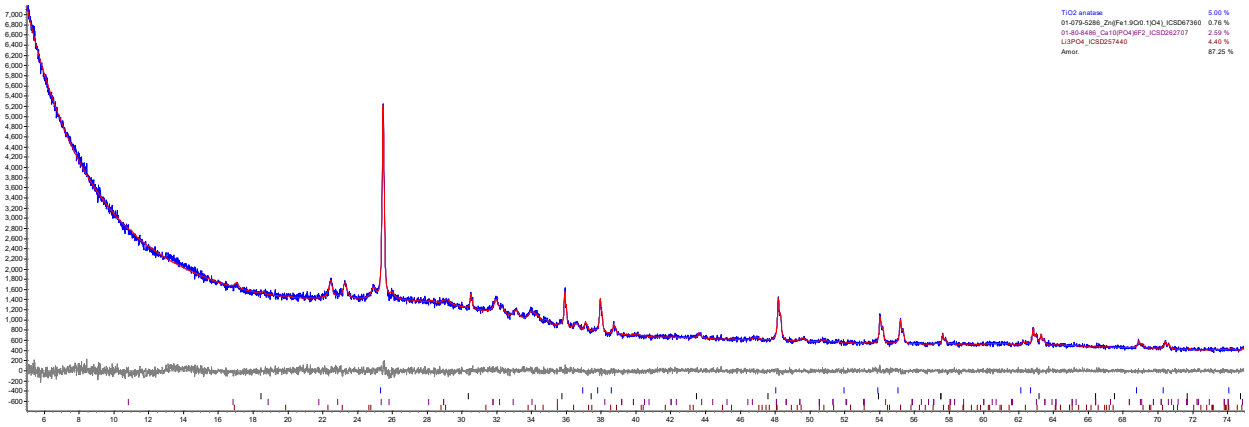

Phase Name	Wt% Measured	Wt% Corrected	Wt% Normalized
TiO_2 anatase	5.00	4.56	-
$ZnFe_{1.9}Cr_{0.1}O_4$	0.76	0.69	0.73
$Ca_{10}(PO_4)_6F_2$	2.59	2.36	2.49
Li_3PO_4	4.41	4.02	4.23

Figure F.25. XRD scan of glass HS24-28 after CCC.

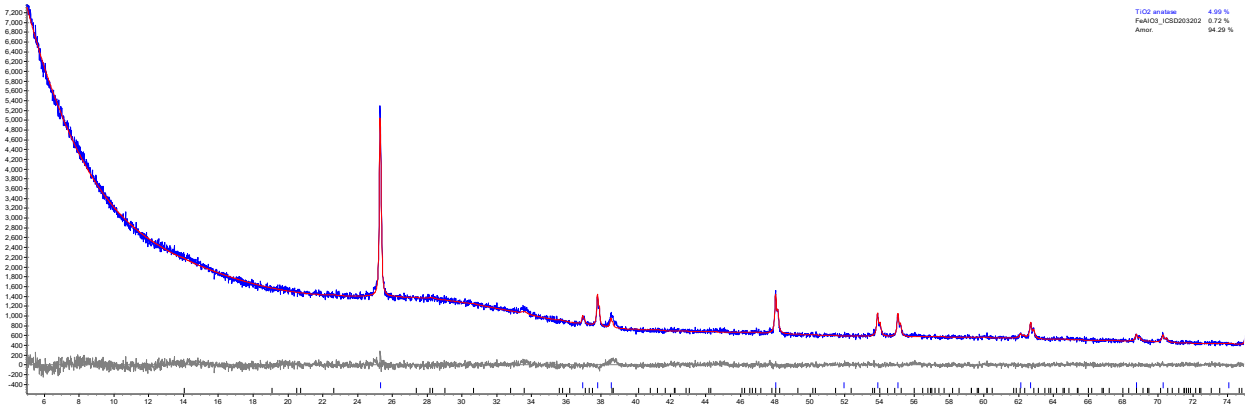

Phase Name	Wt% Measured	Wt% Corrected	Wt% Normalized
TiO_2 anatase	4.99	4.55	-
$FeAlO_3$	0.72	0.66	0.70

Figure F.26. XRD scan of glass HS24-29 after CCC.

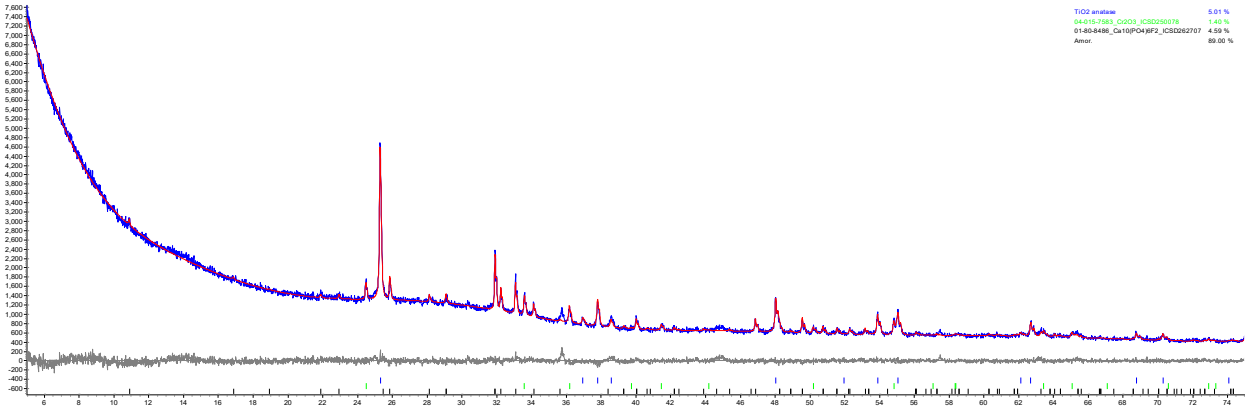

Phase Name	Wt% Measured	Wt% Corrected	Wt% Normalized
TiO_2 anatase	5.01	4.57	-
Cr_2O_3	1.40	1.28	1.35
$Ca_{10}(PO_4)_6F_2$	4.59	4.19	4.41

Figure F.27. XRD scan of glass HS24-30 after CCC.

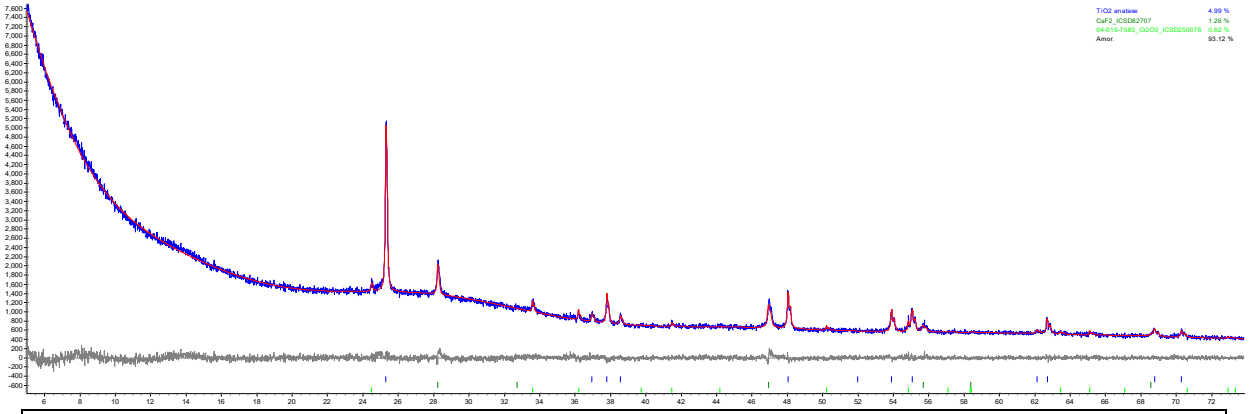

Phase Name	Wt% Measured	Wt% Corrected	Wt% Normalized
TiO_2 anatase	4.99	4.56	-
CaF_2	1.26	1.15	1.21
Cr_2O_3	0.62	0.57	0.60

Figure F.28. XRD scan of glass HS24-31 after CCC.

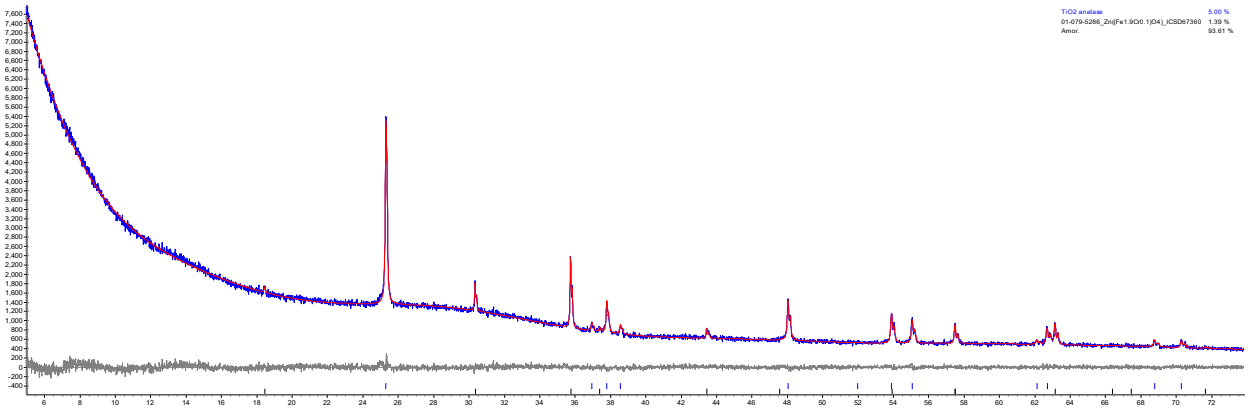

Phase Name	Wt% Measured	Wt% Corrected	Wt% Normalized
TiO_2 anatase	5.00	4.56	-
$ZnFe_{1.9}Cr_{0.1}O_4$	1.39	1.27	1.33

Figure F.29. XRD scan of glass HS24-32 after CCC.

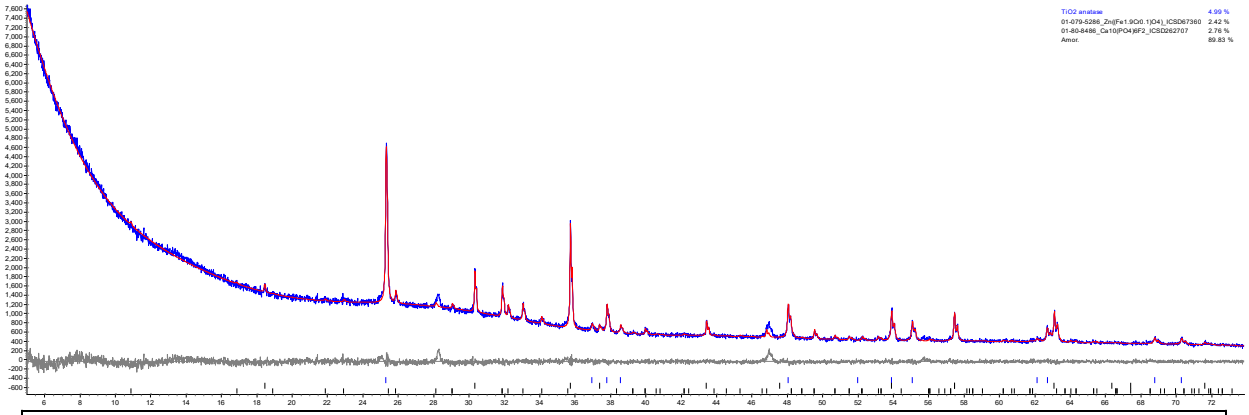

Phase Name	Wt% Measured	Wt% Corrected	Wt% Normalized
TiO_2 anatase	4.99	4.55	-
$ZnFe_{1.9}Cr_{0.1}O_4$	2.42	2.21	2.33
$Ca_{10}(PO_4)_6F_2$	2.76	2.51	2.65

Figure F.30. XRD scan of glass HS24-33 after CCC.

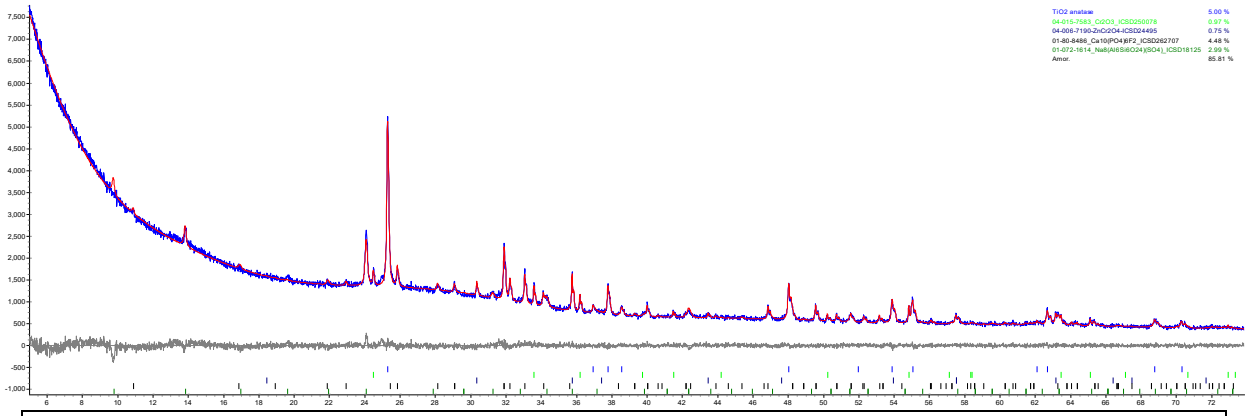

Phase Name	Wt% Measured	Wt% Corrected	Wt% Normalized
TiO_2 anatase	5.00	4.56	-
Cr_2O_3	0.97	0.88	0.93
$Ca_{10}(PO_4)_6F_2$	4.48	4.09	4.30
$ZnCr_2O_4$	0.75	0.69	0.72
$Na_8(Al_6Si_6O_{24})(SO_4)$	2.99	2.73	2.87

Figure F.31. XRD scan of glass HS24-34 after CCC.

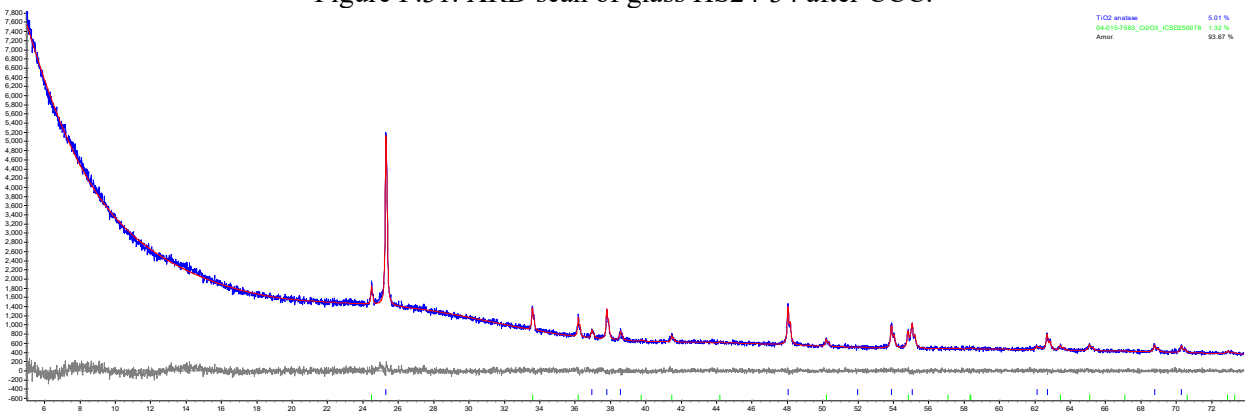

Phase Name	Wt% Measured	Wt% Corrected	Wt% Normalized
TiO_2 anatase	5.01	4.57	-
Cr_2O_3	1.32	1.21	1.27

Figure F.32. XRD scan of glass HS24-35 after CCC.

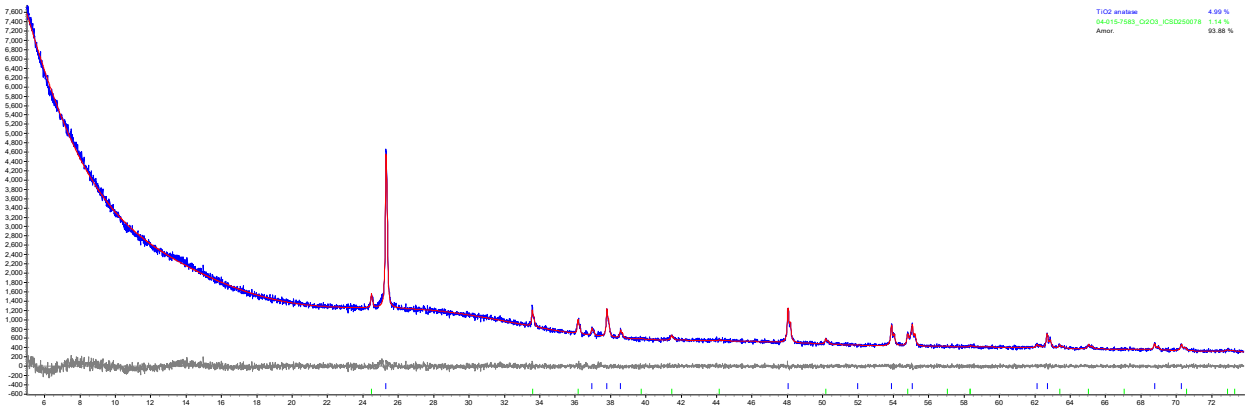

Phase Name	Wt% Measured	Wt% Corrected	Wt% Normalized
TiO_2 anatase	4.99	4.55	-
Cr_2O_3	1.14	1.04	1.09

Figure F.33. XRD scan of glass HS24-36 after CCC.

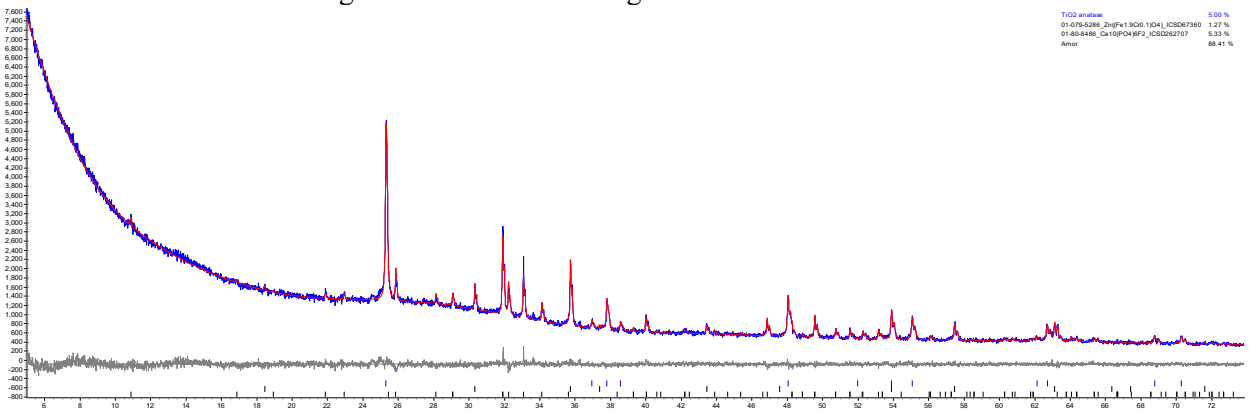

Phase Name	Wt% Measured	Wt% Corrected	Wt% Normalized
TiO_2 anatase	5.00	4.56	-
$ZnFe_{1.9}Cr_{0.1}O_4$	1.27	1.16	1.22
$Ca_{10}(PO_4)_6F_2$	5.33	4.87	5.12

Figure F.34. XRD scan of glass HS24-38 after CCC.

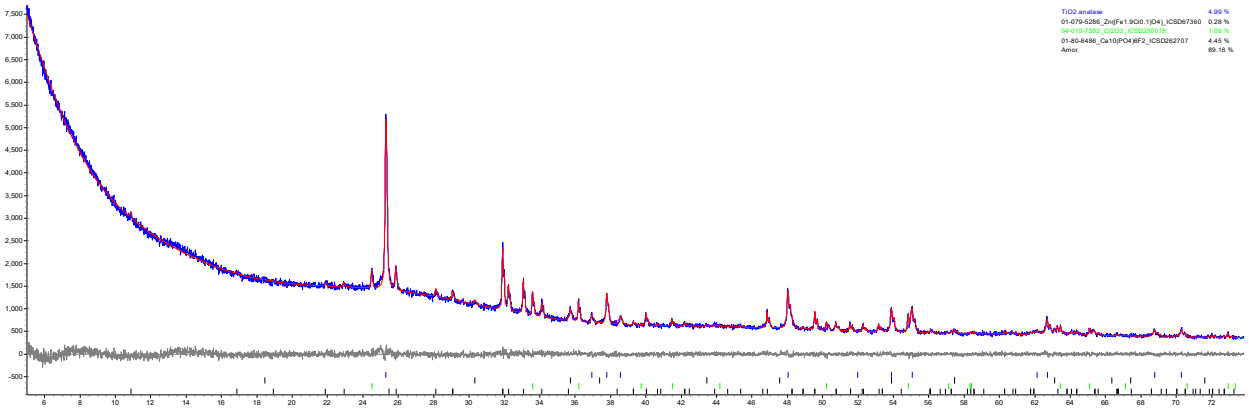

Phase Name	Wt% Measured	Wt% Corrected	Wt% Normalized
TiO_2 anatase	4.99	4.56	-
Cr_2O_3	1.09	1.00	1.05
$Ca_{10}(PO_4)_6F_2$	4.45	4.06	4.27
$ZnFe_{1.9}Cr_{0.1}O_4$	0.28	0.26	0.27

Figure F.35. XRD scan of glass HS24-39 after CCC.

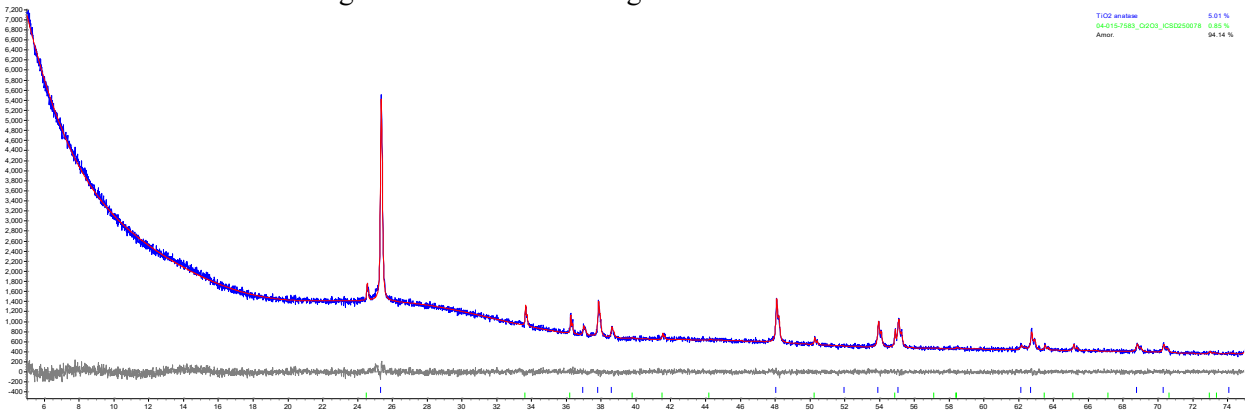

Phase Name	Wt% Measured	Wt% Corrected	Wt% Normalized
TiO_2 anatase	5.01	4.57	-
Cr_2O_3	0.85	0.78	0.82

Figure F.36. XRD scan of glass HS24-40 after CCC.

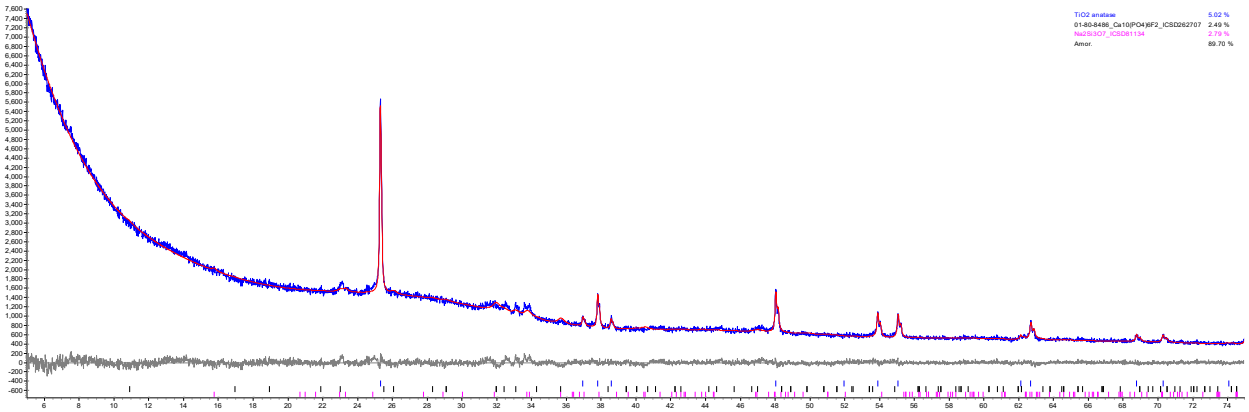

Phase Name	Wt% Measured	Wt% Corrected	Wt% Normalized
TiO_2 anatase	5.02	4.58	-
$Na_2Si_3O_7$	2.79	2.55	2.69
$Ca_{10}(PO_4)_6F_2$	2.49	2.27	2.39

Figure F.37. XRD scan of glass HS24-41 after CCC.

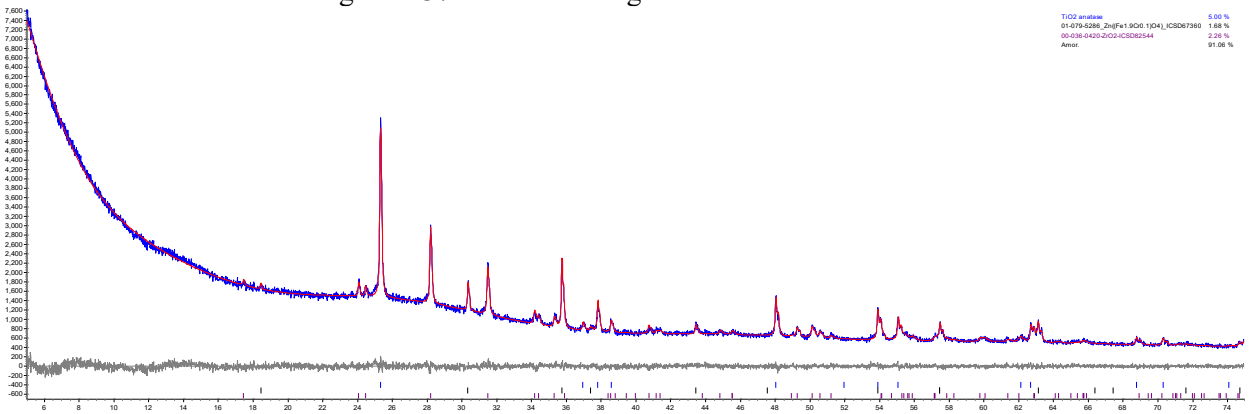

Phase Name	Wt% Measured	Wt% Corrected	Wt% Normalized
TiO_2 anatase	5.00	4.56	-
$ZnFe_{1.9}Cr_{0.1}O_4$	1.68	1.53	1.61
ZrO_2	2.26	2.06	2.17

Figure F.38. XRD scan of glass HS24-42 after CCC.

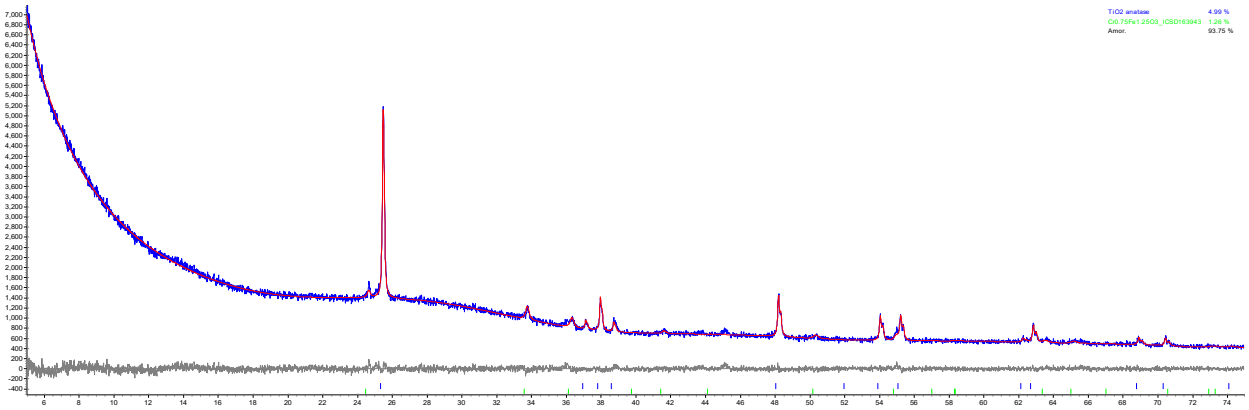

Phase Name	Wt% Measured	Wt% Corrected	Wt% Normalized
TiO_2 anatase	4.99	4.56	-
$Cr_{0.75}Fe_{1.25}O_3$	1.26	1.15	1.21

Figure F.39. XRD scan of glass HS24-43 after CCC.

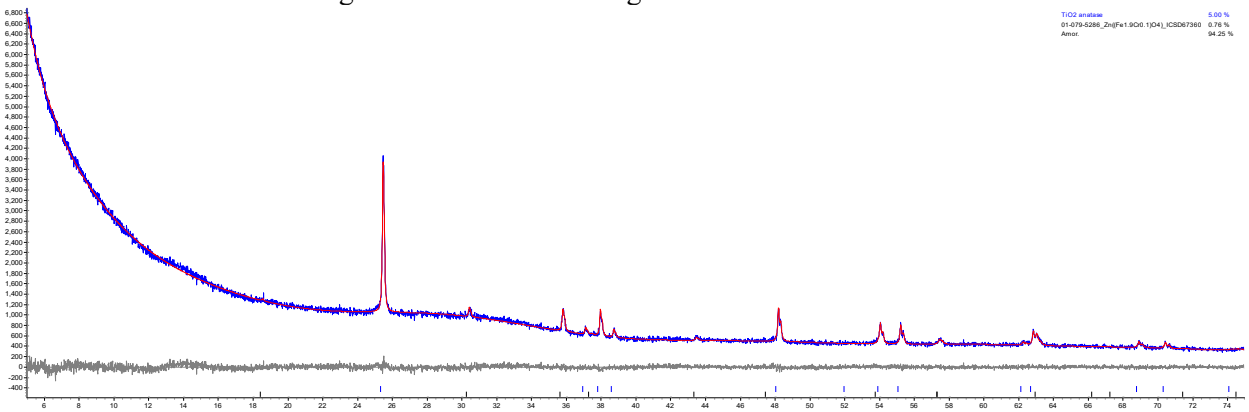

Phase Name	Wt% Measured	Wt% Corrected	Wt% Normalized
TiO_2 anatase	5.00	4.56	-
$ZnFe_{1.9}Cr_{0.1}O_4$	0.76	0.69	0.73

Figure F.40. XRD scan of glass HS24-44 after CCC.

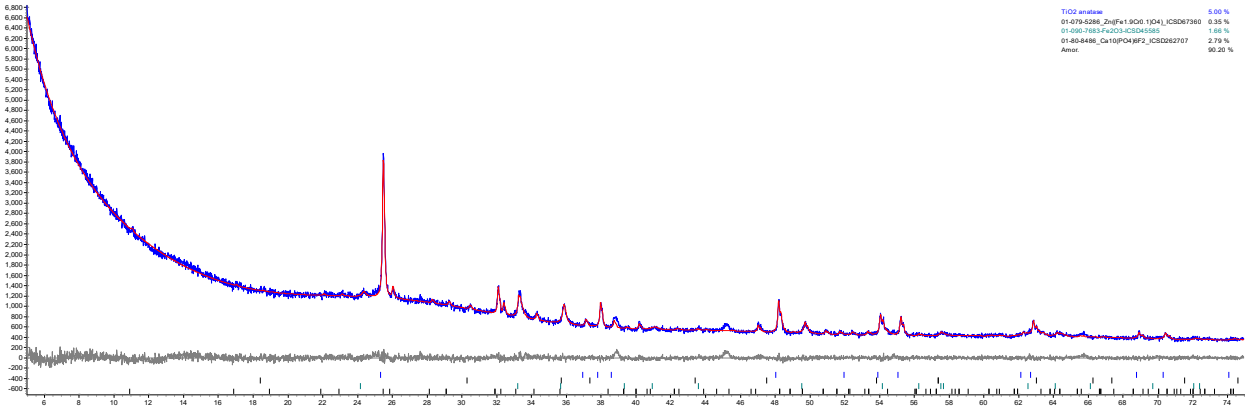

Phase Name	Wt% Measured	Wt% Corrected	Wt% Normalized
TiO_2 anatase	5.00	4.57	-
$ZnFe_{1.9}Cr_{0.1}O_4$	0.35	0.32	0.34
$Ca_{10}(PO_4)_6F_2$	2.79	2.54	2.68
Fe_2O_3	1.66	1.51	1.59

Figure F.41. XRD scan of glass HS24-45 after CCC.

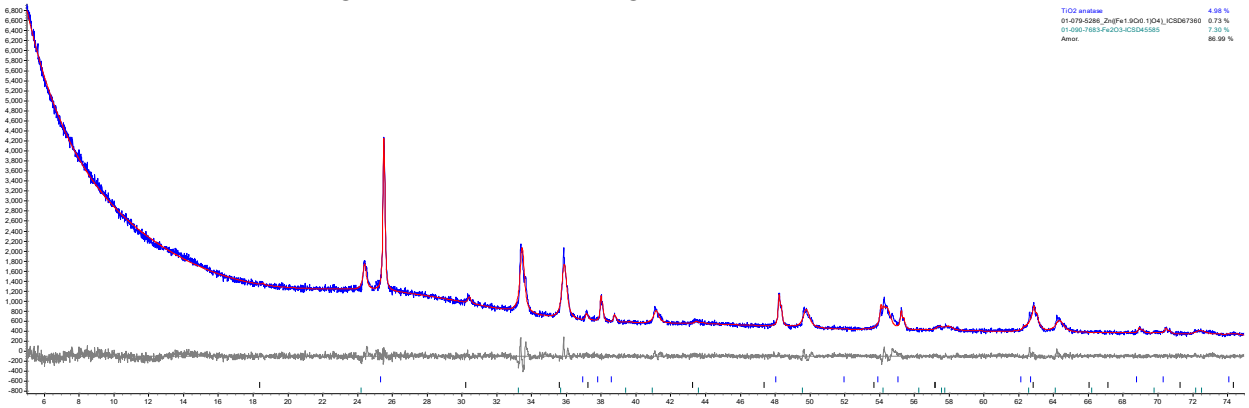

Phase Name	Wt% Measured	Wt% Corrected	Wt% Normalized
TiO_2 anatase	4.98	4.55	-
$ZnFe_{1.9}Cr_{0.1}O_4$	0.73	0.66	0.70
Fe_2O_3	7.30	6.66	7.01

Figure F.42. XRD scan of glass HS24-46 after CCC.

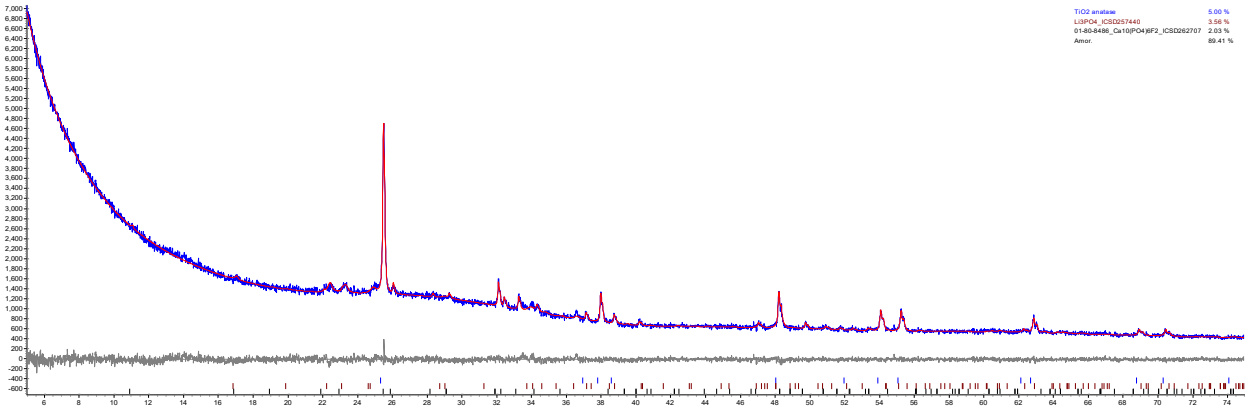

Phase Name	Wt% Measured	Wt% Corrected	Wt% Normalized
TiO_2 anatase	5.00	4.57	-
$Ca_{10}(PO_4)_6F_2$	2.03	1.85	1.95
Li_3PO_4	3.56	3.25	3.42

Figure F.43. XRD scan of glass HS24-47 after CCC.

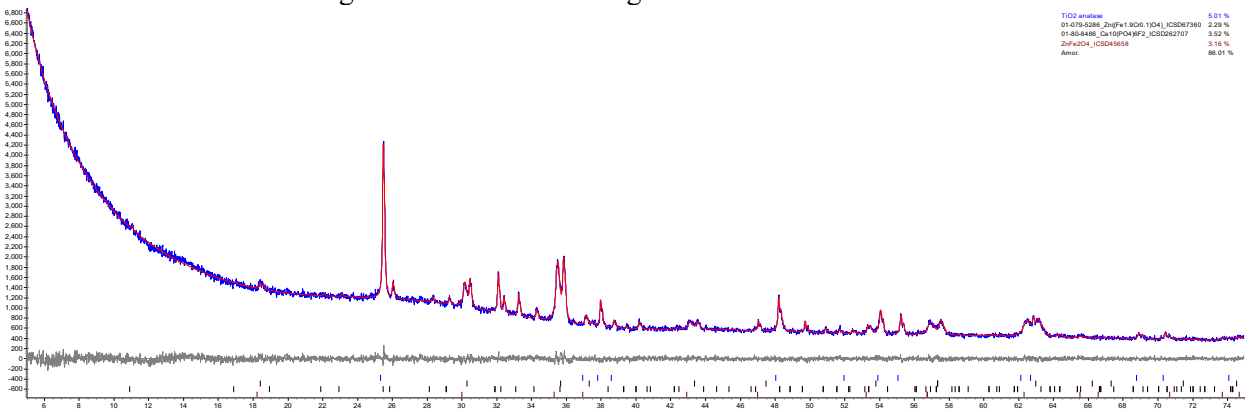

Phase Name	Wt% Measured	Wt% Corrected	Wt% Normalized
TiO_2 anatase	5.01	4.57	-
$ZnFe_{1.9}Cr_{0.1}O_4$	2.29	2.09	2.20
$Ca_{10}(PO_4)_6F_2$	3.52	3.22	3.39
$ZnFe_2O_4$	3.16	2.89	3.04

Figure F.44. XRD scan of glass HS24-48 after CCC.

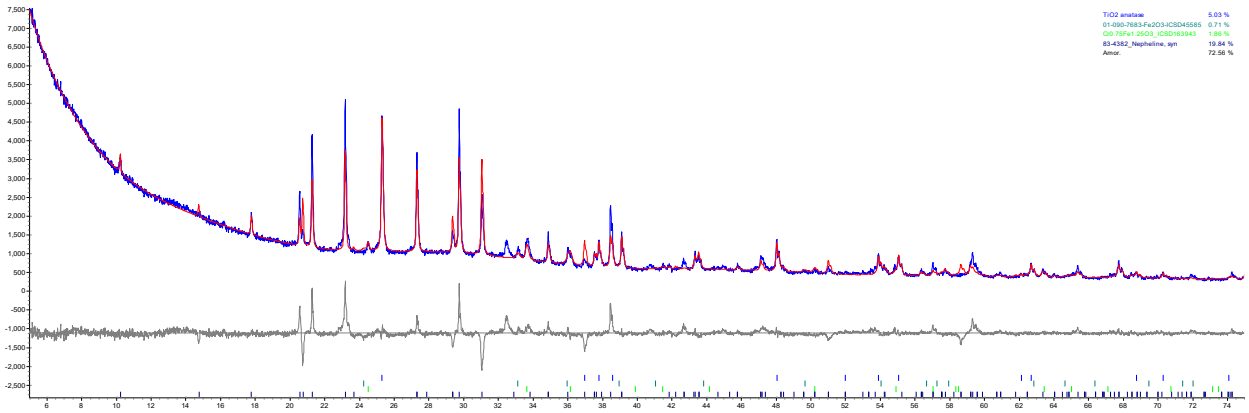

Phase Name	Wt% Measured	Wt% Corrected	Wt% Normalized
TiO_2 anatase	5.03	4.59	-
Nepheline	19.84	18.11	19.07
Fe_2O_3	0.71	0.64	0.68
$Cr_{0.75}Fe_{1.25}O_3$	1.86	1.70	1.79

Figure F.45. XRD scan of glass HS24-50 after CCC.

Appendix G – XRD results of isothermally heat-treated glasses

This appendix contains XRD scans of the HS24 glasses after they were heat-treated at 950 °C for 24 h, except for fully amorphous samples. The crystal fraction (wt%) in the XRD images reported before adjustment was made from spiking with 5 wt% high purity TiO_2 anatase as an internal standard. The T_L value was determined on the primary crystalline phase by linear fitting and non-linear fitting except for glasses with abnormal CF trends. Non-linear curve is not shown if the non-linear fitting function hits B_L limit (see Section 3.4).

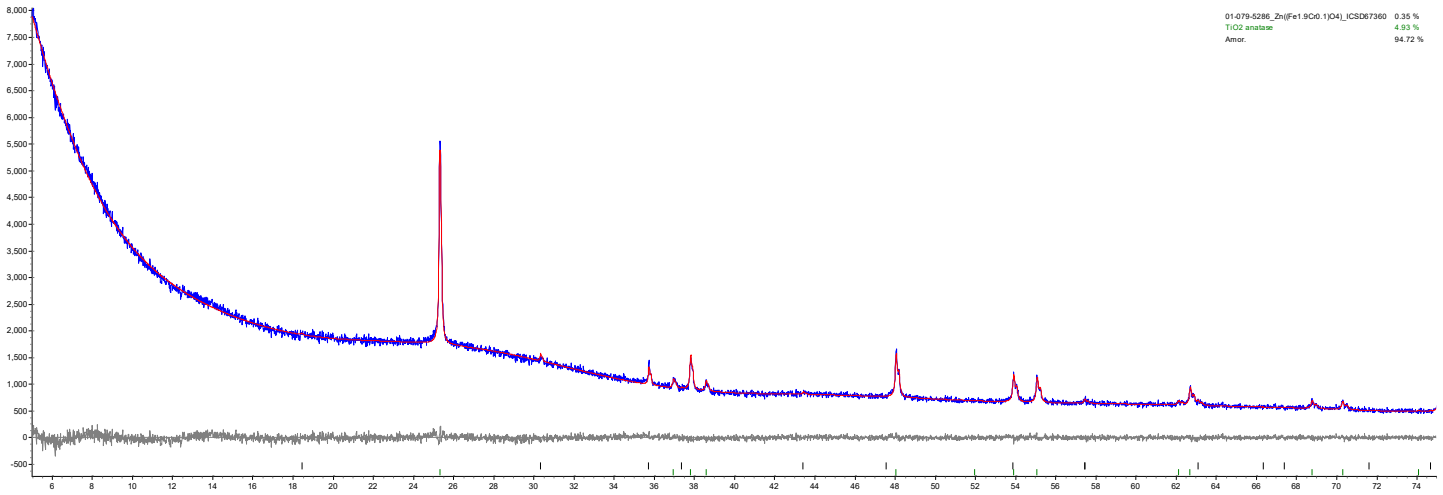

Figure G.1. XRD scan of glass HS24-01 after isothermal heat treatment at 950 °C for 24 h. The crystalline phase is $ZnFe_{1.9}Cr_{0.1}O_4$.

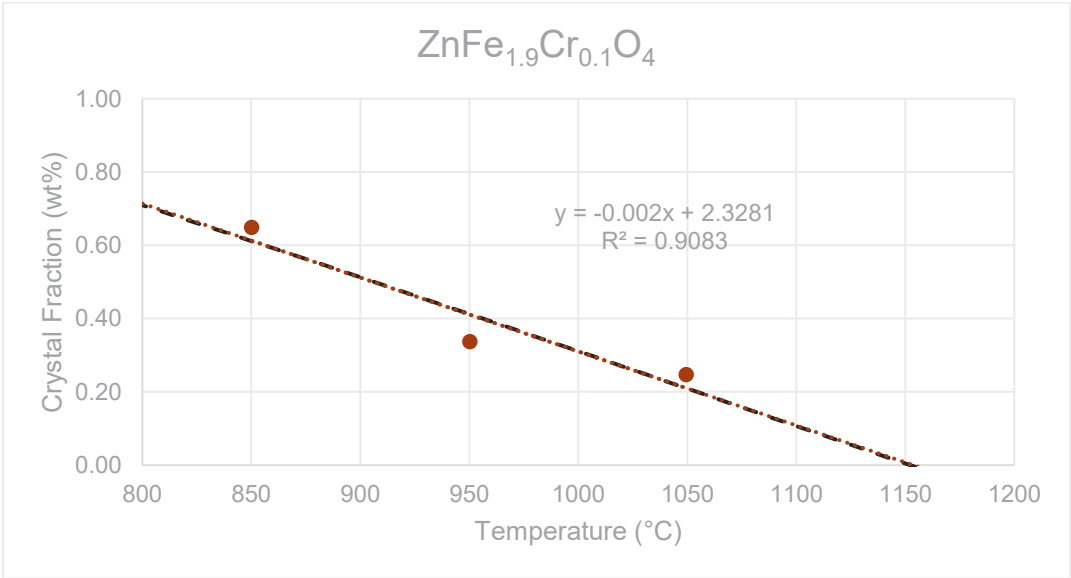

Figure G.2. The liquidus temperature plot for $ZnFe_{1.9}Cr_{0.1}O_4$ in glass HS24-01 showing the linear T_L at 1154 °C (R^2 = 0.9083) and the non-linear (black dash line) T_L at 1152 °C.

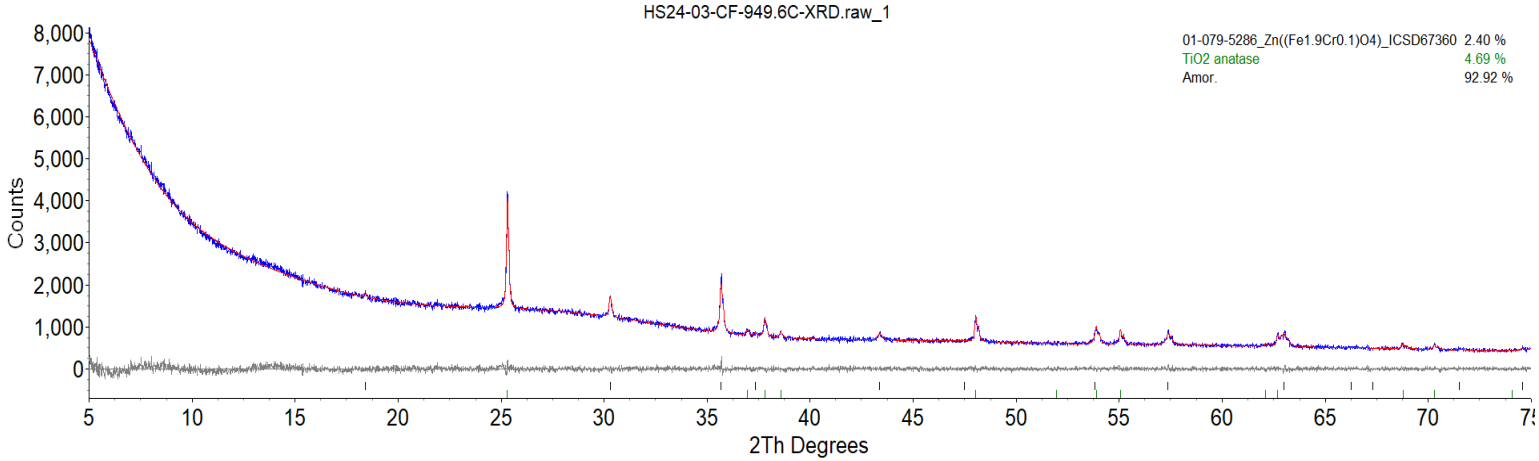

Figure G.3. XRD scan of glass HS24-03 after isothermal heat treatment at 950 °C for 24 h. The crystalline phase is $ZnFe_{1.9}Cr_{0.1}O_4$.

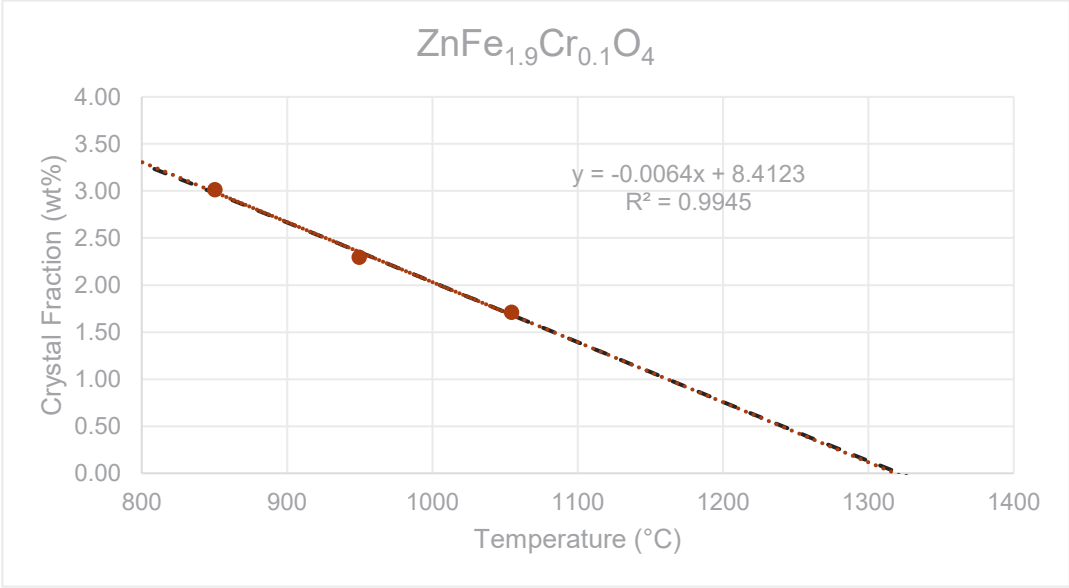

Figure G.4. The liquidus temperature plot for $ZnFe_{1.9}Cr_{0.1}O_4$ in glass HS24-03 showing the linear T_L at 1318 °C (R^2 = 0.9945) and the non-linear (black dash line) T_L at 1321 °C.

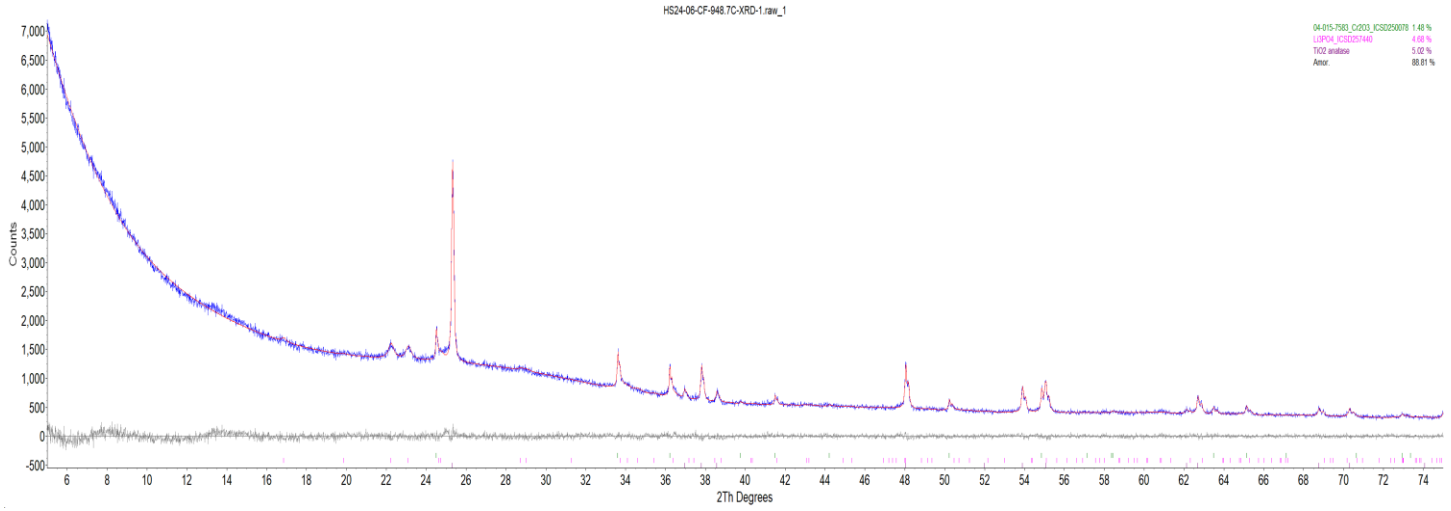

Figure G.5. XRD scan of glass HS24-06 after isothermal heat treatment at 950 °C for 24 h. The crystalline phases are Li_3PO_4 and Cr_2O_3.

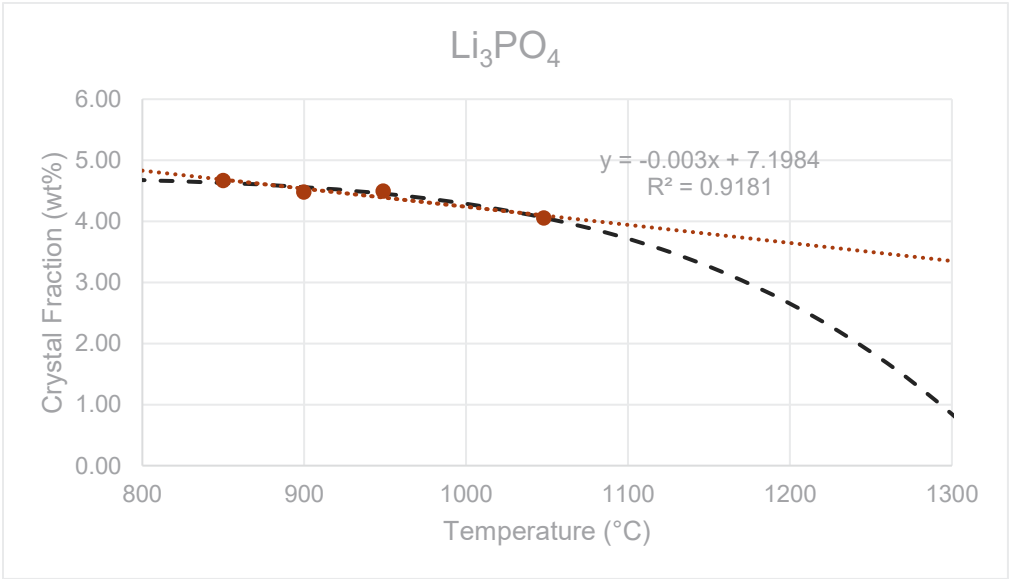

Figure G.6. The liquidus temperature plot for Li_3PO_4 in glass HS24-06 showing the linear T_L at 2432 °C (R^2 = 0.9181) and the non-linear (black dash line) T_L at 1334 °C.

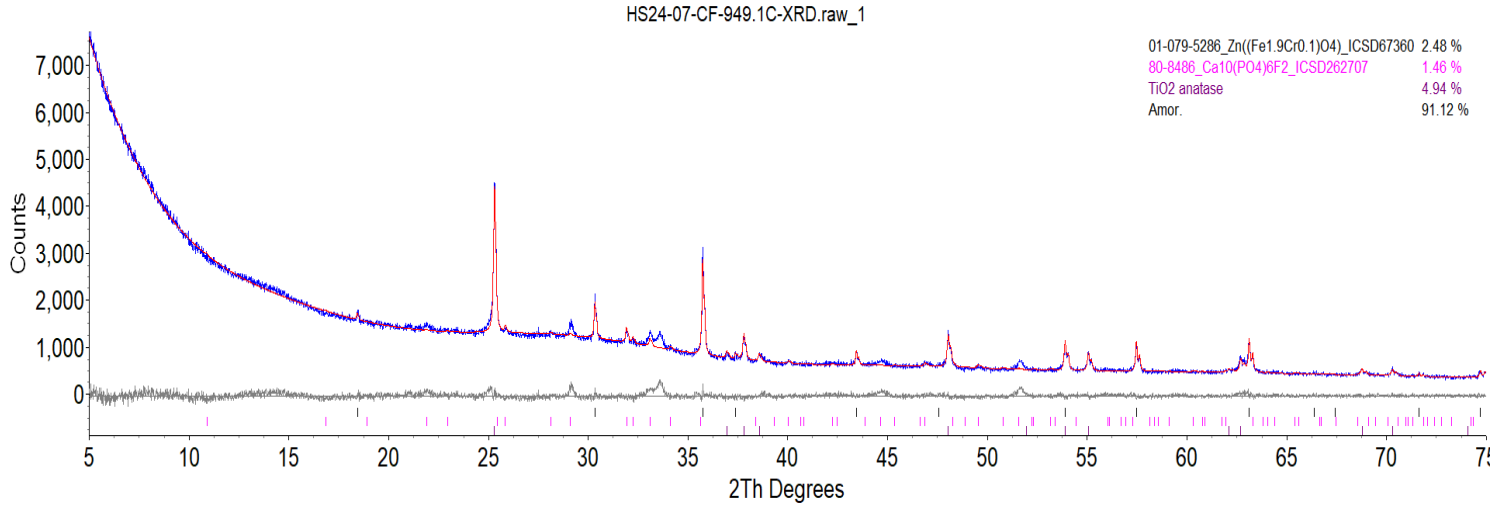

Figure G.7. XRD scan of glass HS24-07 after isothermal heat treatment at 950 °C for 24 h. The crystalline phases are $Ca_{10}(PO_4)_6F_2$ and $ZnFe_{1.9}Cr_{0.1}O_4$.

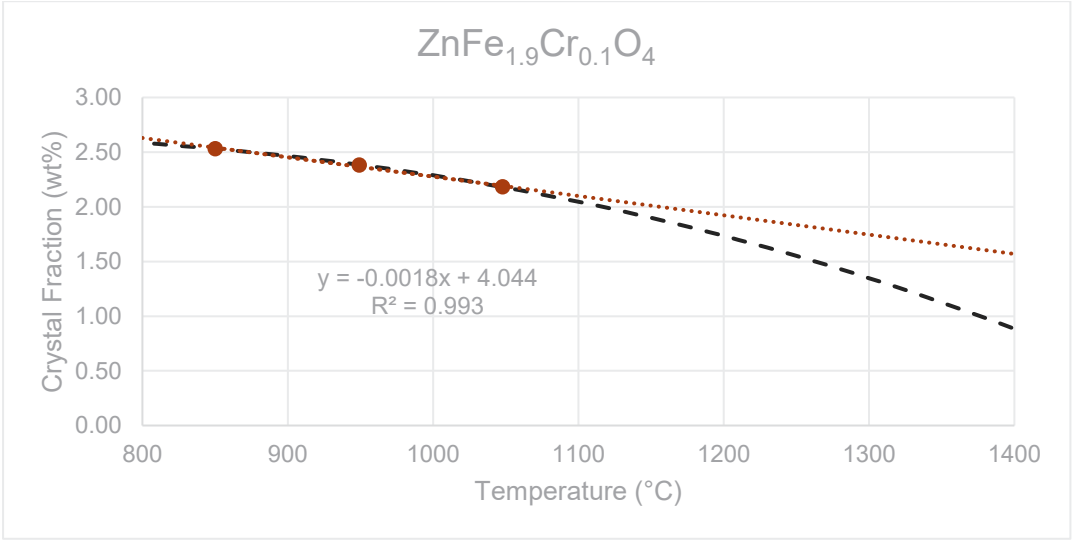

Figure G.8. The liquidus temperature plot for $ZnFe_{1.9}Cr_{0.1}O_4$ in glass HS24-07 showing the linear T_L at 2287 °C (R^2 = 0.993) and the non-linear (black dash line) T_L at 1558 °C.

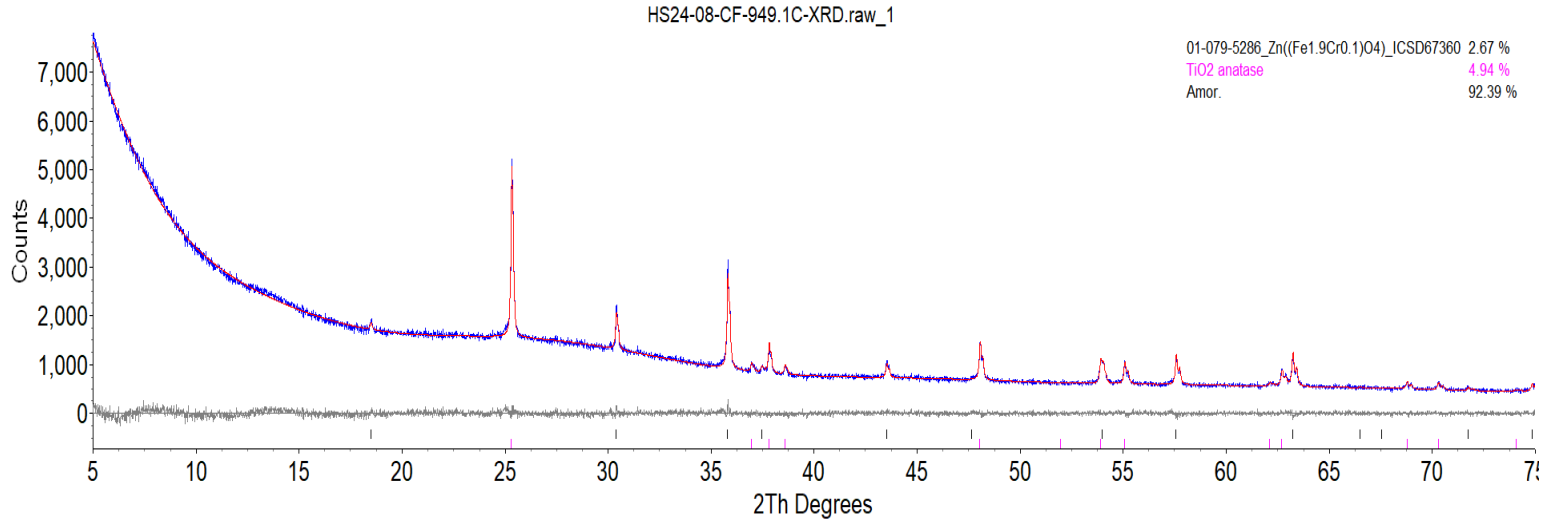

Figure G.9. XRD scan of glass HS24-08 after isothermal heat treatment at 950 °C for 24 h. The crystalline phase is $ZnFe_{1.9}Cr_{0.1}O_4$.

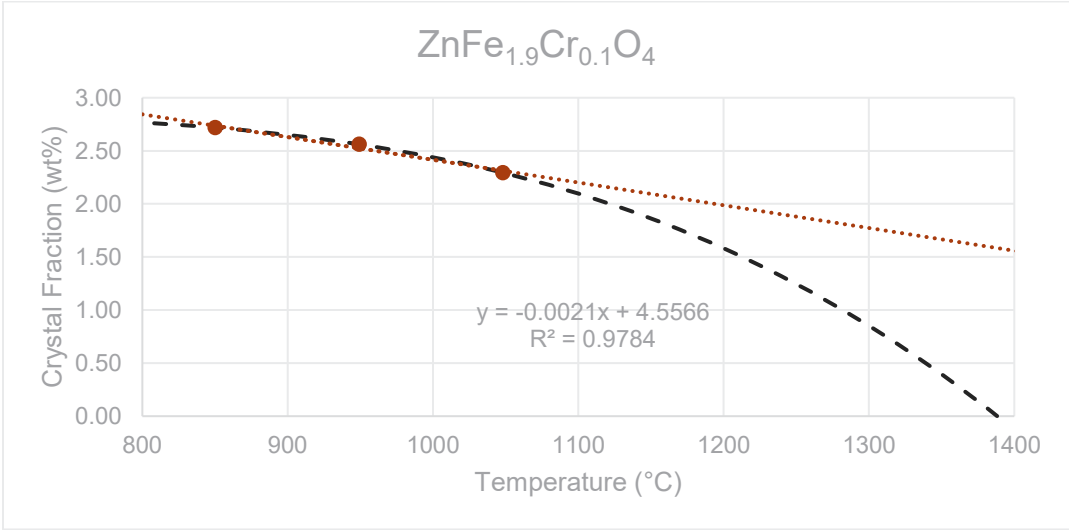

Figure G.10. The liquidus temperature plot for $ZnFe_{1.9}Cr_{0.1}O_4$ in glass HS24-08 showing the linear T_L at 2128 °C (R^2 = 0.9784) and the non-linear (black dash line) T_L at 1388 °C.

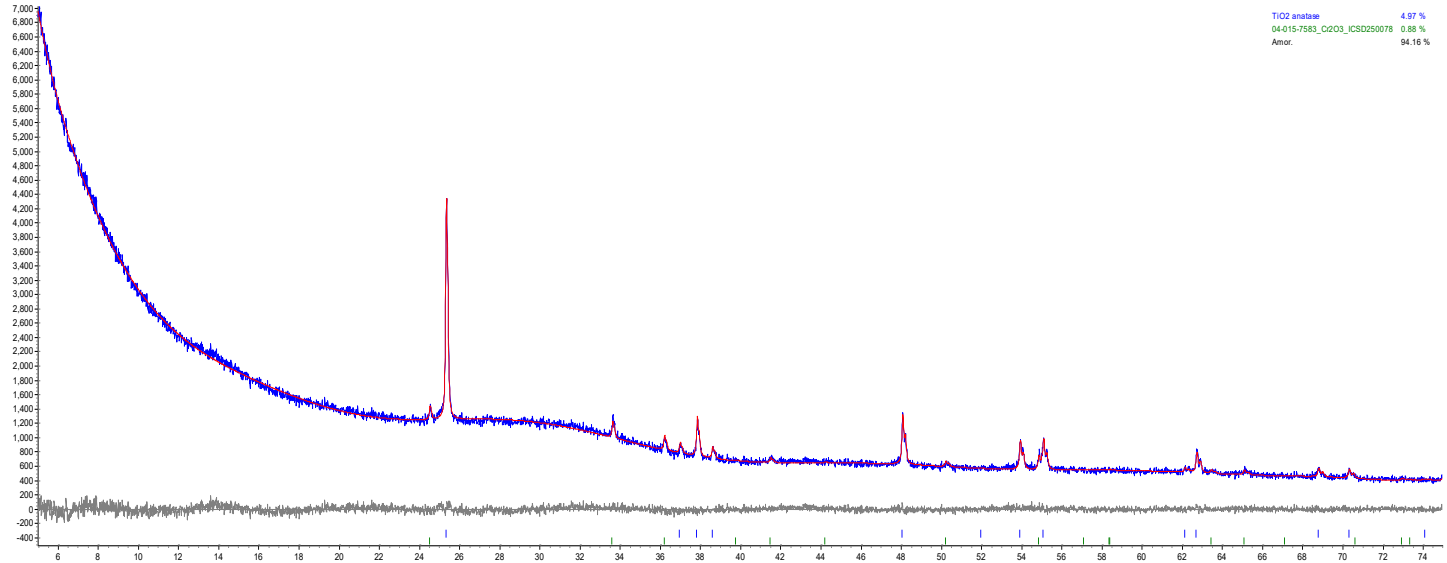

Figure G.11. XRD scan of glass HS24-09 after isothermal heat treatment at 950 °C for 24 h. The crystalline phase is Cr_2O_3.

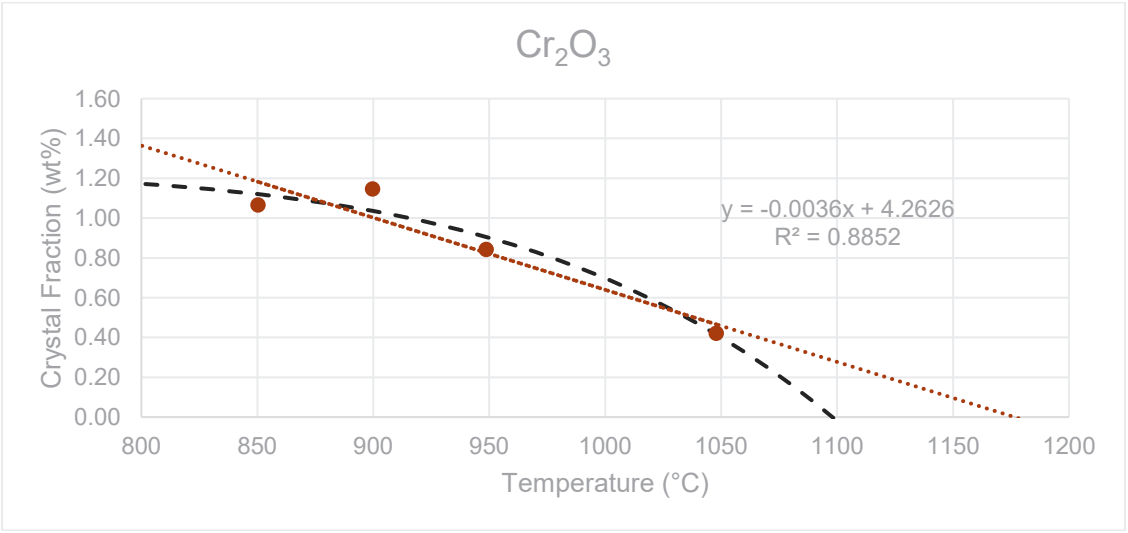

Figure G.12. The liquidus temperature plot for Cr_2O_3 in glass HS24-09 showing the linear T_L at 1177 °C (R^2 = 0.8852) and the non-linear (black dash line) T_L at 1098 °C.

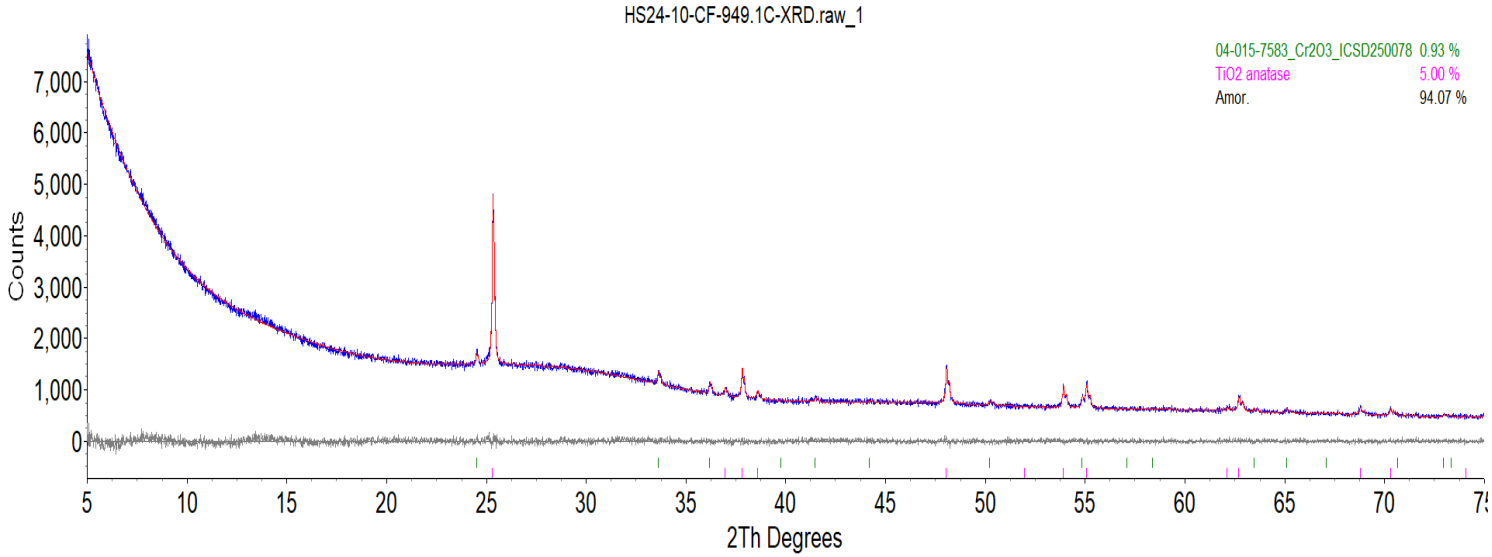

Figure G.13. XRD scan of glass HS24-10 after isothermal heat treatment at 950 °C for 24 h. The crystalline phase is Cr_2O_3.

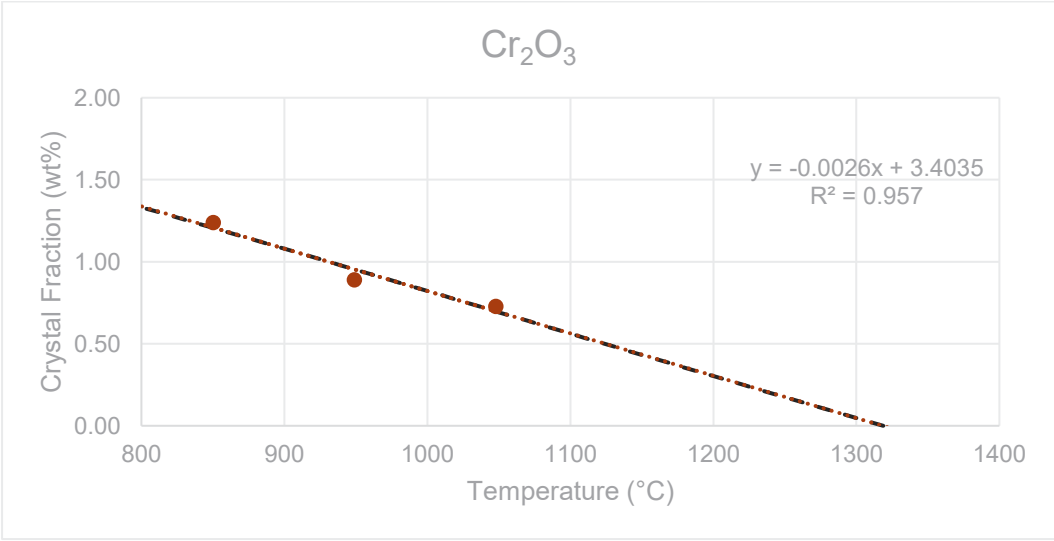

Figure G.14. The liquidus temperature plot for Cr_2O_3 in glass HS24-10 showing the linear T_L at 1318 °C (R^2 = 0.957) and the non-linear (black dash line) T_L at 1319 °C.

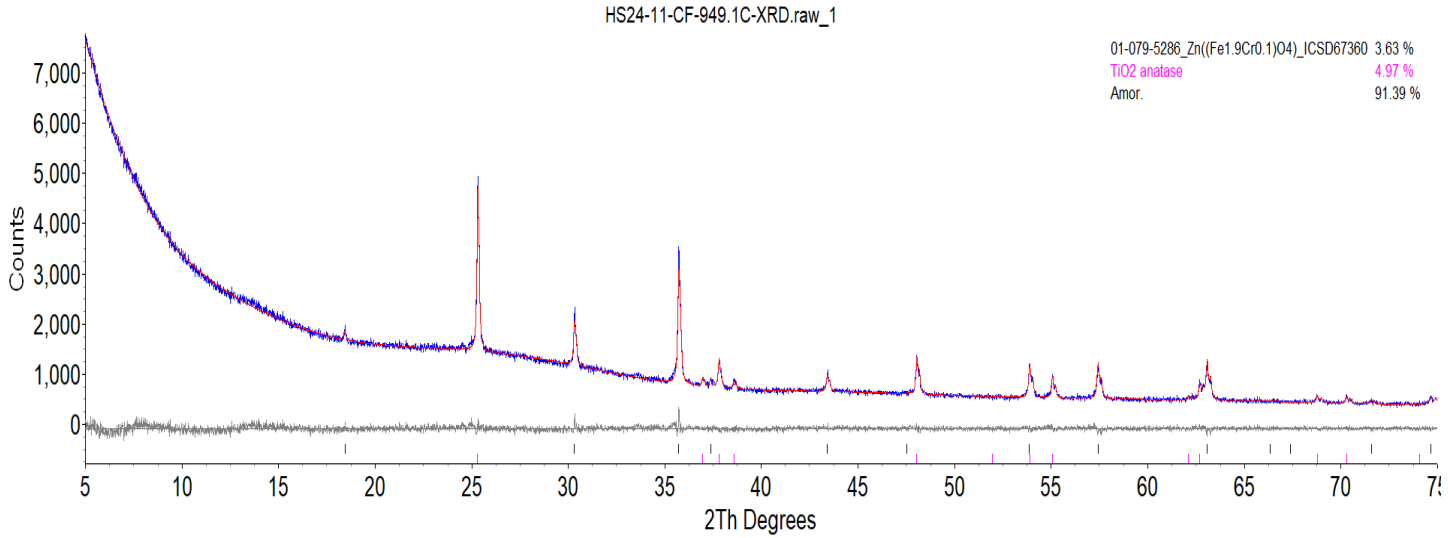

Figure G.15. XRD scan of glass HS24-11 after isothermal heat treatment at 950 °C for 24 h. The crystalline phase is $ZnFe_{1.9}Cr_{0.1}O_4$.

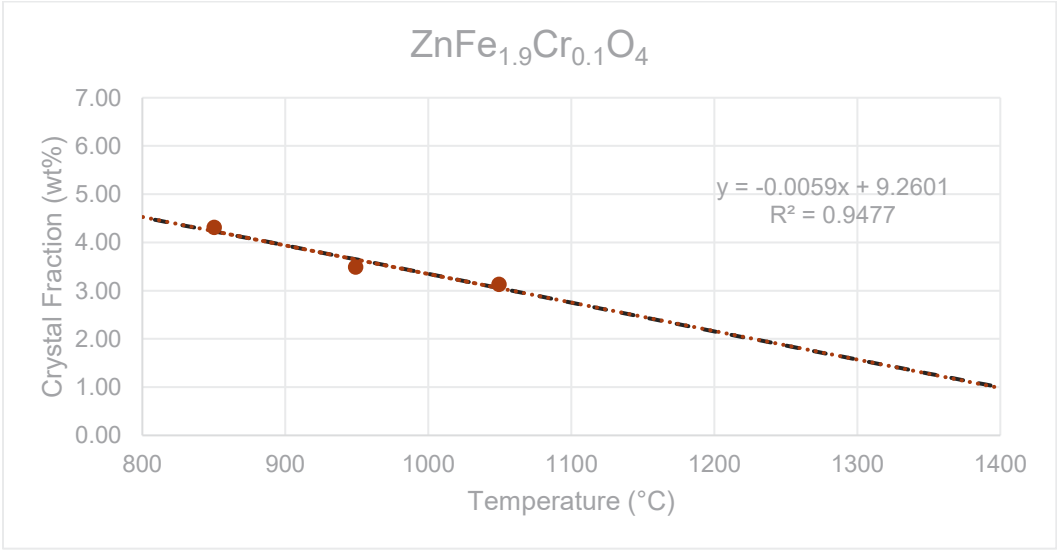

Figure G.16. The liquidus temperature plot for $ZnFe_{1.9}Cr_{0.1}O_4$ in glass HS24-11 showing the linear T_L at 1566 °C (R^2 = 0.9477) and the non-linear (black dash line) T_L at 1579 °C.

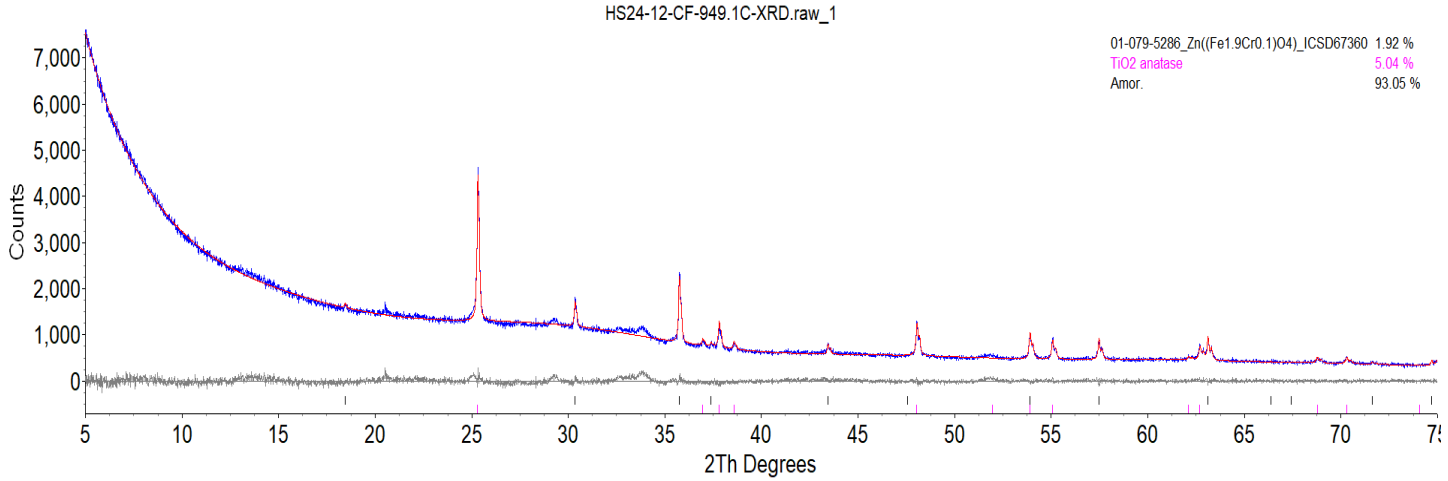

Figure G.17. XRD scan of glass HS24-12 after isothermal heat treatment at 950 °C for 24 h. The crystalline phase is $ZnFe_{1.9}Cr_{0.1}O_4$.

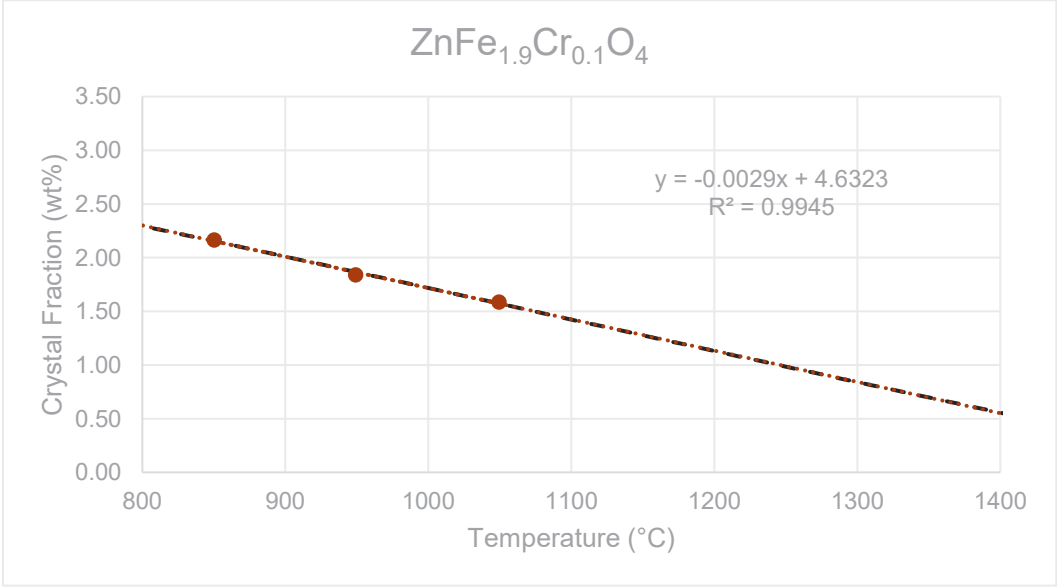

Figure G.18. The liquidus temperature plot for $ZnFe_{1.9}Cr_{0.1}O_4$ in glass HS24-12 showing the linear T_L at 1589 °C (R^2 = 0.9945) and the non-linear (black dash line) T_L at 1604 °C.

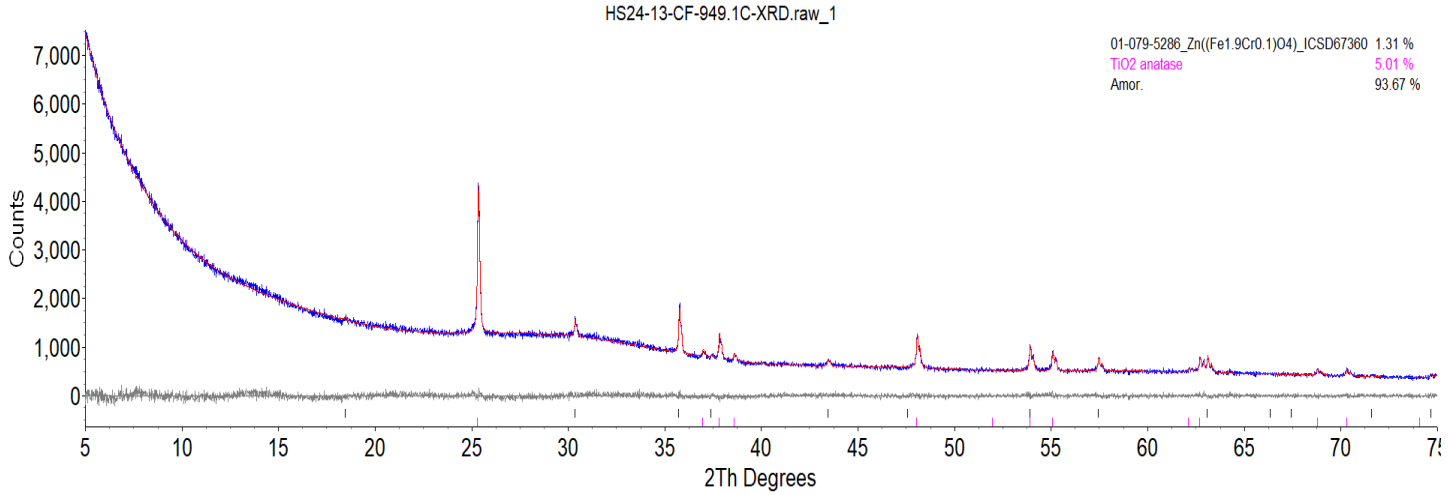

Figure G.19. XRD scan of glass HS24-13 after isothermal heat treatment at 950 °C for 24 h. The crystalline phase is $ZnFe_{1.9}Cr_{0.1}O_4$.

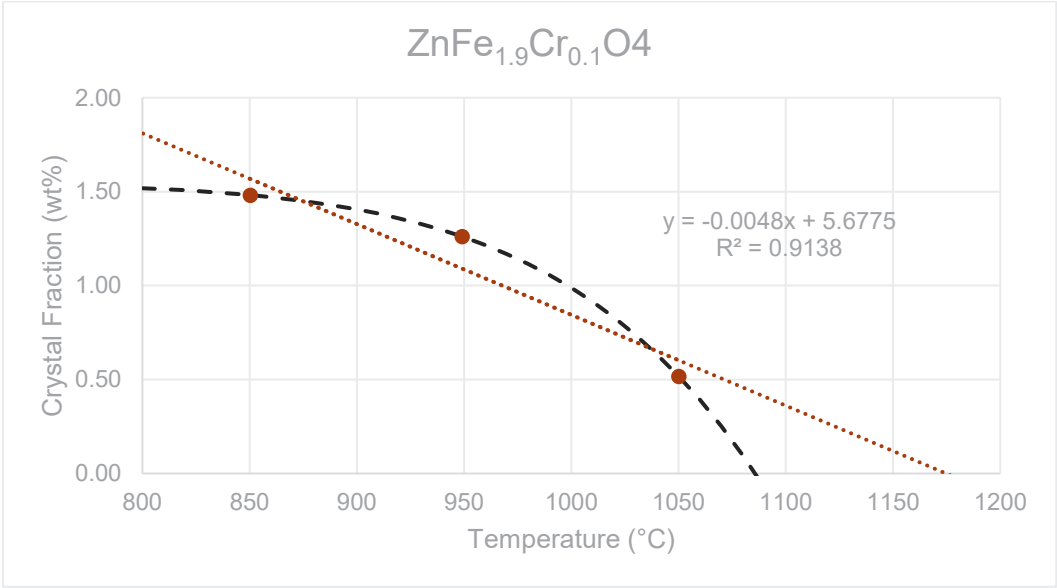

Figure G.20. The liquidus temperature plot for $ZnFe_{1.9}Cr_{0.1}O_4$ in glass HS24-13 showing the linear T_L at 1175 °C ($R^2 = 0.9138$) and the non-linear (black dash line) T_L at 1086 °C.

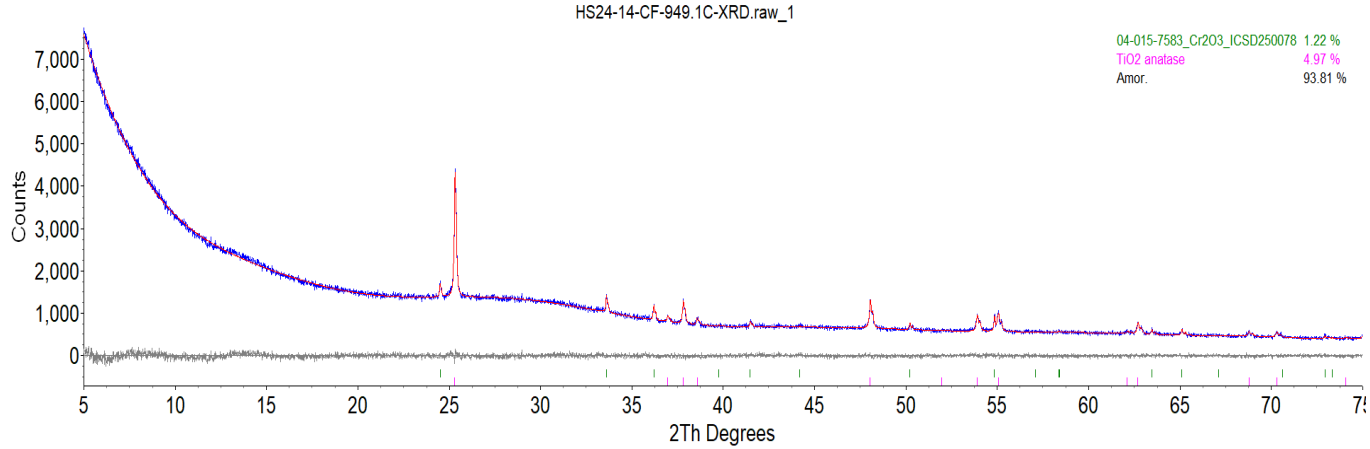

Figure G.21. XRD scan of glass HS24-14 after isothermal heat treatment at 950 °C for 24 h. The crystalline phase is Cr_2O_3.

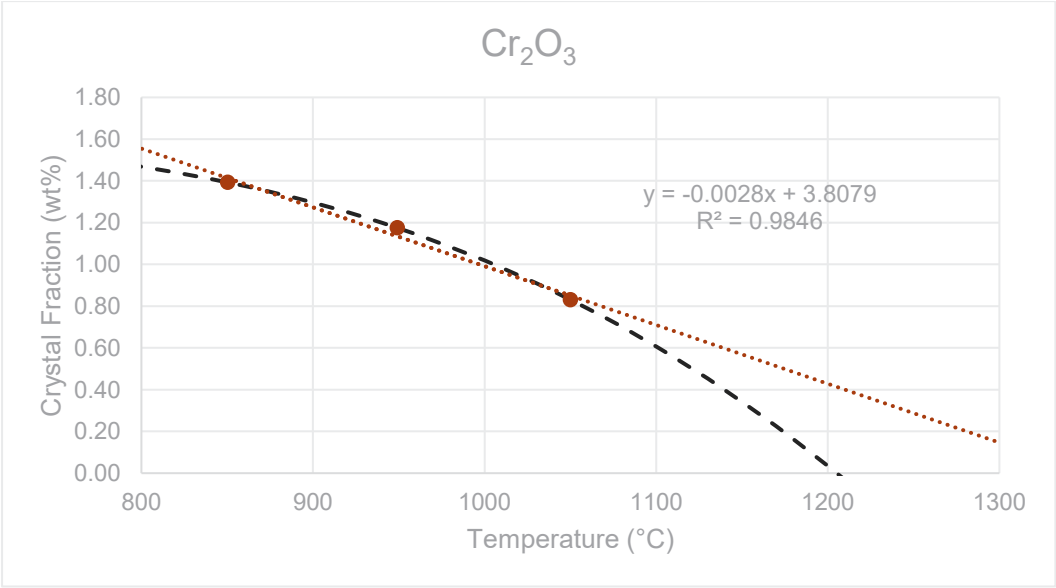

Figure G.22. The liquidus temperature plot for Cr_2O_3 in glass HS24-14 showing the linear T_L at 1352 °C (R^2 = 0.9846) and the non-linear (black dash line) T_L at 1205 °C.

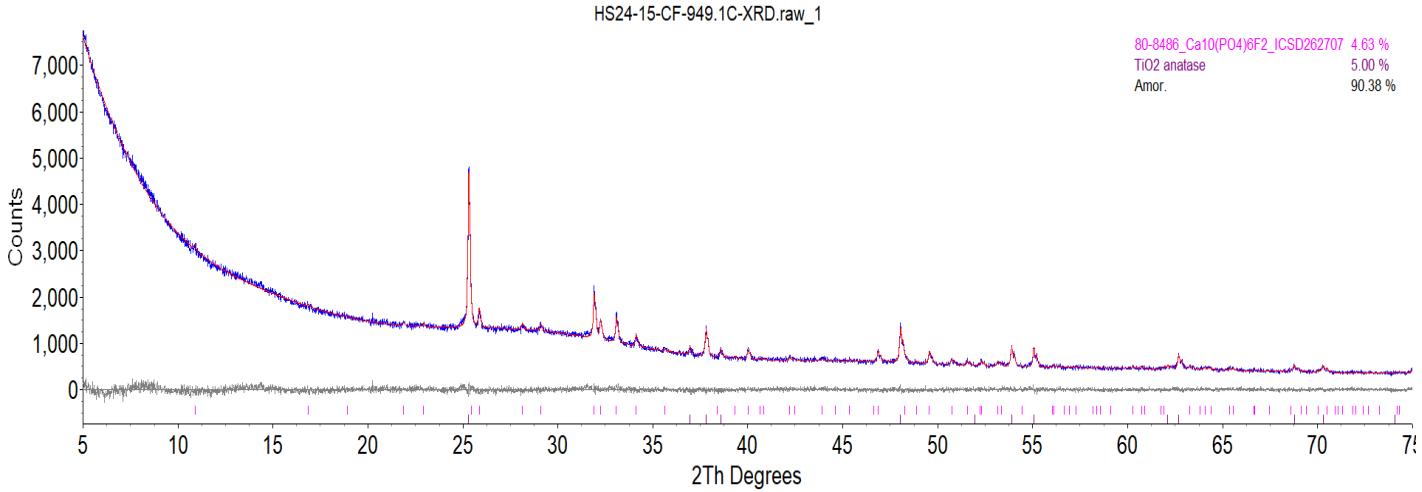

Figure G.23. XRD scan of glass HS24-15 after isothermal heat treatment at 950 °C for 24 h. The crystalline phase is $Ca_{10}(PO_4)_6F_2$.

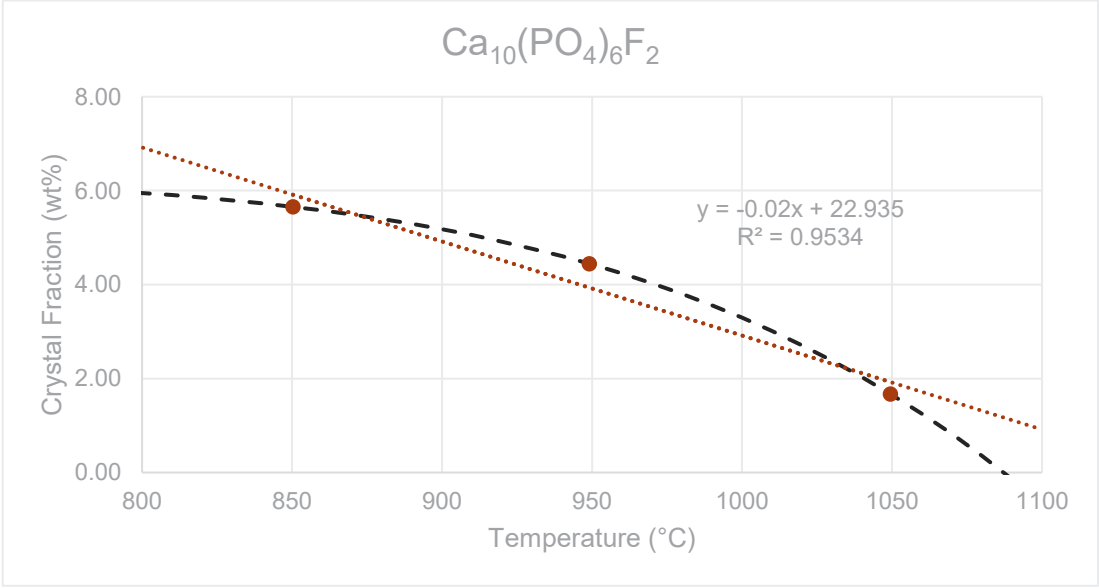

Figure G.24. The liquidus temperature plot for $Ca_{10}(PO_4)_6F_2$ in glass HS24-15 showing the linear T_L at 1146 °C (R^2 = 0.9534) and the non-linear (black dash line) T_L at 1087 °C.

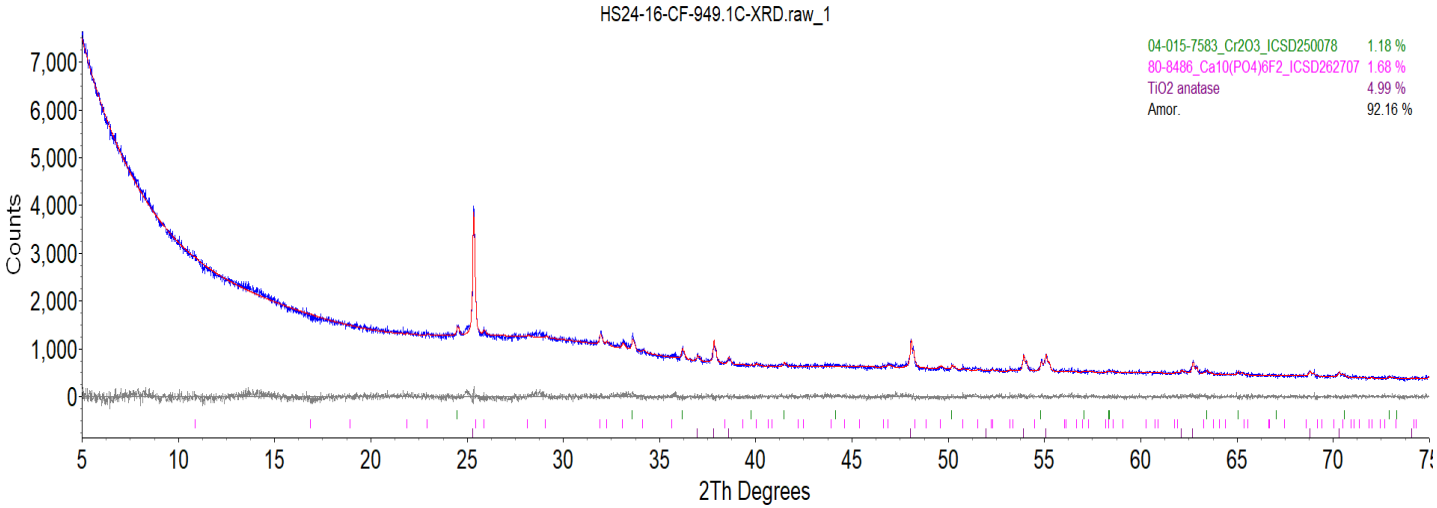

Figure G.25. XRD scan of glass HS24-16 after isothermal heat treatment at 950 °C for 24 h. The crystalline phases are $Ca_{10}(PO_4)_6F_2$ and Cr_2O_3.

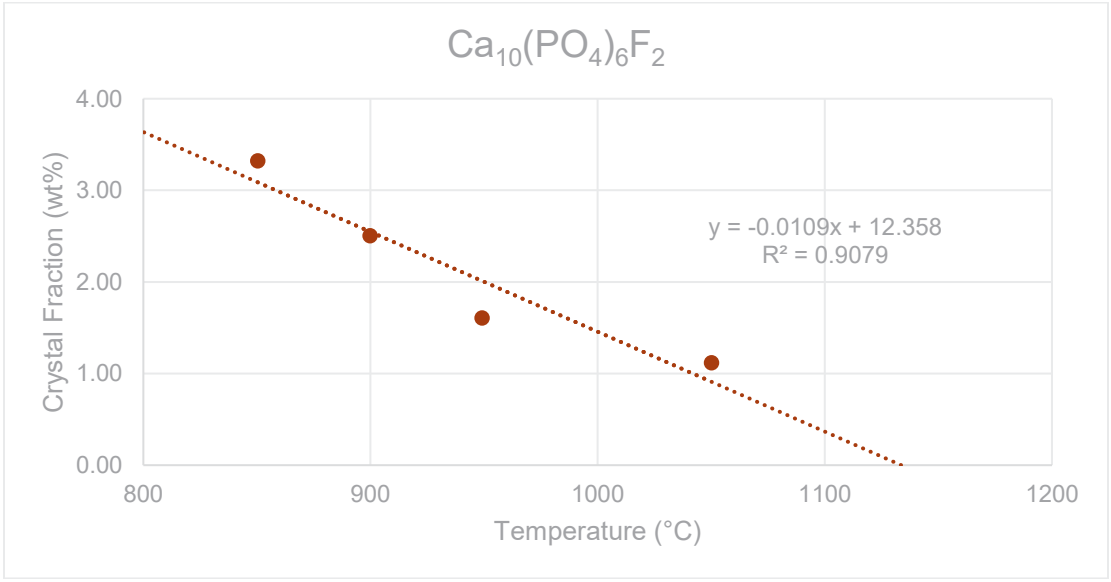

Figure G.26. The liquidus temperature plot for $Ca_{10}(PO_4)_6F_2$ in glass HS24-16 showing the linear T_L at 1134 °C ($R^2 = 0.9079$).

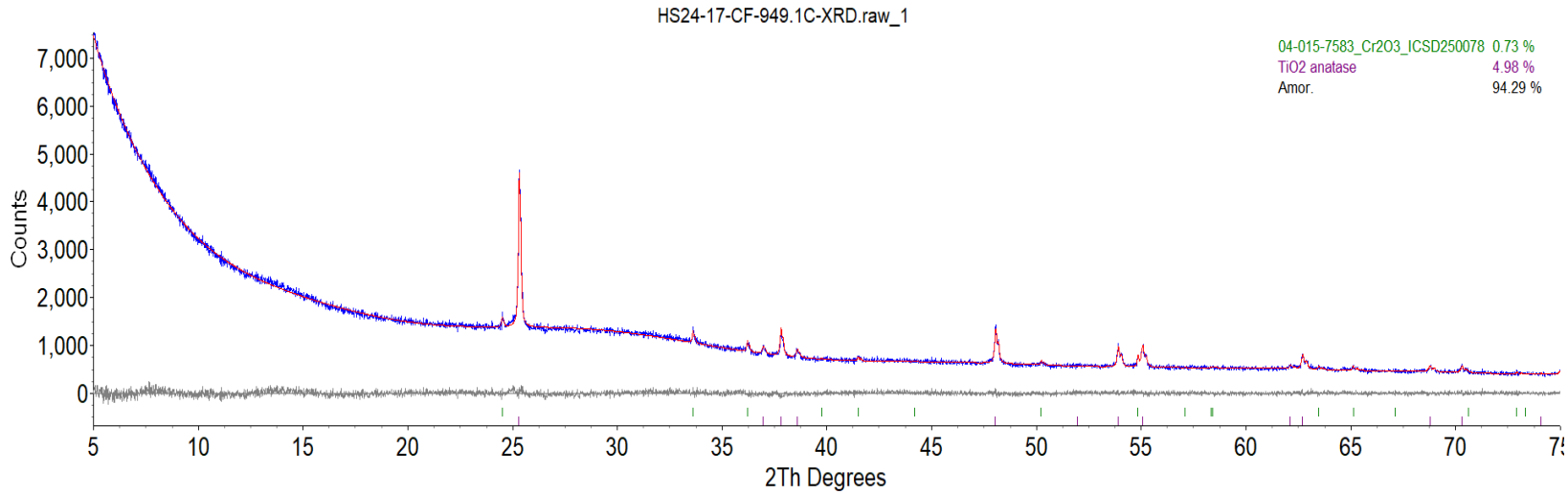

Figure G.27. XRD scan of glass HS24-17 after isothermal heat treatment at 950 °C for 24 h. The crystalline phase is Cr_2O_3. T_L was not determined due to the abnormal CF trend as function of temperature.

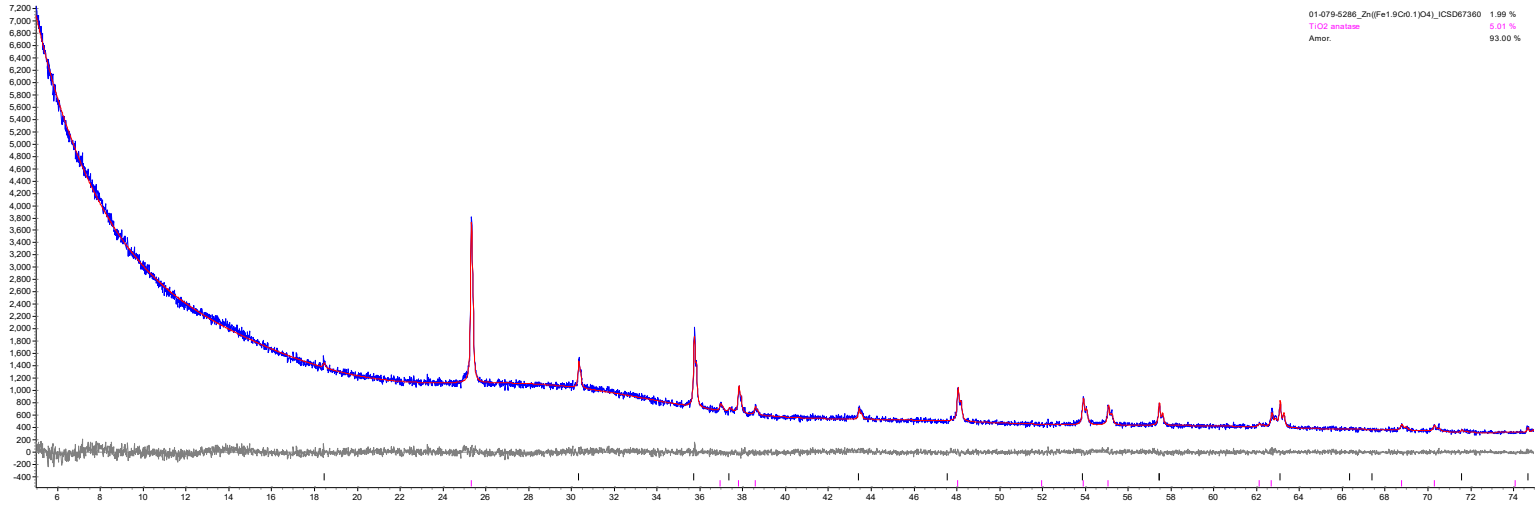

Figure G.28. XRD scan of glass HS24-19 after isothermal heat treatment at 950 °C for 24 h. The crystalline phase is $ZnFe_{1.9}Cr_{0.1}O_4$.

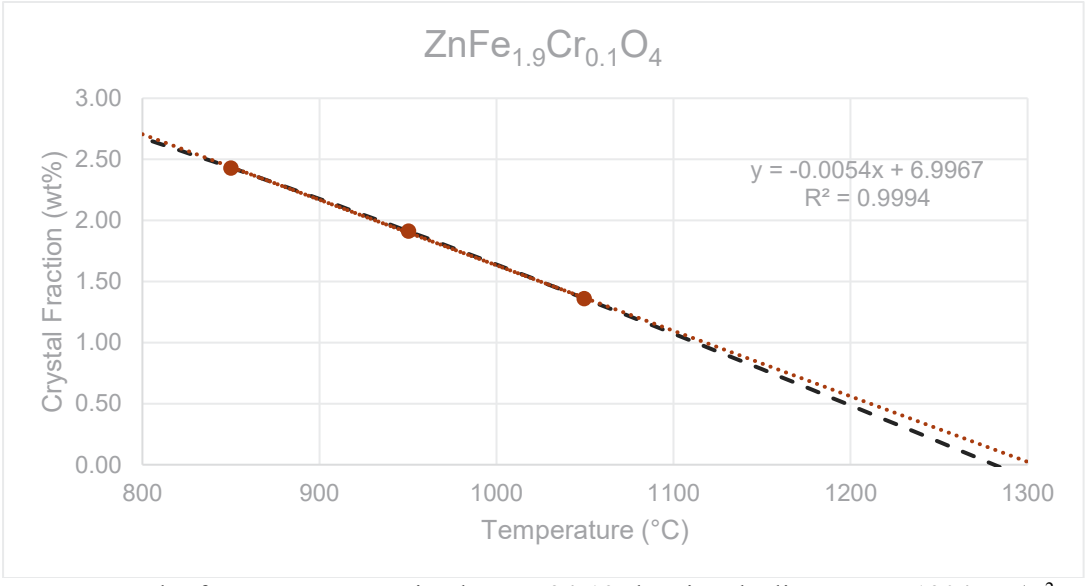

Figure G.29. The liquidus temperature plot for $ZnFe_{1.9}Cr_{0.1}O_4$ in glass HS24-19 showing the linear T_L at 1304 °C (R^2 = 0.9994) and the non-linear (black dash line) T_L at 1281 °C.

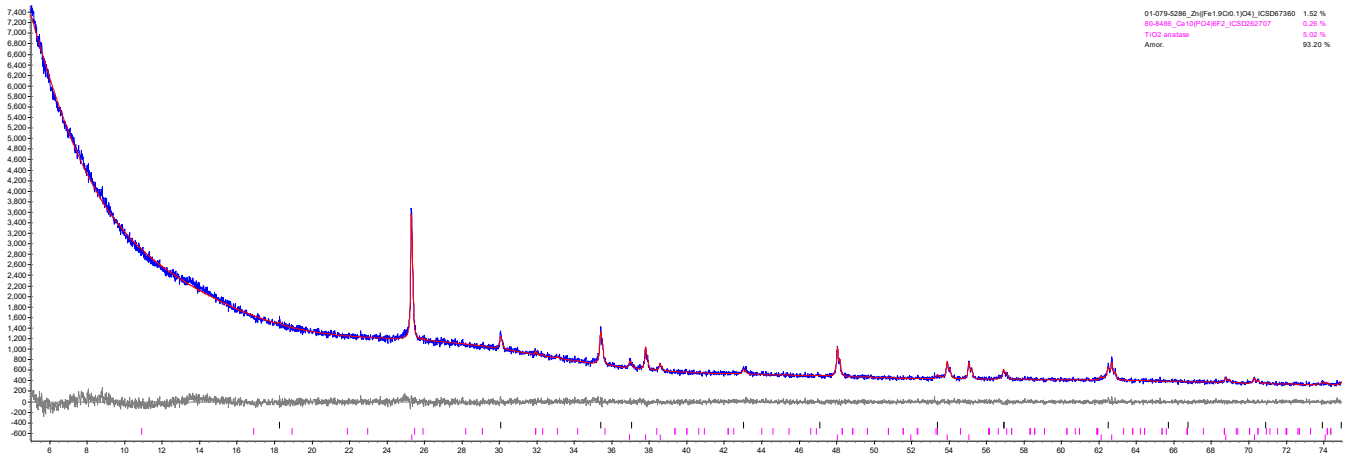

Figure G.30. XRD scan of glass HS24-21 after isothermal heat treatment at 950 °C for 24 h. The crystalline phases are $Ca_{10}(PO_4)_6F_2$ and $ZnFe_{1.9}Cr_{0.1}O_4$.

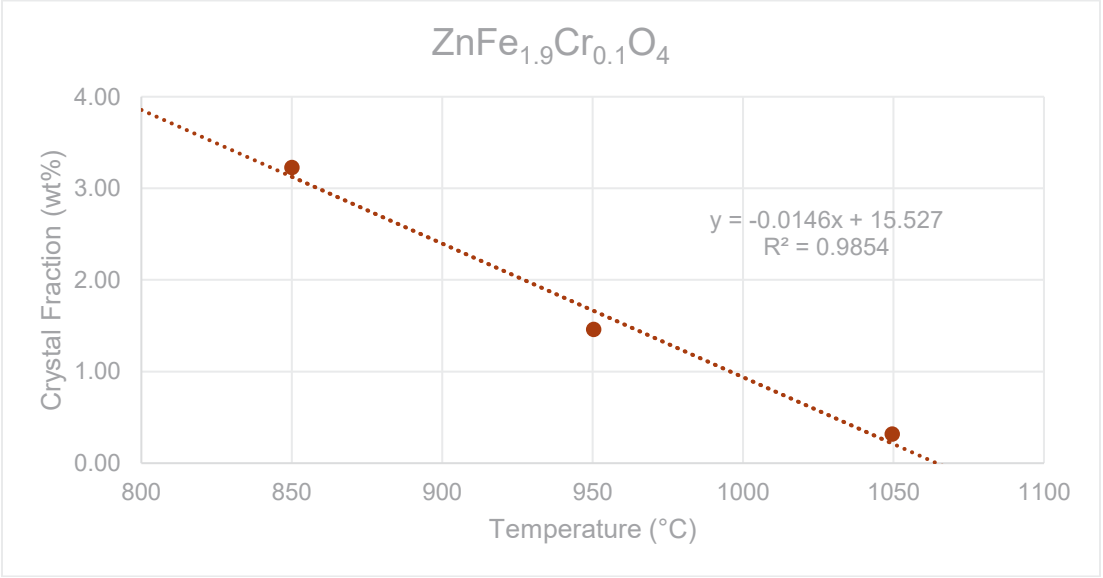

Figure G.31. The liquidus temperature plot for $ZnFe_{1.9}Cr_{0.1}O_4$ in glass HS24-21 showing the linear T_L at 1064 °C (R^2 = 0.9854).

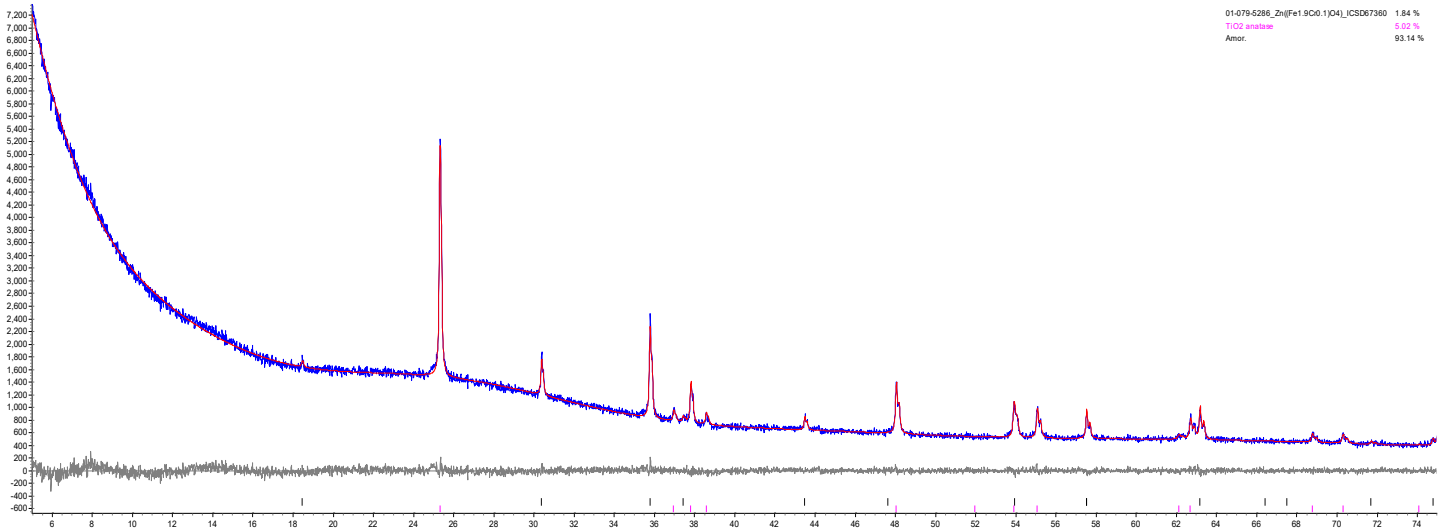

Figure G.32. XRD scan of glass HS24-22 after isothermal heat treatment at 950 °C for 24 h. The crystalline phase is $ZnFe_{1.9}Cr_{0.1}O_4$.

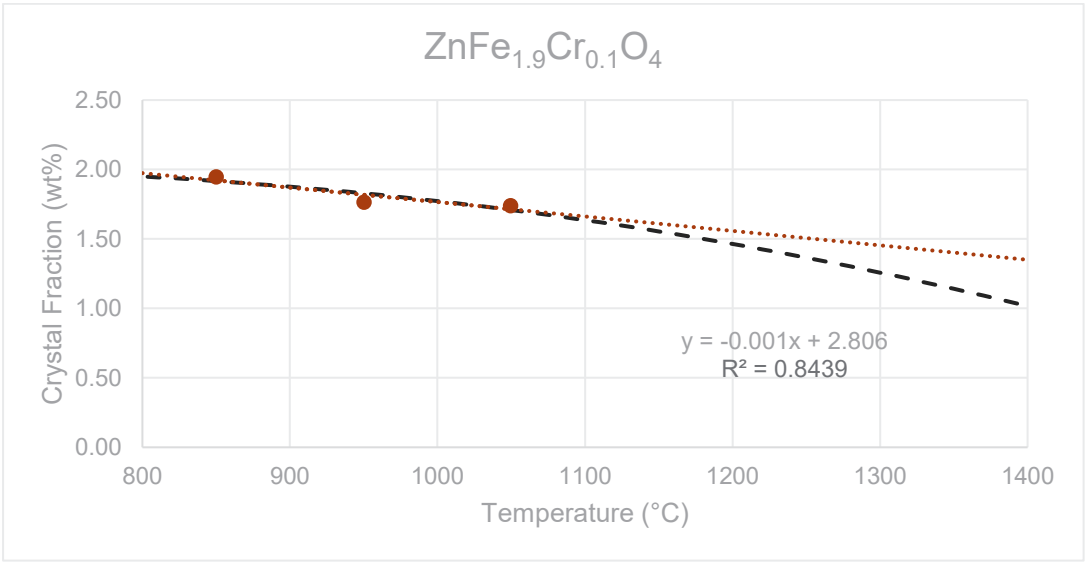

Figure G.33. The liquidus temperature plot for $ZnFe_{1.9}Cr_{0.1}O_4$ in glass HS24-22 showing the linear T_L at 2698 °C (R^2 = 0.8439) and the non-linear (black dash line) T_L at 1727 °C.

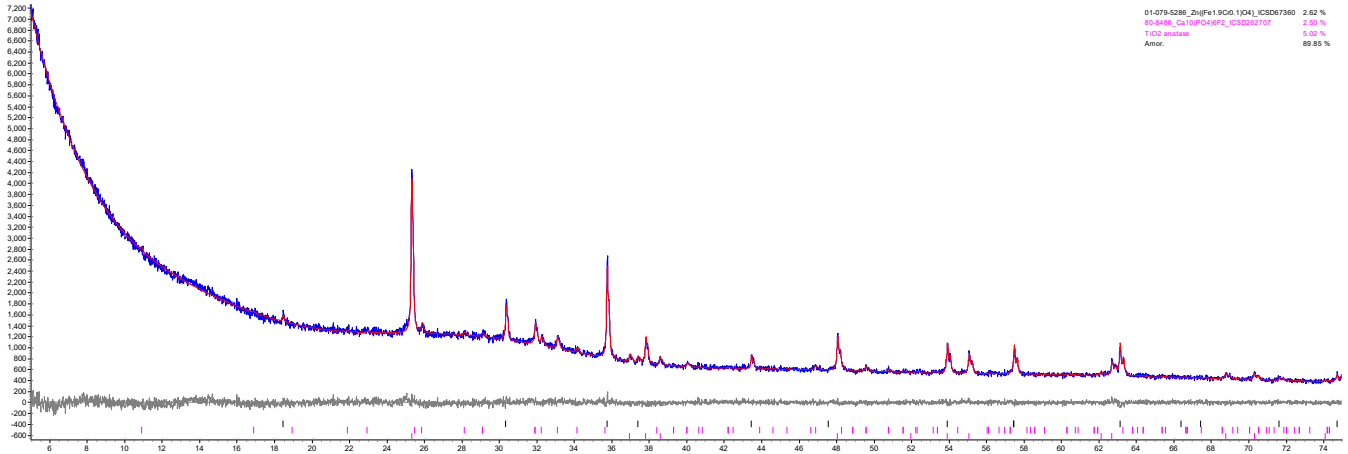

Figure G.34. XRD scan of glass HS24-23 after isothermal heat treatment at 950 °C for 24 h. The crystalline phases are $Ca_{10}(PO_4)_6F_2$ and $ZnFe_{1.9}Cr_{0.1}O_4$.

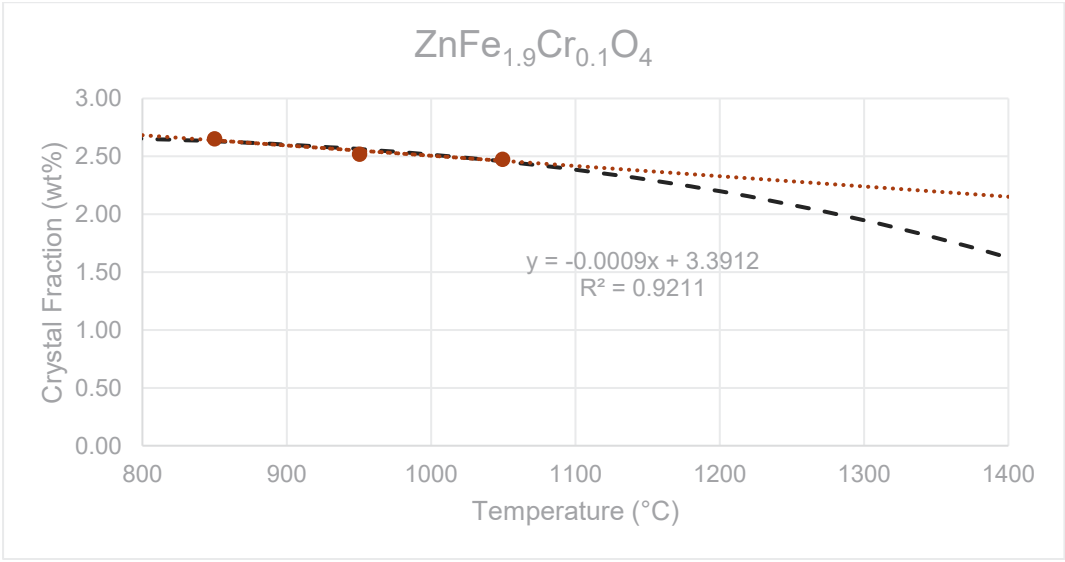

Figure G.35. The liquidus temperature plot for $ZnFe_{1.9}Cr_{0.1}O_4$ in glass HS24-23 showing the linear T_L at 3828 °C (R^2 = 0.9211) and the non-linear (black dash line) T_L at 1727 °C.

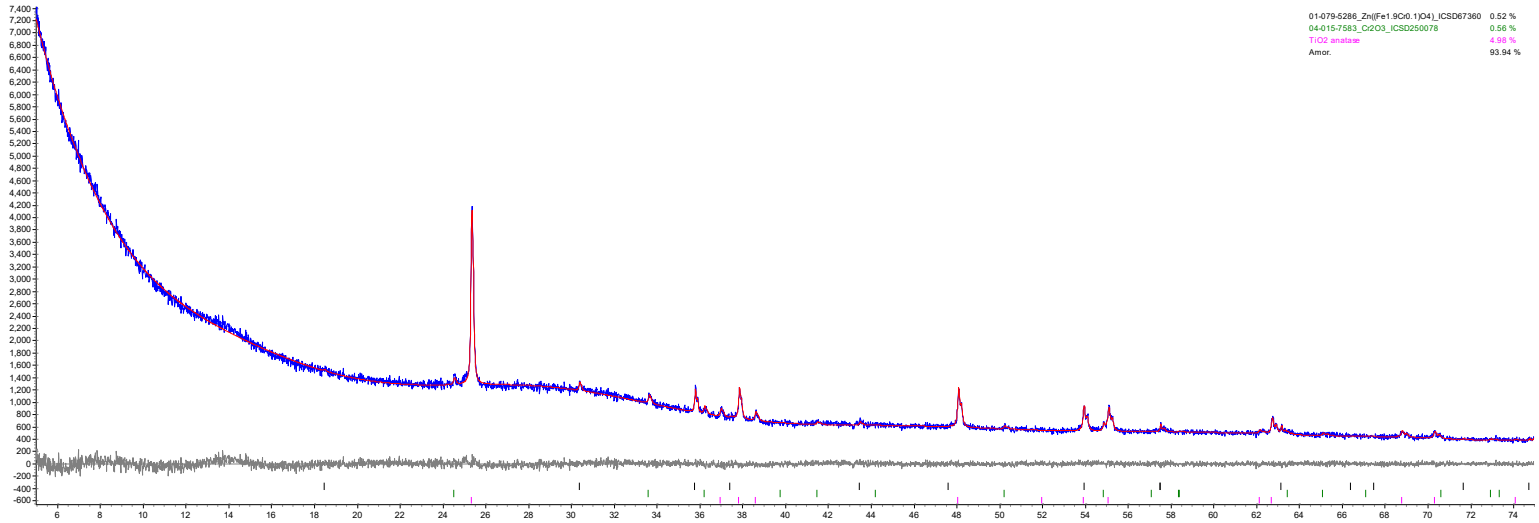

Figure G.36. XRD scan of glass HS24-24 after isothermal heat treatment at 950 °C for 24 h. The crystalline phases are Cr_2O_3 and $ZnFe_{1.9}Cr_{0.1}O_4$. T_L was not determined due to the abnormal CF trend as function of temperature.

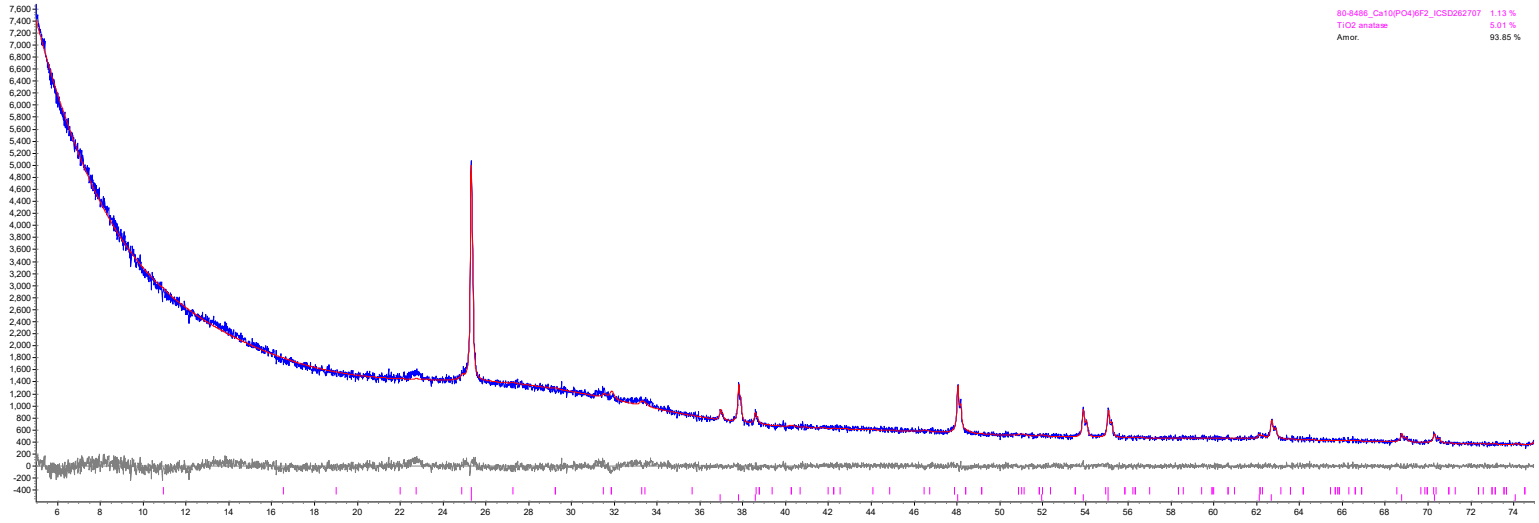

Figure G.37. XRD scan of glass HS24-25 after isothermal heat treatment at 950 °C for 24 h. The crystalline phase is $Ca_{10}(PO_4)_6F_2$.

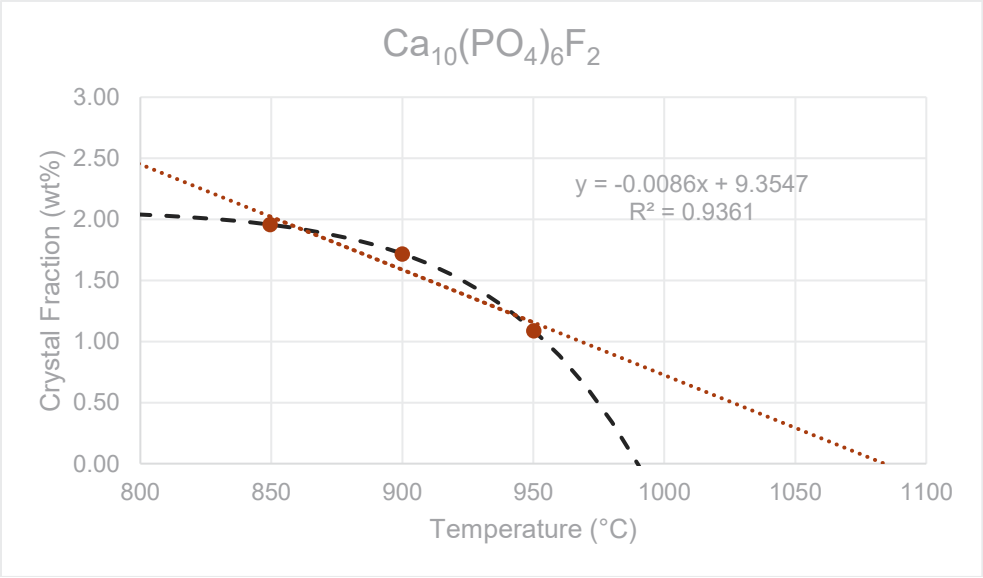

Figure G.38. The liquidus temperature plot for $Ca_{10}(PO_4)_6F_2$ in glass HS24-25 showing the linear T_L at 1084 °C (R^2 = 0.9361) and the non-linear (black dash line) T_L at 990 °C. The non-linear fitting T_L was accepted as no crystal was observed at 1000 °C.

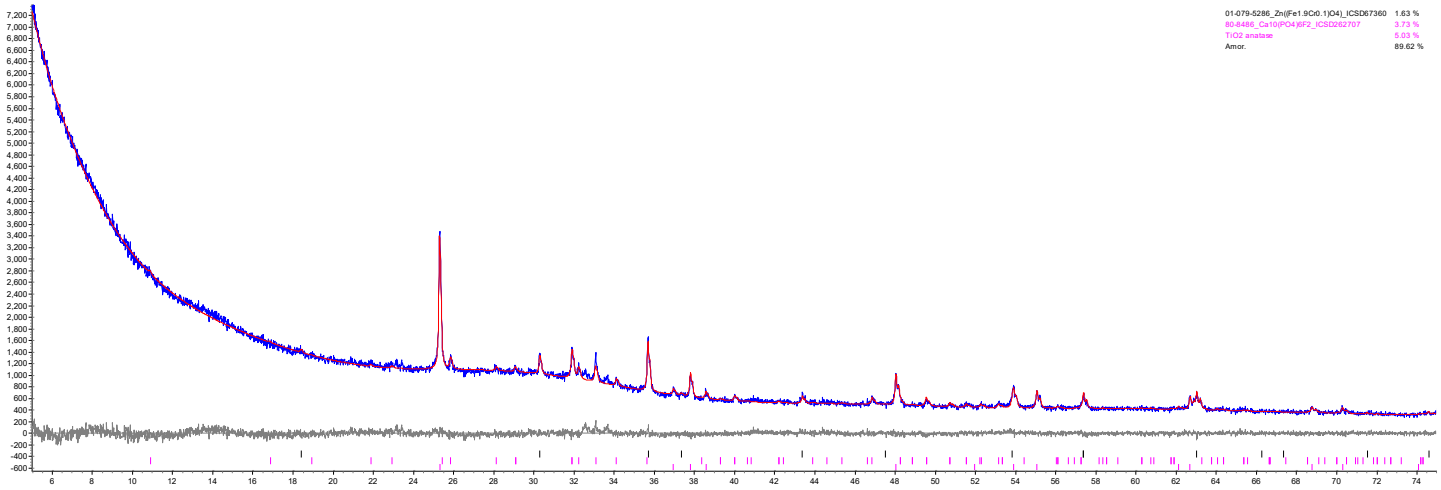

Figure G.39. XRD scan of glass HS24-26 after isothermal heat treatment at 950 °C for 24 h. The crystalline phases are $Ca_{10}(PO_4)_6F_2$ and $ZnFe_{1.9}Cr_{0.1}O_4$.

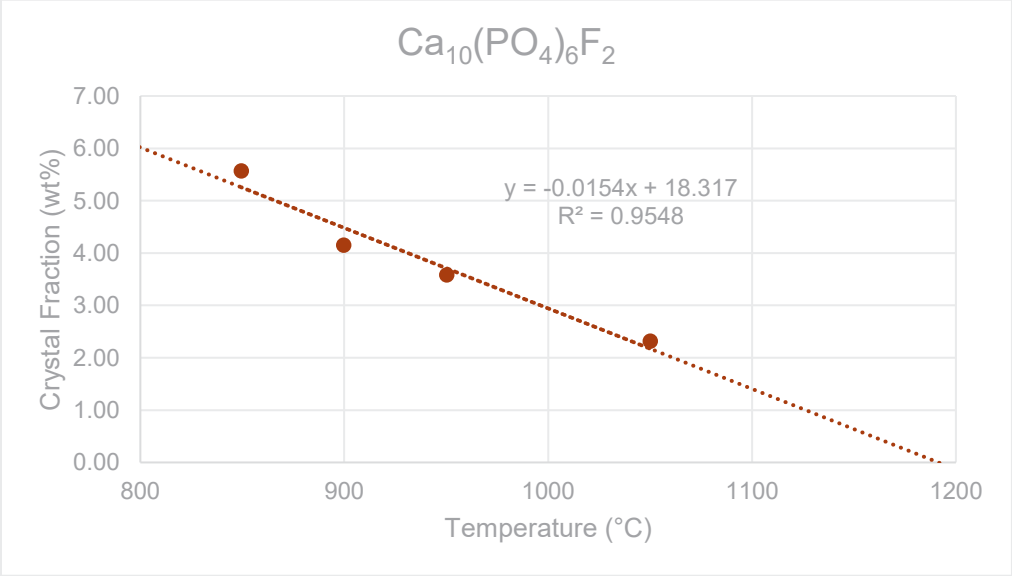

Figure G.40. The liquidus temperature plot for $Ca_{10}(PO_4)_6F_2$ in glass HS24-26 showing the linear T_L at 1191 °C ($R^2 = 0.9548$)

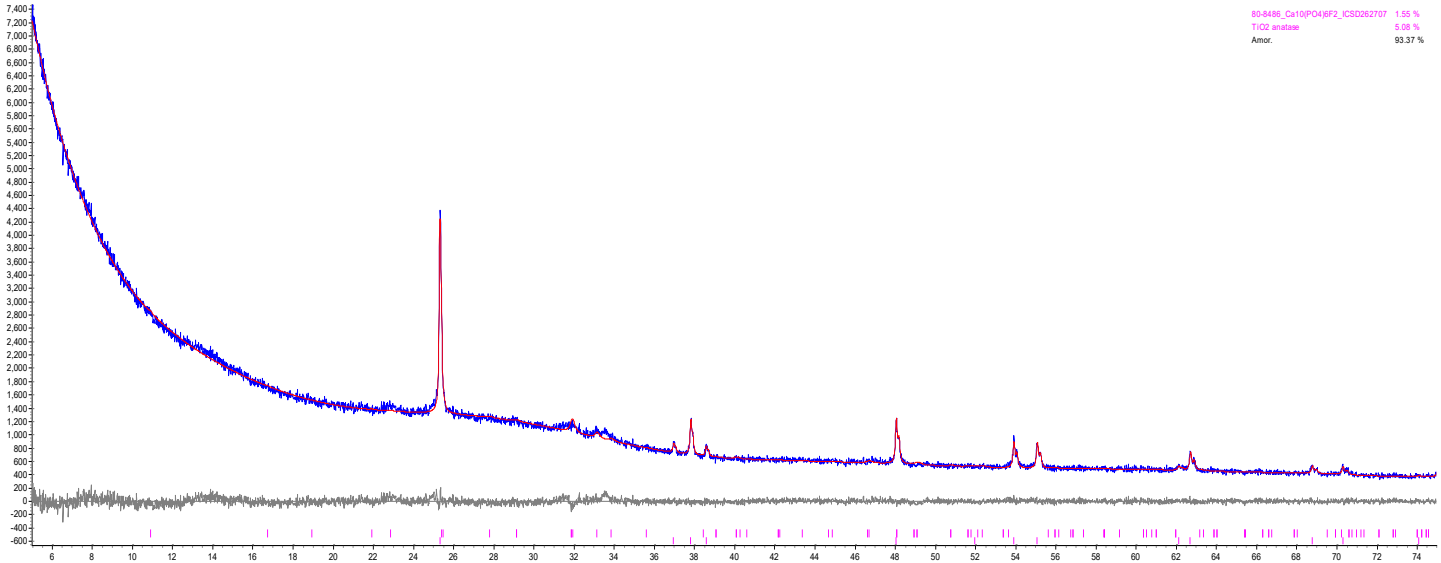

Figure G.41. XRD scan of glass HS24-27 after isothermal heat treatment at 950 °C for 24 h. The crystalline phase is $Ca_{10}(PO_4)_6F_2$.

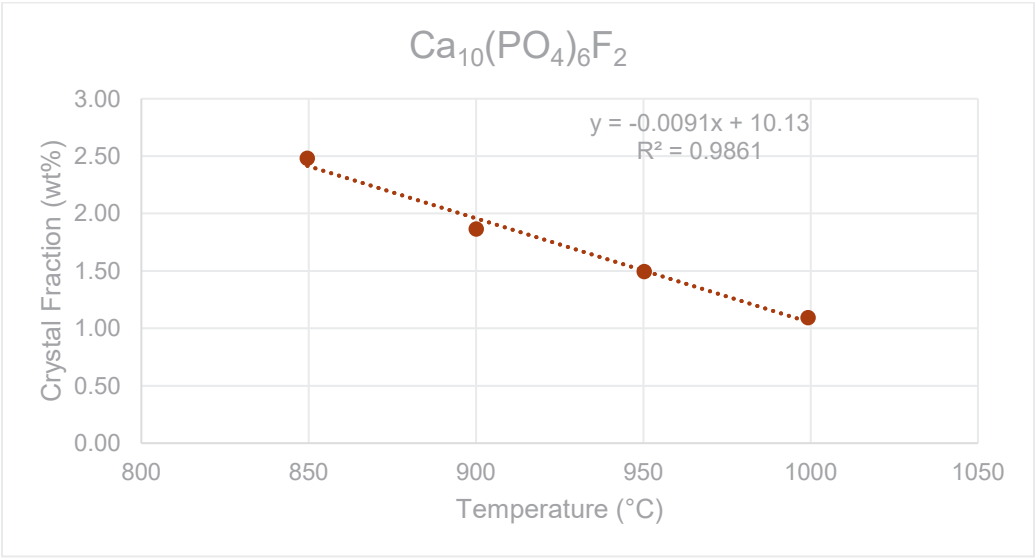

Figure G.42. The liquidus temperature plot for $Ca_{10}(PO_4)_6F_2$ in glass HS24-27 showing the linear T_L at 1116 °C ($R^2 = 0.9861$)

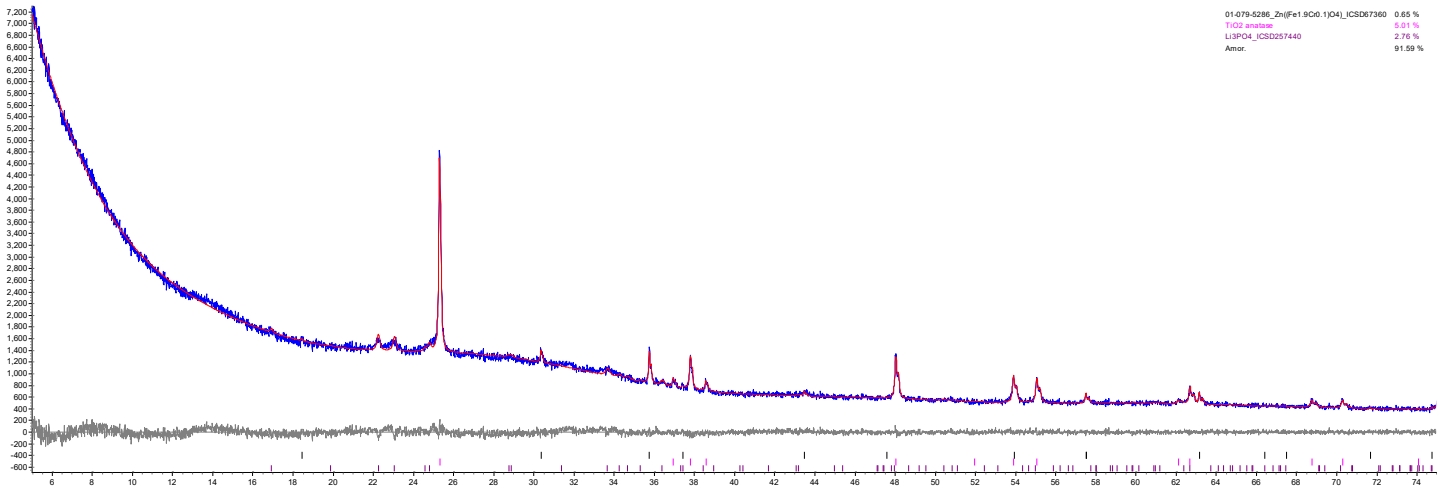

Figure G.43. XRD scan of glass HS24-28 after isothermal heat treatment at 950 °C for 24 h. The crystalline phases are Li_3PO_4 and $ZnFe_{1.9}Cr_{0.1}O_4$.

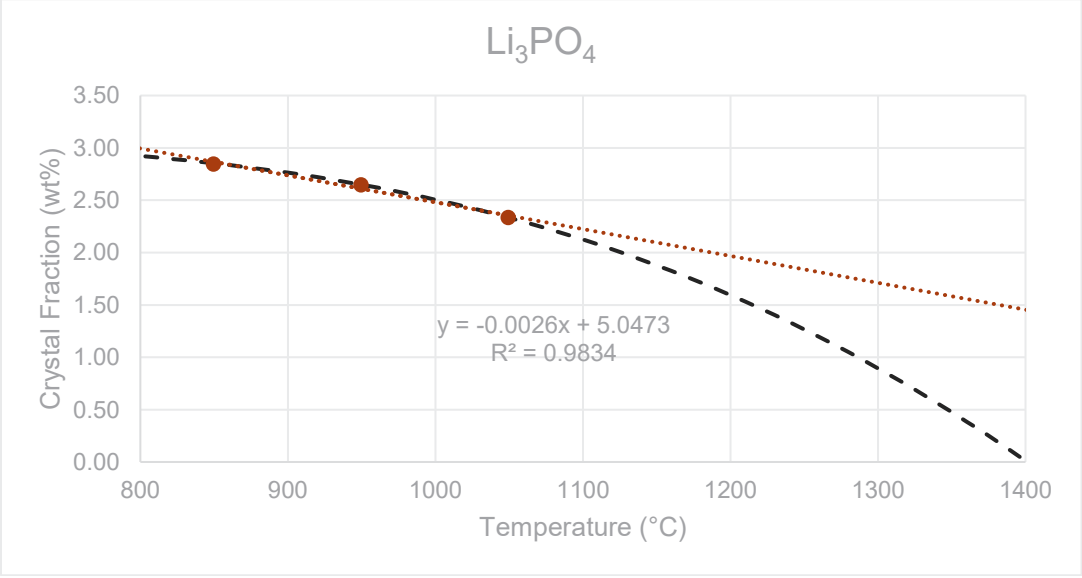

Figure G.44. The liquidus temperature plot for Li_3PO_4 in glass HS24-28 showing the linear T_L at 1967 °C (R^2 = 0.9834) and the non-linear (black dash line) T_L at 1401 °C.

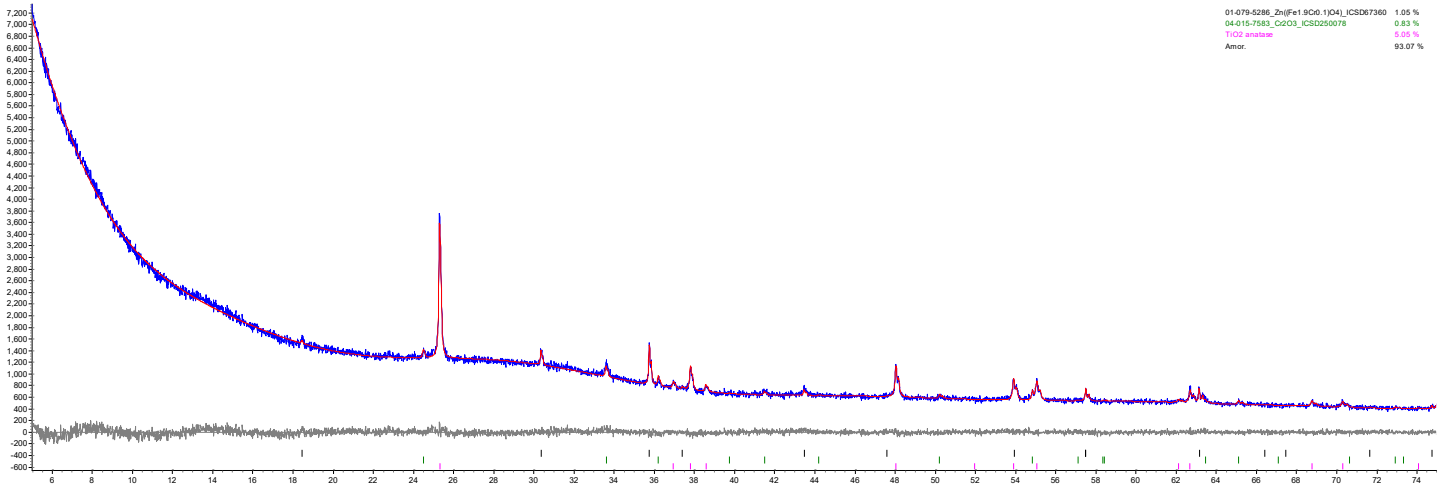

Figure G.45. XRD scan of glass HS24-30 after isothermal heat treatment at 950 °C for 24 h. The crystalline phases are Cr_2O_3 and $ZnFe_{1.9}Cr_{0.1}O_4$. T_L was not determined due to the abnormal CF trend as function of temperature.

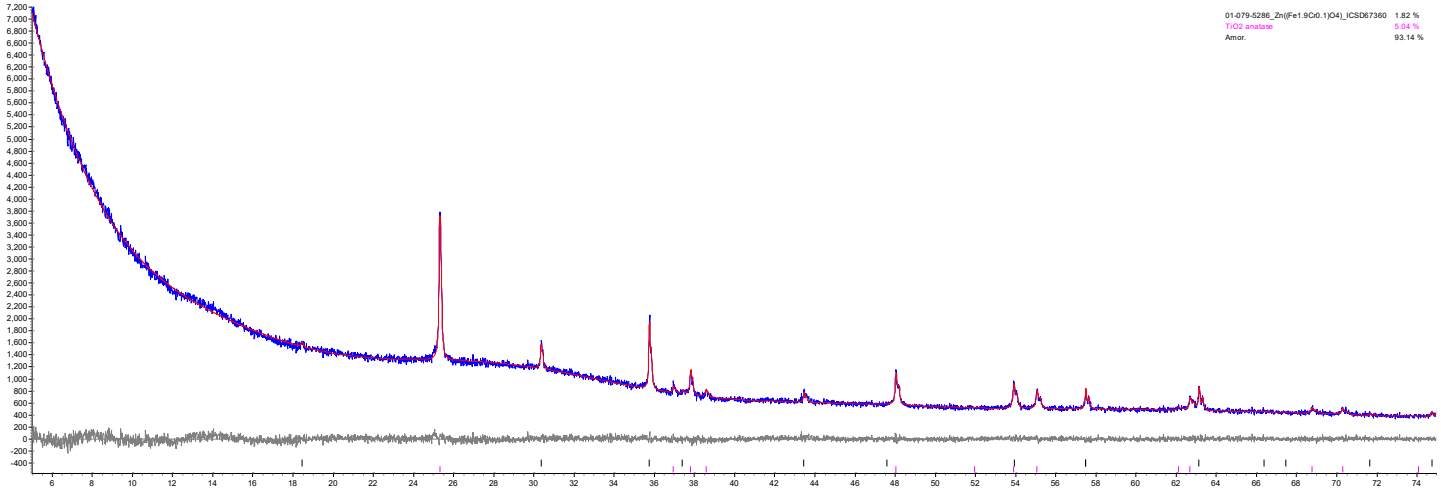

Figure G.46. XRD scan of glass HS24-31 after isothermal heat treatment at 950 °C for 24 h. The crystalline phase is $ZnFe_{1.9}Cr_{0.1}O_4$.

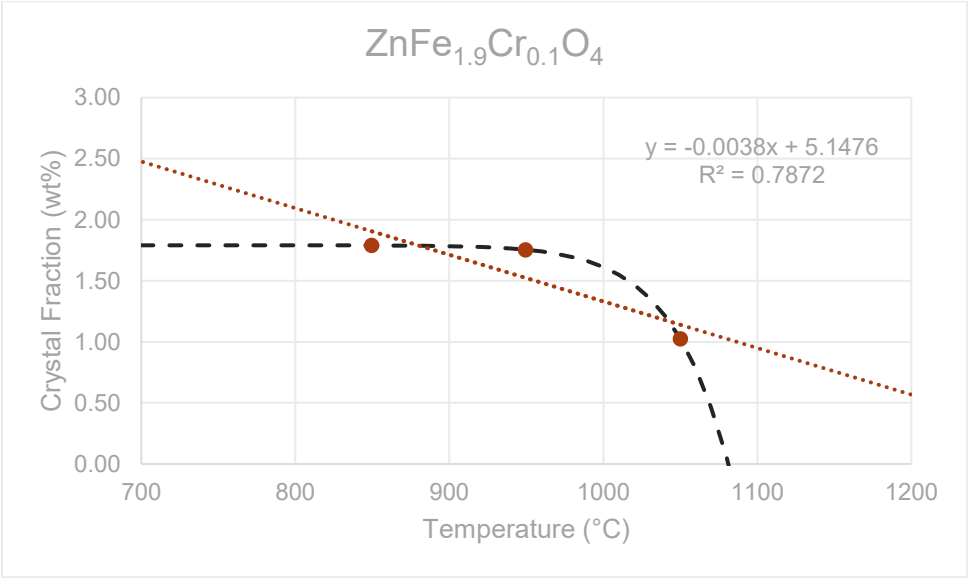

Figure G.47. The liquidus temperature plot for $ZnFe_{1.9}Cr_{0.1}O_4$ in glass HS24-31 showing the linear T_L at 1349 °C ($R^2 = 0.7872$) and the non-linear (black dash line) T_L at 1081 °C.

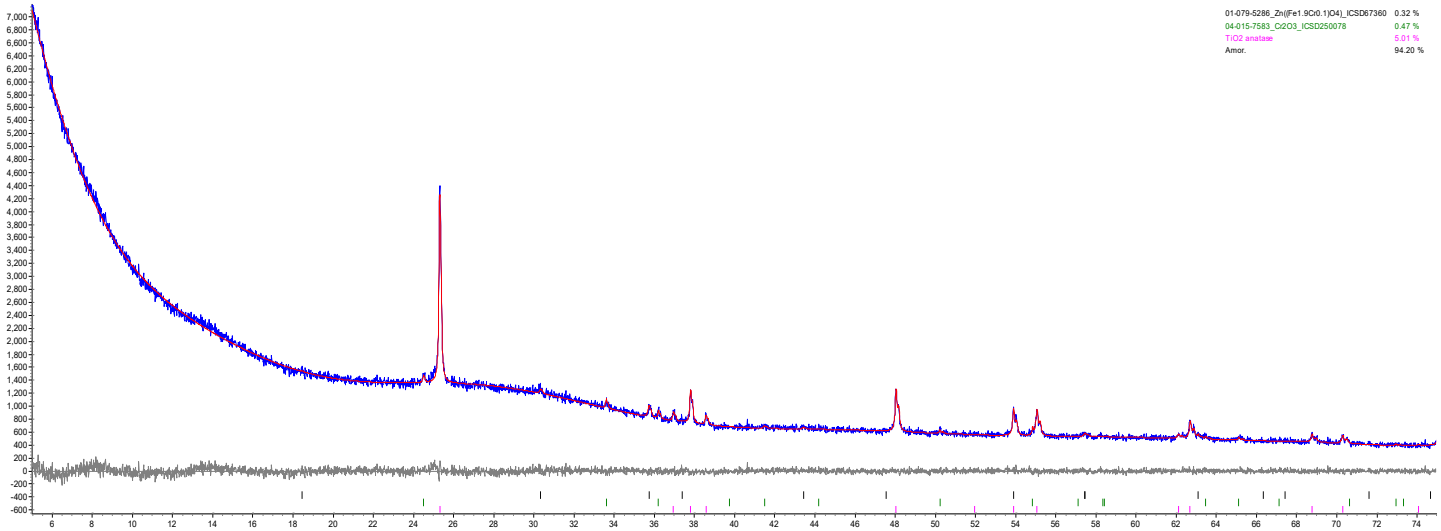

Figure G.48. XRD scan of glass HS24-32 after isothermal heat treatment at 950 °C for 24 h. The crystalline phases are Cr_2O_3 and $ZnFe_{1.9}Cr_{0.1}O_4$.

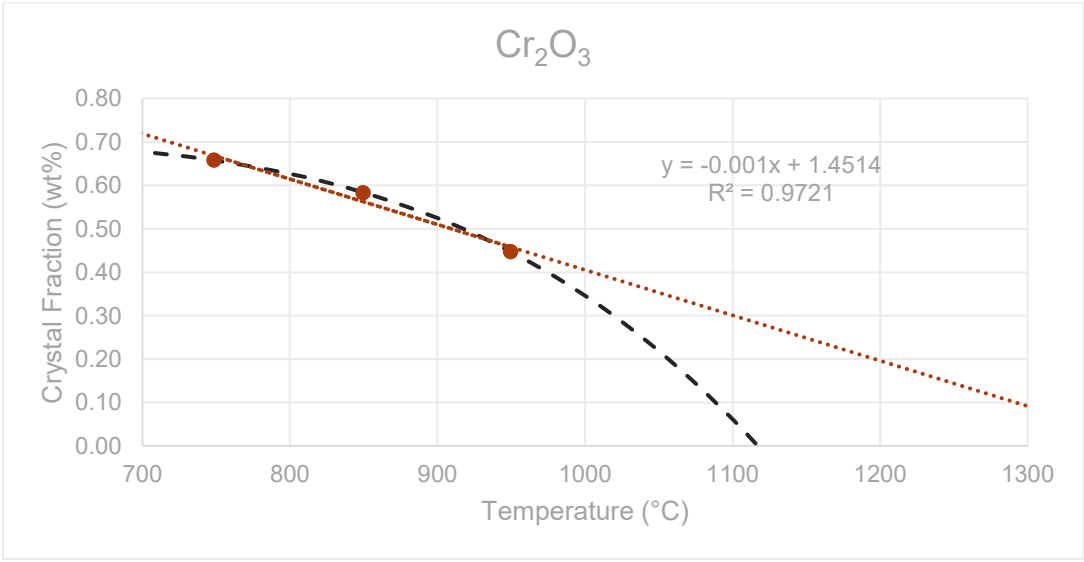

Figure G.49. The liquidus temperature plot for Cr_2O_3 in glass HS24-32 showing the linear T_L at 1387 °C (R^2 = 0.9721) and the non-linear (black dash line) T_L at 1117 °C.

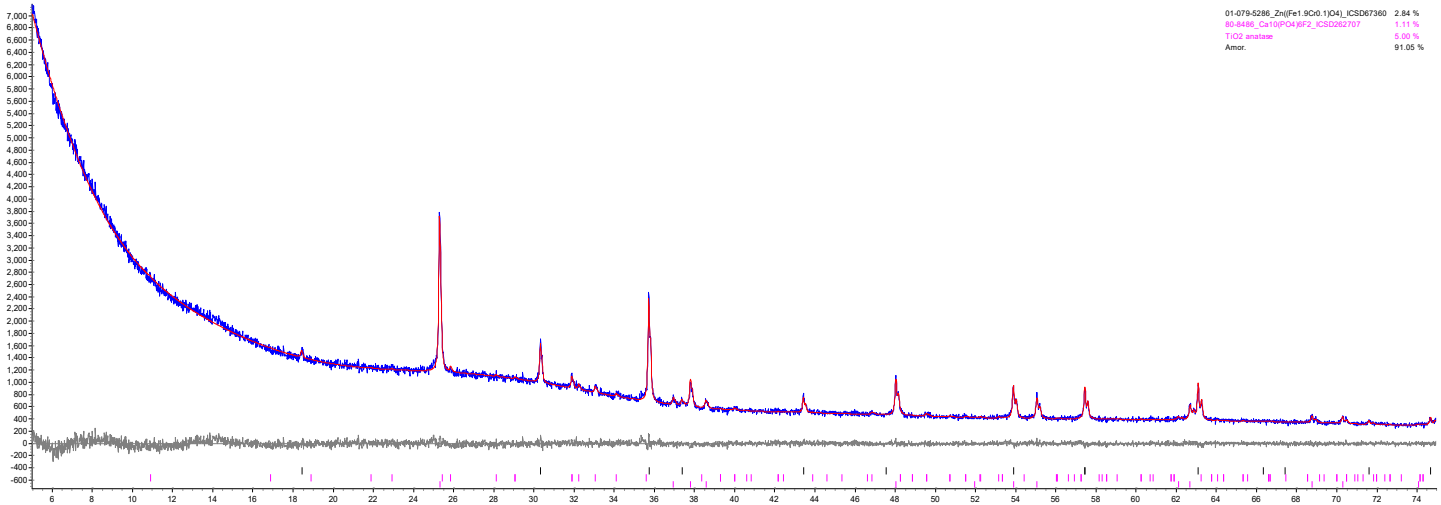

Figure G.50. XRD scan of glass HS24-33 after isothermal heat treatment at 950 °C for 24 h. The crystalline phases are $Ca_{10}(PO_4)_6F_2$ and $ZnFe_{1.9}Cr_{0.1}O_4$.

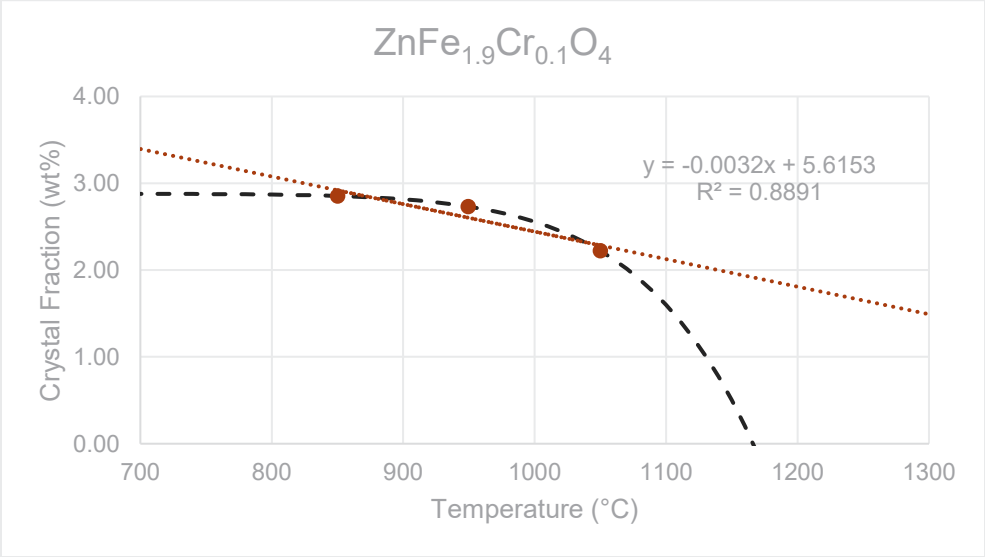

Figure G.51. The liquidus temperature plot for $ZnFe_{1.9}Cr_{0.1}O_4$ in glass HS24-33 showing the linear T_L at 1770 °C (R^2 = 0.8891) and the non-linear (black dash line) T_L at 1166 °C.

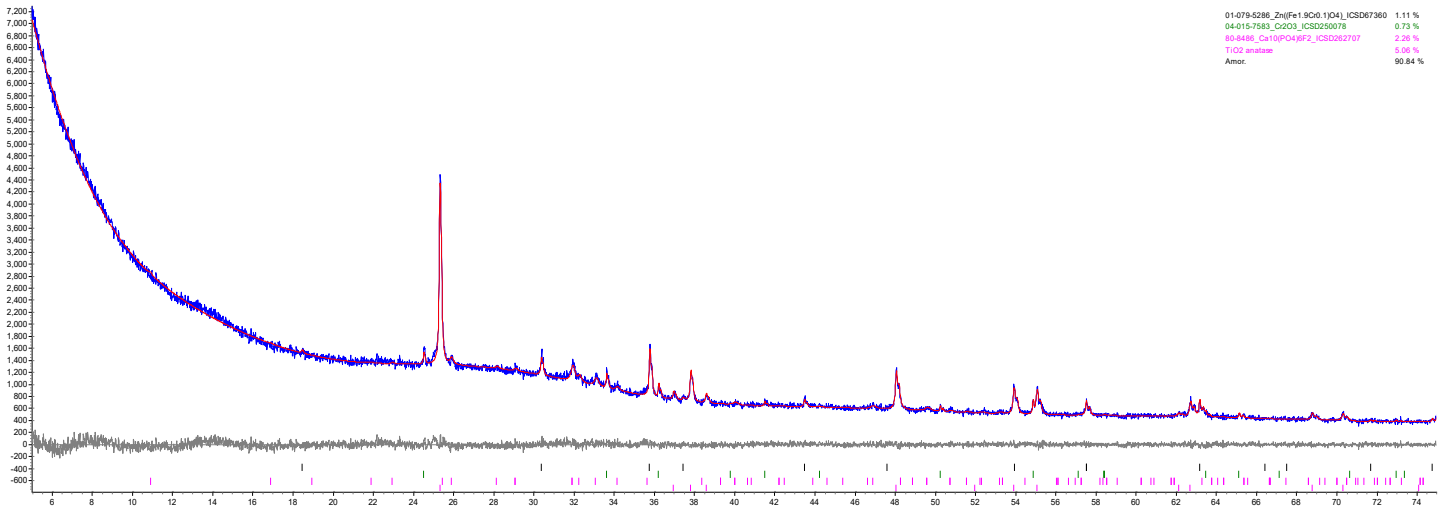

Figure G.52. XRD scan of glass HS24-34 after isothermal heat treatment at 950 °C for 24 h. The crystalline phases are $Ca_{10}(PO_4)_6F_2$, Cr_2O_3 and $ZnFe_{1.9}Cr_{0.1}O_4$.

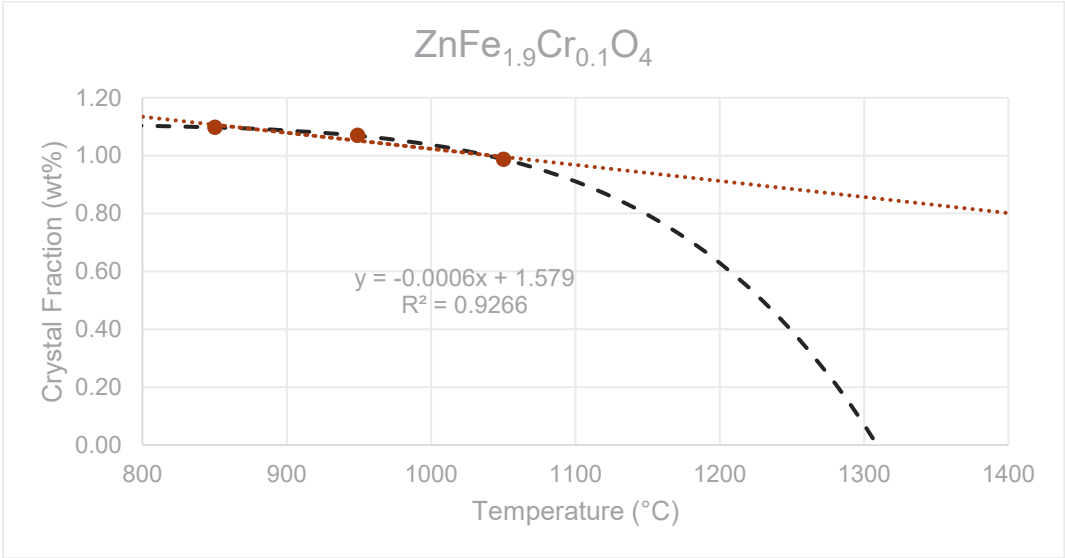

Figure G.53. The liquidus temperature plot for $ZnFe_{1.9}Cr_{0.1}O_4$ in glass HS24-34 showing the linear T_L at 2843 °C (R^2 = 0.9266) and the non-linear (black dash line) T_L at 1309 °C.

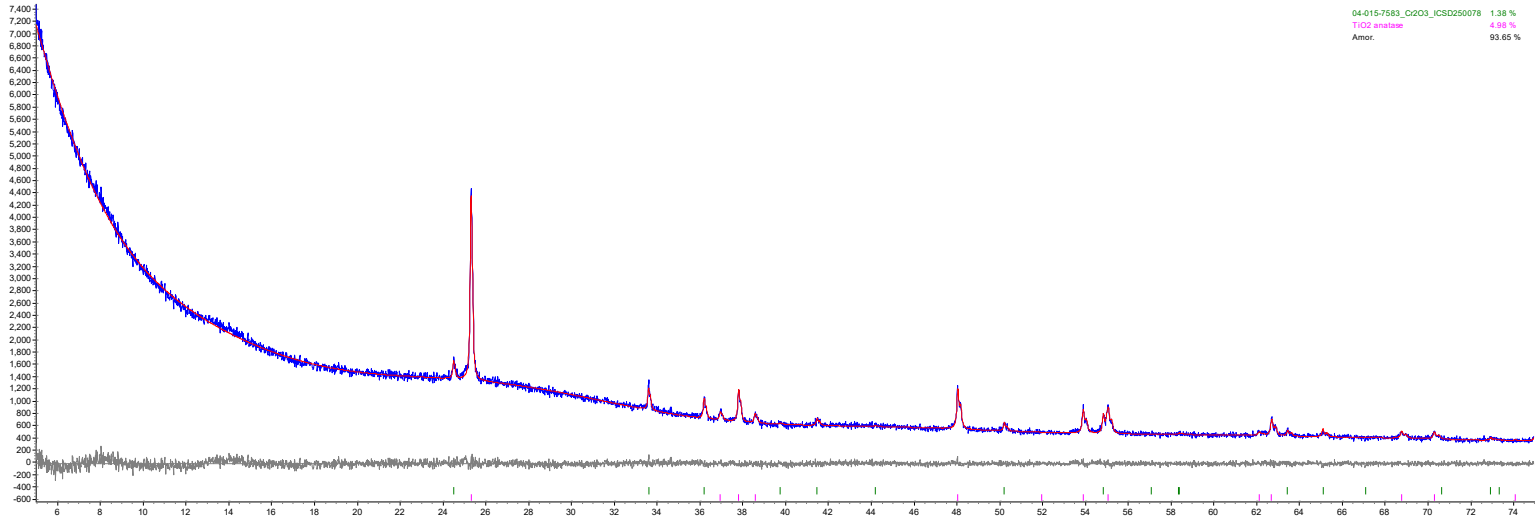

Figure G.54. XRD scan of glass HS24-35 after isothermal heat treatment at 950 °C for 24 h. The crystalline phase is Cr_2O_3.

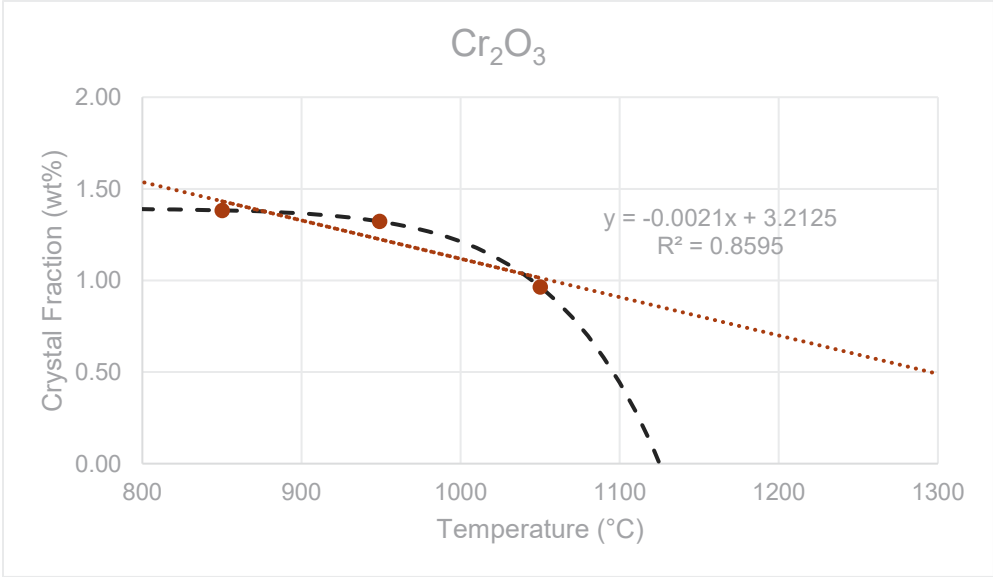

Figure G.55. The liquidus temperature plot for Cr_2O_3 in glass HS24-35 showing the linear T_L at 1534 °C (R^2 = 0.8595) and the non-linear (black dash line) T_L at 1125 °C.

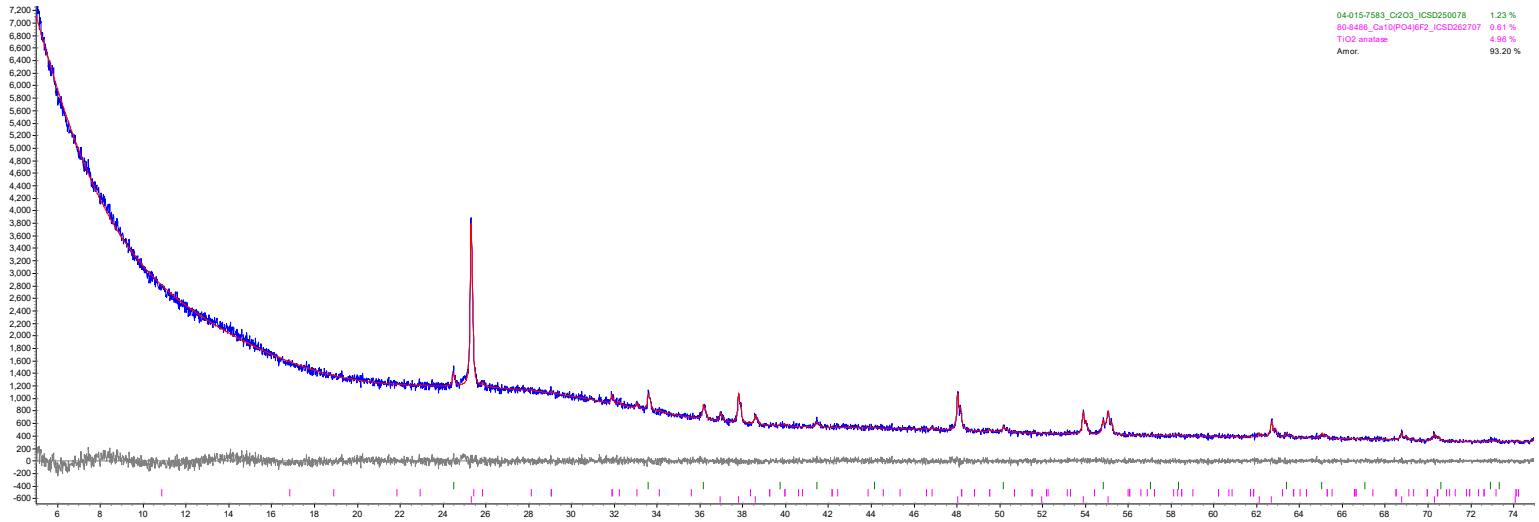

Figure G.56. XRD scan of glass HS24-36 after isothermal heat treatment at 950 °C for 24 h. The crystalline phases are $Ca_{10}(PO_4)_6F_2$ and Cr_2O_3.

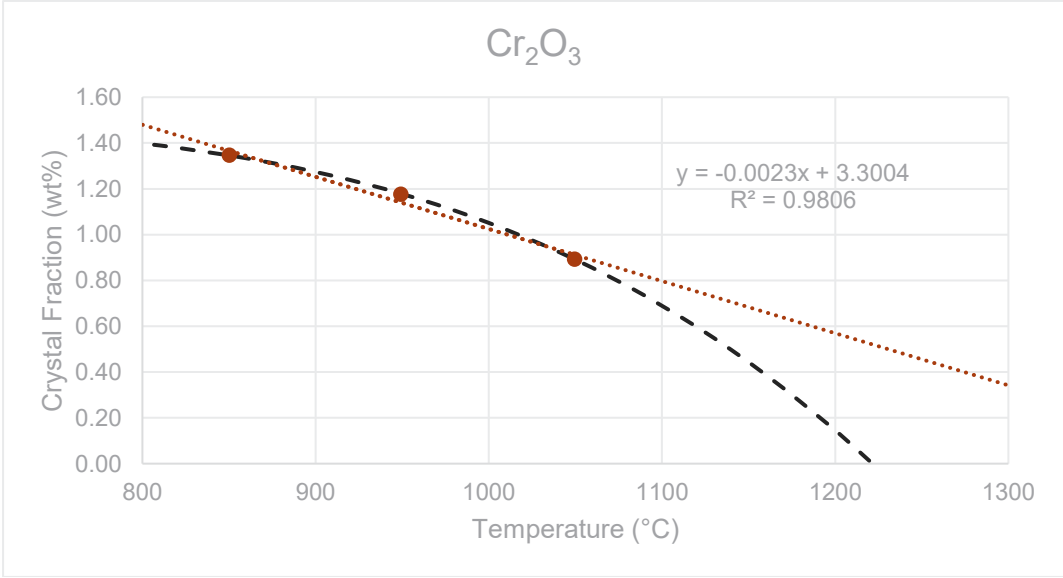

Figure G.57. The liquidus temperature plot for Cr_2O_3 in glass HS24-36 showing the linear T_L at 1450 °C ($R^2 = 0.9806$) and the non-linear (black dash line) T_L at 1222 °C.

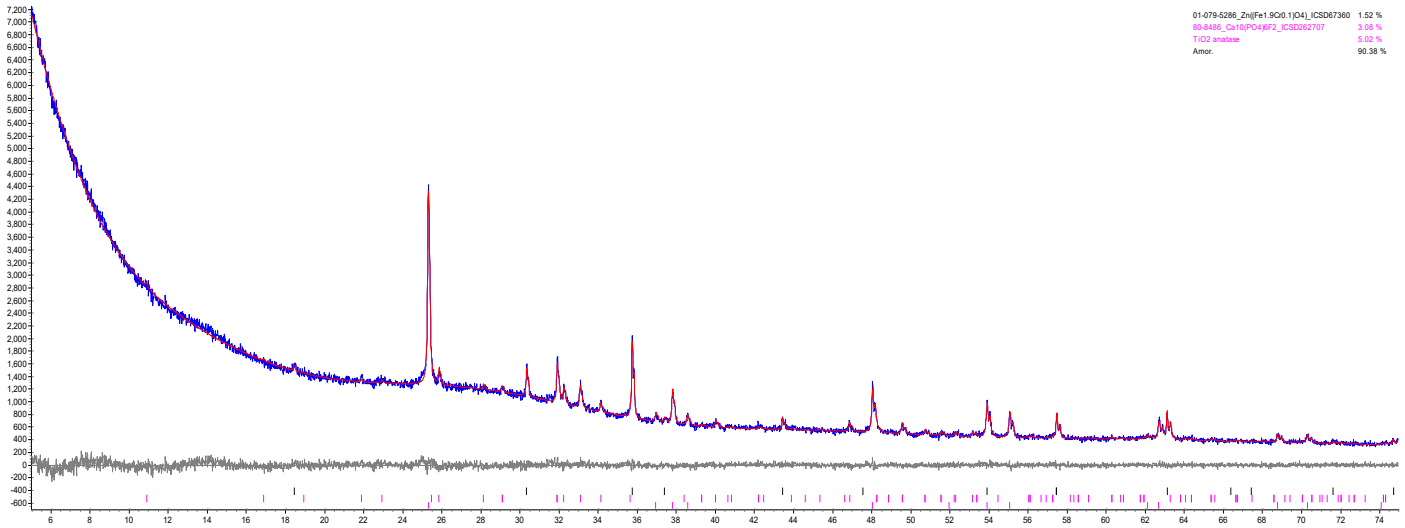

Figure G.58. XRD scan of glass HS24-38 after isothermal heat treatment at 950 °C for 24 h. The crystalline phases are $Ca_{10}(PO_4)_6F_2$ and $ZnFe_{1.9}Cr_{0.1}O_4$.

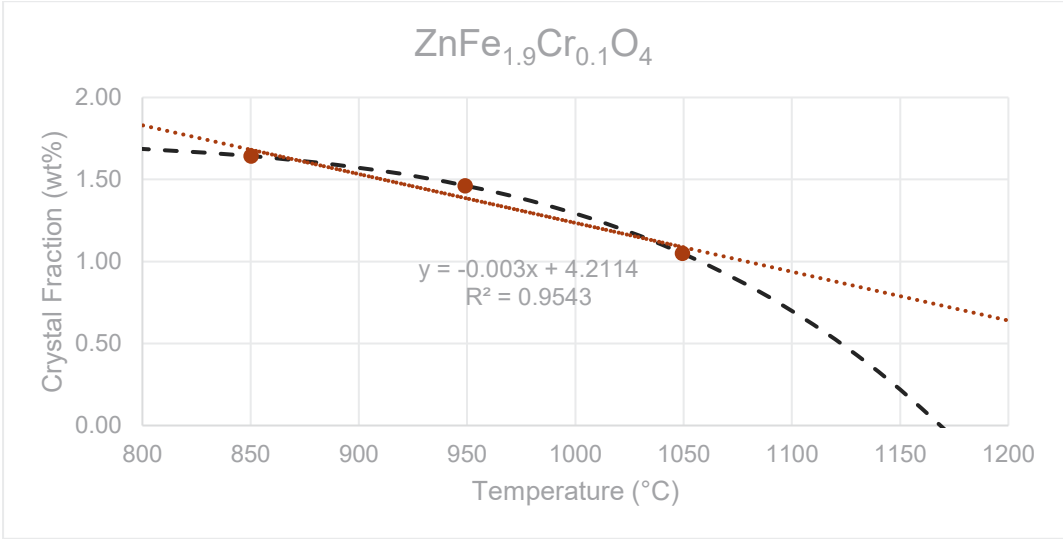

Figure G.59. The liquidus temperature plot for $ZnFe_{1.9}Cr_{0.1}O_4$ in glass HS24-38 showing the linear T_L at 1415 °C (R^2 = 0.9543) and the non-linear (black dash line) T_L at 1169 °C.

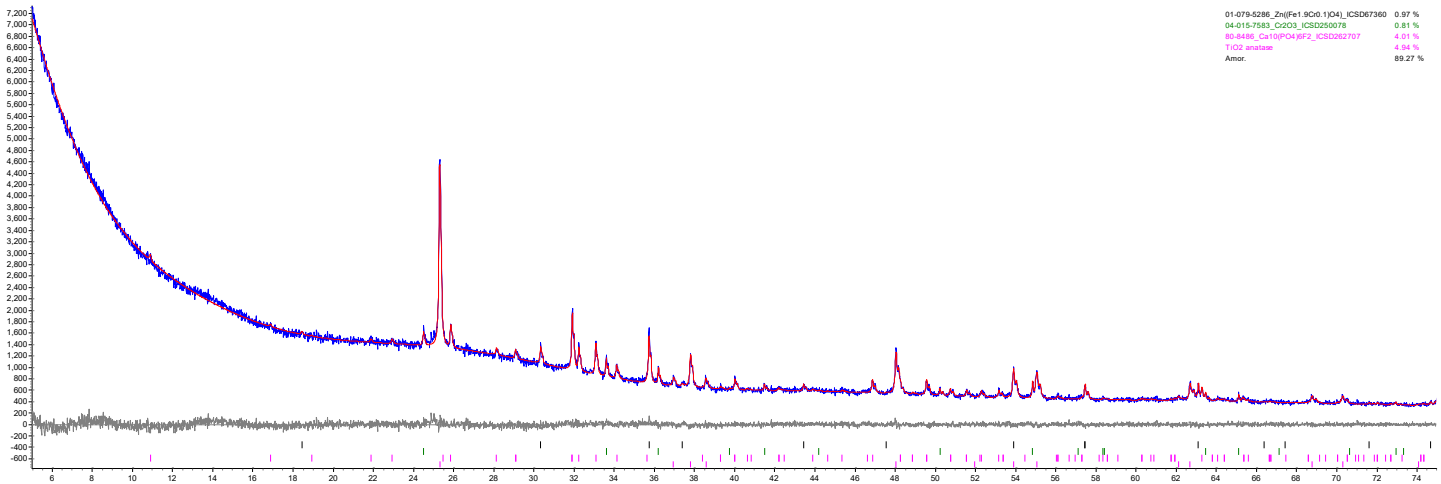

Figure G.60. XRD scan of glass HS24-39 after isothermal heat treatment at 950 °C for 24 h. The crystalline phases are $Ca_{10}(PO_4)_6F_2$, Cr_2O_3 and $ZnFe_{1.9}Cr_{0.1}O_4$.

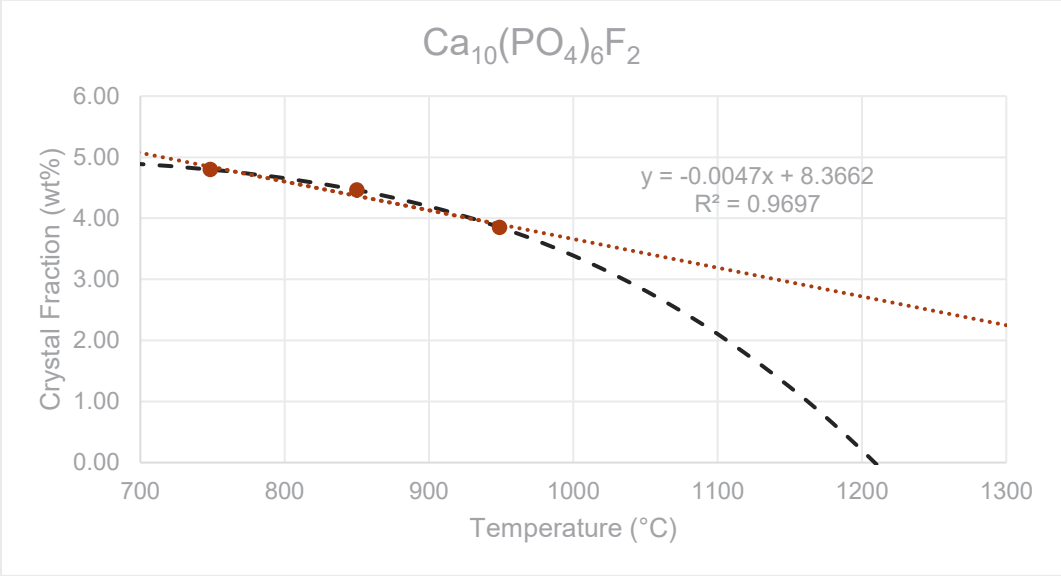

Figure G.61. The liquidus temperature plot for $Ca_{10}(PO_4)_6F_2$ in glass HS24-39 showing the linear T_L at 1778 °C (R^2 = 0.9697) and the non-linear (black dash line) T_L at 1209 °C.

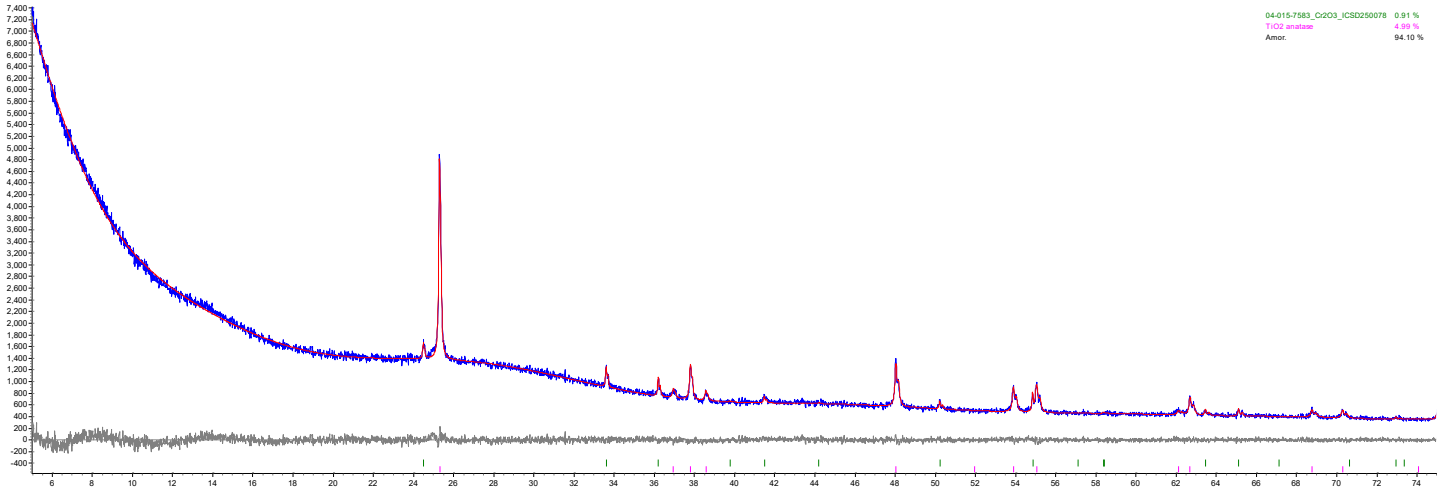

Figure G.62. XRD scan of glass HS24-40 after isothermal heat treatment at 950 °C for 24 h. The crystalline phase is Cr_2O_3.

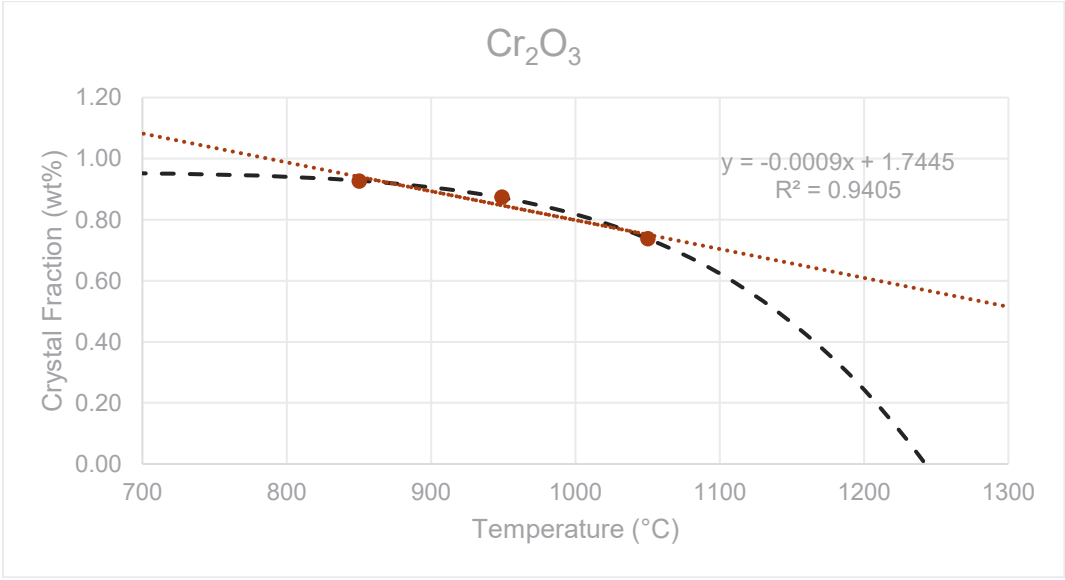

Figure G.63. The liquidus temperature plot for Cr_2O_3 in glass HS24-40 showing the linear T_L at 1844 °C (R^2 = 0.9405) and the non-linear (black dash line) T_L at 1242 °C.

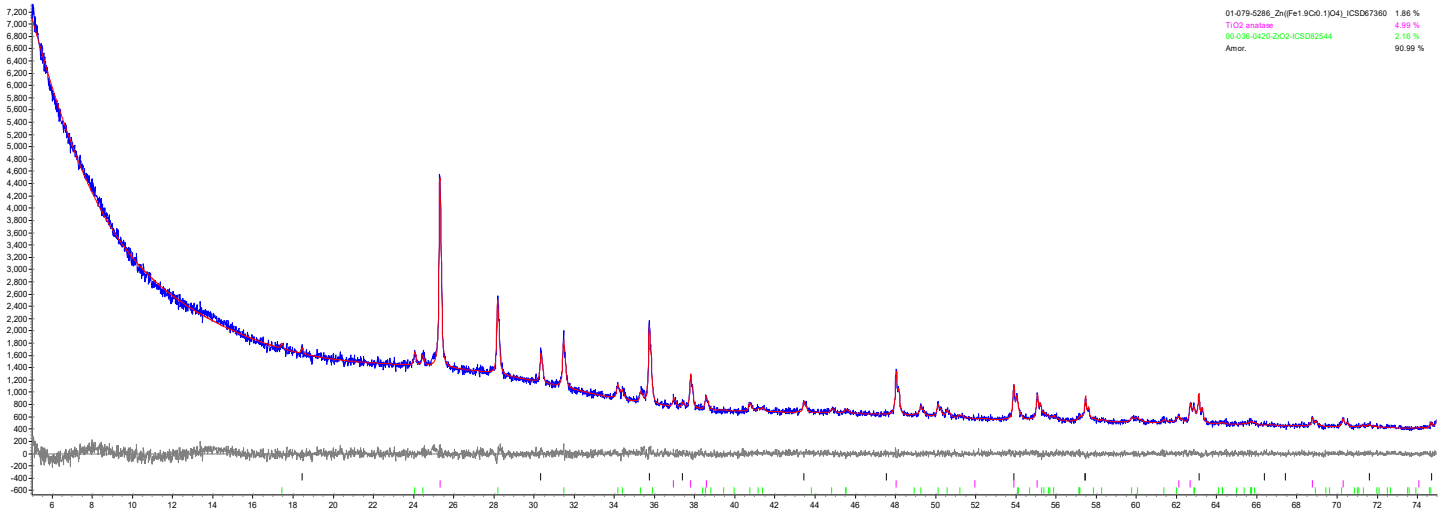

Figure G.64. XRD scan of glass HS24-42 after isothermal heat treatment at 950 °C for 24 h. The crystalline phases are ZrO_2 and $ZnFe_{1.9}Cr_{0.1}O_4$.

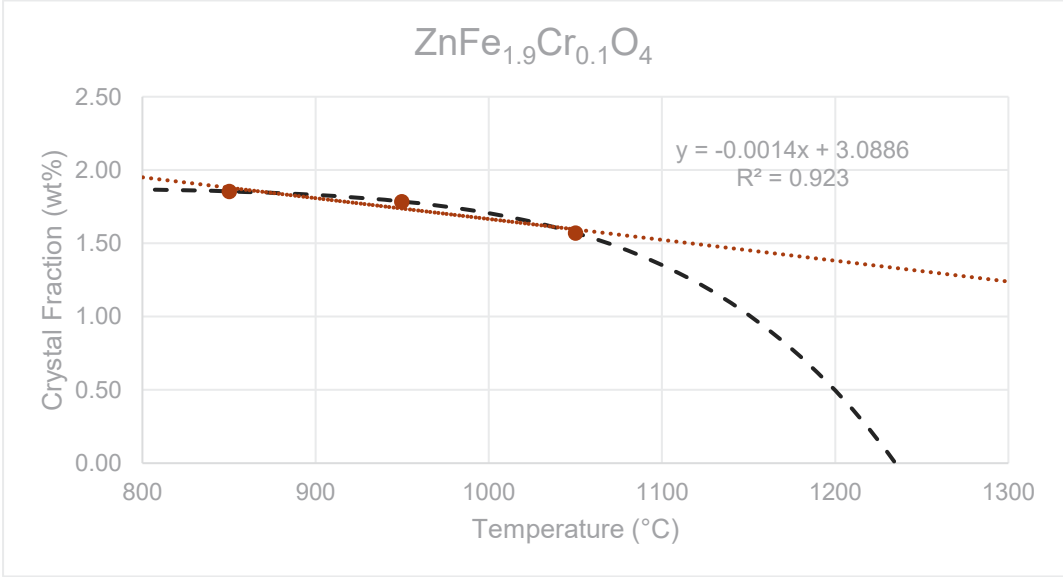

Figure G.65. The liquidus temperature plot for $ZnFe_{1.9}Cr_{0.1}O_4$ in glass HS24-42 showing the linear T_L at 2171 °C (R^2 = 0.923) and the non-linear (black dash line) T_L at 1235 °C.

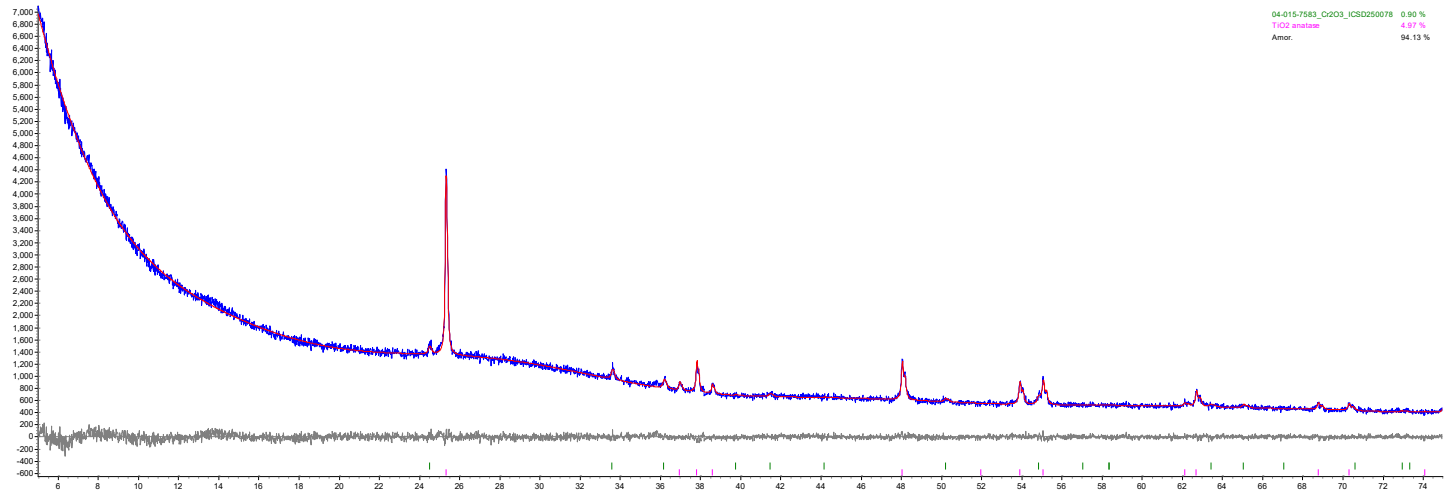

Figure G.66. XRD scan of glass HS24-43 after isothermal heat treatment at 950 °C for 24 h. The crystalline phase is Cr_2O_3.

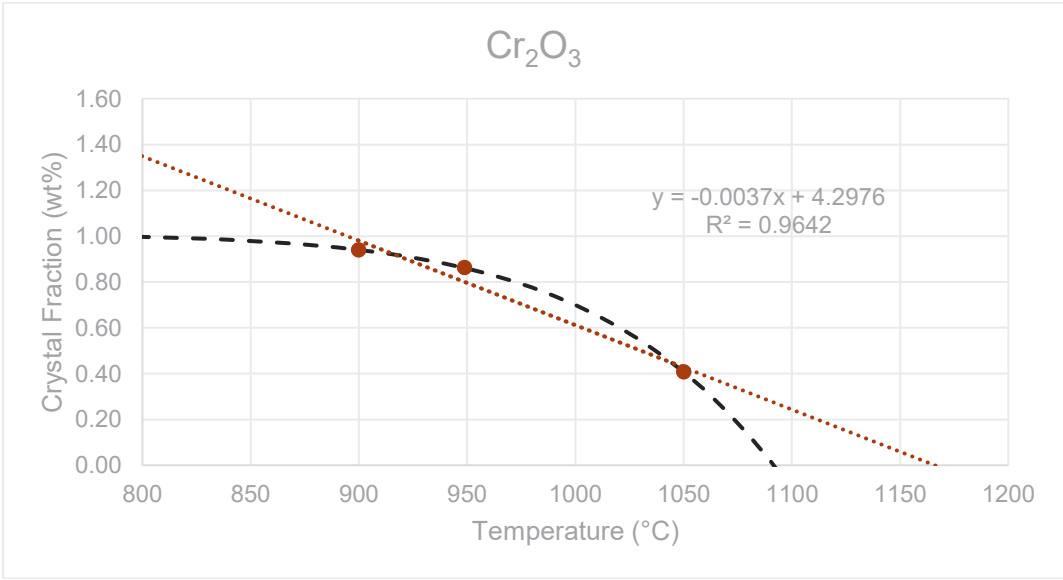

Figure G.67. The liquidus temperature plot for Cr_2O_3 in glass HS24-43 showing the linear T_L at 1166 °C (R^2 = 0.9642) and the non-linear (black dash line) T_L at 1092 °C.

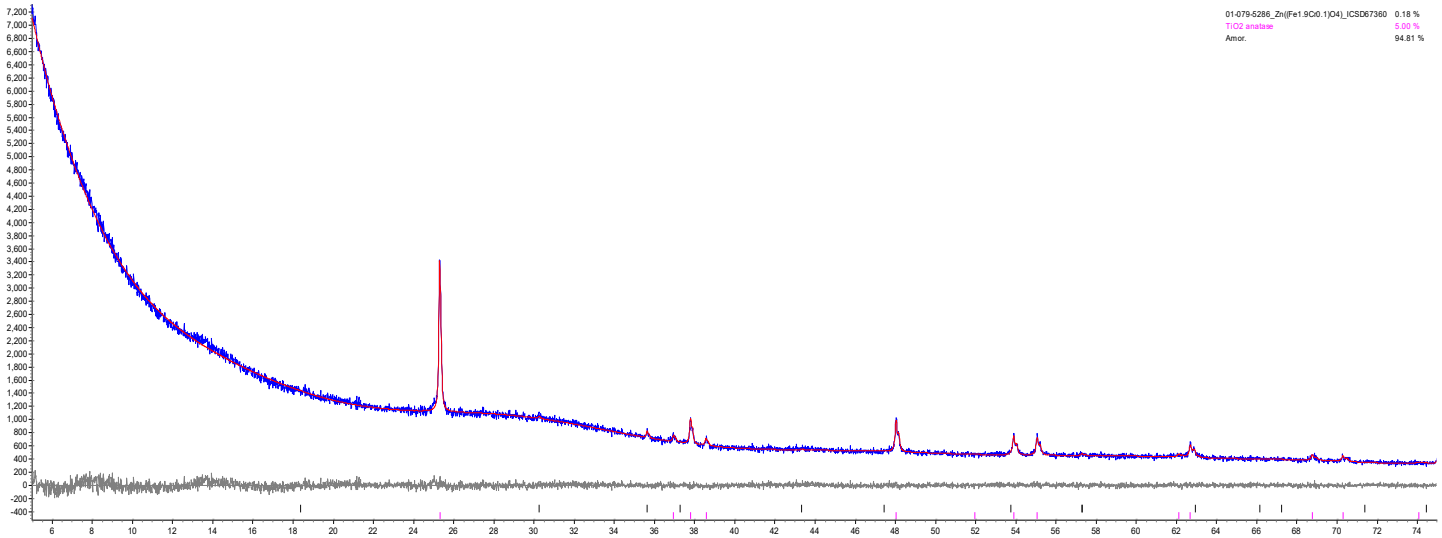

Figure G.68. XRD scan of glass HS24-44 after isothermal heat treatment at 950 °C for 24 h. The crystalline phase is $ZnFe_{1.9}Cr_{0.1}O_4$.

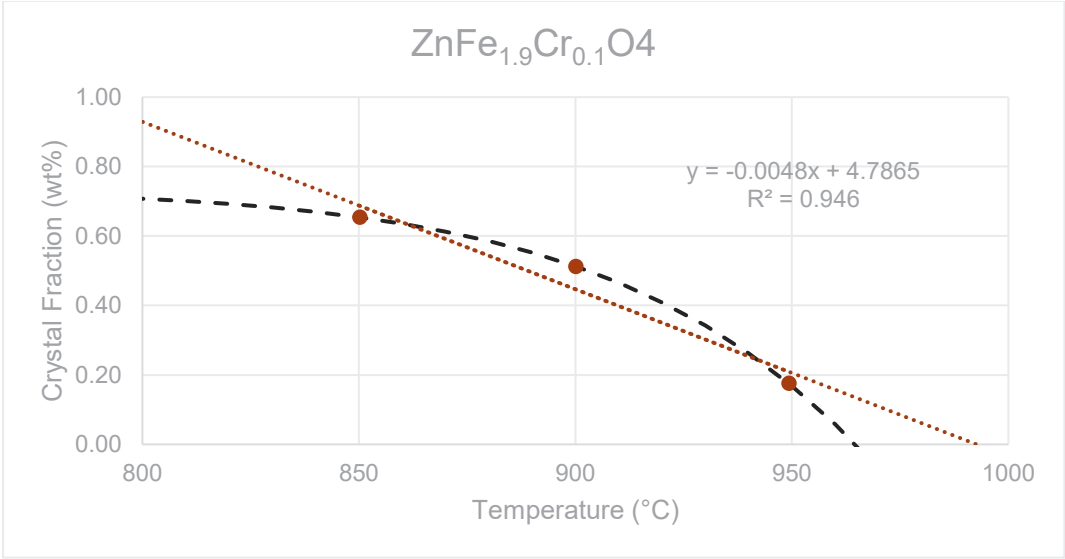

Figure G.69. The liquidus temperature plot for $ZnFe_{1.9}Cr_{0.1}O_4$ in glass HS24-44 showing the linear T_L at 993 °C (R^2 = 0.946) and the non-linear (black dash line) T_L at 965 °C.

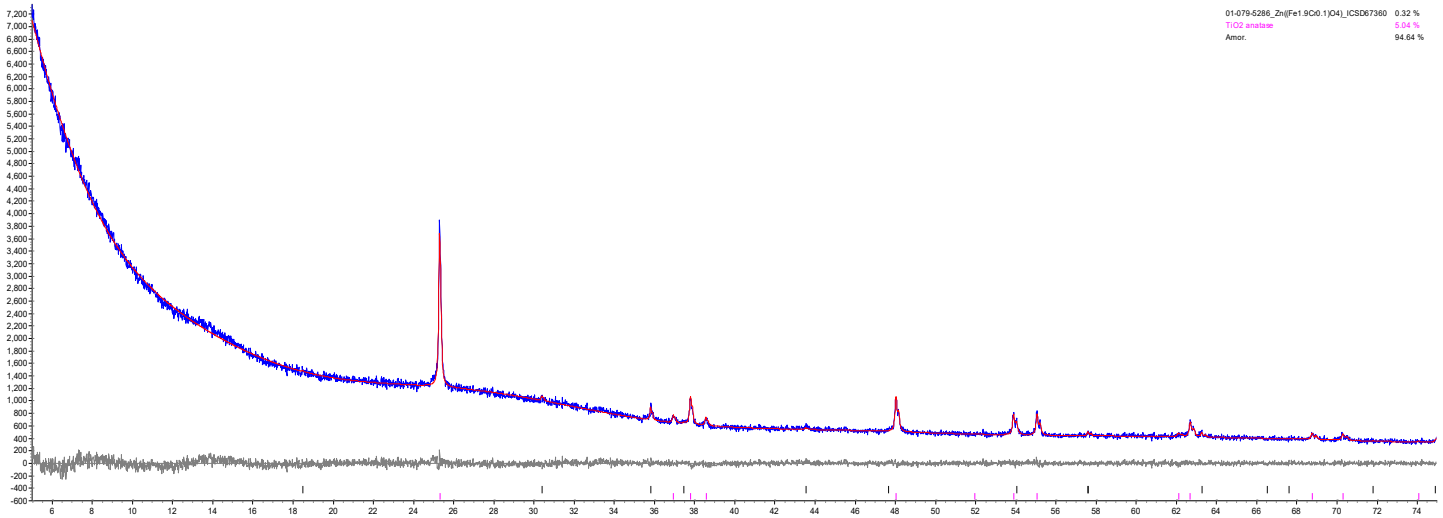

Figure G.70. XRD scan of glass HS24-45 after isothermal heat treatment at 950 °C for 24 h. The crystalline phase is $ZnFe_{1.9}Cr_{0.1}O_4$.

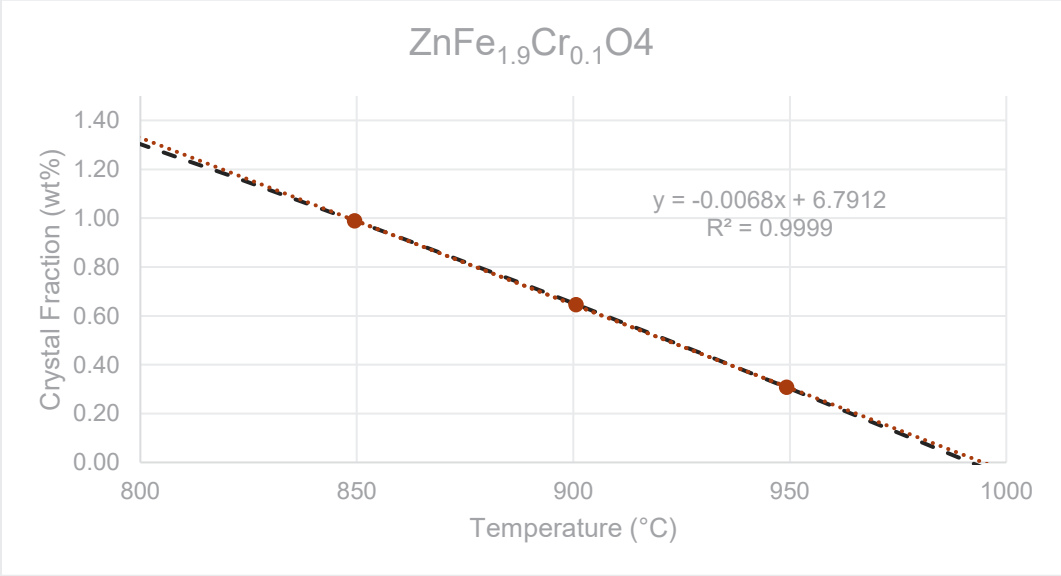

Figure G.71. The liquidus temperature plot for $ZnFe_{1.9}Cr_{0.1}O_4$ in glass HS24-45 showing the linear T_L at 995 °C (R^2 = 0.9999) and the non-linear (black dash line) T_L at 992 °C.

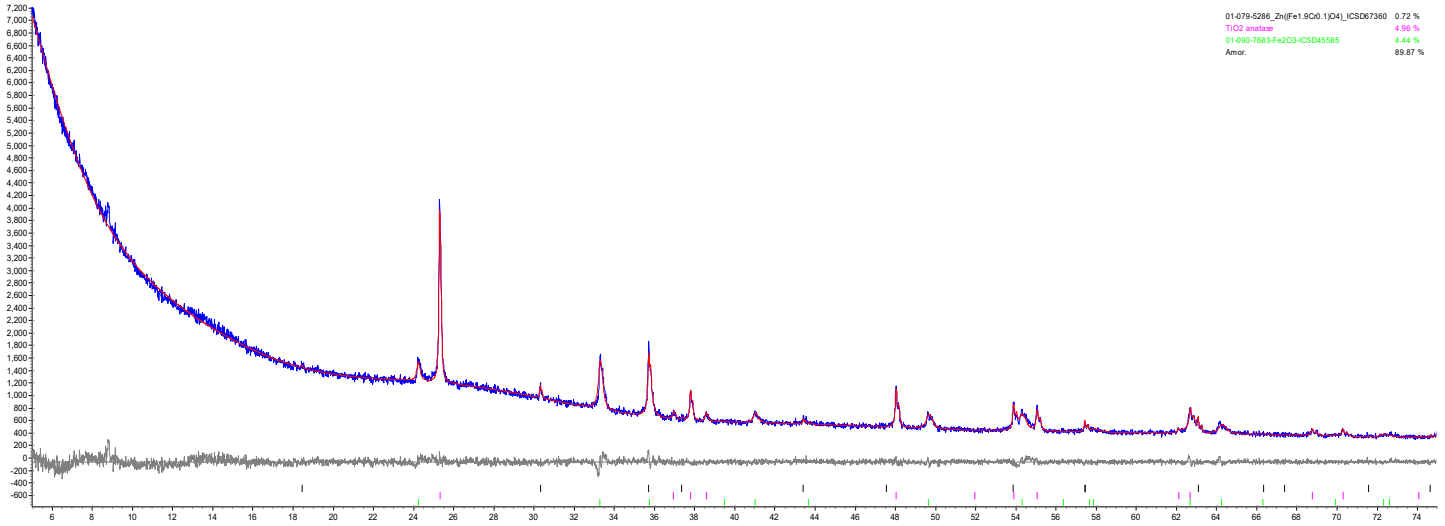

Figure G.72. XRD scan of glass HS24-46 after isothermal heat treatment at 950 °C for 24 h. The crystalline phases are Fe_2O_3 and $ZnFe_{1.9}Cr_{0.1}O_4$.

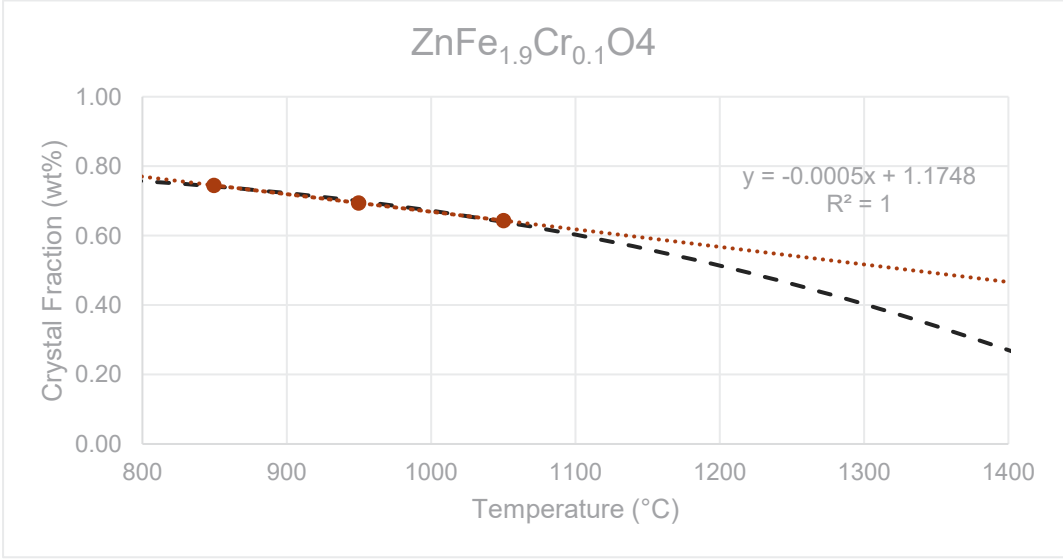

Figure G.73. The liquidus temperature plot for $ZnFe_{1.9}Cr_{0.1}O_4$ in glass HS24-46 showing the linear T_L at 2322 °C ($R^2 = 1$) and the non-linear (black dash line) T_L at 1567 °C.

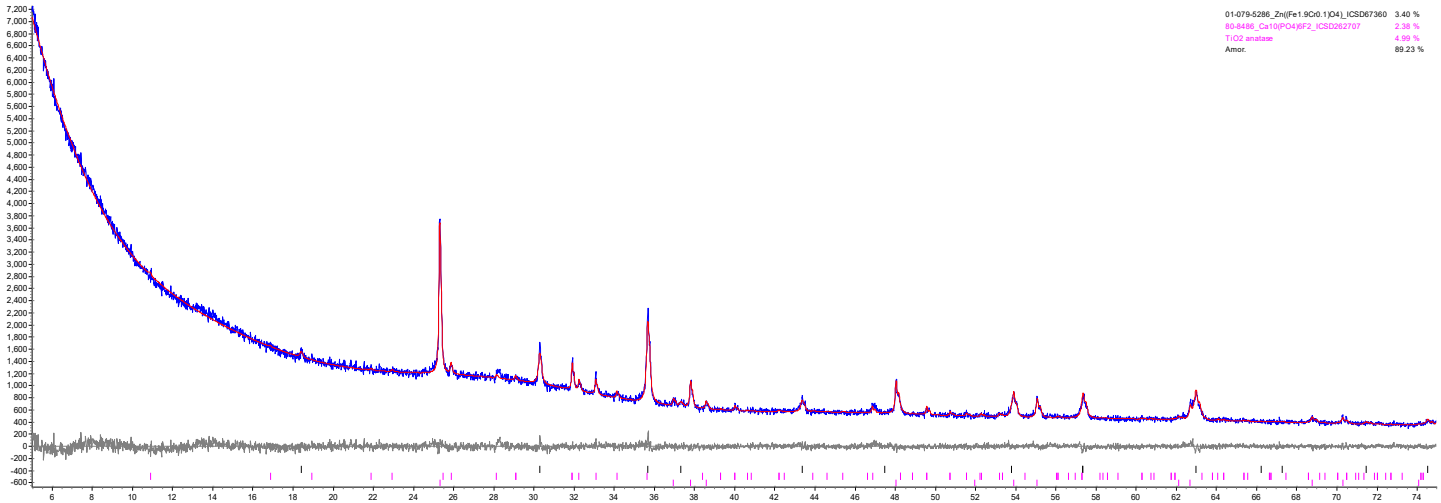

Figure G.74. XRD scan of glass HS24-48 after isothermal heat treatment at 950 °C for 24 h. The crystalline phases are $Ca_{10}(PO_4)_6F_2$ and $ZnFe_{1.9}Cr_{0.1}O_4$.

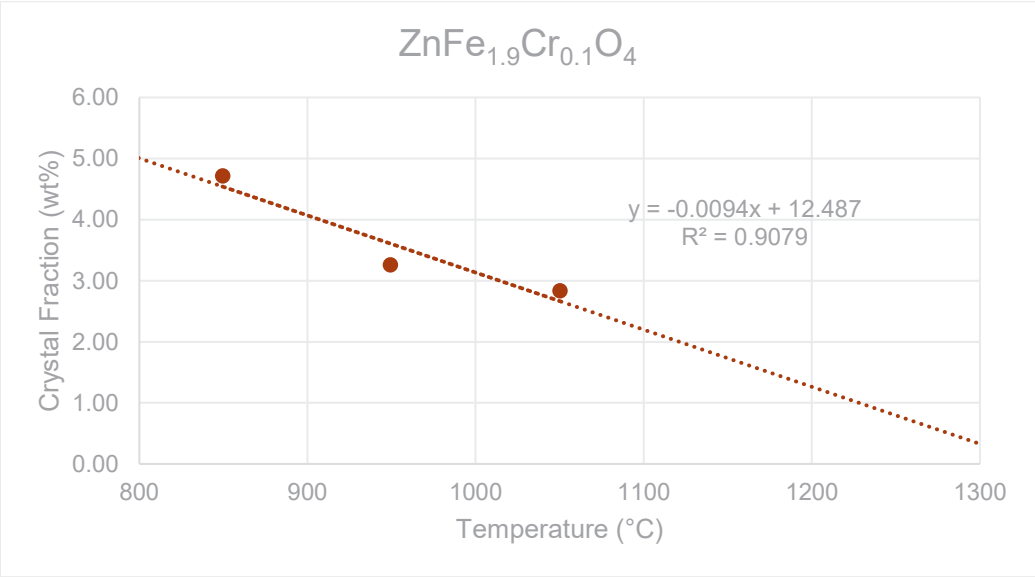

Figure G.75. The liquidus temperature plot for $ZnFe_{1.9}Cr_{0.1}O_4$ in glass HS24-48 showing the linear T_L at 1335 °C (R^2 = 0.9079).

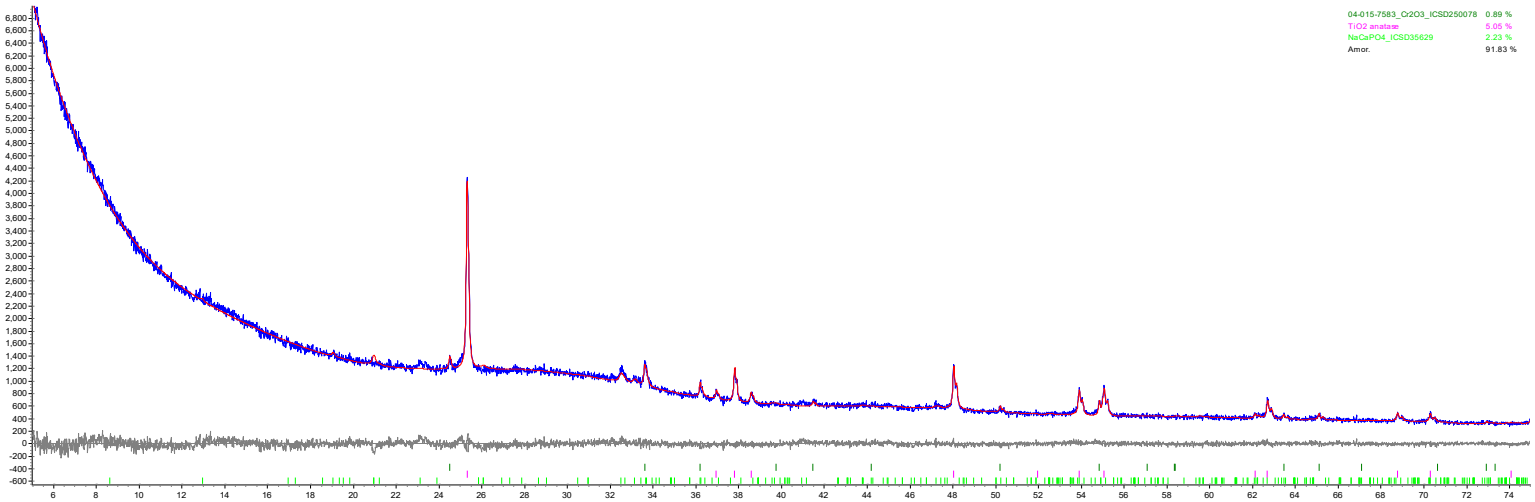

Figure G.76. XRD scan of glass HS24-50 after isothermal heat treatment at 950 °C for 24 h. The crystalline phases are $NaCaPO_4$ and Cr_2O_3.

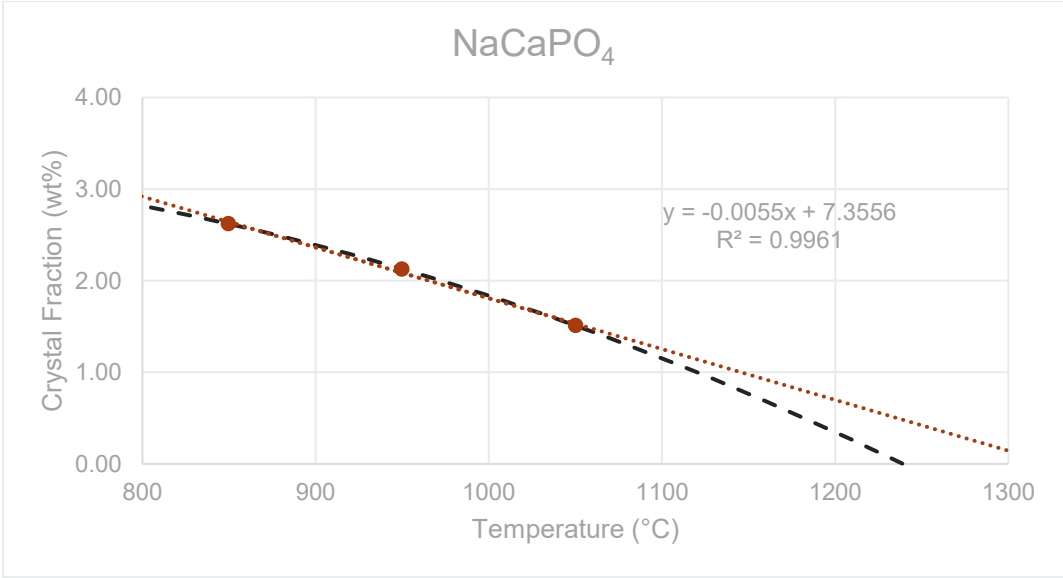

Figure G.77. The liquidus temperature plot for $NaCaPO_4$ in glass HS24-50 showing the linear T_L at 1326 °C (R^2 = 0.9961) and the non-linear (black dash line) T_L at 1239 °C.

Appendix H – Measured SO_3 concentrations in SSM glasses

This section provides the measured SO_3 concentrations in SSM glasses determined by ICP-OES and IC.

Table H.1. Measured SO_3 concentrations of SSM via ICP-OES and IC in wt%

Glass ID	ICP-OES	IC	Glass ID	ICP-OES	IC
HS24-01-SSM	0.83	1.11	HS24-26-SSM	1.37	1.35
HS24-02-SSM	1.59	1.53	HS24-27-SSM	1.02	0.99
HS24-03-SSM	1.08	1.07	HS24-28-SSM	1.48	1.49
HS24-04-SSM	1.41	1.37	HS24-29-SSM	1.08	1.02
HS24-05-SSM	1.44	1.40	HS24-30-SSM	0.97	0.95
HS24-06-SSM	1.65	1.60	HS24-31-SSM	1.40	1.46
HS24-07-SSM	1.14	1.15	HS24-32-SSM	1.48	1.49
HS24-08-SSM	1.08	1.22	HS24-33-SSM	1.39	1.35
HS24-09-SSM	1.07	1.01	HS24-34-SSM	1.37	1.34
HS24-10-SSM	1.48	1.40	HS24-35-SSM	1.08	1.14
HS24-11-SSM	0.87	0.90	HS24-36-SSM	1.77	1.86
HS24-12-SSM	1.14	1.09	HS24-37-SSM	1.42	1.46
HS24-13-SSM	1.30	1.44	HS24-38-SSM	1.76	1.74
HS24-14-SSM	1.46	1.42	HS24-39-SSM	1.45	1.49
HS24-15-SSM	2.12	1.85	HS24-40-SSM	1.14	1.24
HS24-16-SSM	1.39	1.19	HS24-41-SSM	0.94	1.05
HS24-17-SSM	1.06	1.02	HS24-42-SSM	0.85	0.96
HS24-18-SSM	1.45	1.50	HS24-43-SSM	0.82	0.79
HS24-19-SSM	1.29	1.27	HS24-44-SSM	1.12	1.17
HS24-20-SSM	1.58	1.54	HS24-45-SSM	1.03	0.98
HS24-21-SSM	1.26	1.26	HS24-46-SSM	0.89	0.90
HS24-22-SSM	0.94	1.44	HS24-47-SSM	0.93	1.28
HS24-23-SSM	1.15	1.23	HS24-48-SSM	1.07	1.21
HS24-24-SSM	1.63	1.57	HS24-49-SSM	1.19	1.22
HS24-25-SSM	1.36	1.31	HS24-50-SSM	1.24	1.25

Appendix I – Viscosity Results

This appendix contains the temperatures at which viscosity was measured (Table I.1), and the measured viscosity data, also found in Table 5.6, for each of the glasses in this matrix.

The graphs shown in this appendix are fitted to the Arrhenius equation (Equation 4.2), referenced in Section 4.6.

Table I.1. Temperatures (°C) at which the viscosities have been measured in order of measurement.

Glass ID	Temperature (°C)					
HS24-01	1139	1054	963	1131	1228	1146
HS24-02	1136	1052	961	1134	1228	1145
HS24-03	1125	1053	958	1139	1230	1148
HS24-04	1134	1054	966	1138	1231	1146
HS24-05	1132	1054	963	1145	1232	1147
HS24-06	1140	1054	962	1142	1232	1145
HS24-07	1147	1059	965	1144	1234	1149
HS24-08	1143	1058	966	1141	1235	1149
HS24-09	1136	1059	966	1145	1234	1150
HS24-10	1141	1057	966	1142	1237	1149
HS24-11	1133	1057	968	1145	1235	1150
HS24-12	1156	1059	968	1146	1237	1151
HS24-13	1145	1057	967	1146	1236	1150
HS24-14	1147	1060	971	1149	1240	1154
HS24-15	1149	1063	NM	1149	1240	1153
HS24-16	1146	1063	968	1148	1239	1153
HS24-17	1147	1061	969	1150	1241	1153
HS24-18	1137	1053	965	1139	1228	1143
HS24-19	1141	1054	964	1137	1229	1145
HS24-20	1139	1053	964	1139	1230	1144
HS24-21	1142	1056	966	1139	1231	1145
HS24-22	1142	1055	964	1140	1232	1146
HS24-23	1139	1055	1004	1142	1231	1146
HS24-24	1142	1053	966	1138	1229	1144
HS24-25	1143	1056	966	1140	1233	1145
HS24-26	1143	1056	995	1144	1234	1148
HS24-27	1143	1057	967	1142	1233	1146
HS24-28	1153	1064	973	1153	1243	1154
HS24-29	1150	1060	969	1150	1241	1152
HS24-30	1153	1062	970	1153	1243	1153
HS24-31	1150	1060	964	1151	1242	1152
HS24-32	1150	1064	972	1153	1244	1154
HS24-33	1152	1062	972	1152	1243	1154
HS24-34	1153	1063	NM	1151	1243	1153
HS24-35	1149	1061	970	1151	1248	1153
HS24-36	1150	1061	969	1150	1241	1151

Glass ID	Temperature (°C)					
HS24-37	1151	1061	969	1150	1241	1152
HS24-38	1150	1061	NM	1150	1242	1152
HS24-39	1152	1063	NM	1155	1247	1156
HS24-40	1151	1062	971	1153	1244	1153
HS24-41	1148	1061	970	1151	1242	1153
HS24-42	1152	1061	969	1152	1244	1154
HS24-43	1148	1062	970	1151	1243	1152
HS24-44	1152	1061	970	1151	1243	1153
HS24-45	1150	1061	969	1151	1242	1153
HS24-46	1150	1061	971	1150	1243	1153
HS24-47	1151	1061	969	1152	1241	1151
HS24-48	1151	1062	NM	1152	1243	1153
HS24-49	1149	1060	969	1151	1242	1151
HS24-50	1151	1061	970	1151	1242	1153

NM = not measured

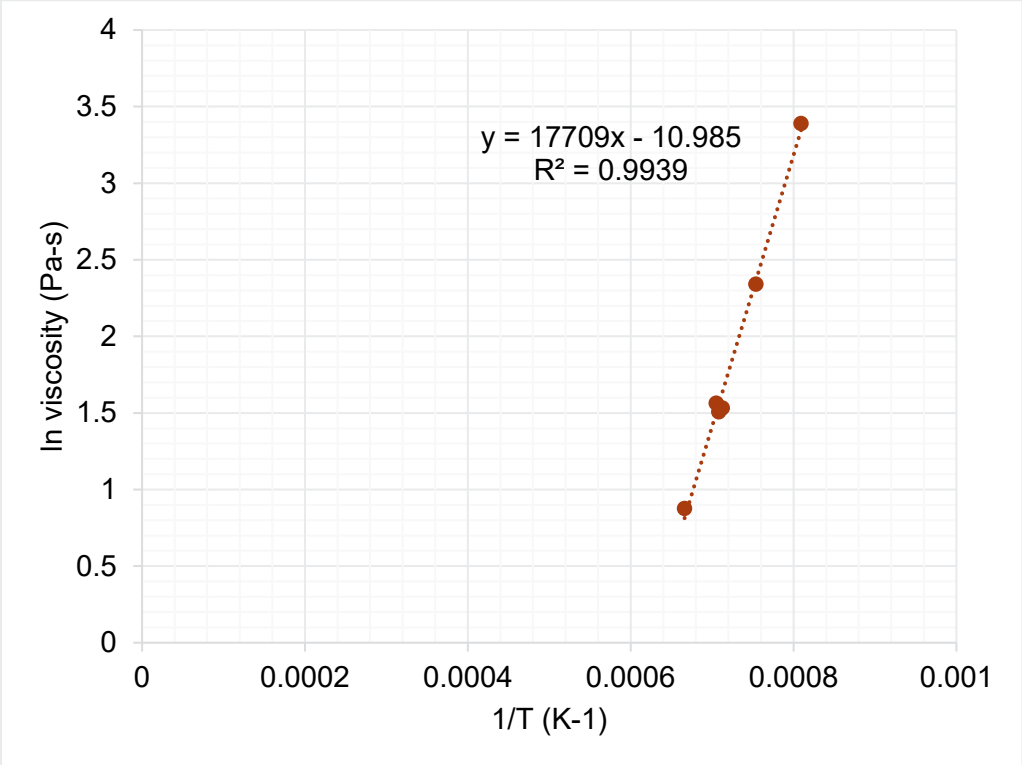

Figure I.1. Viscosity-temperature data and Arrhenius equation fit for HS24-01.

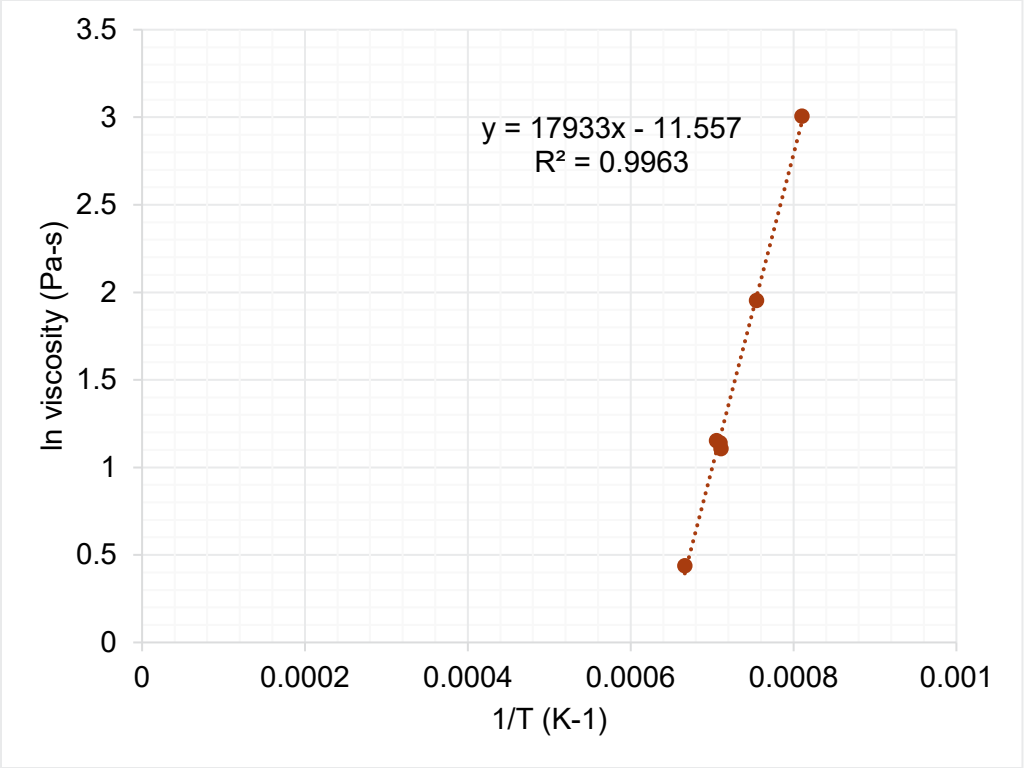

Figure I.2. Viscosity-temperature data and Arrhenius equation fit for HS24-02.

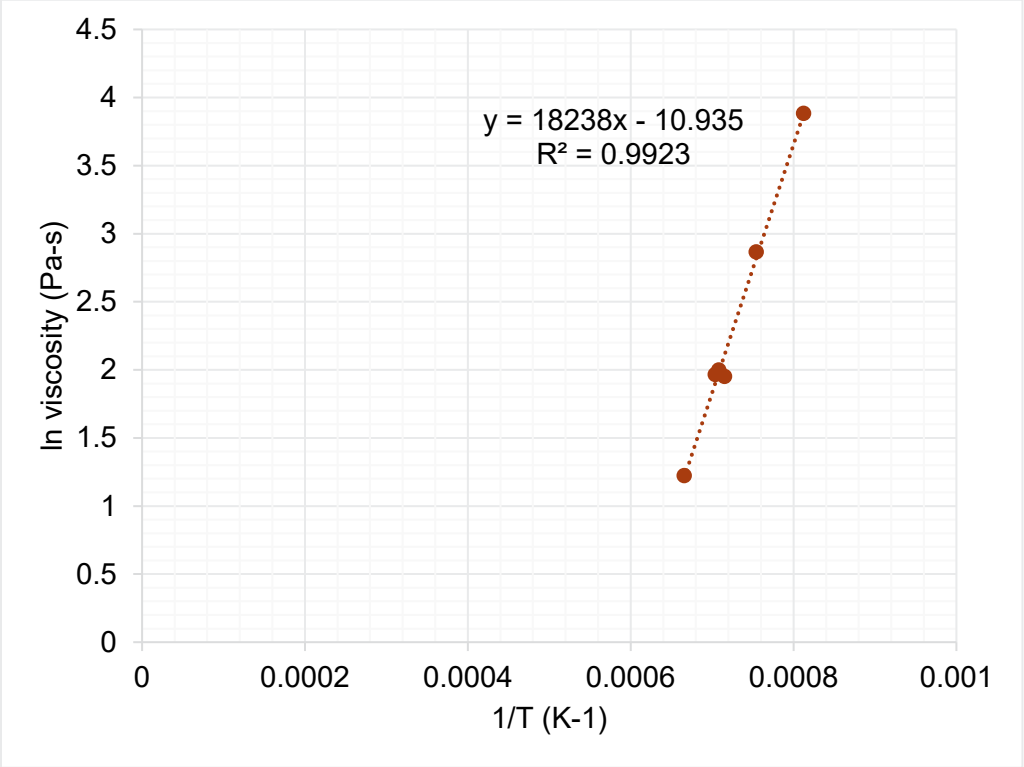

Figure I.3. Viscosity-temperature data and Arrhenius equation fit for HS24-03.

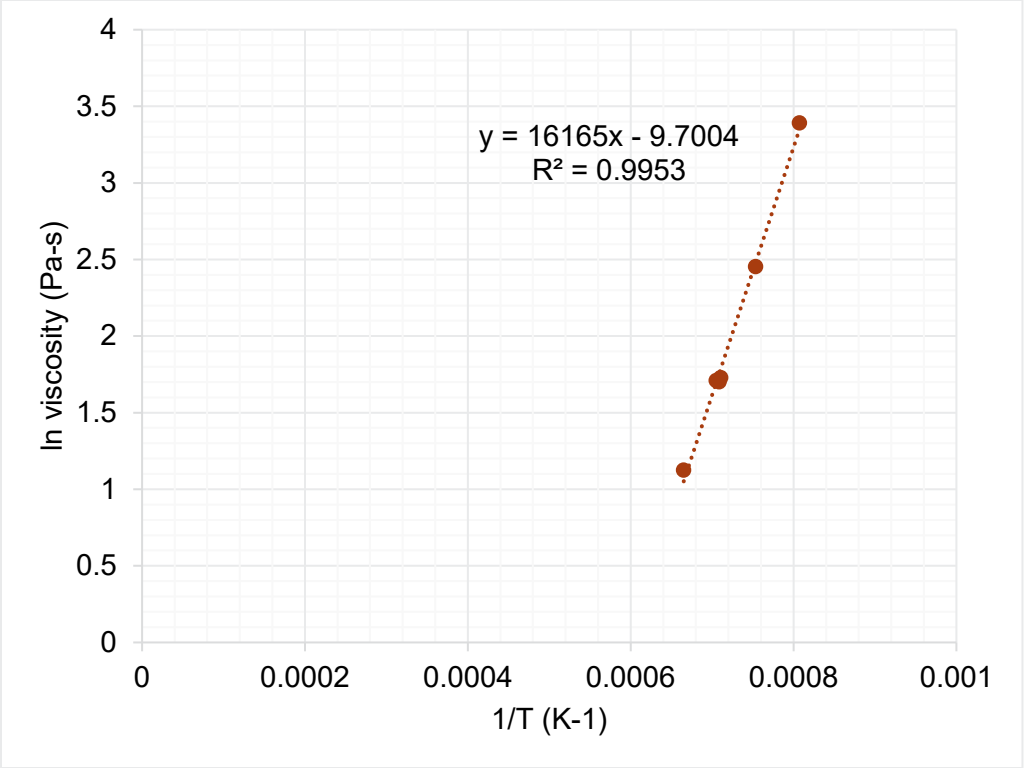

Figure I.4. Viscosity-temperature data and Arrhenius equation fit for HS24-04.

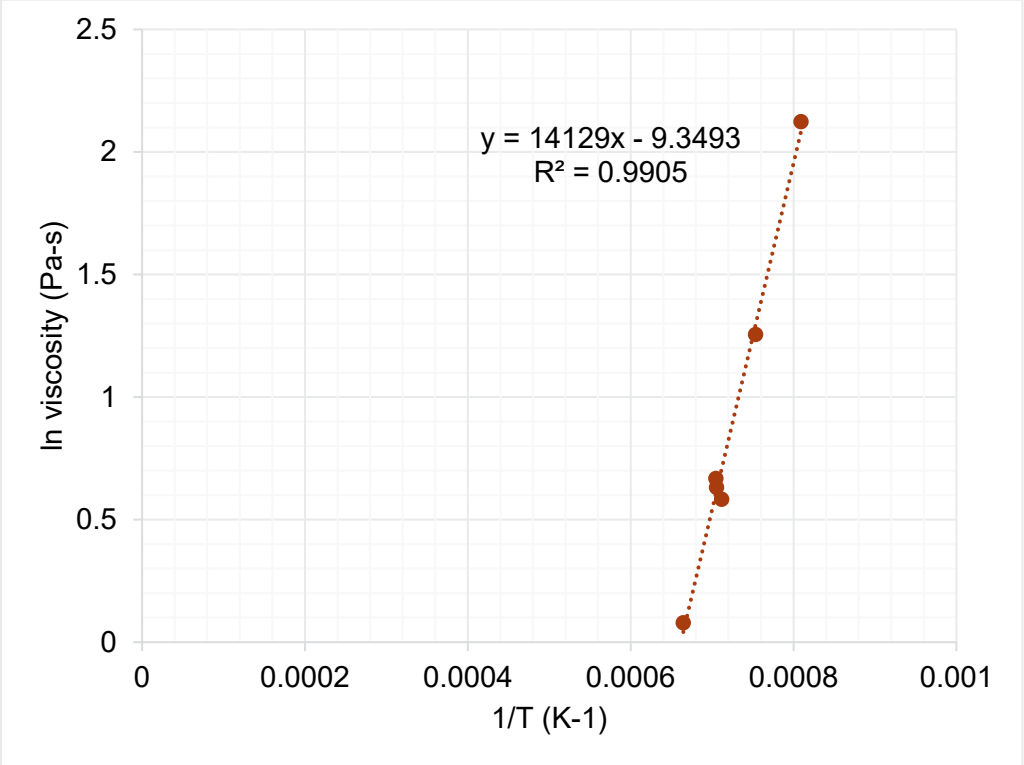

Figure I.5. Viscosity-temperature data and Arrhenius equation fit for HS24-05.

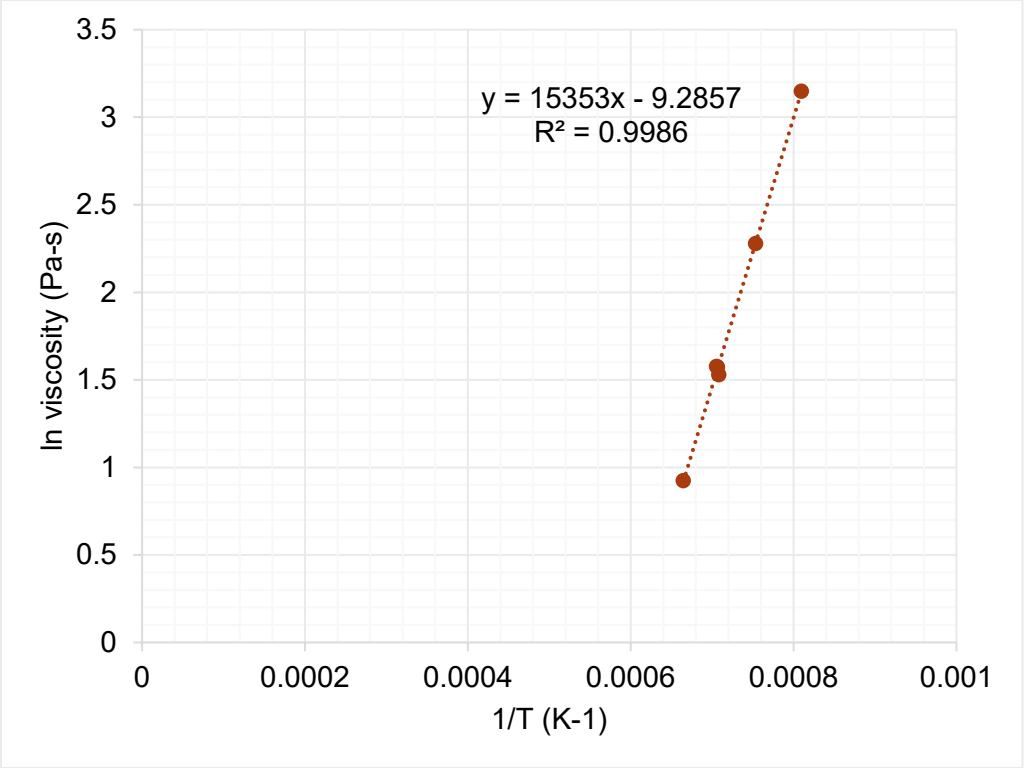

Figure I.6. Viscosity-temperature data and Arrhenius equation fit for HS24-06.

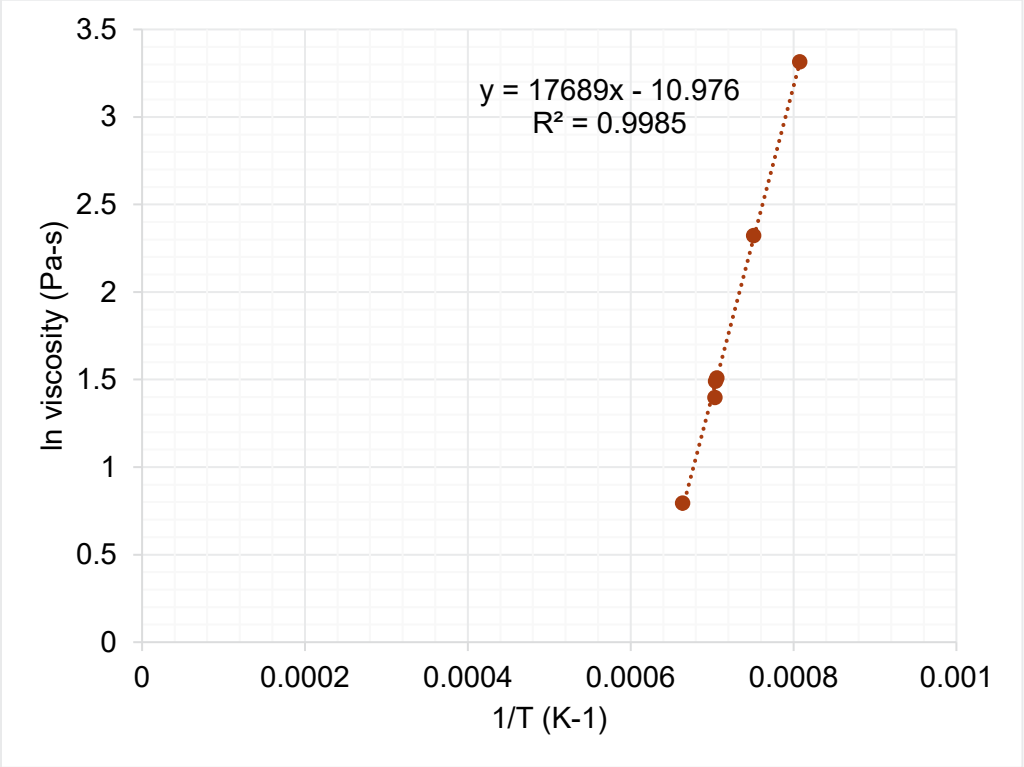

Figure I.7. Viscosity-temperature data and Arrhenius equation fit for HS24-07.

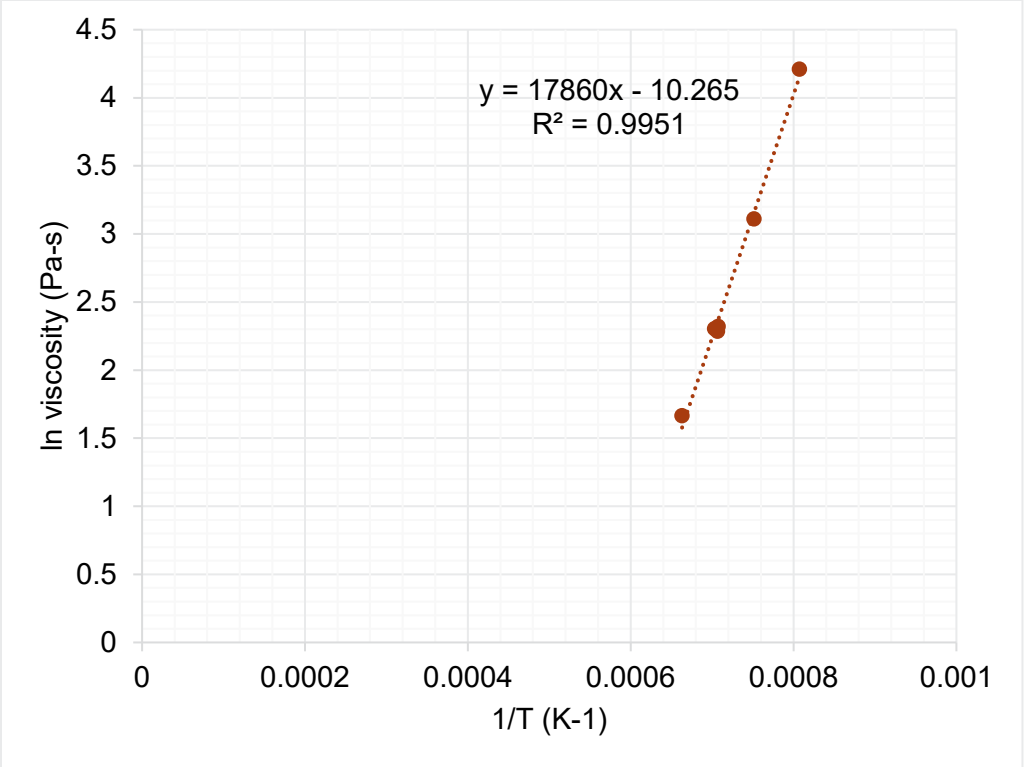

Figure I.8. Viscosity-temperature data and Arrhenius equation fit for HS24-08.

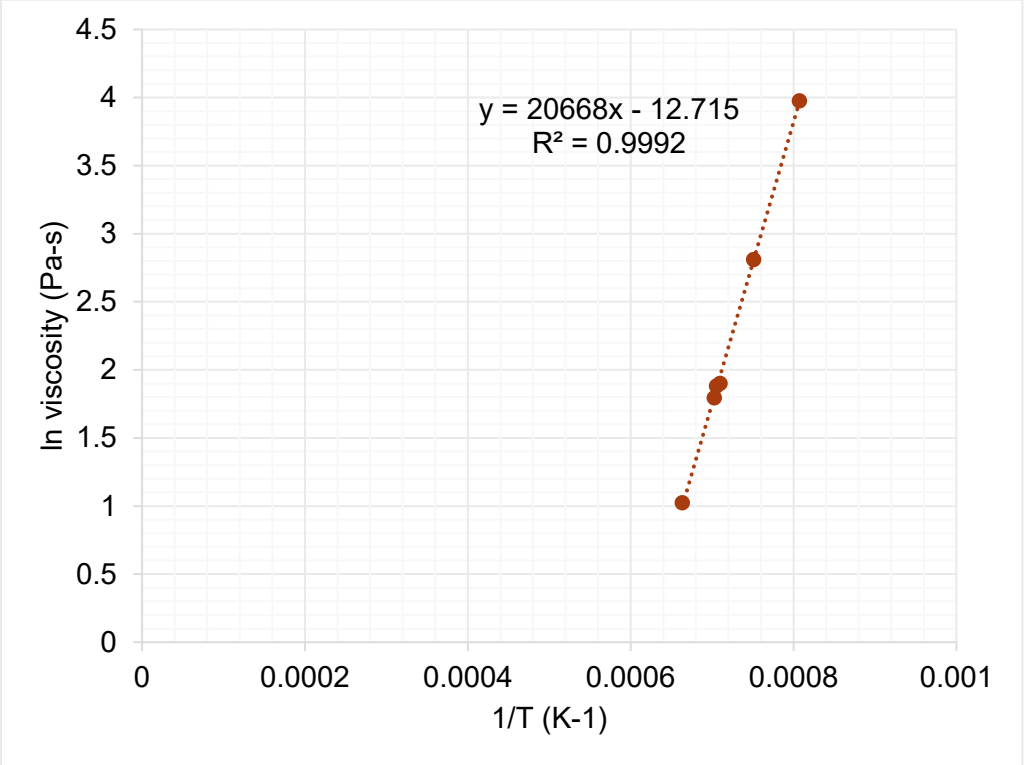

Figure I.9. Viscosity-temperature data and Arrhenius equation fit for HS24-09.

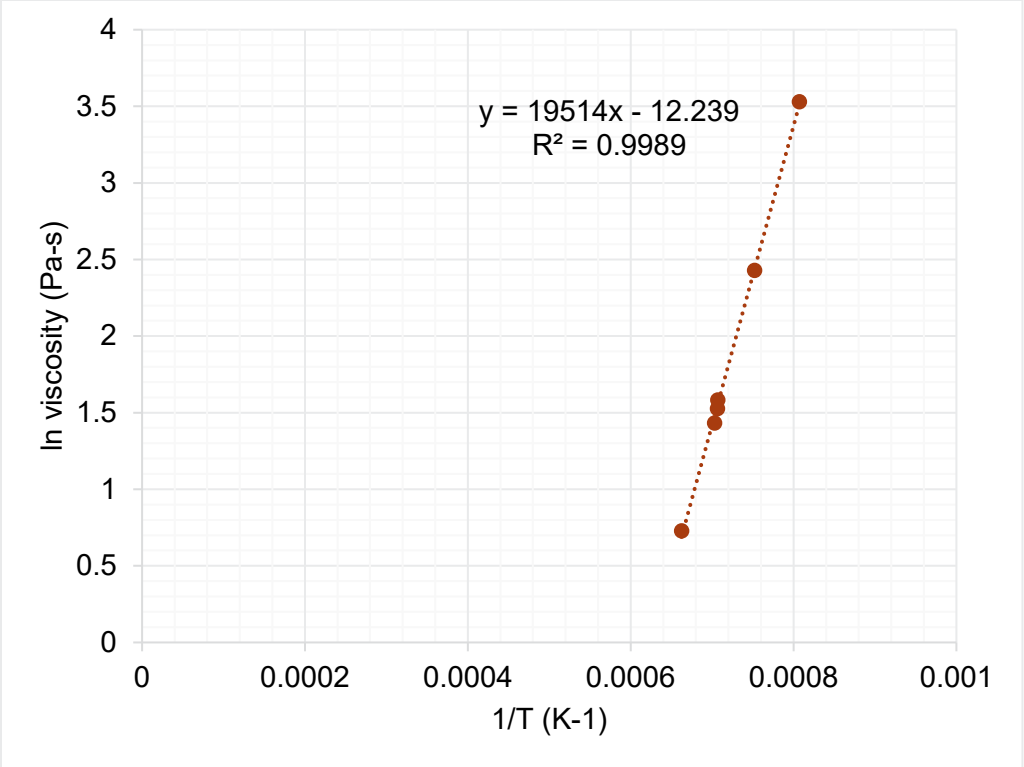

Figure I.10. Viscosity-temperature data and Arrhenius equation fit for HS24-10.

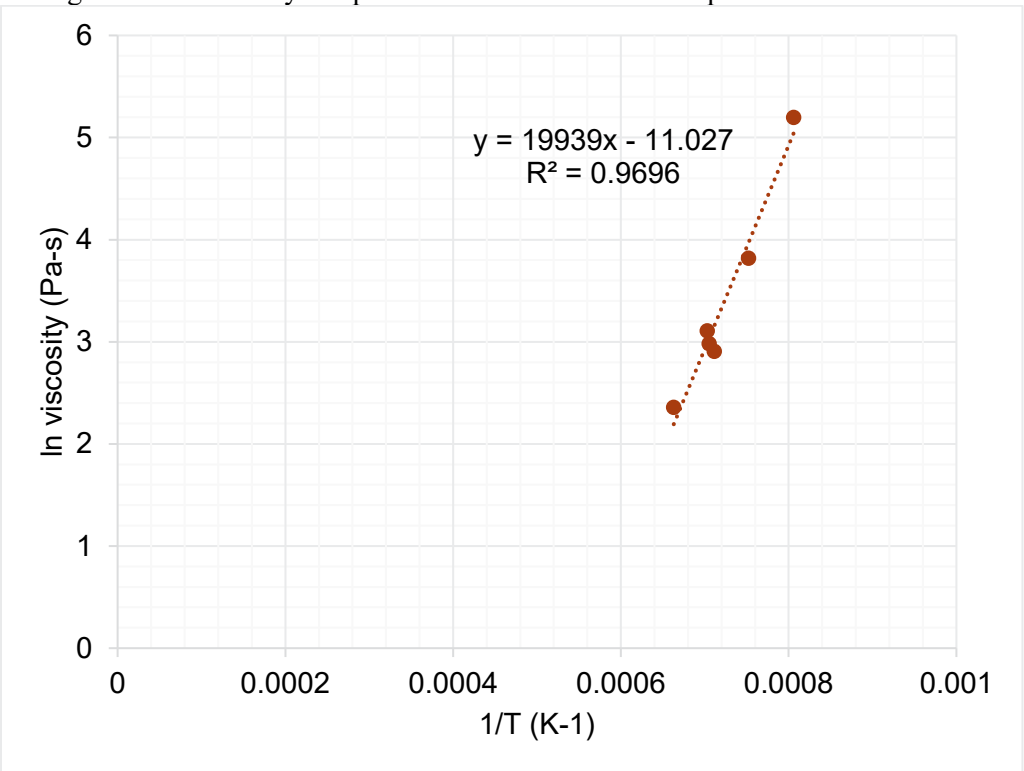

Figure I.11. Viscosity-temperature data and Arrhenius equation fit for HS24-11.

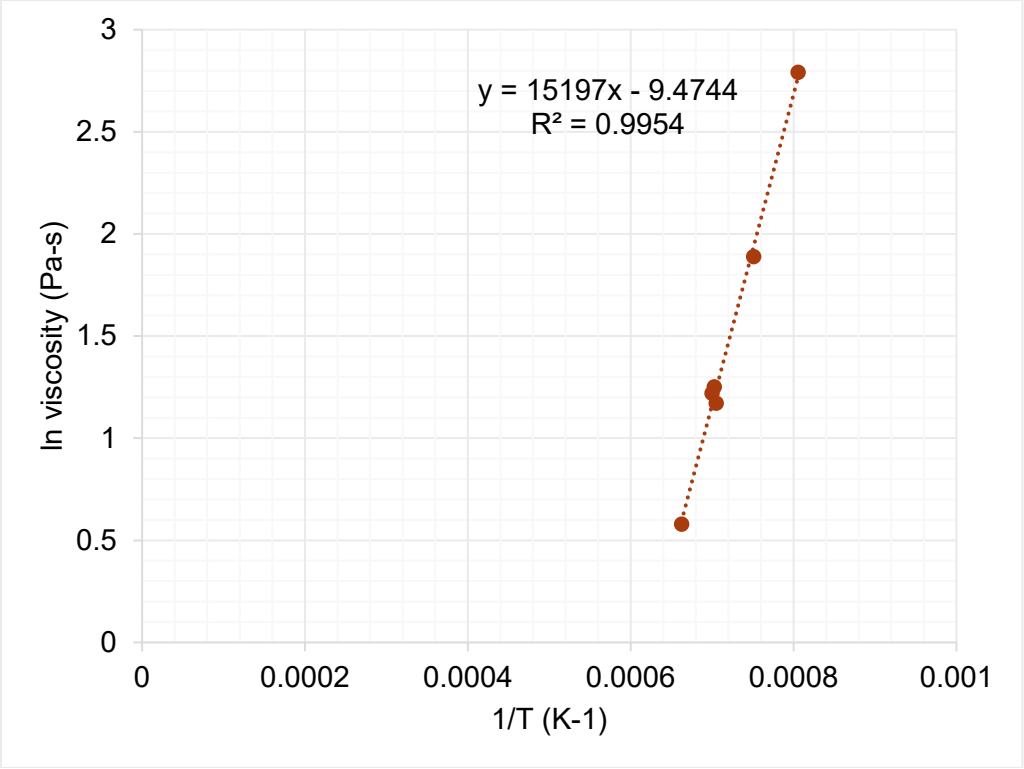

Figure I.12. Viscosity-temperature data and Arrhenius equation fit for HS24-12.

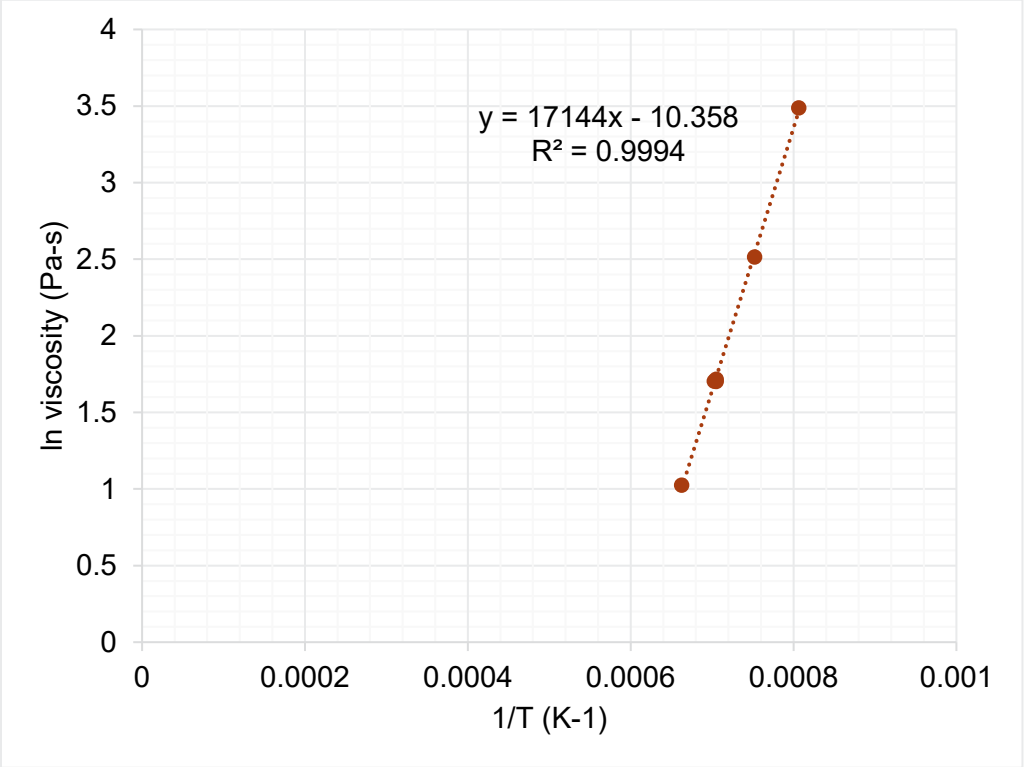

Figure I.13. Viscosity-temperature data and Arrhenius equation fit for HS24-13.

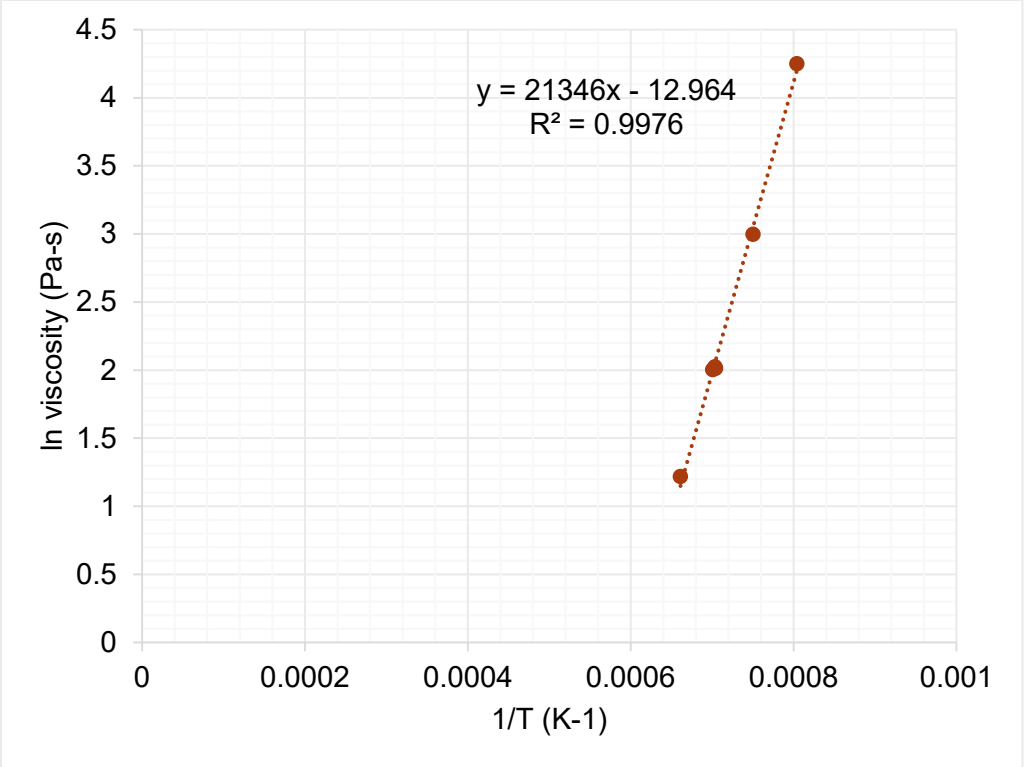

Figure I.14. Viscosity-temperature data and Arrhenius equation fit for HS24-14.

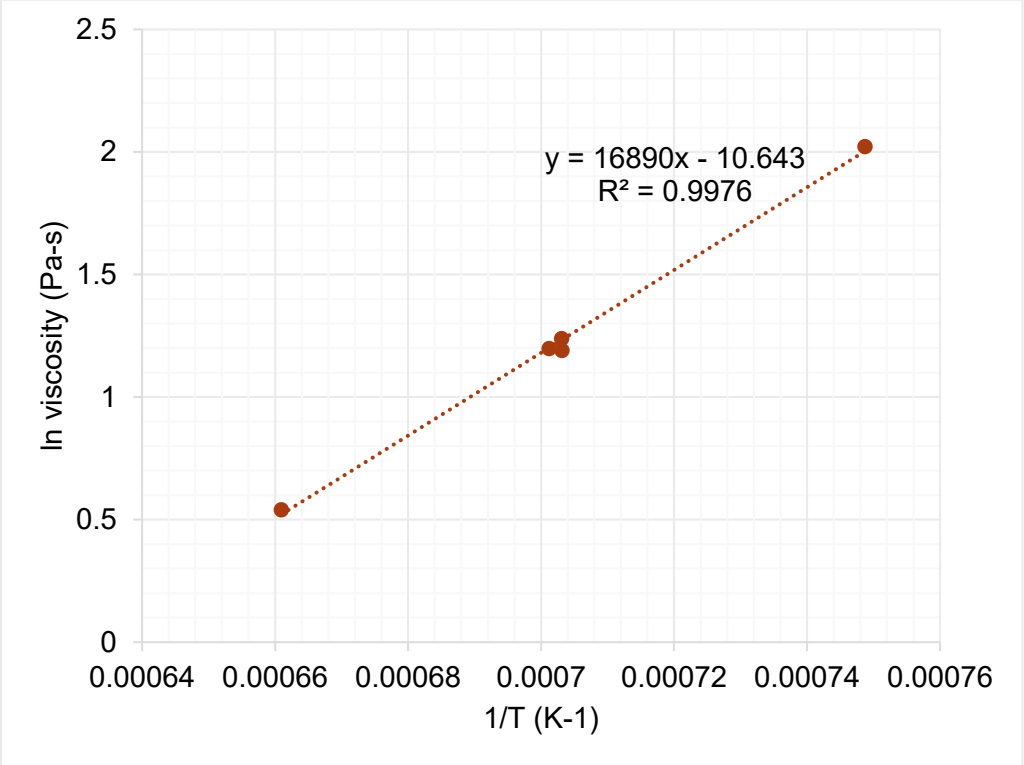

Figure I.15. Viscosity-temperature data and Arrhenius equation fit for HS24-15.

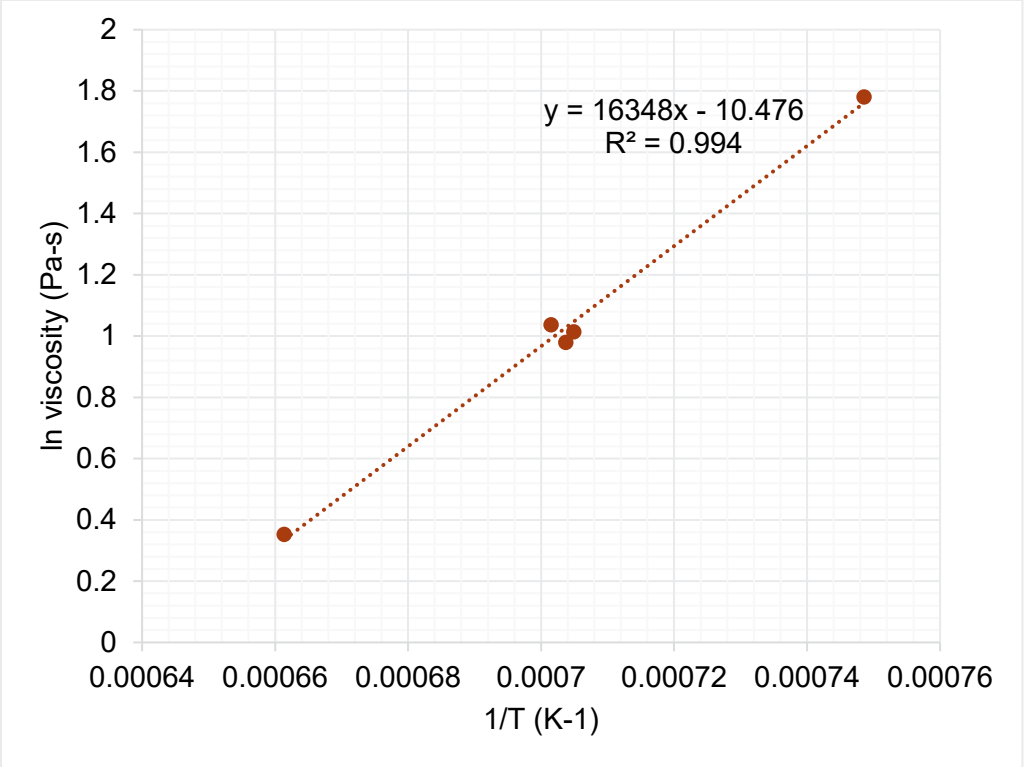

Figure I.16. Viscosity-temperature data and Arrhenius equation fit for HS24-16.

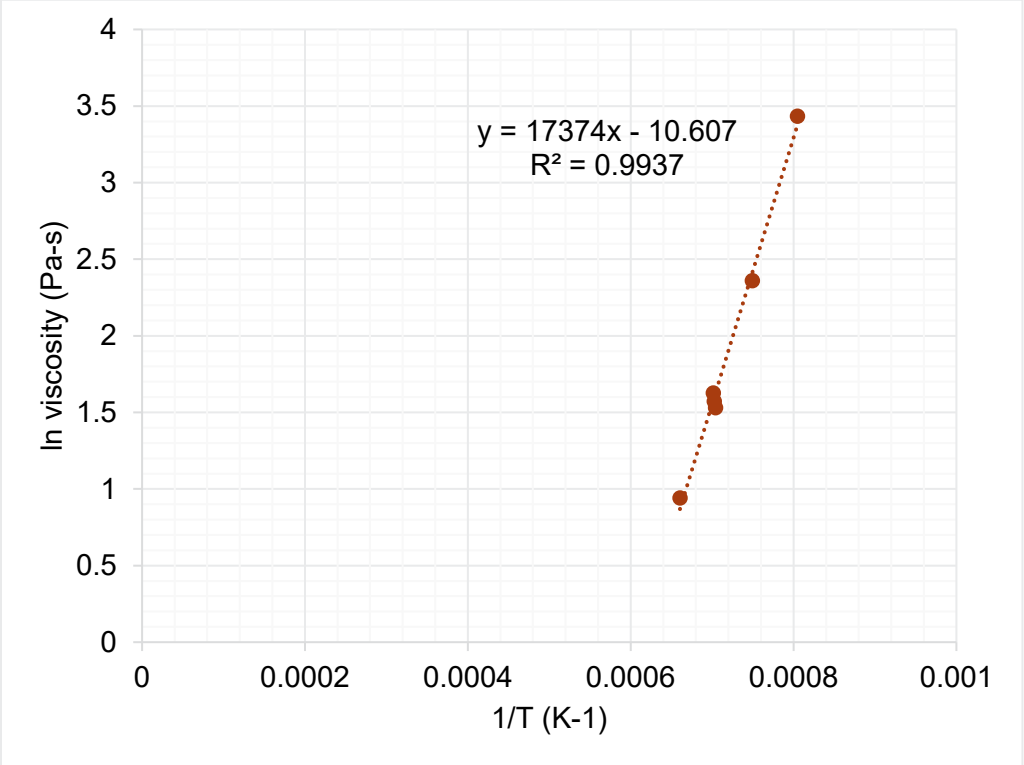

Figure I.17. Viscosity-temperature data and Arrhenius equation fit for HS24-17.

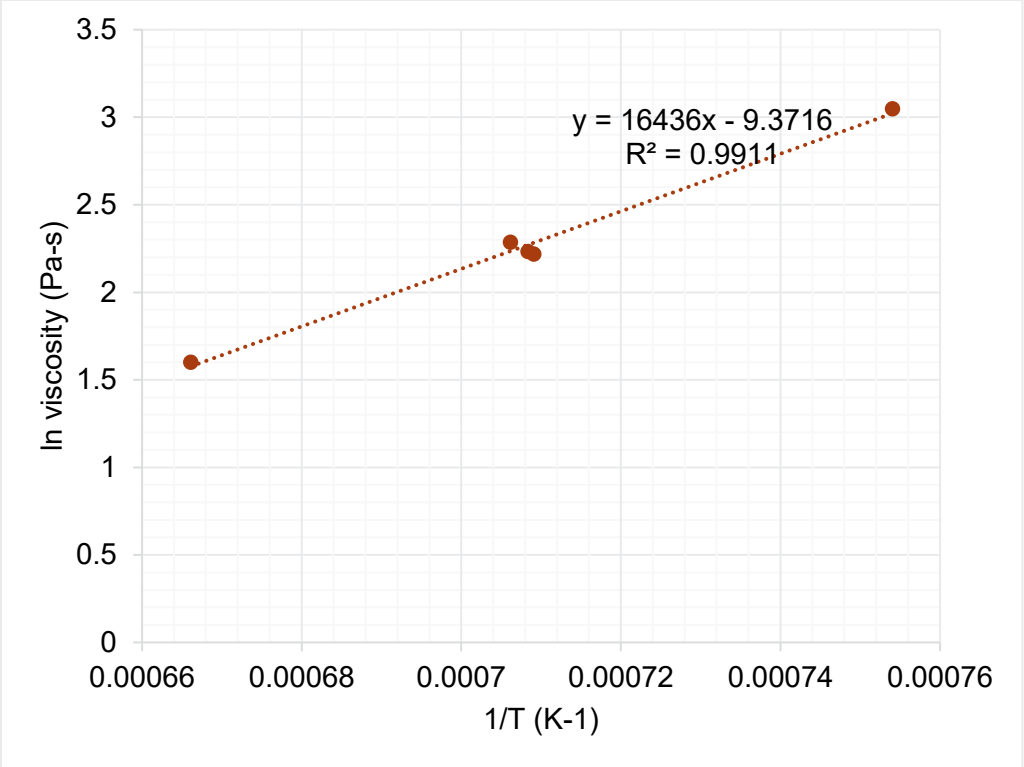

Figure I.18. Viscosity-temperature data and Arrhenius equation fit for HS24-18.

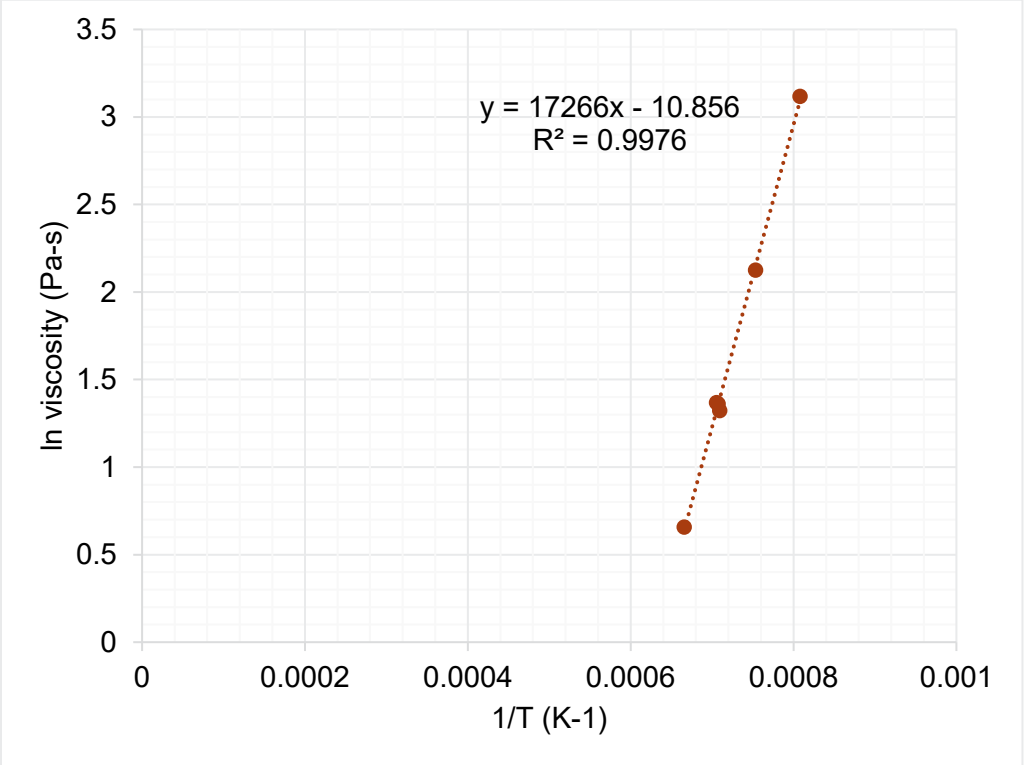

Figure I.19. Viscosity-temperature data and Arrhenius equation fit for HS24-19.

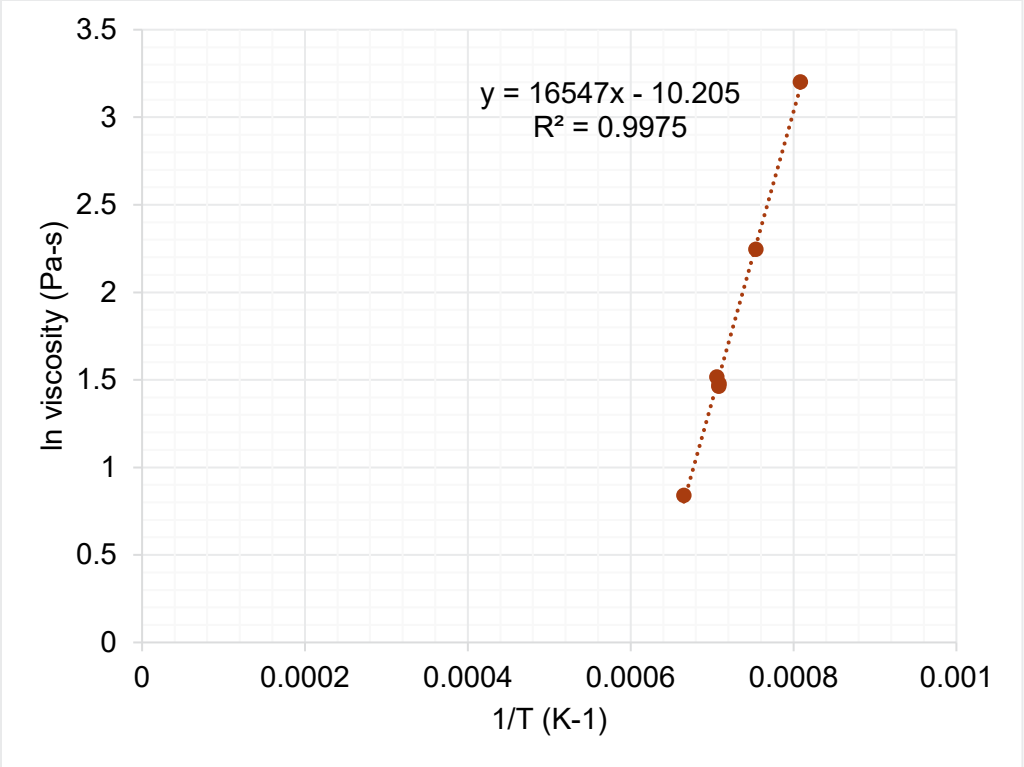

Figure I.20. Viscosity-temperature data and Arrhenius equation fit for HS24-20.

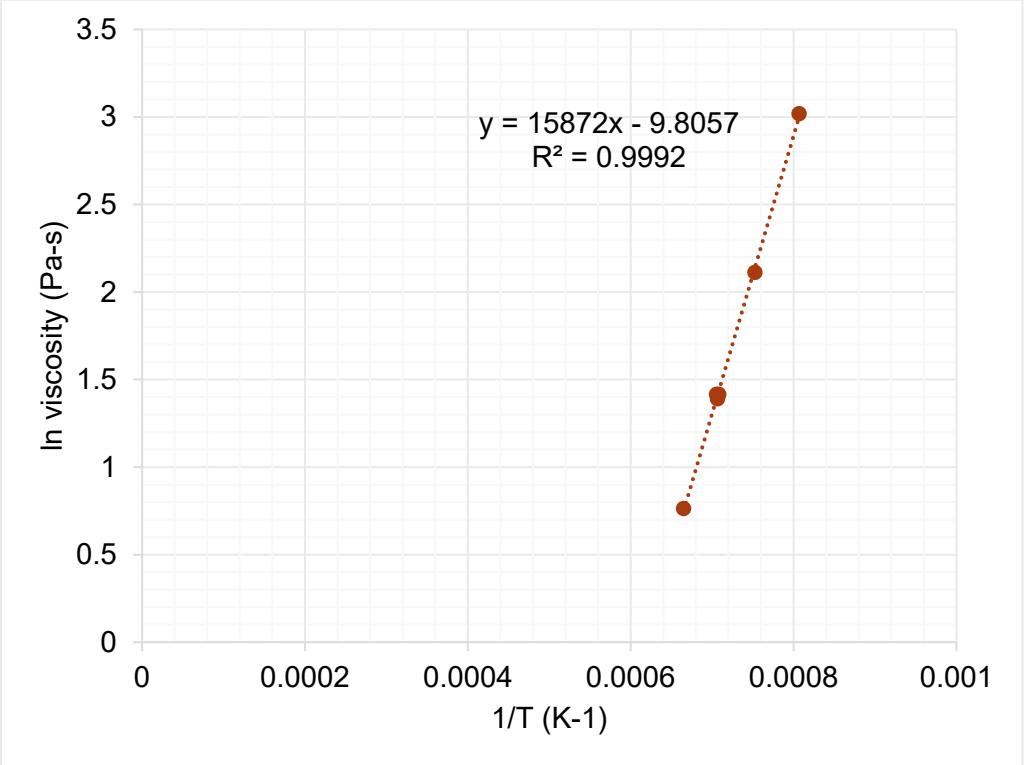

Figure I.21. Viscosity-temperature data and Arrhenius equation fit for HS24-21.

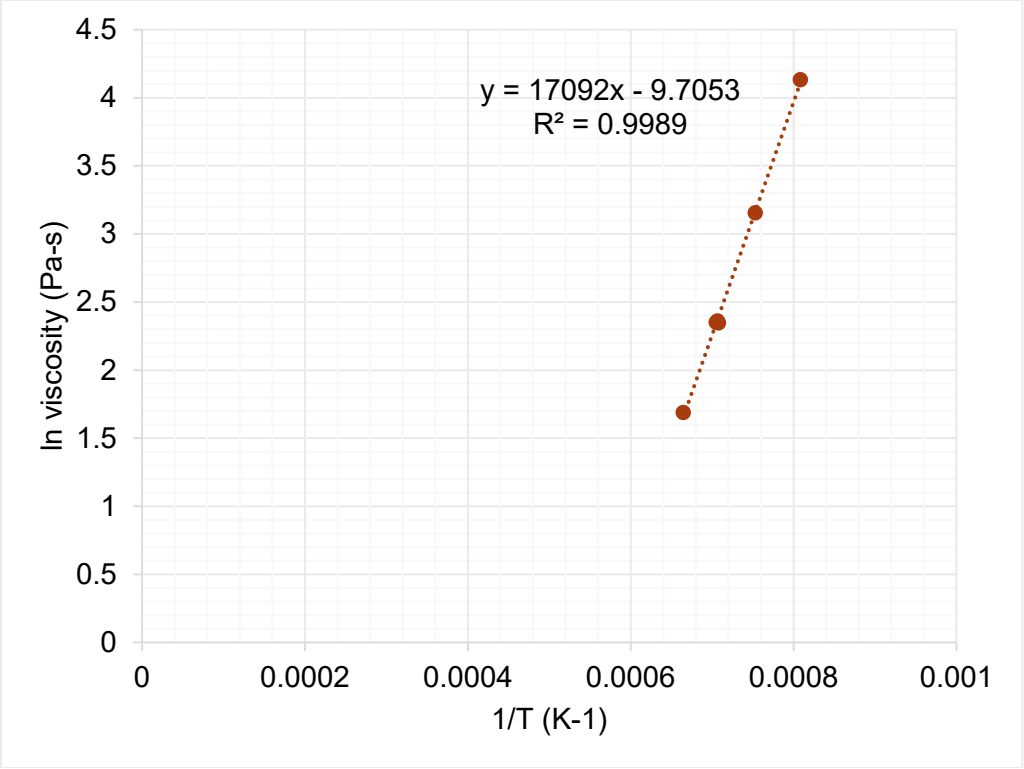

Figure I.22. Viscosity-temperature data and Arrhenius equation fit for HS24-22.

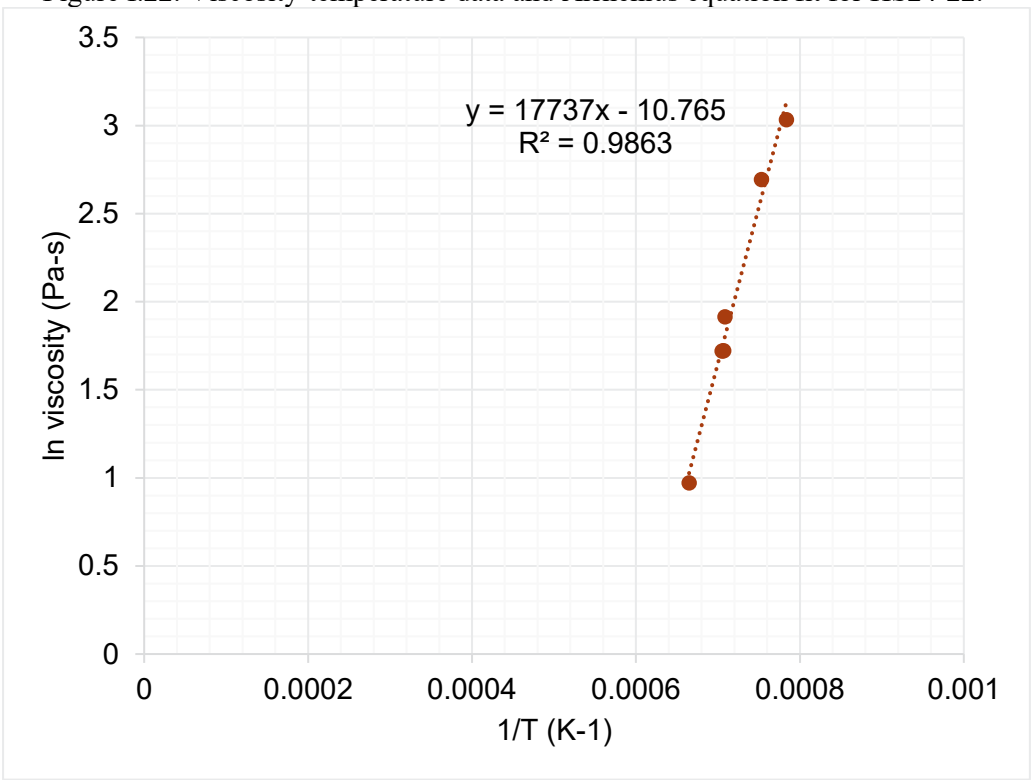

Figure I.23. Viscosity-temperature data and Arrhenius equation fit for HS24-23.

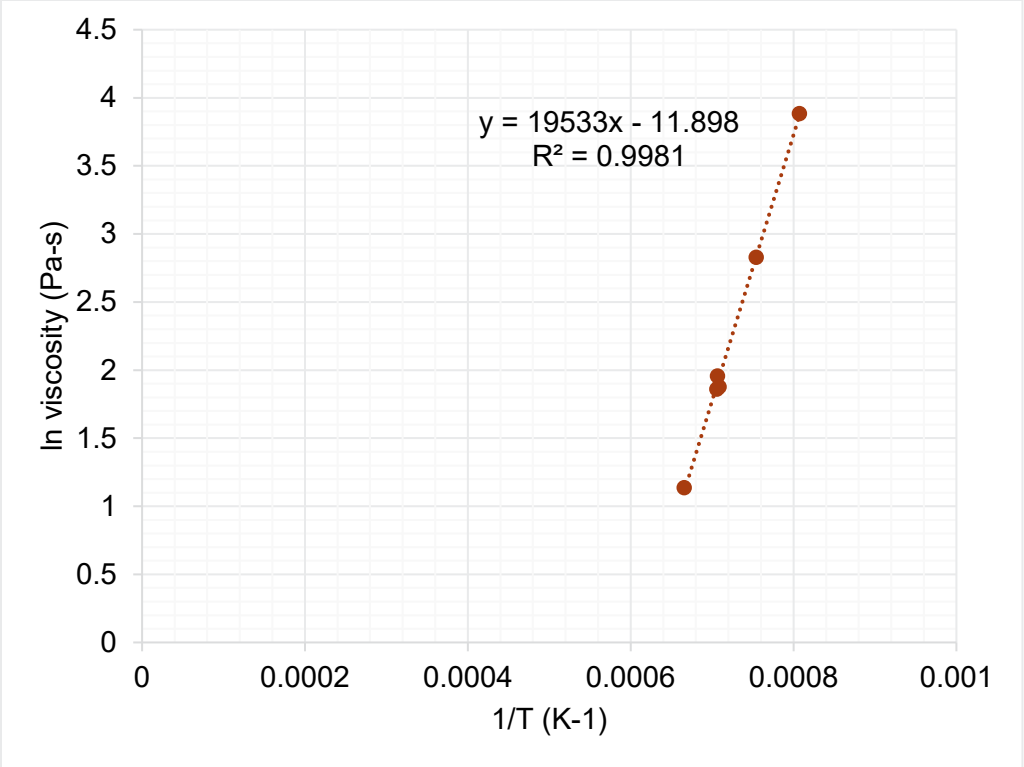

Figure I.24. Viscosity-temperature data and Arrhenius equation fit for HS24-24.

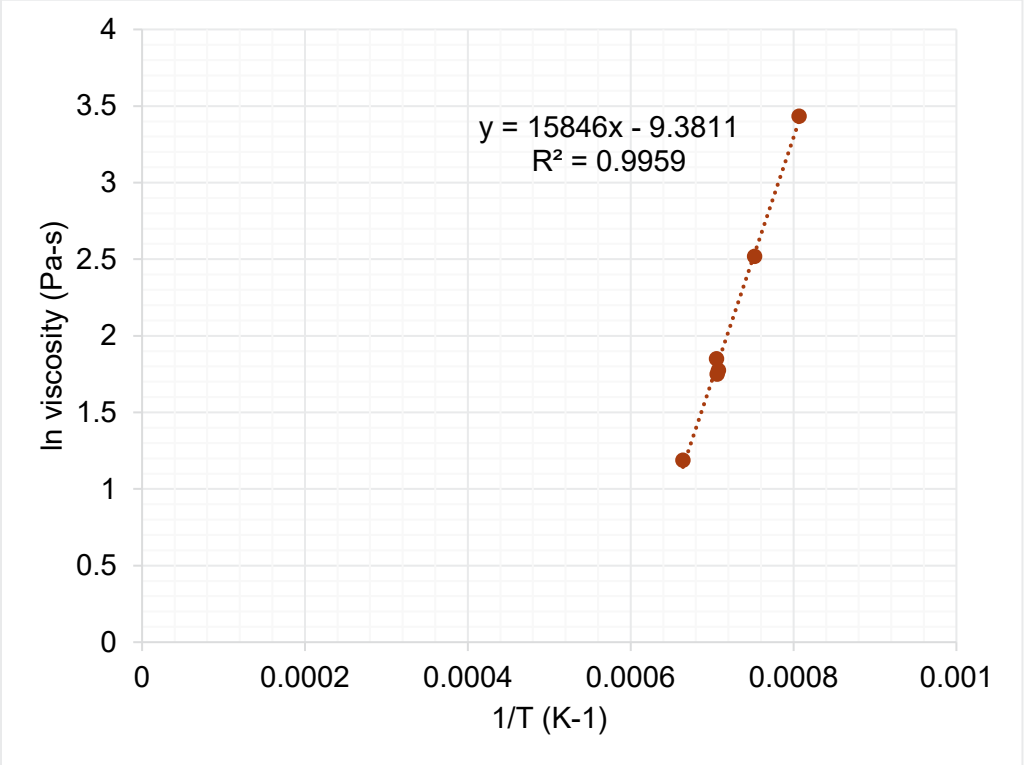

Figure I.25. Viscosity-temperature data and Arrhenius equation fit for HS24-25.

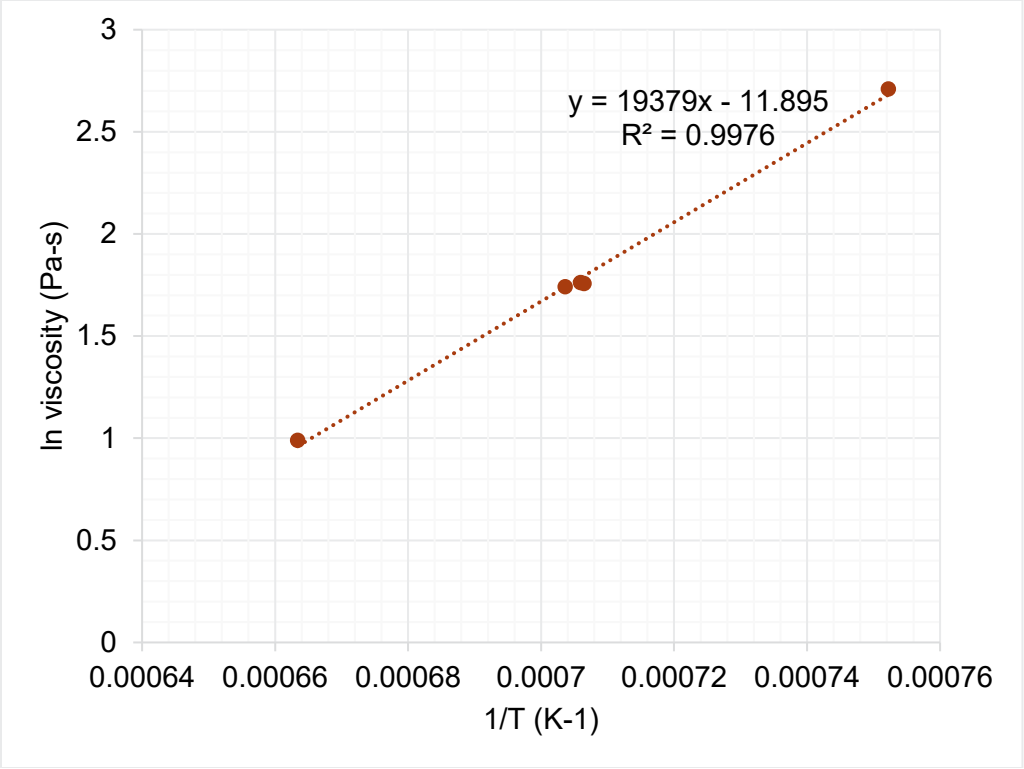

Figure I.26. Viscosity-temperature data and Arrhenius equation fit for HS24-26.

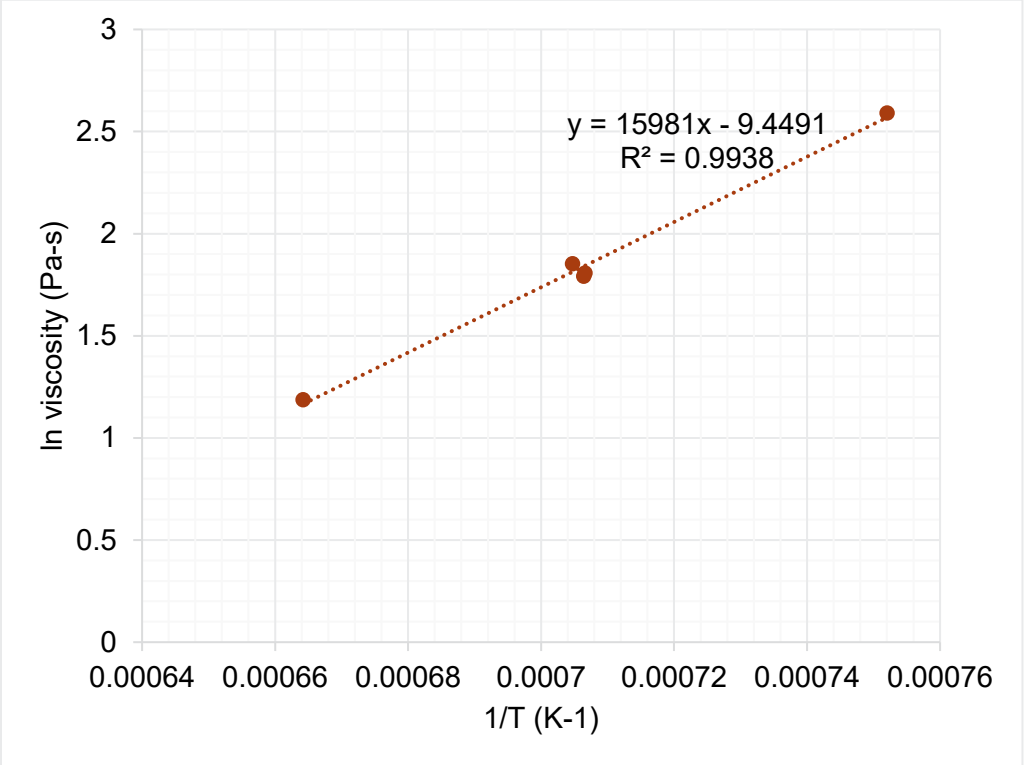

Figure I.27. Viscosity-temperature data and Arrhenius equation fit for HS24-27.

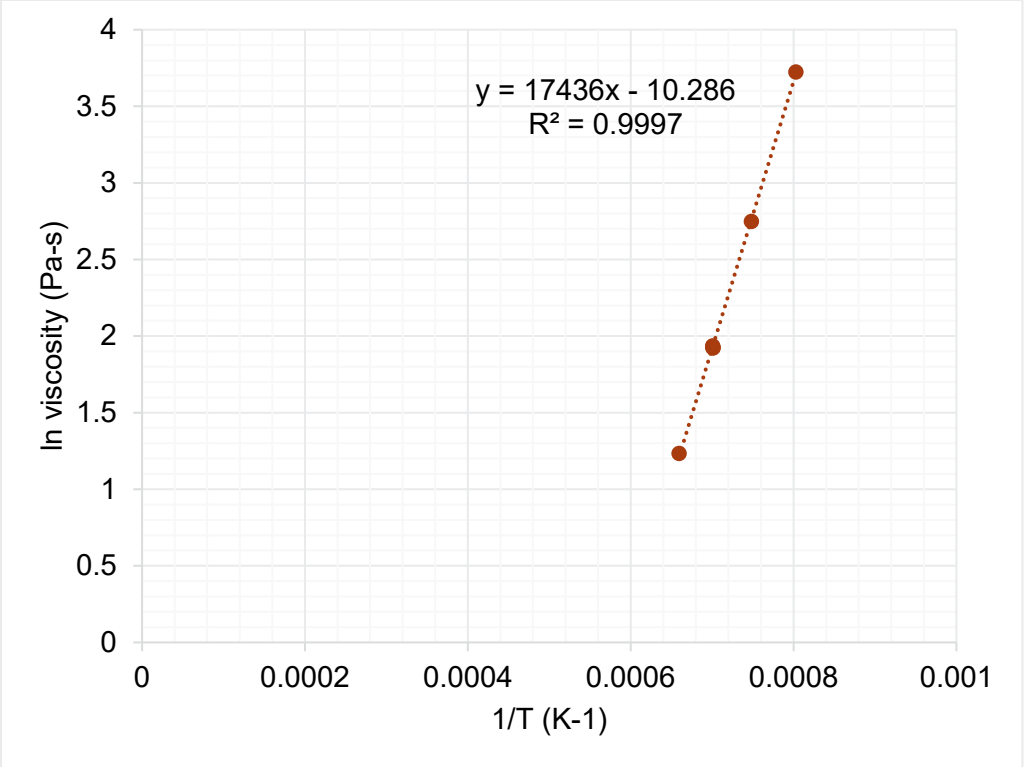

Figure I.28. Viscosity-temperature data and Arrhenius equation fit for HS24-28.

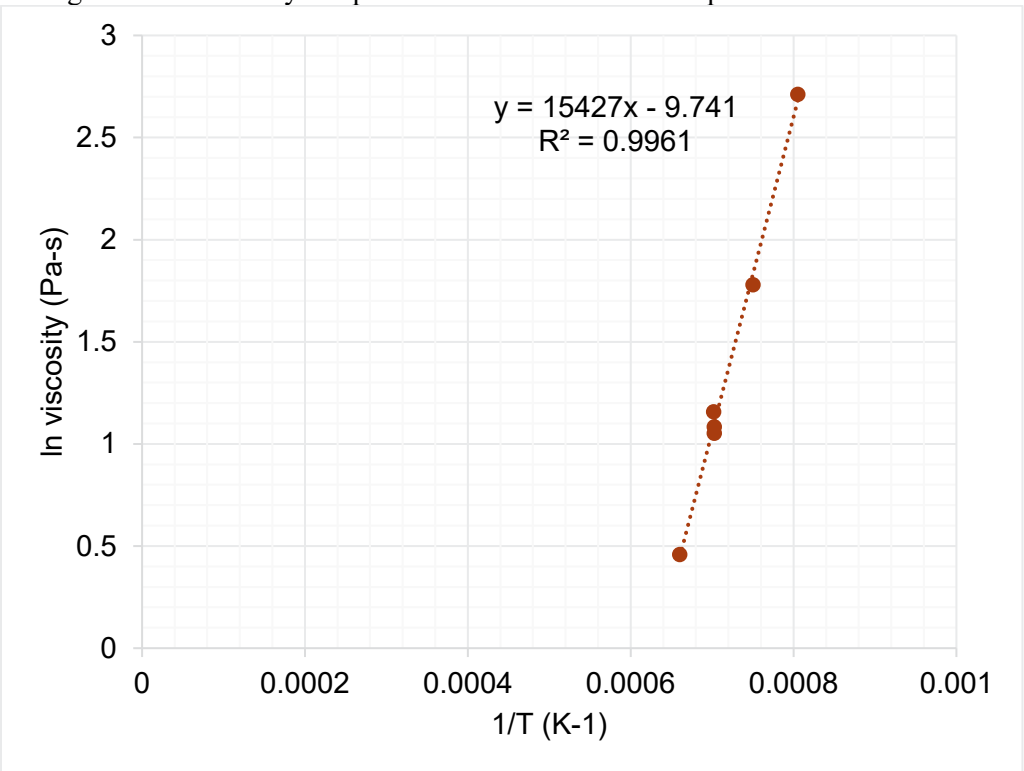

Figure I.29. Viscosity-temperature data and Arrhenius equation fit for HS24-29.

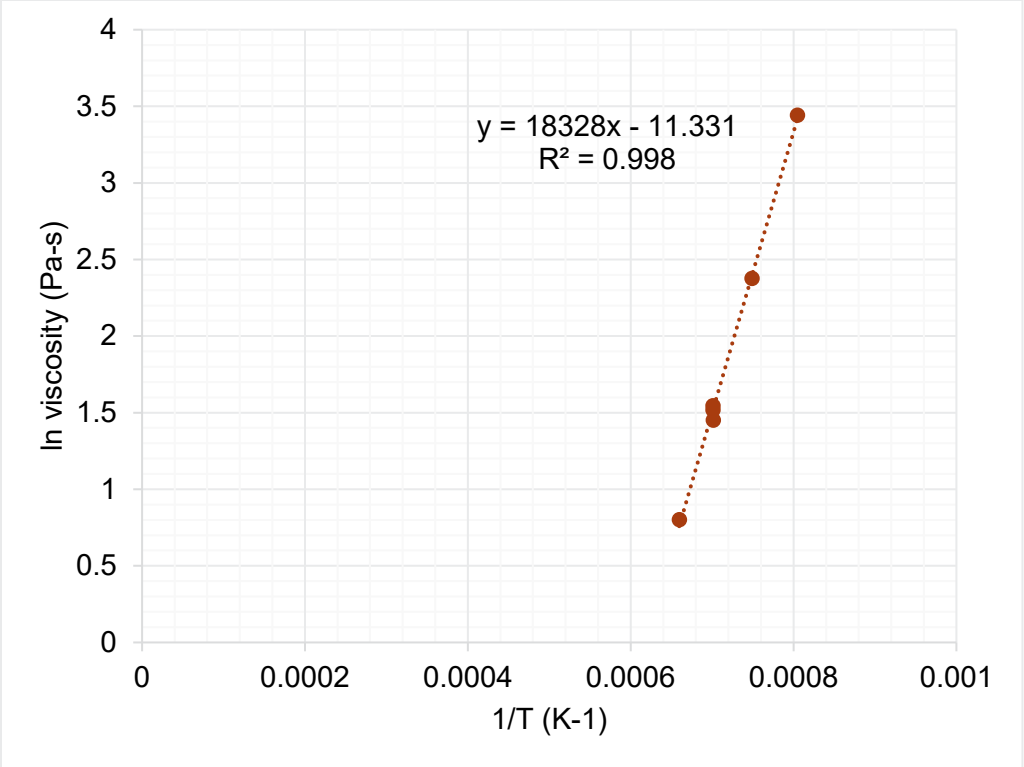

Figure I.30. Viscosity-temperature data and Arrhenius equation fit for HS24-30.

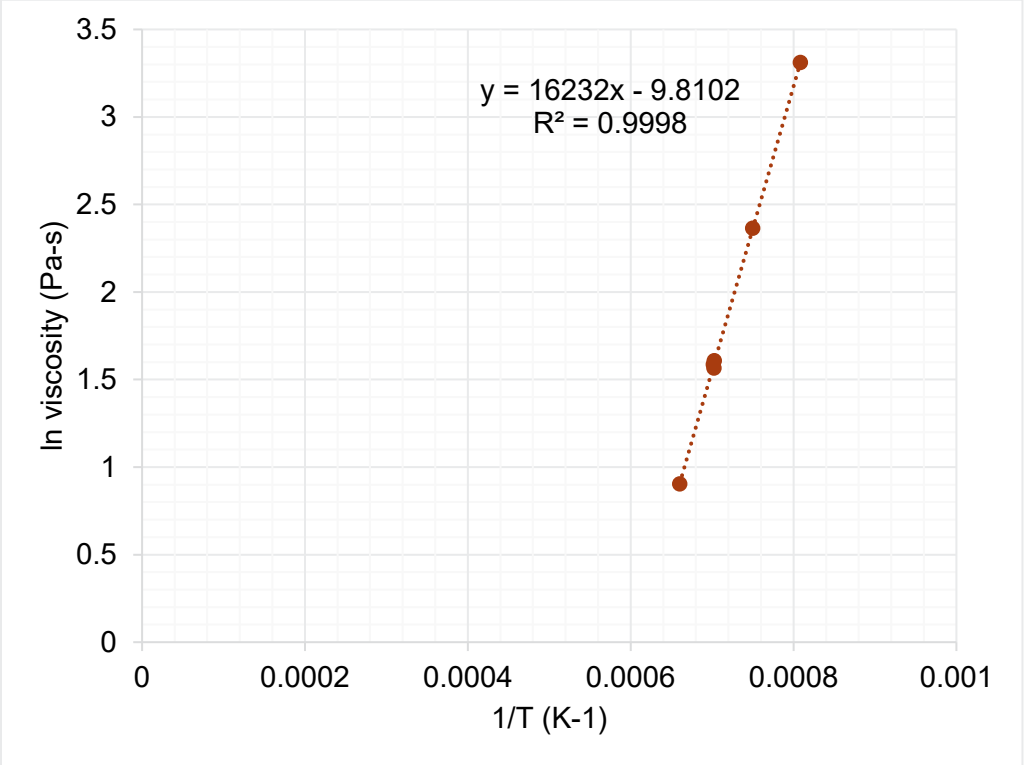

Figure I.31. Viscosity-temperature data and Arrhenius equation fit for HS24-31.

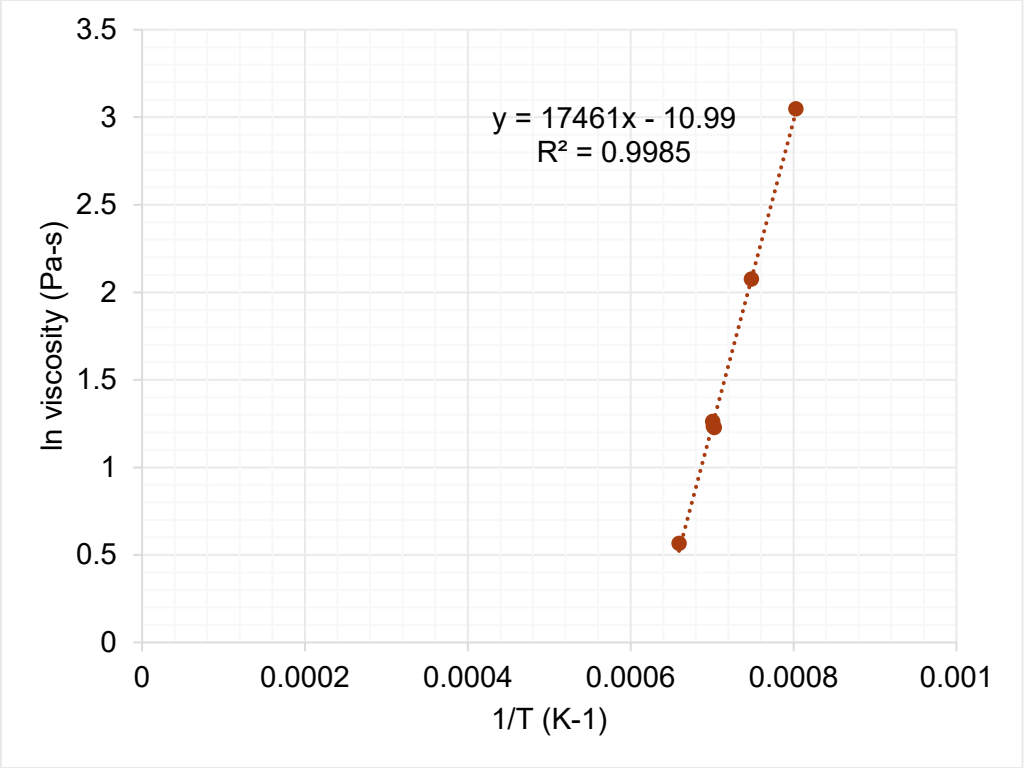

Figure I.32. Viscosity-temperature data and Arrhenius equation fit for HS24-32.

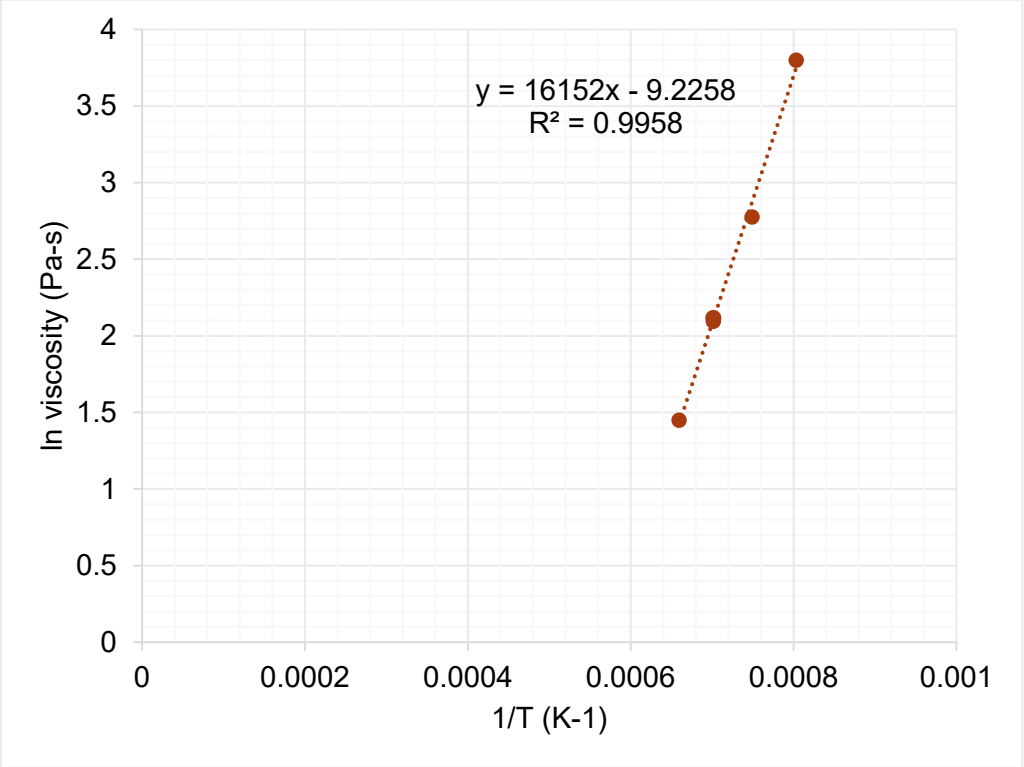

Figure I.33. Viscosity-temperature data and Arrhenius equation fit for HS24-33.

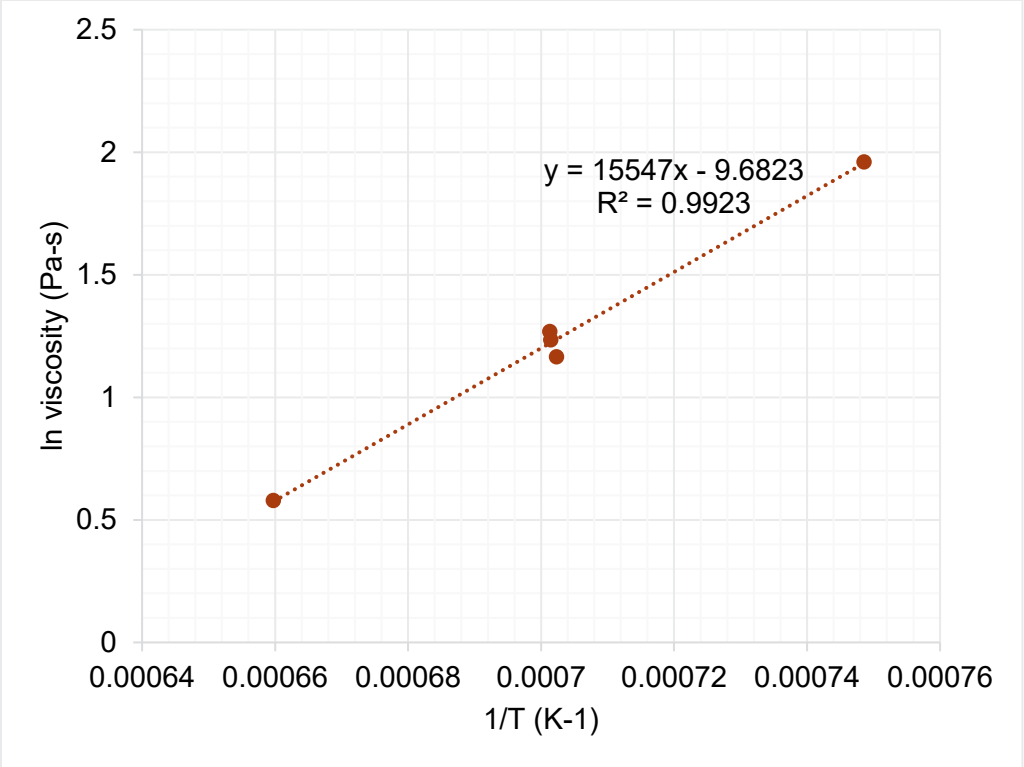

Figure I.34. Viscosity-temperature data and Arrhenius equation fit for HS24-34.

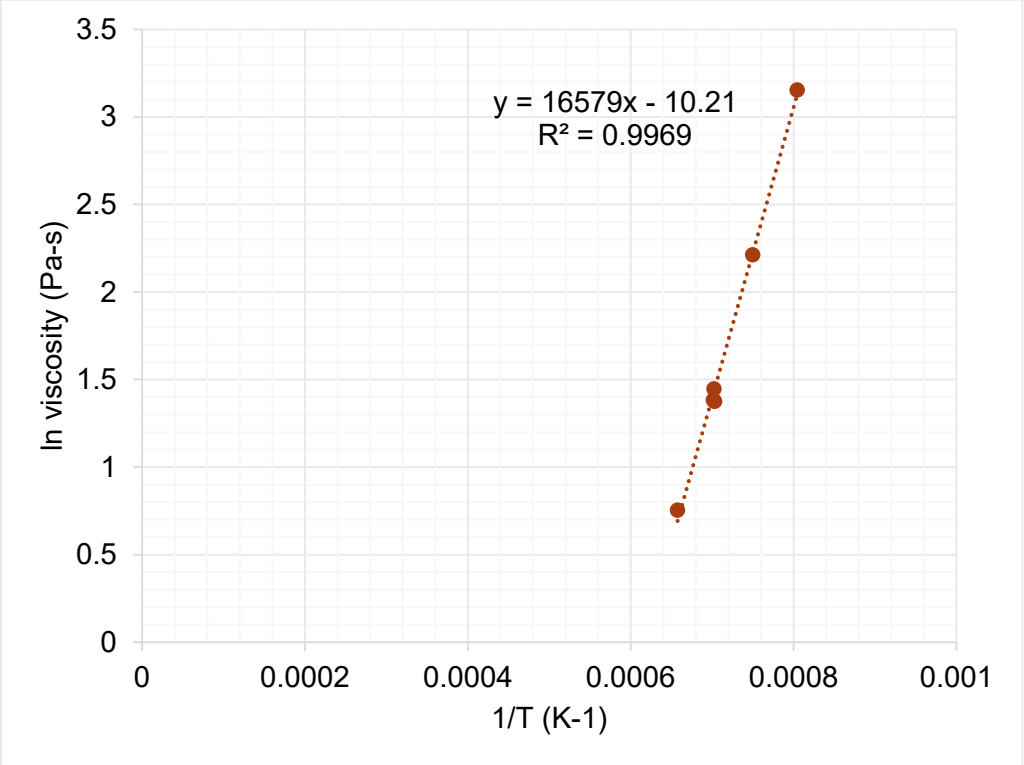

Figure I.35. Viscosity-temperature data and Arrhenius equation fit for HS24-35.

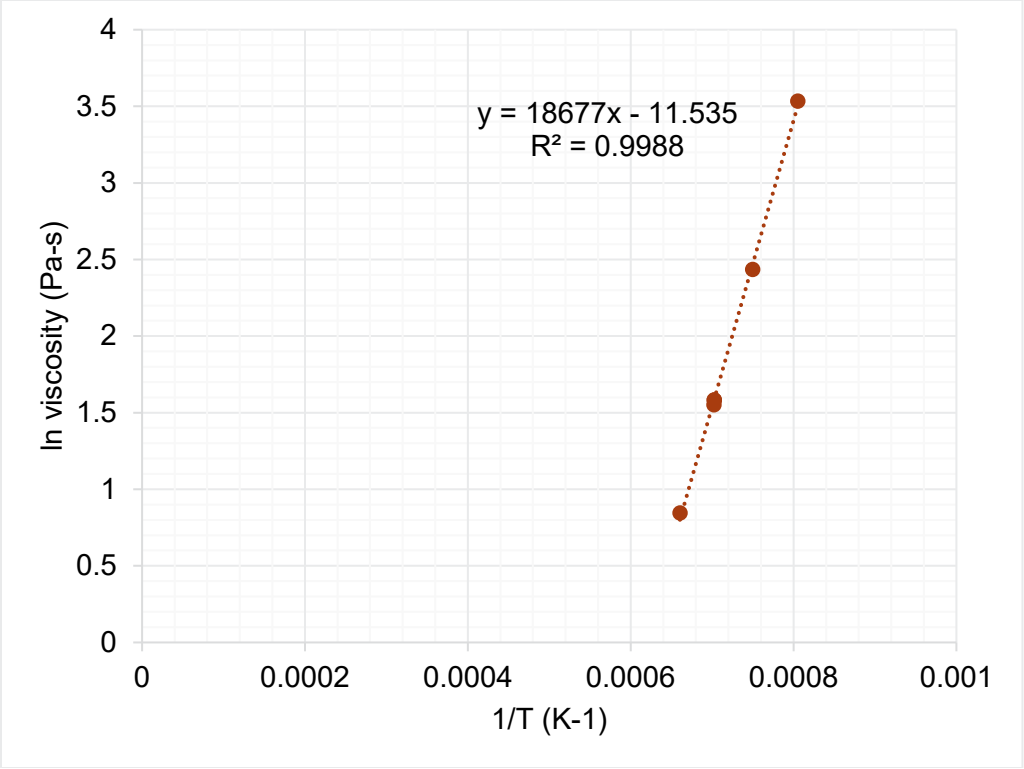

Figure I.36. Viscosity-temperature data and Arrhenius equation fit for HS24-36.

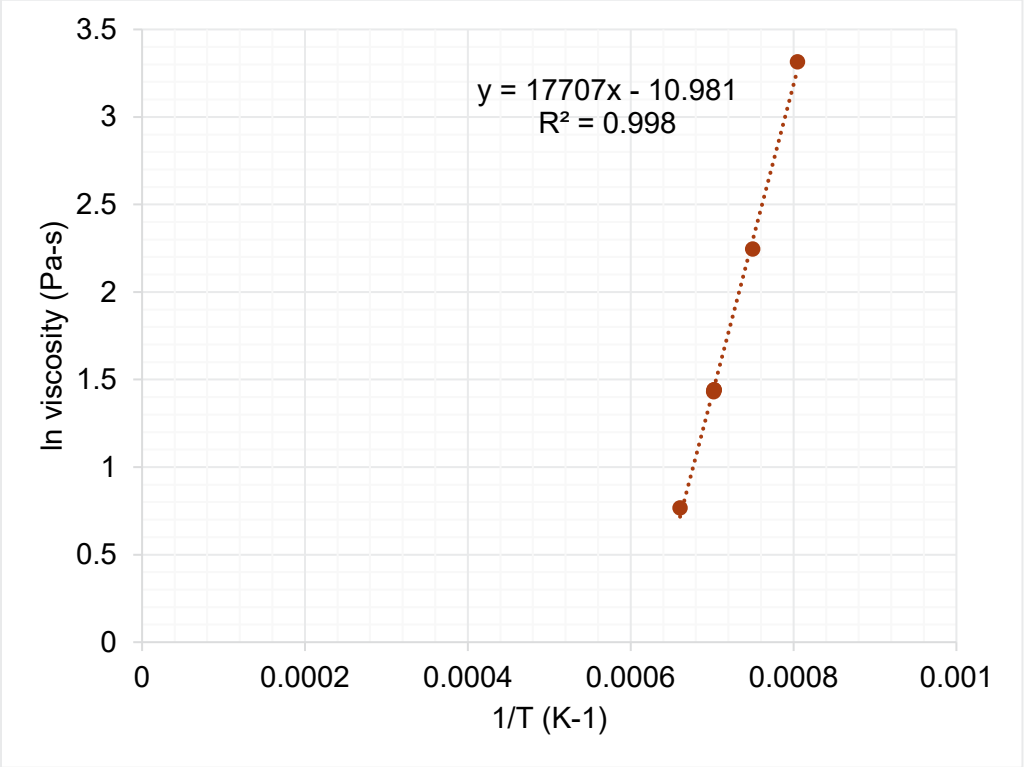

Figure I.37. Viscosity-temperature data and Arrhenius equation fit for HS24-37.

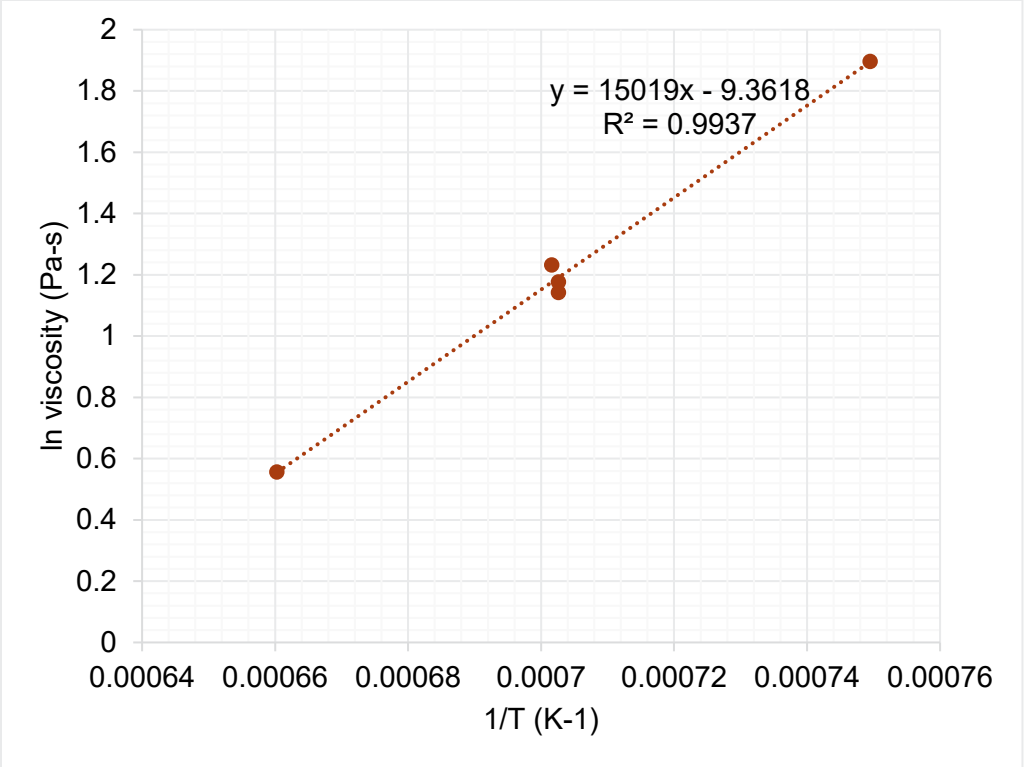

Figure I.38. Viscosity-temperature data and Arrhenius equation fit for HS24-38.

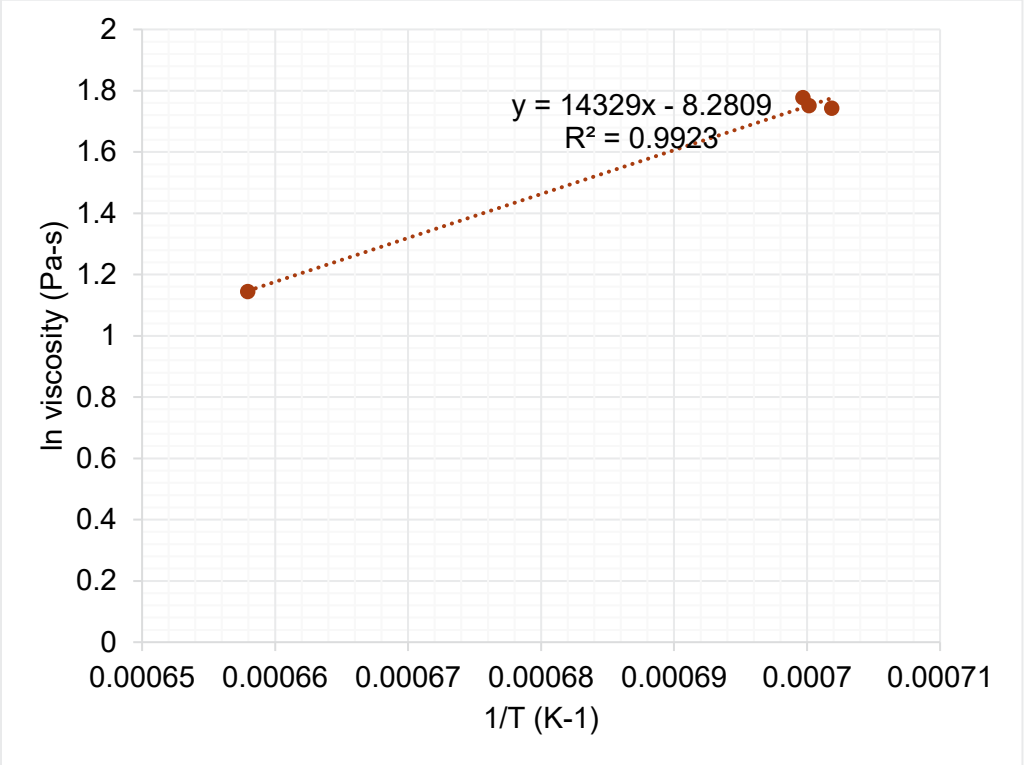

Figure I.39. Viscosity-temperature data and Arrhenius equation fit for HS24-39.

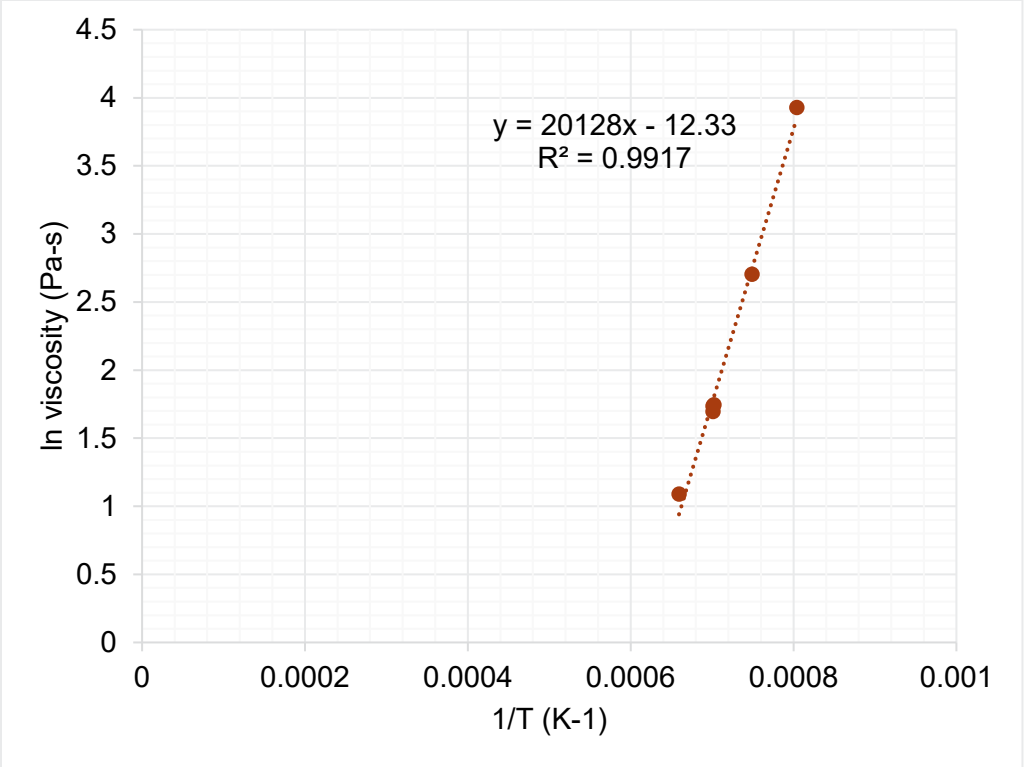

Figure I.40. Viscosity-temperature data and Arrhenius equation fit for HS24-40.

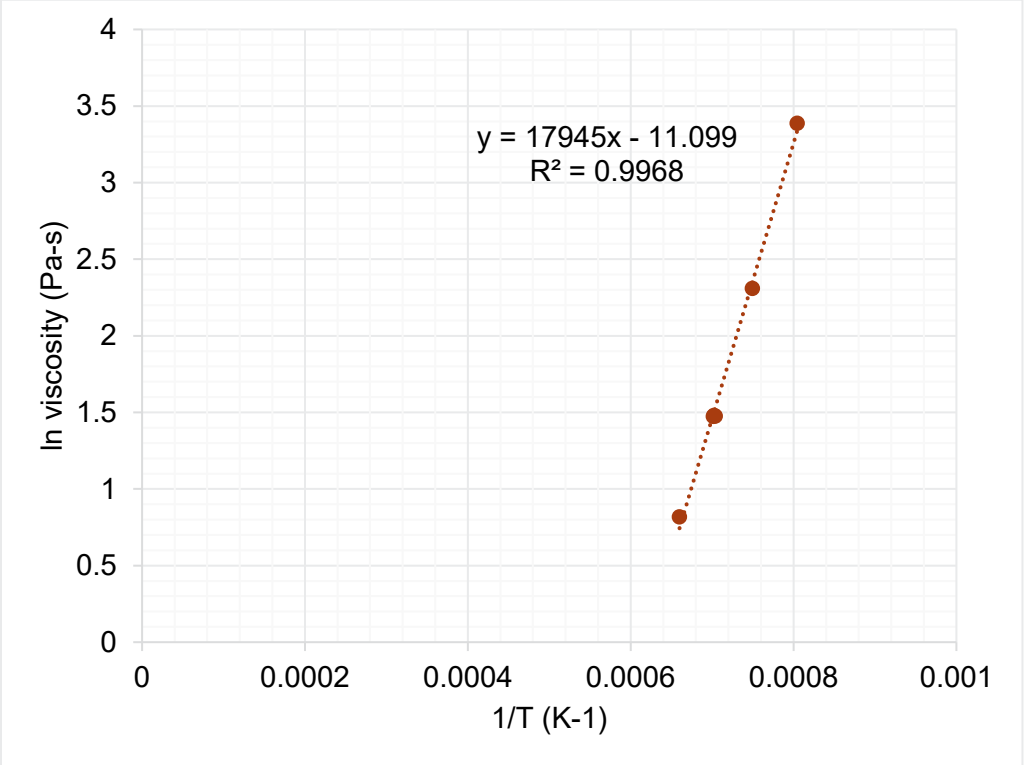

Figure I.41. Viscosity-temperature data and Arrhenius equation fit for HS24-41.

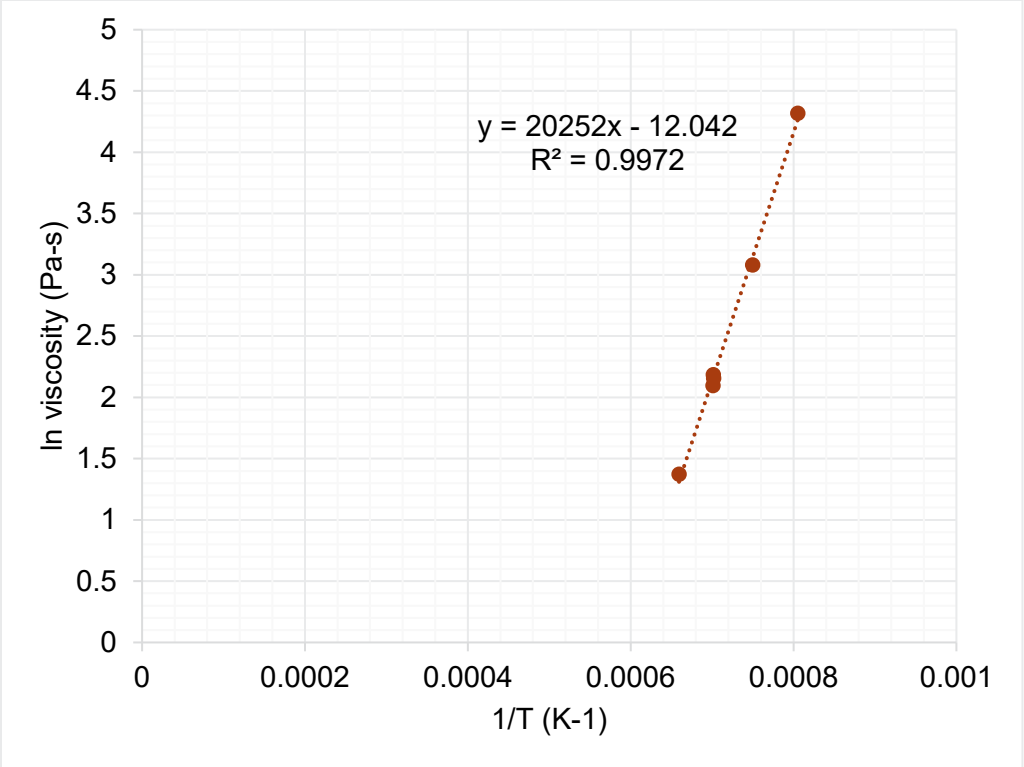

Figure I.42. Viscosity-temperature data and Arrhenius equation fit for HS24-42.

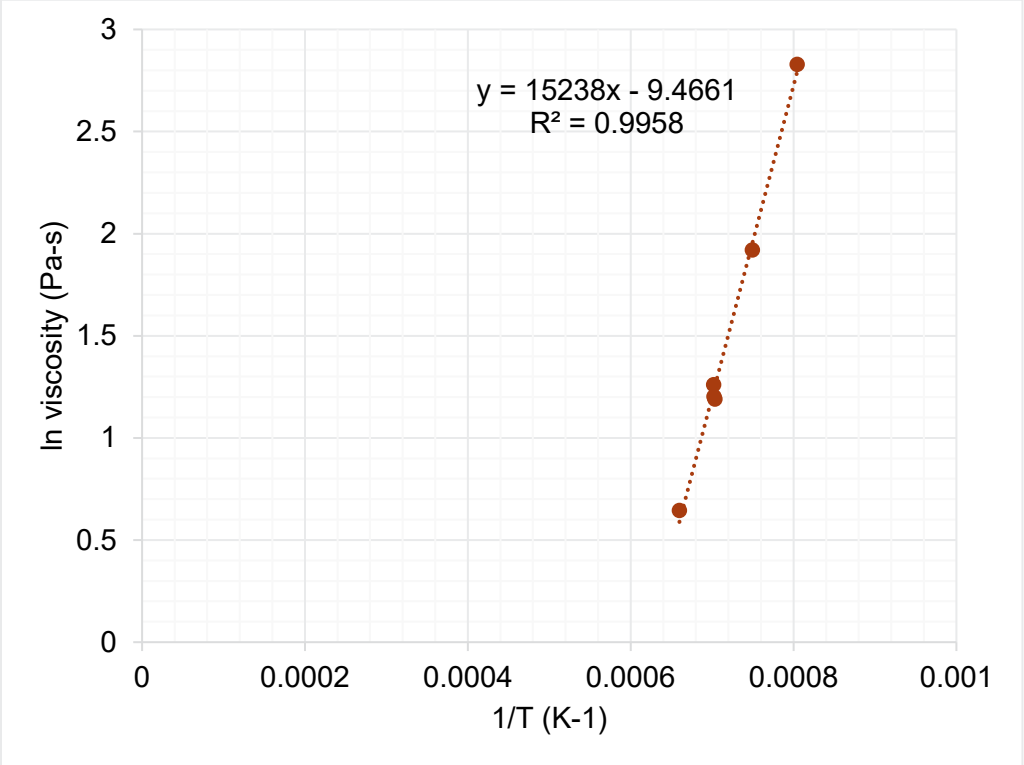

Figure I.43. Viscosity-temperature data and Arrhenius equation fit for HS24-43.

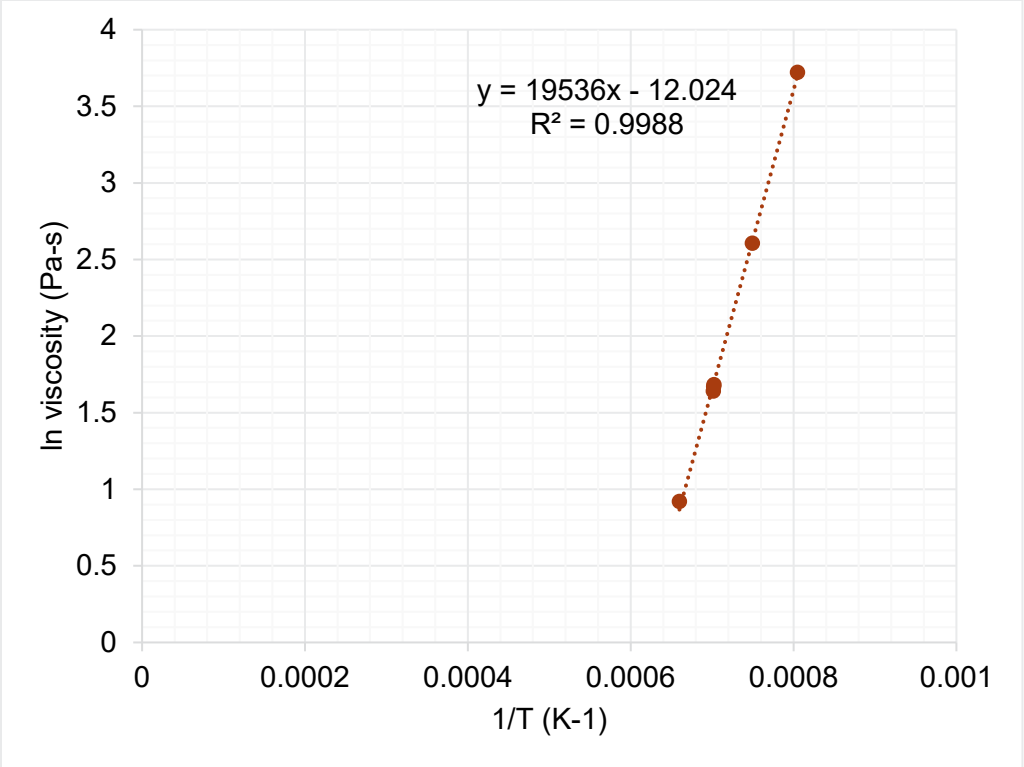

Figure I.44. Viscosity-temperature data and Arrhenius equation fit for HS24-44.

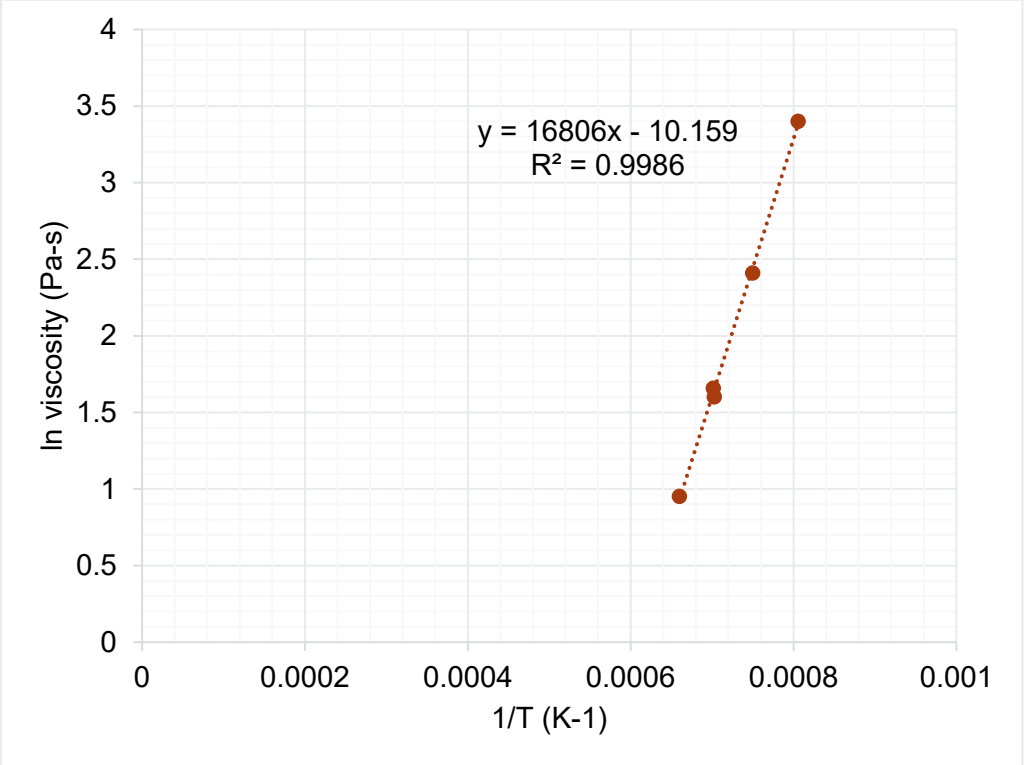

Figure I.45. Viscosity-temperature data and Arrhenius equation fit for HS24-45.

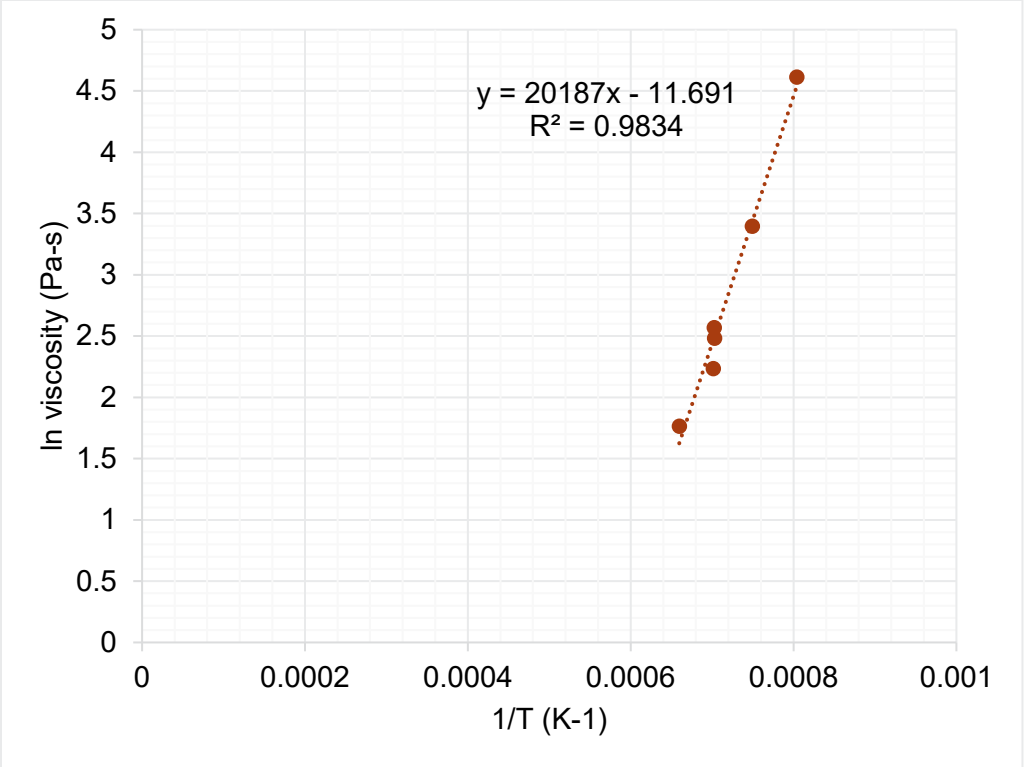

Figure I.46. Viscosity-temperature data and Arrhenius equation fit for HS24-46.

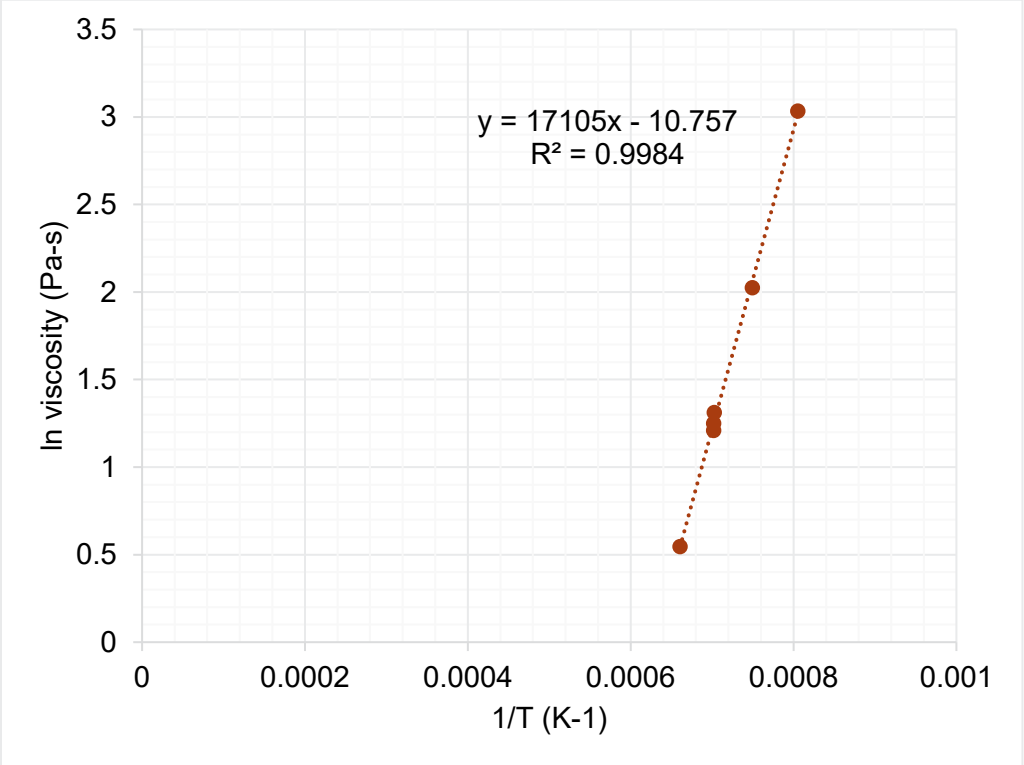

Figure I.47. Viscosity-temperature data and Arrhenius equation fit for HS24-47.

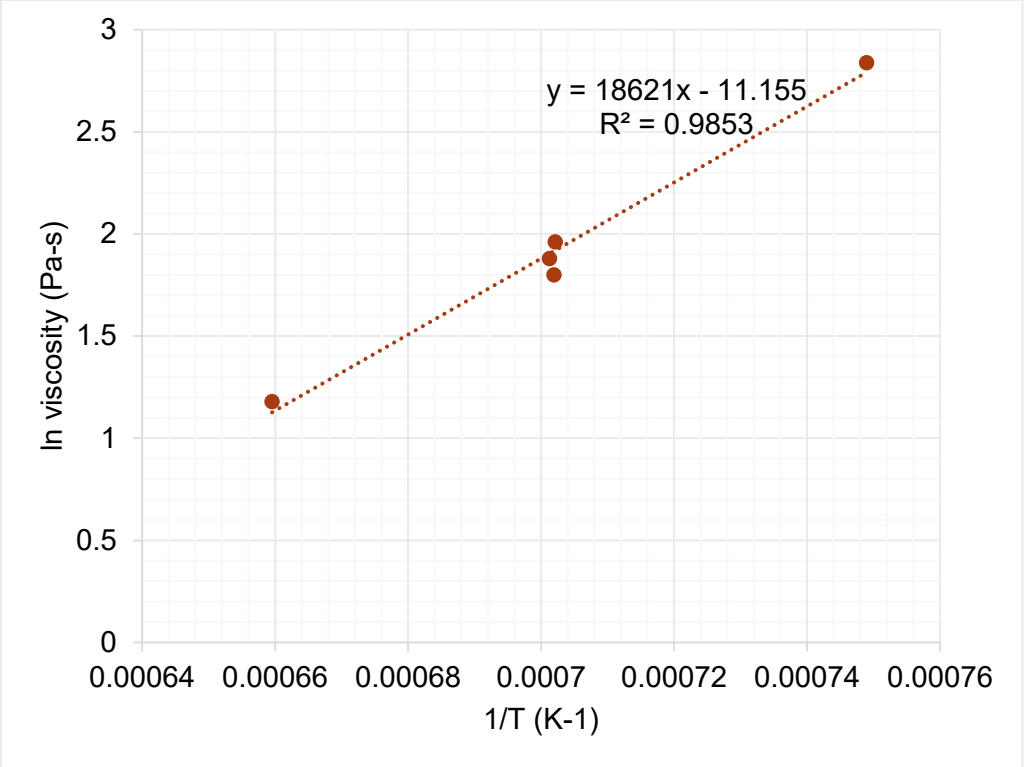

Figure I.48. Viscosity-temperature data and Arrhenius equation fit for HS24-48.

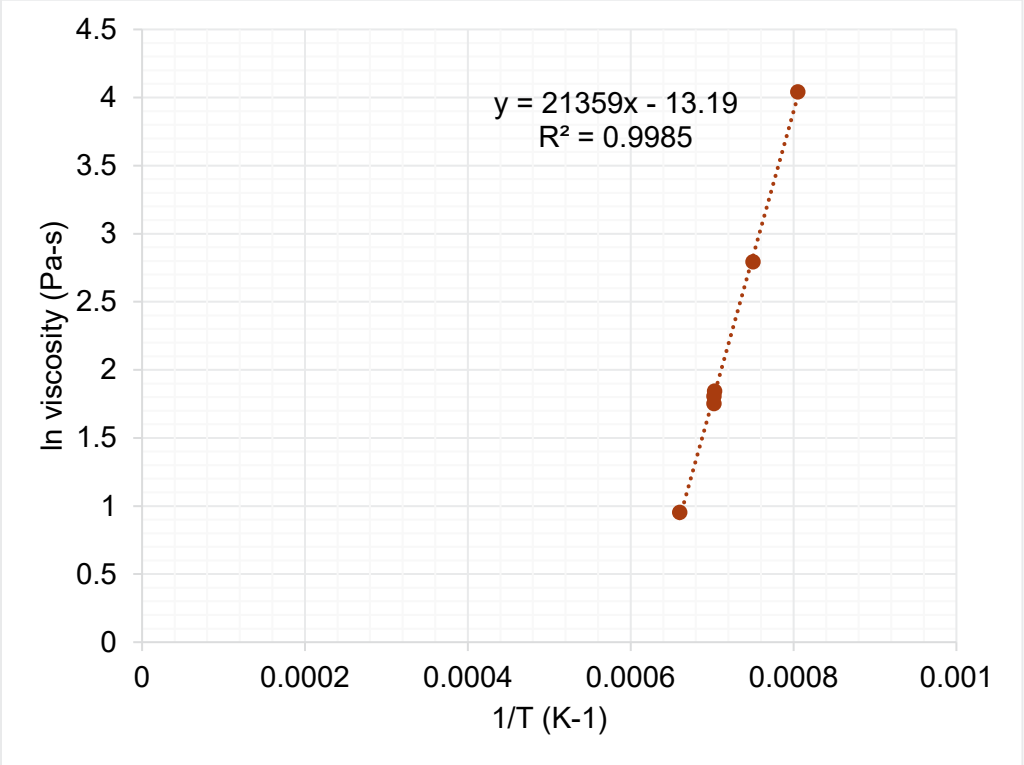

Figure I.49. Viscosity-temperature data and Arrhenius equation fit for HS24-49.

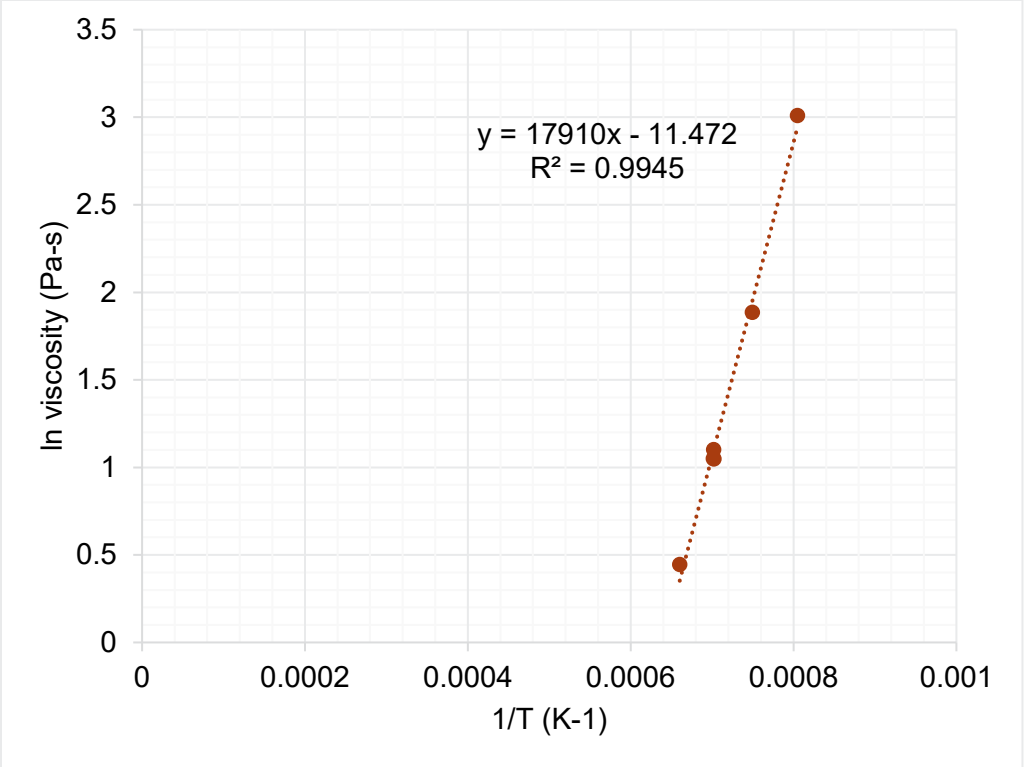

Figure I.50. Viscosity-temperature data and Arrhenius equation fit for HS24-50.

Appendix J – EC Results

This appendix contains the measured electrical conductivity data for each of the glasses in the HS24 matrix described in Section 3.7.

The graphs shown in this appendix are fitted to the Arrhenius equation (Equation 4.2), referenced in Section 4.6.

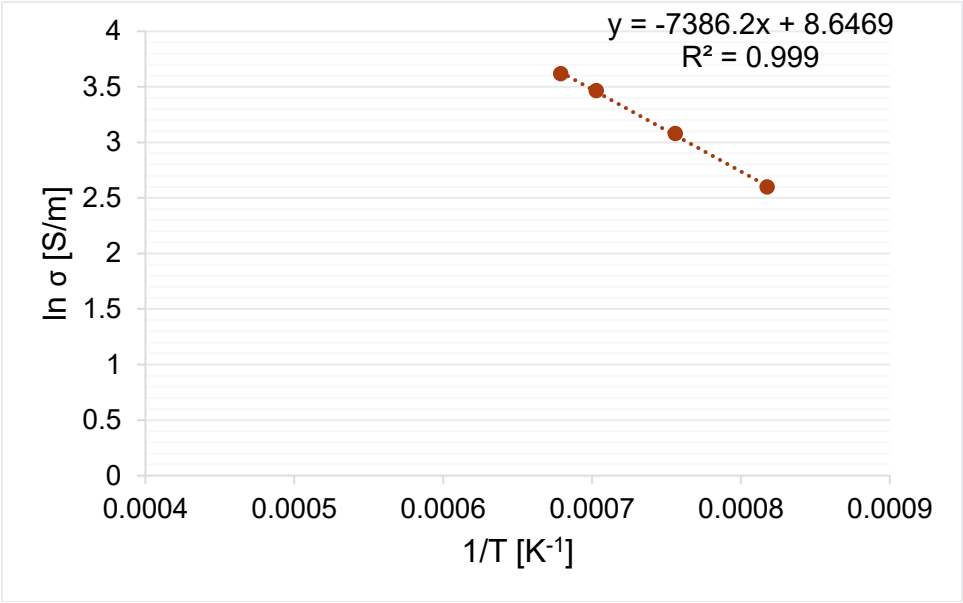

Figure J.1. Electrical conductivity-temperature data and Arrhenius equation fit for glass HS24-01.

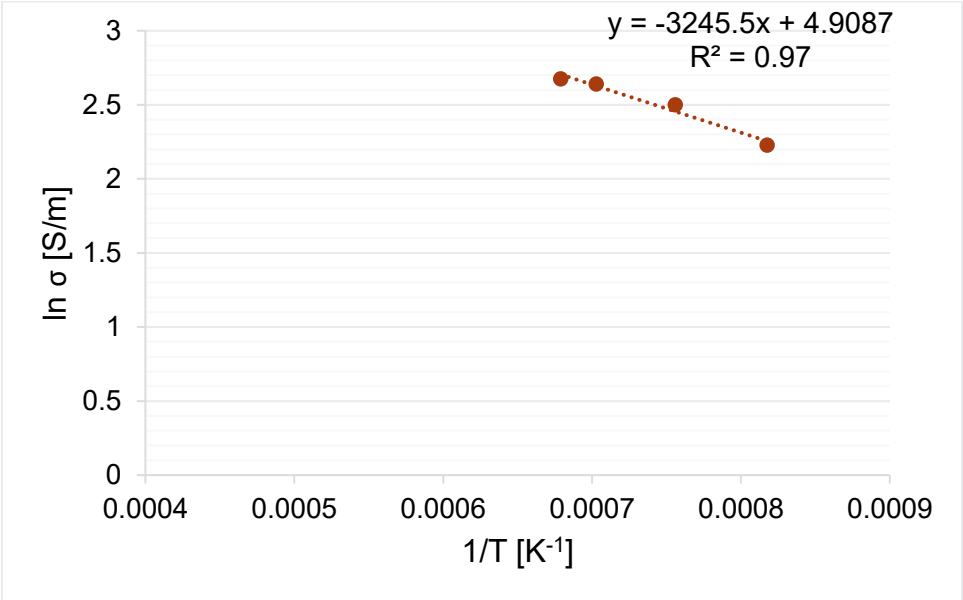

Figure J.2. Electrical conductivity-temperature data and Arrhenius equation fit for glass HS24-02.

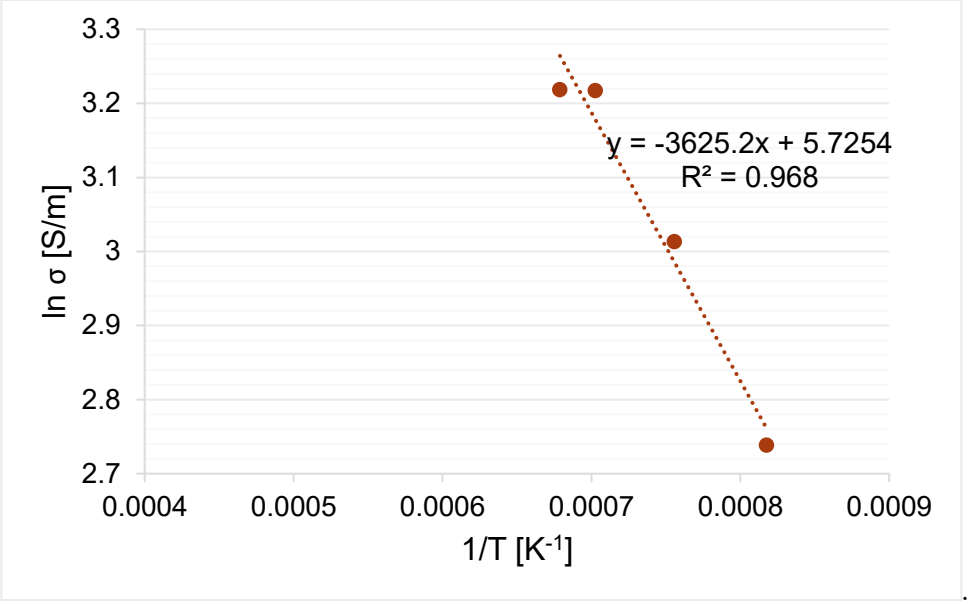

Figure J.3. Electrical conductivity-temperature data and Arrhenius equation fit for glass HS24-03.

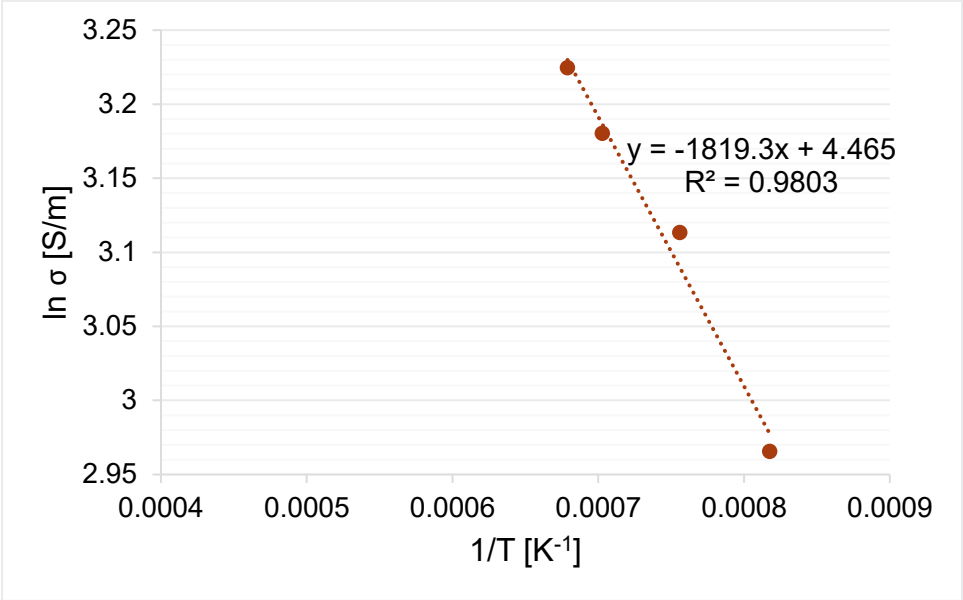

Figure J.4. Electrical conductivity-temperature data and Arrhenius equation fit for glass HS24-04.

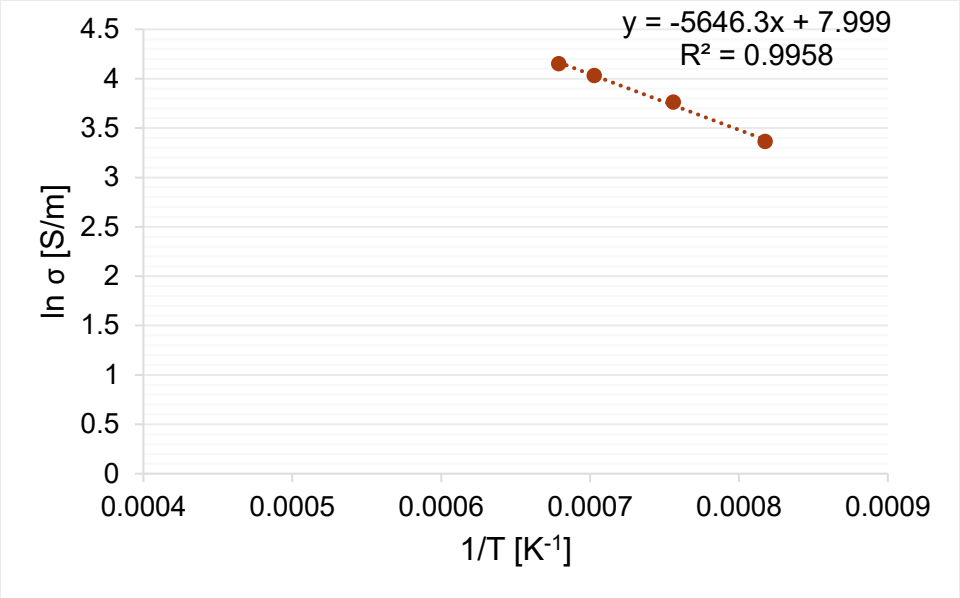

Figure J.5. Electrical conductivity-temperature data and Arrhenius equation fit for glass HS24-05.

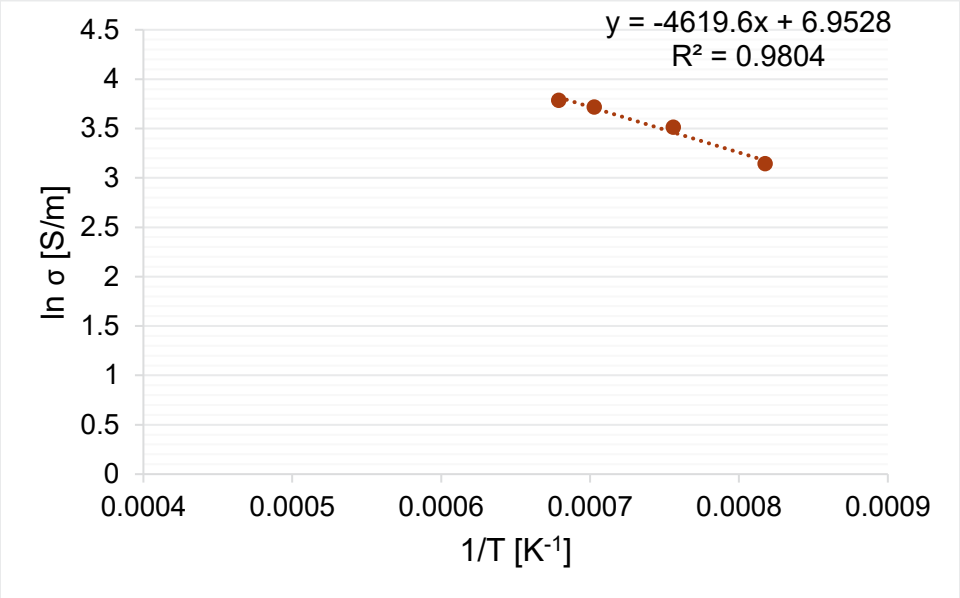

Figure J.6. Electrical conductivity-temperature data and Arrhenius equation fit for glass HS24-06.

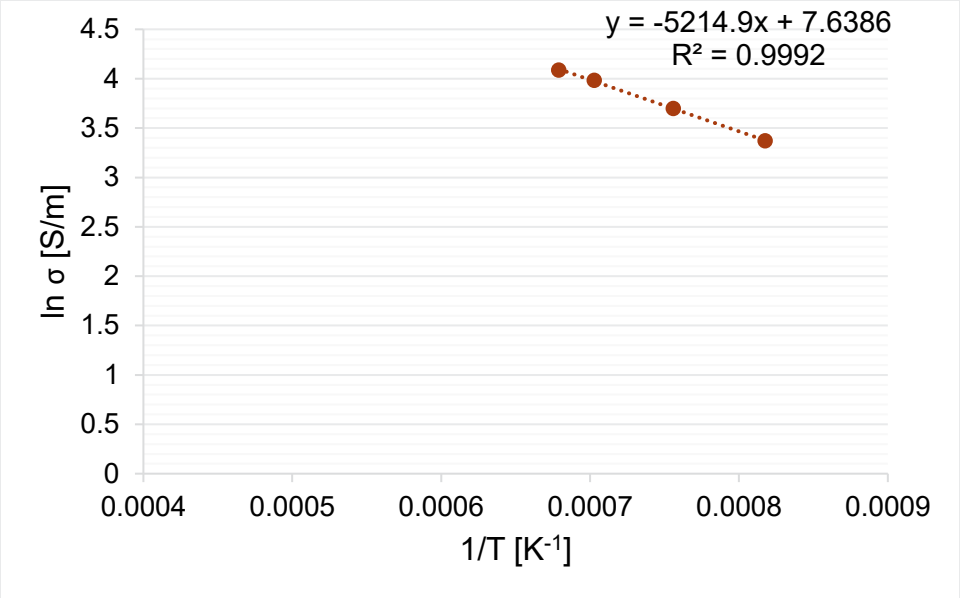

Figure J.7. Electrical conductivity-temperature data and Arrhenius equation fit for glass HS24-07.

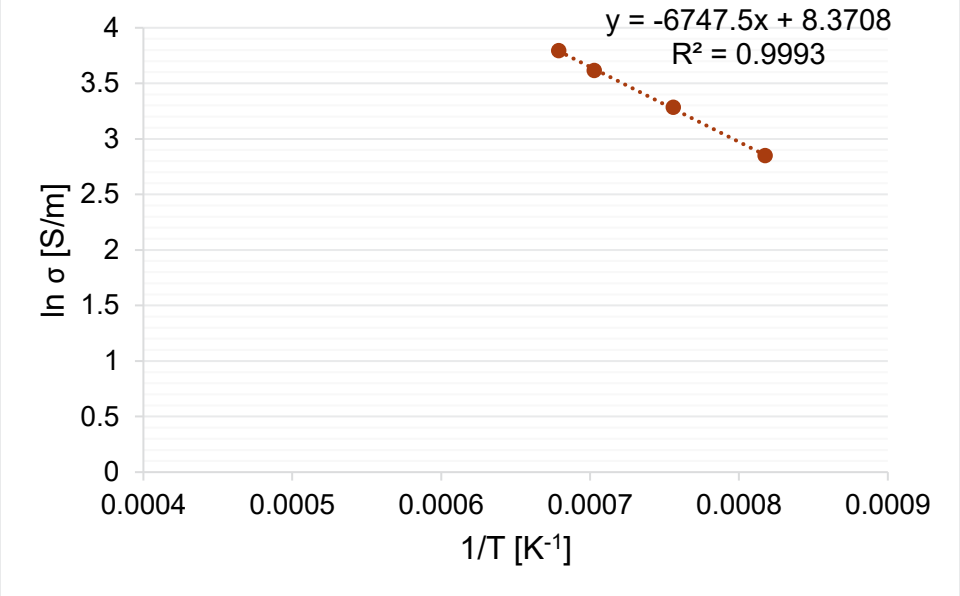

Figure J.8. Electrical conductivity-temperature data and Arrhenius equation fit for glass HS24-08.

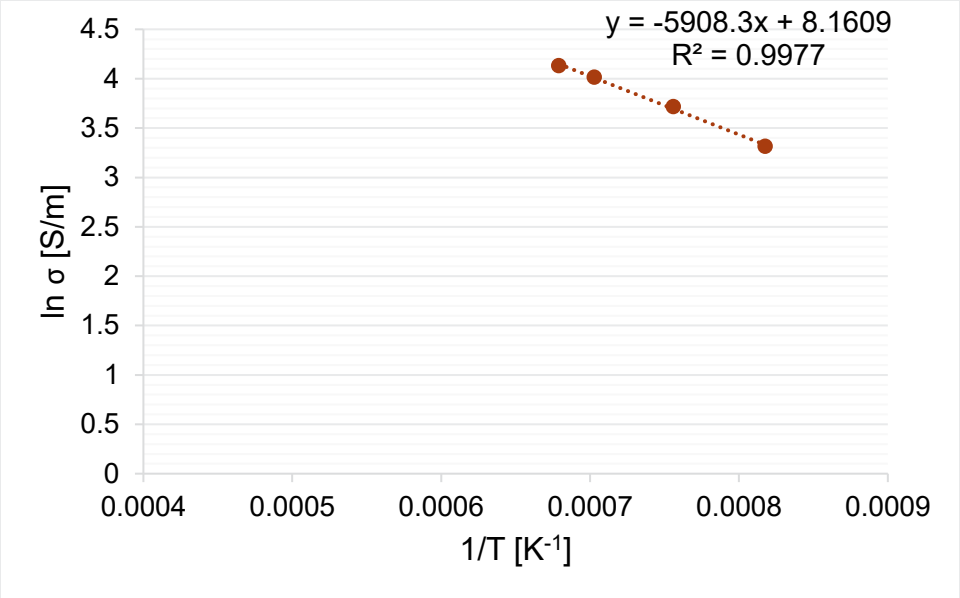

Figure J.9. Electrical conductivity-temperature data and Arrhenius equation fit for glass HS24-09.

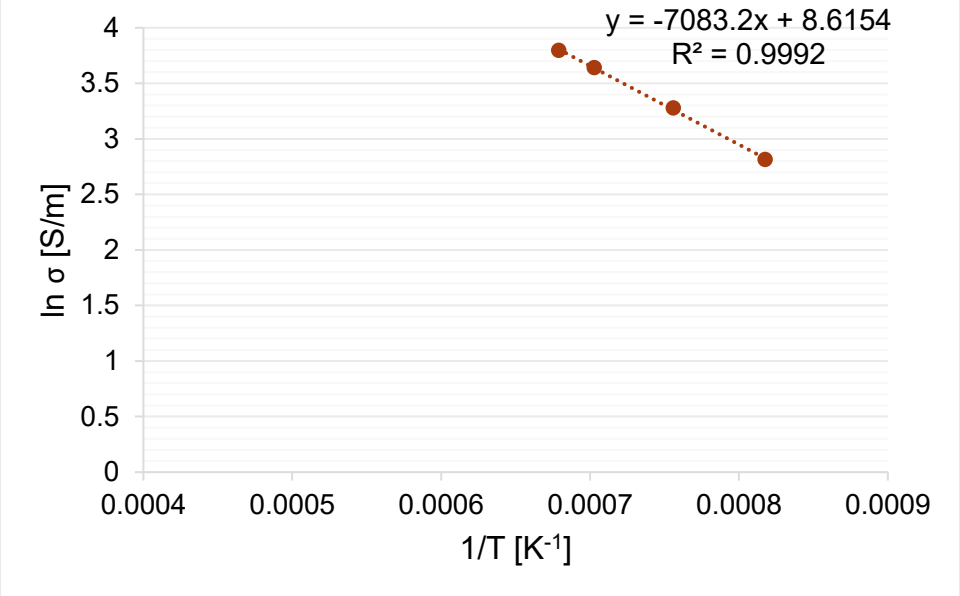

Figure J.10. Electrical conductivity-temperature data and Arrhenius equation fit for glass HS24-10.

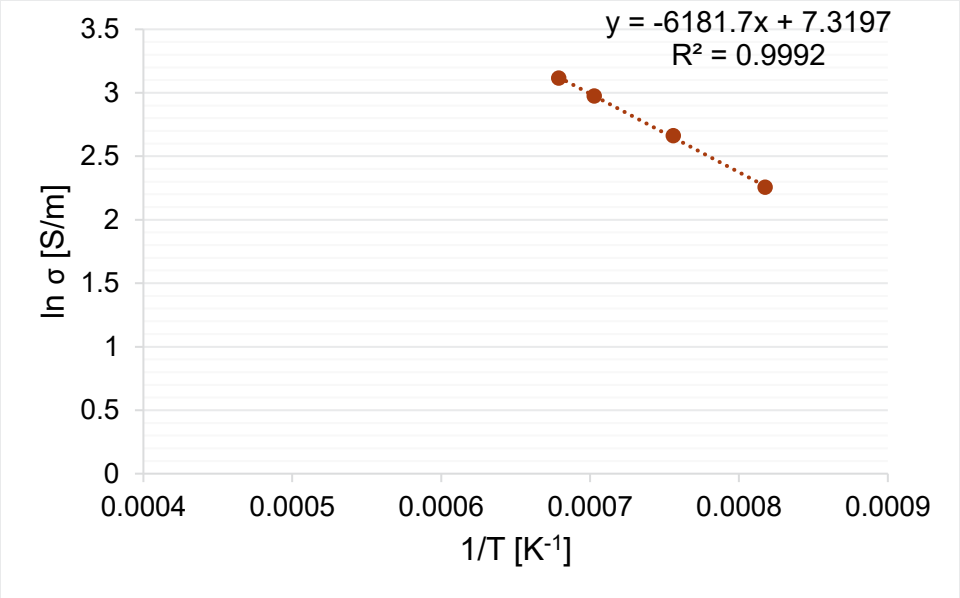

Figure J.11. Electrical conductivity-temperature data and Arrhenius equation fit for glass HS24-11.

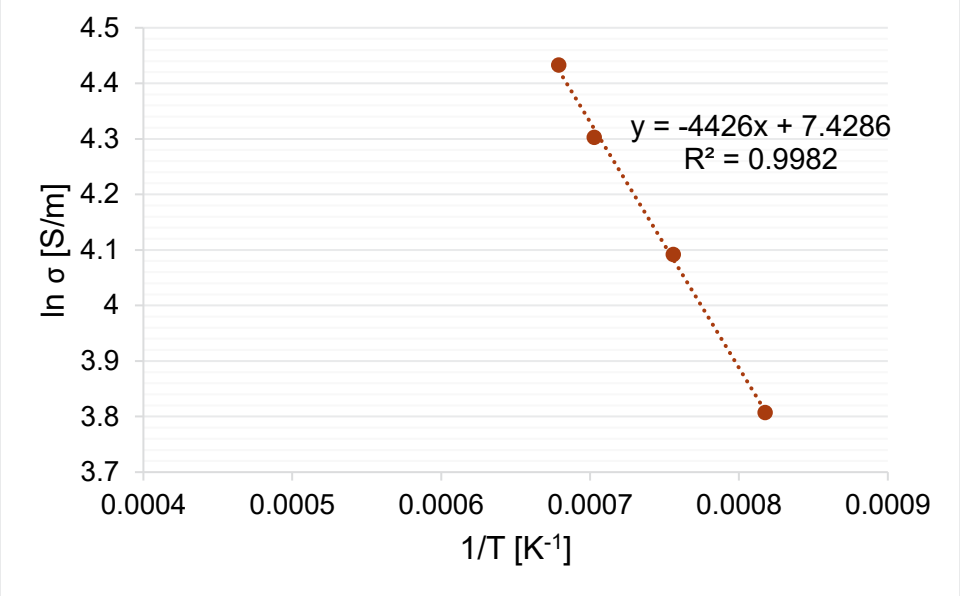

Figure J.12. Electrical conductivity-temperature data and Arrhenius equation fit for glass HS24-12.

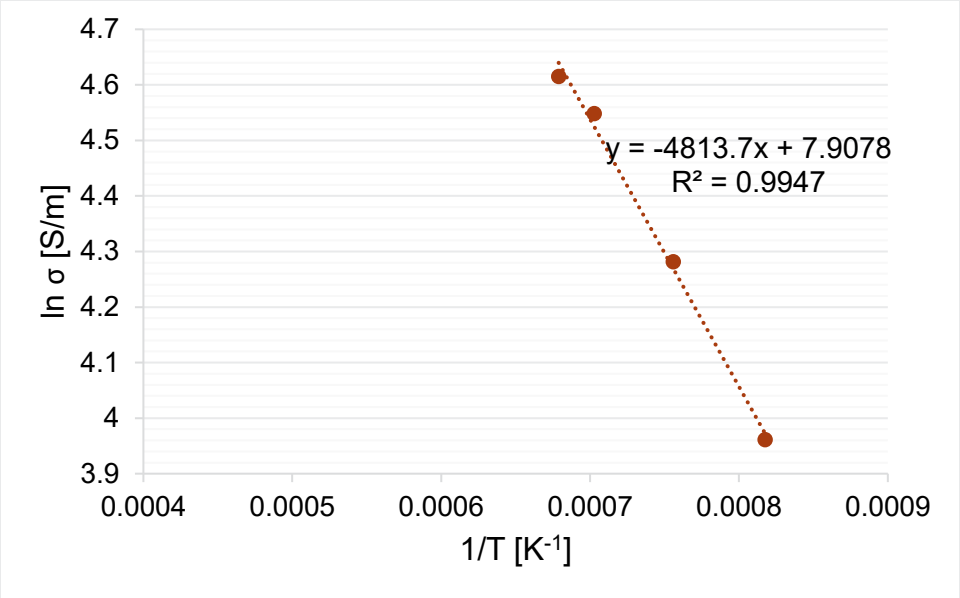

Figure J.13. Electrical conductivity-temperature data and Arrhenius equation fit for glass HS24-13.

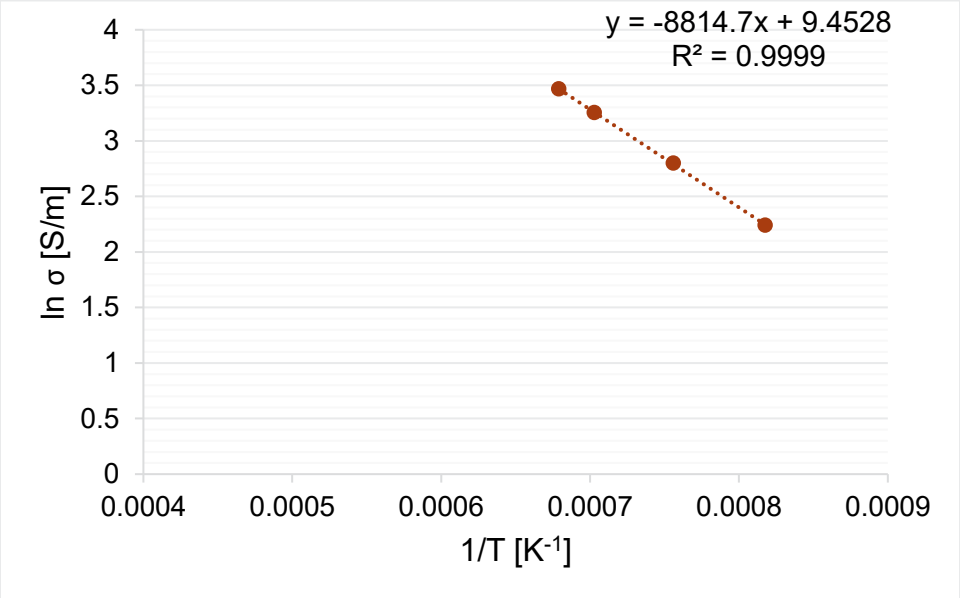

Figure J.14. Electrical conductivity-temperature data and Arrhenius equation fit for glass HS24-14.

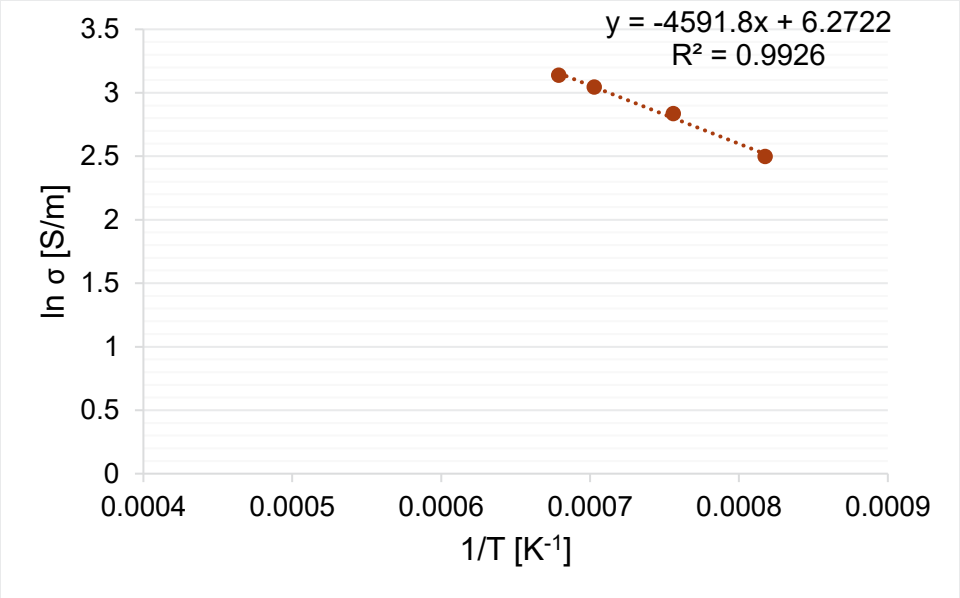

Figure J.15. Electrical conductivity-temperature data and Arrhenius equation fit for glass HS24-15.

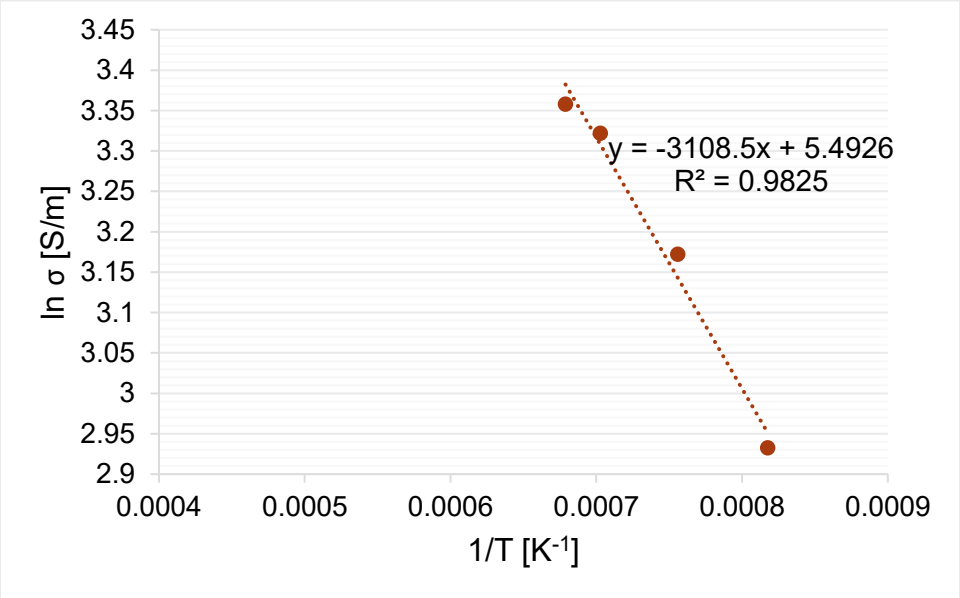

Figure J.16. Electrical conductivity-temperature data and Arrhenius equation fit for glass HS24-16.

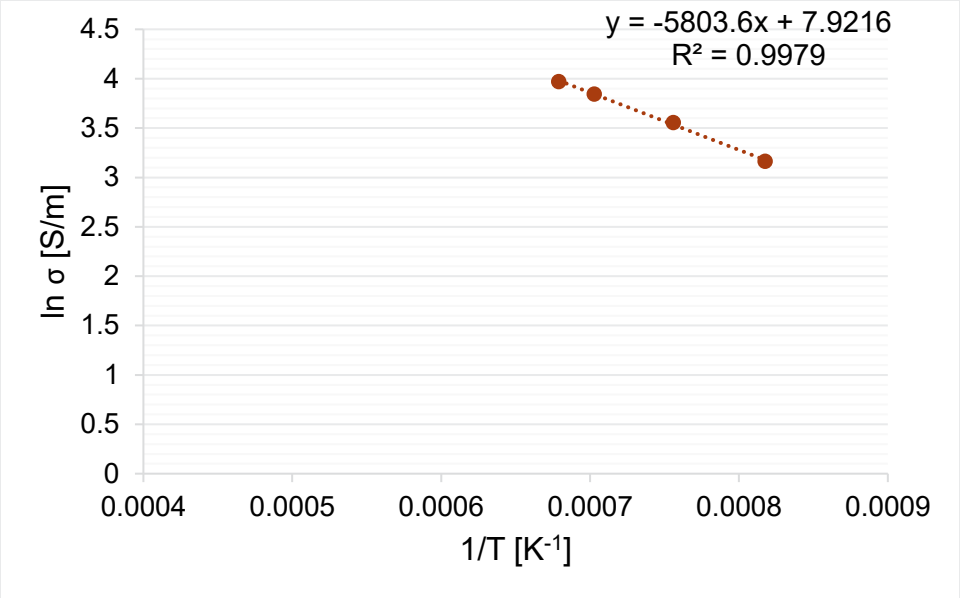

Figure J.17. Electrical conductivity-temperature data and Arrhenius equation fit for glass HS24-17.

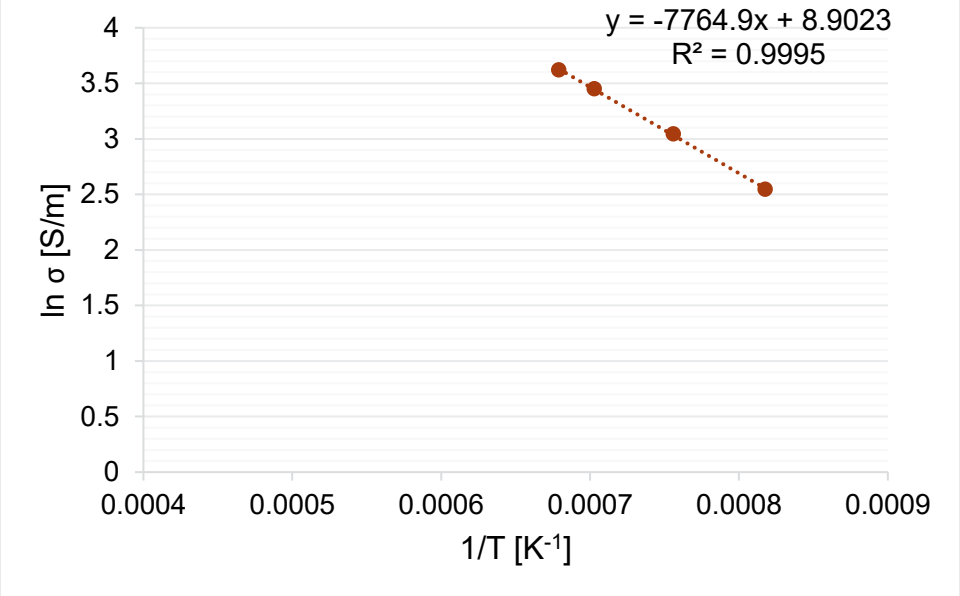

Figure J.18. Electrical conductivity-temperature data and Arrhenius equation fit for glass HS24-18.

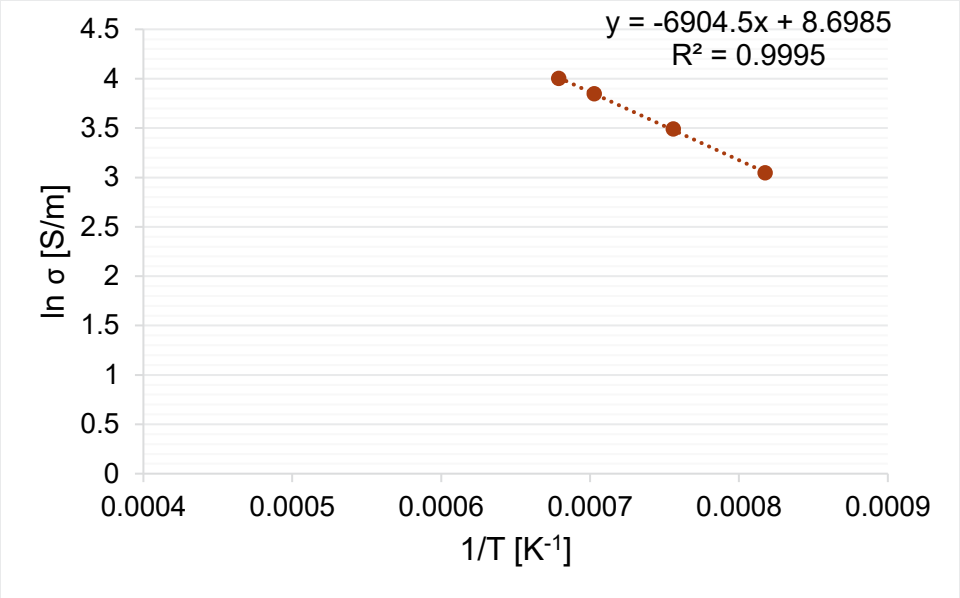

Figure J.19. Electrical conductivity-temperature data and Arrhenius equation fit for glass HS24-19.

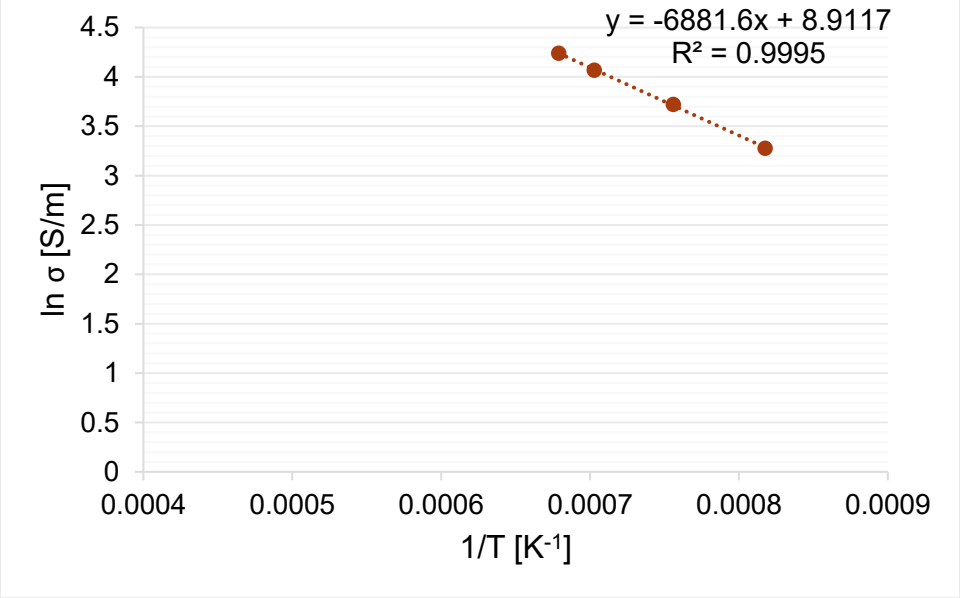

Figure J.20. Electrical conductivity-temperature data and Arrhenius equation fit for glass HS24-20.

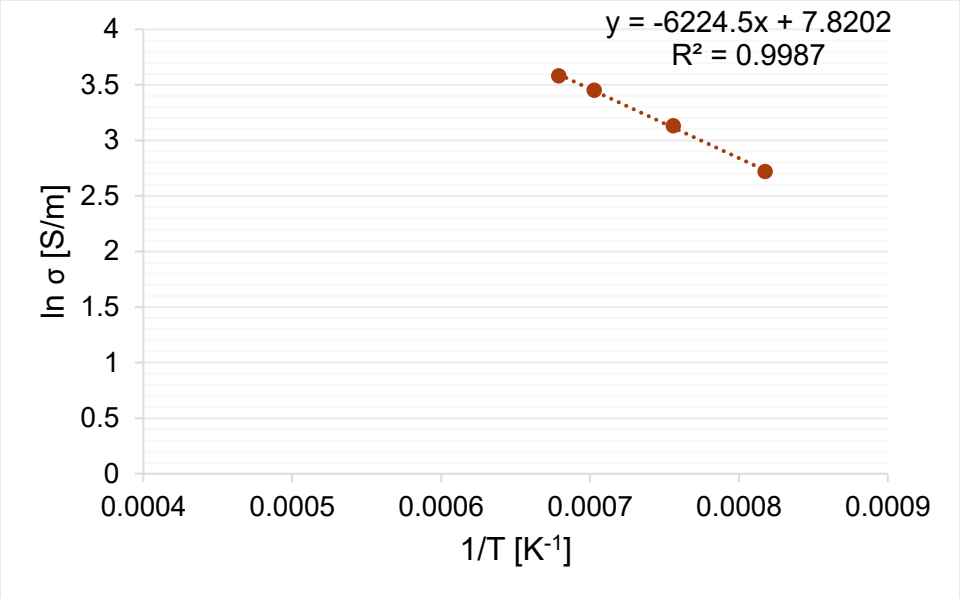

Figure J.21. Electrical conductivity-temperature data and Arrhenius equation fit for glass HS24-21.

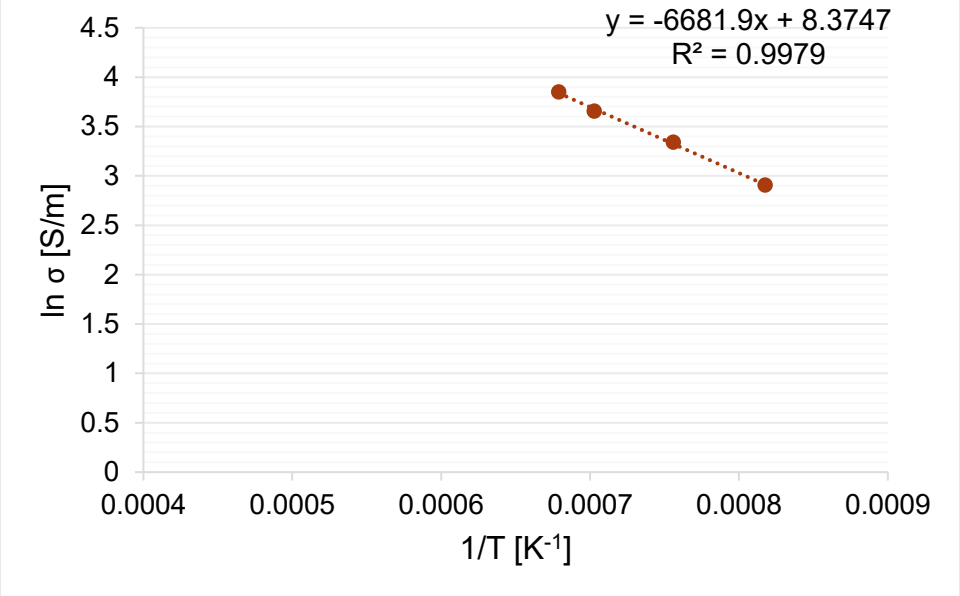

Figure J.22. Electrical conductivity-temperature data and Arrhenius equation fit for glass HS24-22.

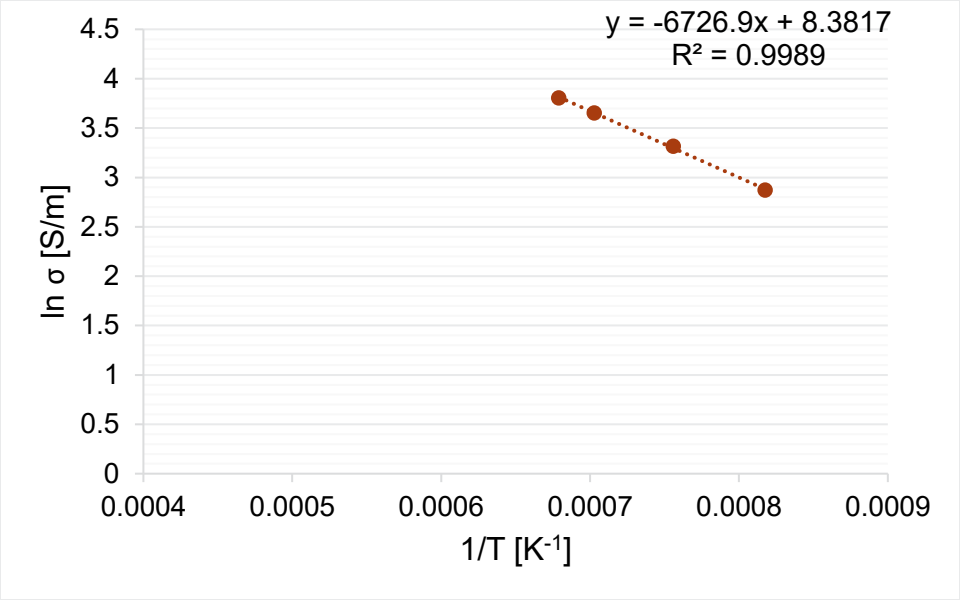

Figure J.23. Electrical conductivity-temperature data and Arrhenius equation fit for glass HS24-23.

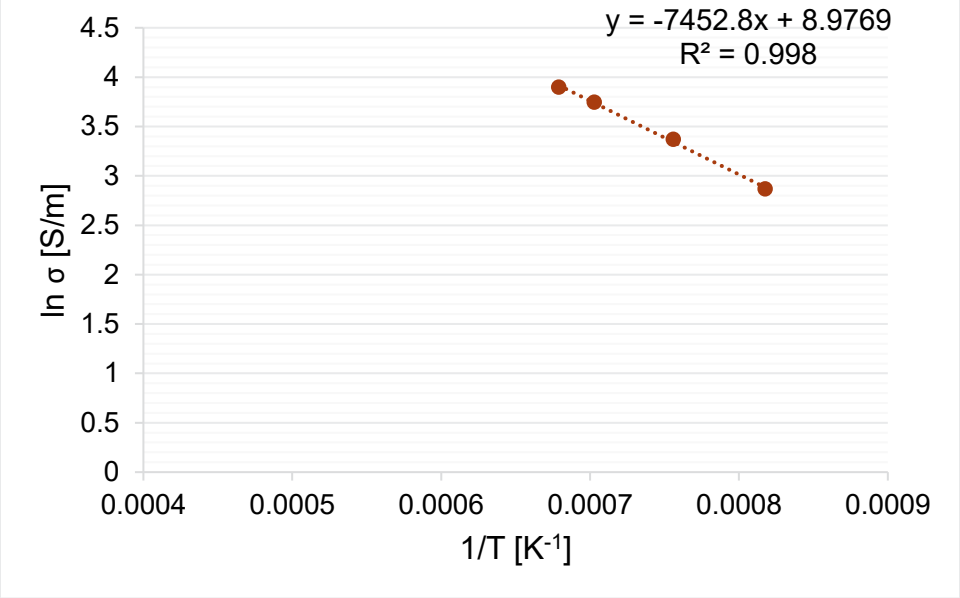

Figure J.24. Electrical conductivity-temperature data and Arrhenius equation fit for glass HS24-24.

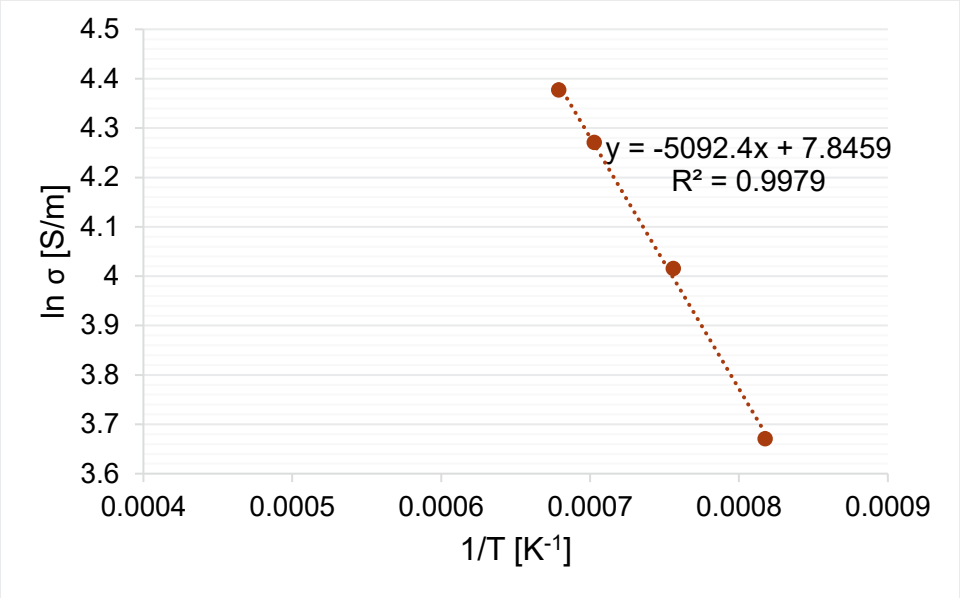

Figure J.25. Electrical conductivity-temperature data and Arrhenius equation fit for glass HS24-25.

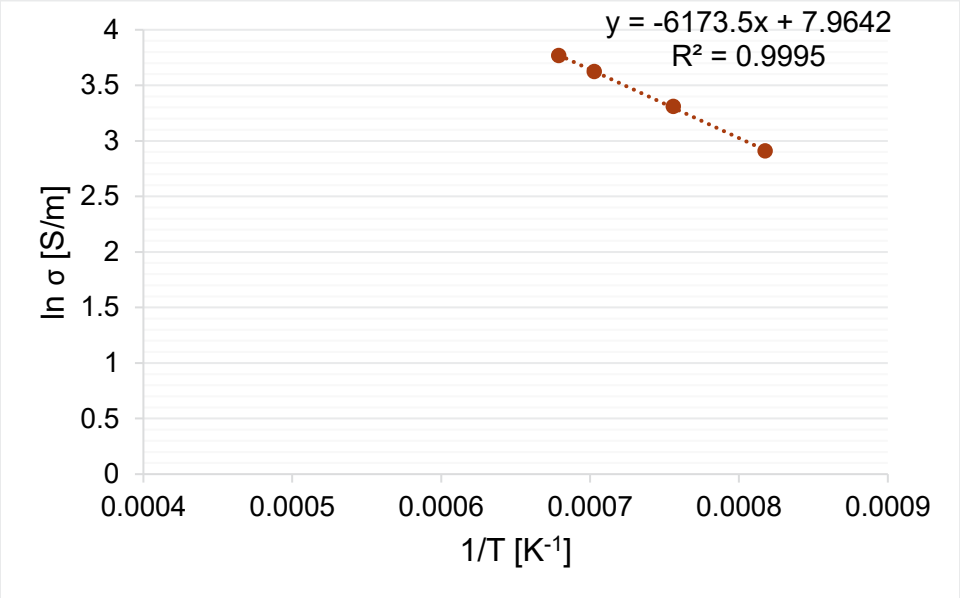

Figure J.26. Electrical conductivity-temperature data and Arrhenius equation fit for glass HS24-26.

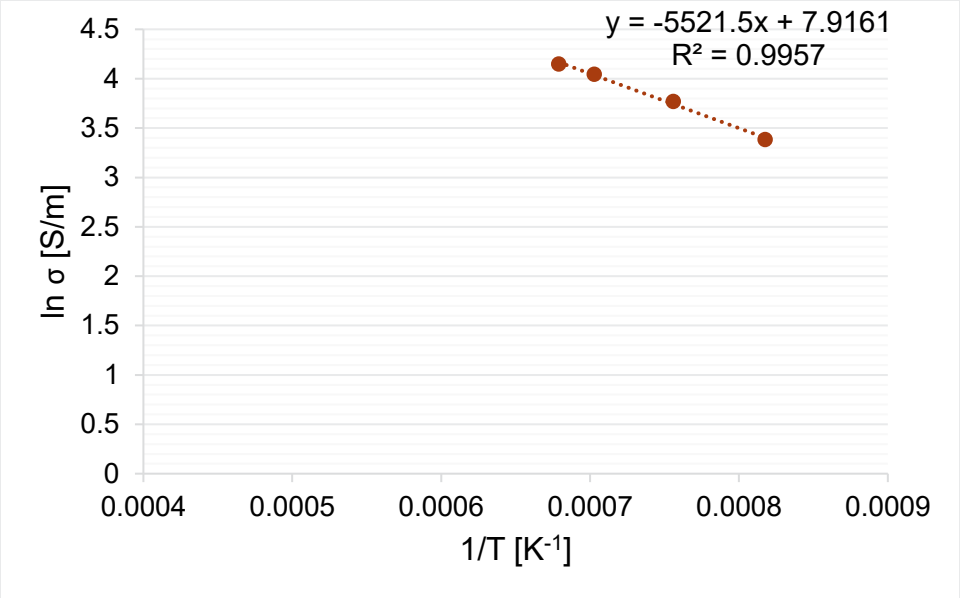

Figure J.27. Electrical conductivity-temperature data and Arrhenius equation fit for glass HS24-27.

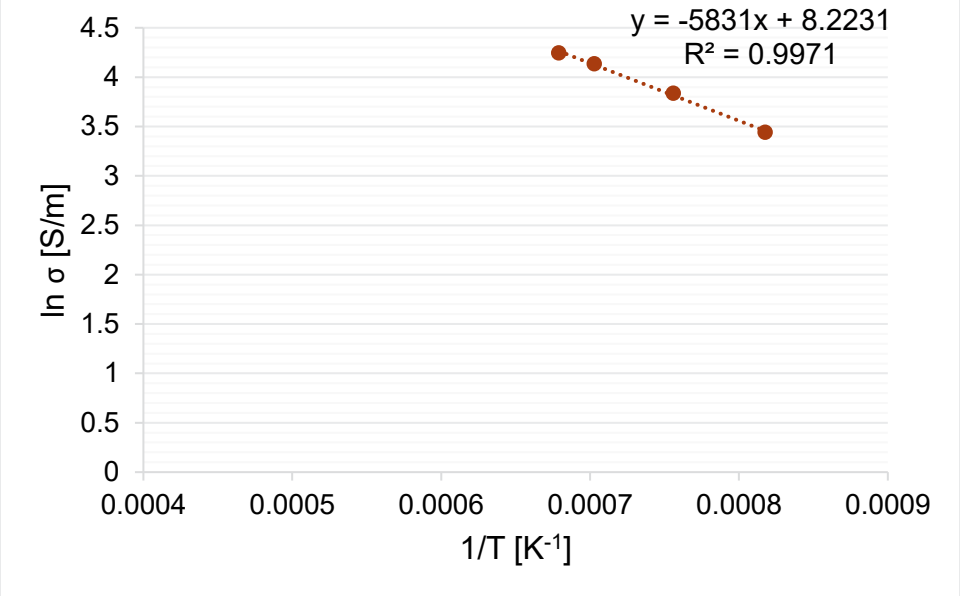

Figure J.28. Electrical conductivity-temperature data and Arrhenius equation fit for glass HS24-28.

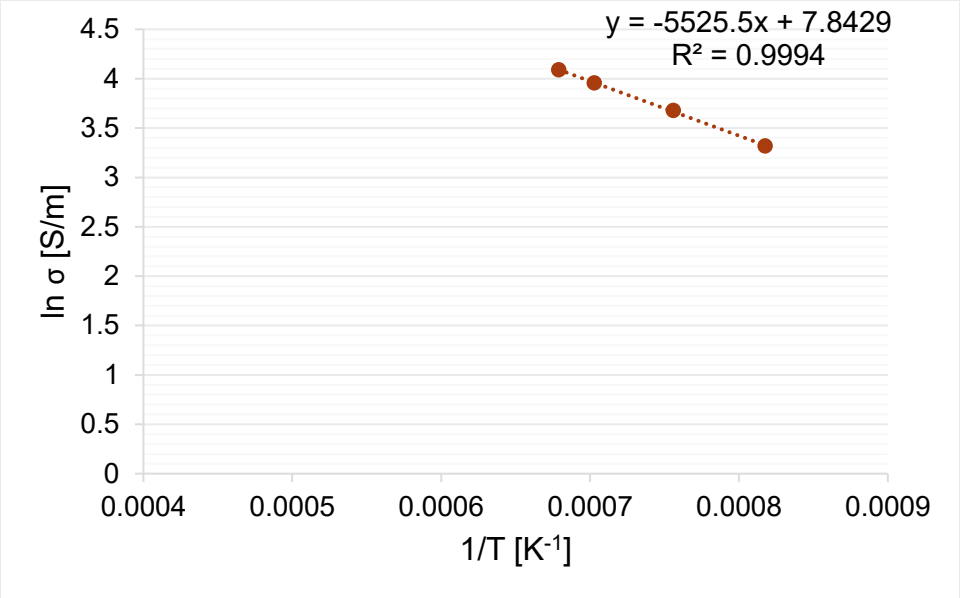

Figure J.29. Electrical conductivity-temperature data and Arrhenius equation fit for glass HS24-29.

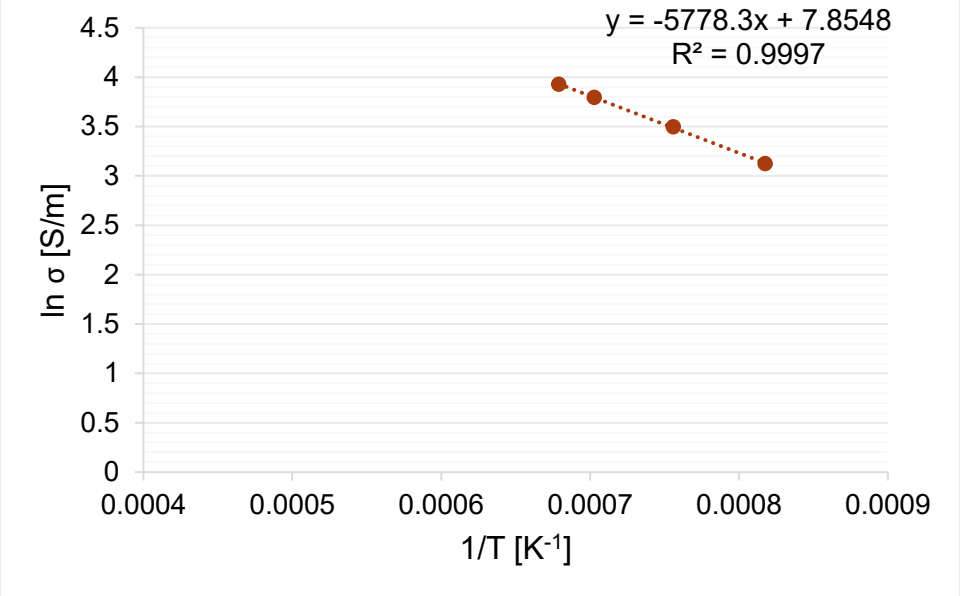

Figure J.30. Electrical conductivity-temperature data and Arrhenius equation fit for glass HS24-30.

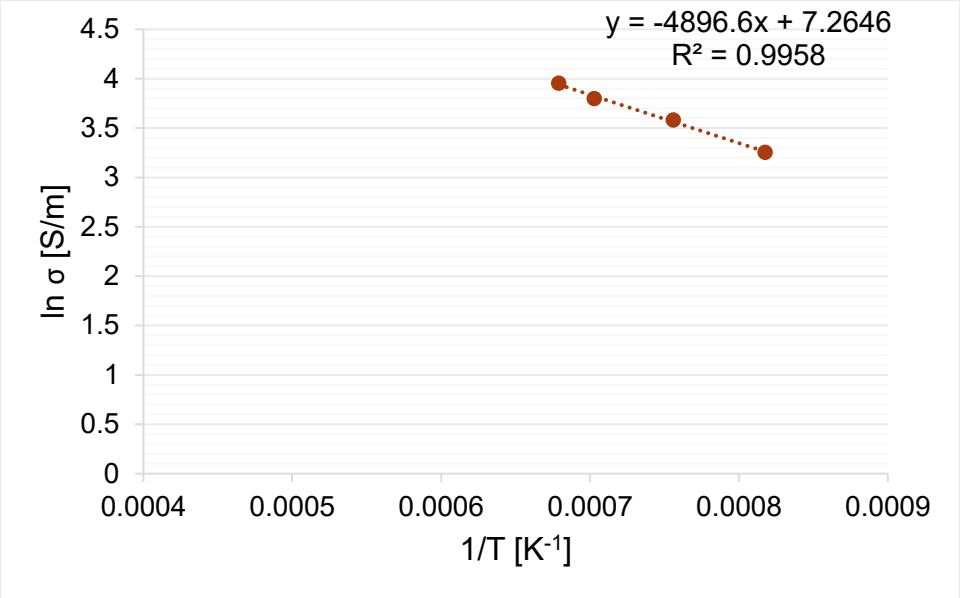

Figure J.31. Electrical conductivity-temperature data and Arrhenius equation fit for glass HS24-31.

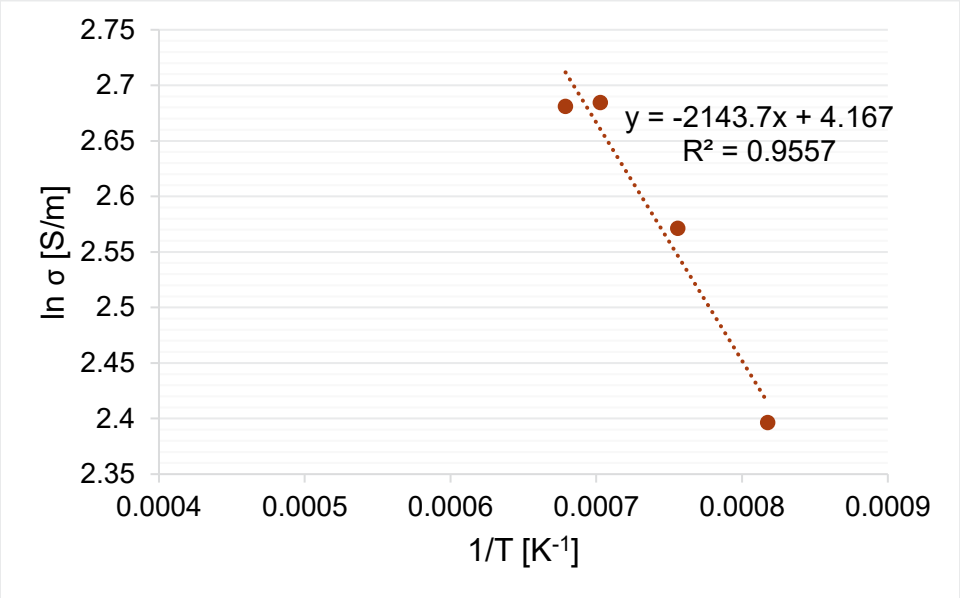

Figure J.32. Electrical conductivity-temperature data and Arrhenius equation fit for glass HS24-32.

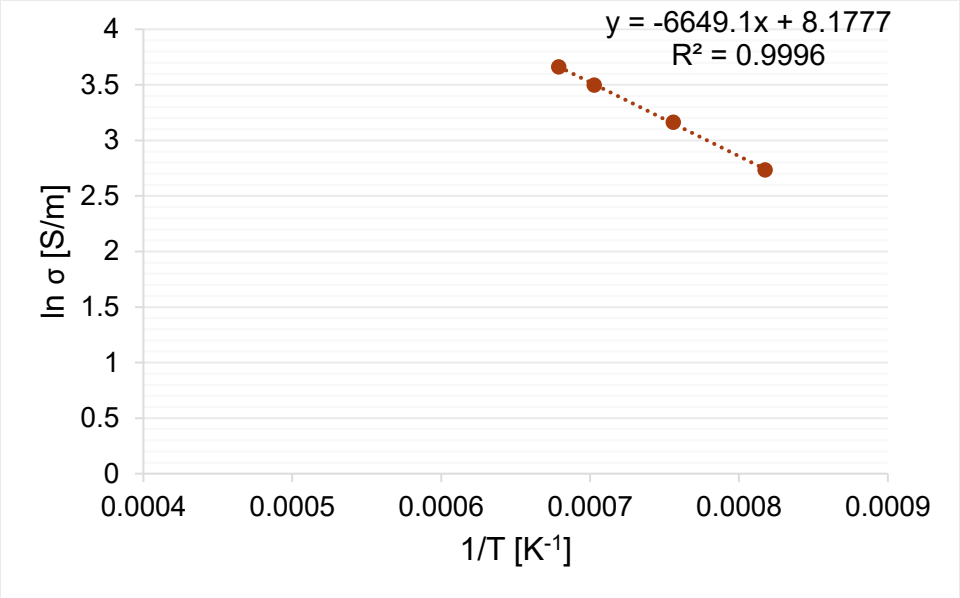

Figure J.33. Electrical conductivity-temperature data and Arrhenius equation fit for glass HS24-33.

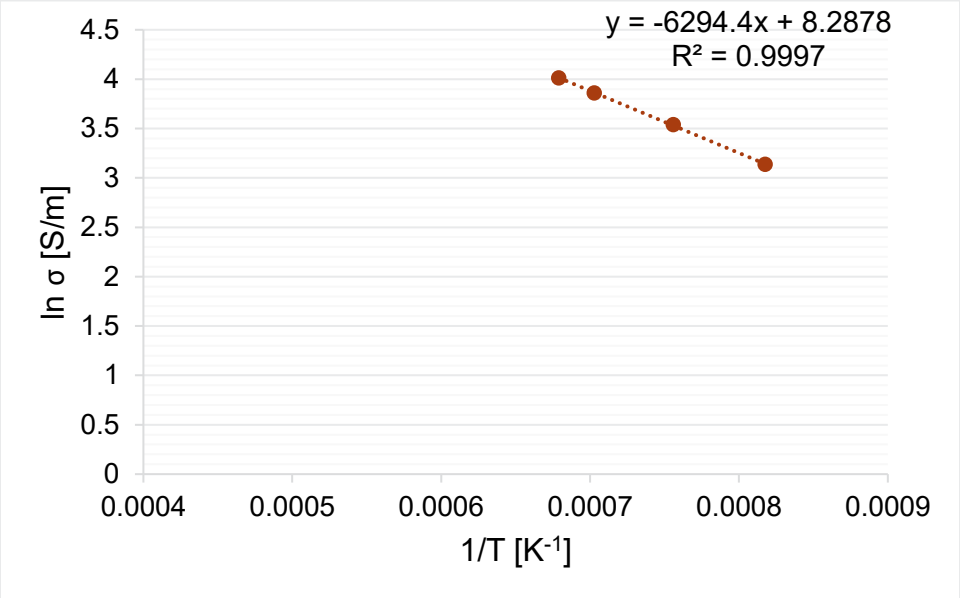

Figure J.34. Electrical conductivity-temperature data and Arrhenius equation fit for glass HS24-34.

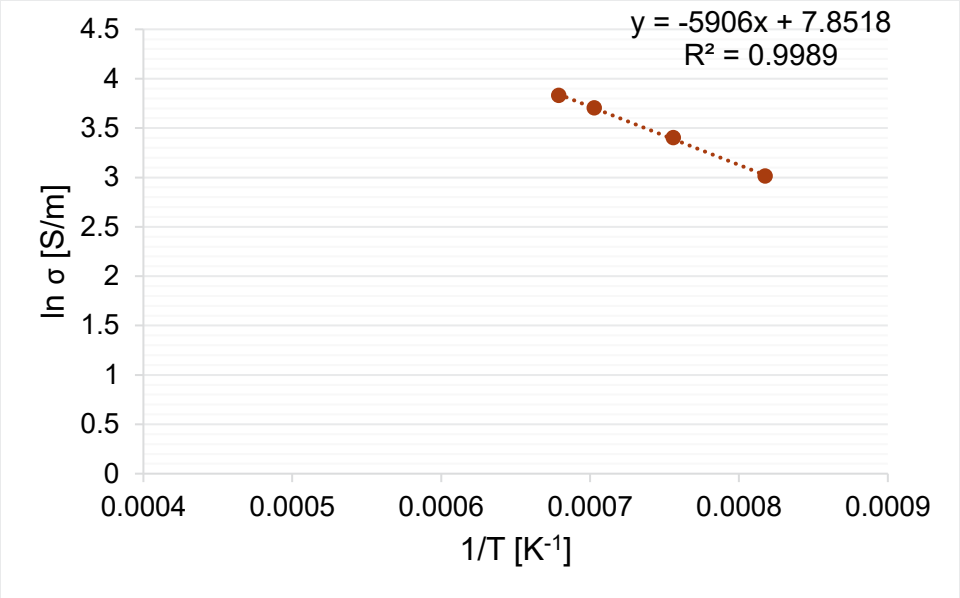

Figure J.35. Electrical conductivity-temperature data and Arrhenius equation fit for glass HS24-35.

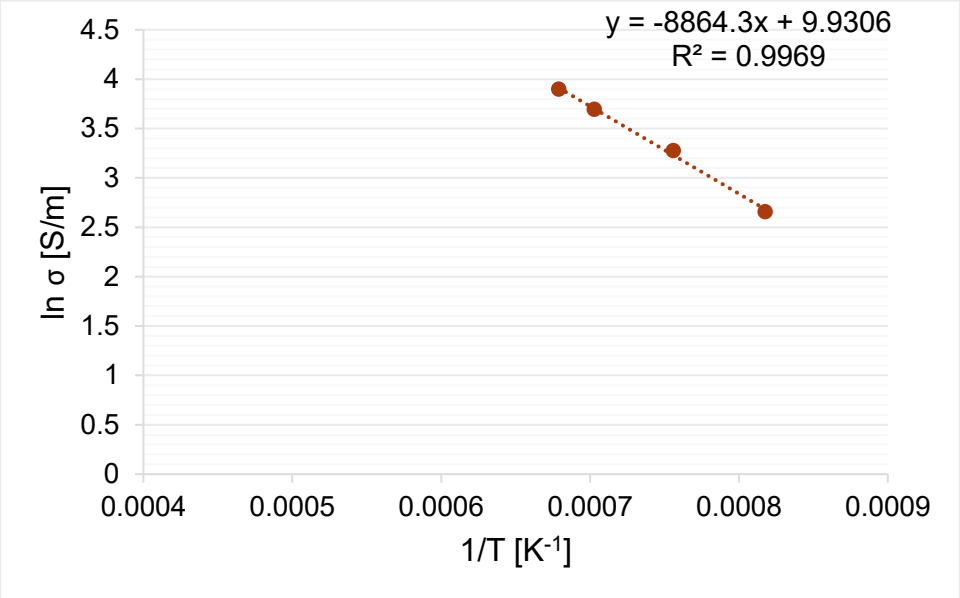

Figure J.36. Electrical conductivity-temperature data and Arrhenius equation fit for glass HS24-36.

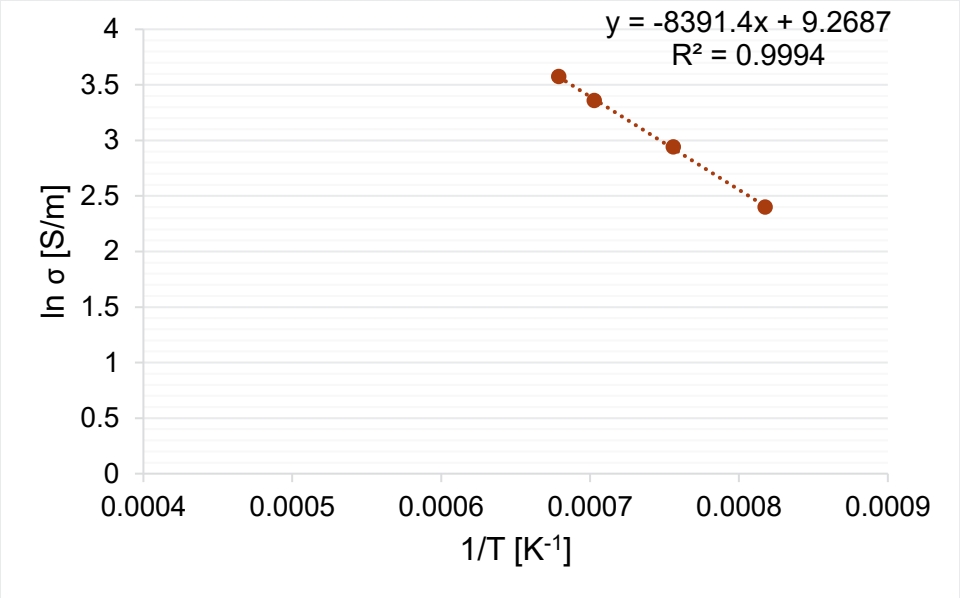

Figure J.37. Electrical conductivity-temperature data and Arrhenius equation fit for glass HS24-37.

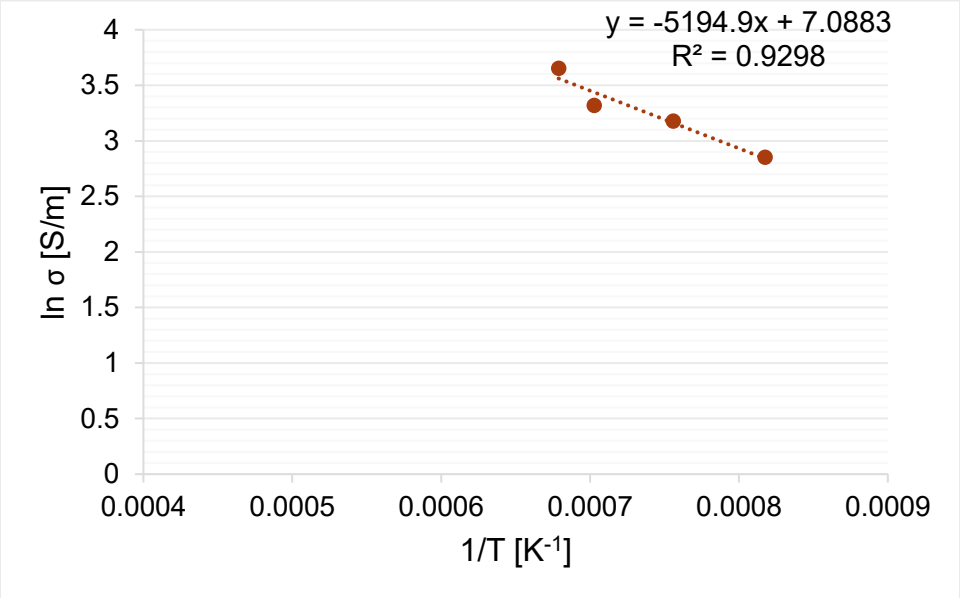

Figure J.38. Electrical conductivity-temperature data and Arrhenius equation fit for glass HS24-38.

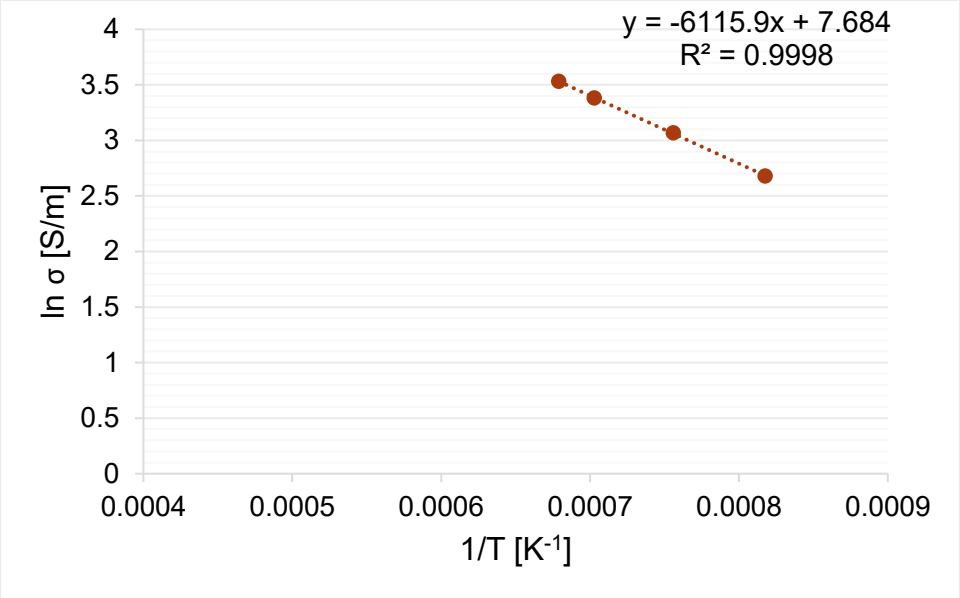

Figure J.39. Electrical conductivity-temperature data and Arrhenius equation fit for glass HS24-39.

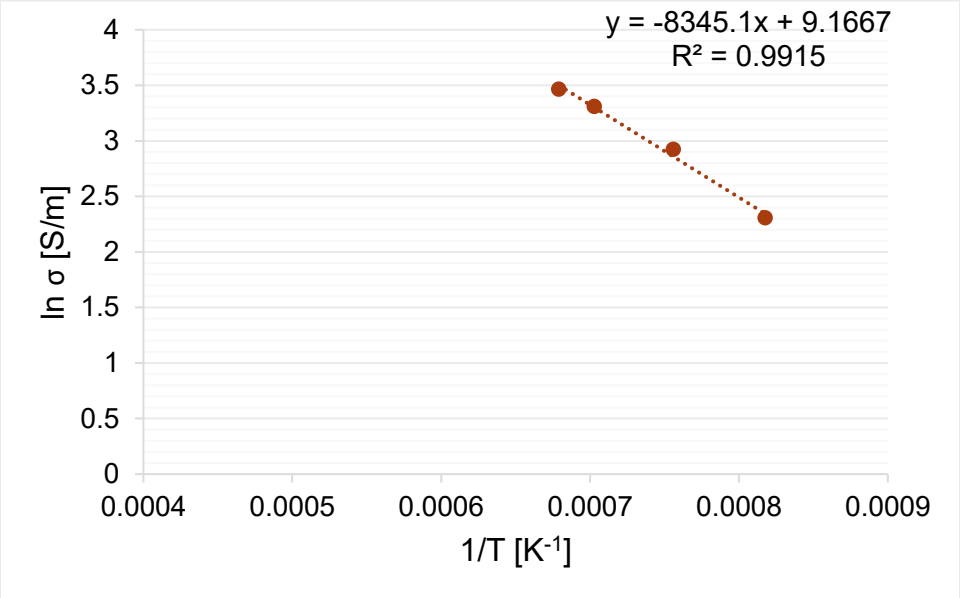

Figure J.40. Electrical conductivity-temperature data and Arrhenius equation fit for glass HS24-40.

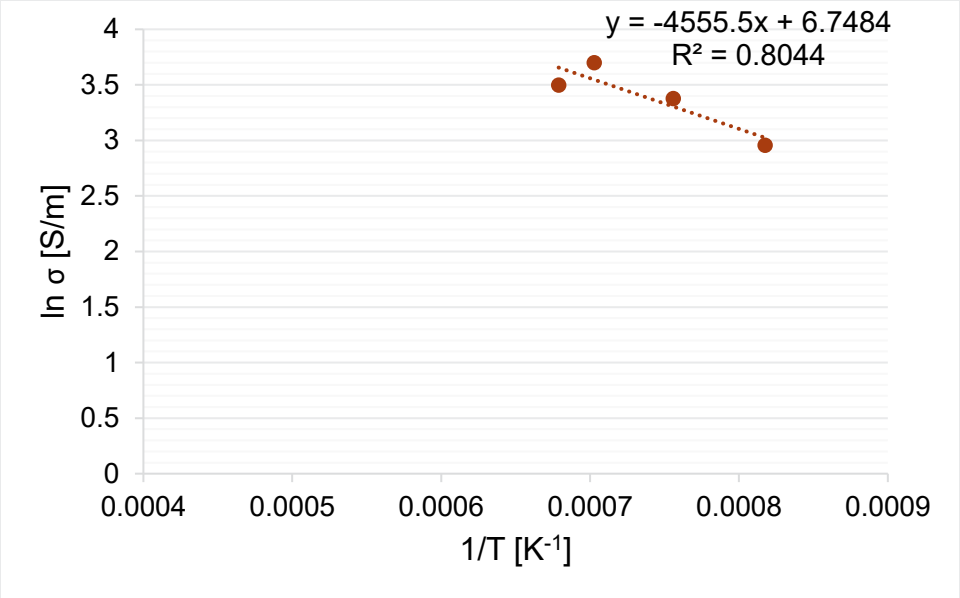

Figure J.41. Electrical conductivity-temperature data and Arrhenius equation fit for glass HS24-41.

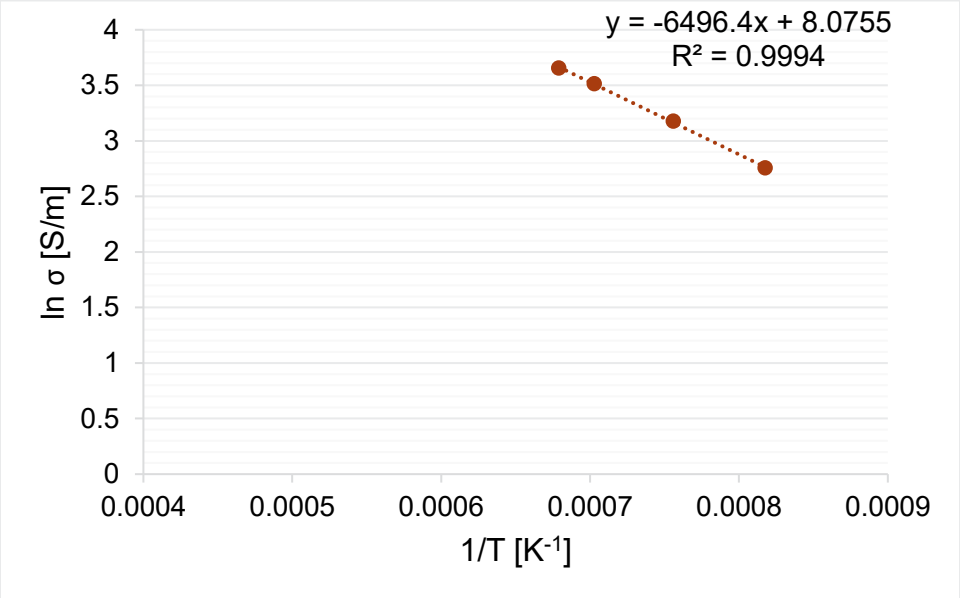

Figure J.42. Electrical conductivity-temperature data and Arrhenius equation fit for glass HS24-42.

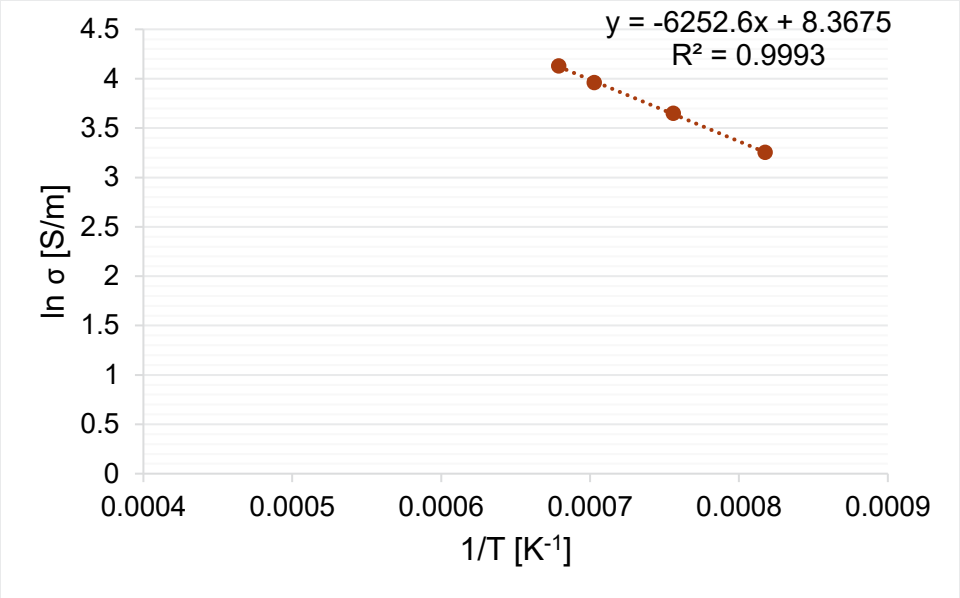

Figure J.43. Electrical conductivity-temperature data and Arrhenius equation fit for glass HS24-43.

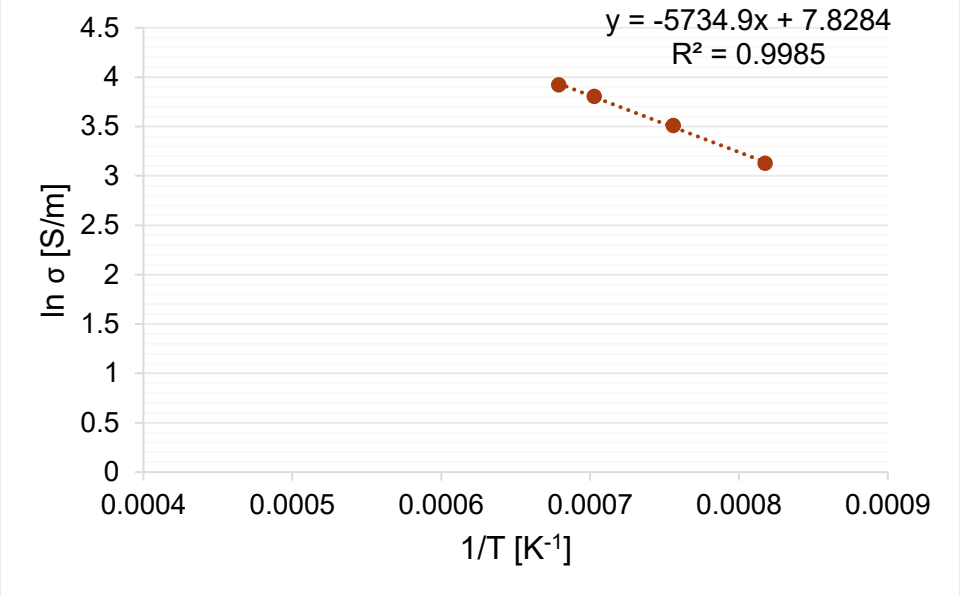

Figure J.44. Electrical conductivity-temperature data and Arrhenius equation fit for glass HS24-44.

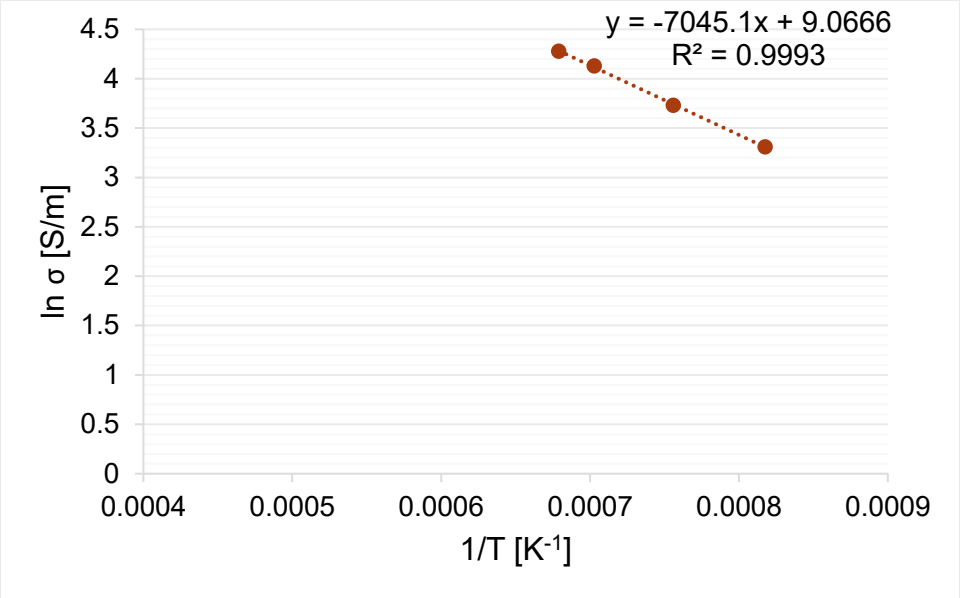

Figure J.45. Electrical conductivity-temperature data and Arrhenius equation fit for glass HS24-45.

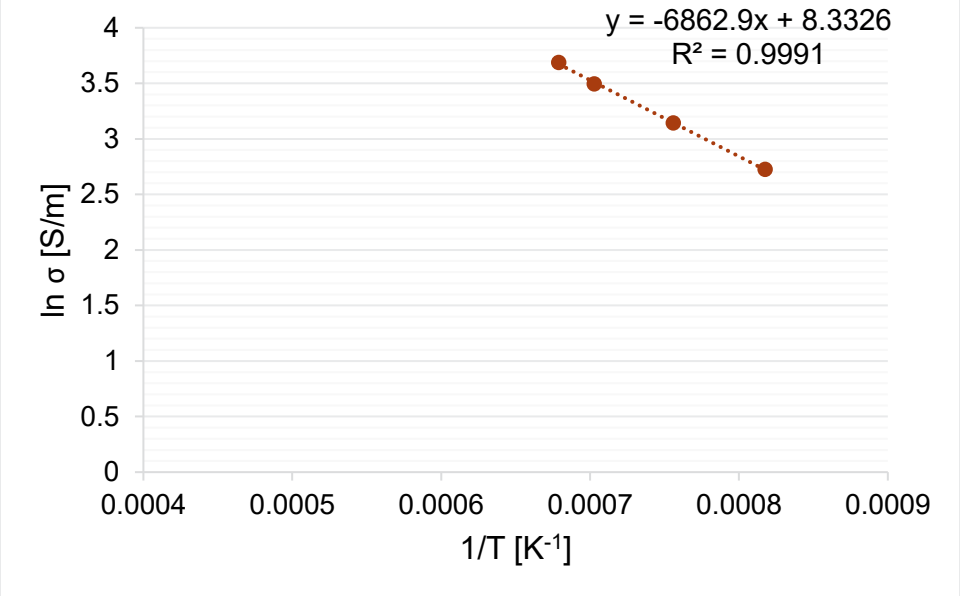

Figure J.46. Electrical conductivity-temperature data and Arrhenius equation fit for glass HS24-46.

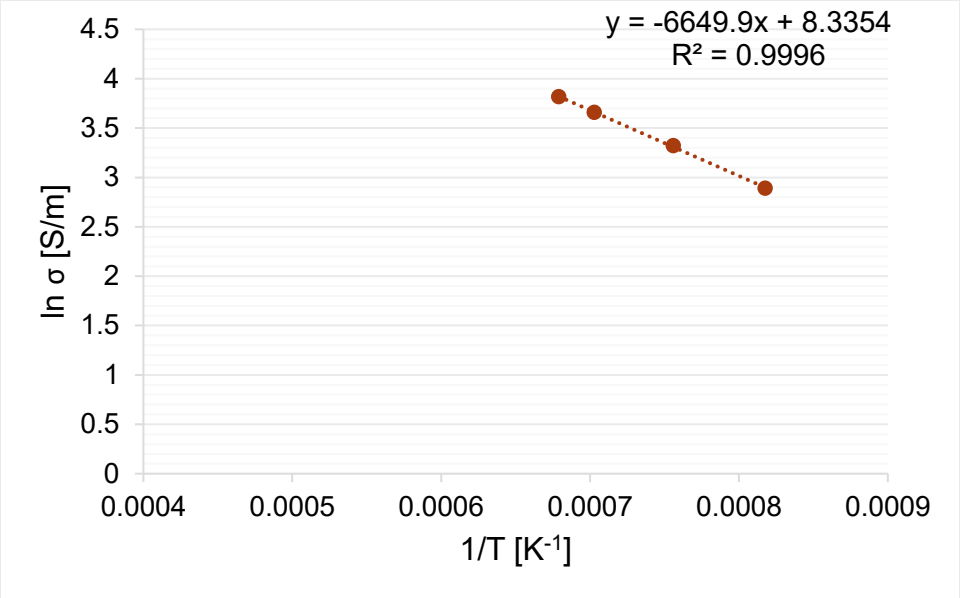

Figure J.47. Electrical conductivity-temperature data and Arrhenius equation fit for glass HS24-47.

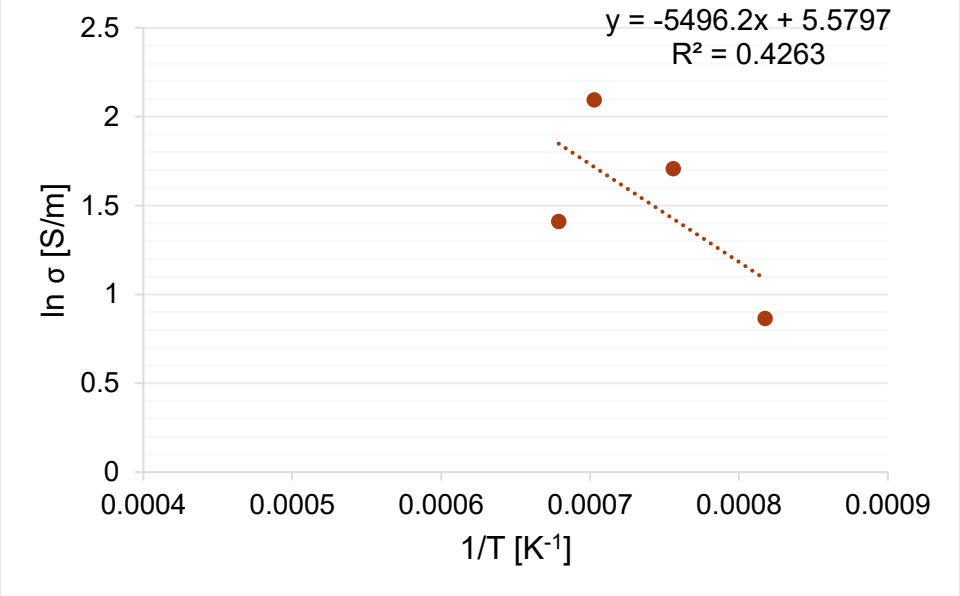

Figure J.48. Electrical conductivity-temperature data and Arrhenius equation fit for glass HS24-48.

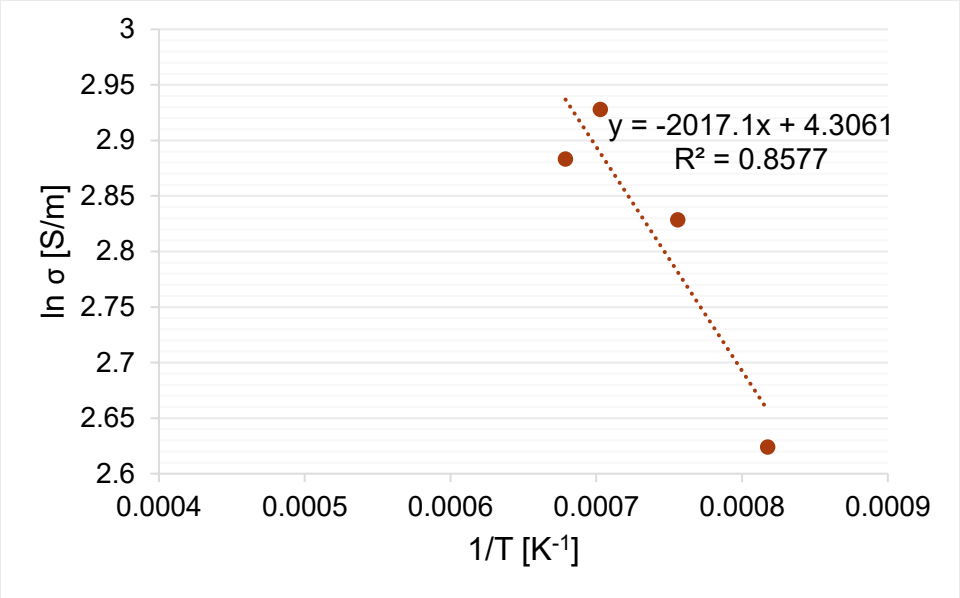

Figure J.49. Electrical conductivity-temperature data and Arrhenius equation fit for glass HS24-49.

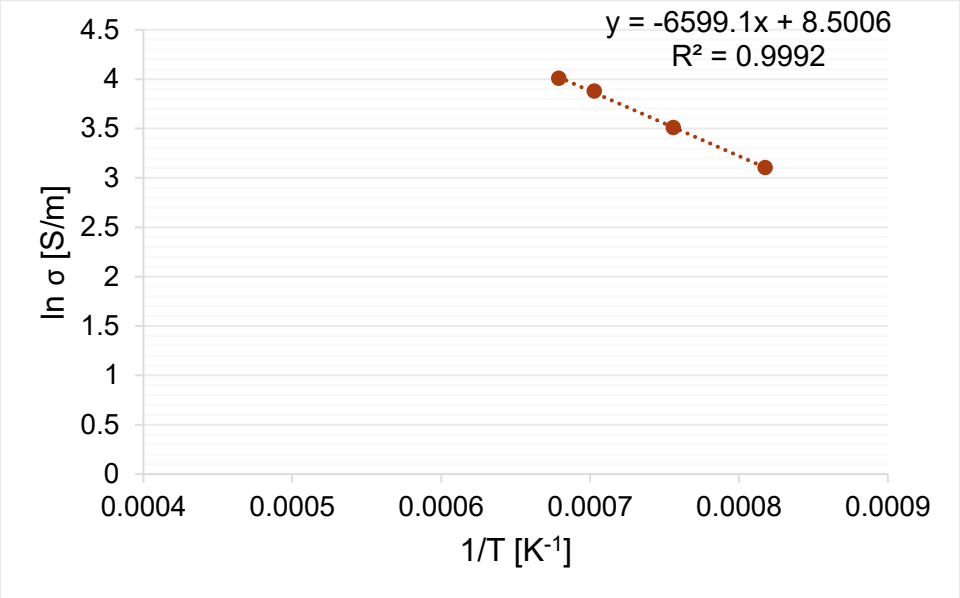

Figure J.50. Electrical conductivity-temperature data and Arrhenius equation fit for glass HS24-50.

Appendix K – PCT results

The list of triplicate product consistency test (PCT) results for all quenched (Q) and canister centerline cooled (CCC) glasses reported in the present study are presented in this Appendix.

Table K.1. PCT normalized concentrations (g/L) of B, Si, and Na for Q and CCC HS24 glasses.

	Normalized Concentration (NC_i) in g/L			
	Boron	Silicon	Sodium	Lithium
HS24_01_Q_PCT_A	14.98	0.44	8.99	12.61
HS24_01_Q_PCT_B	14.30	0.44	9.02	12.67
HS24_01_Q_PCT_C	14.14	0.44	9.00	12.56
HS24_01_CCC_PCT_A	4.72	0.28	6.04	0.43
HS24_01_CCC_PCT_B	4.80	0.29	6.12	0.44
HS24_01_CCC_PCT_C	4.72	0.29	6.06	0.43
HS24_02_Q_PCT_A	6.01	0.28	4.99	6.20
HS24_02_Q_PCT_B	5.88	0.28	4.92	5.96
HS24_02_Q_PCT_C	5.84	0.28	4.87	5.86
HS24_02_CCC_PCT_A	13.32	0.52	5.58	122.43
HS24_02_CCC_PCT_B	12.92	0.51	5.43	119.68
HS24_02_CCC_PCT_C	12.56	0.51	5.30	115.33
HS24_03_Q_PCT_A	0.56	0.17	0.59	0.66
HS24_03_Q_PCT_B	0.62	0.18	0.64	0.69
HS24_03_Q_PCT_C	0.60	0.18	0.63	0.67
HS24_03_CCC_PCT_A	0.62	0.20	0.64	0.68
HS24_03_CCC_PCT_B	0.56	0.20	0.61	0.62
HS24_03_CCC_PCT_C	0.55	0.20	0.60	0.62
HS24_04_Q_PCT_A	1.38	0.43	1.44	0.62
HS24_04_Q_PCT_B	1.38	0.43	1.41	0.63
HS24_04_Q_PCT_C	1.42	0.44	1.45	0.65
HS24_04_CCC_PCT_A	0.52	0.34	0.97	0.64
HS24_04_CCC_PCT_B	0.57	0.36	1.05	0.70
HS24_04_CCC_PCT_C	0.55	0.36	1.02	0.68
HS24_05_Q_PCT_A	2.12	0.54	2.08	1.53
HS24_05_Q_PCT_B	2.08	0.51	2.07	1.51
HS24_05_Q_PCT_C	2.09	0.55	2.05	1.49
HS24_05_CCC_PCT_A	1.98	0.54	2.01	1.60
HS24_05_CCC_PCT_B	2.00	0.55	2.02	1.63
HS24_05_CCC_PCT_C	2.00	0.56	2.01	1.63
HS24_06_Q_PCT_A	2.38	0.51	2.12	1.28
HS24_06_Q_PCT_B	2.31	0.50	2.06	1.25
HS24_06_Q_PCT_C	2.32	0.50	2.07	1.25
HS24_06_CCC_PCT_A	2.51	0.54	2.32	2.78
HS24_06_CCC_PCT_B	2.50	0.55	2.29	2.80
HS24_06_CCC_PCT_C	2.51	0.55	2.33	2.82
HS24_07_Q_PCT_A	0.66	0.27	0.87	0.45
HS24_07_Q_PCT_B	0.66	0.27	0.87	0.44
HS24_07_Q_PCT_C	0.64	0.27	0.86	0.45

	Normalized Concentration (NC_i) in g/L			
	Boron	Silicon	Sodium	Lithium
HS24_07_CCC_PCT_A	1.33	0.25	2.39	1.20
HS24_07_CCC_PCT_B	1.32	0.26	2.38	1.21
HS24_07_CCC_PCT_C	1.34	0.26	2.41	1.24
HS24_08_Q_PCT_A	0.38	0.24	0.45	0.60
HS24_08_Q_PCT_B	0.38	0.24	0.46	0.60
HS24_08_Q_PCT_C	0.38	0.24	0.45	0.60
HS24_08_CCC_PCT_A	0.40	0.26	0.49	0.81
HS24_08_CCC_PCT_B	0.42	0.27	0.51	0.86
HS24_08_CCC_PCT_C	0.42	0.27	0.50	0.86
HS24_09_Q_PCT_A	0.53	0.24	0.86	0.30
HS24_09_Q_PCT_B	0.53	0.24	0.85	0.30
HS24_09_Q_PCT_C	0.53	0.24	0.85	0.30
HS24_09_CCC_PCT_A	0.53	0.23	0.81	0.38
HS24_09_CCC_PCT_B	0.51	0.23	0.79	0.36
HS24_09_CCC_PCT_C	0.51	0.23	0.79	0.36
HS24_10_Q_PCT_A	0.63	0.18	0.73	0.69
HS24_10_Q_PCT_B	0.60	0.18	0.70	0.66
HS24_10_Q_PCT_C	0.61	0.18	0.70	0.67
HS24_10_CCC_PCT_A	0.96	0.20	0.90	1.03
HS24_10_CCC_PCT_B	0.98	0.21	0.91	1.05
HS24_10_CCC_PCT_C	1.00	0.21	0.93	1.07
HS24_11_Q_PCT_A	14.64	0.17	6.57	10.67
HS24_11_Q_PCT_B	14.34	0.17	6.52	10.64
HS24_11_Q_PCT_C	14.38	0.17	6.50	10.73
HS24_11_CCC_PCT_A	15.74	0.17	6.93	11.21
HS24_11_CCC_PCT_B	15.99	0.17	6.89	11.39
HS24_11_CCC_PCT_C	14.34	0.15	6.17	10.05
HS24_12_Q_PCT_A	1.41	0.42	1.28	1.06
HS24_12_Q_PCT_B	1.36	0.42	1.27	1.06
HS24_12_Q_PCT_C	1.33	0.42	1.26	1.06
HS24_12_CCC_PCT_A	1.12	0.35	1.87	1.06
HS24_12_CCC_PCT_B	1.13	0.37	1.89	1.06
HS24_12_CCC_PCT_C	1.10	0.37	1.85	1.06
HS24_13_Q_PCT_A	3.35	1.26	3.41	1.66
HS24_13_Q_PCT_B	3.32	1.28	3.42	1.66
HS24_13_Q_PCT_C	3.31	1.26	3.38	1.64
HS24_13_CCC_PCT_A	2.27	1.03	2.70	1.32
HS24_13_CCC_PCT_B	2.28	1.11	2.70	1.30
HS24_13_CCC_PCT_C	2.29	1.07	2.70	1.34
HS24_14_Q_PCT_A	1.06	0.31	1.29	1.16
HS24_14_Q_PCT_B	0.99	0.30	1.22	1.10
HS24_14_Q_PCT_C	0.98	0.30	1.20	1.07
HS24_14_CCC_PCT_A	0.98	0.33	1.19	1.19
HS24_14_CCC_PCT_B	0.93	0.30	1.14	1.13
HS24_14_CCC_PCT_C	0.91	0.29	1.12	1.14
HS24_15_Q_PCT_A	6.68	1.19	6.58	5.43

	Normalized Concentration (NC_i) in g/L			
	Boron	Silicon	Sodium	Lithium
HS24_15_Q_PCT_B	6.68	1.24	6.57	5.54
HS24_15_Q_PCT_C	6.70	1.25	6.59	5.40
HS24_15_CCC_PCT_A	6.01	1.16	5.94	6.06
HS24_15_CCC_PCT_B	6.46	1.30	6.30	6.32
HS24_15_CCC_PCT_C	7.42	1.42	7.33	7.41
HS24_16_Q_PCT_A	0.57	0.23	0.74	0.47
HS24_16_Q_PCT_B	0.60	0.24	0.77	0.51
HS24_16_Q_PCT_C	0.60	0.24	0.77	0.50
HS24_16_CCC_PCT_A	1.01	0.24	1.13	0.76
HS24_16_CCC_PCT_B	1.01	0.24	1.15	0.77
HS24_16_CCC_PCT_C	0.99	0.24	1.12	0.74
HS24_17_Q_PCT_A	2.16	0.52	2.09	1.43
HS24_17_Q_PCT_B	2.18	0.52	2.10	1.44
HS24_17_Q_PCT_C	2.46	0.57	2.42	1.41
HS24_17_CCC_PCT_A	2.56	0.57	2.41	2.00
HS24_17_CCC_PCT_B	2.57	0.58	2.40	2.04
HS24_17_CCC_PCT_C	2.57	0.57	2.39	2.00
HS24_18_Q_PCT_A	2.99	0.37	2.73	3.32
HS24_18_Q_PCT_B	2.95	0.37	2.68	3.25
HS24_18_Q_PCT_C	3.04	0.37	2.74	3.34
HS24_18_CCC_PCT_A	3.20	0.43	2.87	3.54
HS24_18_CCC_PCT_B	2.58	0.38	2.34	2.88
HS24_18_CCC_PCT_C	2.58	0.38	2.32	2.86
HS24_19_Q_PCT_A	1.19	0.48	1.70	1.27
HS24_19_Q_PCT_B	1.16	0.48	1.67	1.24
HS24_19_Q_PCT_C	0.98	0.43	1.47	1.07
HS24_19_CCC_PCT_A	1.22	0.44	1.59	1.33
HS24_19_CCC_PCT_B	1.19	0.44	1.57	1.29
HS24_19_CCC_PCT_C	0.97	0.39	1.36	1.10
HS24_20_Q_PCT_A	0.42	0.28	0.83	0.69
HS24_20_Q_PCT_B	0.42	0.28	0.82	0.70
HS24_20_Q_PCT_C	0.40	0.27	0.80	0.68
HS24_20_CCC_PCT_A	0.39	0.25	0.74	0.68
HS24_20_CCC_PCT_B	0.42	0.27	0.78	0.73
HS24_20_CCC_PCT_C	0.42	0.27	0.79	0.73
HS24_21_Q_PCT_A	0.58	0.31	0.65	0.73
HS24_21_Q_PCT_B	0.58	0.31	0.64	0.72
HS24_21_Q_PCT_C	0.56	0.30	0.63	0.69
HS24_21_CCC_PCT_A	1.96	0.39	1.75	6.60
HS24_21_CCC_PCT_B	1.97	0.39	1.74	6.58
HS24_21_CCC_PCT_C	1.98	0.40	1.76	6.65
HS24_22_Q_PCT_A	0.59	0.35	0.56	0.15
HS24_22_Q_PCT_B	0.61	0.36	0.58	0.16
HS24_22_Q_PCT_C	0.59	0.36	0.57	0.15
HS24_22_CCC_PCT_A	0.46	0.32	0.55	1.09
HS24_22_CCC_PCT_B	0.51	0.36	0.60	1.20

	Normalized Concentration (NC_i) in g/L			
	Boron	Silicon	Sodium	Lithium
HS24_22_CCC_PCT_C	0.49	0.35	0.58	1.17
HS24_23_Q_PCT_A	0.62	0.32	0.91	0.64
HS24_23_Q_PCT_B	0.62	0.32	0.91	0.64
HS24_23_Q_PCT_C	0.62	0.32	0.92	0.65
HS24_23_CCC_PCT_A	0.86	0.37	0.98	0.82
HS24_23_CCC_PCT_B	0.82	0.37	0.96	0.80
HS24_23_CCC_PCT_C	0.81	0.36	0.95	0.79
HS24_24_Q_PCT_A	1.28	0.59	1.74	1.44
HS24_24_Q_PCT_B	1.37	0.62	1.82	1.52
HS24_24_Q_PCT_C	1.41	0.64	1.87	1.59
HS24_24_CCC_PCT_A	1.29	0.58	1.58	1.43
HS24_24_CCC_PCT_B	1.17	0.54	1.48	1.33
HS24_24_CCC_PCT_C	1.15	0.53	1.45	1.31
HS24_25_Q_PCT_A	0.44	0.36	0.93	0.43
HS24_25_Q_PCT_B	0.44	0.35	0.91	0.42
HS24_25_Q_PCT_C	0.43	0.35	0.91	0.43
HS24_25_CCC_PCT_A	0.87	0.47	1.59	4.45
HS24_25_CCC_PCT_B	0.86	0.47	1.59	4.45
HS24_25_CCC_PCT_C	0.86	0.47	1.58	4.46
HS24_26_Q_PCT_A	0.66	0.37	1.01	0.87
HS24_26_Q_PCT_B	0.92	0.45	1.50	0.87
HS24_26_Q_PCT_C	0.65	0.36	1.00	0.86
HS24_26_CCC_PCT_A	0.69	0.44	1.21	0.86
HS24_26_CCC_PCT_B	0.68	0.44	1.19	0.86
HS24_26_CCC_PCT_C	0.68	0.44	1.18	0.86
HS24_27_Q_PCT_A	0.42	0.26	0.61	0.38
HS24_27_Q_PCT_B	0.42	0.26	0.61	0.37
HS24_27_Q_PCT_C	0.42	0.26	0.61	0.37
HS24_27_CCC_PCT_A	0.47	0.28	1.19	2.76
HS24_27_CCC_PCT_B	0.47	0.27	1.19	2.77
HS24_27_CCC_PCT_C	0.47	0.28	1.19	2.80
HS24_28_Q_PCT_A	0.47	0.34	0.97	0.46
HS24_28_Q_PCT_B	0.46	0.34	0.95	0.46
HS24_28_Q_PCT_C	0.46	0.34	0.96	0.46
HS24_28_CCC_PCT_A	0.52	0.39	1.03	1.51
HS24_28_CCC_PCT_B	0.51	0.39	1.03	1.51
HS24_28_CCC_PCT_C	0.52	0.40	1.04	1.53
HS24_29_Q_PCT_A	0.74	0.26	0.88	0.40
HS24_29_Q_PCT_B	0.76	0.26	0.89	0.41
HS24_29_Q_PCT_C	0.76	0.26	0.88	0.41
HS24_29_CCC_PCT_A	0.55	0.27	0.76	0.49
HS24_29_CCC_PCT_B	0.55	0.27	0.76	0.49
HS24_29_CCC_PCT_C	0.56	0.27	0.76	0.49
HS24_30_Q_PCT_A	0.37	0.22	0.76	0.36
HS24_30_Q_PCT_B	0.38	0.23	0.75	0.35
HS24_30_Q_PCT_C	0.38	0.23	0.76	0.36

	Normalized Concentration (NC_i) in g/L			
	Boron	Silicon	Sodium	Lithium
HS24_30_CCC_PCT_A	0.45	0.30	1.09	2.14
HS24_30_CCC_PCT_B	0.44	0.29	1.09	2.14
HS24_30_CCC_PCT_C	0.44	0.30	1.09	2.13
HS24_31_Q_PCT_A	0.94	0.48	1.45	0.76
HS24_31_Q_PCT_B	0.95	0.48	1.45	0.76
HS24_31_Q_PCT_C	0.95	0.49	1.46	0.77
HS24_31_CCC_PCT_A	2.40	0.45	1.14	1.42
HS24_31_CCC_PCT_B	2.40	0.45	1.14	1.41
HS24_31_CCC_PCT_C	2.29	0.43	1.08	1.33
HS24_32_Q_PCT_A	1.69	0.50	1.72	1.70
HS24_32_Q_PCT_B	1.67	0.50	1.71	1.68
HS24_32_Q_PCT_C	1.65	0.50	1.69	1.68
HS24_32_CCC_PCT_A	1.19	0.51	1.99	1.07
HS24_32_CCC_PCT_B	1.21	0.52	2.01	1.09
HS24_32_CCC_PCT_C	1.21	0.53	2.01	1.10
HS24_33_Q_PCT_A	0.40	0.27	0.70	0.52
HS24_33_Q_PCT_B	0.41	0.28	0.71	0.53
HS24_33_Q_PCT_C	0.40	0.27	0.69	0.52
HS24_33_CCC_PCT_A	0.70	0.37	0.84	0.70
HS24_33_CCC_PCT_B	0.57	0.34	0.76	0.63
HS24_33_CCC_PCT_C	0.58	0.34	0.78	0.63
HS24_34_Q_PCT_A	0.69	0.22	0.70	0.59
HS24_34_Q_PCT_B	0.68	0.22	0.70	0.60
HS24_34_Q_PCT_C	0.67	0.22	0.69	0.59
HS24_34_CCC_PCT_A	2.18	0.27	1.44	2.26
HS24_34_CCC_PCT_B	2.17	0.27	1.44	2.26
HS24_34_CCC_PCT_C	2.20	0.27	1.45	2.30
HS24_35_Q_PCT_A	9.55	0.27	4.85	7.74
HS24_35_Q_PCT_B	9.40	0.27	4.83	7.77
HS24_35_Q_PCT_C	9.28	0.27	4.75	7.61
HS24_35_CCC_PCT_A	7.33	0.28	3.99	6.29
HS24_35_CCC_PCT_B	7.38	0.28	3.99	6.35
HS24_35_CCC_PCT_C	7.27	0.28	3.94	6.26
HS24_36_Q_PCT_A	0.44	0.20	0.59	0.54
HS24_36_Q_PCT_B	0.43	0.20	0.58	0.53
HS24_36_Q_PCT_C	0.43	0.20	0.58	0.54
HS24_36_CCC_PCT_A	0.36	0.20	0.55	0.54
HS24_36_CCC_PCT_B	0.36	0.20	0.55	0.54
HS24_36_CCC_PCT_C	0.34	0.20	0.53	0.51
HS24_37_Q_PCT_A	0.32	0.17	0.52	0.48
HS24_37_Q_PCT_B	0.32	0.17	0.52	0.48
HS24_37_Q_PCT_C	0.32	0.17	0.51	0.48
HS24_37_CCC_PCT_A	0.31	0.17	0.49	0.47
HS24_37_CCC_PCT_B	0.29	0.17	0.46	0.44
HS24_37_CCC_PCT_C	0.29	0.16	0.46	0.44
HS24_38_Q_PCT_A	1.59	0.40	1.50	1.38

	Normalized Concentration (NC_i) in g/L			
	Boron	Silicon	Sodium	Lithium
HS24_38_Q_PCT_B	1.58	0.40	1.49	1.36
HS24_38_Q_PCT_C	1.55	0.40	1.48	1.35
HS24_38_CCC_PCT_A	2.17	0.46	1.90	2.09
HS24_38_CCC_PCT_B	2.19	0.46	1.92	2.12
HS24_38_CCC_PCT_C	2.20	0.46	1.94	2.13
HS24_39_Q_PCT_A	22.91	0.19	10.39	18.02
HS24_39_Q_PCT_B	20.43	0.19	10.20	17.80
HS24_39_Q_PCT_C	22.34	0.19	10.30	17.98
HS24_39_CCC_PCT_A	20.80	0.19	9.64	17.19
HS24_39_CCC_PCT_B	20.62	0.19	9.71	17.47
HS24_39_CCC_PCT_C	20.61	0.19	9.71	17.51
HS24_40_Q_PCT_A	1.09	0.18	1.07	1.26
HS24_40_Q_PCT_B	1.12	0.18	1.09	1.27
HS24_40_Q_PCT_C	1.06	0.18	1.04	1.23
HS24_40_CCC_PCT_A	0.93	0.18	0.90	1.05
HS24_40_CCC_PCT_B	0.94	0.18	0.94	1.10
HS24_40_CCC_PCT_C	0.88	0.18	0.88	1.03
HS24_41_Q_PCT_A	18.00	0.17	9.36	14.28
HS24_41_Q_PCT_B	17.84	0.17	9.20	14.09
HS24_41_Q_PCT_C	17.52	0.17	9.12	13.82
HS24_41_CCC_PCT_A	16.10	0.17	8.80	13.72
HS24_41_CCC_PCT_B	16.09	0.17	8.56	13.26
HS24_41_CCC_PCT_C	15.42	0.17	8.48	13.25
HS24_42_Q_PCT_A	18.84	0.14	8.11	13.52
HS24_42_Q_PCT_B	19.90	0.15	8.61	14.35
HS24_42_Q_PCT_C	19.74	0.15	8.56	14.30
HS24_42_CCC_PCT_A	20.92	0.16	8.67	15.76
HS24_42_CCC_PCT_B	20.61	0.16	8.62	15.64
HS24_42_CCC_PCT_C	20.47	0.16	8.76	15.89
HS24_43_Q_PCT_A	3.02	0.20	1.89	2.72
HS24_43_Q_PCT_B	2.93	0.20	1.89	2.71
HS24_43_Q_PCT_C	3.00	0.21	1.92	2.78
HS24_43_CCC_PCT_A	1.99	0.22	1.30	1.78
HS24_43_CCC_PCT_B	1.93	0.22	1.29	1.77
HS24_43_CCC_PCT_C	1.93	0.22	1.28	1.78
HS24_44_Q_PCT_A	0.67	0.33	1.00	0.56
HS24_44_Q_PCT_B	0.66	0.33	1.00	0.54
HS24_44_Q_PCT_C	0.62	0.34	0.99	0.54
HS24_44_CCC_PCT_A	0.60	0.31	0.88	0.69
HS24_44_CCC_PCT_B	0.60	0.31	0.88	0.69
HS24_44_CCC_PCT_C	0.58	0.31	0.87	0.68
HS24_45_Q_PCT_A	0.36	0.23	0.52	0.49
HS24_45_Q_PCT_B	0.36	0.23	0.52	0.49
HS24_45_Q_PCT_C	0.36	0.24	0.52	0.49
HS24_45_CCC_PCT_A	0.34	0.24	0.90	8.39
HS24_45_CCC_PCT_B	0.34	0.24	0.91	8.45

	Normalized Concentration (NC_i) in g/L			
	Boron	Silicon	Sodium	Lithium
HS24_45_CCC_PCT_C	0.33	0.24	0.90	8.59
HS24_46_Q_PCT_A	7.05	0.19	3.92	6.06
HS24_46_Q_PCT_B	6.93	0.20	3.83	5.90
HS24_46_Q_PCT_C	6.88	0.19	3.82	5.90
HS24_46_CCC_PCT_A	9.29	0.19	4.47	7.28
HS24_46_CCC_PCT_B	9.02	0.19	4.33	7.06
HS24_46_CCC_PCT_C	9.04	0.19	4.30	7.02
HS24_47_Q_PCT_A	0.49	0.26	0.58	0.63
HS24_47_Q_PCT_B	0.48	0.26	0.57	0.63
HS24_47_Q_PCT_C	0.48	0.26	0.58	0.64
HS24_47_CCC_PCT_A	0.49	0.27	0.59	1.40
HS24_47_CCC_PCT_B	0.47	0.26	0.57	1.38
HS24_47_CCC_PCT_C	0.46	0.27	0.57	1.36
HS24_48_Q_PCT_A	0.94	0.20	0.85	1.11
HS24_48_Q_PCT_B	0.91	0.21	0.84	1.11
HS24_48_Q_PCT_C	0.99	0.21	0.89	1.11
HS24_48_CCC_PCT_A	2.60	0.17	1.79	2.57
HS24_48_CCC_PCT_B	2.52	0.17	1.75	2.58
HS24_48_CCC_PCT_C	2.51	0.17	1.74	2.52
HS24_49_Q_PCT_A	1.39	0.47	2.04	0.00
HS24_49_Q_PCT_B	1.40	0.47	2.06	0.00
HS24_49_Q_PCT_C	1.41	0.47	2.07	0.00
HS24_49_CCC_PCT_A	1.01	0.40	1.57	0.00
HS24_49_CCC_PCT_B	0.99	0.40	1.57	0.00
HS24_49_CCC_PCT_C	1.01	0.40	1.57	0.00
HS24_50_Q_PCT_A	5.13	0.26	4.11	32.53
HS24_50_Q_PCT_B	5.09	0.26	4.10	32.51
HS24_50_Q_PCT_C	5.05	0.26	4.05	32.56
HS24_50_CCC_PCT_A	60.32	0.44	33.59	50.60
HS24_50_CCC_PCT_B	61.28	0.44	33.53	52.36
HS24_50_CCC_PCT_C	59.93	0.44	33.52	51.46

Appendix L – TCLP results

This appendix presents the extraction fluid used for each glass (Table L.1) and the complete list of results for both the quenched (Table L.2) and canister centerline cooling (Table L.3) toxicity characteristic leaching procedure (TCLP) analysis for the HS24 glasses in this study. Average measured TCLP concentrations with uncertainties are provided in Table L.4

Table L.1. Extraction fluid (EF) used for each Q and CCC glass

Sample ID	EF	Sample ID	EF	Sample ID	EF	Sample ID	EF	Sample ID	EF
HS24-01-Q	1	HS24-11-Q	1	HS24-21-Q	1	HS24-31-Q	1	HS24-41-Q	1
HS24-02-Q	1	HS24-12-Q	1	HS24-22-Q	1	HS24-32-Q	1	HS24-42-Q	1
HS24-03-Q	1	HS24-13-Q	1	HS24-23-Q	1	HS24-33-Q	1	HS24-43-Q	1
HS24-04-Q	1	HS24-14-Q	1	HS24-24-Q	1	HS24-34-Q	1	HS24-44-Q	1
HS24-05-Q	1	HS24-15-Q	2	HS24-25-Q	1	HS24-35-Q	1	HS24-45-Q	1
HS24-06-Q	1	HS24-16-Q	1	HS24-26-Q	1	HS24-36-Q	1	HS24-46-Q	1
HS24-07-Q	1	HS24-17-Q	1	HS24-27-Q	1	HS24-37-Q	1	HS24-47-Q	1
HS24-08-Q	1	HS24-18-Q	1	HS24-28-Q	1	HS24-38-Q	1	HS24-48-Q	1
HS24-09-Q	1	HS24-19-Q	1	HS24-29-Q	1	HS24-39-Q	1	HS24-49-Q	1
HS24-10-Q	1	HS24-20-Q	1	HS24-30-Q	1	HS24-40-Q	1	HS24-50-Q	1
Sample ID	EF	Sample ID	EF	Sample ID	EF	Sample ID	EF	Sample ID	EF
HS24-01-CCC	1	HS24-11-CCC	1	HS24-21-CCC	1	HS24-31-CCC	1	HS24-41-CCC	1
HS24-02-CCC	1	HS24-12-CCC	1	HS24-22-CCC	1	HS24-32-CCC	1	HS24-42-CCC	1
HS24-03-CCC	1	HS24-13-CCC	1	HS24-23-CCC	1	HS24-33-CCC	1	HS24-43-CCC	1
HS24-04-CCC	1	HS24-14-CCC	1	HS24-24-CCC	1	HS24-34-CCC	1	HS24-44-CCC	1
HS24-05-CCC	1	HS24-15-CCC	2	HS24-25-CCC	1	HS24-35-CCC	1	HS24-45-CCC	1
HS24-06-CCC	1	HS24-16-CCC	1	HS24-26-CCC	1	HS24-36-CCC	1	HS24-46-CCC	1
HS24-07-CCC	1	HS24-17-CCC	1	HS24-27-CCC	1	HS24-37-CCC	1	HS24-47-CCC	1
HS24-08-CCC	1	HS24-18-CCC	1	HS24-28-CCC	1	HS24-38-CCC	1	HS24-48-CCC	1
HS24-09-CCC	1	HS24-19-CCC	1	HS24-29-CCC	1	HS24-39-CCC	1	HS24-49-CCC	1
HS24-10-CCC	1	HS24-20-CCC	1	HS24-30-CCC	1	HS24-40-CCC	1	HS24-50-CCC	2

Table L.2. Measured TCLP concentrations for replicates A and B of the quenched (Q) glasses. Values in red are the detection limits.

	Replicate A						Replicate B					
Sample ID	B	Cr	Ni	Pb	V	Zn	B	Cr	Ni	Pb	V	Zn
HS24-01-Q-TCLP	4.35	*0.25*	*0.25*	*0.51*	1.14	2.67	4.52	*0.25*	*0.25*	*0.51*	1.16	2.67
HS24-02-Q-TCLP	13.39	*0.25*	*0.25*	*0.51*	5.03	1.99	13.59	*0.25*	*0.25*	*0.51*	4.95	1.89
HS24-03-Q-TCLP	*1.27*	*0.25*	*0.25*	*0.51*	0.48	0.78	*1.27*	*0.25*	*0.25*	*0.50*	0.48	*0.50*
HS24-04-Q-TCLP	*1.27*	*0.25*	*0.25*	*0.51*	0.38	*0.51*	*1.27*	*0.25*	*0.25*	*0.51*	0.37	*0.51*
HS24-05-Q-TCLP	*1.27*	*0.25*	*0.25*	*0.51*	0.41	*0.51*	*1.27*	*0.25*	*0.25*	*0.51*	0.41	*0.51*
HS24-06-Q-TCLP	*1.27*	*0.25*	*0.25*	*0.51*	0.45	*0.51*	*1.27*	*0.25*	*0.25*	*0.51*	0.47	*0.51*
HS24-07-Q-TCLP	*1.27*	*0.25*	*0.25*	*0.51*	*0.25*	0.92	*1.27*	*0.25*	*0.25*	*0.51*	*0.25*	0.92
HS24-08-Q-TCLP	*1.27*	*0.25*	*0.25*	*0.51*	*0.25*	*0.51*	*1.27*	*0.25*	*0.25*	*0.51*	*0.25*	*0.51*
HS24-09-Q-TCLP	*1.26*	*0.25*	*0.25*	*0.50*	*0.25*	*0.50*	*1.27*	*0.25*	*0.25*	*0.51*	*0.25*	*0.51*
HS24-10-Q-TCLP	1.71	*0.25*	*0.25*	*0.51*	*0.25*	*0.51*	1.68	*0.25*	*0.25*	*0.50*	*0.25*	*0.50*
HS24-11-Q-TCLP	1.90	*0.25*	*0.25*	*0.50*	*0.25*	0.59	1.96	*0.25*	*0.25*	*0.50*	*0.25*	0.59
HS24-12-Q-TCLP	*1.26*	*0.25*	*0.25*	*0.50*	0.89	0.59	*1.27*	*0.25*	*0.25*	*0.51*	0.88	0.59
HS24-13-Q-TCLP	*1.26*	*0.25*	*0.25*	*0.50*	0.31	0.88	*1.26*	*0.25*	*0.25*	*0.51*	0.31	0.89
HS24-14-Q-TCLP	*1.26*	*0.25*	*0.25*	*0.50*	0.41	0.82	*1.26*	*0.25*	*0.25*	*0.50*	0.45	0.92
HS24-15-Q-TCLP	113.60	4.15	6.15	*0.50*	7.33	3.90	117.66	4.16	6.32	*0.51*	7.11	4.03
HS24-16-Q-TCLP	*1.27*	*0.25*	*0.25*	*0.51*	1.06	*0.51*	*1.27*	*0.25*	*0.25*	*0.51*	1.04	*0.51*
HS24-17-Q-TCLP	*1.27*	*0.25*	*0.25*	*0.51*	*0.25*	0.78	*1.27*	*0.25*	*0.25*	*0.51*	*0.25*	0.84
HS24-18-Q-TCLP	1.55	*0.25*	*0.25*	*0.51*	0.32	*0.51*	2.05	*0.25*	*0.25*	*0.51*	0.34	*0.51*
HS24-19-Q-TCLP	*1.26*	*0.25*	*0.25*	*0.50*	*0.25*	*0.50*	*1.26*	*0.25*	*0.25*	*0.50*	*0.25*	*0.50*
HS24-20-Q-TCLP	*1.27*	*0.25*	*0.25*	*0.51*	*0.25*	0.68	*1.27*	*0.25*	*0.25*	*0.50*	*0.25*	0.64
HS24-21-Q-TCLP	*1.26*	*0.25*	*0.25*	*0.51*	0.46	0.63	*1.27*	*0.25*	*0.25*	*0.51*	0.46	0.60
HS24-22-Q-TCLP	*1.27*	*0.25*	*0.25*	*0.51*	*0.25*	*0.51*	*1.27*	*0.25*	*0.25*	*0.51*	*0.25*	*0.51*
HS24-23-Q-TCLP	*1.27*	*0.25*	*0.25*	*0.51*	*0.25*	*0.51*	*1.27*	*0.25*	*0.25*	*0.51*	*0.25*	*0.51*
HS24-24-Q-TCLP	*1.27*	*0.25*	*0.25*	*0.51*	*0.25*	*0.51*	*1.27*	*0.25*	*0.25*	*0.51*	*0.25*	*0.51*
HS24-25-Q-TCLP	*1.27*	*0.25*	*0.25*	*0.51*	*0.25*	*0.51*	*1.26*	*0.25*	*0.25*	*0.50*	*0.25*	*0.50*
HS24-26-Q-TCLP	*1.27*	*0.25*	*0.25*	*0.51*	0.32	*0.51*	*1.26*	*0.25*	*0.25*	*0.50*	0.31	*0.50*
HS24-27-Q-TCLP	*1.26*	*0.25*	*0.25*	*0.50*	*0.25*	*0.50*	*1.26*	*0.25*	*0.25*	*0.50*	*0.25*	*0.50*
HS24-28-Q-TCLP	2.85	*0.25*	*0.25*	*0.50*	*0.25*	*0.50*	*1.26*	*0.25*	*0.25*	*0.50*	*0.25*	*0.50*
HS24-29-Q-TCLP	*1.26*	*0.25*	*0.25*	*0.50*	0.25	0.55	*1.27*	*0.25*	*0.25*	*0.51*	0.26	0.59
HS24-30-Q-TCLP	*1.27*	*0.25*	*0.25*	*0.51*	*0.25*	*0.51*	*1.27*	*0.25*	*0.25*	*0.51*	*0.25*	*0.51*
HS24-31-Q-TCLP	*1.27*	*0.25*	*0.25*	*0.51*	*0.25*	0.57	*1.27*	*0.25*	*0.25*	*0.51*	*0.25*	0.55
HS24-32-Q-TCLP	*1.27*	*0.25*	*0.25*	*0.51*	*0.25*	*0.51*	*1.27*	*0.25*	*0.25*	*0.51*	*0.25*	*0.51*
HS24-33-Q-TCLP	*1.27*	*0.25*	*0.25*	*0.50*	0.43	*0.51*	*1.27*	*0.25*	*0.25*	*0.51*	0.41	*0.51*

	Replicate A						Replicate B					
Sample ID	B	Cr	Ni	Pb	V	Zn	B	Cr	Ni	Pb	V	Zn
HS24-34-Q-TCLP	2.39	*0.25*	*0.25*	*0.50*	*0.25*	0.68	2.38	*0.25*	*0.25*	*0.50*	*0.25*	0.70
HS24-35-Q-TCLP	*1.27*	*0.25*	*0.25*	*0.51*	0.68	*0.51*	*1.27*	*0.25*	*0.25*	*0.50*	0.68	*0.51*
HS24-36-Q-TCLP	*1.27*	*0.25*	*0.25*	*0.50*	0.33	*0.51*	*1.27*	*0.25*	*0.25*	*0.50*	0.32	*0.51*
HS24-37-Q-TCLP	*1.27*	*0.25*	*0.25*	*0.51*	*0.25*	*0.51*	*1.27*	*0.25*	*0.25*	*0.51*	*0.25*	*0.51*
HS24-38-Q-TCLP	1.30	*0.25*	*0.25*	*0.51*	0.59	0.63	1.31	*0.25*	*0.25*	*0.51*	0.59	0.60
HS24-39-Q-TCLP	3.29	*0.25*	*0.25*	*0.50*	1.73	0.72	3.46	*0.25*	*0.25*	*0.51*	1.81	0.82
HS24-40-Q-TCLP	2.73	*0.25*	*0.25*	*0.51*	*0.25*	*0.51*	2.62	*0.25*	*0.25*	*0.51*	*0.25*	*0.51*
HS24-41-Q-TCLP	5.33	*0.25*	*0.25*	*0.51*	0.36	1.68	5.67	*0.25*	*0.25*	*0.51*	0.37	1.78
HS24-42-Q-TCLP	4.15	*0.25*	*0.25*	*0.51*	1.20	*0.51*	3.99	*0.25*	*0.25*	*0.51*	1.19	*0.51*
HS24-43-Q-TCLP	1.49	*0.25*	*0.25*	*0.51*	*0.25*	*0.51*	1.58	*0.25*	*0.25*	*0.51*	*0.25*	*0.51*
HS24-44-Q-TCLP	*1.27*	*0.25*	*0.25*	*0.51*	0.34	*0.51*	*1.27*	*0.25*	*0.25*	*0.51*	0.34	*0.51*
HS24-45-Q-TCLP	*1.27*	*0.25*	*0.25*	*0.51*	0.39	*0.51*	*1.28*	*0.26*	*0.26*	*0.51*	0.37	*0.51*
HS24-46-Q-TCLP	3.34	*0.26*	*0.26*	*0.53*	0.54	*0.53*	3.12	*0.25*	*0.25*	*0.51*	0.51	*0.51*
HS24-47-Q-TCLP	*1.27*	*0.25*	*0.25*	*0.50*	*0.25*	0.53	*1.27*	*0.25*	*0.25*	*0.51*	*0.25*	*0.51*
HS24-48-Q-TCLP	*1.27*	*0.25*	*0.25*	*0.51*	0.46	0.88	*1.27*	*0.25*	*0.25*	*0.51*	0.45	0.80
HS24-49-Q-TCLP	2.14	*0.25*	*0.25*	*0.51*	*0.25*	1.96	2.32	*0.25*	*0.25*	*0.51*	*0.25*	2.07
HS24-50-Q-TCLP	4.60	*0.25*	*0.25*	*0.51*	*0.25*	*0.51*	4.46	*0.25*	*0.25*	*0.51*	*0.25*	*0.51*

Table L.3. Measured TCLP concentrations for replicates A and B of the CCC glasses. Values in red are the detection limits. Values in pink are above the delisting limits reported in Table 3.5.

	Replicate A						Replicate B					
Sample ID	B	Cr	Ni	Pb	V	Zn	B	Cr	Ni	Pb	V	Zn
HS24-01-CCC-TCLP	9.72	*0.25*	*0.25*	*0.50*	3.94	1.49	8.93	*0.25*	*0.25*	*0.51*	3.66	1.40
HS24-02-CCC-TCLP	3.84	*0.25*	*0.25*	*0.50*	1.10	2.49	4.06	*0.25*	*0.25*	*0.50*	1.13	2.51
HS24-03-CCC-TCLP	*1.26*	*0.25*	*0.25*	*0.50*	0.66	0.55	*1.26*	*0.25*	*0.25*	*0.50*	0.64	0.54
HS24-04-CCC-TCLP	*1.26*	*0.25*	*0.25*	*0.50*	0.48	*0.50*	*1.26*	*0.25*	*0.25*	*0.50*	0.49	*0.50*
HS24-05-CCC-TCLP	*1.26*	*0.25*	*0.25*	*0.50*	1.71	*0.50*	*1.26*	*0.25*	*0.25*	*0.50*	1.65	*0.50*
HS24-06-CCC-TCLP	*1.27*	0.51	*0.25*	*0.50*	1.58	*0.50*	*1.26*	0.55	*0.25*	*0.51*	1.56	*0.51*
HS24-07-CCC-TCLP	8.27	0.49	0.31	*0.51*	1.23	6.00	9.08	0.55	0.35	*0.50*	1.35	6.68
HS24-08-CCC-TCLP	*1.26*	*0.25*	*0.25*	*0.50*	*0.25*	*0.50*	*1.26*	*0.25*	*0.25*	*0.50*	*0.25*	*0.50*
HS24-09-CCC-TCLP	*1.26*	1.33	*0.25*	*0.50*	*0.25*	*0.50*	2.67	1.03	*0.25*	*0.50*	*0.25*	*0.50*
HS24-10-CCC-TCLP	4.20	*0.25*	*0.25*	*0.50*	*0.25*	*0.50*	2.10	*0.25*	*0.25*	*0.50*	*0.25*	*0.50*
HS24-11-CCC-TCLP	2.23	*0.25*	*0.25*	*0.50*	*0.25*	0.56	2.40	*0.25*	*0.25*	*0.50*	*0.25*	0.58
HS24-12-CCC-TCLP	3.34	2.58	0.28	*0.50*	13.79	4.13	3.22	2.70	0.28	*0.50*	13.79	4.53
HS24-13-CCC-TCLP	*1.26*	*0.25*	*0.25*	*0.50*	0.34	1.01	*1.26*	*0.25*	*0.25*	*0.50*	0.35	1.04
HS24-14-CCC-TCLP	*1.26*	*0.25*	*0.25*	*0.50*	0.47	0.90	*1.27*	*0.25*	*0.25*	*0.51*	0.45	0.96
HS24-15-CCC-TCLP	136.91	**6.45**	6.75	*0.50*	9.42	4.44	134.87	**6.42**	6.72	*0.51*	9.47	4.34
HS24-16-CCC-TCLP	5.38	0.89	0.45	*0.50*	5.70	1.47	5.36	0.97	0.45	*0.51*	5.78	1.64
HS24-17-CCC-TCLP	1.32	1.82	*0.25*	*0.50*	0.75	1.29	1.42	1.85	*0.25*	*0.50*	0.72	1.39
HS24-18-CCC-TCLP	1.52	*0.25*	*0.25*	*0.50*	0.31	*0.50*	1.40	*0.25*	*0.25*	*0.50*	0.31	*0.50*
HS24-19-CCC-TCLP	3.58	0.86	0.31	*0.50*	0.61	1.63	3.93	0.96	0.34	*0.50*	0.65	1.77
HS24-20-CCC-TCLP	*1.27*	*0.25*	*0.25*	*0.51*	*0.25*	0.67	*1.27*	*0.25*	*0.25*	*0.51*	*0.25*	0.64
HS24-21-CCC-TCLP	10.54	*0.25*	*0.25*	*0.51*	6.98	10.85	9.53	*0.25*	*0.25*	*0.51*	6.51	10.03
HS24-22-CCC-TCLP	1.29	*0.25*	*0.25*	*0.51*	0.53	9.51	*1.28*	*0.26*	*0.26*	*0.51*	0.54	9.47
HS24-23-CCC-TCLP	*1.28*	0.70	*0.25*	*0.51*	*0.25*	0.66	*1.27*	0.73	*0.25*	*0.51*	*0.25*	0.70
HS24-24-CCC-TCLP	2.42	1.98	*0.25*	*0.51*	*0.25*	0.91	3.82	3.16	*0.25*	*0.51*	*0.25*	1.09
HS24-25-CCC-TCLP	*1.27*	1.38	*0.25*	*0.51*	0.66	*0.51*	*1.27*	1.40	*0.25*	*0.51*	0.73	*0.51*
HS24-26-CCC-TCLP	*1.27*	*0.25*	*0.25*	*0.50*	0.59	*0.51*	*1.27*	*0.25*	*0.25*	*0.50*	0.58	*0.51*
HS24-27-CCC-TCLP	1.34	0.84	*0.25*	*0.50*	1.37	*0.51*	*1.27*	0.81	*0.25*	*0.51*	1.35	*0.51*
HS24-28-CCC-TCLP	2.49	0.85	*0.25*	*0.51*	1.15	*0.51*	*1.27*	0.92	*0.25*	*0.51*	1.09	*0.51*
HS24-29-CCC-TCLP	*1.27*	*0.25*	*0.25*	*0.51*	0.70	1.18	*1.27*	*0.25*	*0.25*	*0.51*	0.77	1.29
HS24-30-CCC-TCLP	*1.27*	0.47	*0.25*	*0.51*	0.39	0.54	*1.26*	0.44	*0.25*	*0.51*	0.35	*0.51*
HS24-31-CCC-TCLP	*1.27*	*0.25*	*0.25*	*0.51*	0.53	0.72	*1.27*	*0.25*	*0.25*	*0.51*	0.53	0.72
HS24-32-CCC-TCLP	*1.27*	0.39	*0.25*	*0.51*	0.31	0.99	*1.27*	0.37	*0.25*	*0.51*	0.31	1.04

	Replicate A						Replicate B					
Sample ID	B	Cr	Ni	Pb	V	Zn	B	Cr	Ni	Pb	V	Zn
HS24-33-CCC-TCLP	*1.28*	*0.26*	*0.26*	*0.51*	0.52	*0.51*	*1.28*	*0.26*	*0.26*	*0.51*	0.50	*0.51*
HS24-34-CCC-TCLP	8.05	1.95	*0.25*	*0.51*	0.72	1.83	8.15	2.00	0.26	*0.51*	0.71	1.88
HS24-35-CCC-TCLP	1.49	0.41	*0.25*	*0.51*	1.10	*0.51*	1.46	0.35	*0.25*	*0.51*	1.03	*0.51*
HS24-36-CCC-TCLP	*1.27*	*0.25*	*0.25*	*0.51*	0.37	0.54	*1.27*	*0.25*	*0.25*	*0.51*	0.40	*0.51*
HS24-37-CCC-TCLP	*1.26*	*0.25*	*0.25*	*0.51*	*0.25*	*0.51*	*1.27*	*0.25*	*0.25*	*0.51*	*0.25*	*0.51*
HS24-38-CCC-TCLP	1.68	*0.25*	*0.25*	*0.50*	0.76	0.87	1.82	*0.25*	*0.25*	*0.50*	0.85	0.73
HS24-39-CCC-TCLP	4.20	*0.25*	*0.25*	*0.50*	2.19	0.86	4.24	*0.25*	*0.25*	*0.50*	2.23	0.90
HS24-40-CCC-TCLP	3.06	*0.25*	*0.25*	*0.50*	*0.25*	*0.50*	2.98	*0.25*	*0.25*	*0.51*	0.25	*0.51*
HS24-41-CCC-TCLP	7.28	*0.25*	0.31	*0.50*	0.39	2.57	6.73	*0.25*	0.28	*0.51*	0.37	2.30
HS24-42-CCC-TCLP	5.57	*0.25*	*0.25*	*0.50*	1.69	0.66	5.50	*0.25*	*0.25*	*0.50*	1.65	0.59
HS24-43-CCC-TCLP	5.22	*0.25*	*0.25*	*0.50*	*0.25*	*0.50*	4.84	*0.25*	*0.25*	*0.50*	*0.25*	*0.50*
HS24-44-CCC-TCLP	*1.26*	*0.25*	*0.25*	*0.50*	0.40	0.79	*1.26*	*0.25*	*0.25*	*0.50*	0.41	*0.50*
HS24-45-CCC-TCLP	4.25	*0.25*	*0.25*	*0.51*	5.15	*0.51*	3.64	*0.25*	*0.25*	*0.50*	4.63	*0.50*
HS24-46-CCC-TCLP	4.24	*0.25*	*0.25*	*0.50*	0.80	*0.50*	4.24	*0.25*	*0.25*	*0.50*	0.81	*0.50*
HS24-47-CCC-TCLP	*1.27*	*0.25*	*0.25*	*0.51*	*0.26*	*3.80*	*1.27*	*0.25*	*0.25*	*0.50*	0.27	3.88
HS24-48-CCC-TCLP	1.96	*0.25*	*0.25*	*0.51*	0.74	0.98	1.98	*0.25*	*0.25*	*0.51*	0.74	0.98
HS24-49-CCC-TCLP	3.42	0.62	*0.25*	*0.51*	*0.25*	2.81	3.53	0.60	*0.25*	*0.50*	*0.25*	2.86
HS24-50-CCC-TCLP	419.82	4.27	7.56	*0.51*	*0.26*	*0.51*	410.71	4.11	7.33	*0.51*	*0.25*	*0.51*

Table L.4. Average TCLP concentrations with uncertainties represented by one standard deviation for the Q and CCC glasses. Values in red are the detection limits, values in blue are estimated results, and values in pink are above the delisting limits reported in Table 3.5.

	Q						CCC					
Glass ID	B	Cr	Ni	Pb	V	Zn	B	Cr	Ni	Pb	V	Zn
HS24-01	4.44 ± 0.12	≤0.25	≤0.25	≤0.51	1.15 ± 0.01	2.67 ± 0	9.33 ± 0.56	≤0.25	≤0.25	≤0.5	3.8 ± 0.2	1.45 ± 0.06
HS24-02	13.49 ± 0.14	≤0.25	≤0.25	≤0.51	4.99 ± 0.06	1.94 ± 0.07	3.95 ± 0.15	≤0.25	≤0.25	≤0.5	1.11 ± 0.02	2.5 ± 0.01
HS24-03	≤1.27	≤0.25	≤0.25	≤0.51	0.48 ± 0	0.64 ± 0.2	≤1.26	≤0.25	≤0.25	≤0.5	0.65 ± 0.02	0.55 ± 0.01
HS24-04	≤1.27	≤0.25	≤0.25	≤0.51	0.37 ± 0.01	≤0.51	≤1.26	≤0.25	≤0.25	≤0.5	0.49 ± 0.01	≤0.5
HS24-05	≤1.27	≤0.25	≤0.25	≤0.51	0.41 ± 0	≤0.51	≤1.26	≤0.25	≤0.25	≤0.5	1.68 ± 0.04	≤0.5
HS24-06	≤1.27	≤0.25	≤0.25	≤0.51	0.46 ± 0.01	≤0.51	≤1.26	0.53 ± 0.03	≤0.25	≤0.5	1.57 ± 0.01	≤0.5
HS24-07	≤1.27	≤0.25	≤0.25	≤0.51	≤0.25	0.92 ± 0	8.68 ± 0.57	0.52 ± 0.04	0.33 ± 0.03	≤0.51	1.29 ± 0.09	6.34 ± 0.48
HS24-08	≤1.27	≤0.25	≤0.25	≤0.51	≤0.25	≤0.51	≤1.26	≤0.25	≤0.25	≤0.5	≤0.25	≤0.5
HS24-09	≤1.26	≤0.25	≤0.25	≤0.5	≤0.25	≤0.5	1.96 ± 1	1.18 ± 0.21	≤0.25	≤0.5	≤0.25	≤0.5
HS24-10	1.7 ± 0.02	≤0.25	≤0.25	≤0.51	≤0.25	≤0.51	3.15 ± 1.48	≤0.25	≤0.25	≤0.5	≤0.25	≤0.5
HS24-11	1.93 ± 0.04	≤0.25	≤0.25	≤0.5	≤0.25	0.59 ± 0	2.32 ± 0.12	≤0.25	≤0.25	≤0.5	≤0.25	0.57 ± 0.02
HS24-12	≤1.26	≤0.25	≤0.25	≤0.5	0.88 ± 0.01	0.59 ± 0	3.28 ± 0.08	2.64 ± 0.09	0.28 ± 0	≤0.5	13.79 ± 0	4.33 ± 0.29
HS24-13	≤1.26	≤0.25	≤0.25	≤0.5	0.31 ± 0	0.88 ± 0	≤1.26	≤0.25	≤0.25	≤0.5	0.35 ± 0	1.03 ± 0.02
HS24-14	≤1.26	≤0.25	≤0.25	≤0.5	0.43 ± 0.03	0.87 ± 0.07	≤1.26	≤0.25	≤0.25	≤0.51	0.46 ± 0.01	0.93 ± 0.04
HS24-15	115.63 ± 2.87	4.15 ± 0.01	6.23 ± 0.12	≤0.5	7.22 ± 0.16	3.97 ± 0.09	135.89 ± 1.44	**6.43 ± 0.02**	6.74 ± 0.02	≤0.51	9.45 ± 0.04	4.39 ± 0.07
HS24-16	≤1.27	≤0.25	≤0.25	≤0.51	1.05 ± 0.01	≤0.51	5.37 ± 0.01	0.93 ± 0.06	0.45 ± 0	≤0.5	5.74 ± 0.06	1.56 ± 0.12
HS24-17	≤1.27	≤0.25	≤0.25	≤0.51	≤0.25	0.81 ± 0.04	1.37 ± 0.07	1.83 ± 0.02	≤0.25	≤0.5	0.73 ± 0.02	1.34 ± 0.07

	Q						CCC					
Glass ID	B	Cr	Ni	Pb	V	Zn	B	Cr	Ni	Pb	V	Zn
HS24-18	1.8 ± 0.35	*≤0.25*	*≤0.25*	*≤0.51*	0.33 ± 0.02	*≤0.51*	1.46 ± 0.09	*≤0.25*	*≤0.25*	*≤0.5*	0.31 ± 0	*≤0.5*
HS24-19	*≤1.26*	*≤0.25*	*≤0.25*	*≤0.5*	*≤0.25*	*≤0.5*	3.76 ± 0.25	0.91 ± 0.07	0.33 ± 0.02	*≤0.5*	0.63 ± 0.03	1.7 ± 0.1
HS24-20	*≤1.27*	*≤0.25*	*≤0.25*	*≤0.51*	*≤0.25*	0.66 ± 0.03	*≤1.27*	*≤0.25*	*≤0.25*	*≤0.51*	*≤0.25*	0.65 ± 0.03
HS24-21	*≤1.26*	*≤0.25*	*≤0.25*	*≤0.51*	0.46 ± 0	0.61 ± 0.02	10.04 ± 0.71	*≤0.25*	*≤0.25*	*≤0.51*	6.74 ± 0.33	10.44 ± 0.58
HS24-22	*≤1.27*	*≤0.25*	*≤0.25*	*≤0.51*	*≤0.25*	*≤0.51*	1.28 ± 0.01	*≤0.26*	*≤0.26*	*≤0.51*	0.53 ± 0	9.49 ± 0.03
HS24-23	*≤1.27*	*≤0.25*	*≤0.25*	*≤0.51*	*≤0.25*	*≤0.51*	≤1.27	0.72 ± 0.02	*≤0.25*	*≤0.51*	*≤0.25*	0.68 ± 0.03
HS24-24	*≤1.27*	*≤0.25*	*≤0.25*	*≤0.51*	*≤0.25*	*≤0.51*	3.12 ± 0.99	2.57 ± 0.84	*≤0.25*	*≤0.51*	*≤0.25*	1 ± 0.13
HS24-25	*≤1.26*	*≤0.25*	*≤0.25*	*≤0.5*	*≤0.25*	*≤0.5*	*≤1.27*	1.39 ± 0.01	*≤0.25*	*≤0.51*	0.7 ± 0.05	*≤0.51*
HS24-26	*≤1.26*	*≤0.25*	*≤0.25*	*≤0.51*	0.32 ± 0.01	*≤0.51*	*≤1.27*	*≤0.25*	*≤0.25*	*≤0.5*	0.59 ± 0.01	*≤0.51*
HS24-27	*≤1.26*	*≤0.25*	*≤0.25*	*≤0.5*	*≤0.25*	*≤0.5*	1.3 ± 0.05	0.82 ± 0.03	*≤0.25*	*≤0.5*	1.36 ± 0.01	*≤0.51*
HS24-28	2.05 ± 1.13	*≤0.25*	*≤0.25*	*≤0.5*	*≤0.25*	*≤0.5*	1.88 ± 0.87	0.89 ± 0.05	*≤0.25*	*≤0.51*	1.12 ± 0.04	*≤0.51*
HS24-29	*≤1.26*	*≤0.25*	*≤0.25*	*≤0.51*	0.26 ± 0	0.57 ± 0.03	*≤1.27*	*≤0.25*	*≤0.25*	*≤0.51*	0.74 ± 0.05	1.23 ± 0.08
HS24-30	*≤1.27*	*≤0.25*	*≤0.25*	*≤0.51*	*≤0.25*	*≤0.51*	*≤1.26*	0.45 ± 0.02	*≤0.25*	*≤0.51*	0.37 ± 0.02	0.52 ± 0.02
HS24-31	*≤1.27*	*≤0.25*	*≤0.25*	*≤0.51*	*≤0.25*	0.56 ± 0.02	*≤1.27*	*≤0.25*	*≤0.25*	*≤0.51*	0.53 ± 0	0.72 ± 0
HS24-32	*≤1.27*	*≤0.25*	*≤0.25*	*≤0.51*	*≤0.25*	*≤0.51*	*≤1.27*	0.38 ± 0.01	*≤0.25*	*≤0.51*	0.31 ± 0	1.02 ± 0.04
HS24-33	*≤1.27*	*≤0.25*	*≤0.25*	*≤0.5*	0.42 ± 0.01	*≤0.51*	*≤1.28*	*≤0.26*	*≤0.26*	*≤0.51*	0.51 ± 0.02	*≤0.51*
HS24-34	*2.39 ± 0.01*	*≤0.25*	*≤0.25*	*≤0.5*	*≤0.25*	*0.69 ± 0.01*	8.1 ± 0.07	1.97 ± 0.04	0.26 ± 0.01	*≤0.51*	0.72 ± 0.01	1.85 ± 0.04
HS24-35	*≤1.27*	*≤0.25*	*≤0.25*	*≤0.5*	*0.68 ± 0*	*≤0.51*	1.48 ± 0.02	0.38 ± 0.04	*≤0.25*	*≤0.51*	1.06 ± 0.04	*≤0.51*

	Q						CCC					
Glass ID	B	Cr	Ni	Pb	V	Zn	B	Cr	Ni	Pb	V	Zn
HS24-36	≤1.27	≤0.25	≤0.25	≤0.5	0.33 ± 0	≤0.51	≤1.27	≤0.25	≤0.25	≤0.51	0.38 ± 0.02	0.52 ± 0.02
HS24-37	≤1.27	≤0.25	≤0.25	≤0.51	≤0.25	≤0.51	≤1.26	≤0.25	≤0.25	≤0.51	≤0.25	≤0.51
HS24-38	1.3 ± 0.01	≤0.25	≤0.25	≤0.51	0.59 ± 0	0.62 ± 0.02	1.75 ± 0.09	≤0.25	≤0.25	≤0.5	0.8 ± 0.06	0.8 ± 0.1
HS24-39	3.37 ± 0.12	≤0.25	≤0.25	≤0.5	1.77 ± 0.05	0.77 ± 0.08	4.22 ± 0.03	≤0.25	≤0.25	≤0.5	2.21 ± 0.03	0.88 ± 0.03
HS24-40	2.67 ± 0.08	≤0.25	≤0.25	≤0.51	≤0.25	≤0.51	3.02 ± 0.06	≤0.25	≤0.25	≤0.51	0.25 ± 0	≤0.51
HS24-41	5.5 ± 0.24	≤0.25	≤0.25	≤0.51	0.36 ± 0.01	1.73 ± 0.07	7.01 ± 0.39	≤0.25	0.29 ± 0.02	≤0.51	0.38 ± 0.01	2.43 ± 0.19
HS24-42	4.07 ± 0.11	≤0.25	≤0.25	≤0.51	1.19 ± 0.01	≤0.51	5.53 ± 0.05	≤0.25	≤0.25	≤0.5	1.67 ± 0.03	0.63 ± 0.05
HS24-43	1.54 ± 0.06	≤0.25	≤0.25	≤0.51	≤0.25	≤0.51	5.03 ± 0.27	≤0.25	≤0.25	≤0.5	≤0.25	≤0.5
HS24-44	≤1.27	≤0.25	≤0.25	≤0.51	0.34 ± 0	≤0.51	≤1.26	≤0.25	≤0.25	≤0.5	0.41 ± 0.01	0.65 ± 0.2
HS24-45	≤1.27	≤0.25	≤0.25	≤0.51	0.38 ± 0.01	≤0.51	3.94 ± 0.43	≤0.25	≤0.25	≤0.51	4.89 ± 0.37	≤0.51
HS24-46	3.23 ± 0.15	≤0.26	≤0.26	≤0.52	0.53 ± 0.02	≤0.52	4.24 ± 0	≤0.25	≤0.25	≤0.5	0.81 ± 0.01	≤0.5
HS24-47	≤1.27	≤0.25	≤0.25	≤0.51	≤0.25	0.52 ± 0.01	≤1.27	≤0.25	≤0.25	≤0.51	0.27 ± 0	3.84 ± 0.06
HS24-48	≤1.27	≤0.25	≤0.25	≤0.51	0.46 ± 0	0.84 ± 0.05	1.97 ± 0.01	≤0.25	≤0.25	≤0.51	0.74 ± 0	0.98 ± 0
HS24-49	2.23 ± 0.13	≤0.25	≤0.25	≤0.51	≤0.25	2.01 ± 0.08	3.47 ± 0.08	0.61 ± 0.01	≤0.25	≤0.5	≤0.25	2.83 ± 0.04
HS24-50	4.53 ± 0.1	≤0.25	≤0.25	≤0.51	≤0.25	≤0.51	415.26 ± 6.44	4.19 ± 0.11	7.45 ± 0.16	≤0.51	≤0.25	≤0.51

Pacific Northwest National Laboratory

902 Battelle Boulevard
P.O. Box 999
Richland, WA 99354

1-888-375-PNNL (7665)

www.pnnl.gov